THE BEHAVIOUR OF AIR POCKETS IN HYDRAULIC STRUCTURES WITH PARTICULAR REFERENCE TO DROPSHAFT/TUNNEL BENDS

By

SAWSAN KHALID MOHAMAD HIMMO
B.Sc. (University of Baghdad) 1976

A thesis submitted to the University of Glasgow in fulfillment of the requirements for the Degree of Doctor of Philosophy

October 1986

Department of Civil Engineering
University of Glasgow
GLASGOW
UNITED KINGDOM

TO MY PARENTS

ACKNOWLEDGEMENTS

The author would like to express her gratitude to the Iraqi Government for awarding a scholarship to pursue this research.

The author would like to express her grateful appreciation to Professor H.B. Sutherland, Head of Department of Civil Engineering, for his help and encouragement.

The author is deeply grateful to Dr. D.A. Ervine for his supervision, guidance, help and encouragement throughout the course of this research.

Appreciation is extended to the technical staff, to Mr. A. Gray for building the physical model and Mr. W. Henderson for his help in carrying out the changes to the physical model during the course of work. Thanks should also go to members of the Computer Advisory Service for their help, and to members of the photography unit for their help in part of this work.

The author expresses her thanks to Miss I.P. Campbell for her excellent typing.

Finally, the author expresses her sincere thanks to her husband, Adnan, her son, Mazin, and all her family, without whose encouragement and support this work would not have been completed.

Sawsan K.M. Himmo
Glasgow, U.K.
October 1986

ABSTRACT

This thesis investigates the behaviour of large air pockets forming at the junction bend of a vertical dropshaft and a horizontal or slightly inclined outlet tunnel. A secondary thrust of the work concerns the behaviour of air pockets in straight pipe sections inclined at a shallow slope both upwards and downwards from the horizontal. These aims were achieved by constructing a physical model of the situation and also by deriving theoretical models of each physical situation arising. The experimental data is compared with the derived theoretical models, and both are compared with past research in this field.

The physical model was tested over a range of nine different geometries. The radius of the junction bend (R'/D) was tested at values 0.5, 1.0 and 1.5, the tunnel slope (θ) was varied between +1.5°, 0° and -1.5°, the water flow rate was varied from 0 to 0.04 m^3/s, and the air flow rate, in the form of independent injection of air bubbles down the dropshaft, was varied from 0 to 0.02 m^3/s.

The ultimate aims of the work were as follows:

(a) to obtain a deeper understanding of air pocket behaviour at vertical bends and in straight pipes.

(b) to ascertain if simplified theoretical models can be made realistic enough to describe air pocket behaviour, especially the chaotic behaviour of a two-phase flow at a dropshaft/tunnel bend.

(c) to provide insight and information for the designers of such hydraulic structures.

In the first chapter an introduction to air presence in Civil Engineering Hydraulic Structures is given, with reference to the benefits and problems associated with air presence and the structures which have experienced problems. A state-of-the-art review of past research work on air pockets in closed conduit hydraulic structures is given in Chapter (2).

Chapter (3) is concerned with producing theoretical models for air pockets at the dropshaft/tunnel bend. This includes air pockets blowing back, air pockets with a drowned jump, air pockets with a hydraulic jump and air pockets clearing downstream from the bend. Also, theoretical models are produced for air pockets in straight pipes inclined above and below the horizontal.

Chapter (4) contains a description of the design of the experimental apparatus, the instrumentation used, as well as details of the experimental procedure.

Chapter (5) includes the experimental results for the behaviour of air pockets at the nine dropshaft/tunnel bend geometries tests. The experimental results for each geometry tested are presented graphically, covering the various flow regimes found to exist at the bend, the depth of air pocket forming at the bend, the upper limits of air pocket blowback up the dropshaft, the lower limits of air pocket clearing downstream from the bend, as well as information on the velocity and Froude number of flow under the air pocket forming at the bend. A comparison is carried out between the three bend radii used as well as the three angles of outlet tunnel.

Chapter (6) includes the results of air pockets in straight pipes. Most of the data was obtained for air pockets rising in an upward sloping straight pipe. The design of the experimental apparatus permitted only a few data points to be taken for the case of the downward sloping straight pipe, for reasons outlined in Chapter (6).

Chapter (7) contains the comparison between the theoretical models and experimental data for both air pockets at the bend and in straight pipes. Empirical equations are derived for the case of air pockets clearing downstream from the bend, where no theoretical model was attempted due to the flow complexities involved. A comparison is also carried out between the author's data and theoretical models and most of the available previous research data.

Chapter (8) includes a discussion on the findings of this work, conclusions and suggestions for the future work.

In the broadest terms, this work shows that four stable regimes of flow are identifiable at a dropshaft/tunnel bend and these regimes can be represented with reasonable accuracy by theoretical models of the flow, based on force-momentum and energy principles. The work also shows that the bend radius (R'/D), the outlet tunnel slope (θ), the Froude number of the flow (Fr_o), and the ratio of air to water (β) are all important parameters affecting whether or not an air pocket will blow back, remain trapped at the bend or clear downstream.

Air pocket behaviour can now be accurately predicted for the case of upward sloping straight pipes, although further work is required for the case of downward sloping straight pipes.

TABLE OF CONTENTS

LIST OF SYMBOLS AND ABBREVIATIONS

A or A_p	area of the pipe
a	half the angle of the free water surface with the axis of a circular pipe
A_1, A_2, A_3	area of flowing water at sections 1, 2 and 3 respectively
A_2	area of the flowing water below the free surface
A_b	air pocket area
b	width of the free surface in a circular pipe
C_1	air pocket speed in horizontal conduit for stationary water, or water moving under transient effects
C_2	velocity of water below the air pocket in horizontal conduit
C_1, C_2	coefficients to account for a weighted average liquid velocity and the velocity profile respectively in equation (2.43)
C_o , C_1	distribution parameter and factor depending on fluid properties respectively in equation (2.49)
C	basic correction factor in equation (4.4)
C_d	drag coefficient ; coefficient of discharge
D	pipe diameter
d	depth of water upstream of the air pocket ; depth of channel ; diameter of orifice throat in equation (4.4)
D_e	equivalent pocket diameter
d_b	bubble diameter
E	velocity of approach factor
f	$C_1/\sqrt{gd}$; friction factor
F	$C_2/\sqrt{gh}$
Fr_o	full pipe Froude number = $V_o/\sqrt{gD}$

Fr_1	Froude number below the air pocket = $V_1/\sqrt{gy_e}$
F_{oc}	Froude number above which air pockets clear from the bend
F_{or}	Froude number below which air pockets vent back up the shaft
F_s	Force required for clearing the bend pocket
G_g	mass velocity of gas
G_ℓ	mass velocity of liquid
g	acceleration
H	maximum depth of air pocket
H_{abs}	absolute pressure head
h	depth of water below the pocket in horizontal conduit; difference in pressure (mm water) between upstream and downstream pressure tappings in equation (4.4) ; vertical distance from the nose of the pocket to a point on the air pocket surface ; depth of water in tank above the weir; the depth below water surface to the element of integration.
j	volumetric flux $(Q_W + Q_A)/A$
<j>	average volumetric flux
K	constant = $1.62\sqrt{\zeta}$
K_1	constant for the rising velocity in vertical pipes for inertia flow ; dimensionless parameter = K_1 $(N_f , N_{E\ddot{o}} , \theta)$
K_2	constant for the rising velocity in vertical pipes for viscous flow ; factor depending on flow rates, flow geometries and velocity distribution
K_3	parameter to allow for the effect of inclination
K_a	the bulk modulus of air
L	air pocket length ; length of weir in equation (4.3)
L_s	separation distance between air pockets
m	a function of N_f ; water factor distribution

N_{Ar}	Archimedes number
$N_{Eö}$	Eötvös number = $(\rho_1-\rho_2)gD^2/\sigma$
N_f	dimensionless inverse viscosity
N	$3\sqrt{14.5\ \rho_1^2 g/\mu_1^2}$
N_{Re_b}	bubble Reynolds number
n	air volume/$(\pi D^3/4)$
P_{air} or P	the pressure along the air pocket surface
P_1, P_2, P_3	pressure at sections 1, 2 and 3 respectively
P_A, P_B, P_C	pressure at points A, B and C respectively
Q	discharge through the orifice meter in equation (4.4)
Q_A or Q_a	air flow rate
Q_C	water discharge required for clearing air pockets
Q_w	water flow rate
q	liquid velocity in the bubble
R	pipe radius
R'	bend radius
R_C	radius of curvature of the bubble nose
R'_C	equilibrium cylindrical radius
Re	Reynolds number = $\rho VD/\mu$
r	radius of bend at any point
r_e	equivalent radius of air pocket
S_1, S_2	the flow forces upstream the cavity and below the cavity respectively
S_o	pipe slope = Sinθ
V	bubble volume
V_{air}	air volume
$\bar{V}$ or $\bar{V}_L$	mean velocity of water = $(Q_w + Q_A)/A$

V_b	air pocket speed in horizontal conduit for moving water
V_b'	rising velocity for a string of air bubbles
V_{br}	bubble rise velocity
V_c	water velocity required to clear the air pocket from a straight pipe, either by entrainment or bodily sweeping
V_{c_1}	clearing velocity in a pipe of 1.0 m diameter
V_e	minimum water velocity required to entrain air
V_o	pipe full velocity
V_r	air pocket rising velocity in inclined pipes, both for stationary and moving water
V_s	air pocket velocity in vertical pipes for moving water
V_∞	air pocket velocity in vertical pipes for stationary water
V_1	water velocity below the air pocket
V_1, V_2, V_3	water velocities at sections 1, 2 and 3 respectively
Wb or We	Weber number
Y	property group
y_e	effective depth of the flowing water below the pocket
y_1	depth of water below the pocket in circular pipe
Z	Reynolds number correction factor in equation (4.4)
Z_1	vertical depth to the datum
α	void fraction
α_o	correction factor to the kinetic energy head ($V^2/2g$)
α'	correction factor to the hydrostatic pressure head (y)
β	air-water ratio (Q_A/Q_W)

β_o	correction factor to the momentum flux (ρQV)
β'	correction factor to the pressure forces $\rho g(D/2)A_p$
Δ	energy losses
δ	indication for the direction of flowing water
δ_o	film thickness
ϵ	expansibility factor in equation (4.4)
ζ	shape factor
θ	angle of inclination of conduit with horizontal
λ	$[(\rho_g/\rho_a)(\rho_\ell/\rho_w)]^{1/2}$; friction coefficient
μ	dynamic viscosity
μ_a	air viscosity
μ_w	water viscosity
ν	kinematic viscosity (μ/ρ)
π	natural constant
ρ_a	air density (at 101.3 KPa and 20°C)
ρ_g or ρ_2	gas density
ρ_ℓ or ρ_1	liquid density
ρ_w	water density (at 101.3 kPa and 20°C)
Σ	surface tension parameter = $\sigma/(\rho_1-\rho_2)gR^2$
σ	surface tension
σ_{aw}	air-water surface tension (at 101.3 kPa and 20°C)
τ_o	shear stress = $(f/4)(\rho_1/2)V^2$
Φ	angle between the tangent at air pocket nose and horizontal for air pockets at bend ; angle between the tangent at air pocket nose and pipe wall in straight inclined pipes
Ψ	$(\rho_w/\rho_\ell)[\mu(\rho_w/\rho_\ell)^2]^{1/3}$
Γ	factor determined experimentally

Chapter One

INTRODUCTION TO AIR POCKET BEHAVIOUR IN HYDRAULIC STRUCTURES

1.1 GENERAL INTRODUCTION

In many Civil Engineering Hydraulic structures there is an interaction between the flowing water through the structure and the adjacent air. Sometimes this interaction can be beneficial or it can cause problems and the alleviation of these problems can be costly.

The objective of this work is to study the interaction between pockets of air and flowing water in closed conduits, with particular reference to dropshaft/tunnel systems. Typical examples of dropshaft/tunnel systems are illustrated in Fig. (1.1) and can be used for the following purposes:

1. Diverting water from the main stream when building a dam, where it is used later as a flood control device to reduce the water level in the reservoir at times of high flood.

2. To transfer water from a high level to a lower level, such as diverting a stream outside a catchment area through the dropshaft/tunnel system to a reservoir, or transferring water from a high reservoir to a low reservoir.

3. In the circulating water systems used in cooling water from

thermal power stations.

The interaction between the flowing water and the adjacent air can develop in the following cases:

1. Morning-glory spillways which must be designed to have a capacity to convey both of the design flood and its entrained air, as in Fig. (1.1.a).

2. Vertical shafts where the falling jet of water will entrain large quantities of air at small water discharges, as in Fig. (1.1.b).

3. Measuring weirs that need adequate ventilation to prevent sub-atmospheric pressures, false readings and to eliminate surging.

4. Inverted siphons that can be damaged due to blowback of entrained air, as in Fig. (1.1.c).

5. Long pipelines that require air release and vacuum relief valves especially at high points in the pipeline.

6. Outlet gates that require adequate aeration to prevent the development of low-pressures which can lead to cavitation damaged, as in Fig. (1.1.d).

1.2 PRESENCE OF AIR IN WATER LINES

Air present in water lines can take many forms, ranging from minute bubbles to large air pockets. This presence can either be beneficial or can cause problems in the water line. For each case examples will be given with the causes of air presence in water

lines.

1.2.1 Forms of Air in Water Lines

Air may be present in water lines in the following forms:

(a) Minute bubbles which arise in a water line from a turbulent action due to a falling nappe. These are generally very small bubbles with a diameter of about 0.10 mm. Their presence in water lines is considered to be insignificant, because they can be removed out of the lines easily by the flowing water.

(b) Bubbles which arise also from the turbulent action of a falling nappe, hydraulic jump, and air separation at low pressures. The diameter of bubbles ranges between 1-5 mm and are mostly ellipsoidal in shape. Their rising velocity in stationary water is about 0.23 m/s which is independent of conduit size[180]. In moving water conditions, bubbles with effective diameter less than 3 mm will have a velocity which varies non-systematically with different flow rates. Bubbles with effective diameter between 3-4.5 mm will have a velocity which is slightly increased from that in stationary water to about 0.26 m/s[16,180].

(c) Pockets can be defined as air cavities formed as a result of a coalescence of "bubbles" and "minute bubbles". They can also be formed by entrapment of large quantities of air as occurs during the filling of a pipeline, at high points of pipelines where vents are used to reduce sub-atmospheric pressure, and in siphons where the negative pressure allows the dissolved air to come out of solution.

1.2.2 Causes of Air Presence in Water Lines

The air can be present in a water line due to the following:

1. Vortices at the intake structure

Vortices generated at the intake often lead to air introduction into the system, and the quantity of air introduced depends on intensity of vortex. The formation of these vortices at the intake depends on inlet geometry, depth of submergence of intake and the flow rate. Such vortices have a longitudinal axis parallel to the direction of flow as in pump intakes (Fig. 1.2.a) and flow under a sluice gate (Fig. 1.2.b).

2. The Pumps

The low pressures at pump impellers may be a source of air introduction into the system. When a pipeline is supplied by a centrifugal pump there is initially a physical disturbance in the flow of water at pump impeller which causes air to be extracted from water near the pump.

3. Dropshaft

Water allowed to fall freely some distance down a vertical shaft entrains air when it impinges on an ambient water surface. The lower part of the shaft will contain air bubbles which will either rise up to the water surface and be released, or will be transported down the shaft to the tunnel system, depending on the flow rate (Fig. 1.3).

4. Filling of lines

Large quantities of air can be entrapped during filling a pipeline, or when increasing the discharge of a pipeline which is running partially full.

5. Air separation at low pressure

In areas of low pressure the dissolved air in water usually comes out of solution, as is the case in topographic high points in a pipeline or siphons, which are a typical example of hydraulic structures working under negative pressure (Fig. 1.4).

6. Vents

Vents used at high points to reduce sub-atmospheric pressure are often a source of entrapment of large quantities of air (Fig. 1.5).

7. Other causes

Leakage in water lines may be a source of air introduction into the line. Steam power plants which circulate large quantitites of hot water will introduce air into the system due to the separation of dissolved air.

1.2.3 Benefits of Air Presence in Water Lines

The air present in water lines can be beneficial in reducing cavitation, reducing large negative pressures, priming siphons and supplying ventilation to water lines.

(a) Cavitation reduction

Cavitation is induced by surface irregularities and low pressures in a turbulent shear layer, and can be reduced by using steel linings, high quality surface finishes, and using aeration devices. The first method is very expensive so it is used only in special areas such as outlet gates. The second method may present some difficulties during the life of the hydraulic structure, in that defects may still occur on the concrete surface. The only relatively cheap method is the third one of using aeration devices, such as air slot ramps.

The low pressures in the flowing water are used to induce large quantitites of air from the atmosphere, which is broken into small bubbles and dispersed over the full depth of flow. When water reaches vapour pressure, vapour bubbles (cavities) will start to form and move downstream, until they reach an area of higher pressure where the cavities will condense and suddenly collapse. This collapse gives rise to extremely high pressures, which causes cavitation erosion if it happens against a solid boundary.

The entrained air in the flowing water affects the compressibility of air-water mixtures so that as vapour cavities collapse, the resulting pressures will be smaller than those occurring in water without free air due to the compressibility effect.

(b) Priming siphons

A siphon is a pipe bent to form two limbs of unequal length so that a liquid may be transferred from a higher to a lower level at a rate proportional to the difference in head (Fig. 1.6). A siphon spillway is used to pass flood water from a reservoir and can also act as a control for sudden surges in

canals and forebays[88]. The siphon will run full when all the air in the siphon barrel is removed. The process of removal of air and filling the siphon with water is called priming.

Air in the siphon barrel can be removed by the natural flow of water through the siphon, and is said to be self-priming. It can also be removed by using air pumps, where the siphon will run from zero discharge to full bore (black water siphon) with no intervening stable range of flows.

When air is allowed to enter a siphon (in controlled volumes) during the priming process, then the siphon will prime in a slow controlled rate. This siphon is called an air-regulated siphon, where it will automatically adjust its discharge over the full range to maintain a virtually constant water level on the upstream side. This type of siphon is more flexible in its uses, less violent in operation, and safer than a black water siphon, both from the point of view of preventing the inevitable flood wave that results from sudden priming, to full-bore discharge, and because air regulation eradicates the hunting and vibration problems that occur in black water siphons.

(c) Ventilation

Ventilation is the process of allowing air to enter or escape from a closed hydraulic system. Air vents are usually used at the base of dropshafts or morning-glory spillways to remove air pockets (1.1.a), at high points in water lines to reduce sub-atmospheric pressure and air accumulations (Fig. 1.4),
and in outlets from high head dams to stabilise the hydraulic jump in the outlet tunnel (Fig. 1.1.d). In this case the flow is aerated, thus preventing the formation of

sub-atmospheric pressures and cavitation damage.

Air vent structures used in pipelines have three primary purposes:

1. Evacuation of air during filling

2. Removal of air during operation, and

3. Preventing pipe collapse during draining

1.2.4 Problems Arising from Air Presence in Water Lines

The presence of free air in water lines may give rise to a range of problems and may cause difficulties in operating hydraulic structures. The following are the most important problems:

(a) Reduction of capacity

The presence of air pockets in waterlines restricts the flow and increases the head losses. This is especially true if an hydraulic jump forms at the d/s end of an air pocket. This is reflected in a reduction in the capacity of the flow of the structure and reduction in its efficiency. Figure (1.7) indicates the effect of the presence of an air pocket on the energy line given by Richards[136]. This problem is usually common just downstream of high points in water lines, and also at the junction of a dropshaft/tunnel system.

(b) Surges and blow backs

The presence of air in water lines may also give rise to surges and blow backs of considerable magnitude. When the water flows under an air pocket present at a high point in a water line (Fig.

1.8), it may sweep some of the generated bubbles at the end of the pocket. The swept bubbles may coalesce into large air pockets which periodically blow back upstream to the high point causing pressure fluctuation.

(c) Oscillation of water in shaft/tunnel systems

This usually occurs in power stations where a plunging water nappe into the shaft entrains air bubbles which may be transported down to the junction of the shaft/tunnel system. These air bubbles usually accumulate at the bend forming an air pocket which may periodically collapse and cause oscillation in the water level in the shaft and may also cause vibration (Fig. 1.9).

(d) White water

This is the water which has a milky appearance due to the presence of large quantities of minute bubbles and it is chemically corrosive.

(e) Reduction of pump efficiency

When a pump is pumping water which carries air, or when air-water mixture is fed into a turbine, their efficiences are significantly reduced. Supplying a turbine with air-water mixture affects its operation by a drop in its output and hence its efficiency, also it may cause water hammer pressures. Air carried into a pump by a vortex at its inlet delays pump priming. It was reported by Denny and Young[39] that a presence of 1% of air reduces the pump efficiency by 15%. Tests were carried out by Mitsukiyo et al[114] on the performance of three centrifugal pumps, which was reduced by increasing the entrained air. When the entrained air reached 15% of water volume the three pumps lost prime and ceased to function.

(f) Difficulties in filter operation

Entrapped air in water lines may sometimes interfere with the operation of filtration plants causing serious effects. The surges produced by air presence make it difficult to maintain a good filter cake. The settling basins, which are present before the filtration plants, allow much of the dissolved air to come out of solution forming minute bubbles which then get bound to the sand filters and thus reduce the filter efficiency.

(g) Corrosion

The presence of air in ferrous water lines causes corrosion by making more oxygen available for the process. The corrosion deteriorates the pipe wall and increases friction which increases the head losses through the line.

(h) Biological effects

Constant air presence in water lines encourages the growth of certain aeroboic organisms.

1.3 SOME HYDRAULIC STRUCTURES WHICH EXPERIENCED THE PROBLEM OF AIR PRESENCE

In the previous section some general problems caused by air presence in water lines have been outlined. It is also important to look at some practical examples of hydraulic structures where damage has been caused to either the structure itself or its operation.

The main problems seem to be oscillation, surges and blowback, blowout and vibration.

(a) Hunterston "B" Power Station outfall

The Hunterston "B" Power Station outfall in Scotland (Fig. 1.10) exhibited flow instability in the water filled shaft/tunnel system which took the form of oscillations in both land and seal pit shafts. This was reported by Townson[165] 1975. These oscillations increased gradually until the seal pit weir was submerged and spillage occurred at the land shaft. The problem was not excessive but nevertheless warranted model investigations. The fall from the seal pit weir crest to the standing water level in the shaft below caused entrainment of air bubbles. From model scale tests it was found that this entrained air was the main cause of the oscillations. In the shaft, air bubbles circulated in a vertical downward direction according to their size and position in the flow. Some of this air returned to the surface while the rest was carried around the bend into the roof of the tunnel.

This air tended to form a cavity downstream of the bend. The oscillation occurred due to the periodic collapse of the cavity frontal head when the cavity reached a certain size. The cavity collapse also caused a variation in shaft density and oscillation of the cavity interface. In order to avoid oscillation, model tests showed that this may be achieved by the following:

- Adjustment of length of shaft sizes so that natural frequencies are small compared to cavity oscillation in separating zones.

- Control of separation zone size by local conduit geometry and/or venting.

- Allowing the air to be swept through the system to a point where it could be released.

(b) The Canadian River project

In 1966 Colgate[35] reported on the Canadian River project. This project included an aqueduct system, pumping plants and regulating reservoirs. In one of the main pipelines from a regulating reservoir water was flowing under gravity. This pipeline was designed so that at normal flow the hydraulic gradient will be parallel to the average ground profile and the water pressure will be less than 30 m head. While filling or draining the pipeline, or discharging less than normal flow through the system, there was a danger of surging, air entrainment and water hammer.

A tower-type check structure was designed to prevent adverse conditons such as over-pressures and water hammer when discharging less than normal flow, and to maintain the proper hydraulic gradient during normal flow (Fig. 1.11). Each tower consisted of 90° bend to turn the water vertically upwards, a 180° return bend with a pipe open to atmosphere at the top, and a 90° bend at the bottom of the downstream leg to return the flow to the main conduit. These towers were installed so that during normal operation the hydraulic gradient will be above the top of each tower causing the system to run full.

For flow less than normal, or no flow, this alignment also kept the conduit full between towers. The open pipe at the top of the tower prevented overpressure damage when there was surging in the conduit during changing flows and also allowed air entrainment at low discharges in downstream leg of tower. Model studies were carried out to devise a vent structure to remove the entrained air downstream the check tower when the tower is flowing partially full. Air which passed the vent formed bubbles. These bubbles moved either upstream or downstream, depending on the pipe slope, discharge,

and bubble size. Studies were carried out to get the best conduit slope to allow the air bubbles to move upstream to the vent and to be removed from the line. It was found that a downward conduit slope of 0.087 downstream from the vent will ensure the return upstream of the amount of air which may pass the air vent, or to be pumped into the conduit.

(c) Littlebrook 'D' Power Station

In 1979, Goldring[62] reported on Littlebrook 'D' Power Station. The cooling water system of the power station draws its condenser cooling water from a body of water and pumps it through the condenser to be heated by the condensing steam. The top of the condenser was about 10-20 m above the lowest water level and the cooling water in the condenser's water box was at sub-atmospheric pressure. Thus the cooling water system was run as a siphon, see Fig. (1.12). It was necessasry to provide a seal at the outlet, both to limit the minimum pressure in the condenser's outlet water box to a value above vapour pressure of the cooling water, and to prevent air moving back into the condenser and breaking the siphon. The siphon seal at Littlebrook 'D' is shown in Fig. (1.12).

Air was drawn into the siphon as dissolved air in the incoming water. This air came out of solution in sub-atmospheric pressure areas in condensers. Also air leakage from faulty joints was possible. The air started to form an air-void on the sloping roof of the down leg, and to grow in size, thus causing additional head loss across the siphon which was approximately equal to the drop in water level from the crest to the free surface.

Model studies were carried out to specify the ability of the siphon to pass this air with minimum head los. It was found

that air-void removal from the siphon crown could be achieved by either:

1. Entrainment by the plunging nappe, which is similar to the void length adjustment process. or

2. Entire void removal from the siphon, making use of Gandenberger's[59] experimental results on the minimum water velocity needed to clear an air-void from a high point in a pipeline for various slopes of the pipe downstream of the high point.

(d) San Pablo Dam in California

Hall[86] reported on San Pablo Dam near Oakland, California, which was constructed in 1917-1920 and was provided with both an open-channel spillway and an auxiliary vertical shaft spillway equipped with outlet gates below full reservoir level. The horizontal leg of the shaft spillway was laid on a re-entrant grade, and a weir was built below the outlet to assure submergence of the tunnel. The falling water down the shaft entrained air into the horizontal leg when it impacted the water surface. The behaviour of the entrained air was considered dangerous. The lower part of the shaft contained air bubbles which either rose up the shaft or were transported to the tunnel system. These air bubbles accumulated as air pockets at the roof of the tunnel and moved slowly along the grade of the tunnel toward the outlet, discharging periodically with explosive violence, throwing water as spray in the air to a height of 15 m. This explosive violence caused vibration in the tunnel which was also a serious problem.

(e) Chabot Dam near Oakland

Hall[86] also reported on the tunnel spillway at the Chabot Dam,

constructed of masonry in 1889 and has a side-channel spillway discharging into a tunnel. The operation of the tunnel spillway under full discharge has never been satisfactory because of the poor hydraulic properties of the tunnel inlet and outlet.

When the maximum carrying capacity was approached, the tunnel mouth was submerged, and air entrained in the water at the drop over the weir was carried into the tunnel. This air rose up to the roof of the tunnel within 122 m of the inlet, and a portion escaped through the downstream portal. A section of the tunnel, 30-60 m long below the inlet, was under pressure of the air and water mixture, and when sufficient pressure was created, a portion of the air accumulated along the roof discharged violently back through the inlet, throwing spray into the air. The water which was rushing in to replace the discharged air, caused severe vibrations in the masonry of the tunnel.

1.4 FLOW PATTERNS IN CLOSED CONDUITS

Flow patterns in closed conduits depend on the air flow rate relative to the water flow rate and the slope of the conduit[55]. Flow patterns which can occur in a horizontal conduit were described according to the physical appearance of flow by Alves[8] as follows, see Fig. (1.13):

- Bubble Flow: The air forms in bubbles at the upper surface of the pipe. The bubbles and water velocities are about equal.
  If the bubbles are dispersed through the water, the flow is called "Froth Flow".

- Plug Flow: For increased air flow rates the air bubbles

coalesce with plugs of air and water alternately flowing along the top of the pipe. This represents typical air pocket flow regimes as experienced in Civil Engineering structures.

- Stratified Flow: Increasing air flow rates produces a horizontal interface separating the air and water flows.

- Wave Flow: As the airflow rate is increased, surface waves appear on the stratified flow interface.

- Slug Flow: Wave amplitudes are large enough to seal the conduit. The wave forms a frothy slug where it touches the roof of the conduit.

- Annular Flow: For greater air flow rates the water flows as a film on the wall of the pipe, while the air flows in a high speed core down the axis of the pipe.

- Spray Flow: For very great airflow rates, the annular film is stripped from the pipe walls and is carried in the air as entrained droplets.

In hydraulic structures, conduits are often placed on a slope, which will cause changes in the flow patterns and shape of the flowing air pockets. Flow patterns in horizontal conduits also have been defined by Baker[16] as in Fig. (1.14). The given correlation can be used for other gases and liquids by substituting the appropriate quantities into the following parameters:

G_g = mass velocity of gas, $Kg/(m^2\text{-}s)$

G_ℓ = mass velocity of liquid, $Kg/(m^2\text{-}s)$

λ = $[(\rho_g/\rho_a)(\rho_\ell/\rho_w)]^{1/2}$, $\lambda = 1.0$ for air water mixtures

μ = dynamic viscosity, Pa.s (N-sec/m^2)

ρ_g = gas density, Kg/m^3

ρ_a = air density (at 101.3 KPa and 20°C) = 1.20 Kg/m^3

ρ_ℓ = liquid density, Kg/m^3

ρ_w = water density (at 101.3 KPa and 20°C) = 988 Kg/m^3

σ = interfacial surface tension, N/m

σ_{aw} = air-water surface tension (at 101.3 KPa and 20°C) = 0.0728 N/m

ψ = $(\rho_w/\rho_\ell)\ [\mu(\rho_w/\rho_\ell)^2]^{1/3}$, $Pa^{1/3}.S^{1/3}$

ψ = 0.10 $Pa^{1/3}.S^{1/3}$ if the liquid used is water.

Typical values of G_g/λ and $G_\ell\lambda\psi/G_g$, shown in Fig. (1.14), are worked out below for the case of air/water mixtures in a pipe of 152 mm inside diameter. The value of $G_\ell\lambda\psi/G_g$ varies from 4116.65 for β = 0.02 to 164.66 for β = 0.50, where β = air water ratio, i.e. Q_A/Q_W. On the other hand, the value of G_g/λ varies from 0.011027 for Q_A = 0.1667 x 10^{-3} m^3/s to 0.9922 for Q_A = 15 x 10^{-3} m^3/s. The above values indicate that the expected flow regimes can be bubble flow, plug flow and stratified flow, depending on the airflow and waterflow rates.

Wallis[177] presented flow patterns for vertical upward flow of air and water for a 25.4 mm diameter tube, as shown in Fig. (1.15). Wallis notified that different flow patterns can be obtained for different variables. The areas covered by a particular regime can alter in size and shape when some variables are changed, such as pressure and pipe diameter. For certain combinations of parameters,

an entire regime may disappear from the graph altogether.

1.5 THE OBJECTIVE OF THE INVESTIGATION

To investigate the behaviour of a two phase bubbly mixture descending a vertical dropshaft and subsequently entering a horizontal or slightly inclined tunnel section via a right angled bend. The major thrust of the work is to investigate the nature of air pocket (or air cavity) formation and behaviour at the dropshaft/tunnel bend, including air-pocket blow-back, air-pocket trapped at the bend and air-pocket clearing along the tunnel section. Secondary thrusts of the work include an investigation of the rise velocity of air-pockets in the straight tunnel section and also the conditions necessary to clear air-pockets along straight pipes inclined slightly downwards. In all cases experimental results are compared with simple theoretical models.

A schematic representation of the physical system is shown in Fig. (1.1.b). A total of four independent parameters will be varied in the experimental work. These are:

1. The air flow rate through the system which will vary between zero and 20 ℓ/s. This is adequate to give an air/water ratio up to 50% which is comparable to that found in the prototype.

2. The water flow rate through the system which can be increased up to 60 ℓ/s, the limit flow capacity of the pump used.

3. The tunnel inclination to the horizontal which will be changed from:

+1.50° for an upward slope of tunnel

0° for a horizontal tunnel

-1.50° for a downward slope of tunnel

4. The radius of the 90° bend where three bends will be tested for each angle of inclination of tunnel with the horizontal. The non-dimensional bend radius $\acute{R}/D$ used will be 0.5, 1.0, 1.50.

There are other physical parameters which will not be varied in the experimental work. These include: Pipe diameter, tunnel and dropshaft lengths, other gases and liquids apart from air/water, and surfactants.

For each experimental test run the author has attempted to establish:

i) The regime of flow

ii) Physical dimensions of the air-pockets such as length and depth of the pockets

iii) Stability of the air-pocket, i.e. if the pocket is stationary, blowing back or clearing

iv) Air-pocket velocity in the tunnel section

v) Water velocities acting upstream, downstream and under the pocket

vi) The relationship between experimental data and quasi-steady theoretical models based on energy, force-momentum and continuity principles

The ultimate aim of the work is:

i) To develop an understanding of the behaviour of such hydraulic systems

ii) To recommend design criteria for similar systems, such as dam outlets, power station outlets

iii) To obtain an understanding of scale effects involved in modelling such systems

iv) To determine the effectiveness of simple theoretical models in predicting such complex two phase flow problems.

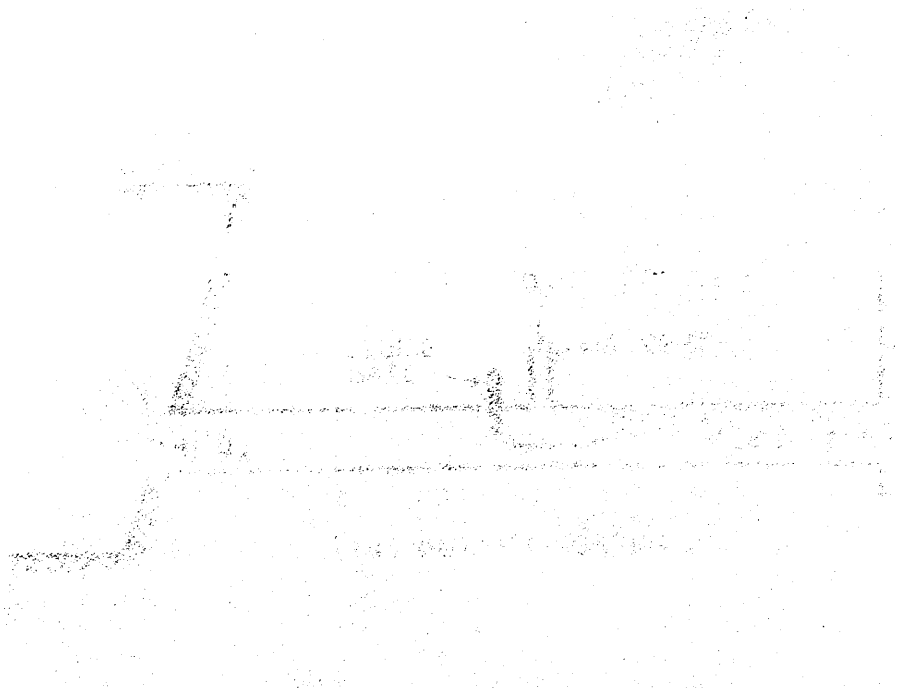

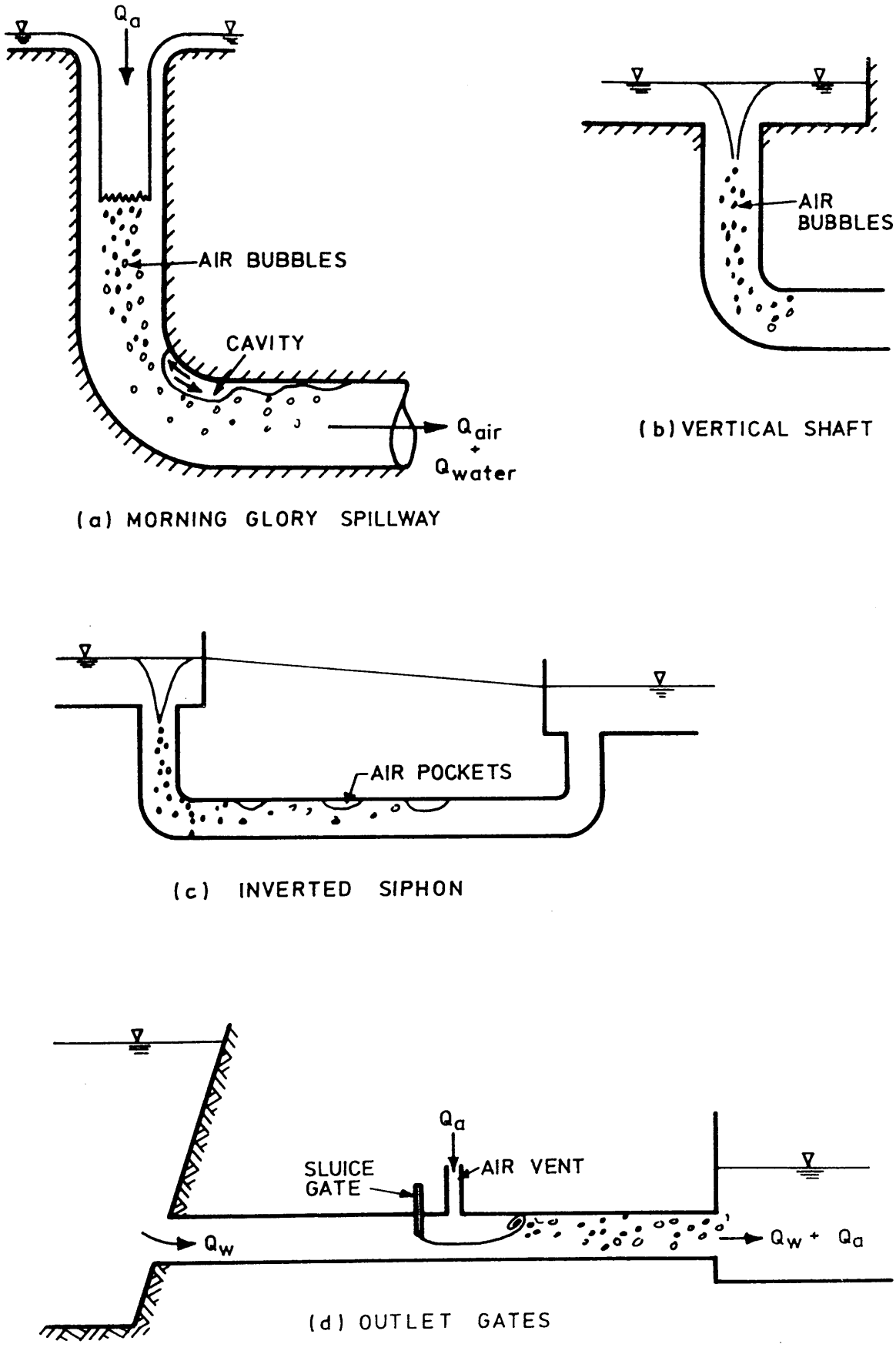

FIG. (1.1) EXAMPLES OF AIR/WATER MIXTURE IN HYDRAULIC STRUCTURES

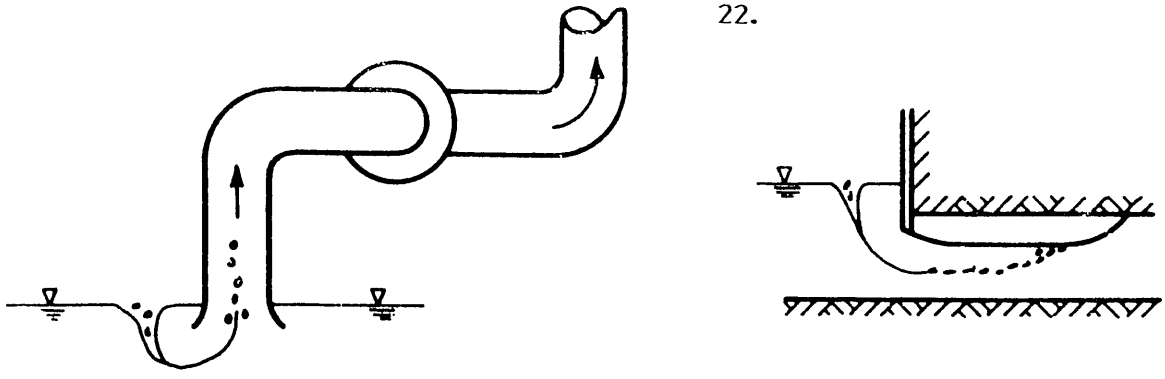

(a) PUMP INTAKE

(b) SLUICE GATE

FIG (1.2) VORTICES AT THE INTAKE

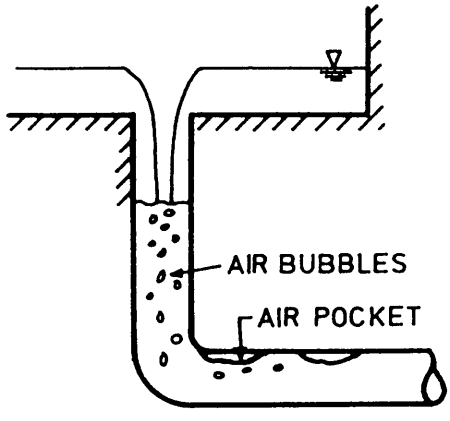

FIG. (1.3) VERTICAL SHAFTS

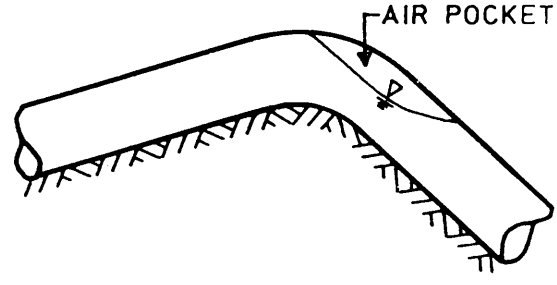

FIG. (1.4) AIR SEPARATION AT HIGH POINTS

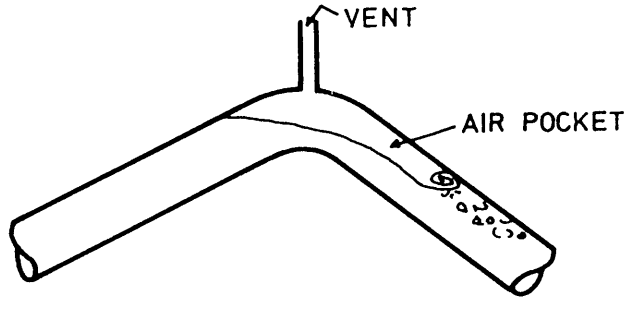

FIG. (1.5) VENTS AT HIGH POINTS

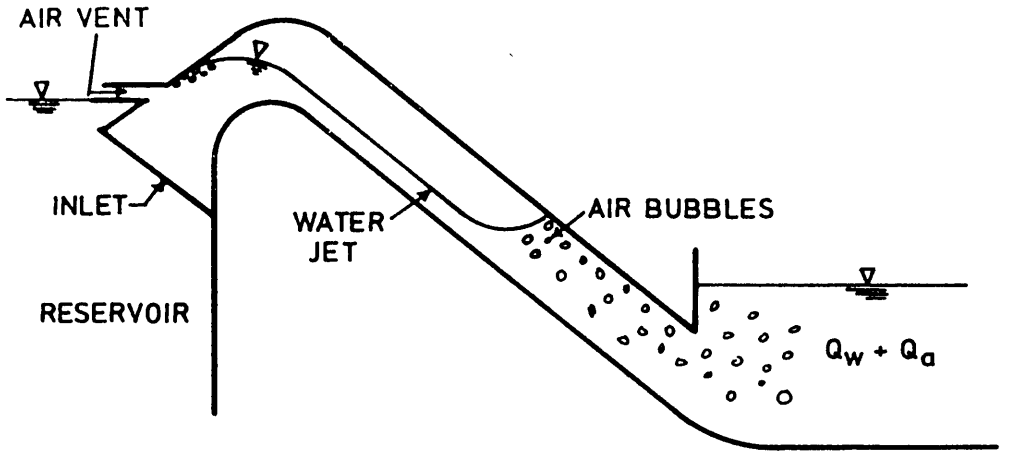

FIG. (1.6) SIPHON

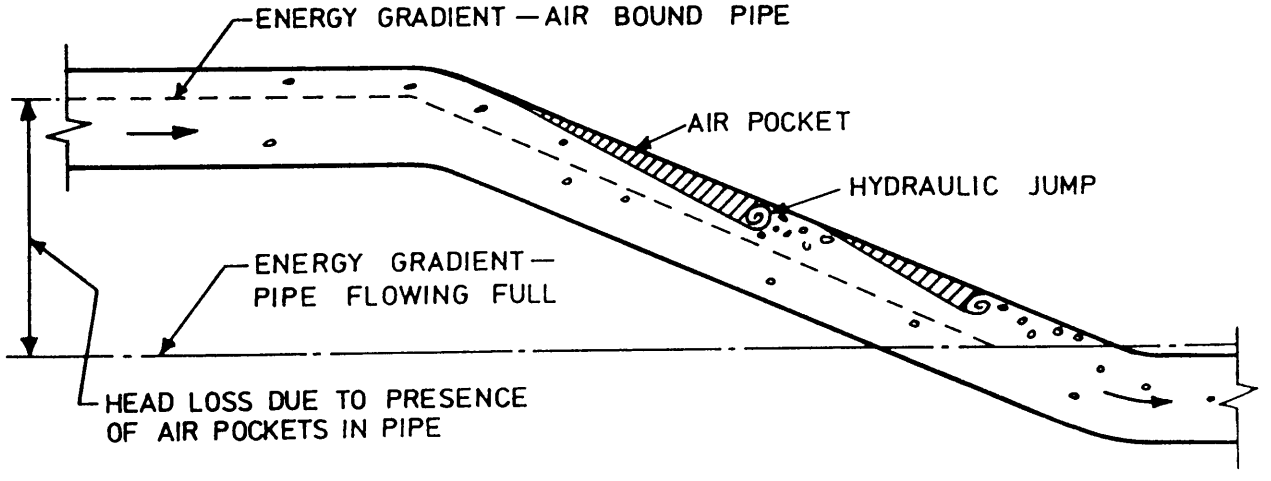

FIG. (1.7) THE EFFECT OF PRESENCE OF AIR POCKET ON ENERGY GRADIENT

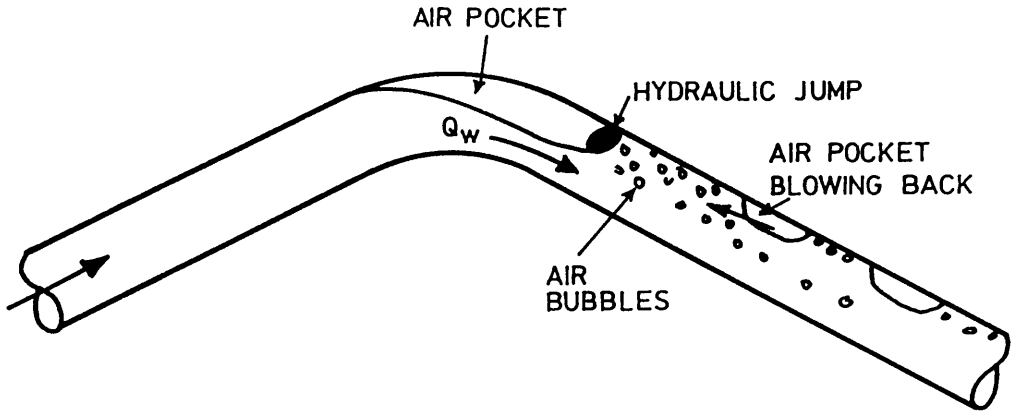

FIG. (1.8) AIR POCKETS BLOWING BACK TO THE HIGH POINT

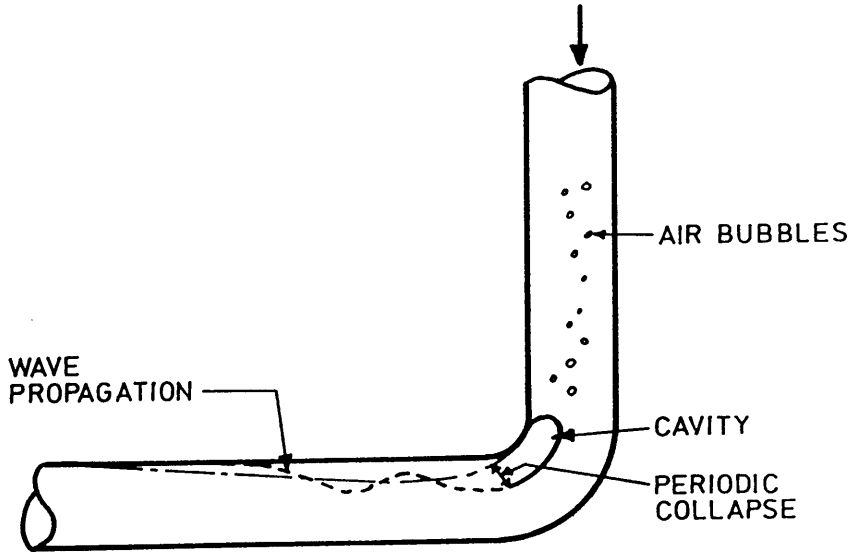

FIG. (1.9) PERIODIC COLLAPSE OF AIR CAVITIES AT THE JUNCTION OF SHAFT/TUNNEL SYSTEM

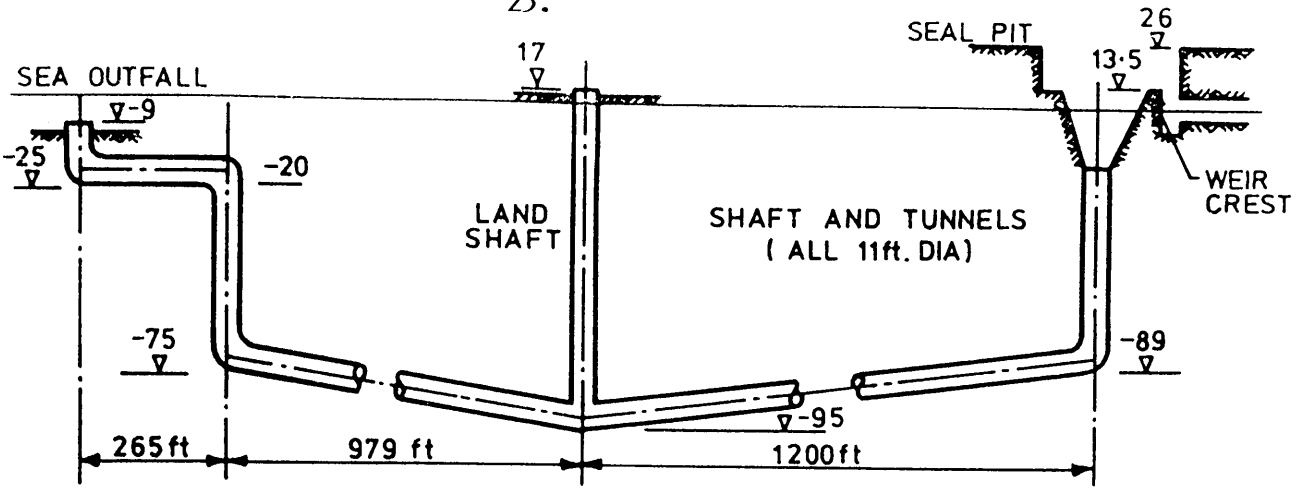

FIG. (1.10) LONGITUDINAL PROFILE OF OUTFALL SYSTEM (not to scale)

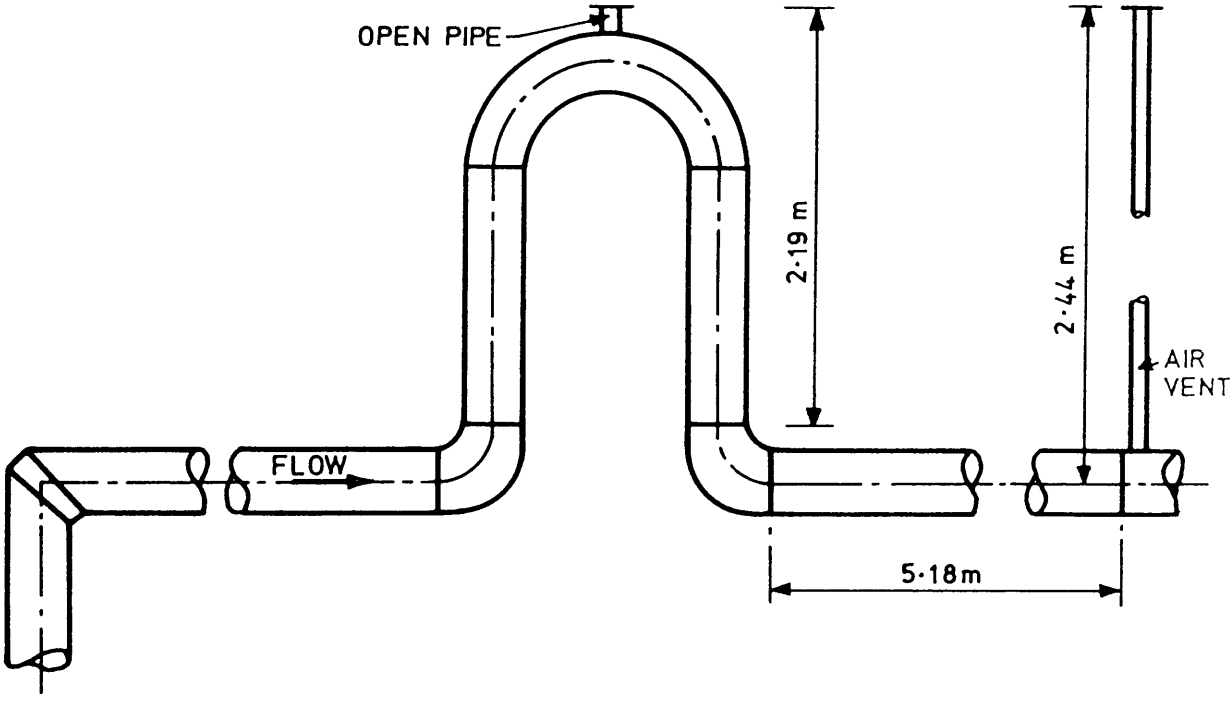

FIG. (1.11) CHECK TOWER OF THE CANADIAN RIVER MAIN AQUEDUCT

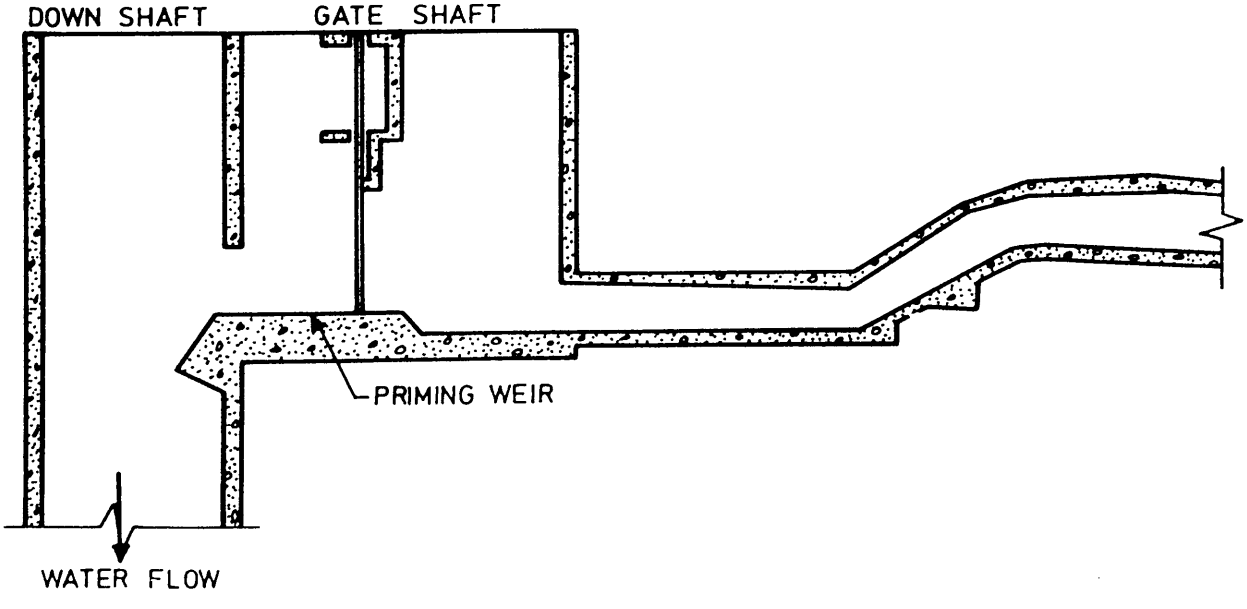

FIG. (1.12) LITTLEBROOK "D" SIPHON SEAL WEIR

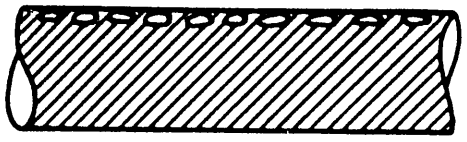

BUBBLY FLOW

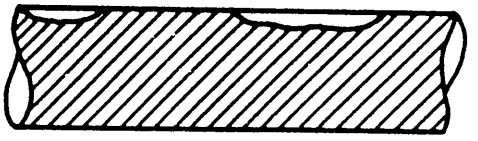

PLUG FLOW

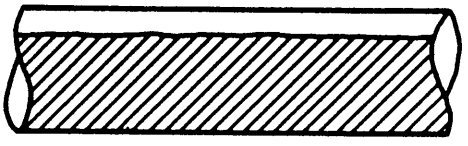

STRATIFIED FLOW

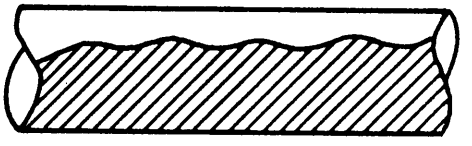

WAVE FLOW

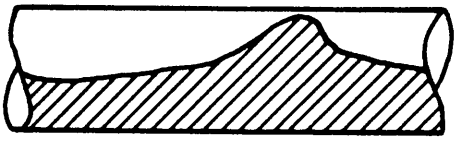

SLUG FLOW

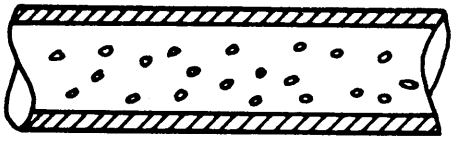

ANNULAR FLOW

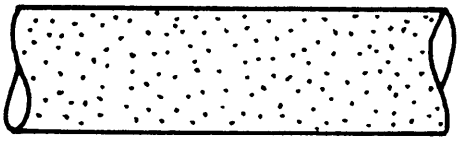

SPRAY FLOW

FIG. (1.13) FLOW PATTERNS OBSERVED IN A HORIZONTAL CONDUIT, ALVES

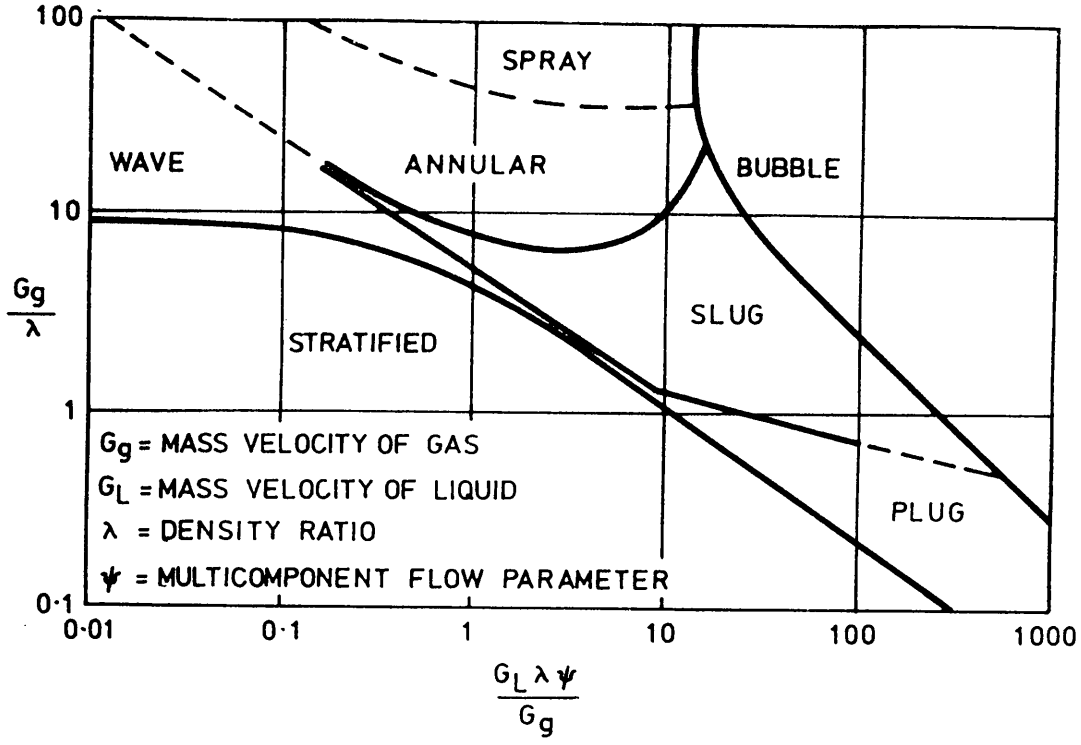

FIG. (1.14) FLOW PATTERNS IN HORIZONTAL PIPE, BAKER (Ref.16)

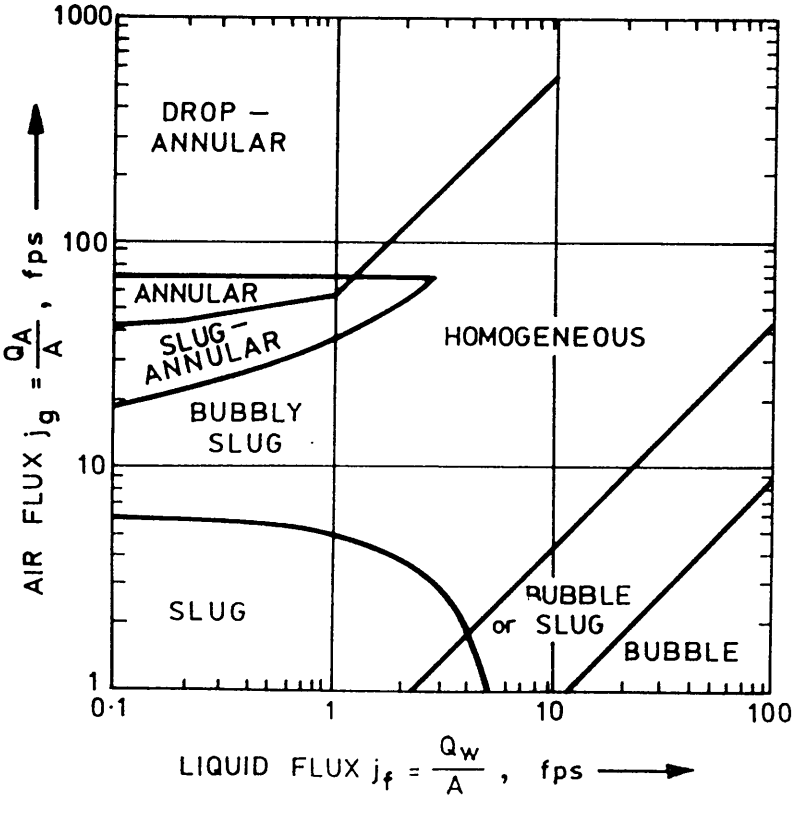

FIG. (1.15) FLOW PATTERN BOUNDARIES FOR VERTICAL UPFLOW OF AIR AND WATER AT 15 psia IN A 1 IN. DIA. TUBE, WALLIS (Ref. 177)

Chapter Two

REVIEW OF PREVIOUS RESEARCH ON THE BEHAVIOUR OF AIR-POCKETS

2.1 INTRODUCTION AND DEFINITION OF TERMS

In this chapter a review of previous research on the behaviour of air pockets will be carried out. This will include the behaviour of air pockets in both stationary and moving water, for vertical, horizontal and inclined conduits. The review will also include the effect of the direction of the flowing water on the air pocket and other factors which affect the air pocket rising velocity such as inertia, viscosity and surface tension forces.

The review will also include air pocket behaviour at the junction of dropshaft/tunnel systems, which essentially is the subject of this thesis, as well as blowing back of air pockets and clearing of pockets in inclined conduits.

The following are definitions of terms used in this review for the rising velocity of air pockets and related parameters, given in a schematic form:

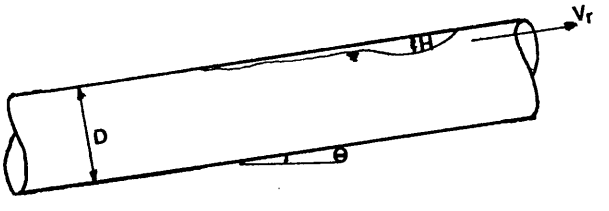

An air pocket, sometimes referred to as an air cavity, plug flow,or slug flow if H/D > 0.5.

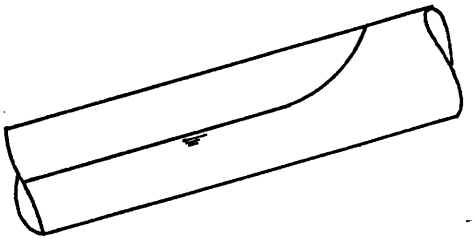

Continuous air pocket

Single air pocket

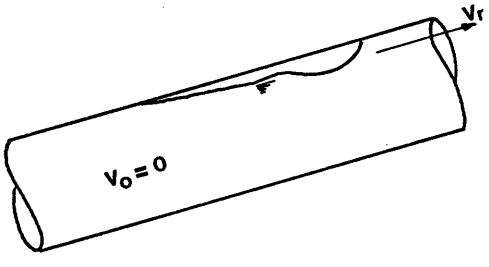

Air pocket rising in stationary water

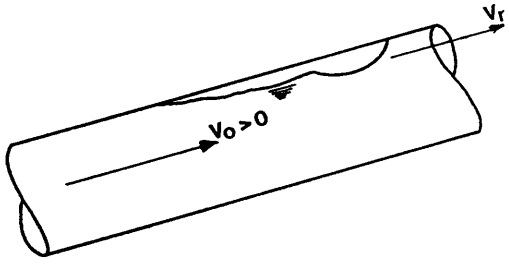

Air pocket rising in moving water

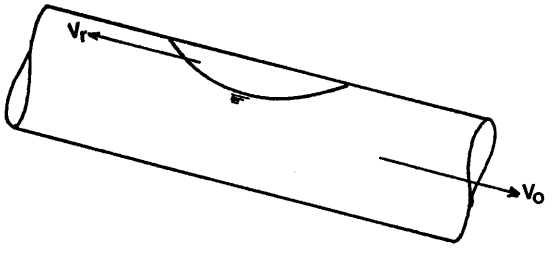

Air pocket rising in water moving in the opposite direction, i.e. blowback

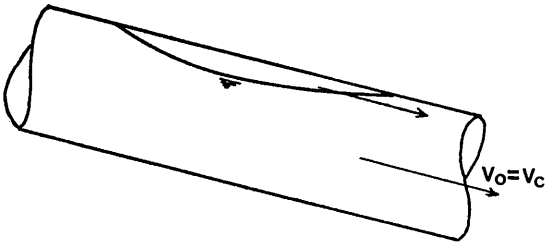

Air pocket clearing in the downward direction by bodily sweeping

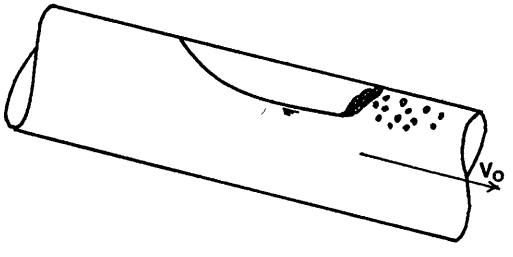

Air pocket gradually clearing by entrainment

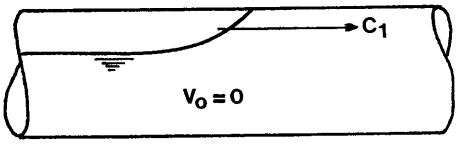

Air pocket speed in stationary water for a horizontal conduit

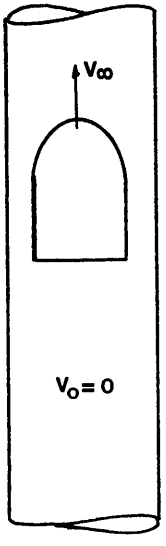

Air pocket rising in stationary water for a vertical conduit

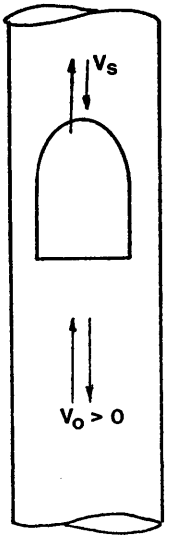

Air pocket rising in upward water flow, and ascending or descending in downward waterflow

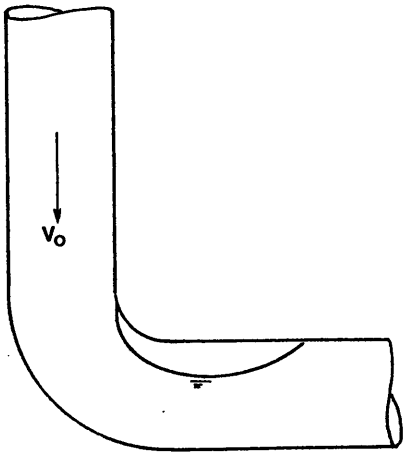

Air pocket trapped at the junction of a dropshaft/ tunnel system

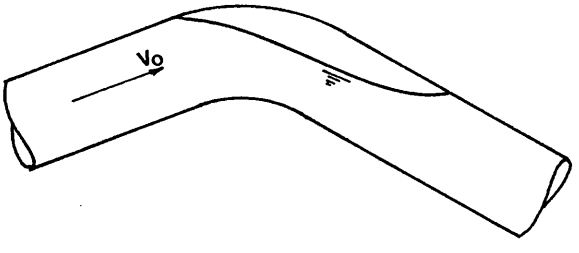

Air pocket trapped at a high point in a pipe-line

2.2 THE BEHAVIOUR OF AIR POCKETS IN VERTICAL PIPES

Many investigators have studied the rising velocity of air pockets in vertical pipes, although mainly in the field of Chemical Engineering. In this context most of the work has been done using liquids of different viscosities and pipes of very small diameter. Some investigators have proposed theoretical models for the pocket itself, including the shape of the pocket and have given extensive details of the nose region of the pocket, which appears to have a significant effect on the rise velocity of the air pocket. The review will include; the rise velocity of air pockets in stationary and moving water, the behaviour of expanding air pockets, and also the effect of the direction of the flowing liquid on the rising velocity of air pockets. The general solution for the rising velocity of air pockets will be given and to what extent this solution can be applied for the case of Civil Engineering structures.

2.2.1 The Rising Velocity of Air Pockets in Stationary Water

The behaviour of an air pocket in a vertical conduit depends on the size of the bubble. When the bubble is quite small it will be spherically shaped and will rise along a vertical rectilinear path[181]. Larger bubbles become ellipsoidal in shape and tend to rise along helical paths. A further increase in the bubble size gives the bubble a spherical capped shape and will rise along a rectilinear path. Any further increase in size will cause the bubble to have a cylindrical shape and to be an air pocket or sometimes called slug flow.

An air pocket will rise through a denser liquid due to its buoyancy. There are some factors which will affect this movement, such as liquid inertia, air compressibility, liquid viscosity and surface tension. The velocity (V_∞) with which a single air pocket will rise is governed by the interaction between buoyancy and the

above mentioned factors which are acting on the air pocket as a result of its shape and motion. Wallis[177] expressed the balance between buoyancy and these three factors in terms of the following three dimensionless groups:

$$\frac{\text{Inertia}}{\text{buoyancy}} \qquad \frac{\rho_1 \ V_\infty^2}{Dg(\rho_1 - \rho_2)} \tag{2.1}$$

$$\frac{\text{Viscosity}}{\text{buoyancy}} \qquad \frac{V_\infty \ \mu_1}{D^2 g(\rho_1 - \rho_2)} \tag{2.2}$$

$$\frac{\text{Surface tension}}{\text{buoyancy}} \qquad \frac{\sigma}{D^2 g(\rho_1 - \rho_2)} \tag{2.3}$$

Solutions were obtained when only one dimensionless group governs the motion, and subsequently a general solution was obtained incorporating all three parameters.

First if viscosity and surface tension were considered negligible, then from equation (2.1) the rising velocity will be as follows:

$$V_\infty = K_1 \sqrt{\frac{\rho_1 - \rho_2}{\rho_1}} \ \sqrt{gD} \tag{2.4}$$

For the case of air pocket in water $\rho_2 << \rho_1$ so equation (2.4) becomes:

$$V_\infty = K_1 \sqrt{gD} \tag{2.5}$$

An approximate analytical solution for vertical flow in a circular tube was obtained by Dumitrescu[42] and by Davies and Taylor[38]. Values of the constant (K_1) obtained by these authors were:

$$\text{Dumitrescu} \qquad K_1 = 0.351 \tag{2.6}$$

$$\text{Davies \& Taylor} \qquad K_1 = 0.328 \tag{2.7}$$

Experimental results obtained by Dumitrescu[42] and White and Beardmore[181] were as follows:

$$\text{Dumitrescu} \qquad K_1 = 0.346 \tag{2.8}$$

$$\text{White \& Beardmore} \qquad K_1 = 0.345 \tag{2.9}$$

Experiments done by Nicklin et al[123] for air pockets rising relative to the liquid ahead of them gave a value of the rising velocity of air pockets equal to that found by Dumitrescu. Fig. (2.1) shows the experimental results found by Nicklin where the rising velocity is plotted as a function of the air pocket length. It can be noted from the results that the non-expanding pockets where the liquid take-off is below the pocket, i.e. there is no liquid velocity, all rise at the same velocity and according to the following equation:

$$V_\infty = 0.35 \sqrt{gD} \tag{2.10}$$

For the case of single air bubbles rising in an infinite body of water, Davies & Taylor[38] found that bubbles have a spherical shape, based on a series of successive photographs for bubbles rising in nitrobenzene. This spherical shape enabled them to find the conditions which must be satisfied at its surface, and by applying Bernoulli's equation to steady flow relative to the bubble, they found the equation for the rising velocity of the bubble related to the radius of curvature of the bubble nose as follows:

$$V_\infty = \frac{2}{3} \sqrt{gR_C} \qquad (2.11)$$

This equation is applied only near the stagnation point where an assumption is made that the flow over the forward part of the bubble is the same as that calculated for a sphere moving in a frictionless liquid. Further calculations based on the pressure distribution measured over the surface of a solid of nearly the same shape as the bubble, produced the following equation:

$$V_\infty = 0.78 \sqrt{gR_C} \qquad (2.12)$$

In their experimental values for (V_∞), which is plotted in Fig. (2.2), against $\sqrt{R_C}$, it is noted that they lie closely around the line of equation (2.11) which means that the flow near the front of a bubble is close to the theoretical flow near the front of a complete sphere in an inviscid fluid.

Davies & Taylor[38] also introduced an expression for the rising velocity in terms of the bubble volume (V), as follows:

$$V_\infty = 24.8\ V^{1/6} \qquad (2.13)$$

Collins[36] found that the radius of curvature (R_C) can be correlated to the bubble volume (V) in the following equation:

$$R_C = 1.465\ V^{1/3} \qquad (2.14)$$

Collins examined this result with equation (2.13), after rearranging it as follows:

$$V_\infty = 0.792\ (g\ V^{1/3})^{1/2} \qquad (2.15)$$

Substituting the value of (V) from equation (2.14) into equation (2.15) the following is obtained:

$$V_\infty = 0.654\ \sqrt{gR_C} \qquad (2.16)$$

It is noted that equation (2.16) is very close to equation (2.11), and that (V_∞) is a function of the bubble volume.

For the case when viscosity is the dominant force, as the case in highly viscous flows, from equation (2.2) the rising velocity will be as follows:

$$V_\infty = K_2\ \frac{gD^2(\rho_1 - \rho_2)}{\mu_1} \qquad (2.17)$$

From experimental results the value of the constant (K_2) for vertical round tubes was as follows:

Wallis[177] $K_2 = 0.010$ (2.18)

White & Beardmore[181] $K_2 = 0.0096$ (2.19)

When surface tension is the dominant force equation (2.3) can be arranged as follows:

$$N_{E\ddot{o}} = \frac{gD^2(\rho_1 - \rho_2)}{\sigma} \qquad (2.20)$$

where $N_{E\ddot{o}}$ is a surface tension parameter, known as the Eötvös number. It is a type of Weber number for air/water mixtures. Bretherton[28] found that for vertical round tubes surface tension will dominate if the Eötvös number $N_{E\ddot{o}} < 3.37$ which, for air/water mixtures, gives a pipe diameter up to 4.95 mm below which surface tension is the dominant force.

Zukoski[192] combined the effect of viscosity and surface tension on the rising velocity of air pockets. Zukoski gave the surface tension parameter in terms of the radius of tube as follows:

$$\Sigma = \frac{\sigma}{gR^2(\rho_1 - \rho_2)} \qquad (2.21)$$

where he gave $\Sigma \leq 1.20$ as the criterion for surface tension to be the dominant force. For air/water this corresponds to pipe of 4.93 mm diameter, as suggested by Bretherton[28]. For the criterion of viscosity dominance Zukoski used the Reynolds number as a parameter, which can be obtained by dividing equation (2.1) by equation (2.2) as follows:

$$Re = \frac{\rho_1 V_\infty D}{\mu_1} \qquad (2.22)$$

Zukoski found that a value of Reynolds Number greater than 400 was required for independence from viscous effects. When using equation (2.10) to substitute for (V_∞) in equation (2.22) for the suggested value of (Re), the required pipe diameter for the rising velocity to be independent of viscous effects is about 5 mm.

To obtain a general solution Wallis[177] rearranged the three parameters in equations (2.1),(2.2) and (2.3) in order to get a two dimensional plot of any two parameters with the third one as the independent parameter. The dimensionless bubble velocity defined by equation (2.9) is plotted versus a dimensionless inverse viscosity (N_f) (obtained from equations (2.1) and (2.2)) and is shown in Fig. (2.3), where N_f is given as:

$$N_f = \frac{[D^3 g(\rho_1 - \rho_2)\rho_1]^{1/2}}{\mu_1} \qquad (2.23)$$

Another dimensionless parameter was obtained by Wallis by eliminating both (V_∞) and (D) from equations (2.1), (2.2) and (2.3). This is called the Archimedes Number (N_{Ar}) as:

$$N_{Ar} = \frac{\sigma^{3/2}\,\rho_1}{\mu_1^2 g^{1/2}(\rho_1 - \rho_2)^{1/2}} \qquad (2.24)$$

Experimental data shown in Fig. (2.3) yields three solutions equivalent to equations (2.9), (2.18) and (2.21). They are:

Inertia dominant	$N_f > 300$, $N_{E\ddot{o}} > 100$	
	$K_1 = 0.345$	
Viscosity dominant	$N_f < 2$, $N_{E\ddot{o}} > 100$	
	$K_1 = 0.01\ N_f$	(2.25)
Surface tension dominant	$N_{E\ddot{o}} = 3.37$	
	$N_f^2 = 6.2\ N_{Ar}$	(2.26)

If we calculate the pipe diameters required for each of the three criteria above, it is clear that inertia is the main consideration in the Civil Engineering context as viscous effects are only important up to a pipe diameter of 2 mm (for air/water mixtures) and surface tension up to 27 mm diameter pipe. Neither size would be used even in model studies of vertical pipes and thus is of academic interest only. It may be of interest here to refer to Fig. (2.4) indicating the surface tension effect for vertical, horizontal and inclined pipes, the latter two categories showing surface tension effects up to diameters of 150 mm to 200 mm corresponding to an Eötvös Number of 3000. This is an order of magnitude greater than vertical pipes, and mainly due to the fact that in vertical pipes the rising air pocket is assumed to have no contact with the pipe wall.

White and Beardmore[181] used an alternative method for plotting their results using another parameter called the property group (Y).

$$Y = \frac{g\,\mu_1^4}{\sigma^3 \rho_1} \tag{2.27}$$

which is a ratio of surface tension/viscosity and is constant for air/water mixtures. (Y) is equal to $(1/N^2_{Ar})$ when the gas density is low compared to liquid density. A plot of (K_1) versus $(N_{E\ddot{o}})$ as a function of (Y) is shown in Fig. (2.5), indicating that when (Y) is reduced the inertia force will dominate the air pocket rising velocity. When considering the effect of all parameters (K_1) could be expressed by the following equation given by Wallis[177] as:

$$K_1 = 0.345(1 - e^{-0.01\,N_f/0.345})(1-e^{(3.37 - N_{E\ddot{o}})/m}) \tag{2.28}$$

where (m) is a function of (N_f) and takes the following values:

$$m = 10 \qquad 250 < N_f$$

$$m = 69\, N_f^{-0.35} \qquad 18 < N_f < 250$$

$$m = 25 \qquad N_f < 18$$

It is of interest to note the equations of the rising velocity of air pockets obtained by Brown[31] which correlates the velocity to the film thickness, and accounts for liquid viscosity. Brown found that, although the air pocket shapes are different in the transition region, they are similar in the nose region. He also found that the frontal radius of the pocket is equal to 0.75 of the equilibrium cylindrical radius (R_c'). Brown defined R_c' as:

$$R_c' = R - \delta_o \tag{2.29}$$

where δ_o is the equilibrium film thickness. Then Brown presented a correlation for the pocket velocity independent of liquid velocity using (R_c') instead of tube radius (R) as follows:

$$V_\infty = 0.496 \sqrt{gR_c'} \tag{2.30}$$

and to get a general solution Brown derived a correlation for the film thickness (δ_o) as follows:

$$\delta_o = \frac{-1 + \sqrt{1 + 2\,NR}}{N} \tag{2.31}$$

where

$$N = \sqrt[3]{14.5\,\frac{\rho_1^2\,g}{\mu_1^2}} \tag{2.32}$$

Substituting into equation (2.30) the rising velocity of an air pocket can be written as:

$$V_\infty = 0.496\,\sqrt{gR}\,\sqrt{1 - \frac{-1 + \sqrt{1+2\,NR}}{NR}} \tag{2.33}$$

The limits to which equation (2.33) can be applied were derived empirically as:

Surface tension:

$$\frac{\rho_1 gR^2}{\sigma}\left(1 - \frac{-1 + \sqrt{1+2\,NR}}{NR}\right)^2 > 5.0 \tag{2.34}$$

Viscosity:

$$2\,NR > 60 \tag{2.35}$$

and the minimum size of pocket which behaves according to equation (2.33) must satisfy the following condition:

$$r_e > 0.75\,R\left(1 - \frac{-1 + \sqrt{1 + 2\,NR}}{NR}\right) \tag{2.36}$$

where (r_e) is the equivalent radius of pocket.

It can be noted from the previous research on the rise velocity of air pockets in vertical pipes that for the case of Civil Engineering structures, inertia forces will only dominate. Most of the research above was carried out for Chemical Engineering where small diameter tubes were used and also liquids of different viscosities.

For most Civil Engineering structures the diameters of conduits or tunnel systems are large enough to neglect the effect of surface tension, also the liquid used is water so viscosity effects can also be neglected. Therefore, for this case the only equation which will be applied to the rising velocity of an air pocket in stationary water for vertical conduit is equation (2.10), i.e.

$$V_\infty = 0.35 \sqrt{gD} \qquad (2.10)$$

However, the general equation (2.28) should be applied in modelling air pocket movement, especially when the model conduit is less than 150 mm diameter.

Equation (2.10) represents the rising velocity of air pockets in vertical shafts for stationary water, and at the same time gives an indication for the minimum downward water velocity in vertical dropshafts to prevent an air pocket from blowing back. Hence we might say that the minimum non-dimensional water velocity $V_o/\sqrt{gD}$ to prevent air pocket blowing back is approximately 0.35, and it should be greater than 0.35 in order to transport the air pocket down the vertical dropshaft. Equation (2.10) can be applied for air pockets in the range $0.4 < D_e/D < 1.0$, where D_e is the equivalent pocket diameter.

2.2.2 The Rising Velocity of Expanding Air Pockets

Dumitrescu[42] and Davies and Taylor[38] derived equations (2.6) and (2.7) respectively as a theoretical result for the rising velocity of a non-expanding pocket using potential flow theory. This velocity is determined by the conditions near the nose of the

pocket, and hence the theory should be applicable to finite pockets, provided the flow around the nose does not affect the shape of the nose region.

Griffith and Wallis[77] found that finite pockets do in fact follow equation (2.10) except that for tubes of small diameters, viscous effects became important, and the velocity of rise increased with slug length.

Experimental work carried out by Nicklin et al [123] showed that the increase of rising velocity with slug length is due to the expansion of the rising pocket. Fig. (2.1) shows the experimental results found by Nicklin et al, where it can be noted that the rising velocity of expanding pockets increases with slug length. When any expansion of the pocket causes a displacement of liquid above the pocket, the pocket will be rising in moving liquid, and thus will move faster. If the liquid displaced by the expansion is taken below the pocket, the nose will be rising in stationary liquid and will follow equation (2.10). In the case of expanding slugs in which the liquid is taken off above the slug, the increase in the rising velocity with slug length varies with the absolute pressure of the system. It was found that this increase is related to the rate of expansion of the slug, that is, to the mean velocity $\bar{V}_L$ of the liquid across any section in front of the slug. From their experimental results for expanding slugs the following expression was found for the rising velocity:

$$V_S = 1.48\ \bar{V}_L + V_\infty \qquad (2.37)$$

Griffith and Wallis[77] found that the mean velocity of water $\bar{V}_L$ is:

$$\bar{V}_L = \frac{Q_W + Q_A}{A} \qquad (2.38)$$

2.2.3 The Rising Velocity of Air Pockets in Moving Water

In section (2.2.1) the rising velocity of air pockets in stationary water was given in equation (2.10). For the case of air pockets rising in moving water a modification is required for equation (2.10) in order for it to be applied.

Nicklin et al[123] indicated that an air pocket rising in moving liquid stream will move at a velocity made up of its basic rising velocity in stationary water, plus a component due to the motion of the liquid. This component depends upon the mean velocity and the form of the velocity profile. The rising velocity was given as follows:

$$V_S = V_\infty + \Gamma V_L \qquad (2.39)$$

where (Γ) is a factor determined experimentally and shown in Fig. (2.6) plotted against liquid velocity with air pocket length as a parameter. It can be noted that there is a scatter in the value of (Γ). For downward flows of water (indicated as negative velocities), the motion of the air pocket in this region was unsteady and the pocket had great changes in shape avoiding the fast moving liquid in the centre of the tube. For small upward flows there is also a scatter in the values of (Γ) due to experimental difficulties in this region[123]. For values of water velocity $V_L > 0.3$ m/s (Re > 8000), (Γ) has a constant value of 1.2, and independent of both the air pocket length and the liquid velocity. The absolute velocity of the pocket therefore for upward flows was given by Niclin et al[123] as:

$$V_S = 1.2\ \bar{V}_L + 0.35\ \sqrt{gD} \qquad (2.40)$$

where $\bar{V}_L$ is given in equation (2.38).

For upward flow case, Wallis[177] used the drift flux model to obtain the slug velocity when there is net flow, the slug velocity is:

$$V_s = j + V_\infty \tag{2.41}$$

where j is the volumetric flux given as:

$$j = \frac{Q_w + Q_A}{A} \tag{2.42}$$

which is exactly the same as $\bar{V}_L$ given in equation (2.38). Wallis[177] applied improvements to equation (2.41) because the bubble drift velocity is not strictly constant since it is influenced by the velocity profile in the liquid. This profile is a function of Reynolds Number, and is influenced by the wake of a preceding pocket. These effects may be taken into account by applying correction factors to equation (2.41). Thus the upward air pocket velocity is given by:

$$V_s = C_1\, j + C_2\, V_\infty \tag{2.43}$$

The coefficient (C_1) is a measure of the fact that the air pocket does not move relative to the average liquid velocity but relative to a weighted average value. (C_2) is a measure of the change in relative velocity due to the approaching velocity profile. For the case of fully developed turbulent flow in the liquid (Reynolds Number greater than 8000) the results is as follows:

$$Re_j > 8000\ ,\ C_1 = 1.20\ ,\ C_2 = 1.0 \tag{2.44}$$

where

$$Re_j = \frac{j\, D\rho_1}{\mu_1} \tag{2.45}$$

it can be noted that equation (2.44) is exactly the same as equation (2.40).

Accepted correlations for C_1 and C_2 in the laminar flow region are not available. Griffith and Wallis[77] observed that equation (2.10) is not applicable for low air pocket velocity Reynolds Number, even when the liquid is stationary. Griffith and Wallis[77] observed that V_∞ depends on water velocity, or the shape of the liquid velocity profile. In an attempt to rationalize the effect of low Reynolds Number and velocity profile, the constant of Taylor and Dumitrescu was split up into two parts C_1 C_2, so the expression for the rising velocity was given as:

$$V_\infty = C_1 C_2 \sqrt{gD} \qquad (2.46)$$

C_1 is the governing coefficient in static water, it is a function of the Reynolds Number based on air pocket velocity, tube diameter and liquid viscosity. The relationship between C_1 and Reynolds Number N_{Re_b} is shown in Fig. (2.7).

C_2 depends both on air pocket velocity and the velocity profile of the liquid. Its variation has been rationalized by plotting values of C_2 against a Reynolds Number based on liquid velocity with a Reynolds Number based on air pocket velocity as a parameter. This plot is shown in Fig. (2.8). It was observed from experimental results that for $N_{Re_b} < 3000$, the results agree with the curve. For $3000 < N_{Re_b} < 5000$ there was a scatter in the results possibly due to a transition region where turbulent flow is starting to be initiated. At higher N_{Re_b} the results are more consistent and C_2 tends to approach unity. This means that it is very difficult to separate the effects of the two correction factors.

For the case when a string of air pockets follows one another, Moissis and Griffith[116] found the air pocket rise velocity is a function of separation distance between the pockets (L_s) and the

pipe diameter. Fig. (2.9) shows a plot of the air pocket velocity against separation distance for three circular pipes of 1 inch, 3/4 inch and 2 inches diameter. Moissis gave the following relationship for the rising velocity of a string of bubbles:

$$\frac{V_b'}{V_\infty} = 1 + 8 \exp(-1.06\ L_s/D) \qquad (2.47)$$

This means that the following air pocket is continually tending to catch up the preceding one and coalescing with it.

Martin[107] analysed vertically downward slug flow and compared the results with upward flow. Martin used an expression similar to equation (2.39) for the rising velocity in upward flow of water as follows:

$$V_s = C_o \frac{Q_w + Q_A}{A} + C_1 \frac{\sqrt{g\Delta\rho D}}{\rho_1} \qquad (2.48)$$

which can be written as:

$$V_s = C_o < j > + C_1 \sqrt{gD} \qquad (2.49)$$

where C_o is a distribution parameter, C_1 is a factor that depends on fluid properties, and <j> is the average volumetric flux for the entire mixture and similar to $\bar{V}_L$ given in equation (2.38). The coefficient C_o has been defined by Zuber and Findlay[191] to be a distribution parameter, which reflects both the flow and concentration distribution across the pipe, and given as:

$$C_o = \frac{< \alpha j >}{<\alpha><j>} \qquad (2.50)$$

where α is the local void fraction, and j the local volumetric flux density. Zuber and Findlay[191] demonstrated that by using equation

(2.50), (C_o) will be greater than unity if the void fraction at the wall is less than it is on the pipe axis, and that (C_o) is less than unity if the wall void fraction is greater than that on the pipe axis.

Experiments carried out by Martin[107] gave the value of C_o = 1.2 only for upward water flow. The value of the constant (C_1) was the same as given by the previous investigators (i.e. C_1 = 0.35) only when the air pocket remains in the centre of the pipe. If the pockets tend to move away from the middle of the conduit, the rising velocity will increase above that for an air pocket rising in stationary water. In certain cases of air pockets rising in fluidized beds, Kehoe and Davidson[107] found that the pockets tended to move up the wall at a velocity greater than that given by equation (2.10) and C_1 = 0.35. They were able to correlate these results only if (D) in equation (2.10) was replaced by (2D), resulting in an effective value of C_1 = 0.495. That means air pockets rising vertically along the pipe wall have a rising velocity of:

$$V_s = 1.2 \frac{Q_w + Q_A}{A} + 0.495 \sqrt{gD} \qquad (2.51)$$

For downward water flow the air pocket may either rise or descend, depending on the relative magnitudes of air and water velocities. Martin[107] indicated that equations (2.48) and (2.49) may be valid, but the coefficients (C_o) and (C_1) will only be identical to the values of upward flow if the air pockets remain centred on the pipe axis. If the air pockets move away from the centre of the pipe, C_o will decrease because the pocket is travelling relative to a fluid velocity less than the maximum on the pipe axis, while C_1 will increase because the drift velocity increases as the pocket becomes closer to the boundary.

Martin[107] carried out his experiments on three different pipe diameters for vertically downward flow, where the air pockets will either descend, ascend or remain stationary. Fig. (2.10) shows a typical result for a pipe of 0.14 m diameter, where the air pocket velocity is plotted against total volumetric flux. Both V_s and <j> are positive for upward directed velocities. It can be noted from Fig. (2.10) that for D = 0.14 m, C_o = 0.86 and C_1 = 0.58. The results for a pipe of 0.026 m diameter are shown in Fig. (2.11), where both ascending and descending air pockets in downward flow and ascending air pockets in upward flow are included for comparison. It can be seen from Fig. (2.11) that C_o = 1.20 for upward flow ascending air pockets and that C_o = 0.93 for descending air pockets in downward flow. It can be concluded from Martin's experimental results that:

a - $C_o < 1.0$ for downward flow and descending air pockets

b - $C_1 > 0.35$ for descending air pockets in large diameter pipes

c - A stable Taylor bubble is only possible for downward flow for small pipe diameters, an average value of C_o = 1.14 is obtained from the results of three investigators for D = 0.026m

d - The air pockets become more eccentric relative to the pipe axis as the downward flow is increased and the pipe diameter is increased

e - Above a certain pipe diameter the rising velocity becomes independent of (D) as in the case of air bubbles movement

f - From the results of ascending air pockets in a downward water flow, it can be noted that a balanced air pocket can be obtained if the term accounting for effect of water velocity equals that of buoyancy, i.e. $0.86 < j > =$

$0.58\sqrt{gD}$. When substituting for the mixture velocity <j> by $V_o(1+\beta)$, it can be noted that the non-dimensional water velocity $V_o/\sqrt{gD}$ required to prevent the air pocket from blowing back is approximately $0.674/(1+\beta)$ in a downward flowing water.

g - Combining the result notified in (f) above with that notified at the end of section (2.2.1), we find that the non-dimensional water velocity required to keep the air pocket from blowing back in a vertical shaft should be in the following range:

$$0.35 < \frac{V_o}{\sqrt{gD}} \leq \frac{0.674}{1+\beta}$$

The behaviour of air pockets in vertical pipes for stationary and moving water, for water flowing upwards or downwards, and for pipe diameters greater than 27 mm so that surface tension and viscosity effects are negligible, can be summarized as follows:

(i) For stationary water:

(a) - Air pocket at the centre of pipe:

$$V_\infty = 0.35\sqrt{gD} \qquad (2.10)$$

(b) - Air pocket at pipe wall:

$$V_\infty = 0.495\sqrt{gD}$$

(ii) For upward flowing water with (Re > 8000):

(a) - Air pocket at the centre of pipe:

$$V_s = 1.2\ V_o\ (1+\beta) + 0.35\ \sqrt{gD} \qquad (2.40)$$

(b) - Air pocket at pipe wall:

$$V_s = 1.2\ V_o\ (1+\beta) + 0.495\ \sqrt{gD} \qquad (2.51)$$

(iii) For downward flowing water with (Re > 8000):

(a) - Air pocket ascending the pipe:

$$V_s = 1.2\ V_o\ (1+\beta) + 0.35\ \sqrt{gD} \qquad (2.40)$$

where V_o is (-ve) for downward flowing water

(b) - Air pocket descending:

$$V_s = 0.86\ V_o\ (1+\beta) + 0.58\ \sqrt{gD} \qquad (2.49)$$

where V_o is also (-ve)

2.3 THE BEHAVIOUR OF AIR POCKETS IN HORIZONTAL CONDUITS

In horizontal conduits the air pocket velocity is not affected by buoyancy. In stationary water the air pocket will not move unless there is a transient effect such as raising a gate at the end of a horizontal conduit where the water will start emptying from the end of the conduit and air pockets start advancing into the conduit. Past research work in horizontal conduits has been investigated mainly for detailed studies of gravity currents. The effect of surface tension will also be illustrated, where a minimum size of conduit is given for both circular and rectangular conduits. The air pocket velocity in moving water will also be given which, as

is the case in vertical conduits, is higher than the average liquid velocity.

2.3.1 Air Pockets Moving Under Transient Effects

In order to analyse the movement of air pockets in horizontal conduits, the theory developed by Benjamin[24] for gravity currents will be considered. A gravity current consists of a wedge of denser fluid intruding into an expansion of lighter fluid. If the effects of viscosity and mixing of the fluids at the interface are ignored the hydrodynamical problem is formally the same as that for an air cavity advancing along the upper boundary of a liquid. Fig. (2.12) shows a gravity current where a stream of heavy fluid is flowing along the horizontal bottom and replacing the lighter fluid. The front of the current is observed to progress with a nearly constant speed and maintain its shape which means that the motive force is balanced by the hydrodynamic drag. This means that the balance between momentum and hydrostatic force can be used to analyse the problem. Benjamin [24] used continuity and force-momentum balance to derive an expression for the cavity speed which is shown in Fig. (2.13) for a steady flow with a free boundary. The analysis was carried out for the flow with and without energy losses, and assuming that viscosity and surface tension can be ignored. Upstream of the cavity the liquid has a depth (d), and a constant relative velocity (C_1). Downstream, the flow under the free cavity boundary is uniform and of depth (h) and velocity (C_2). The cavity shown in Fig. (2.13) is similar to a continuous air pocket, such as the case of liquid emptying from a long horizontal two-dimensional conduit.

For the case of flow without energy losses, Benjamin[24] assumed that point (0) in Fig. (2.13) is a stagnation point, and the pressure is zero along the free boundary. Then, by applying Bernoulli's theorem along the free boundary, it follows that:

$$C_2^2 = 2g(d-h) \tag{2.52}$$

Then the flow forces for upstream and downstream flows are derived by adding the pressure forces to the momentum flux. The flow forces are represented as follows:

$$S_1 = \frac{1}{2}\rho_1(C_1^2 d + gd^2) \tag{2.53}$$

$$S_2 = \rho_1(C_2^2 h + \frac{1}{2} gh^2) \tag{2.54}$$

But $S_1 = S_2$, because the flow force is an invariant in any steady flow in the absence of external horizontal forces. Equating equations (2.53) and (2.54) and considering the following equation of continuity where:

$$C_1 d = C_2 h \tag{2.55}$$

the following expression is obtained:

$$C_2^2 = \frac{g(d^2 - h^2)d}{(2d - h)h} \tag{2.56}$$

From equations (2.52) and (2.56) the following two solutions are

obtained, the first root being h = d and the other:

$$h = \frac{1}{2} d \tag{2.57}$$

Equation (2.57) is the only solution for the flow to be steady and free from energy dissipation. Using the result of equation (2.57) the following is obtained from equations (2.52) and (2.55):

$$f = \frac{C_1}{\sqrt{gd}} = \frac{1}{2} \tag{2.58}$$

$$F = \frac{C_2}{\sqrt{gh}} = \sqrt{2} \tag{2.59}$$

Equation (2.58) gives the speed of an air pocket propagating in a horizontal conduit to be $C_1 = 0.5\sqrt{gD}$, for the case of zero energy loss. Equation (2.59) means that the receding stream is supercritical, indicating that stationary waves cannot rise upon the stream without energy loss, but a dissipative hydraulic jump may occur.

This type of flow can be realized in a long rectangular box filled with liquid, closed at both ends and fixed horizontally as in Fig. (2.14). If one end is opened, the liquid will flow under the action of gravity. After the initial transient effects disappear, the air filled cavity replacing the ejected liquid will move steadily along the box. When a reference is travelling with the front of the cavity, the liquid motion will appear to be steady, as in Fig. (2.13). If the effects of viscosity and surface tension are ignored, the velocity of the cavity relative to a stationary observer will be (C_1) as given in equation (2.58). Since h = d/2 the liquid

will discharge from the open end with the same velocity. The rate of discharge will be the same as the rate at which the volume of cavity increases. The discharge per unit span is as follows:

$$Q_w = C_1(d - h) \tag{2.60}$$

Benjamin[24] extended his work to the flow with energy loss and found that the velocity far downstream will be as follows:

$$C_2^2 = 2g(d-h-\Delta) \tag{2.61}$$

Equating equations (2.56) and (2.61) the following is obtained:

$$\Delta = \frac{(2h-d)(d-h)^2}{2h(2d-h)} \tag{2.62}$$

Equation (2.62) confirms that:

(a) - $\Delta = 0$ for $h = 1/2\ d$, i.e. steady flow with no energy loss when the receding stream fills half the space between planes.

(b) - Δ is positive for $h > 1/2\ d$, i.e. steady flow is possible when the receding stream fills more than half the conduit depth but with energy loss.

(c) - Δ is negative for $h < 1/2\ d$, i.e. steady flow is impossible when the cavity occupies more than half the conduit depth unless an external supply of energy is used to sustain steady flow.

From equations (2.55) and (2.56) it follows that:

$$\frac{C_1}{\sqrt{gd}} = \left[\frac{h(d^2 - h^2)}{d^2(2d-h)}\right]^{1/2} \tag{2.63}$$

combining equation (2.63) with equation (2.60) it follows that:

$$\frac{Q_w}{\sqrt{gd^3}} = \left[\frac{(d-h)^2\ h(d^2-h^2)}{d^4\ (2d-h)}\right]^{1/2} \qquad (2.64)$$

Fig. (2.15) presents graphs of the dimensionless quantities Δ/d, $C_1/\sqrt{gd}$ and $Q_w/\sqrt{gd^3}$ plotted against h/d in the range $0.5 \leq h/d \leq 1.0$.

The maximum value of $C_1/\sqrt{gd}$ is 0.5273 when h/d is equall to 0.6527. This is the highest air cavity speed in a two-dimensional conduit with energy losses included.

Equation (2.63) can be expressed in terms of the depth of cavity H = d-h as follows:

$$\frac{C_1}{\sqrt{gH}} = \left[\frac{(d-H)\ (2d-H)}{d(d+H)}\right]^{1/2} \qquad (2.65)$$

This equation is plotted against H/d in Fig. (2.16) which shows that $C_1/\sqrt{gH}$ varies from $1/\sqrt{2} \rightarrow \sqrt{2}$ as H/d varies from 0.5 to zero.

For a liquid emptying from a horizontal pipe with a circular cross section, as in Fig. (2.17), Benjamin[24] assumed the flow to be uniform far upstream and far downstream. The free surface downstream has an angle 2a at the axis, so that the breadth b = 2R Sina and the cross section area is given by:

$$A_2 = (\pi - a + 1/2\ \mathrm{Sin}2a) \qquad (2.66)$$

and continuity will have the following form:

$$\frac{C_1}{C_2} = \frac{A_2}{\pi R^2} \qquad (2.67)$$

Applying Bernoulli's theorem along the free surface, between the stagnation point 0 and the asymptotic level far downstream, the following is obtained:

$$C_2^2 = 2gR(1 - \text{Cosa}) \tag{2.68}$$

For a circular section the flow force upstream and downstream are given as follows:

$$S_1 = \rho_1(gR + \frac{1}{2} C_1^2)\pi R^2 \tag{2.69}$$

$$S_2 = \rho_1[gR(A_2\text{Cosa} + \frac{2}{3} R^2\text{Sin}^3\text{a}) + A_2C_2^2] \tag{2.70}$$

When equating the flow forces, it was found that the only solution for zero energy loss is when the angle a = 82.78°. The following values are obtained:

$$C_2/\sqrt{gR} = 1.322 \tag{2.71}$$

$$C_1/\sqrt{gR} = 0.767 \tag{2.72}$$

Equation (2.72) can be written in terms of the pipe diameter (D) as follows:

$$C_1/\sqrt{gD} = 0.542 \tag{2.73}$$

It can be noted from equation (2.73) that the air pocket speed in horizontal pipes is higher than the rising velocity of air pocket for vertical pipes ($V_\infty = 0.35\sqrt{gD}$) which is given by equation (2.10).

Zukoski[192] observed long bubbles for different angles including horizontal conduits where he studied the effect of

viscosity and surface tension on the air pocket velocity. Zukoski found the surface tension parameter (Σ) given in equation (2.22) still has an effect on the pocket velocity until it reaches a value of $\Sigma = 0.001$ for horizontal conduits. This corresponds to pipe diameters of the order 150-200 mm diameter. His result for a pipe of 17.8 cm diameter was comparable with the theoretical result found by Benjamin[24] and given in equation (2.72). Zukoski found experimentally that for a 17.8 cm diameter horizontal pipe the pocket velocity is:

$$C_1/\sqrt{gR} = 0.752 \qquad (2.74)$$

which is only 2.2% less than the theoretical value predicted by Benjamin. Zukoski also found from his experiments that the cavity will not propagate steadily along emptying horizontal pipes. The reason for the non-steady flow, which was observed when $C_1/\sqrt{gR} < 0.5$, is due to the velocity of the fluid passing under the cavity near the pipe exit. If this velocity is less than half the critical speed for the flow, disturbances originating at the exit can overtake the cavity and hence prevent steady flow from being established. When the exit velocity is greater than half the critical speed, disturbances from the exit move upstream slower than the cavity and hence steady motion can be maintained at least at the front nose of the cavity. The critical speed was given roughly by Zukoski, when the fluid occupies the lower half of the tube, to be equal to $\sqrt{gR}$ which means that the Froude Number there is equal to (1.0). Von Karman[96] discussed a model for gravity currents at great depths of submergence. Fig. (2.18) shows the shape of the surface separating larger density (ρ_1) muddy water and lower density (ρ_2) clear water. The front of the muddy water progresses with approximately constant speed and keeps its permanent shape. He considered the flow relative to a co-ordinate system moving with the heavier fluid, which means that it can be assumed to be at rest while the lighter fluid (of density ρ_2) to be moving steadily over the interface with a velocity C_1. Von Karman applied Bernoulli's theorem after

determining the shape of the discontinuity surface in a similar method used by Stokes for determination of the steepest slope occurring in waves of finite height. That is, if the frictional effects are neglected, the slope of the discontinuity surface at the intersection with the bottom must be equal to $\pi/3$ (or 60°). Thus by applying Bernoulli's theorem between the stagnation point and points on the interface downstream, supposing that the interface becomes horizontal and the velocity of flow along it tends towards a constant value C_1, Von Karman found that:

$$C_1^2 = 2gH \frac{(\rho_1 - \rho_2)}{\rho_2} \qquad (2.75)$$

A similar result was obtained by Benjamin[24] but using different reasoning. For great depths, the flow velocity cannot have a uniform distribution with depth, because the liquid in the upper layer has a considerable loss of head when passing through the breaking or hydraulic jump zone just downstream of the cavity nose. The velocity distribution will have the form of a wake, with the maximum velocity defect at the free surface, as shown in Fig. (2.19). To find the velocity (C_1) in terms of cavity depth (H), a path which starts at the upstream boundary is taken to great depths and brought up again to the free surface through the wake zone. The pressure variation along this path is hydrostatic and equating the pressure upstream with the cavity pressure results in a value of C_1 as follows:

$$C_1 = \sqrt{2gH} \qquad (2.76)$$

Benjamin argued that the model suggested by Von Karman is not theoretically possible because the hydrostatic forces far upstream and downstream are not balanced by a hydrodynamic drag in Von Karman's model to obtain a steady state of flow. To obtain the balance the head wave must break and produce turbulence to form a

wake which has the required momentum. This is the case realised in practice.

Gardner and Crow[60] investigated large air pockets moving into stationary water in a horizontal channel of rectangular cross-section. They studied the influence of surface tension on the air pocket velocity and also the variation of the radius of curvature of the air pocket interface with varying depth of channel. The channel used was 1830 mm long, 100 mm wide and with a variable depth from zero to 175 mm. They used the surface tension parameter (Σ) in the following form:

$$\Sigma = \frac{4\sigma}{\Delta\rho g d^2} \qquad (2.77)$$

where d is the channel depth. They found that for deep channels with $\Sigma < 0.02$ or $d > 38.7$ mm the flow was the same as given by Benjamin[24] except for the curved nose near the top wall. For Σ between 0.02 - 0.105 or 16.9 mm $< d <$ 38.7 mm, large waves formed downstream of the bubble nose, beyond the point at which the bubble attained its maximum depth. For $\Sigma > 0.105$ the flow was much more quiescent and the fraction of the channel depth occupied by the liquid downstream of the bubble nose increased. The channel finally blocked and $C_1/\sqrt{gd}$ equalled zero when Σ reached a critical value of 0.368 which corresponds to d = 9 mm. The blocked system is shown in Fig. (2.20) where a substantial layer of water of depth h_s remained undrained from the bottom of the channel due to surface tension. Their experimental results are shown in Fig. (2.21) for square-ended and chamferred sills, where $F = C_1/\sqrt{gd}$ is plotted against the surface tension parameter Σ. The bubble nose profiles found by Gardner and Crow[60] are shown in Fig. (2.22), and compared with the profile predicted by Benjamin[24]. It can be seen that for the case of h = 107 mm, when the air pocket speed is in close agreement with that predicted by Benjamin, that the front nose of the cavity is not identical to Benjamin's model. This is a surface tension effect.

Gardner and Crow[60] followed Benjamin[24] in using momentum and energy principles but they also included the terms involving surface tension. They solved the equations to find the radius of curvature for the bubble nose and the effect of surface tension on it. They found that surface tension still has a substantial effect upon the bubble velocity for air-water system in channels as deep as 175 mm, i.e. $\Sigma = 10^{-4}$, given by equation (2.77). This result agrees with that found by Zukoski[192] and shown in Fig. (2.4), where it is clear that a pipe diameter of 150 mm to 200 mm is required in order to have negligible effect of surface tension. In Civil Engineering structures pipe diameters used are usually large enough to neglect the effect of surface tension. It seems that the analysis used by Benjamin[24] might provide a useful tool, at least for horizontal or slightly inclined conduits. If Benjamin's analysis can be modified to take into account velocity profiles, the inclination angles of conduits, single air pockets, rather than continuous air pockets, both for the case of stationary and moving water, then a useful tool for analysis has been provided.

Extension of Benjamin's work has been carried out recently by Bacopolous[14] who derived theoretical models for both single and continuous air pockets in slightly inclined and horizontal pipes. Considering only the case of horizontal pipes, Bacopolous analysed the case of rectangular and non-rectangular velocity profiles with energy losses also introduced into the analysis. For the case of rectangular velocity profile, Bacopolous applied Bernoulli's theorem between the stagnation point and the free surface far downstream in the same way as Benjamin[24], also introducing the head loss term (Δ) into the equations. His theoretical result is shown in Fig. (2.23) where $C_1/\sqrt{gD}$ is plotted against H/D. It is noted from the figure that a maximum value of $C_1/\sqrt{gD} = 0.567$, which is obtained for a cavity depth H/D = 0.319. This is different from the results found by Benjamin for a liquid filling the space between two horizontal boundaries where, for two dimensional flow $(C_1/\sqrt{gD})$ max. = 0.5273, and for circular pipe $C_1/\sqrt{gD} = 0.542$ for the case of no energy loss.

Bacopolous then assumed that a non-rectangular velocity profile appears downstream, which he confirmed using photographs from his experimental work. Bacopolous adjusted the terms of the velocity downstream and the momentum according to this non-rectangular velocity profile in the Force momentum equations, and solved the equations to end with a result similar to the case of a rectangular velocity profile. His results are shown in Fig. (2.24) where the maximum air cavity velocity $C_1/\sqrt{gD} = 0.563$ for $H/D = 0.315$. This means that air cavity velocity exhibits negligible change due to the change in velocity profile far downstream from rectangular to non-rectangular.

2.3.2 Air Pocket Velocity in Moving Water

In Civil Engineering structures the behaviour of air pockets in horizontal conduits under moving water conditions is of great interest. Usually single air pockets appear in such structures rather than continuous cavities described by Benjamin[24] and Bacopolous[14]. This situation has not yet been analysed, but it seems that the application of force-momentum equations could yield a solution for the air pocket velocity for different air pocket depths and different water velocities.

Wallis[177] analysed horizontal slug flow with $H/D > 0.5$ which involves much larger air pockets than those found in Civil Engineering. He used the continuity equation to find the air pocket velocity, and indicated that the air pockets do not move at the same speed as the average liquid velocity. A sketch is shown in Fig. (2.25). Since there is no pressure drop along the length of pocket, the liquid film on the wall will be stationary. If this film has a thickness of δ_o, the air pocket area will be:

$$A_b = \pi(D/2 - \delta_o)^2 \qquad (2.78)$$

Then from continuity at this section:

$$V_b A_b = \bar{V}_L A \tag{2.79}$$

and if the film is very thin:

$$V_b \simeq (1 + 4\delta_o/D)\, \bar{V}_L \tag{2.80}$$

which means that $V_b > \bar{V}_L$ or that the air pocket speed is greater than the average liquid velocity. It was found for high velocities and high Reynolds Numbers that:

$$V_b = 1.19\, \bar{V}_L \tag{2.81}$$

The value of the coefficient in equation (2.81) is very close to the value of ($C_o = 1.20$) for vertical upward flow at high Reynolds Numbers. A simple expression for the air pocket velocity in terms of the overall flow rates for Re > 3000 can be given as:

$$V_b = 1.2 \left(\frac{Q_w + Q_A}{A}\right) \tag{2.82}$$

It is not known if the above equation can be applied to the velocity of air pockets which are usually found in Civil Engineering structures, when the air pocket depth H/D is generally less than 0.5.

The behaviour of air pockets in horizontal conduits for stationary or moving water can be summarized as follows:

1 - The speed of air pockets is not affected by buoyant forces. In stationary water the air pocket will only move under transient effects.

2 - The air pocket speed is a function of the maximum depth of the air pocket and is affected by viscosity and surface tension, i.e.

$$\frac{C_1}{\sqrt{gD}} = f(H/D \ , \ Re \ , \ Wb)$$

3 - If viscosity and surface tension are neglected, which is the case for pipes with diameters > 150 mm - 200 mm, and water as the flowing liquid, the speed of air pockets is:

$$\frac{C_1}{\sqrt{gD}} = f(H/D)$$

4 - The speed of air pocket for two dimensional flow is represented by equation (2.65) as:

$$\frac{C_1}{\sqrt{gH}} = \left[\frac{(d-H)(2d-H)}{d(d+H)}\right]^{1/2} \qquad (2.65)$$

5 - The maximum speed of an air pocket for two dimensional flow with energy loss in stationary water is as follows:

$$\left(\frac{C_1}{\sqrt{gd}}\right)_{max} = 0.5273 \quad \text{for} \quad \frac{H}{d} = 0.3473$$

6 - The maximum speed of an air pocket for three dimensional flow in stationary water is:

(a) for flow without energy loss:

$$\frac{C_1}{\sqrt{gD}} = 0.542$$

(b) for flow with energy loss:

$$\frac{C_1}{\sqrt{gD}} = 0.567 \quad \text{for} \quad \frac{H}{D} = 0.319$$

7 - The speed of air pockets in moving water is greater than the average liquid velocity, and for Re > 3000 and large air pockets with H/D > 0.5 it is given by equation (2.82) as:

$$V_b = 1.2 \left(\frac{Q_w + Q_A}{A}\right) \qquad (2.82)$$

8 - In Civil Engineering the air pockets are usually with H/D < 0.50 and it is not known if equation (2.82) can be applied. But it is thought that the speed can be represented as:

$$\frac{C_1}{\sqrt{gD}} = f\left(\frac{H}{D}\right) + 1.2 \left(\frac{Q_w + Q_A}{A}\right)$$

for flow with energy loss. The constant (1.2) might also be different and a proper value for the above speed can be obtained experimentally if air fed pockets were introduced in the flowing water.

9 - The speed of air pockets increases with increasing the depth of air pocket until a maximum speed is reached and then it starts decreasing, which is clearly shown in Figs. (2.15) and (2.23).

2.4 THE BEHAVIOUR OF AIR POCKETS IN INCLINED CONDUITS

Most of the past research work done on air pocket behaviour in inclined conduits has been experimental, with the analysis mainly concerned with air pockets blowing back or clearing out of the conduit rather than the rise velocity of the air pocket itself. In this section the available information about the rising velocity of

air pockets will be illustrated for both stationary and moving water conditions. This will be related as far as possible to part of the investigation carried out in this research.

2.4.1 The Rising Velocity of Air Pockets in Stationary Water

An air pocket will rise in an inclined conduit due to its buoyancy. In order to find the rise velocity most theoretical expressions assure the pocket is stationary and the water is moving at the air pocket rising velocity. Falvey[55] derived an equation for the rising velocity of an air pocket by equating the buoyant force to the drag force on a stationary pocket, shown in Fig. (2.26). This gives:

$$(\rho_1 - \rho_2) \frac{\pi D_e^3}{6} (gS_o) = C_d \frac{\pi D_e^2}{4} \frac{(\rho_1 V_r^2)}{2} \qquad (2.83)$$

where D_e = equivalent pocket diameter

C_d = drag coefficient on the pocket

S_o = pipe slope = Sinθ

and V_r = rise velocity in pipe inclined at angle θ above horizontal

Rearranging terms and dividing by pipe diameter:

$$\frac{V_r^2}{gD} = \frac{4}{3} \left[1 - \frac{\rho_2}{\rho_1}\right] \left(\frac{D_e}{D}\right) \left(\frac{S_o}{C_d}\right) \qquad (2.84)$$

Eq. (2.84) indicates that the rising velocity depends on the drag coefficient and the pocket shape. Kent[97] used the same principal of holding the pocket stationary in a moving water to get a minimum water velocity to clear an air pocket out of a downward sloping pipe. This model can also be used to represent the rising

velocity of air pockets in stationary water. By equating the buoyancy and the drag forces on a stationary pocket the following was obtained:

$$V\rho_1 g \mathrm{Sin}\theta = \frac{C_d A_b \rho_1 V_r^2}{2} \qquad (2.85)$$

where V is the air pocket volume and A_b the air pocket area exposed to oncoming flow.

By substituting for the drag force C_d from his experimental results, Kent was able to reduce equation (2.85) into the following equation:

$$V_r = K\sqrt{gD\mathrm{Sin}\theta} \qquad (2.86)$$

where K is a constant given as a component of two constants, the first is the drag coefficient and the second is a shape factor, where K can be written as:

$$K = 1.62\sqrt{\zeta} \qquad (2.87)$$

Kent suggested from his experimental results that ζ becomes constant and equal to 0.58 for L/D > 1.50. (L is the air pocket length and D the pipe diameter).

Runge and Wallis[139] studied slug flow H/D > 0.5 in inclined pipes and indicated that the parameters which describe this regime are precisely those which were used to describe vertical flow together with angle θ made between the axis of the pipe and the vertical. They suggested that for bubble rise velocity one can obtain curves similar to those in Fig. (2.3) at each value of θ. The rising velocity is given by using the dimensionless parameter K_1 as follows:

$$K_1 = K_1 (N_f , N_{E\ddot{o}} , \theta) \qquad (2.88)$$

where N_f and $N_{E\ddot{o}}$ are the same as given in equations (2.23) and (2.20) respectively.

The ratios of the rising velocity in inclined conduit to the rising velocity in vertical pipe were plotted against angle of inclination for different values of N_f and $N_{E\ddot{o}}$. A typical plot is shown in Fig. (2.27) for $N_f > 300$ and $N_{E\ddot{o}} > 100$, which is the case in Civil Engineering structures, when inertia force is the dominant factor and viscous and surface tension effects are negligible.

Zukoski[192] studied the rising velocity for continuous air pockets in inclined conduits. He indicated that the air pocket velocity is complex because of the change in air pocket geometry in response to change in inclination angle. He obtained the bubble rise velocity for a wide range of the surface tension parameter (Σ) and Reynolds Numbers (Re), defined by equations (2.21) and (2.22) respectively. His experimental results are shown in Fig. (2.28) for various pipe diameters and different angles of inclination, where $V_r/\sqrt{gD}$ has been plotted against (θ) the angle of inclination with the horizontal. Also in Fig. (2.28) the experimental results found by Runge and Wallis[139], Bonnecaze[26], Davies and Taylor[38] and White and Beardman[181] are plotted to give a clearer idea about the effect of surface tension and angle of inclination on the rising velocity of air pockets.

Zukoski[192] indicated that viscous effects are not important for $V_r/\sqrt{gD} > 0.10$, because in this region the Reynolds Number Re > 400 and hence the rising velocity is likely to be independent of viscous effects as for the vertical case. The effect of surface tension has already been shown in Fig. (2.24) where the rising velocity is plotted against pipe diameter for three different angles of inclination. It can be noted that surface tension still has an effect on the rising velocity up to a pipe diameter between 150 mm and 200 mm as for the horizontal case.

Wisner et al[187] carried out experimental work for the clearing velocities of air pockets from downward sloping pipes, but he also studied the rising velocity of air pockets in stationary water. The experimental work was performed in a pipe inclined at 18.5° with horizontal and a pipe diameter of 244 mm. The results are shown in Fig. (2.29), where the non-dimensional rise velocity is plotted against the Reynolds Number for different air pocket volumes (n) defined as Air Volume/($\pi D^3/4$). Wisner's results indicate that the rising velocity $V_r/\sqrt{gD}$ will be independent of viscous effects for Re $> 10^5$ where $Re = V_r D/\nu$. When substituting for V_r value as $0.5\sqrt{gD}$, a diameter in excess of 159 mm will be required for the rising velocity to be independent of viscous effects. This value of $Re > 10^5$ is far away from the value suggested by Zukoski[192] for Re to be in excess of 400 to get a velocity independent of viscous effects. Also, it can be noted that for larger air pockets with $n \geq 0.80$, where n = air pocket volume/($\pi D^3/4$), and $Re > 10^5$, the rising velocity will be a function of the angle of inclination only. It is of interest that Wisner correlated his data with the air volume rather than H/D as Benjamin and Bacopolous, or the air pocket length L as Kent.

For mildly sloping pipes, Bacopolous[14] formulated a theoretical model for both single and continuous air pockets by extending Benjamin's analysis[24]. He also carried out experimental work to confirm his model for a pipe slope of 1.65%. Fig. (2.30) illustrates the motion of a single air cavity with its front moving at a velocity C_1. The cavity was divided into four zones to simplify the analysis, where zone OA is a second degree curve with maximum cavity depth H at point A. The second zone is AE where something between a hydraulic jump and undular jump occurs. The third zone EZ has an arbitrary length $L_3 = 2D$, so that force-momentum equation can be applied between sections AA_1 and ZZ_1. Finally, the fourth zone has a horizontal interface and is the tail of the pocket.

The velocity profile at section AA_1 in Fig. (2.30) is assumed to be rectangular, and the drag force between water pipe wall is included in the force balance equations. Three conditions for resistance were examined between OO_1 and AA_1 as follows:

a - no resistance present

b - the resistance balances 2/3 of water weight component between OO_1 and AA_1 sections

c - the resistance determined by shear stress from turbulent flow formula for steady incompressible flow

$$\tau_o = \frac{f}{4}\frac{\rho_1}{2} V^2 \quad \text{with} \quad f = 0.009$$

The velocity profile at section ZZ_1 in Fig. (2.30) is assumed parabolic. The analysis was carried out by applying continuity equation between sections AA_1 and BB_1, applying Bernoulli's theorem between points B and O, and also incorporating the force balance equation between sections BB_1 and AA_1. In the analysis consideration for angle of inclination, weight of water, and three different kinds of resistance mentioned above, was taken into account in solving the equations for $C_1/\sqrt{gD}$ in terms of H/D. The final result is given in Table (2.1) below, which illustrates the air cavity velocity for different values of H/D and for three different resistance conditions for a pipe slope of 1.65%.

TABLE 2.1: Variation of dimensionless air cavity velocity $C_1/\sqrt{gD}$ with resistance condition

	H/D →	0.10	0.20	0.30	0.40
a.	no resistance present	0.4239	0.5367	0.5716	0.5597
b.	2/3 of water weight component is balanced by resistance	0.4213	0.5335	0.5682	0.5565
c.	resistance is given by the equation of turbulent flow	0.4239	0.5367	0.5716	0.5597

It can be noted from Table (2.1) that the flow resistance makes no difference to the cavity velocity. Bacopolous also showed that the cavity velocity is more related to H/D than other parameters such as the cavity volume or the cavity length. The theoretical results will be plotted in Chapter (7) for comparison with experimental results from the author's research. Bacopolous continued his theoretical analysis and found the length of the air cavity in terms of cavity depth H/D. His results for a pipe slope of 1.65% are shown in Fig. (2.31) for three different resistances. Finally, Bacopolous fitted a second degree curve for his results of $C_1/\sqrt{gD}$ and H/D for "no resistance present". where the equation is as follows:

For H/D varying from 0.06 to 0.49

$$\frac{C_1}{\sqrt{gD}} = 0.259 + 1.9292 \times \frac{H}{D} - 2.9036 \times \left(\frac{H}{D}\right)^2 \qquad (2.89)$$

In his experimental work for the rising velocity of single air cavities in stationary water, Bacopolous tested the pocket rise velocity for different slopes of 1.25%, 1.5%, 1.65% in a pipe of 0.219 m inside diameter. His results are shown in Fig. (2.32) where $C_1/\sqrt{gD}$ is plotted against H/D. It can be noted that the maximum rising velocity is very close to the result obtained by Zukoski[192] shown in Fig. (2.28) for the same angle, and higher than the velocity obtained by Benjamin[24] for a horizontal conduit.

2.4.2 The Rising Velocity of Air Pockets in Moving Water

The rising velocity of an air pocket in moving water in an inclined conduit has similar characteristics to that for vertical flow, in the sense that it is composed of two components, the first due to air pocket buoyancy and the second due to liquid velocity.

Bonnecaze et al[26] studied slug flow (H/D > 0.5) in pipes inclined at ± 10° with horizontal. It was found that slug flow regime predominates in upward and horizontal flows, while stratified flow tends to dominate in the downward situation, but even for this situation slug flow can exist if the flow rate is sufficiently large. Bonnecaze et al gave the following expression for the rising velocity of an air pocket in moving water:

$$\frac{V_r}{\bar{V}_L} = C_1 + \frac{\delta V_\infty}{\bar{V}_L} \qquad (2.90a)$$

which can be written as:

$$V_r = C_1\bar{V}_L + \delta V_\infty \qquad (2.90b)$$

where δ indicates the direction in which the buoyancy force is acting. For horizontal pipe, $\delta = 0$ because the buoyancy force does

not act in the direction of flow. For upward slug flow, $\delta = +1$ because the buoyancy force is acting so as to force the air pocket up the pipe. In downward slug flow the same phenomenon occurs, but in this case the flow is down the pipe and therefore $\delta = -1$. The value of C_1 found in this work was (1.20) for pipes inclined from +10° to -10° with horizontal, which is very similar to the constant for vertical conduits found by Nicklin et al[123] and for horizontal conduits found by Wallis[177]. The term V_∞ in equation (2.90b) is the same as that for vertical conduits which is given in equation (2.7) derived by Davies and Taylor[38]. The experimental results of Bonnecaze have shown this constant to be (0.35) which is close to the value in equation (2.7) of (0.328). The result can be written as:

$$V_r = 1.2\left(\frac{Q_w + Q_A}{A}\right) \pm 0.35\sqrt{gD} \qquad (2.91)$$

It is interesting to note that the component due to buoyancy in inclined conduits is the same as that for vertical conduits, while the experimental results of Wisner et al[187] and Bacopolous[14] for stationary water showed that the rising velocity depends on the angle of conduit as well as either the volume of air pocket or H/D. Wisner and Bacopolous both worked with air pockets with $H/D < 0.5$ whereas Bonnecaze' slug flow regime has $H/D > 0.5$. Parakh[125] carried out slug flow experiments for air pocket speeds in moving water for conduit angles up to 30°. The result was given by:

$$V_r = K_2 \bar{V}_L + 0.35\, K_3 \sqrt{gD} \qquad (2.92)$$

where K_2 was found to vary linearly with the mixture velocity and has the following values for different angles of inclination:

θ	0°	5°	10°	15°	20°	25°	30°
K_2	1.26	1.24	1.24	1.24	1.16	1.30	1.18

K_2 does not vary systematically with inclination because it also depends on flow rates, flow geometries and velocity distribution. The parameter K_3 allows for the effect of inclination, with experimental values of (K_3) shown in Fig. (2.33) plotted against angle of inclination. The curve between 0° and 5° is arbitrary as there is no data in this region. Also, the experimental results of the present research show that this parameter is higher than the value of K_3 given by Parakh and is dependent on the angle of inclination and H/D. This will be shown in Chapter (6) where the value of K_3 varies between 1.14-1.66 for H/D between 0.1-0.35.

2.5 THE EFFECT OF ANGLE OF INCLINATION ON THE RISING VELOCITY OF AIR POCKETS

Runge and Wallis[139] noticed an interesting phenomenon which arises when the pipe is tilted from the vertical position. The air pocket velocity in an inclined pipe exceeds that of the same pipe placed vertically, provided the air pocket rises up the centre of the vertical pipe. When the pipe is tilted from the vertical the rising velocity increases until a certain angle is reached, then it starts decreasing again. Experimental work carried out by Bonnecaze[26], Zukoski[192] and Spedding and Nguyen[154] defined this phenomenon, with their results shown in Fig. (2.28) as the rising velocity against inclination angle. Spedding and Nguyen[154] carried out tests for bubble rise velocity for horizontal and inclined pipes where they found that the air bubble volume can be important in determining the actual bubble rise velocity, but it does not affect the angle at which the maximum bubble rise occurs. Fig. (2.34) shows the $Fr = V_r/\sqrt{gD}$ plotted against angle of inclination for different bubble volumes, where it can be noted that for any bubble volume the maximum rise velocity is occurring at an angle of 35° with

horizontal. The basic reason appears to be due to the shape of the air pocket in the nose region. As the angle is increased from horizontal the buoyancy force is also increased. The force is opposed by the drag force originating from the draining of the liquid past the rising pocket. When the inclination is under 30° the acute contact angle of the air pocket to the wall, and the downstream air/water interface which is parallel to the tube wall allows the water to drain away from the pocket with little resistance. As the angle is increased to 40° the pocket nose has an obtuse contact angle with the wall and the interface tends to lie at an angle to the lower tube wall in such a way as to restrict the down flow of water. In the vertical position there is no contact angle but the pocket is totally surrounded by water flowing down the tube. In this case the vertical rise of the pocket is opposed by the liquid passing down the annular space between the gas and the solid wall. The effect of the tube inclination on the bubble shape is shown in Fig. (2.35).

Bonnecaze et al[26] defined the co-ordinates for the model used in their experiments as shown in Fig. (2.36). The air pocket is assumed to be at rest and liquid is flowing past the air pocket. Applying Bernoulli's equation to a streamline defining the pocket shape yields:

$$\frac{P}{\rho_1} - gh + \frac{q^2}{2} = E_L \qquad (2.93)$$

where $h = y\text{Cos}\theta + x\text{Sin}\theta$, and equal to the vertical distance from the nose of the pocket to a point on the air pocket surface, and q = liquid velocity in the bubble. For the air pocket:

$$\frac{P}{\rho_2} - gh = E_G \qquad (2.94)$$

subtracting equation (2.93) and (2.94) and recognising that at the pocket nose there is a stagnation point with (q = 0), then the following is obtained:

$$q^2 = 2(1 - \frac{\rho_2}{\rho_1})gh$$

$$= 2(1 - \frac{\rho_2}{\rho_1})g(y\,\mathrm{Cos}\theta + x\mathrm{Sin}\theta) \qquad (2.95)$$

Equation (2.95) shows that the liquid velocity for a point on the air pocket is proportional to its vertical distance from the nose of the pocket. For small angles from vertical this vertical distance is greater than that for the vertical case as shown in Fig. (2.36). Since $h' > h''$, then the liquid velocity at point (P) will increase when the tube is tilted from the vertical. When the air pocket is nearly horizontal, i.e. $h < h''$ the liquid velocity at (P) will be less than the vertical case. This gives an explanation of why the rise velocity first increases and then decreases when the pipe is tilted from the vertical position. One point should be noticed here when the pipe is near the horizontal, and according to the above explanation, the rise velocity should be less than that for the vertical case while Wallis[177] and Spedding and Nguyen[154] noticed from their experimental work that the rise velocity for angles of 2°-3° from horizontal was still greater than that for the vertical case. This was also noticed by Bacopolous[14] for an angle of 0.945° with horizontal for air pockets rising in stationary water, and in the present research for an angle of +1.5° with horizontal for air pockets rising in moving water.

2.6 AIR POCKET BLOWBACK AND CLEARING PHENOMENA

In this section the behaviour of air pockets in sloping conduits will be examined in the context of blow back up a sloping conduit and air pocket clearing in downward sloping conduits. Blowback generally occurs when a coalescence of air bubbles produces an air pocket large enough to blowback in the opposite direction to the oncoming flow. Clearing or "blow out" is the term generally given to air pockets moving in the same direction as the flowing water with most problems occurring in downward sloping pipes. Most of the previous work in this area has been carried out for air pockets at a high point of a sloping conduit where the minimum water velocity required to clear the air pocket has been investigated. Little attention has been given to air pockets blowing back, where these pockets usually form due to the coalescence of small air bubbles entrained at the end of a hydraulic jump and grow in size until the water velocity is insufficient to overcome the pocket buoyant force. Air pocket formation at a high point was studied by Kalinske and Bliss[93], Mohsen[115], Wisner et al[187] and Edmunds[43]. Air pocket formation below a sluice gate in a downward sloping conduit was studied by Kalinske and Robertson[94]. Kent[97] and Gandenberger[59] studied air pockets held stationary in a downward sloping conduit. Fig. (2.37) shows a configuration of the air pocket at a high point, below a gate and an equilibrium pocket. Each of the above cases will be investigated in detail and a comparison between different results will be shown.

Kalinske and Robertson[94] were the first to study the air removal characteristics of a hydraulic jump formed at the end of an air pocket which can be formed at the summit of a pipe line or beyond a partly open gate (see Fig. 2.37). They outlined two methods for removing the air:

(a) mechanically by using air valves; but this is not feasible if the pipe is under sub-atmospheric pressure, and

(b) hydraulically by the flowing water.

Their main concern was to study the ability of the hydraulic jump to entrain air and pump this air along the conduit beyond the jump. Their experiments were carried out using a transparent "Lucite" circular pipe of 0.49 ft (0.149 m) inside diameter, which was laid at different angles ranging from 0° - 16.70° with the horizontal. Kalinske and Robertson [94] noticed that for any given initial depth of flow and slope of pipe, there is a point up to which the air entrained into the jump will exceed the rate at which the air is carried along the pipe beyond the jump. The air entrained by the jump will form a large bubble just beyond the jump, where it periodically blows back over the jump causing the jump to drop downstream; then another jump forms and the process will be repeated. They suggested that for discharge below critical value the average rate of air removal is controlled by the flow conditions below the jump and not by the jump itself. They found that the rate of air entrainment was mainly dependent on the Froude Number below the jump, where their results are shown in Fig. (2.38) as air water ratio (β) against the Froude Number ($Fr_1 = V_1/\sqrt{gy_e}$). The relationship of Fig. (2.38) can be expressed by the following equation:

$$\beta = \frac{Q_A}{Q_W} = 0.0066\ (Fr_1 - 1)^{1.4} \qquad (2.96)$$

Their experimental results for the limiting Froude Number, beyond which equation (2.96) applies, are shown in Fig. (2.39), where y_1/D is plotted against Fr_1. For any value of y_1/D, there is a value of Froude Number Fr_1 below which the pipe line will carry only a part of the air pumped into the water by the jump. This means that blowback can occur up to this limiting value of Froude Number Fr_1.

Sailer[143] reported on the problem of blowbacks in the San Diego Aqueduct which incorporates several long siphons. Fig. (2.40) shows a typical plan and profile of a long siphon where a hydraulic jump occurs near the point of intersection of inlet leg and hydraulic gradient for partial flow. This hydraulic jump may cause trouble in long siphons, because the entrained air accumulates into large air pockets downstream the jump blowing back with great force taking water up with them. These forces, on the Belle Fourche Project in South Dakota, were sufficient to completely destroy the reinforced concrete platform on the inlet structure. Sailer[143] analysed 21 different siphons ranging from 24 inches (0.61 m) to 111 inches (2.82 m) diameter, and plotted the results on the same graph of Kalinske and Robertson[94]. His results are shown in Fig. (2.41) where he indicated that siphon inlets with upstream Froude Number values falling on or below Kalinske and Robertson's curves gave no trouble, whilst the siphon inlets that fell above the curves had given trouble with blowbacks. This is the reverse of Kalinske and Robertson's findings who experienced blowback problems with upstream Froude Numbers less than the curves shown on Fig. (2.41). Recently Goldring[66] made an attempt to compare all the available results of blowback, where he plotted all the comparable data on a common graph, shown in Fig. (2.42). This graph includes only equilibrium void and blowback data. The equilibrium void is the void which is held stationary by flowing water in a downward sloping pipe, see Fig. (2.37). Any small increase in water flow causes it to move downstream, while a small decrease in water flow allows it to move upstream. Sailer's prototype data shown on the graph, where the upstream Froude Number has been translated into the pipe full Froude Number ($Fr_o = V_o/\sqrt{gD}$), indicates that blowbacks occur at non-dimensionalised velocities ($V_o/\sqrt{gD}$) of 0.99 and over. This means that critical flow occurs when the pipe runs full, and a hydraulic jump cannot form at the end of the air pocket. Hence the pocket cannot be cleared by air entrainment at its end, and may only be removed by bodily sweeping.

Kalinske and Bliss[93] investigated air removal from a high point by the flowing water, as shown in Fig. (2.37). Their main concern was to indicate the water discharge required to maintain air removal from any given size of pipe laid at any slope. Their experimental work was performed using two pipes of 4 in. (0.102 m) and 6 in. (0.152 m) diameter and laid at downward sloping angles up to 30°. They found from their data that the rate of air removal was controlled by two different hydraulic phenomena. For lower discharges the air removal was controlled by the flow characteristics beyond the jump which are described by Q^2_w/gD^5. At higher discharges the air removal was controlled by the hydraulic jump, which gives Q_A/Q_w as a function of the Froude Number of the supercritical approaching flow. To find the limiting conditon above which blowback would not occur, Kalinkse and Bliss[93] equated the buoyant and drag force on an equilibrium air pocket giving the velocity required to clear the pocket downstream. This is given by the following equation:

$$\frac{V_c^2}{gD} = \frac{KS}{C_d} \qquad (2.97)$$

where K is a constant, S is the pipe slope and C_d is the drag coefficient. Then replacing V_c by the water discharge Q_c, they obtained:

$$\frac{Q_c^2}{gD^5} = \frac{K_2 S}{C_d} \qquad (2.98)$$

indicating that the non-dimensional clearing discharge should vary linearly with the downward pipe slope. Fig. (2.43) showing their experimental data confirms that this is not the case, at least for small pipe slopes, this being due to the fact that hydraulic jumps in

this region do not fill the pipe. It can be noted from Fig. (2.42) plotted by Goldring[66] that there is a discrepancy between the results of Kalinske and Bliss and Kalinske and Robertson and this may be due to the fact that Kalinske and Robertson considered a long air pocket formed by a sluice gate whose upstream end is already at the high point of the pipe, while Kalinske and Bliss got a trapped pocket at the summit of a pipe line when water flows over the summit. Also in Kalinske and Bliss data there is no measurement of Y_1/D in order to compare their results for clearing with those obtained by Kalinske and Robertson, where it is noted from Fig. (2.42) that their clearing velocities are within the blowback data of Kalinske and Robertson.

Kent[97] investigated the entrainment of air by flowing water in circular pipes with downgrade slopes, as shown in Fig. (2.37c). He studied the velocity of flow to remove air from the pipe summit and indicated that accumulated air can be removed wither bodily with enough water velocity so that the drag force can overcome the buoyant force and hence moving the pocket downstream, or by the formation of a hydraulic jump at the end of the air pocket where the violent eddy action will entrain small bubbles into the conduit beyond the jump. These bubbles are small and usually their buoyant force is less than the drag force which enables them to move downstream. During their movement they may coalesce to form a larger pocket which may grow until it reaches a size where it will be stationary and form a further jump similar to the original pocket. He indicated that irrespective of the method used, the velocity of flow must be above a certain minimum value or even small bubbles will not move downstream. Kent[97] carried out his experimental work using two pipes of 1.5 in. (0.038 m) and 4 in. (0.101 m) diameter, with the first pipe laid at angles ranging from 0° - 90° while the second pipe was laid at angles ranging from 15° - 60° to the horizontal. The analysis used by Kent was based on equilibrium pockets, where he equated the drag force to the buoyant force to obtain a theoretical model for the drag coefficient and the minimum velocity for removal of air. He obtained the following for C_d and V_c:

$$C_d = f(\frac{L}{D}, \frac{H}{D}, \theta) \quad \text{for We} < 40 \tag{2.99}$$

$$C_d = f(\frac{L}{D}, \frac{H}{D}) \quad \text{for We} > 40 \text{ and } 15^\circ < \theta < 60^\circ \tag{2.100}$$

where We = Weber Number = $V\sqrt{\frac{\rho L}{\sigma}}$, L = air pocket length and H = max. depth of pocket.

The minimum water velocity to transport an air pocket down the pipe was given by:

$$V_c = K\sqrt{gDSin\theta} \tag{2.101}$$

where $K = 1.62\sqrt{\zeta}$ and is dependent on the drag coefficient and the shape of the air pocket. Equation (2.101) is the same as equation (2.86) used for the rising velocity of air pockets in inclined pipes for stationary water, where the same criteria has been used. Again the value of $\zeta = 0.58$ for air pockets with L/D > 1.50. Kent produced two graphs for the velocity to keep smaller air bubbles and larger air pockets stationary in the larger pipe of (0.101 m) diameter for different angles of inclination. These are shown in Figs. (2.44) and (2.45) respectively. Kent indicated that for each angle there is a critical size of air bubble in order to be swept bodily. Any size greater than the critical will require removal by pumping action at the end of the air pocket. This critical size is shown in Fig. (2.44) in which the largest bubble diameter at each angle represents the critical size for that angle. In Fig. (2.45) for larger air pockets, equation (2.101) is also shown in addition to Kent's experimental data. It can be noted from the Fig. (2.45) that for a conduit angle of 60° with horizontal, a supercritical pipe-full Froude Number is required to keep the pocket stationary. Kent[97]

explained the effect of increasing the air flow rate (Q_A) on the pumping action of the jump, where he stated that increasing (Q_A) will increase the pumping action until the depth under the pocket reaches the normal depth for that discharge and flow. When the normal depth is reached any further increase in (Q_A) will only increase the air pocket length until it fills the whole length of pipe and separation flow or stratified flow develops. Essentially this is using the incoming air discharge to push the jump out of the conduit.

Mohsen[115] and Wisner et al[187] investigated the removal of air from a downward sloping pipe of an angle of 18.5° with horizontal and a pipe diameter of (0.244 m). Using dimensional analysis to define the factors that affect the sweeping velocity, the following relation was obtained:

$$\frac{V_c}{\sqrt{gD}} = f(\frac{L}{D}, Re, \theta) \qquad (2.102)$$

assuming that L/D can be replaced by the non-dimensional air volume, $n = V/(\pi D^3/4)$, then for a given n and θ:

$$\frac{V_c}{\sqrt{gD}} = f(Re) \qquad (2.103)$$

Wisner et al proposed that data obtained for the rising velocity of air pockets Fig. (2.29) could be assumed to be the same velocity to bodily sweep air pockets down along a conduit. It can be noted that the sweeping velocity becomes indpendent of Re (viscous effects) when $Re > 10^5$. This means that the clearing velocity will only depend on angle of inclination (θ) which agrees with the results of Gandenberger[59] for large air pockets. They also carried out experiments to define the "limit bubble", originally discussed by Veronese[174] where a large pocket is introduced into the downward sloping pipe with flowing water. The water velocity was changed continuously to keep the pocket in equilibrium, as disruption

progresses. It was found that the pocket was reduced to a small size where any increase in the velocity will sweep the pocket out of the pipe. Their results are shown in Fig. (2.46) where the limit velocity is plotted against the diameter of pipe. The results confirm that for a particular diameter and slope there is one stable length and corresponding velocity, and that the limit velocity does not become a constant with increasing diameter.

Wisner et al[187] plotted all the available experimental data on one graph, shown in Fig. (2.47), to provide an upper envelope for the minimum velocity required to clear an air pocket in a downward sloping pipe as the following:

$$\frac{V_c}{\sqrt{gD}} = 0.25\sqrt{\sin\theta} + 0.825 \qquad (2.104)$$

They suggested that the velocity required for removal of air pocket should not be much higher than the upper envelope as this will paradoxically introduce further problems of blowback. They recommended that the clearing velocity should be kept within +5% of the upper envelope.

Mohsen[115] indicated an important point about this type of blowback, in that the air pocket is not completely steady at the clearing velocity. There is some generation of air bubbles at its downstream end, with some of the generated air swept out whilst the remainder coalesces in a pocket and travels back to join the original pocket. Thus the size of the air pocket at clearing velocity is ranging between two limits and not completely steady. The difference of volume at the two limits is equal to the blowback pocket. It was observed that the size of the blowback pocket increases with decreasing the depth of flow at clearing velocity. In a subsequent discussion Wiser et al[187] indicated that increasing the velocity much higher than the lower bound will develop a

different flow pattern, where large parts of the air pocket would tear quickly and rise up to the high point. This air at the summit will again be forced down in smaller sizes. This movement up and down the pipe causes significant pressure pulsations.

Gandenberger[59] carried out experimental work after developing theoretical expressions for the velocity of air pockets in pipes with stationary and moving water. His work was published in German (1953 and 1957) and a translation to his work is given by Mechler[110]. Gandenberger noted that the determination of all the factors which affect air pocket movement requires extensive experiments, and that the best way to represent his results will be in the form of graphs. He carried out his experiments in glass tubes of 45 mm, 26 mm and 10.5 mm diameter, and in a steel pipe of 100 mm diameter, having varying pipe inclinations between 0° and 90°, and with water flowing upward and downward. Based on these experiments, together with some prototype data, Gandenberger developed a graph which gives the minimum average water velocity (V_{c_1}) required to clear a given volume of air pocket from a high point in the profile of a pipe of 1 m diameter for various angles of inclination of the downstream leg, as shown in Fig. (2.48). The air pocket is defined as a fraction or multiple of the air volume of a unit pocket, n = 1, defined for any diameter (D) as having the volume $\pi D^3/4$. Gandenberger shows that, for pipe diameters greater than 0.1 m, the corresponding minimum velocity for transport of a pocket of the same relative size in a pipe of diameter D (in meters) can be calculated from:

$$V_c = V_{c_1}\sqrt{D} \qquad (2.105)$$

The available experimental results have been plotted in a non-dimensional form, as shown in Fig. (2.49) where $V_c/\sqrt{gD}$ is plotted against the angle from horizontal. It is noted that clearing from high points is most difficult at downward slopes at 45° - 60° and for large air volume pockets. This graph has also been plotted as

Q_w^2/gD^5 against the angle from horizontal, as shown in Fig. (2.50), together with the curve given by Falvey (USBR)[55] for the limit of air pocket movement, where Q_w is the minimum flow rate to clear the air pockets. Falvey[55] indicated that additional studies are required to define the bubble motion curve in Fig. (2.50) for slopes greater than 45°, since Martin[105] had shown that a stationary air pocket forms when Q_w^2/gD^5 is equal to 0.30 for vertically downward flow, this result is also shown in Fig. (2.50). This means that the increasing trend of this curve probably does not continue past the 45° slope. In fact it could be argued that Falvey's graph is a complete over-estimate of clearing discharges for angles greater than about 10°. Falvey[55] has plotted different results for clearing, blowback and stationary air bubbles and air pockets on one graph, which is shown in Fig. (2.51), where the reverse flow region has been delineated using the data of Colgate[35] and the slug flow curve given by Runge and Wallis[139] and shown in Fig. (2.27).

Gandenberger results have also been plotted in Fig. (2.42) on Goldring's graph, for $n \geq 1$, where it can be noted that Gandenberger limiting Froude Number is less than Kent's and Wisner's et al data, and it fits very closely the results of Kalinske and Robertson for $Y_1/D = 0.150$. Unfortunately it is difficult to compare the results directly because Gandenberger did not use depth of the air pocket, instead he used total volume of the pocket.

It is noted from this review that there is no definite answer for air pocket blowback and clearing phenomena. For air pocket blowback mainly the air pockets were forming due to coalescence of entrained air bubbles and grow in size until their buoyant force overcomes the water velocity when they then blow back. The blowback phenomena was either defined from an equilibrium void or based on prototype data where different criteria were used in each case. For the case of air pockets clearing also different criteria were used to define the water velocity required to clear an air pocket down a sloping conduit. Some investigators used air

entrainment at the end of the pocket as the criteria for reducing the size of air pocket until the pocket reaches a size where the water velocity can overcome the air pocket buoyancy and remove the pocket. Other investigators used the equilibrium void to define the clearing or bodily sweeping of the air pocket. It can be outlined that no definitive answer has been produced because each investigator was:

(1) trying to solve a different specific problem, such as an air pocket at a high point, an air pocket forming below a gate, and air pockets fed into the flowing water.

(2) using different apparatus, with different dimensions and using different physical configuration. Some investigators were using the volume of the air pocket, others were using either the depth of flow or the depth of the air pocket itself.

To obtain a definitive answer, a more general and comprehensive procedure must be used after defining the parameters which affect the behaviour of air pockets in sloping conduits. This will allow the use of more accurate procedures in obtaining the required data such as the depth of flow below the air pockets, velocity profiles, the angle the nose of the air pocket forms with the conduit, the inclination angle of the conduit and the direction of the flowing water.

2.7 AIR POCKET BEHAVIOUR AT THE JUNCTION OF A DROPSHAFT/TUNNEL SYSTEM

Dropshaft/tunnel systems are usually used in the outlets of dams, power stations and the outfall systems of nuclear power stations. In Chapter (1) an outline of the problems caused by the presence of air in dropshaft/tunnel systems has been given, together with a description of some hydraulic structures which experienced the problem of air presence. In this section a review of mainly the

experimental work which has been carried out on the subject will be outlined.

When water is allowed to fall freely some distance down a shaft, it will entrain small air bubbles when the nappe impinges on the standing water surface in the shaft. These entrained air bubbles may descend the shaft and coalesce, forming an air pocket at the junction of the dropshaft/tunnel system. The behaviour of these pockets falls into three basic categories, namely, a trapped stationary air pocket at the bend, blowback up the shaft, or clearing of the pocket along the tunnel. The presence of such air pockets will usually reduce the capacity of the system, produce head losses, and may also lead to mass oscillation, vibration and the damage to the structure itself when they blowback.

Miller[112] carried out model tests to investigate the oscillations which occurred in Hunterston "B" Power Station. Additional work on the same problem was reported by Townson[165] as already outlined in section (1.3). A 1 to 11 scale model of outfall with a 12 inch inside diameter tunnel was used and the tunnel was laid at a down slope of 1 in 200. Operating the model with clear water did not reveal any significant instabilities on a comparable scale of prototype oscillations. This was largely because large air bubbles were entrained whose rising velocity was similar to that of the downward water velocity in the shaft and tunnel. Additives were added to reduce the size of the entrained air bubbles which allowed the bubbles to reach the bend, although the addition of additives caused other problems in the transport of air along the tunnel. Miller found from the tests that the entrained bubbles which accumulate at the bend in the form of air pockets, cannot pass through the system because of the adverse (downward) slope of the tunnel, and the free surface disturbances at the air pocket pump the air back to the vertical shaft. Entrapped air along the tunnel roof represented a considerable store of energy which can only be dissipated by the air escaping up the shaft. With low water

discharges the only way that air could escape was by bringing the system into oscillation close to its natural frequency. In some cases the water velocities fell near to zero or even reversed during part of each cycle. At higher flows the coupling between the release of air from the tunnel and the systems natural period of oscillation was destroyed as air release became dependent on surface disturbances generated by the higher water velocities in the tunnel. Introduction of air vents at the bend provided a means by which the energy stored in the air pocket could be dissipated without disturbing the system.

Goldring, Mawer, and Thomas[63] carried out a preliminary study of air void at the junction of dropshaft/tunnel system while investigating air entrainment in Thameside Power Station. They also noticed that the void will form at the dropshaft/tunnel bend at low water discharges. Tests were conducted on a circular bend of radius ratio ($\acute{R}/D$) 0.75, with their results shown in Fig. (2.52). Water velocities are scaled up to prototype values. They outlined two situations, the first being when suddenly reducing the water velocity below 3.0 m/s the air void will vent back up the shaft rising to the free surface; the second situation existed under steady operation at water velocities below 3.0 m/s where the void startsto form but vents before it can reach a large size. As it vents and rises up the shaft it breaks up into small bubbles and then these bubbles are carried back down and around the bend by the flowing water. They suggested that the problem at low discharges will only be of air bubbles recirculating in the area of the bend, and the problems associated with violent venting will not be present.

Goldring[64,65] has carried out tests to investigate the behaviour of air pockets at the bend which connects a vertical shaft to a horizontal tunnel. The pipe sizes were 0.072 m, 0.10 m, 0.14 m and 0.19 m inside diameter. Four bends were used with bend radii $\acute{R}/D$ = 0.5, 0.75, 1.0 and 1.5. Air flow ranges between 0% - 2% of water flow, which is much lower than the actual percentage of

entrained air in dropshaft spillways where this percentage can be as high as 40%.

Goldring specified four basic modes for the behaviour of the air pocket at the bend:

(1) At low water flow rates, any void which starts to form on the inside of the bend would vent back up the downshaft before it could grow to an appreciable size.

(2) At higher water flow rates a stable void is formed at the bend with its nose located somewhere on the curved inside radius and its downstream end in the form of a hydraulic jump. This void is called partly ventilated void (PVV), which is usually a short air pocket with the jump at its end drowning back to the bend.

(3) If the air flow at this stage is increased the void will grow in length and passes the working section which is 1.2 m from the bend and is called fully ventilated void (FVV). Actually increasing air flow rate will increase the size of the air pocket i.e. its length and depth as will be observed in this research.

(4) Further increase in the water flow causes the FVV to be swept away downstream and the conduit flows full of water, with the air dispersed and carried along as small air bubbles.

The four basic modes are shown in Fig. (2.53) where the air/water ratio (β) is plotted against upstream non-dimensionalised water velocity (Froude Number). The "void vents" line and "void comes" line were obtained by holding Q_A constant and decreasing the water flow. While "FVV" line was obtained by holding the water flow constant and increasing air discharge.

Goldring investigated the effect of bend radius on behaviour of the void at the bend, his results are shown in Fig. (2.54), for 0.14 m diameter pipe. It can be noted that the void will vent back and clear out of the pipe at a lower water velocity for the bend with $\acute{R}/D = 0.50$ than that for the smoothest radius of $\acute{R}/D = 1.50$. Thus the sharpest possible bend is the most desirable situation. Goldring derived empirical expressions for the void vents and void comes lines as shown below:

$$F_{ov} = 0.28 + 0.36 \sqrt{\acute{R}/D} \qquad (2.106)$$

below which an air pocket will vent back up the shaft, and:

$$F_{oc} = \frac{(0.50 + 0.25\sqrt{\acute{R}/D} + 20 \frac{Q_A}{Q_w})V_e}{\sqrt{gD}} \qquad (2.107)$$

above which air voids will continuously clear from the bend.

F_{ov} is non-dimensional velocity for venting and F_{oc} is a non-dimensional velocity for clearing. Equation (2.107) is plotted with experimental data in Fig. (2.54) and shows a deviation for the tightest bend. This may be due to the fact that secondary currents occurring at a sharp bend are stronger and allow the air bubbles to be transported downstream, so that they will not contribute to the growth of the void at the bend.

Tunstall and Harvey[172] had studied secondary currents in a 90° single-mitre bend ($\acute{R}/D = 0.5$), and found that the secondary currents downstream the bend had a periodic component, where swirling flow occurs at the bend and closes the inner separation zone. This swirling flow may be affecting the formation of the hydraulic jump which closes the void, and thus delaying the formation of FVV.

Goldring also studied the effect of the pipe diameter on the behaviour of the air pocket at the bend. His results for different diameters with a bend radius of $\acute{R}/D = 1.0$ is shown in Fig. (2.55). It is clear from this Figure that air pockets will clear at a lower water velocity in large diameter than in small diameter pipes. The effect of pipe diameter on clearing an air void is not clear yet, because the results of Kent for 100 mmΦ and Wisner et al for 244 mmΦ shown in Fig. (2.42) are roughly comparable. This might be due to the face that clearing of the air pocket in Goldring's results was by hydraulic jump entrainment at the tail of the pocket, while Kent's and Wisner's data was for equilibrium void. Removal of the air void by entrainment at the jump is more substantial at larger model sizes.

Ervine and Himmo[53] investigated the scale effect on clearing an air pocket from the junction of a dropshaft/tunnel system. They outlined that if clearing is by bodily sweeping the pocket, and if the pocket can be accurately modelled in the first place, then the water velocity required to bodily clear an air pocket is correctly modelled by Froude scaling, or $V_c/\sqrt{gD}$ is constant, as indicated by the results of Kent and Wisner et al. If the clearing of an air pocket takes place by the air entrained from the hydraulic jump at the end of the pocket, the clearing will be essentially a velocity dominated phenomenon and not modelled accurately by Froude Scaling alone. In order to get a hydraulic jump entraining air, a combination of the underflow Froude Number Fr_1, and the under flow water velocity V_1 must be reached. It is more likely that a dual combination of $Fr_1 > 1.0$ and $V_1 > 0.8$–1.0 m/s is required as the minimum condition for this type of void removal. The rate of air removed at the end of the pocket was given by Goldring[65] who used Thomas' equation[162] for air-entrainment, shown below:

$$\beta = K(Fr_1 - 1)\left[\left(1 - \frac{1}{V_1}\right)^2\left(1 - \frac{1}{3}V_1\right)^{-1}\right] \qquad (2.108)$$

The above equation includes a scale dependent term, which indicates that for hydraulic jump removal of air, the prototype will remove

much more air than the model. This will give an explanation for the results in Fig. (2.55) where larger pipe diameter appears to clear at lower velocities than smaller pipe diameters.

2.8 SUMMARY

Most of the previous work has concentrated on the rising velocity of air pockets in stationary and moving water, with some work done for the required water velocity to clear an air pocket out of a downward sloping pipe. The main point which can be outlined is that in Civil Engineering structures inertia forces and buoyancy will dominate the behaviour of air pockets. Since the liquid is usually water, viscous effects can reasonably be neglected, and for large pipe diameter (D > 150 mm), surface tension can also be neglected. Little work has been done for the case of an air pocket at the junction of a dropshaft/tunnel system which relates to this research. Most of the work has concentrated on clearing an air pocket from a high point in a pipe line, and also on the behaviour of the air pocket in the straight part of a sloping pipe.

For the case of air pocket rising in moving water through inclined pipes, the rising velocity, as indicated in section (2.4.2), will consist of two components, the first component is due to the mixture velocity and the second component is due to angle of inclination of the pipe and the size of the air pocket which is as indicated by Bacopolous is best represented by the air pocket depth (H). In inclined pipes the air pocket can ascend or descend for downward water flow, depending on the drag on the pocket relative to the buoyancy.

The most interesting aspect of the behaviour of air pockets in sloping conduits is the analysis of blowback of air pockets and the minimum velocity required to clear an air pocket downstream. Little attention has been given to the case of blowback, as most of the available experimental and prototype data has been generated for

the case of the stationary equilibrium pocket. Even in the case of tests giving data for blowback, details of the blowback pocket have not been given, such as its shape, depth and the angle of the nose with the conduit, etc.

Clearing air pockets from a downward sloping pipe can take place either by bodily sweeping or by air entrainment due to the hydraulic jump at the end of the air pocket. If the pocket is clearing bodily it can be accurately modelled by Froude scaling, while if it is clearing by entrainment it cannot be modelled accurately. This means that at larger scale models the pocket will clear at low Froude Numbers than smaller models if the clearing is by air entrainment only. However, the air pocket can clear by both entrainment at its downstream end and bodily sweeping. This is almost similar to Veronese[174] and Lara[102] who noted that the air pocket can be reduced by generation and entrainment at its end until it reaches a size where it can be swept bodily and this size is called "limit bubble". This result was also examined by Wisner et al[187] and shown previously in Section (2.6).

The work carried out by Goldring[65] on air pocket formation at the junction of a dropshaft/tunnel system is also the main subject of this thesis. It appears that the radius of the bend has a great effect on the air pocket which forms at the bend and that the tighter bend is better than any other configuration of bend because blowback occurs over a narrower range of Froude Number than other bends, and also clearing of the existing air pocket requires less water velocity than the radiused bend. Thus the aims of this thesis could be summarised as follows:

(1) To investigate the formation and behaviour of air pockets at a dropshaft/tunnel junction. This will include blowback up the shaft, clearing along the tunnel, hydraulic jump formation, comparison between theoretical simple models and

experimental results, and an investigation into the scale effects occurring. This will be carried out by varying the bend radius, the tunnel inclination to the horizontal, the air flow rate and the water flow rate.

(2) To investigate the behaviour of air pockets in a straight length of pipe sloping at an upward angle of +1.5°, primarily to look at how air pockets behave in straight tunnel sections and to see if Benjamin's analysis can be extended to single air pockets under moving water conditions.

(3) To investigate the clearing and blowback characteristics of air pockets in a straight length of pipe sloping at a downward angle of -1.5°.

Thus it is hoped to investigate several aspects of air pocket behaviour in a single piece of apparatus and hopefully provide design rules for such hydraulic structures.

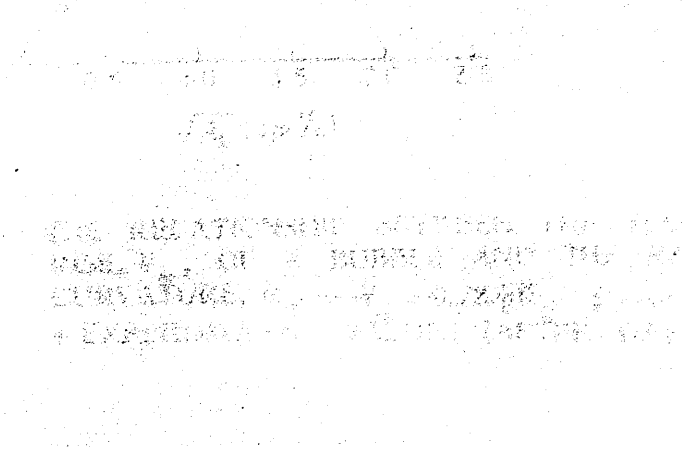

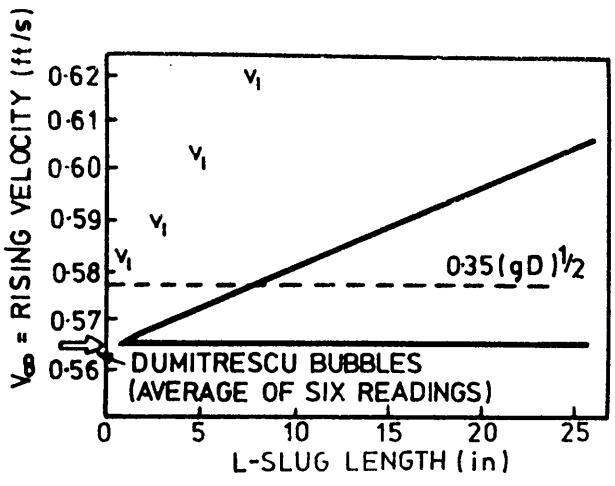

FIG. (2.1) RELATIONSHIP BETWEEN SLUG LENGTH AND THE RISING VELOCITY OF DIFFERENT TYPES OF SLUGS (AFTER NICKLIN ET AL)

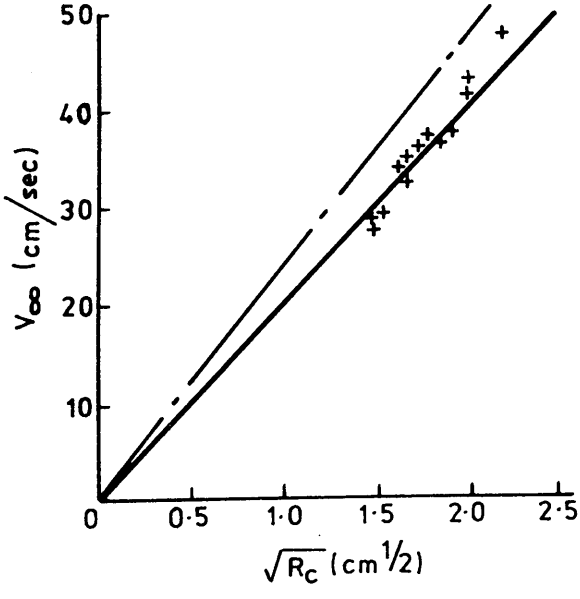

FIG. (2.2) THE RELATIONSHIP BETWEEN THE VELOCITY OF RISE, V_∞, OF A BUBBLE AND THE RADIUS OF CURVATURE, R_c. ---$V_\infty = 0.78\sqrt{gR_c}$; ——$V_\infty = 2/3\sqrt{gR_c}$, + EXPERIMENTAL VALUES (AFTER DAVIES AND TAYLOR)

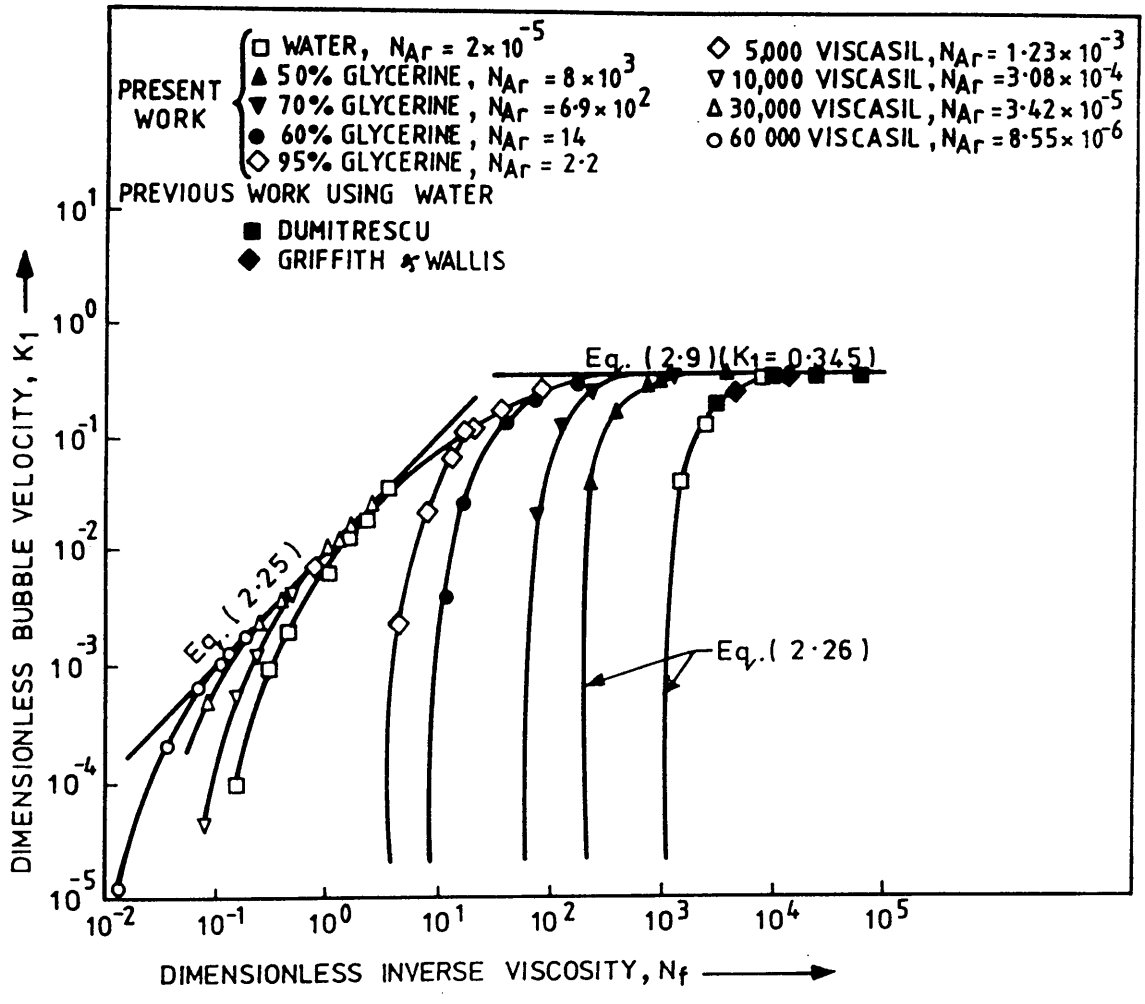

FIG. (2.3) GENERAL DIMENSIONLESS REPRESENTATION OF BUBBLE RISE VELOCITY IN SLUG FLOW (AFTER WALLIS)

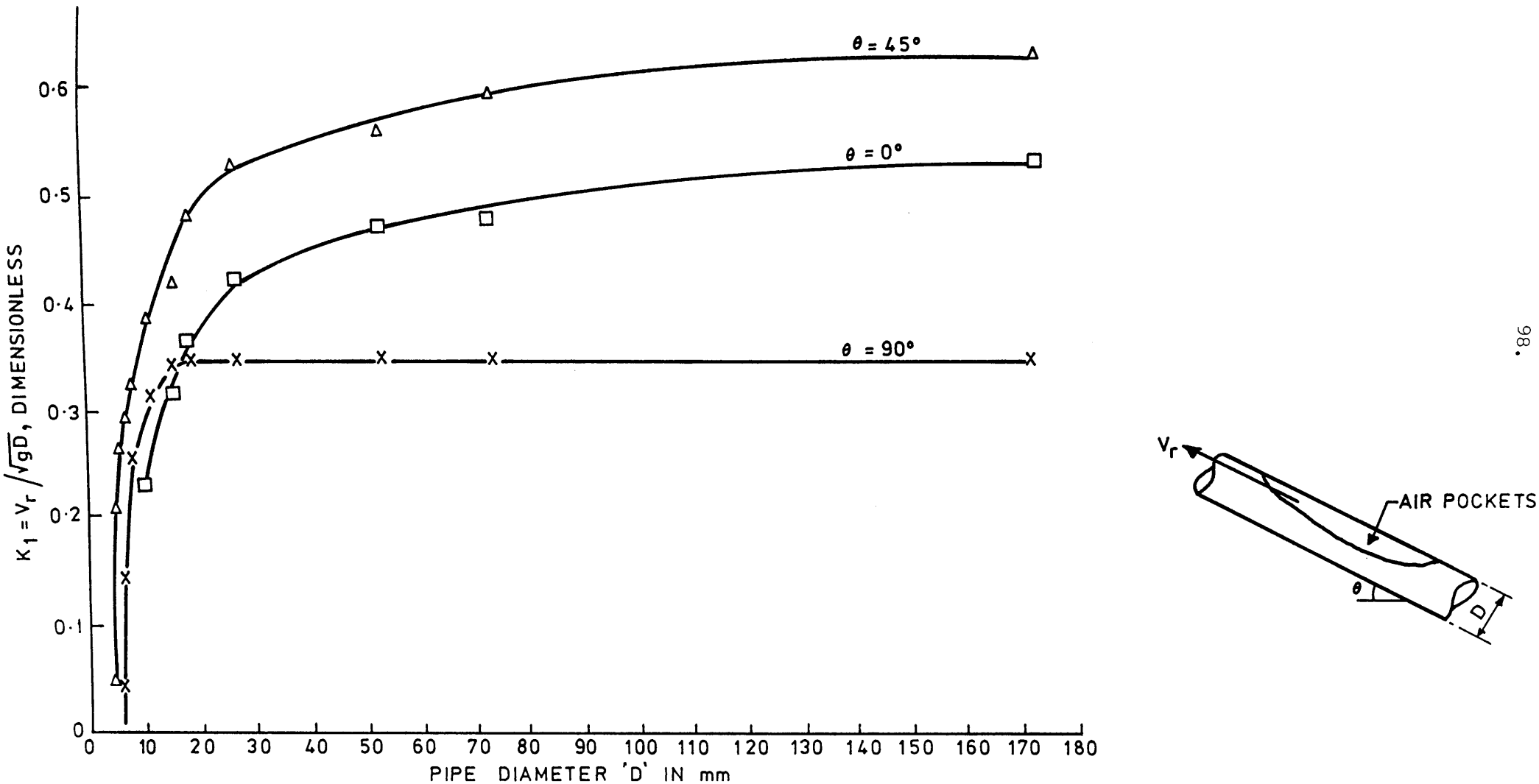

FIG. (2.4) EFFECT OF SURFACE TENSION ON THE RISING VELOCITY OF AIR POCKETS THROUGH STATIONARY WATER IN CLOSED CONDUITS (AFTER ZUKOSKI)

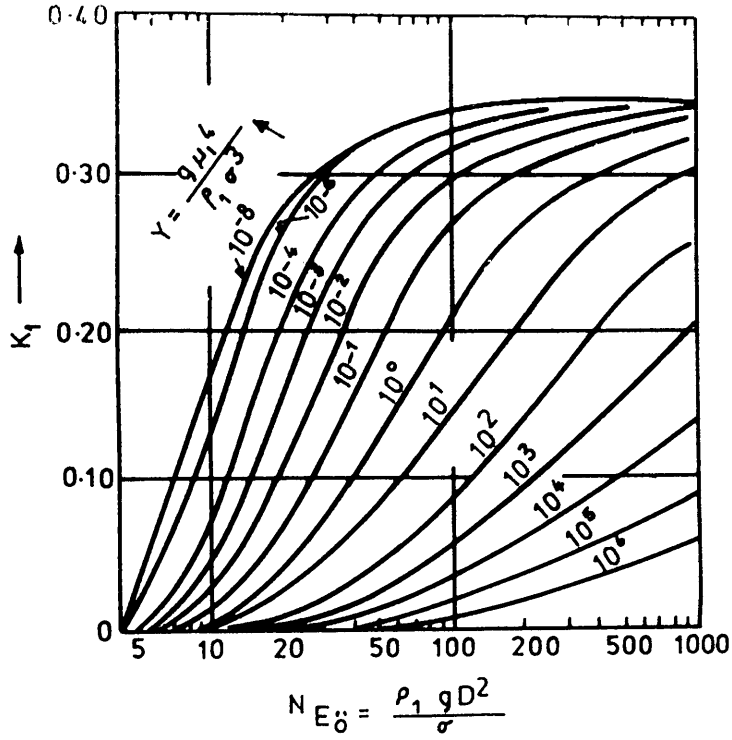

FIG. (2.5) AN ALTERNATIVE REPRESENTATION OF FIG. (2.3), (AFTER WHITE OF BEARDMORE)

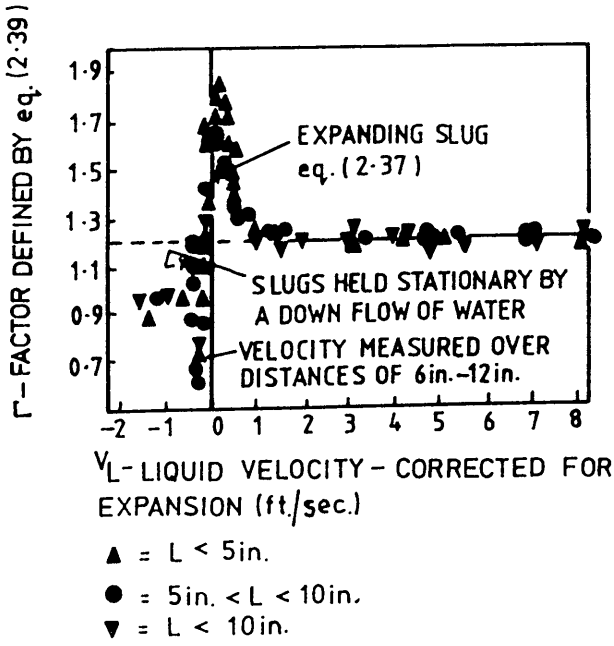

FIG. (2.6) VARIATION OF Γ WITH LIQUID VELOCITY AND SLUG LENGTH (AFTER NICKLIN ET AL)

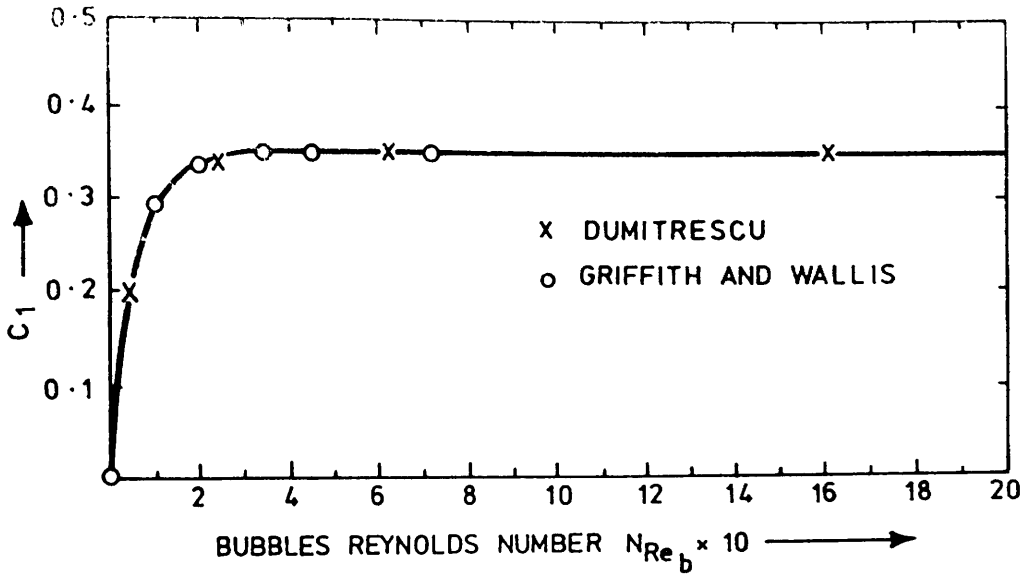

FIG. (2.7) DIMENSIONLESS CONSTANT C_1 AGAINST BUBBLE REYNOLDS NUMBER (AFTER GRIFFITH AND WALLIS)

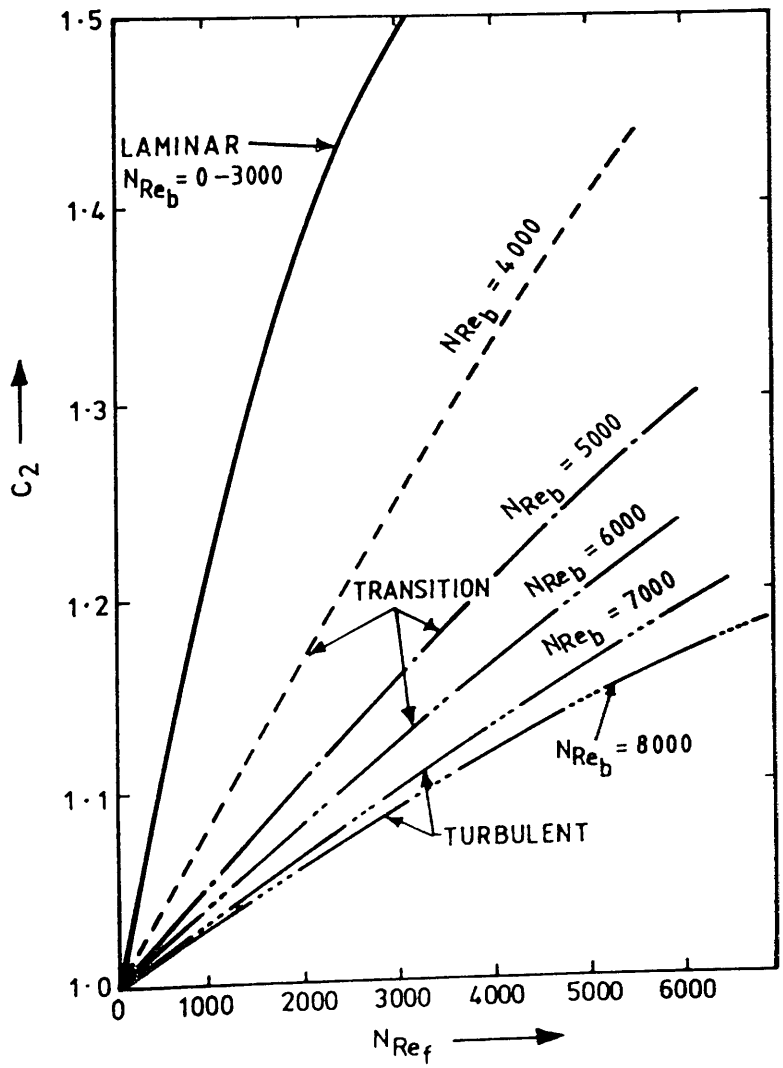

FIG. (2.8) COEFFICIENT C_2 AGAINST LIQUID REYNOLDS NUMBER FOR VARIOUS VALUES OF BUBBLE REYNOLDS NUMBER (AFTER GRIFFITH & WALLIS)

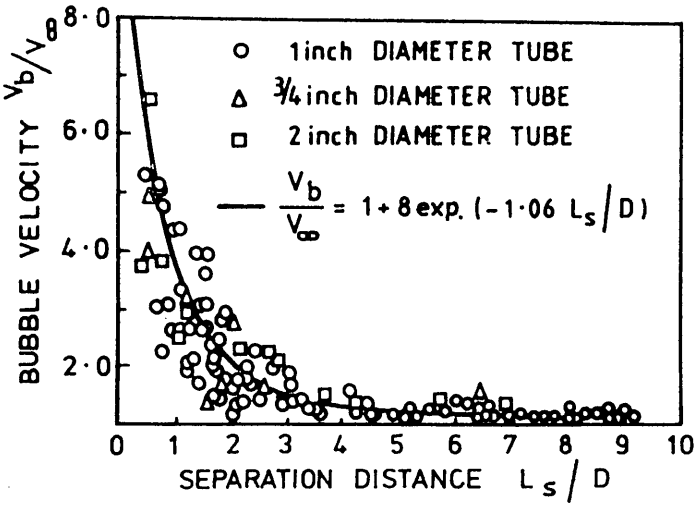

FIG. (2.9) VELOCITY SEPARATION DISTANCE DATA (AFTER MOISSIS AND GRIFFITH)

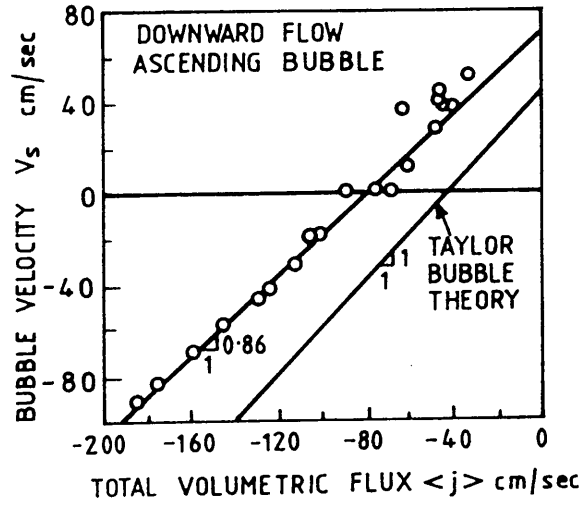

FIG. (2.10) BUBBLE VELOCITY FLUX PLANE FOR D = 14 cm (AFTER MARTIN)

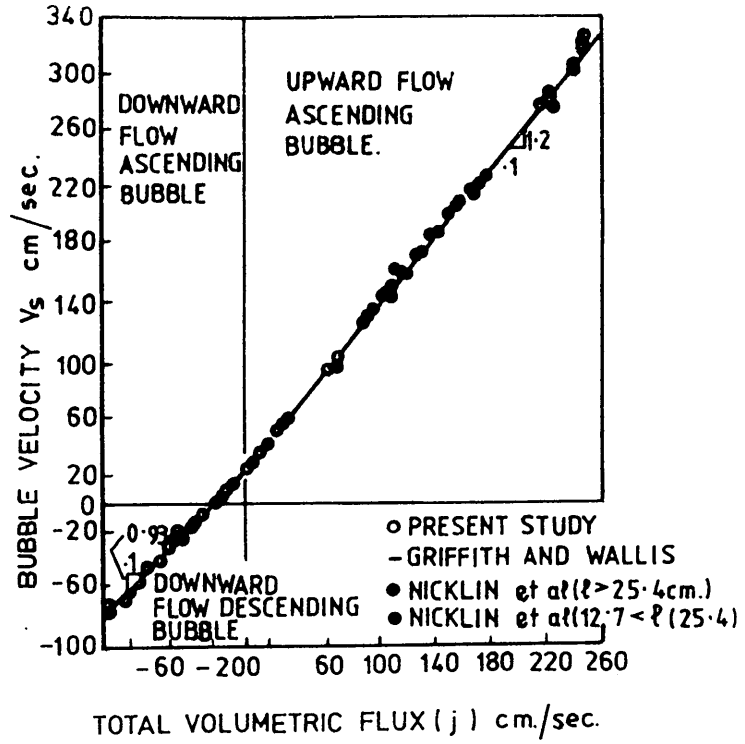

FIG. (2.11) BUBBLE VELOCITY FLUX PLANE FOR D = 2.60 cm (AFTER MARTIN)

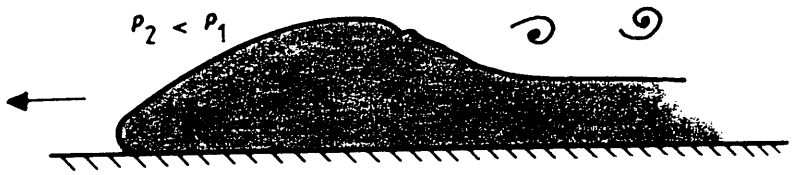

FIG. (2.12) OBSERVED FROM A GRAVITY CURRENT (AFTER KEULEGAN 1958)

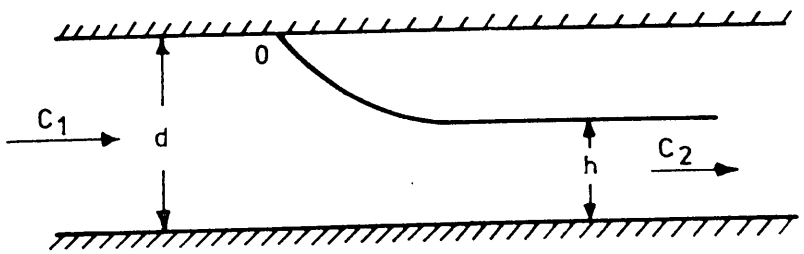

FIG. (2.13) SPECIFICATIONS OF STEADY FLOW PAST A CAVITY (AFTER BENJAMIN)

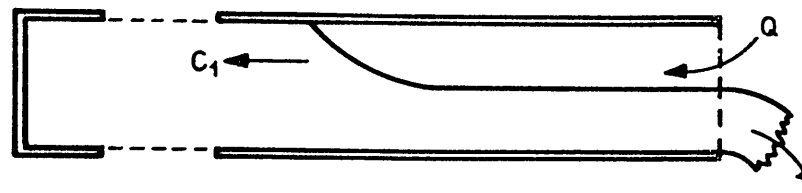

FIG. (2.14) ILLUSTRATION OF THE MOTION WHEN LIQUID FLOWS OUT FROM A HORIZONTAL BOX (AFTER BENJAMIN)

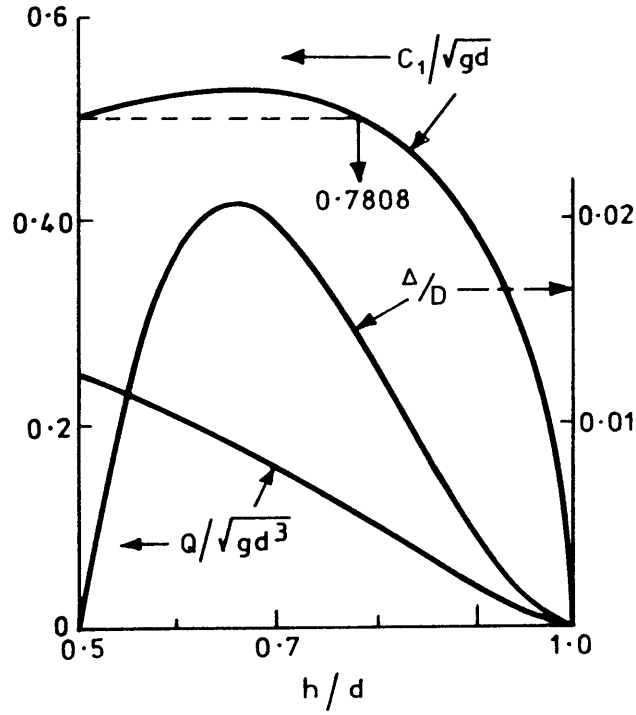

FIG. (2.15) GRAPHS OF NON-DIMENSIONAL PROPAGATION VELOCITY $C_1/\sqrt{gd}$, HEAD LOSS Δ/d, AND CAVITY EXPANSION RATE $Q/\sqrt{gd^3}$ CONSIDERED AS FUNCTIONS OF h/d (AFTER BENJAMIN)

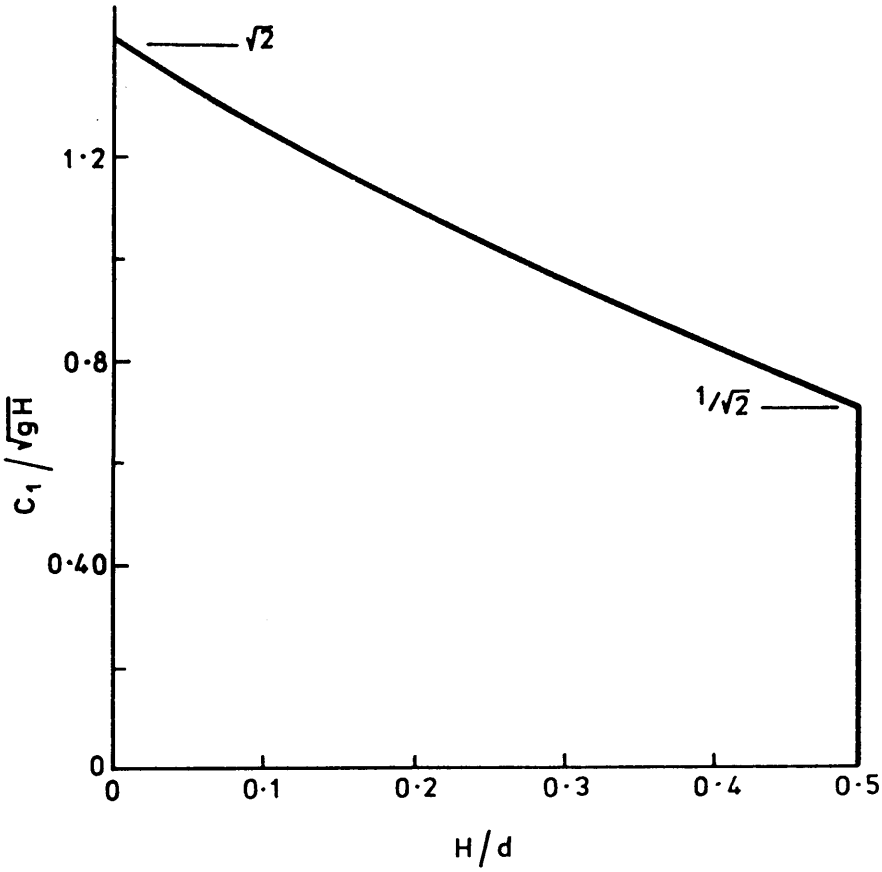

FIG. (2.16) GRAPH OF $C_1/\sqrt{gH}$ AS A FUNCTION OF H/d (AFTER BENJAMIN)

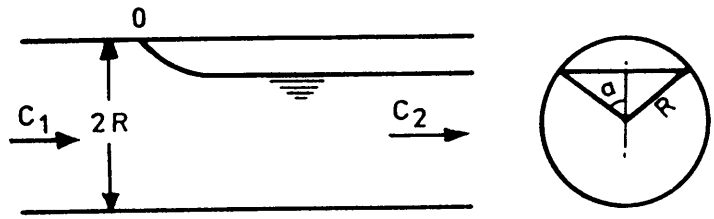

FIG. (2.17) SPECIFICATION OF CAVITY FLOW IN HORIZONTAL TUBE OF CIRCULAR CROSS-SECTION (AFTER BENJAMIN)

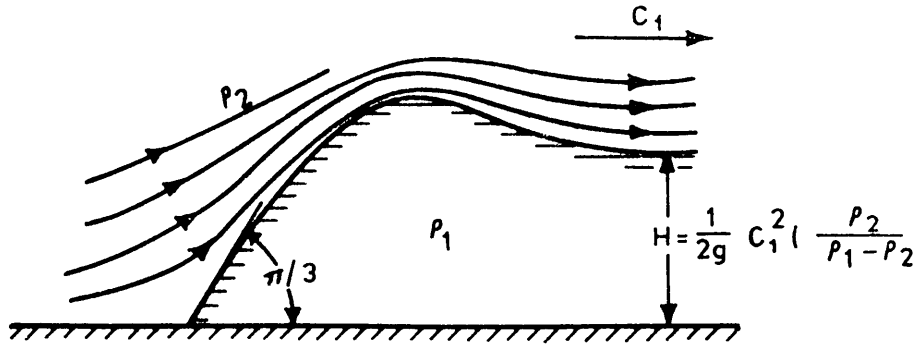

FIG. (2.18) THEORETICAL MODEL PROPOSED BY VON KARMAN

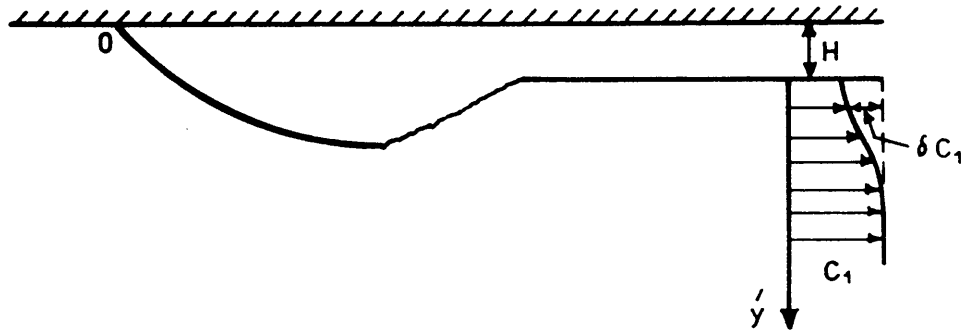

FIG. (2.19) ILLUSTRATION OF REAL FLOW, SHOWING BREAKING HEAD WAVE AND VELOCITY PROFILE OF ENSUING WAKE (AFTER BENJAMIN)

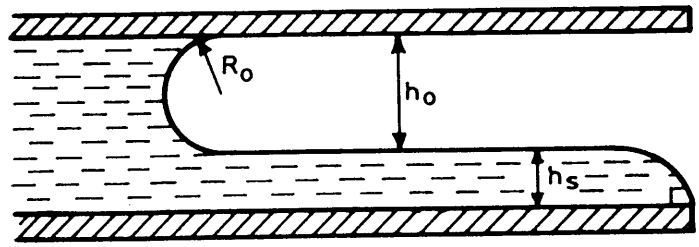

FIG. (2.20) THE BLOCKED CONDITION, SHOWING UNDRAINED WATER (AFTER GARDNER AND CROW)

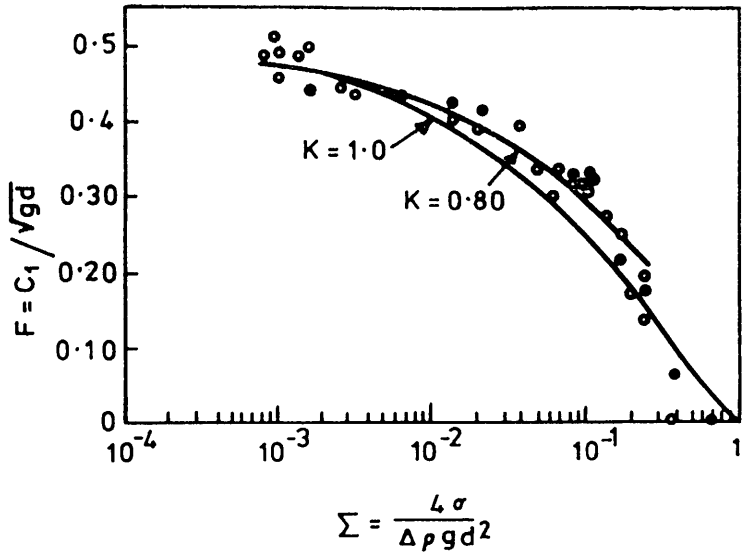

FIG. (2.21) COMPARISON OF EXPERIMENTAL AND CALCULATED VALUES OF (F) FOR A RECTANGULAR CHANNEL. o, SQUARE-ENDED STILL; •, CHAMFERRED SILL (AFTER GARDNER AND CROW)

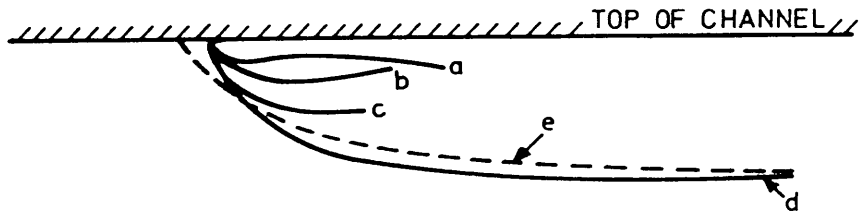

FIG. (2.22) SUPERIMPOSED BUBBLE PROFILES FOR FOUR CHANNEL DEPTHS, TOGETHER WITH THEORETICAL PROFILE OF BENJAMIN FOR A DEPTH OF d = 107 mm.
a,d = 15 mm ; b,d = 27.5 mm ; c,d = 60 mm ; d,d = 107 mm ; e,d = 107 mm, BENJAMIN THEORY, (AFTER GARDNER AND CROW)

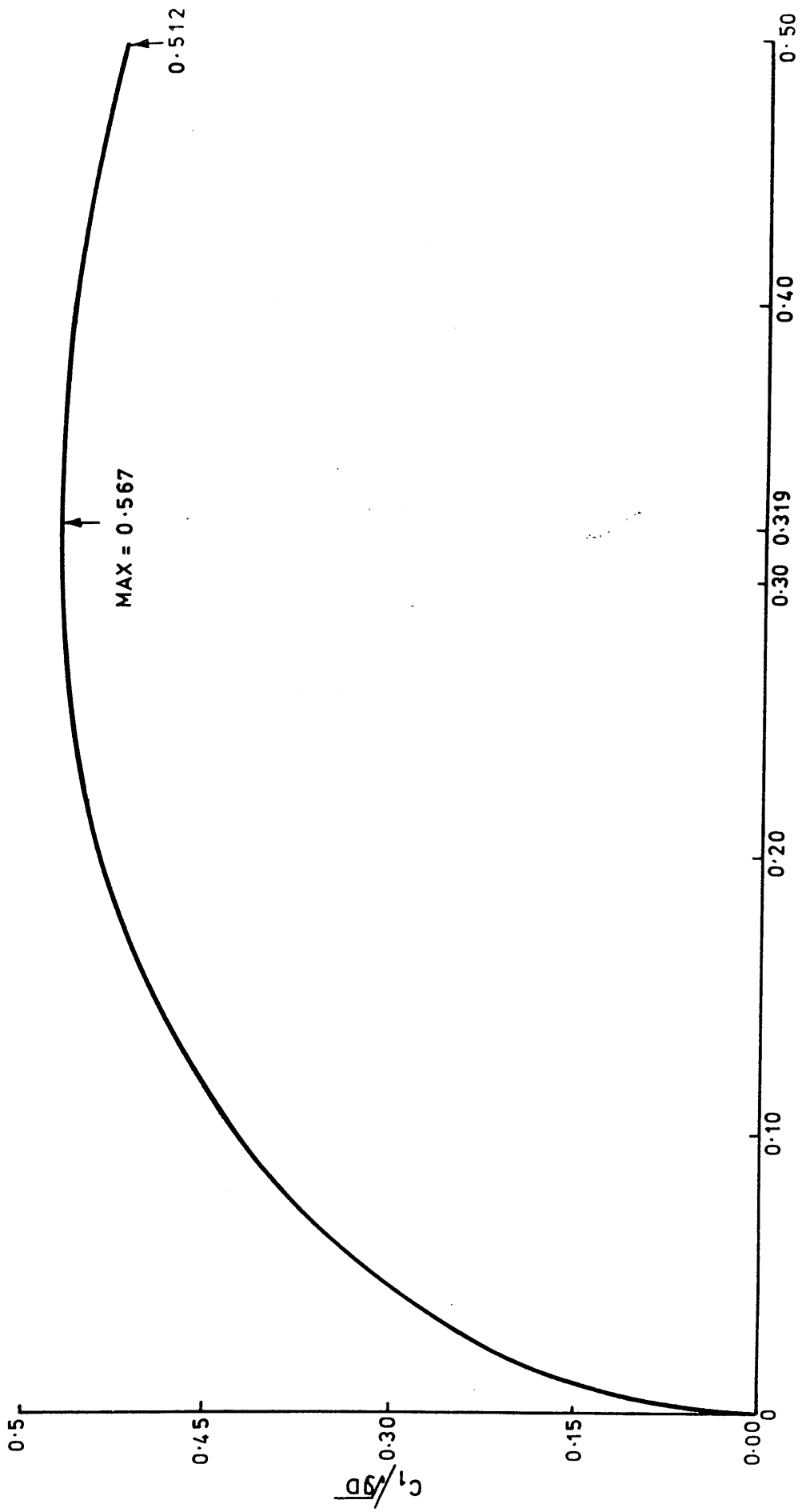

FIG. (2.23) EXTENSION OF BENJAMIN'S THEORY TO HORIZONTAL PIPES, ASSUMING RECTANGULAR VELOCITY PROFILES OF WATER (AFTER BACOPOLOUS)

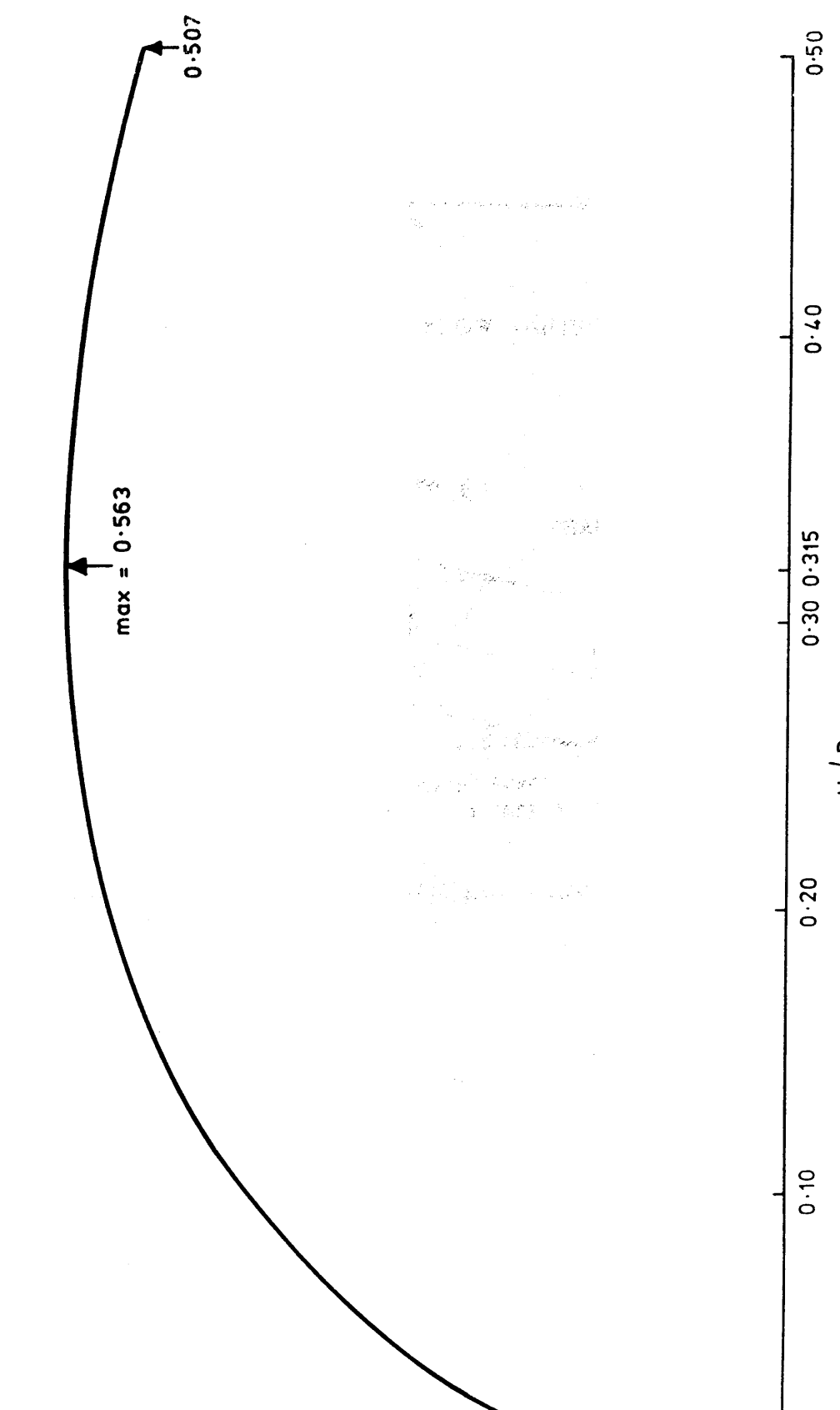

FIG. (2.24) EXTENSION OF BENJAMIN'S THEORY TO HORIZONTAL PIPES, ASSUMING NON-RECTANGULAR VELOCITY PROFILE OF WATER FAR DOWNSTREAM (AFTER BACOPOULOUS)

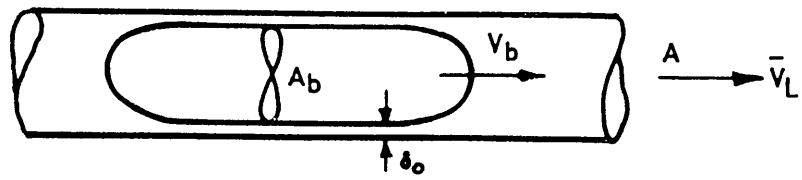

FIG. (2.25) HORIZONTAL SLUG FLOW (AFTER WALLIS)

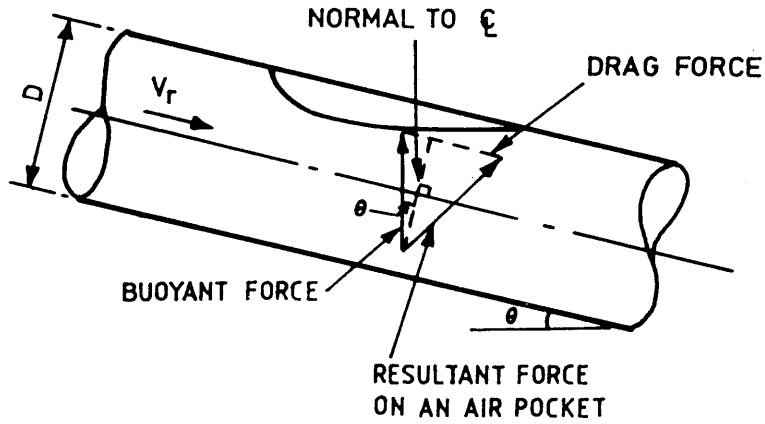

FIG. (2.26) FORCES ON A STATIONARY AIR POCKET (AFTER FALVEY)

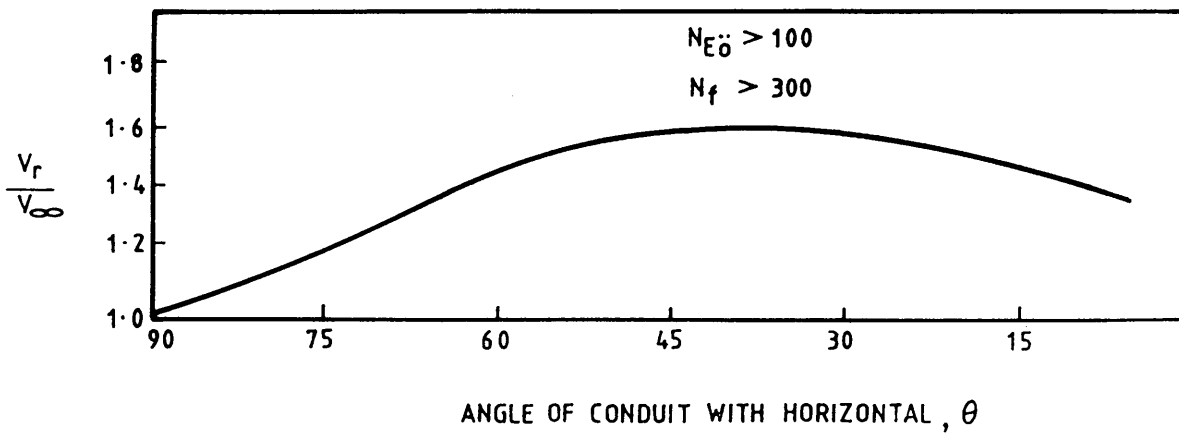

FIG. (2.27) SLUG FLOW IN INCLINED PIPE (AFTER WALLIS)

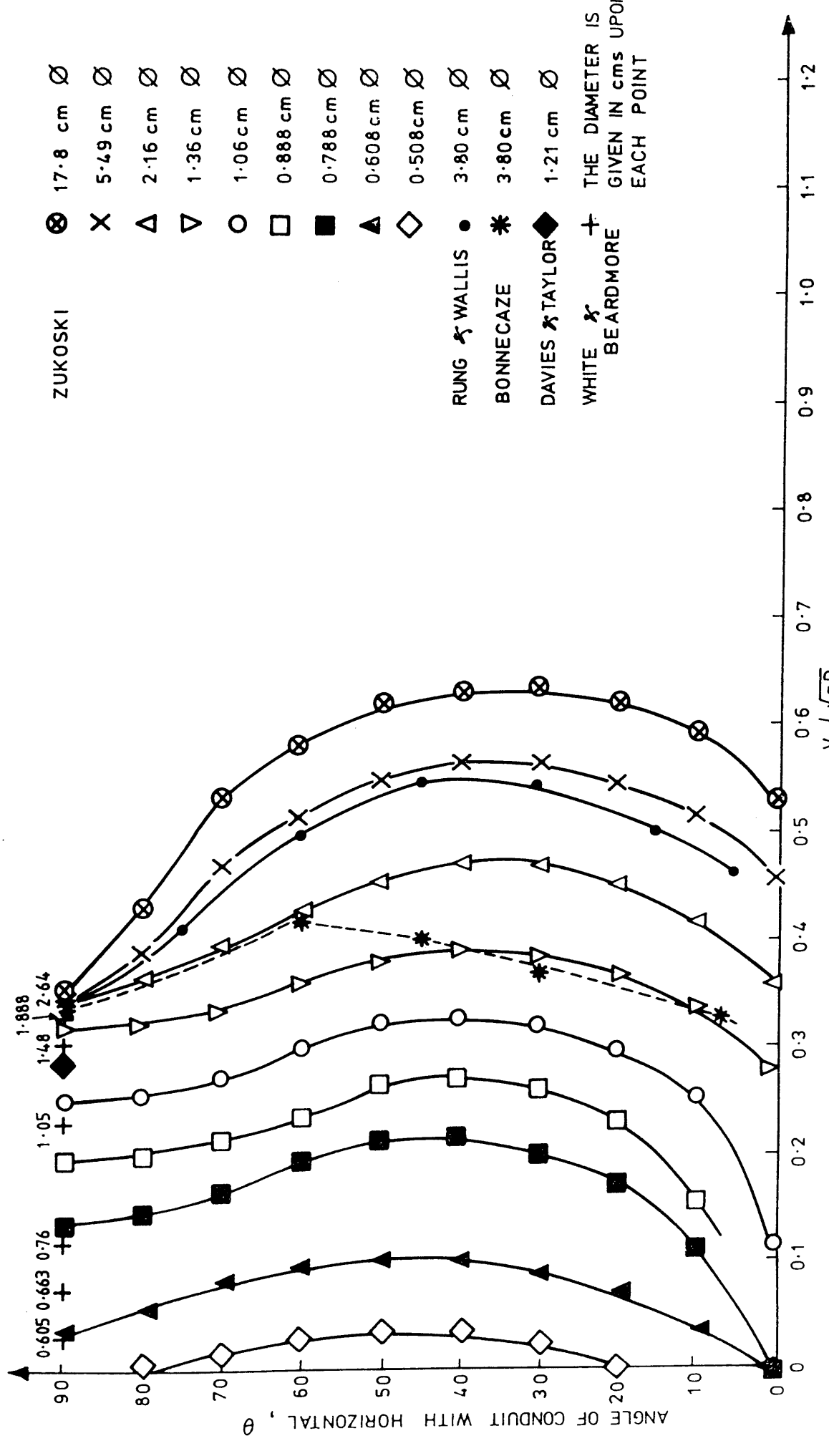

FIG. (2.28) RELATION BETWEEN THE DIMENSIONLESS PARAMETER $V_r/\sqrt{gD}$ AND ANGLE OF CONDUIT WITH HORIZONTAL (OBTAINED FROM RESULTS OF THE ABOVE AUTHORS)

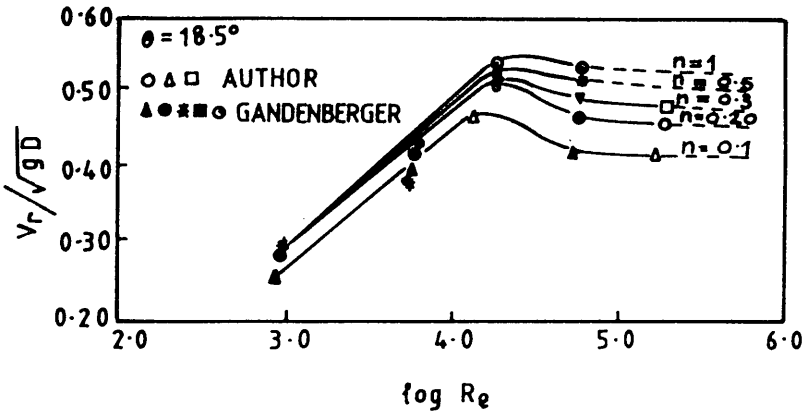

FIG. (2.29) VARIATION OF RISING VELOCITY WITH POCKET SIZE (AFTER WISNER ET AL)

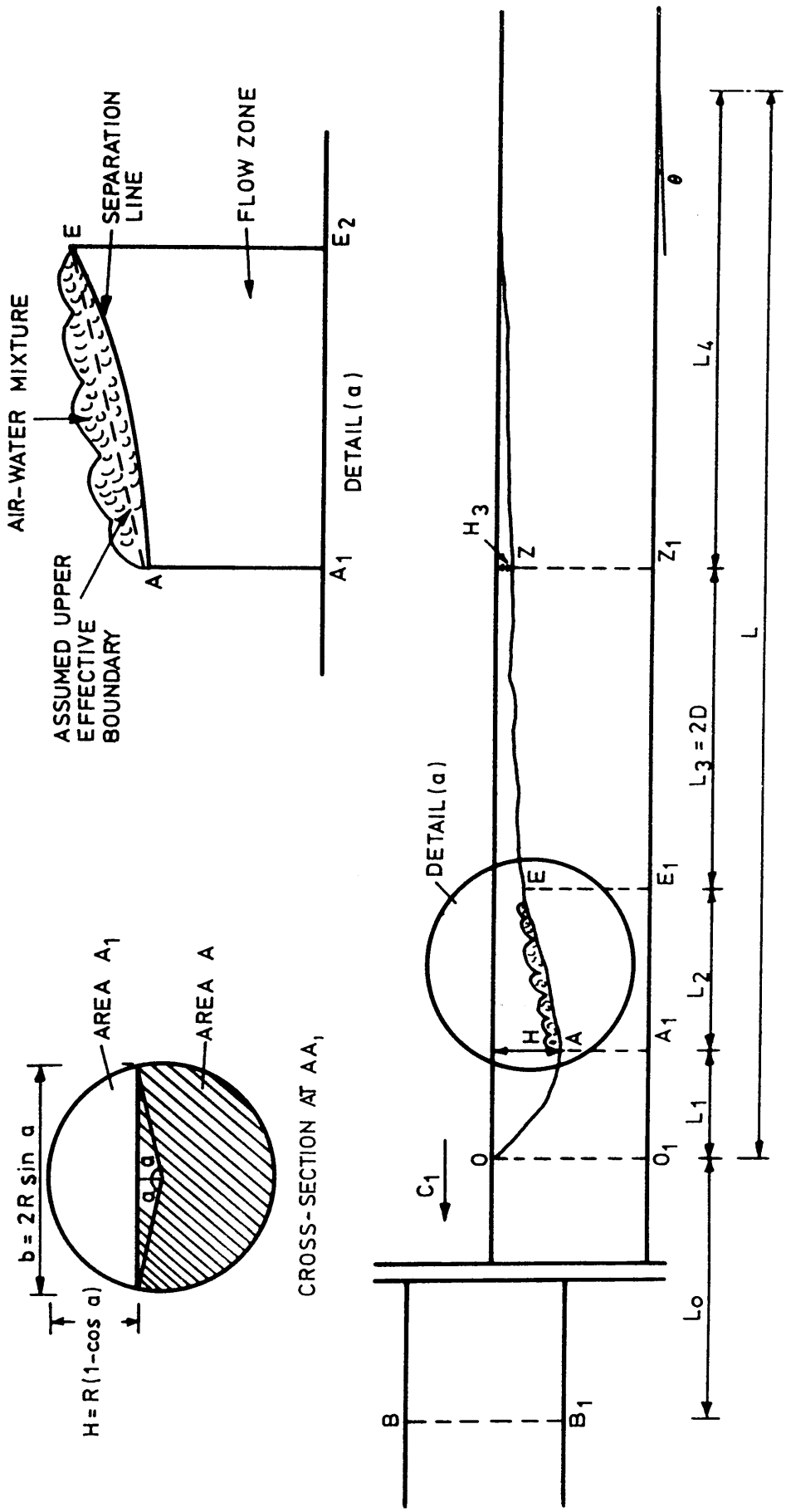

FIG. (2.30) SINGLE AIR CAVITIES, SECTION ALONG THE PIPE AXIS (AFTER BACOPOULOUS)

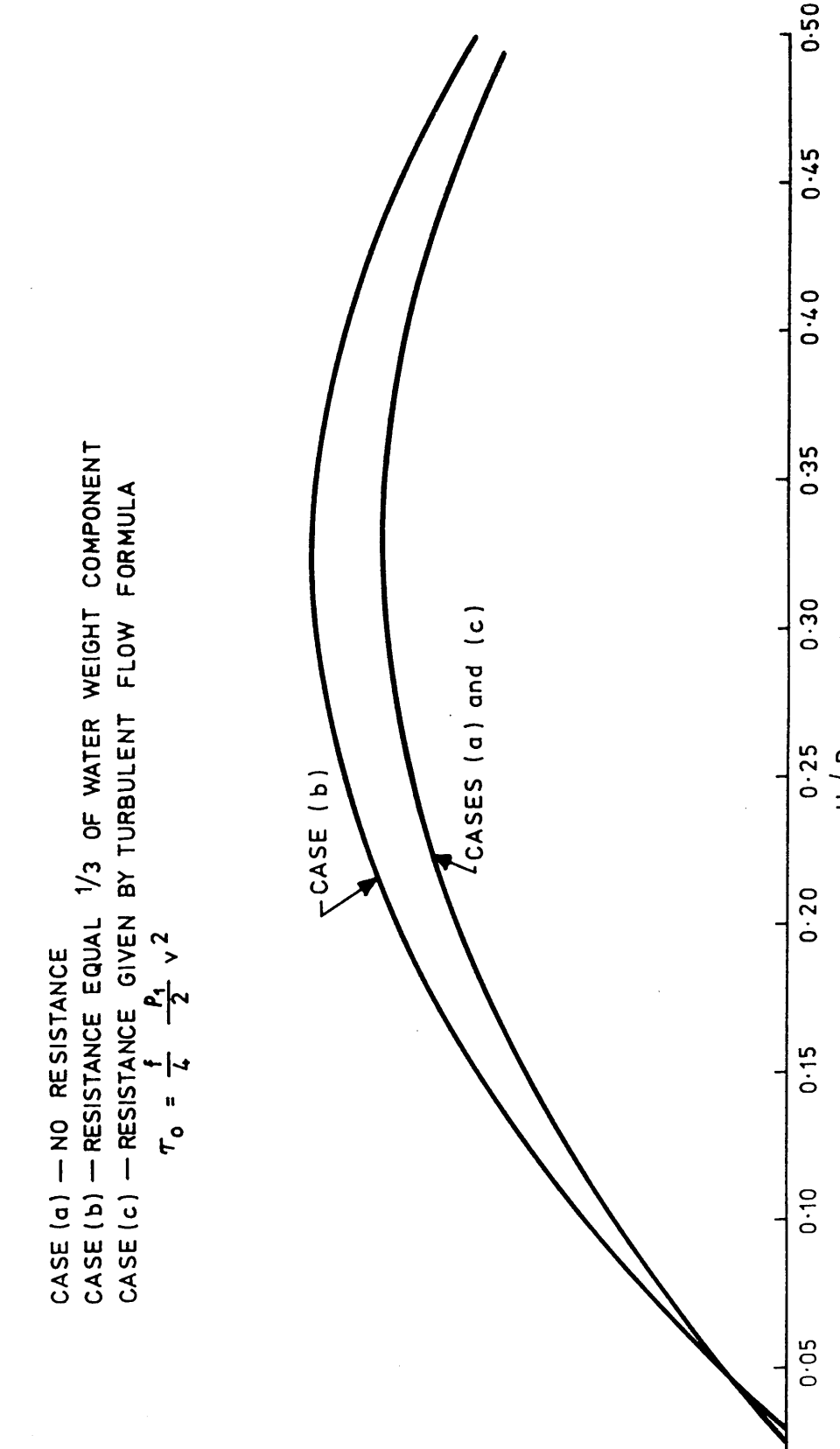

FIG. (2.31) THEORETICAL AIR CAVITY LENGTH IN INCLINED PIPES (AFTER BACOPOULOUS)

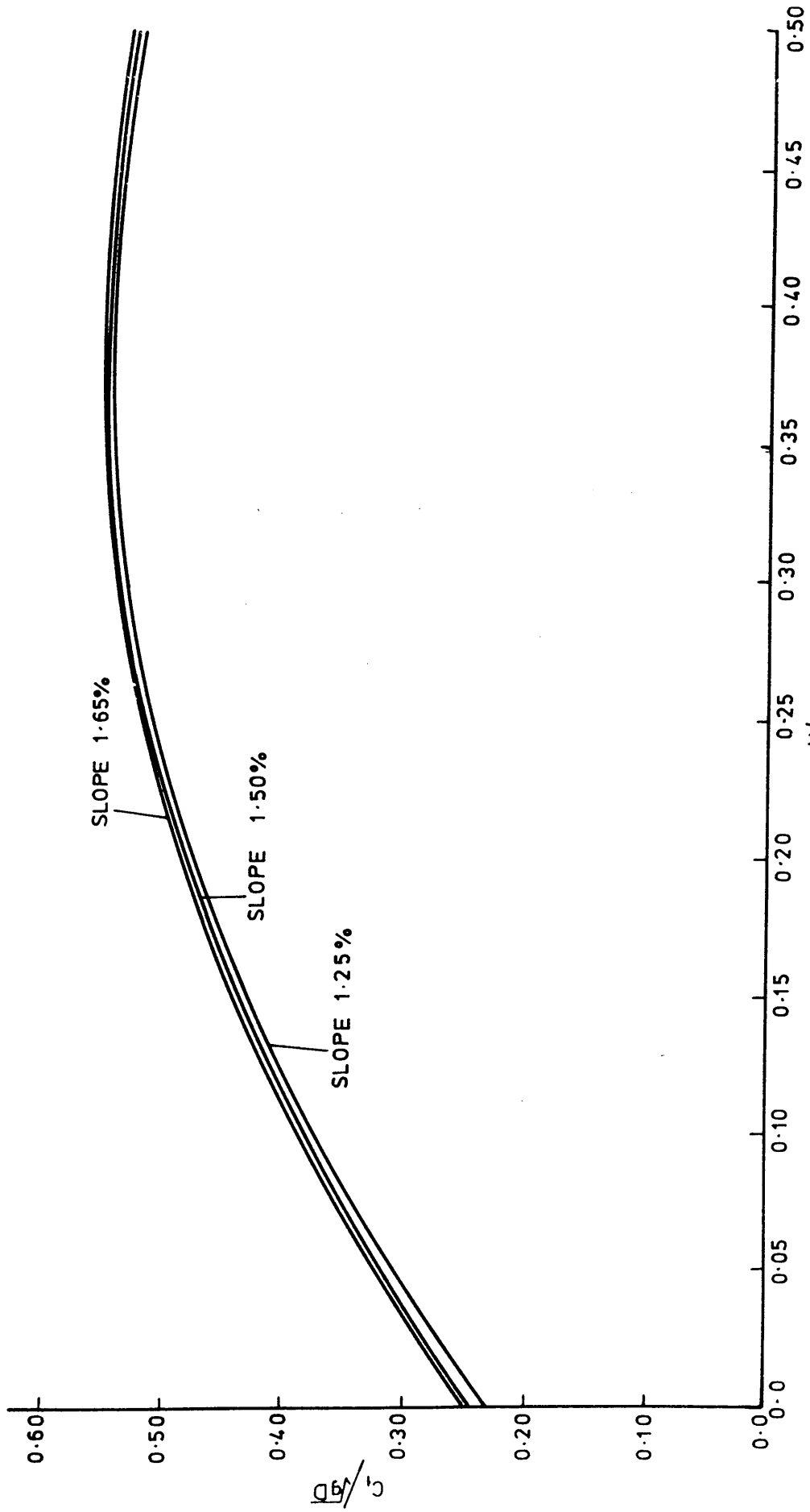

FIG. (2.32) EXPERIMENTAL RESULTS FOR THE RISING VELOCITY OF SINGLE AIR CAVITIES IN STATIONARY WATER FOR DIFFERENT SLOPES (AFTER BACOPOULOUS)

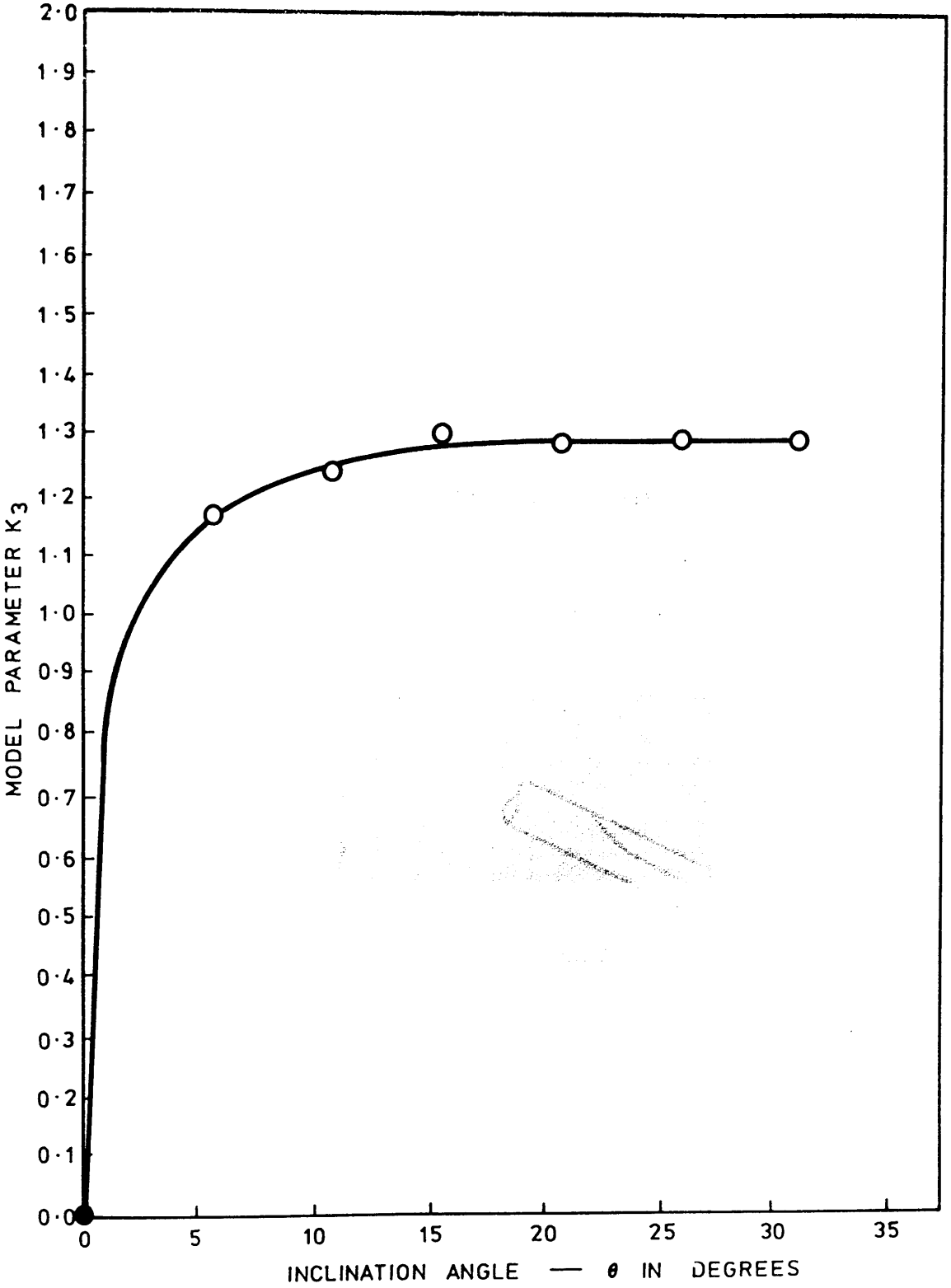

FIG. (2.33) THE EFFECT OF INCLINATION ANGLE ON THE PARAMETER (K_3) (AFTER PARAKH)

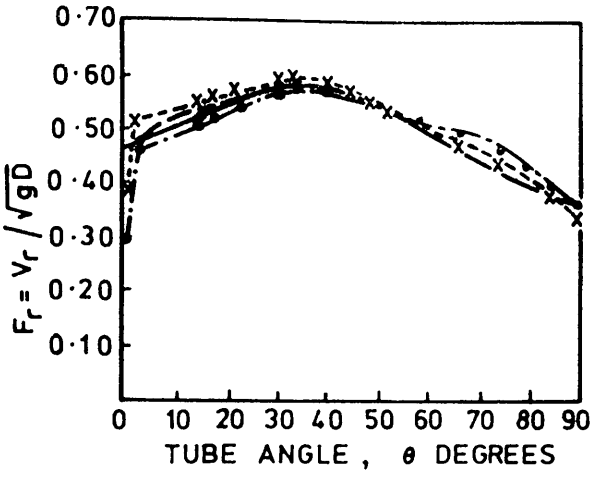

FIG. (2.34) EFFECT OF TUBE INCLINATION ON THE BUBBLE RISE VELOCITY IN WATER AT 20°C FOR DIFFERENT BUBBLE VOLUMES (AFTER SPEDDING AND NGUYAN)

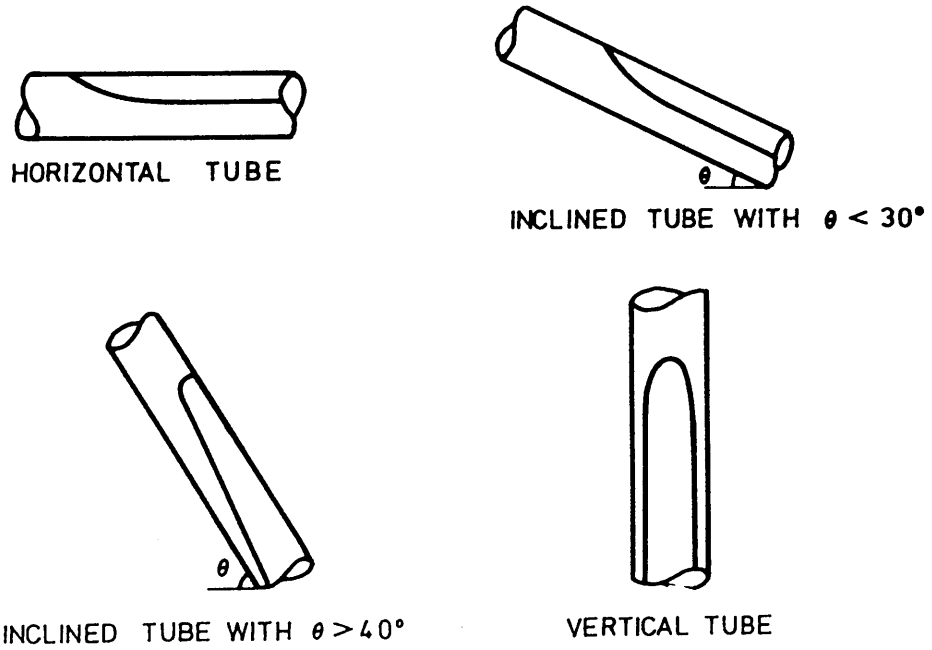

FIG. (2.35) EFFECT OF TUBE INCLINATION ON BUBBLE SHAPE TAKEN FROM PHOTOGRAPHS BY SPEDDING AND NGUYAN

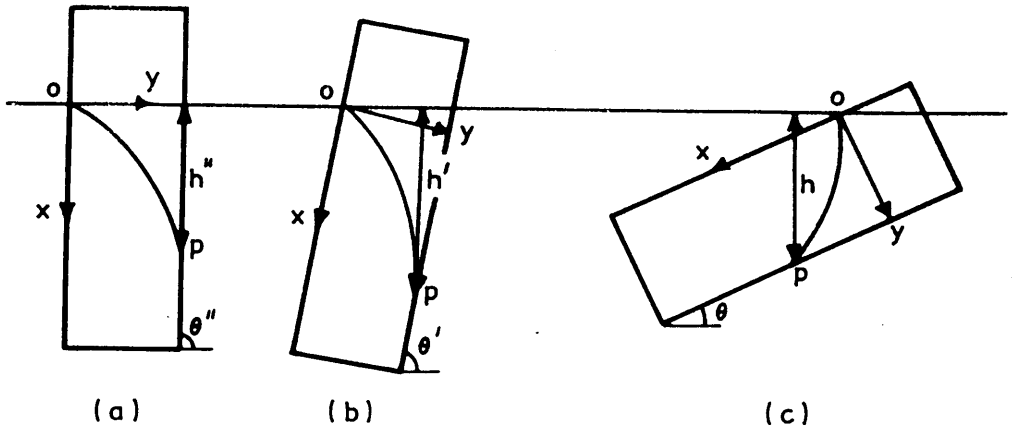

FIG. (2.36) EFFECT OF ROTATION ON AN AIR POCKET RISING IN A TUBE (AFTER BONNECAZE)

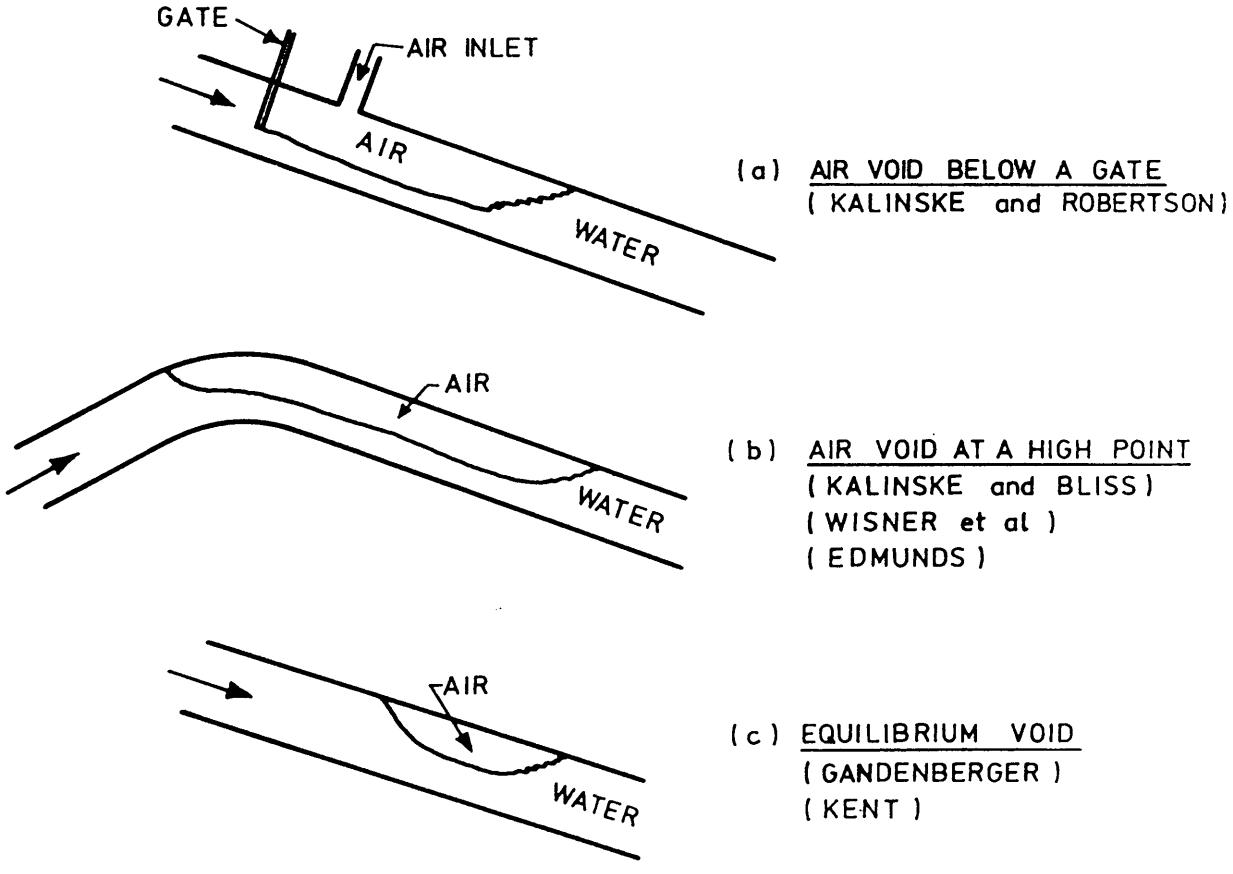

FIG. (2.37) AIR VOID CONFIGURATIONS (AFTER GOLDRING)

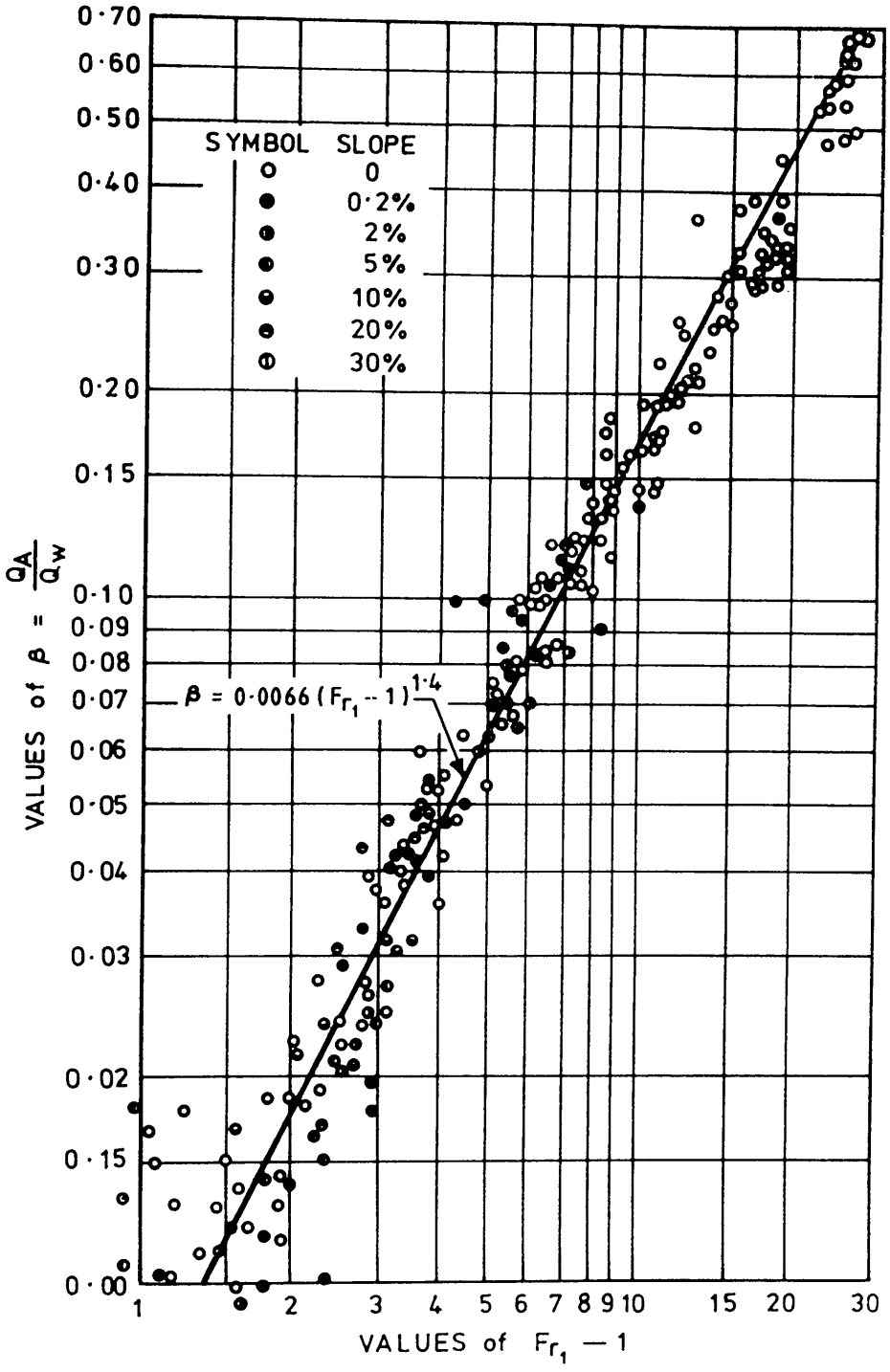

FIG. (2.38) CORRELATION OF DATA ON RATE OF AIR ENTRAINMENT BY HYDRAULIC JUMP (AFTER KALINSKE & ROBERTSON)

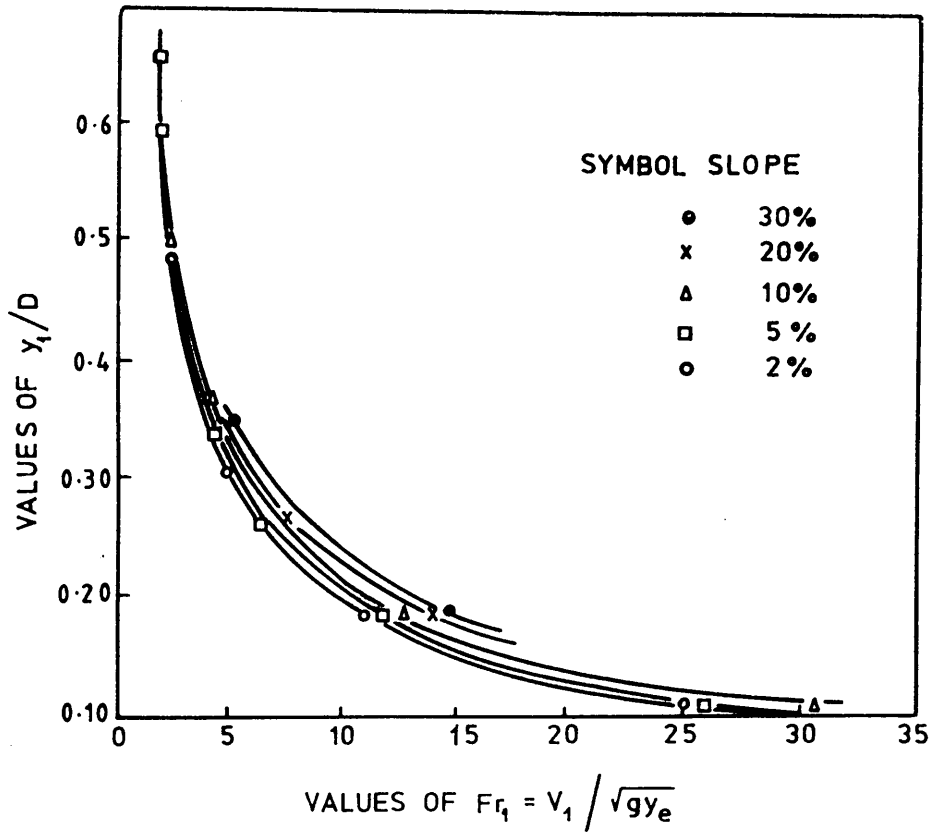

FIG. (2.39) EXPERIMENTAL VALUES OF CRITICAL FROUDE NUMBER (AFTER KALINSKE & ROBERTSON)

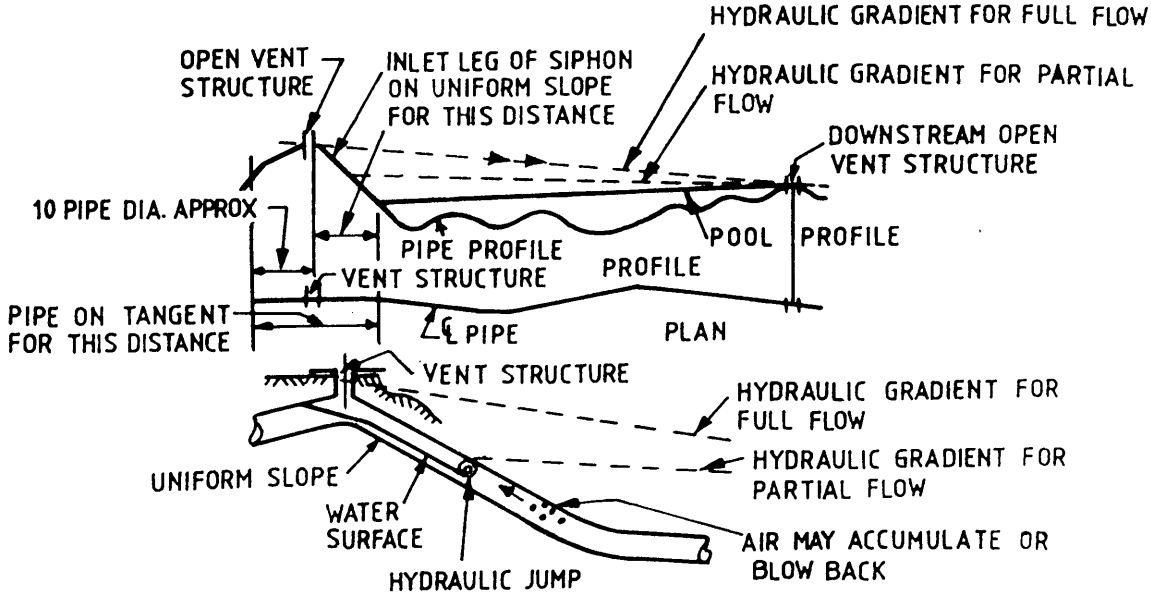

FIG. (2.40) PLAN AND PROFILE OF A TYPICAL LONG SIPHON SHOWING THE HYDRAULIC JUMP (AFTER SAILER)

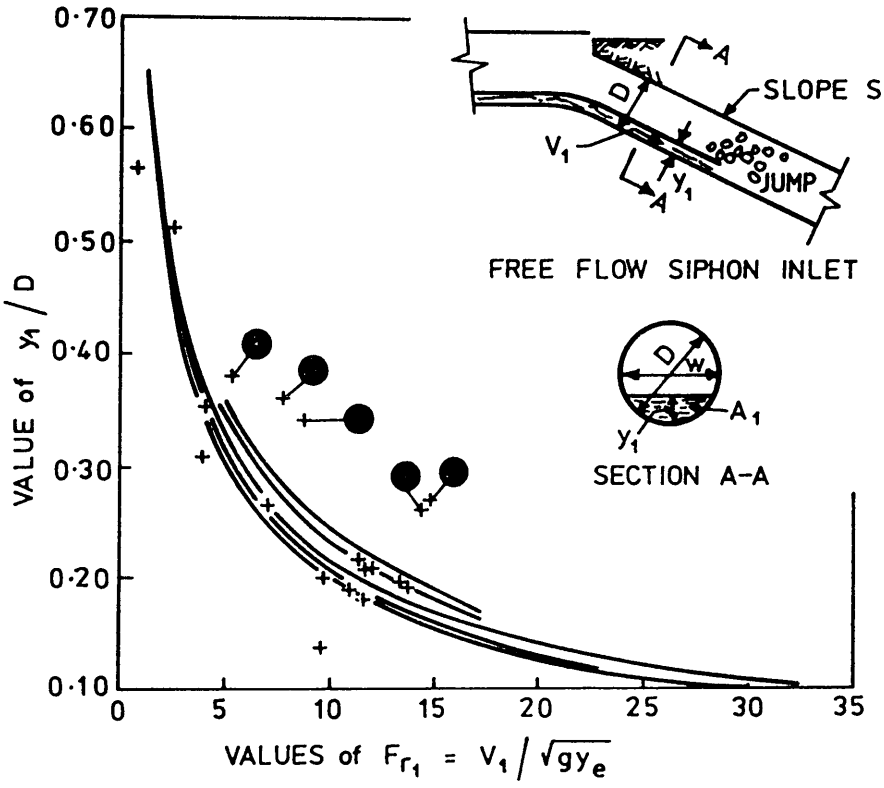

FIG. (2.41) EXPERIMENTAL CURVES OF CRITICAL FROUDE NUMBER OBTAINED BY KALINSKE& ROBERTSON TOGETHER WITH THE RESULTS OF ANALYSING 21 SIPHONS, WHERE THE DARK CIRCLES INDICATE THE SIPHONS WITH BLOWBACK CONDITION (AFTER SAILER)

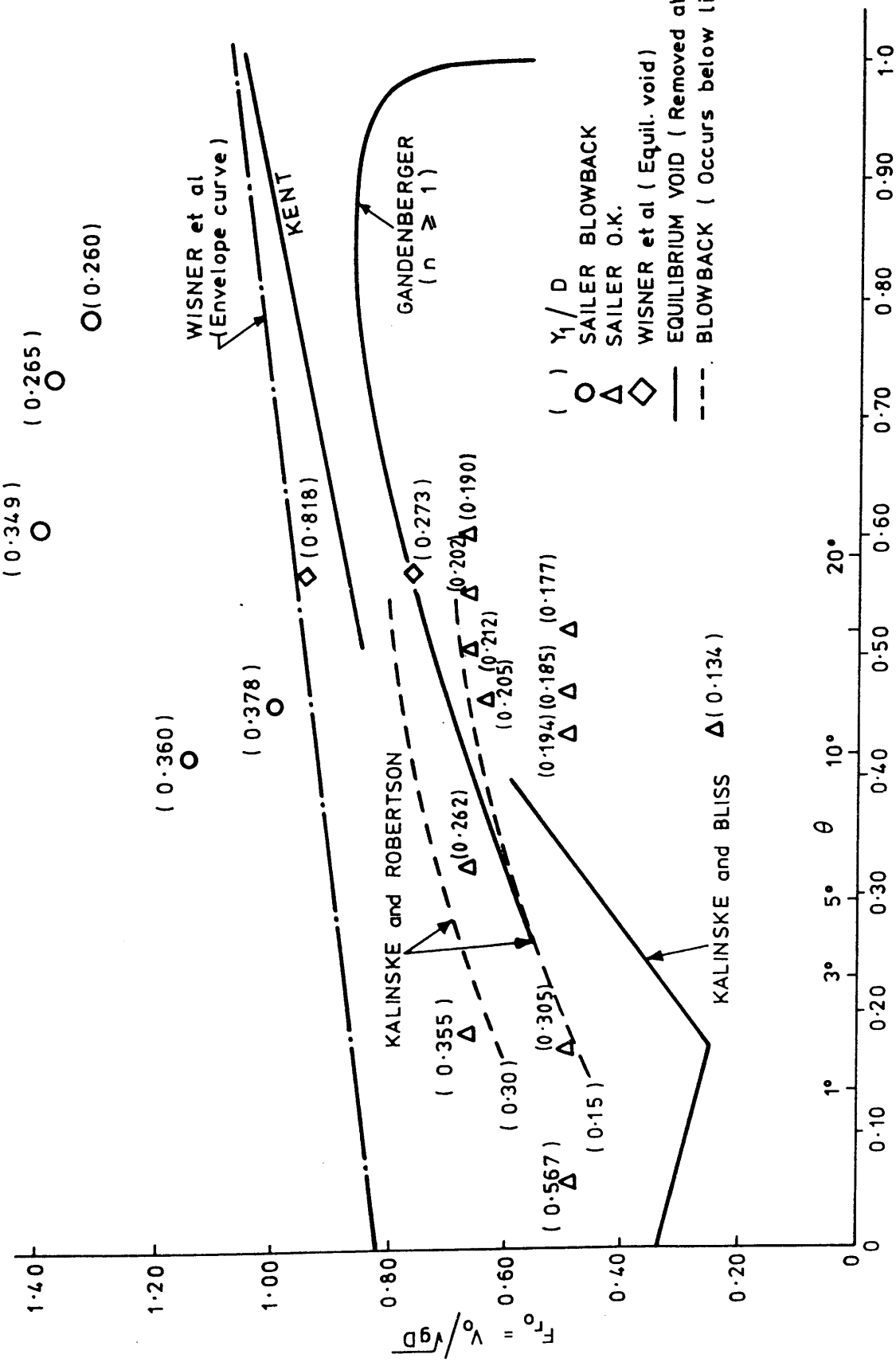

FIG. (2.42) VOID REMOVAL AND BLOWBACK IN CIRCULAR PIPES (AFTER GOLDRING)

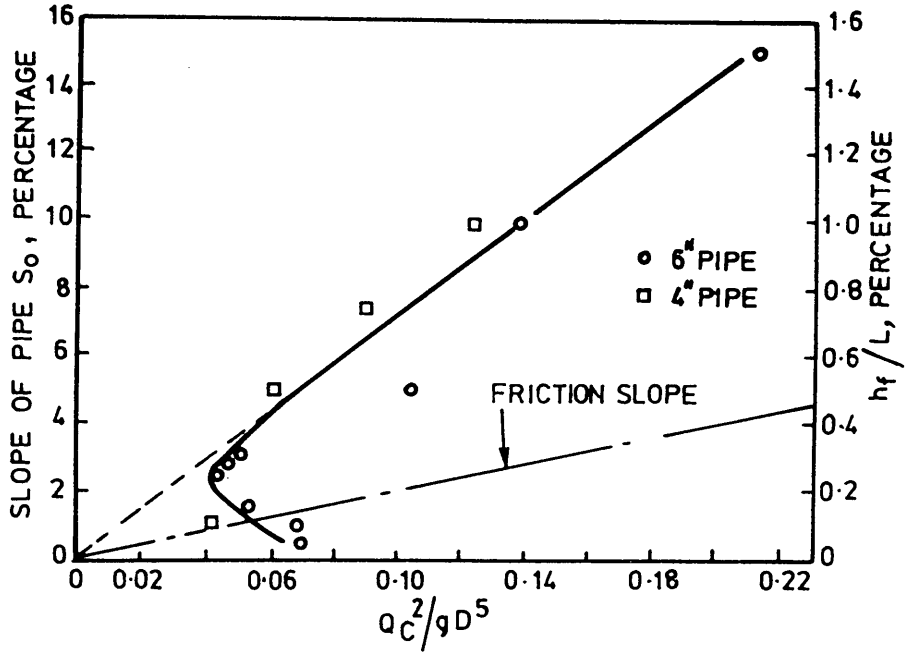

FIG. (2.43) EXPERIMENTAL DATA SHOWING RELATION BETWEEN PIPE SLOPE, PIPE DIAMETER, WATER DISCHARGE, AND HYDRAULIC GRADIENT WHEN AIR REMOVAL STARTS (AFTER KALINSKE & BLISS)

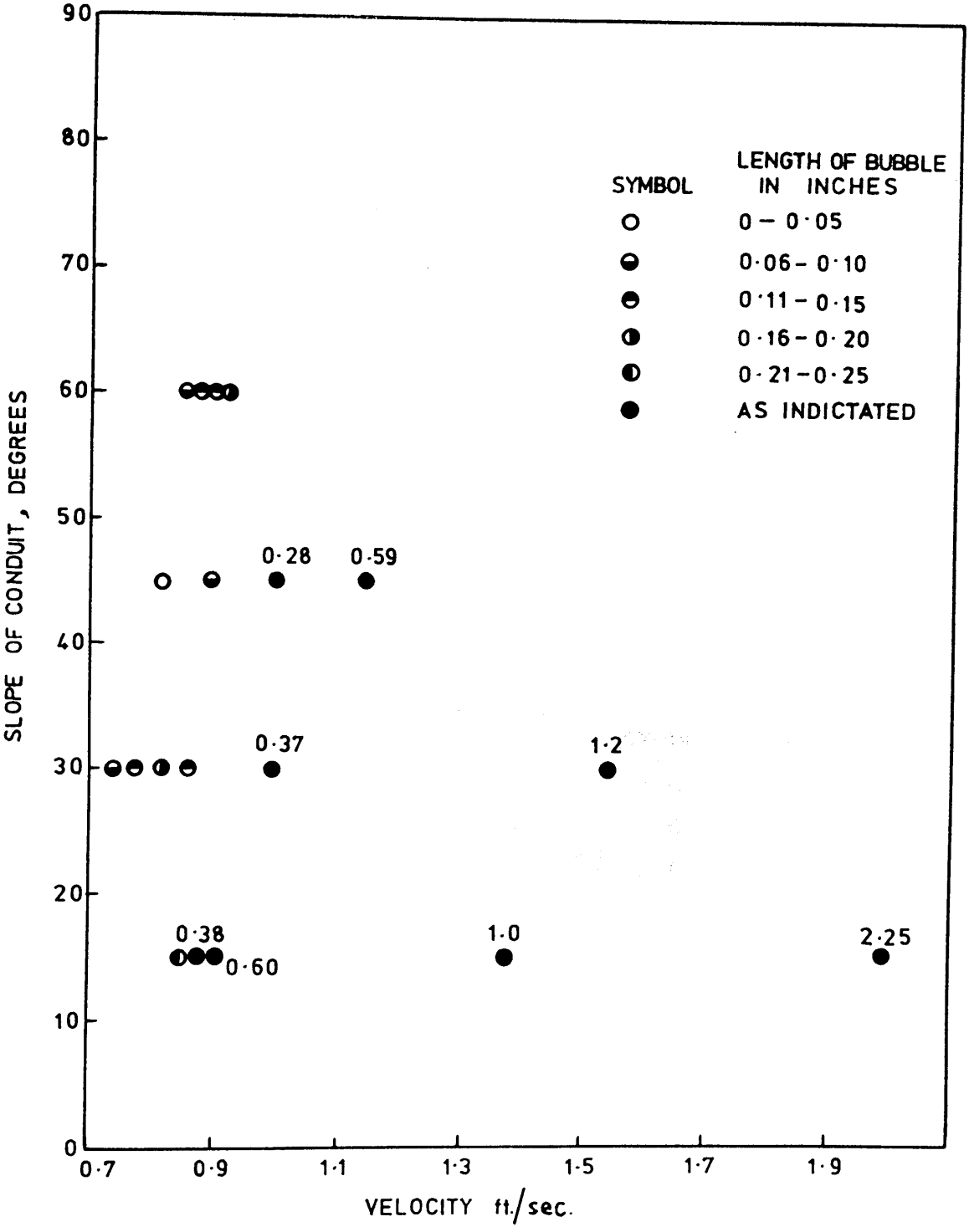

FIG. (2.44) VELOCITY IN CONDUIT REQUIRED TO KEEP BUBBLES STATIONARY IN A 4" (0.101 m) PIPE (AFTER KENT)

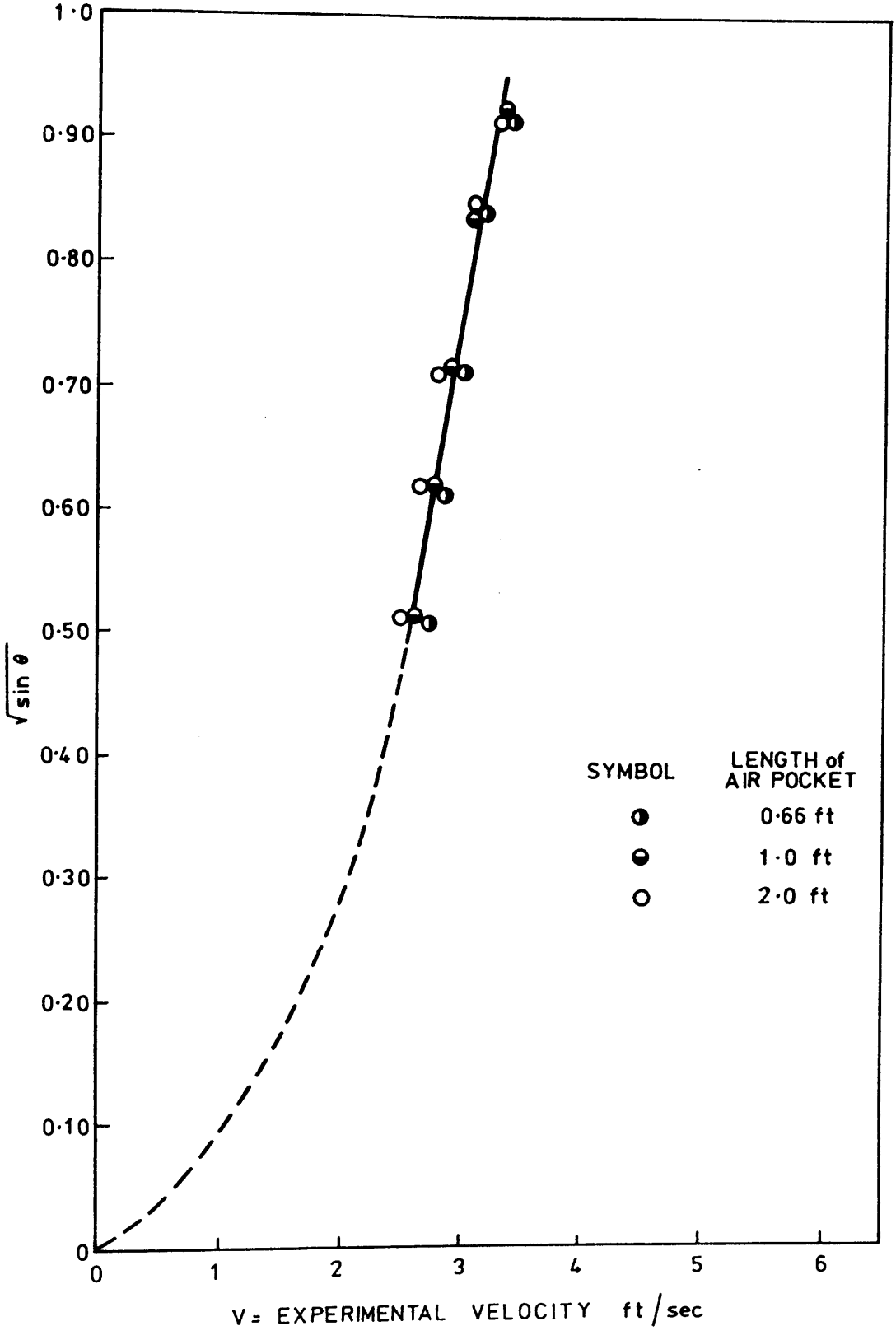

FIG. (2.45) RELATION OF MINIMUM VELOCITY AND THE DOWN-GRADE SLOPE (θ) FOR AIR POCKET TO REMAIN STATIONARY IN A 4 (0.101 m) PIPE (AFTER KENT)

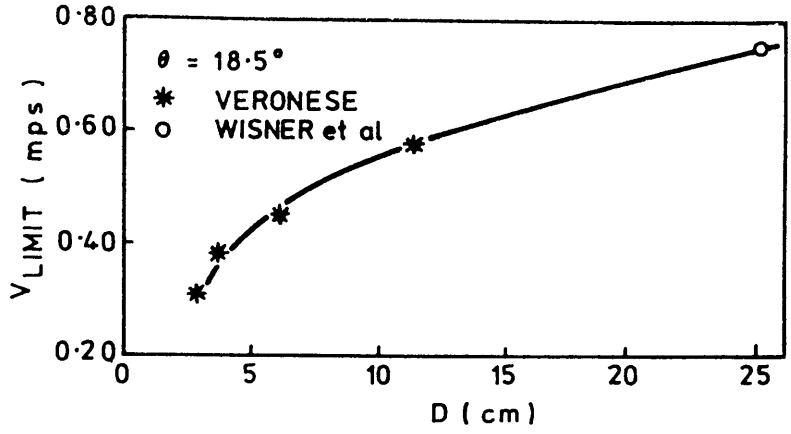

FIG. (2.46) VARIATION OF LIMIT VELOCITY WITH DIAMETER (AFTER WISNER ET AL)

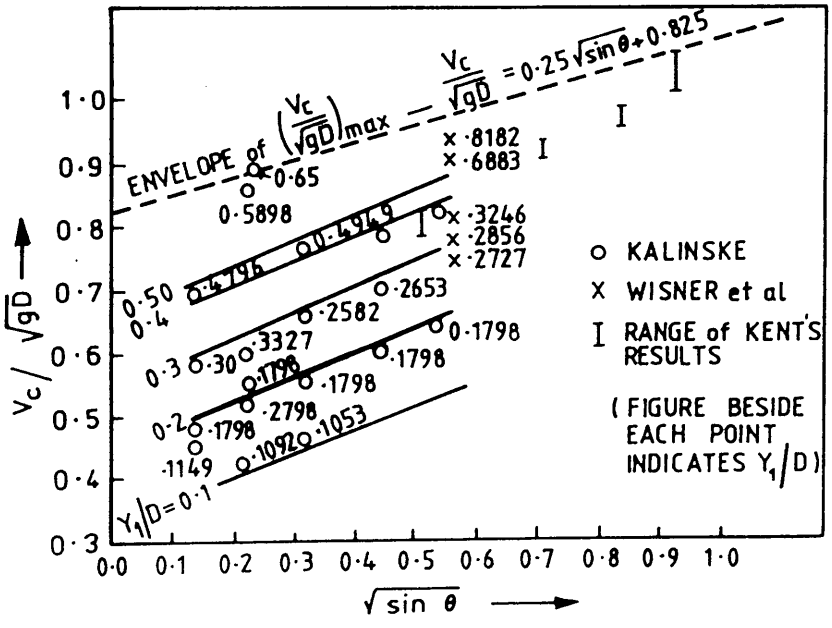

FIG. (2.47) COMPARISON OF THE AVAILABLE EXPERIMENTAL RESULTS AND PROVIDING AN ENVELOPE FOR THE MINIMUM VELOCITY TO CLEAR AIR POCKETS (AFTER WISNER ET AL)

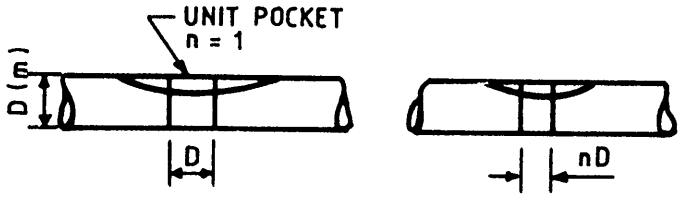

POCKET VOLUME = $n \pi D^{3/4}$

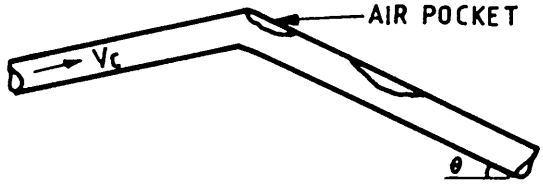

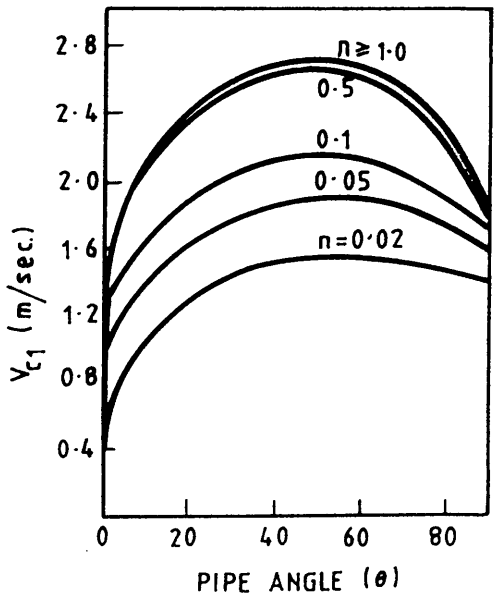

FIG. (2.48) MINIMUM VELOCITY TO MOVE AIR FROM A HIGH POINT IN 1.0 m DIAMETER PIPE (AFTER GANDENBERGER)

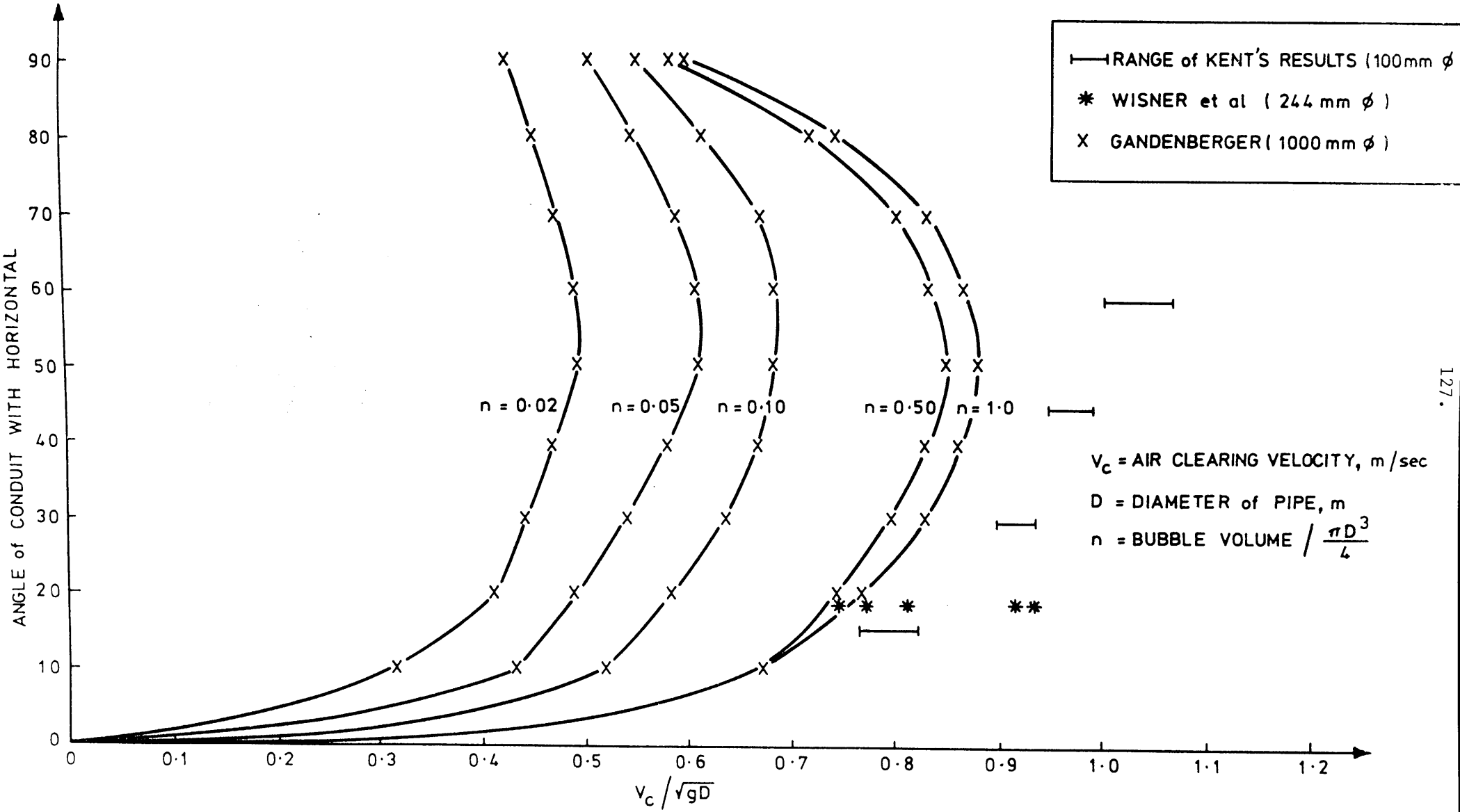

FIG. (2.49) RELATION BETWEEN THE DIMENSIONLESS PARAMETER ($V_c/\sqrt{gD}$) AND ANGLE OF CONDUIT FROM GANDENBERGER'S RESULTS, KENT'S RESULTS, AND WISNER'S RESULTS

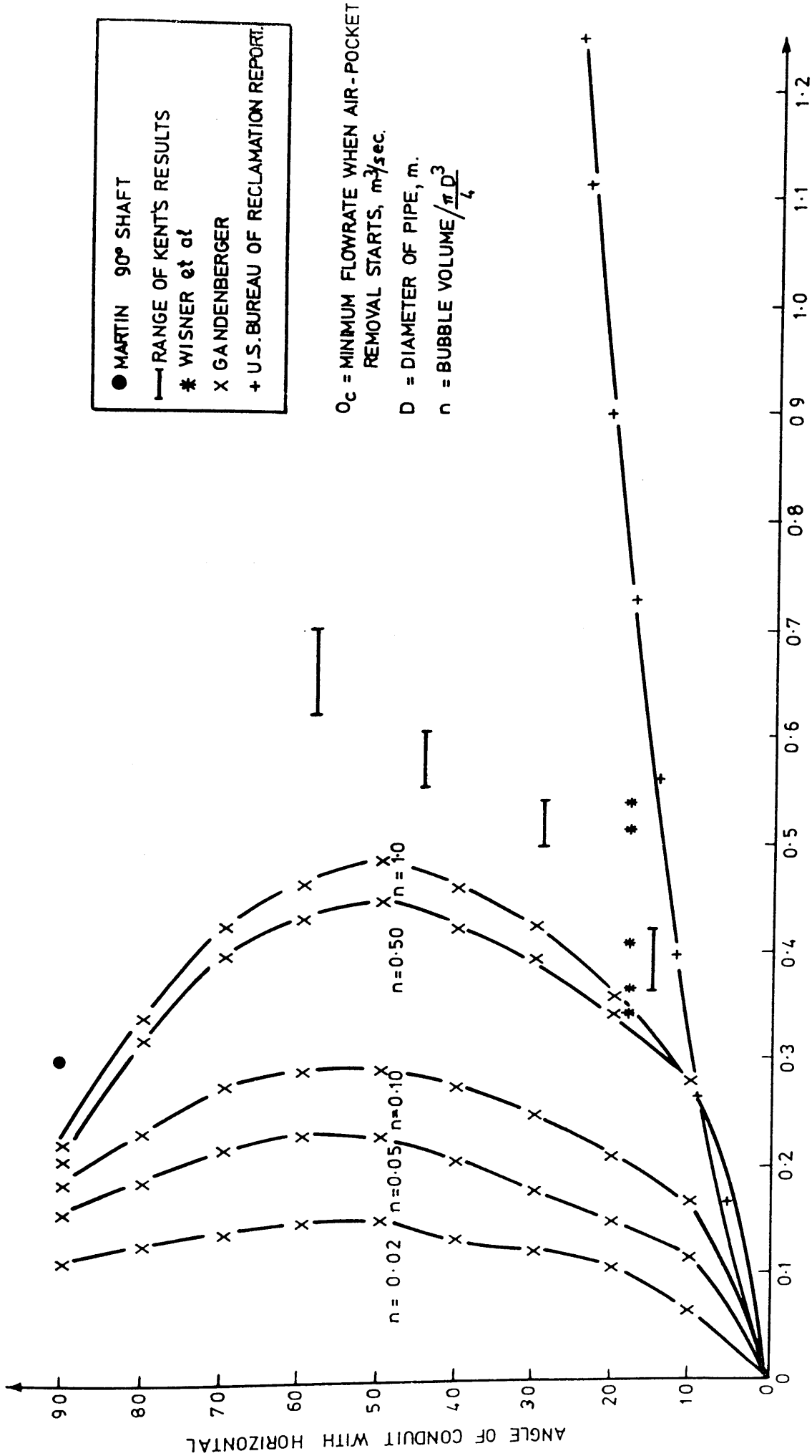

FIG. (2.50) RELATION BETWEEN MINIMUM FLOW RATE WHEN AIR POCKET REMOVAL STARTS AND ANGLE OF CONDUIT

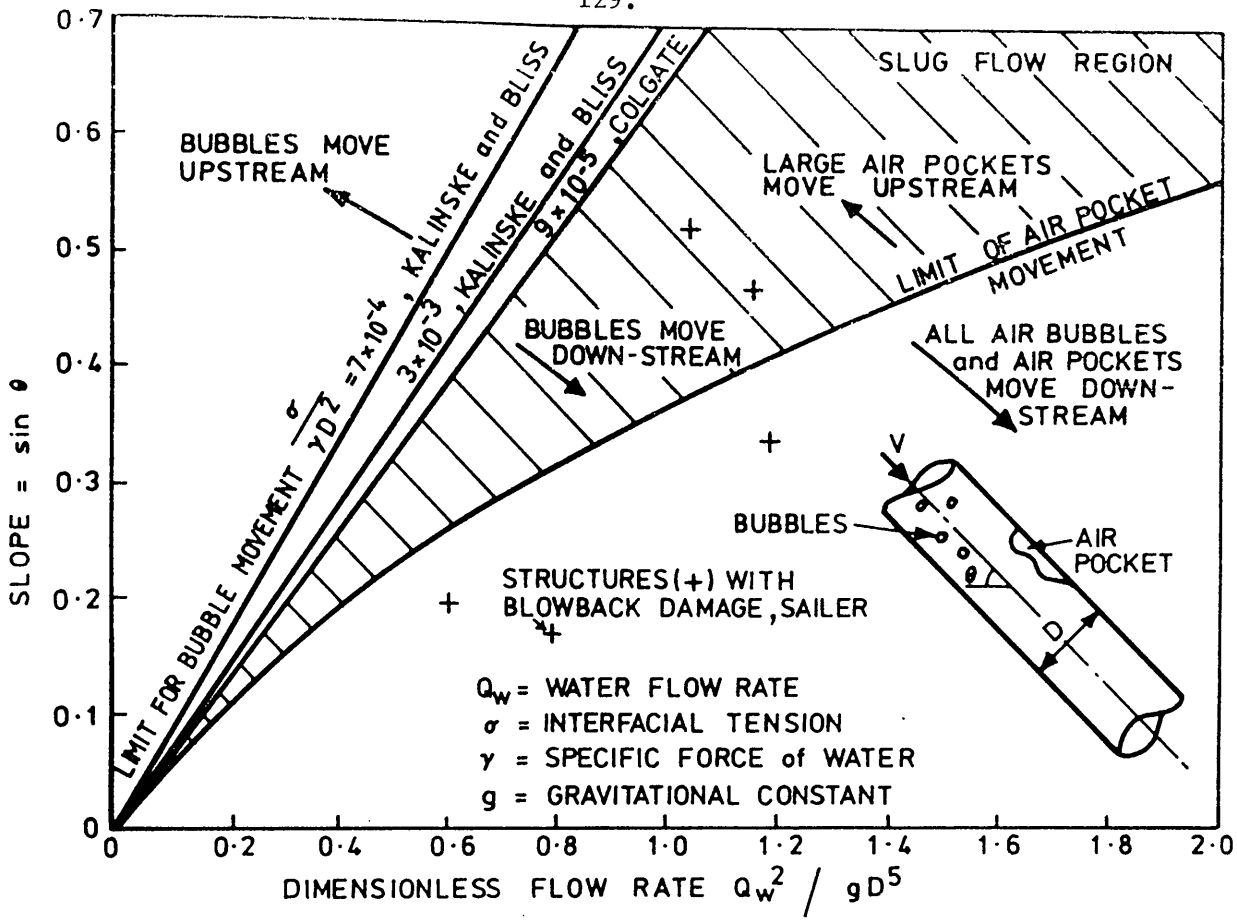

FIG. (2.51) BUBBLE MOTION IN CLOSED CONDUITS FLOWING FULL (AFTER FALVEY)

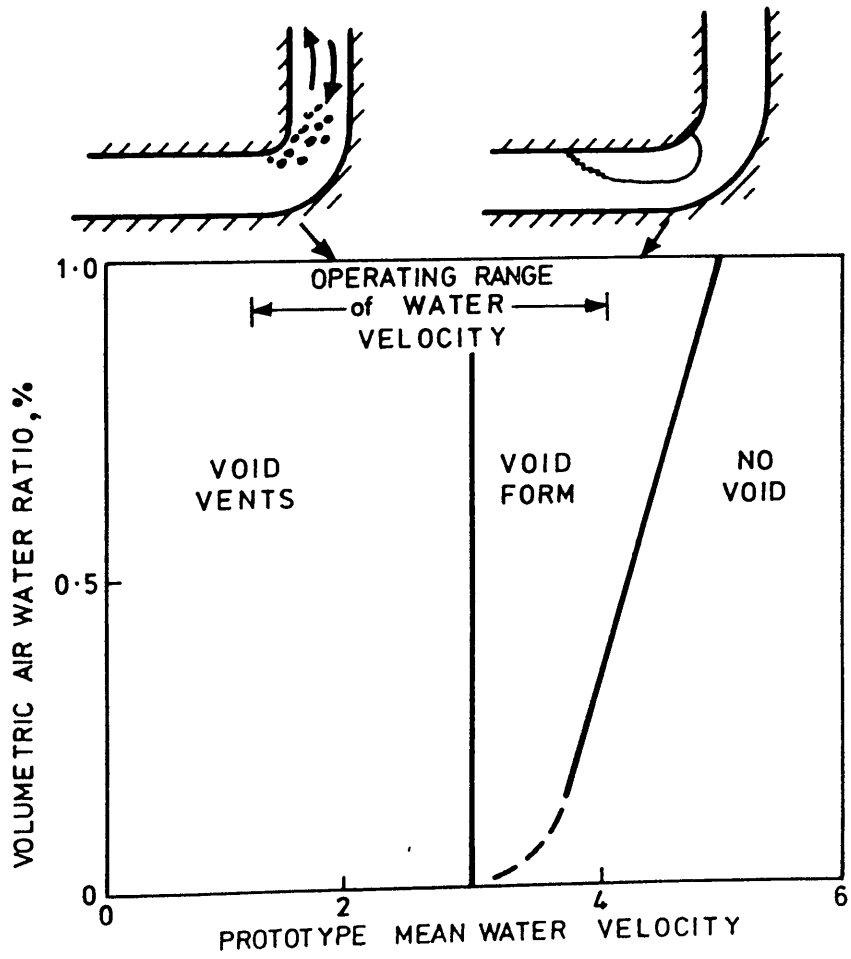

FIG. (2.52) VOID FORMATION AT CIRCULAR BEND OF R'/D = 0.75 (AFTER GOLDRING, MAWER & THOMAS)

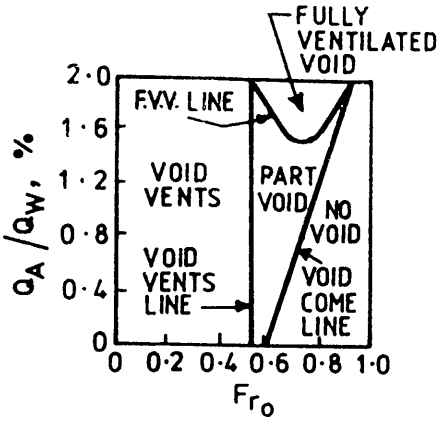

FIG. (2.53) VOID OCCURRENCE IN 5.5 in (0.14 m) DIAMETER BEND OF R'/D = 1.5 (AFTER GOLDRING)

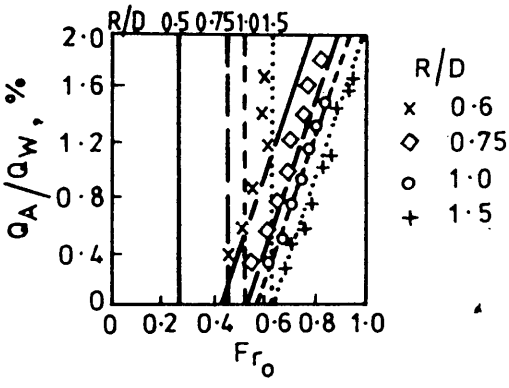

FIG. (2.54) VOID BEHAVIOUR IN BENDS OF VARIOUS R'/D AND 5.5 in (0.14 m) DIAMETER: CORRELATION AND EXPERIMENTAL RESULTS (AFTER GOLDRING)

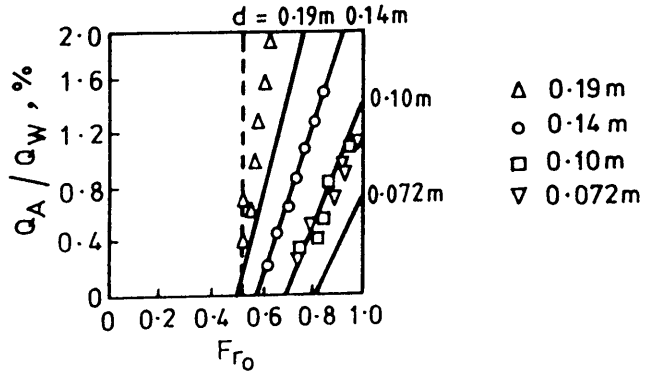

FIG. (2.55) VOID BEHAVIOUR IN BENDS OF R'/D = 1.0 AND VARIOUS PIPE DIAMETERS: CORRELATIONS AND EXPERIMENTAL RESULTS (AFTER GOLDRING)

Chapter Three

THEORETICAL MODELS FOR AIR POCKET BEHAVIOUR IN CLOSED CONDUITS

3.1 INTRODUCTION

The aim of this chapter is to develop simplified theoretical models for the complex situation of:

(a) Air pockets forming at a dropshaft/tunnel bend.

(b) Air pockets in straight pipes inclined above and below the horizontal.

In each case, models developed will be based on force-momentum principles, continuity and the energy principle.

It should be noted that no theoretical models exist at present for case (a), and for case (b), the only existing models have been developed by Benjamin[24] and Bacopoulous[14] for the simplified case of air pockets moving in stationary water, with the conduit either horizontal or inclined slightly upwards.

In a sense it is not possible to formulate a definitive theoretical model especially for case (a) because of the complex nature of the turbulent two-phase flow. The work described in this chapter involves the development of theoretical models of adequate complexity to provide a reasonable correlation with experimental data

and adequate simplicity to be of immediate use to hydraulic designers working in this area.

3.2 COMPLEXITIES INVOLVED IN DEVELOPING A THEORETICAL MODEL FOR AIR POCKETS AT THE DROPSHAFT/TUNNEL BEND

The first complexity involves the chaotic nature of the turbulent two-phase flow descending the dropshaft and approaching the bend. For most dropshafts the formation of air bubbles implies a plunging nappe in the upper part of the dropshaft impinging on the shaft-full condition generating shear layers, as shown in Fig. (3.1). Turbulence levels of the order 15-20% are developed in the shear layer and if the dropshaft is long enough the turbulence level may reduce to the order 5% as in the case of normal pipe flow. The water velocity profile approaching the bend will thus depend on the relative distance (L/D) from the point of impingement to the bend. The simplest assumption is a uniform velocity profile approaching the bend. Even the case of a fully developed pipe flow profile may require 30-50 dropshaft diameters, which is rarely available.

Superimposed on this situation in the dropshaft, is an almost chaotic distribution of entrained air bubbles. This process occurs at the point of impingement, where large quantities of air are entrained (often $\beta \sim 0.5 \rightarrow 2$). Air bubbles descending the shear layer may be detrained back to the atmosphere or alternatively be carried down the shaft, depending on the shaft-full downward velocity.

The relative proportions detrained and transported have been investigated by Ahmed, Ervine and McKeogh[4]. The proportion transported depends primarily on the ratio V_o/V_{br} , the downward shaft water velocity to the bubble rise velocity. Typical air/water ratios transported to the bend are of the order β = 0-70%.

Bubble diameters transported down the shaft are of the order 1-8 mm. Peak turbulence levels entrain bubbles of 1-2 mm and R.M.S. turbulence levels entrain bubbles of order 2-5 mm.

The best assumption would be that air bubbles approaching the bend are uniformly distributed across the shaft diameter, are of mean diameter 2-5 mm, and with air concentration $\alpha = 0 \rightarrow 40\%$ ($\beta = 0 \rightarrow 70\%$), as shown in Fig. (3.2).

A further complexity concerning air bubbles approaching the bend concerns the fact that they will be compressed due to the additional pressure descending the shaft. Assuming isothermal compression we can write $H_{abs} \times V_{air}$ = constant or the absolute pressure head times the air volume = constant. If L is the vertical depth from the impingement point then $H_{abs} \simeq (L + 10.3)$ metres head of water. Furthermore, the air bubble volume can be considered to be proportional to its diameter cubed, $V_{air} = K\, d^3_b$ and hence we obtain:

$$(K\, d^3_b)(L + 10.3) = C \qquad (3.1)$$

where C = constant. Equation (3.1) can be rearranged to obtain the resulting bubble diameter as follows:

$$d_b = \left(\frac{K_1}{L + 10.3}\right)^{1/3} \qquad (3.2)$$

where $K_1 = C/K$. Thus for large dropshaft lengths with $L >>> 10.3$ m, $d_b \propto (1/L)^{1/3}$. Assuming that $d_b = 5$ mm for $L = 0$, the value of K_1 in equation (3.2) will be $K_1 = 1.287 \times 10^{-6}$. Substituting the value of K_1 into equation (3.2) for different vertical depths L, the corresponding bubble diameters are obtained.

For $L = 10$ m , $d_b = 4$ mm

$L = 20$ m , $d_b = 3.5$ mm

$L = 50$ m , $d_b = 2.8$ mm

$L = 100$ m , $d_b = 2.25$ mm

For dropshafts of 50-100 m depth, the bubble diameter is effectively halved, the air bubble volume is an order of magnitude less and hence the air/water ratio. This phenomenon is not considered significant in the model studies described in this thesis, where the droplength is of the order 2 m.

Regarding flow at the dropshaft/tunnel bend, considering first the case of an ideal fluid. The curved flow at the bend produces an outward centrifugal pressure with gradient as follows:

$$\frac{dP}{dr} = \rho \frac{V^2}{r} \qquad (3.3)$$

where r is the radius at any point, as shown in Fig. (3.3).

Applying Bernoulli equation along a streamline, we get:

$$\frac{P}{\rho g} + \frac{V^2}{2g} = \text{Constant} \qquad (3.4)$$

Differentiating equation (3.4) the following is obtained:

$$\frac{dP}{dr} = - \rho V \frac{dv}{dr} \qquad (3.5)$$

Equating equations (3.3) and (3.5) and integrating the following is obtained:

$$Vr = \text{constant} \qquad (3.6)$$

For an ideal fluid a free vortex exists with the velocity at any point inversely proportional to the radius. Ignoring all other effects, it can be seen that if the flow at the bend is considered a free vortex, then the pressure and velocity distributions must be considered distinctly non-uniform and allowance must be made for these non-uniformities in the equations representing force-momentum and energy.

For the case of a real fluid at the bend, a deviation from the classical free vortex analysis must exist. Ignoring the effects of air bubbles and air pockets forming, the first effect is likely to be a separation occurring at the inner bend, as shown in Fig. (3.4). The separation region will produce high intensity turbulent eddies with large energy loss, and a potential recirculating region for air bubbles to accumulate.

Before reaching the bend, a developing boundary layer will ensure that water in contact with the wall will be moving slower than at the shaft centre line. This is combined with an approximate free vortex condition at the bend and outward centrifugal pressures will produce transverse currents, known as secondary currents, transferring momentum from the inner to the outer walls, as shown in Fig. (3.5). These secondary currents will ensure that a perfect free vortex does not exist due to transfer of momentum from the inside to the outside of the bend, as shown in Fig. (3.6). The velocity profile will effectively become more uniform, although in the separation region at the inside of the bend, the net velocity will be zero. It is now apparent that the sources of energy loss at a bend are fourfold:

(a) Pipe wall friction (longitudinal boundary shear)
(b) The high shearing rate at the separation layer at the inside of the bend (longitudinal)
(c) Internal fluid shear due to transverse secondary currents

(d) Additional boundary shear due to the transverse currents in contact with the pipe walls.

When air bubbles are now introduced into the complex three-dimensional situation there now exists the possibility of air pocket formation. This occurs initially in the separation region, but the pocket may extend in length and depth. The formation of the pocket will further disrupt the approximation of:

a - Free vortex velocity profile, where energy and momentum correction factors are required for the flow around the bend, as shown in Fig. (3.7a)

b - Development of secondary currents, where the assumption of a double spiral occurring, even with the introduction of an air pocket, will produce uneven free water surface, as shown in Fig. (3.7b).

c - Pressure distribution at the bend, where the real pressure gradient will be a combination of the hydrostatic and centrifugal pressures and reduced due to air bubble presence, as shown in Fig. (3.7c). The pressure reduction will depend on the air concentration.

d - The path of travel of descending air bubbles, as shown in Fig. (3.7d), where at section 1-1 it can be assumed that all air bubbles passing this section are uniformly distributed, while at section 2-2 the distribution of air bubbles is unknown. For long air pockets, all the air may be assumed to have been released to the air pocket. This is not the case for the majority of shorter pockets forming, where a proportion of the air bubbles will be in the flow and the remainder in the air pocket.

3.3 DIMENSIONAL ANALYSIS FOR AN AIR POCKET FORMING AT THE DROPSHAFT/TUNNEL BEND

The relevant parameters for dimensional analysis of air pocket formation are shown in Fig. (3.8). The depth of the air pocket forming at the bend (H) is thought to be a function of the fluid, flow and geometric parameters, as follows:

$$H = f(\underbrace{\rho a, \rho_w, \mu_a, \mu_w, \sigma, g,}_{\text{fluid parameters}} \underbrace{V_o, Q_A, d_b,}_{\text{flow parameters}} \underbrace{\theta, R', D)}_{\text{geometric parameters}} \qquad (3.7)$$

Equation (3.7) is proposed in the light of observations of past researchers in this field and also experience with the model described later on in this thesis.

For a two-phase flow of this nature it is essential to specify fluid and flow parameters for each phase. In specifying V_o the water velocity and D the pipe diameter, the water discharge is effectively specified in equation (3.7). Specifying the air flow rate Q_A alone, which is varied independently from the water discharge in this work, is not sufficient. The air bubble size descending the shaft (d_b) is also an important parameter in this analysis. From Fig. (3.8) $Q_A \propto V_a \propto D^2$, if we assume $V_a \propto V_o$ and D is already specified, then $Q_a \propto \propto$ the air concentration.

Using the method of synthesis proposed by Barr[22] we are able eventually to form ten non-dimensional groups as follows:

$$H/D = f(\rho_a/\rho_w\ ,\ \mu_a/\mu_w\ ,\ Fr_o,\ Re\ ,\ We,\ R'/D,\ \theta,\ \beta,\ d_b/D) \qquad (3.8)$$

where H/D is the ratio of air pocket depth to pipe diameter

ρ_a/ρ_w is the air/water density ratio

μ_a/μ_w is the air/water absolute viscosity ratio

Fr_o is the Froude Number approaching the bend ($V_o/\sqrt{gD}$)

Re is the Reynolds Number approaching the bend (V_oD/ν)

We is the Weber Number approaching the bend $(\rho V_o^2 D/\sigma)^{1/2}$

R'/D is the bend radius ratio

θ is the inclination of the tunnel section with horizontal

β is the ratio of air flow to water flow rates (Q_A/Q_W)
where $Q_A = \alpha V_a(\pi D^2/4)$, α is the air concentration and
V_a is the air bubble velocity
and $Q_W = (1 - \alpha)V_o (\pi D^2/4)$

Thus when the air bubble speed $\doteq$ water velocity,
$\beta = \alpha/1-\alpha$,
d_b/D is the ratio of air bubble size to pipe diameter.

It can be seen from equation (3.8) that an empirical equation for the air pocket depth at the bend would be almost intractable. There are too many relevant non-dimensional parameters. Equation (3.8) would require to be grossly simplified to obtain a meaningful empirical expression. Consider each of the parameters in turn.

- ρ_a/ρ_w. This parameter is very small and does not vary significantly in the range of experiments carried out in this work. The bulk modulus of air, K_a, is given by:

$$K_a = \Delta P/(\Delta\rho_a/\rho_a) \qquad (3.9)$$

Thus, any change in pressure in the region of the bend will produce a change in air density ($\Delta\rho_a$) as air is compressible. In these experiments the change in pressure is produced by a changing hydraulic gradient, but does not vary significantly. This is in contrast to a normal dropshaft filling arrangement going from low flows to high flows, as shown in Fig. (3.9). In this case $\Delta P = P_2 - P_1$ and $(P_2-P_1)/\rho g$ may be of the order 10-100 m depending on the dropshaft length. The air density will vary significantly

and hence the parameter ρ_a/ρ_w would need to be included in some form.

- μ_a/μ_w. This parameter varies primarily with temperature and it is not significant in this analysis.

- Fr_o. The Froude Number has a significant effect on the air pocket depth (H/D) and hence must be included.

- Re. The influence of Reynolds Number is more difficult. Zukoski[192] has shown that for air pocket flows, Reynolds Number is significant only up to a value of 400. This is in contrast to Wisner's et al work[187] which shows Reynolds Number influence for air pocket flows up to 10^5. For the case of the air pocket at the bend partially clearing by hydraulic jump formation at the toe of the pocket, Kobus[99] has shown Reynolds Number influence up to 10^5. In any case, the experiments outlined are in the range of Reynolds Numbers 3×10^4 to 3×10^5 and are still in the smooth turbulent range of pipe flows. Thus, even though a proportion of the experimental runs have Reynolds Numbers greater than 10^5, we must assume the Reynolds Number is of some significance in this work, although it may well be of second order influence.

- We. The influence of Weber Number has been shown by several experimenters[28,177,181,192] to be insignificant for air pocket flows in pipes with a diameter greater than 150 mm. Thus the Weber Number can be considered of third order significance.

- R'/D. The bend radius is highly significant in air pocket formation at the bend. The value of R'/D will determine:

  a. the centrifugal pressure gradient (dP/dr)

b. the extent of momentum transfer and secondary currents at the bend

c. the value α_o and β_o, the kinetic energy and momentum correction coefficients, for the velocity distribution at the bend

d. the position of the formation of the upstream nose of the air pocket forming at the bend, and

e. the tendency for the air pocket at the bend to blow-back, remain trapped, or be transported downstream.

- θ. The tunnel inclination downstream of the bend is also thought to be significant. Air pockets forming at the bend are likely to have a greater tendency to clear downstream if the tunnel section is inclined in the upward direction, compared with the case of a downward sloping tunnel where blow-back must be a greater risk.

- β. The ratio of air flow rate to water flow rate is also thought to be of first order significance. This is a measure of how much air descends the dropshaft to the bend and hence will have a significant bearing on the size of the air pocket formed; the density of the flowing mixture descending the dropshaft; the ability of an air pocket at the bend to clear itself downstream (too much air may cause the air pocket to extend in size rather than clear); the real water velocity at the bend (for a particular value of water flow rate Q_w).

- d_b/D. This parameter may also be significant in the sense that prototype air bubble sizes are not scaled down in a

Froude model. In fact the reverse occurs in dropshafts. Air bubble sizes are governed by the capilary length $(\sigma/\rho g)^{1/2}$ = 2.7 mm for air/water mixtures, the turbulence intensity at the point of air bubble generation and the pressures on the air bubbles approaching the bend. The prototype with larger pressures and greater turbulence intensity will produce much smaller air bubbles than the model and hence scaling is in the opposite direction. Furthermore, the bubble rise velocity is proportional to its size and hence the velocity vectors for air bubbles approaching the air pocket are as shown in Fig. (3.10) for model/prototype. It can be noted from Fig. (3.10) that $(V_{br})_{model} > (V_{br})_{prototype}$, thus air bubbles in the prototype will have a greater chance of escaping the air pocket at the bend.

Rewriting equation (3.8) including only first and second order significant parameters, we obtain:

$$H/D = f(\overbrace{Fr_o,\ R'/D\ ,\ \theta\ ,\ \beta}^{\text{1st order terms}}\ ,\ \overbrace{\rho_a/\rho_w\ ,\ Re\ ,\ d_b/D}^{\text{2nd order terms}}) \qquad (3.10)$$

For a grossly simplified analysis of air pocket depth at the dropshaft/tunnel bend, and for a given geometrical configuration R'/D and θ, we obtain:

$$H/D \simeq f(Fr_o\ ,\ \beta) \qquad (3.11)$$

In the analysis of experimental data in this thesis, equation (3.11) would be most important for each geometry tested (R'/D and θ), although an attempt will also be made to ascertain the significance of Re and d_b/D. The latter two terms in equation (3.10) are scale effect terms. These can only be properly investigated by testing at different model scales, or comparing with prototype data.

Some attempts have been made, Townson[165], to alter the air bubble diameter d_b with the use of surfactants. This has been largely unsuccessful because, whilst smaller bubble sizes have been produced by altering surface tension and viscosity, the turbulent flow structure is altered and significant air "hold-up" occurs in the tunnel section. That is, the tunnel water velocities are not sufficient to clear the large quantities of "foam" produced and overly large air pocket depths result.

3.4 SIMPLIFIED REGIMES OF FLOW AT THE DROPSHAFT/TUNNEL BEND

The regimes of flow for air pocket formation at the dropshaft/tunnel bend are outlined in detail in Chapter Five of this thesis. It can be seen in Chapter (5) that air pockets of varying depths and lengths form at the bend. The air pockets may blow-back up the shaft, vent-back up the shaft in the form of small bubbles, remain stable, form a hydraulic jump at the downstream end of the pocket, or clear downstream from the bend completely. There are many identifiable regimes of flow, some of which may be stable and others unstable, but because of their great complexity are proposed below in a quasi-steady form.

Four main regimes of flow are chosen for development in theoretical models. These areas have been chosen after extensive visual observation, allowing the air bubbles, in effect, to act as a tracer.

- Model Type 1, shown in Fig. (3.11), which has the following characteristics:

  (1) Subcritical flow under the air pocket

  (2) Lower upstream Froude Numbers

(3) Tendency to vent-back or blow-back up the dropshaft

(4) Nose of pocket may be considered a stagnation point

- Model Type 2, shown in Fig. (3.12), which has the following characteristics:

(1) Drowned hydraulic jump

(2) Nose of pocket is a point of separation

(3) Prelude to stable hydraulic jump forming

(4) Subcritical flows under the air pocket

- Model Type 3, shown in Fig. (3.13), which has the following chracteristics:

(1) Stable hydraulic jump formed ($Fr_1 > 1$)

(2) Nose of pocket is a point of separation

(3) Prelude to air pocket clearing completely

(4) Large H/D and upstream Froude Number values

- Model Type 4, shown in Fig. (3.14), which has the following characteristics:

(1) Pocket is continuously cleared from the bend

(2) Higher Froude Numbers (preceded by hydraulic jump)

3.5 CORRECTION FACTORS FOR THE FLOW AT THE BEND

In developing theoretical models for the flow regimes at the dropshaft/tunnel bend, energy equation and force-momentum balance will be used. This requires the introduction of correction factors to the kinetic energy head ($V^2/2g$) and the momentum flux (ρQV) to account for the non-uniformity spacing of the streamlines. These factors are denoted by α_o and β_o in this thesis to differentiate them from air/water ratio (β) and air concentration (α) used in this work. In addition to the above correction factors, there are two other correction factors which must be applied to account for the curvature of the streamlines at the bend which produces non-linear distribution of pressure. These two factors are applied to the hydrostatic pressure head (y or D) and the pressure force $\rho g A_p D/2$ and denoted by ($\acute{\alpha}$) and ($\acute{\beta}$) respectively. Each of the four correction factors will be considered separately in the derivation of their theoretical values according to the conditions existing at the bend.

3.5.1 Correction Factors for Kinetic Energy Head α_o and Momentum Flux β_o

The equations used for deriving α_o and β_o are as follows[34]:

$$\alpha_o = \int \frac{V^3 dA}{\bar{V}^3 A} \tag{3.12}$$

and

$$\beta_o = \int \frac{V^2 dA}{\bar{V}^2 A} \tag{3.13}$$

where V is the velocity at any point, $\bar{V}$ is the mean water velocity and A is the area of the pipe. Considering the case of a bend in a circular pipe, shown in Fig. (3.15), where air bubbles and air pocket formation, turbulence, momentum transfer and secondary currents are all ignored. In this case the flow around the bend approximates to a

free vortex. That is, the pressure gradient across the bend is due to centrifugal forces $dP/dr = \rho v^2/r$ and the free vortex equation is given by:

$$Vr = C \triangleq \bar{V}R' \tag{3.14}$$

Assuming the mean velocity occurs at the centre line of the pipe (not correct), then the velocity at any other point can be given by:

$$V \simeq \bar{V}R'/r \tag{3.15}$$

the above value of V now can be substituted into equations (3.12) and (3.13) to find α_o and β_o respectively.

(a) The correction factor α_o

Substituting equation (3.15) into equation (3.12) and the area of the pipe $A = \pi D^2/4$ and rearranging, the following is obtained:

$$\alpha_o = \frac{4}{\pi} \frac{R'^3}{D^2} \int (\frac{1}{r})^3 \, dA \tag{3.16}$$

Referring to Fig. (3.16), the value of dA and r can be found as:

$$dA = D \, Sin\theta \, dr \tag{3.17}$$

where $$dr = (D/2) \, Sin\theta \, d\theta \tag{3.18}$$

and

$$r = R' - (D/2)Cos\theta \tag{3.19}$$

Substituting equations (3.17), (3.18) and (3.19) into equation (3.16) and rearranging:

$$\alpha_o = \frac{2}{\pi} \int_o^{\pi} \frac{\mathrm{Sin}^2\theta \, d\theta}{(1 - \frac{D}{2R'}\mathrm{Cos}\theta)^3} \qquad (3.20)$$

let $K = \frac{D}{2R'}$, $Z = \tan(\frac{\theta}{2})$; hence $\mathrm{Cos}\theta = \frac{1-Z^2}{1+Z^2}$, $\mathrm{Sin}\theta = \frac{2Z}{1+Z^2}$ and $d\theta = \frac{2dZ}{1+Z^2}$. Substitute the above values into equation (3.20) with the appropriate integration limits we obtain:

$$\alpha_o = \frac{16}{\pi} \int_o^{\infty} \frac{Z^2}{[(1+Z^2)-K(1-Z^2)]^3} \, dZ \qquad (3.21)$$

assuming that: $a = \sqrt{\frac{1-K}{1+K}}$, $b = (1+K)^{-3}$ and let $Z = a\tan\phi$ then $dZ = a\mathrm{Sec}^2\phi \, d\phi$ and substituting into (3.21):

$$\alpha_o = \frac{16b}{\pi a^3} \int_o^{\pi/2} \frac{\tan^2\phi}{\mathrm{Sec}^4\phi} \, d\phi \qquad (3.22)$$

Integrating (3.22) yields:

$$\alpha_o = \frac{16b}{\pi a^3} (0.196) \qquad (3.23)$$

Substituting for the values of a and b, the value of α_o will be as follows for each bend radius used in this work:

$$\alpha_o = \infty \quad \text{for } R'/D = 0.50 \quad \text{(mitre bend)} \tag{3.24}$$

$$\alpha_o = 1.5368 \quad \text{for } R'/D = 1.0 \tag{3.25}$$

$$\alpha_o = 1.1907 \quad \text{for } R'/D = 1.5 \tag{3.26}$$

(b) The correction factor β_o

Substituting equation (3.15) into equation (3.13), the value of $A = \pi D^2/4$ and the values of dA, dr and r given in equations (3.17), (3.18) and (3.19) respectively, the following is obtained:

$$\beta_o = \frac{2}{\pi} \int_o^{\pi} \frac{\sin^2\theta \, d\theta}{(1 - \frac{D}{2R'} \cos\theta)^2} \tag{3.27}$$

Following the same procedure used in integrating α_o the following is obtained:

$$\beta_o = \frac{16}{\pi} \frac{b'}{a} \int_o^{\pi/2} \frac{\tan^2\phi \; d(\tan\phi)}{(1+\tan^2\phi)^2(1+a\tan^2\phi)} \tag{3.28}$$

Integrating equation (3.28) by parts, the following is obtained:

$$\beta_o = \frac{16}{\pi} \frac{b'}{a} \times (0.78539B + 1.57079D + 1.57079\frac{F}{a}) \tag{3.29}$$

where B, D and F are constants obtained from the integration by parts and depend on bend radius. Their values are given in Table (3.1) below.

TABLE (3.1) Constants from the integration of equation (3.29)

Constants \ R'/D	0.5	1.0	1.5
B	-1.0	-1.4998	-2.0017
D	1.0	2.2496	4.006
F	0	-0.7497	-2.0049

Substituting for $a = \sqrt{(1-K)/(1+K)}$, $b' = (1+K)^{-2}$, $K = D/2R'$, and the values for B, D and F given in Table (3.1), for each bend radius the following is obtained for β_o in this work:

$$\beta_o = \infty \quad \text{for } R'/D = 0.5 \tag{3.30}$$

$$\beta_o = 1.2389 \quad \text{for } R'/D = 1.0 \tag{3.31}$$

$$\beta_o = 1.0868 \quad \text{for } R'/D = 1.5 \tag{3.32}$$

The complete integration of β_o is given in Appendix A.

3.5.2 Correction Factors for Hydrostatic Pressure Head α' and pressure force β'

It has been mentioned earlier in section (3.5) that correction factors are required for the hydrostatic pressure head and pressure force to account for the curvature of the stream lines at

the bend. The effect of curvature is to produce appreciable acceleration components or centrifugal forces normal to the direction of flow[34]. This means that the pressure distribution over the section will deviate from the hydrostatic and non-linear distribution of pressure will occur, as in Fig. (3.7c). In concave flow the centrifugal forces are acting downward to reinforce the gravity action, which means that the actual pressure is greater than the hydrostatic pressure. If the deviation from the hydrostatic pressure in a curvilinear flow is denoted by C, then the actual pressure will be the hydrostatic head +C.

The approximate centrifugal pressure may be computed by Newton's law of acceleration, as:

$$\text{Centrifugal pressure} = \frac{\text{mass}}{\text{unit area}} \times \text{centrifugal acceleration}$$

$$= \frac{\rho g y'}{g} \times \frac{V^2}{r} \qquad (3.33)$$

hence the pressure head correction C is given as:

$$C = \frac{y'}{g} \frac{V^2}{r} \qquad (3.34)$$

where y' is the vertical distance from top of pipe to any point, as shown in Fig. (3.15) and Fig. (3.16). Hence the actual pressure head can be represented by $\alpha' y$, where α' is a correction coefficient known as pressure coefficient and y is the depth of flow. The actual pressure force can be represented by $\beta' P$, where β' is a correction coefficient known as pressure distribution coefficient and P is the pressure force[34]. The following equations are used to derive the values of α' and β' respectively:

$$\alpha' = 1 + \frac{1}{Qy} \int_{o}^{A} CVdA \qquad (3.35)$$

and

$$\beta' = 1 + \frac{1}{A\bar{Z}} \int_{o}^{A} CdA \qquad (3.36)$$

where Q is the total water flow rate, y is the depth of flow = D, V is the velocity at any point, A is the area of flow, $\bar{Z}$ is the depth of the centroid of water area = D/2, and C is the pressure head correction given in equation (3.34). Each coefficient will be considered separately to derive a theoretical value for this work.

(a) The pressure coefficient α'

Substituting equations (3.15), (3.17) and (3.34) into equation (3.35) and rearranging, the following is obtained:

$$\alpha' = 1 + \frac{\bar{V}^3 R'^3 D}{2Qg} \int_{o}^{\pi} \frac{y'}{r^4} \sin^2\theta \, d\theta \qquad (3.37)$$

Now from Fig. (3.16) y' is as follows:

$$y' = (D/2)(1-\cos\theta) \qquad (3.38)$$

Substituting equations (3.19) and (3.38) into equation (3.37) and rearranging:

$$\alpha' = 1 + \frac{\bar{V}^3 D^2}{4QgR'} \int_{o}^{\pi} \frac{(1 - \cos\theta)}{(1 - \frac{D}{2R'} \cos\theta)^4} \sin^2\theta \, d\theta \qquad (3.39)$$

Following the same steps used in integrating equation (3.12), the following equation is obtained:

$$\alpha' = 1 + \frac{4\bar{V}^3D^2}{QgR'} \frac{b}{a^3} \int_0^{\pi/2} \text{Sin}^4\phi \ \text{Cos}^2\phi \ d\phi \qquad (3.40)$$

where $a = \sqrt{\frac{1-K}{1+K}}$, $b = (1+K)^{-4}$, and $K = \frac{D}{2R'}$

Integrating equation (3.40) gives:

$$\alpha' = 1 + \frac{4\bar{V}^3D^2}{QgR'} \times \frac{b}{a^3} \times [0.098] \qquad (3.41)$$

substituting for $Q = \bar{V} \frac{\pi D^2}{4}$

$$\alpha' = 1 + \frac{16}{\pi} \times \frac{\bar{V}^2}{gR'} \times \frac{b}{a^3} \times 0.098 \qquad (3.42)$$

Substituting for each bend radius the equivalent value of R', b, and a, the following values are obtained for α':

$$\alpha' = \infty \qquad \text{for } R'/D = 0.5 \qquad (3.43)$$

$$\alpha' = 1 + 0.5122\ Fr_o^2 \qquad \text{for } R'/D = 1.0 \qquad (3.44)$$

$$\alpha' = 1 + 0.2977\ Fr_o^2 \qquad \text{for } R'/D = 1.5 \qquad (3.45)$$

where $Fr_o = V_o/\sqrt{gD}$

(b) <u>The Pressure Distribution Coefficient β'</u>

Following the same steps used in the substitutions in

equation (3.35), equation (3.36) was reduced to the following form:

$$\beta' = 1 + \frac{2\bar{V}^2}{\pi g R'} \int_o^{\pi} \frac{(1 - \text{Cos}\theta)}{(1 - \frac{D}{2R'}\text{Cos}\theta)^3} \text{Sin}^2\theta \, d\theta \qquad (3.46)$$

Integrating equation (3.46) following the steps used for integrating equation (3.35) yields:

$$\beta' = 1 + \frac{32}{\pi} \frac{\bar{V}^2}{gR'} \times \frac{b}{a} \times \int_o^{\pi/2} \frac{\tan^4\phi \, d(\tan\phi)}{(1 + \tan^2\phi)^3(1 + a^2\tan^2\phi)} \qquad (3.47)$$

Integrating this equation by parts, as for equation (3.28), the following is obtained:

$$\beta' = 1 + \frac{32}{\pi g} \frac{\bar{V}^2}{R'} \times \frac{b}{a} \times [1.5708B + 0.7854D + 0.589F + 1.5708 \frac{H}{a}] \qquad (3.48)$$

where B, D, F and H are constants from the integration by parts and depend on bend radius. Their values are given in Table (3.2) below:

TABLE (3.2) Constants from the integration of equation (3.48)

R'/D / Constants	0.5	1.0	1.50
B	1.0	0.8438	0.800
D	∞	-0.9377	-0.5993
F	∞	0.375	0.1996
H	0	-0.2812	-0.4003

Substituting for $a = \sqrt{(1-K)/(1+K)}$, $b = (1+K)^{-3}$, $K = D/2R'$ and the values for B, D, F and H in Table (3.2) for each bend radius the following is obtained for β' in this work:

$$\beta' = \infty \qquad \text{for } R'/D = 0.5 \qquad (3.49)$$

$$\beta' = 1 + 0.2341\ Fr_o^2 \qquad \text{for } R'/D = 1.0 \qquad (3.50)$$

$$\beta' = 1 + 0.0059\ Fr_o^2 \qquad \text{for } R'/D = 1.50 \qquad (3.51)$$

3.6 THEORETICAL MODELS FOR THE AIR POCKET BEHAVIOUR AT THE DROPSHAFT/TUNNEL BEND

It has been outlined in section (3.4) that four main regimes of flow based on visual observations have been chosen for development of the theoretical models. These models will be developed by using either the energy equation or force momentum balance, or both. To simplify the development, the theory will concentrate mainly on dropshaft/tunnel junctions with a horizontal tunnel outlet, although in some models it will be extended to inclined conduits, especially when using force momentum balance for an air pocket with a hydraulic jump. The effect of air bubbles at different sections will be introduced and the theoretical results will be plotted on graphs to be compared with experimental data in Chapter Seven.

3.6.1 Model Type 1

This model is for the case of air pockets with a tendency to vent back up the vertical shaft where the flow is sub-critical under the air pocket. The nose of the pocket may be considered as a stagnation point where the water velocity at point O, shown in Fig. (3.17), will be zero. At point O the angle between the tangent at the point of contact and the horizontal is denoted by ϕ, where ϕ can

vary between 0° and 90° in theory.

Applying Bernoulli's Equation along the upper streamline between point 0 and 1, we obtain:

$$\frac{P_{air}}{\rho g} + \frac{(0)^2}{2g} + H + h = \frac{P_{air}}{\rho g} + \frac{V_1^2}{2g} + 0 \qquad (3.52)$$

Applying continuity equation between a section upstream the nose of pocket and a section through point 1, we obtain:

$$Q_w = V_1 A_1 = V_o A_p \qquad (3.53)$$

where V_1 and A_1 are the water velocity and water area at the section passing point 1. At this stage, section 1 is assumed to have no air bubbles in the flow. Substituting equation (3.53) into equation (3.52) for the value of V_1, re-arranging and dividing by the pipe diameter, the following is obtained:

$$\frac{H}{D} = 0.5\ Fr_o^2 \left(\frac{Ap}{A_1}\right)^2 - \frac{h}{D} \qquad (3.54)$$

From Fig. (3.17) it can be seen that:

$$h = (R' - D/2)(1 - \cos\Phi) \qquad (3.55)$$

Substituting equation (3.55) into equation (3.54) the following is obtained:

$$\frac{H}{D} = 0.5\ Fr_o^2 \left(\frac{Ap}{A_1}\right)^2 - \left(\frac{R'}{D} - \frac{1}{2}\right)(1 - \cos\Phi) \qquad (3.56)$$

The final term in equation (3.56) can be as small as zero when either R'/D = 1/2 (sharp bend) or Φ = 0°, and can be as high as unity when Φ = 90° and R'/D = 1.5 which is the largest value tested in this work. Equation (3.56) is plotted in Fig. (3.18) for R'/D = 0.5, 1.0 and 1.50

for two different values of ϕ of 20° and 40°. It can be noted from Fig. (3.18) that for a given air pocket depth (H/D), an increasing R'/D and ϕ will require larger Froude Numbers ($V_o/\sqrt{gD}$), to keep the air pocket stable. In other words, tendency to blow back is likely to increase with increasing R'/D and ϕ.

If we now consider the case of a uniform distribution of air bubbles at section 1, (under the air pocket) the real interstitial water velocity at section 1 becomes $V_1/(1-\alpha)$ or $V_1(1+\beta)$. Hence equation (3.56) can be written to incorporate various air concentrations in the form:

$$\frac{H}{D} = 0.5\ Fr_o^2 \left(\frac{A_p}{A_1}\right)^2 (1+\beta)^2 - \left(\frac{R'}{D} - \frac{1}{2}\right)(1 - \cos\phi) \qquad (3.57)$$

Equation (3.57) is plotted in Fig. (3.19) for the particular case of R'/D = 0.5 and for different values of air/water ratio (β) ranging from 0 to 0.3. It can be noted from Fig. (3.19) that increasing β will reduce the air pocket tendency to blow back for a given value of air pocket depth, H/D. Lower Froude Numbers are required to keep the pocket stable. An alternative viewpoint is that for a given Froude Number of flow, the air pocket depth H/D, will be greater as β is increased.

3.6.2 Model Type 2

This model is applicable to the case of air pockets with sub-critical flow under the air pocket, and often occurs as a prelude to the stable hydraulic jump formation. This model can be considered as a drowned hydraulic jump where the nose of the air pockets is a separation point. In order to obtain a solution for this case, the energy equation, continuity and force momentum balance will be applied at three sections along the air pocket. This is necessary because there are too many unknowns involved which require more equations in order to solve. The sections used in this analysis are

shown in Fig. (3.20) where section (1) passes through the nose region, section (2) at the maximum depth of air pocket, and section (3) at the end of the air pocket. It can be noted from Fig. (3.20) that at section (2) the solid line represents the measured air pocket depth at that section, while the dashed line represents the actual path of the top stream line for the flowing water at that section. The energy equation will be applied between sections (1) and (2) along this stream line, while force momentum balance will be applied between sections (2) and (3). Using the energy equation between sections (1) and (2) rather than the force momentum balance is because the latter is a vector quantity which requires all the forces to be in the same direction, where this will encounter more unknowns rather than simplifying the solution. The following assumptions are made:

1. In applying energy equation between sections (1) and (2), the energy losses are neglected and assumed to be concentrated between section (2) and the end of the air pocket. This is not true but it is necessary to reduce the unknowns involved in the solution.

2. At section (2) the stream lines are concentrated in area A_2 rather than the full water area A_2'.

3. The velocity profile at section (2) gives reverse flow, but all the velocity will be assumed concentrating in Area A_2.

4. Correction factors for the velocity head and pressure head α_0 and α' respectively will be applied for the flow at section (1) and correction factor for the velocity head α_2 will be applied for the flow at section (2).

5. Correction factor K_2 for air presence at sections (1) and (2) will be applied, where $K_2 = 0.5+1/[2(1+\beta)]$ (85).

6. At section (3) small separate air pockets are flowing along the tunnel, which means that the pipe flow is alternating between full flow and partial flow. To account for this variation the air will be assumed to flow at the top of the pipe and solid water is flowing with a depth y_3 and in area A_3, as shown in Fig. (3.20), where $A_3 = A_p/(1+\beta)$.

7. The pipe friction will be neglected in the force momentum balance since it is already known that its effect is negligible[14].

8. The solution will be obtained for a horizontal tunnel and for an assumed value of the angle Φ the nose of the air pocket forms with horizontal.

To solve for the air pocket depth (H), the energy equation and force momentum balance will be combined with continuity for the three sections. The solution will include variable air concentration at sections (1) and (2).

Applying Bernoulli's equation along the upper stream line between sections (1) and (2) where the velocity is taken as the average velocity of the section with air presence through the two sections:

$$\alpha_o \frac{\bar{V}_1^2}{2g} + \alpha' K_2 D \cos\Phi + Z_1 = \alpha_2 \frac{\bar{V}_2^2}{2g} + K_2 y_2 \qquad (3.58)$$

where $\bar{V}_1 = V_o(1+\beta)$

$\bar{V}_2 = V_2(1+\beta)$ velocity concentrated in area A_2

$Z_1 = D(1 - \cos\Phi) + h$

$$y_2 = D - H$$

$$K_2 = 0.5 + 1/[2(1+\beta)] \qquad \text{and}$$

h is as given in equation (3.55).

Applying continuity between sections (1), (2) and (3), we obtain by conservation of mass:

$$Q_w = \frac{1}{1+\beta}\bar{V}_1 A_p = \frac{1}{1+\beta}\bar{V}_2 A_2 = V_3 A_3 = V_o A_p \qquad (3.59)$$

hence

$$V_2 = \frac{V_o A_p}{A_2}, \quad \text{and} \qquad (3.60)$$

$$V_3 = \frac{V_o A_p}{A_3} \qquad (3.61)$$

substituting equation (3.60), the values of $\bar{V}_1$, $\bar{V}_2$, Z_1 and y_2 into equation (3.58), the following is obtained:

$$\alpha_o \frac{V_o^2(1+\beta)^2}{2g} + \alpha K_2 D\cos\phi + D(1-\cos\phi) + h = \alpha_2 \frac{V_o^2 A_p^2}{2gA_2^2}(1+\beta)^2 + k_2(D-H) \qquad (3.62)$$

Rearranging equation (3.62) to obtain A_p/A_2 which is required later to simplify the force momentum balance, the following is obtained:

$$\frac{A_p}{A_2} = \left[\left(\alpha_o + \frac{2gD\cos\phi(\alpha' K_2 - 1)}{V_o^2(1+\beta)^2} + \frac{2gD(1-K_2)}{V_o^2(1+\beta)^2} + \frac{2g(K_2 H+h)}{V_o^2(1+\beta)^2}\right) \times \frac{1}{\alpha_2}\right]^{1/2} \qquad (3.63)$$

Applying force momentum balance between sections (2) and (3):

$$P_{air}\,A_p + P_2A_2' + \frac{\rho}{1+\beta}\,Q\,\bar{V}_2 = P_{air}Ap + P_3A_3 + \rho QV_3 \qquad (3.64)$$

The pressure P_2 and P_3 is obtained by integration over the area of each section, as indicated in equations (3.76) to (3.81). Substituting for the pressure P_2 and P_3 from equation (3.81) into equation (3.64), the following is obtained:

$$\frac{\rho gD}{2(1+\beta)}\left(A_2'Cosa_2' + \frac{2}{3}\,\frac{D^2}{4}\,Sin^3a_2'\right) + \frac{\rho}{1+\beta}\,Q\,\bar{V}_2 =$$

$$\frac{\rho gD}{2}\left(A_3Cosa_3 + \frac{2}{3}\,\frac{D^2}{4}\,Sin^3a_3\right) + \rho QV_3 \qquad (3.65)$$

Substituting for $\bar{V}_2$, V_3 and A_3 where $A_3 = A_p/(1+\beta)$ then multiplying by $2/gDA_p$ and rearranging, the following is obtained:

$$2V_o^2\,\frac{(1+\beta)^2}{gD}\left(1-\frac{A_p}{A_2}\right) = \frac{A_2'}{A_p}Cosa_2' + \frac{2}{3\pi}Sin^3a_2' - Cosa_3 - \frac{2(1+\beta)}{3\pi}Sin^3a_3 \qquad (3.66)$$

Substituting equation (3.63) into equation (3.66) assuming that $\alpha_2 = 1.0$ and rearranging:

$$V_o^2\left(1 - \sqrt{\alpha_o + \frac{2gDCos\Phi(\alpha' K_2 - 1)}{V_o^2(1+\beta)^2} + \frac{2gD(1-K_2)}{V_o^2(1+\beta)^2} + \frac{2g(k_2H+h)}{V_o^2(1+\beta)^2}}\right) =$$

$$\frac{gD}{2(1+\beta)^2}\left(\frac{A_2'}{A_p}Cosa_2' + \frac{2}{3\pi}Sin^3a_2' - Cosa_3 - \frac{2(1+\beta)}{3\pi}Sin^3a_3\right) \qquad (3.67)$$

Equation (3.67) can be solved for each bend radius by substituting values for the correction factors α_o and α' obtained in section 3.5, for different values of the air/water ratio β, and hence V_o or Fr_o can be found for each value of air pocket depth H. The above equation is solved for a bend radius R'/D = 1.0 assuming $\Phi = 0°$, where the results

are shown in Fig. (3.21). It can be noted from Fig. (3.21) that increasing β will increase air pocket depth and the transition to a stable hydraulic jump will occur at lower Froude Numbers.

3.6.3 Model Type 3 - Stable Hydraulic Jump

This model is applicable to the air pocket with a stable hydraulic jump at its end, the nose of the air pocket is considered a separation point, the air pocket depth H is often substantially larger than models 1 and 2, and $Fr_1 > 1.0$. This flow regime appeared from initial visual observations to be the most common of the four regimes of flow, covering a wide range of flow Froude Numbers. Two approaches will be used to derive expressions for the air pocket depth, and these are:

a. Applying energy equation at a section through the air pocket nose and a section at maximum depth of air pocket, just upstream of the jump.

b. Applying force momentum balance between two sections, one just before the hydraulic jump and the second just after the hydraulic jump. In this approach the effect of inclination angle of the tunnel will be included.

Each of the above approaches will be plotted separately for different values of air/water ratio (β), and for a given value of β, the two solutions will be plotted on the same graph for comparison purposes. This model is shown in Fig. (3.22).

a. Applying energy equation from nose of pocket to maximum depth of air pocket, i.e. start of jump. The following assumptions are made:

1. Point A is a separation point

2. Air pocket pressure is constant over the air pocket length, hence $P_A = P_B$, and hence the flow between section (1) and (2) may be analysed as a gradually varying flow in a curved open channel under pressure.

3. For long air pockets section (2) will have no air bubbles, but for short air pockets section (2) will have air bubbles distributed throughout its depth.

4. The velocity profile at section (2) will be considered rectangular and hence $\alpha_2 = 1$. This is not the case for section (1).

5. For section (1) the pressure distribution requires correction for centrifugal forces acting outwards and the presence of air bubbles.

Applying Bernoulli's equation between section (1) and (2) for the case of no air bubbles at section 2:

$$Z_1 + \alpha' K_2 D \cos\Phi + \alpha_0 \frac{\bar{V}_1^2}{2g} = y_2 + \frac{\alpha_2 \bar{V}_2^2}{2g} + h_f \qquad (3.68)$$

where K_2 is a factor accounting for air presence at section (1)

α' is the head correction term for streamline curvature at the bend

h_f is the head loss between section 1 and 2

and α_0 and α_2 velocity head correction terms.

K_2 has been derived by Haindl[85] as a factor expressing both the magnitude of air concentration and its distribution in the vertical, where K_2 for aerated open channelflow is:

$$K_2 = 0.5 + \frac{1-\alpha}{m} \tag{3.69}$$

where m accounts for the flow distribution and equals 2 for uniform water distribution. If the flow is assumed uniform, then:

$$K_2 = 0.5 + \frac{1}{2(1+\beta)} \tag{3.70}$$

For a range of β from 0 to 0.5, the value of K_2 will range from 1.0 to 0.8. Substituting for $\bar{V}_2$ using equation (3.60) obtained using continuity and considering that $\bar{V}_2 = V_2$ for no air at section (2), and $\bar{V}_2 = V_2(1+\beta)$ for air present at section (2), and $\bar{V}_1 = V_o(1+\beta)$ for air present at section 1, then the following is obtained, for no air bubbles at section 2:

$$Z_1 + \alpha' K_2 D\cos\Phi + \alpha_o \frac{V_o^2(1+\beta)^2}{2g} = y_2 + \alpha_2 \frac{V_o^2}{2g}\left(\frac{A_p}{A_2}\right)^2 + h_f \tag{3.71}$$

where α_2 might be assumed as 1.0. From Fig. (3.22) we have:

$$Z_1 + D\cos\Phi = h + H + y_2 \tag{3.72a}$$

which can be written as:

$$Z_1 - y_2 = h + H - D\,Cos\phi \qquad (3.72b)$$

Substituting equation (3.72b) into equation (3.71), substituting for $h = (R' - D/2)(1-Cos\phi)$, rearranging and assuming h_f can be considered negligible for the short reach between sections (1) and (2), and dividing by pipe diameter, the following is obtained:

$$\frac{H}{D} = \frac{V_o^2}{2gD}\left[\left(\frac{A_p}{A_2}\right)^2 - \alpha_o(1+\beta)^2\right] + Cos\phi(1-\alpha' K_2) - \left(\frac{R'}{D} - \frac{1}{2}\right)(1-Cos\phi) \qquad (3.73)$$

For the case of air present at both sections (1) and (2) equation (3.73) becomes:

$$\frac{H}{D} = \frac{V_o^2}{2gD}(1+\beta)^2\left[\left(\frac{A_p}{A_2}\right)^2 - \alpha_o\right] + Cos\phi(1-\alpha' K_2) - \left(\frac{R'}{D} - \frac{1}{2}\right)(1-Cos\phi) \qquad (3.74)$$

Equation (3.74) is plotted in Fig. (3.23) for the sharp bend, where $R'/D = 0.5$ and $\phi = 90°$ for different values of air/water ratio β. It can be noted from Fig. (3.23) that substantial air pocket depths are predicted, which decrease with increasing Froude Number, and for a given flow Froude Number, the air pocket depth decreases with increasing air/water ratio β.

b. Applying force momentum between section (2) before the hydraulic jump and section (3) after the jump, as shown in Fig. (3.22), and assuming that the resistance between water and pipewall negligible, the following is obtained:

$$P_2 - P_3 = \rho V_3^2 A_3 \beta_3 - \rho V_2^2 A_2 \beta_2 \qquad (3.75)$$

where β_2 and β_3 are momentum correction factors at sections (2) and (3), P_2 and P_3 are the pressure forces at sections (2) and (3) and are as follows:

$$P_2 = P_B A_p + \int_{a_2}^{\pi} \rho g h \, dA \tag{3.76}$$

$$P_2 = P_C A_p + \int_{a_3}^{\pi} \rho g h \, dA \tag{3.77}$$

where the integration component is used to obtain the actual pressure force for any depth of water flow in a circular section.

The elements used to define this pressure force are shown in Fig. (3.24), where h represents the depth below the water surface to the element of integration, and a is half the angle subtended between free water surface and the vertical. From Fig. (3.24) the following are defined:

$$h = (D/2)\text{Cos}a + (D/2)\text{Cos}(\pi-\theta) = D/2\ (\text{Cos}a - \text{Cos}\theta) \tag{3.78}$$

$$dA = D\ \text{Sin}(\pi-\theta)\ dh = D\ \text{Sin}\theta\ dh \tag{3.79}$$

$$dh = \text{Sin}(\pi-\theta)ds = (D/2)\text{Sin}\theta\ d\theta \tag{3.80}$$

Substituting equations (3.78), (3.79) and (3.80) into the second term of equations (3.76) and (3.77) and integrating, the pressure force can be obtained as follows:

$$\int_{a_2}^{\pi} \rho g h \, dA = \rho g \frac{D^3}{4} \int_{a_2}^{\pi} (\text{Cos}a - \text{Cos}\theta)\ \text{Sin}^2\theta\ d\theta$$

$$= \rho g \frac{D^3}{4} \left[\text{Cos}a \int_{a_2}^{\pi} \text{Sin}^2\theta\ d\theta - \int_{a_2}^{\pi} \text{Cos}\theta\ \text{Sin}^2\theta\ d\theta\right]$$

$$= \rho g \frac{D^3}{4} \left[\text{Cosa}\left(\frac{\theta}{2} - \frac{\text{Sin}2\theta}{4}\right) - \frac{\text{Sin}^3\theta}{3}\right]_{a_2}^{\pi}$$

$$= \rho g \frac{D^3}{4} \left[\frac{\text{Cosa}_2}{2}(\pi - a_2 + \frac{1}{2}\text{Sin}2a_2) + \frac{\text{Sin}^3 a_2}{3}\right]$$

$$= \rho g \frac{D}{2} \left[\text{Cosa}_2 \frac{\pi D^2}{4}\left(1 - \frac{a_2}{\pi} + \frac{\text{Sin}2a_2}{2\pi}\right) + \frac{2}{3}\frac{D^2}{4}\text{Sin}^3 a_2\right]$$

$$= \rho g \frac{D}{2} \left[A_2 \text{Cosa}_2 + \frac{2}{3}\frac{D^2}{4}\text{Sin}^3 a_2\right] \qquad (3.81)$$

Substituting equation (3.81) into equations (3.76) and (3.77) with the correct value of angle (a) and then into equation (3.75), the following force/momentum equation is obtained:

$$P_B A_p + \frac{\rho g D}{2}\left(A_2 \text{Cosa}_2 + \frac{2}{3}\frac{D^2}{4}\text{Sin}^3 a_2\right) - P_C A_p - \frac{\rho g D}{2}\left(A_3 \text{Cosa}_3 + \frac{2}{3}\frac{D^2}{4}\text{Sin}^3 a_3\right) = \rho V_3^2 A_3 \beta_3 - \rho V_2^2 A_2 \beta_2 \qquad (3.82)$$

where $A_2 = (\pi D^2/4)(1 - a_2/180 + \text{Sin}2a_2/2\pi)$ and A_3 is an assumed water flow area downstream of the jump, calculated to account for the continuous stream of air pockets moving downstream of the jump. Thus $A_3 \simeq A_p(1-\alpha)$, where α is the air void fraction and equal to A_{air}/Ap. The area of the flowing air depends on the speed of the flowing water, as well as the speed of air pockets (c) moving downstream of the jump. For horizontal pipes $C = 1 - 1.2\ (Q_A+Q_W)/Ap$ or $C = 1.0 - 1.2\ V_o(1+\beta)$, hence :

$$\alpha = \frac{Q_A}{CA_p} = \frac{Q_A}{Q_W}\frac{Q_W}{CA_p} = \beta \frac{V_o}{C} \qquad (3.82)$$

Hence the value of α is $\beta/(1+\beta)$ for the air pocket speed $C = V_o(1+\beta)$, and α is $\beta/1.2(1+\beta)$ for $C = 1.2\ V_o(1+\beta)$. Two solutions will be given for the above two values of α which defines the value of A_3. From the above V_3 can be given as:

$$V_3 = \frac{Q_w}{A_p(1-\alpha)} = \frac{V_o}{1-\alpha} \tag{3.83}$$

Applying continuity between sections (2) and (3):

$$V_2 = \frac{V_3 A_3}{A_2} = \frac{V_o A_p}{A_2} \tag{3.84}$$

Assuming that $P_C = P_B = P_{air}$, substituting for V_2 and V_3 into equation (3.82), multiplying by $2/gDA_p$ and rearranging, the following is obtained when the air pocket speed downstream of the jump is 1.2 $V_o(1+\beta)$:

$$2Fr_o^2\left[\frac{\beta_3}{1-\frac{\beta}{1.2(1+\beta)}} - \frac{A_p}{A_2}\beta_2\right] = \frac{A_2}{A_p}\mathrm{Cos}a_2 + \frac{2}{3\pi}\mathrm{Sin}^3a_2 - \left[1-\frac{\beta}{1.2(1+\beta)}\right]\mathrm{Cos}a_3 - \frac{2}{3\pi}\mathrm{Sin}^3a_3 \tag{3.85}$$

For the case when the air pocket speed $C = V_o(1+\beta)$ the following is obtained when assuming momentum correction factors $\beta_2 = \beta_3 = 1.0$:

$$2Fr_o^2(1+\beta)\left[1-\frac{A_p}{A_2(1+\beta)}\right] = \frac{A_2}{A_p}\mathrm{Cos}a_2 + \frac{2}{3\pi}\mathrm{Sin}^3a_2 - \frac{\mathrm{Cos}a_3}{1+\beta} - \frac{2}{3\pi}\mathrm{Sin}^3a_3 \tag{3.86}$$

For inclined tunnels a component for the weight of water must be included as well as the effect of inclination angle from horizontal (θ) on the pressure terms ($\mathrm{Cos}\theta$). Introducing the component for water weight and θ into equation (3.82) and rearranging as before,

the following general equation is obtained for a stable hydraulic jump in a closed circular conduit:

$$2Fr_o^2(1+\beta)\left[1-\frac{A_p}{A_2(1+\beta)}\right] = \cos\theta\left[\frac{A_2}{A_p}\cos a_2 + \frac{2}{3\pi}\sin^3 a_2 - \frac{\cos a_3}{1+\beta}\right.$$

$$\left. - \frac{2}{3\pi}\sin^3 a_3\right] - \frac{L}{D}\sin\theta\left(\frac{A_2}{A_p} + \frac{1}{1+\beta}\right) \qquad (3.87)$$

where L is the length of jump. An empirical equation for L has been given by Bacopoulos[14]. Equation (3.87) is plotted in Figs. (3.25), (3.26) and (3.27) for three different angles of tunnel inclination θ, for different air/water ratios β, and for a range of flowing Froude Numbers. It can be noted from the three figures that increasing air/water ratio produces shallower air pocket depths, increasing Froude Number produces shallower air pocket depth, and the variation in tunnel inclination from an upward slope of +1.5° to a downward slope of -1.5° also produces shallower air pockets.

A comparison between the H/ D Fr_o and β relationship using the energy equation (3.74) and comparing with the force momentum equation (3.87) is shown in Fig. (3.28) for an air/water ratio of 0.2. It can be noted that reasonable agreement is achieved in view of the widely different assumptions in each case. Comparison of these two solutions with experimental results will be carried out in chapter (7).

3.6.4 Model Type 4

This regime of flow concerns an air pocket at the dropshaft/tunnel bend being removed completely from the bend and being transported along the tunnel section. This is sketched in Fig. (3.14). Extensive visual observations and photography revealed at least four different components or models of clearing as sketched in Fig. (3.29). These are:

(1) When the pocket is swept bodily down the tunnel by the force of the upstream flow at the bend. This force, as a speculation, may be given by:

$$F_s = K(1/2)\rho_m C_d A_b V_o^2(1+\beta)^2 \qquad (3.88)$$

where ρ_m is the density of the two phase mixture

$V_o(1+\beta)$ is the mean velocity of the flowing mixture

A_b is the area of the air pocket exposed to the oncoming flow at the bend

C_d is the drag coefficient related to the shape of the air pocket, and

K is a constant of proportionality to account for the curvature of the bend and the fact that the oncoming flow is not meeting the air pocket "head on" as in a straight pipe.

The removing force F_s in equation (3.88) is not resisted by air pocket buoyancy in the sharp bend for the cases of a horizontal tunnel ($\theta = 0°$), and upward sloping tunnel ($+\theta°$), but some buoyancy component will exist in the downward sloping tunnel ($-\theta°$). For the radiused bends R'/D = 1.0 and 1.5, the upstream nose of the air pocket is generally located around the bend at an angle ϕ, and hence, some resisting buoyancy component must be present.

(2) Partial clearing by air entrainment at the toe of the jump must constitute a component of air pocket clearing, as shown in Fig. (3.29). Air bubbles are transported downstream from the toe of the jump for the minimum possible conditions:

$$Fr_1 > 1.0 \qquad (3.89)$$

and

$$V_1 > 0.8 \text{ to } 1.0 \text{ m/s} \qquad (3.90)$$

That is, a supercritical flow is required and the water velocity at the toe of the jump must exceed 1.0 m/s for effective entrainment of air[4,50,162,163].

(3) The undulating turbulent roller of the hydraulic jump often "shears-off" a large portion of the air pocket when the roller comes in contact with the roof of the tunnel. This also constitutes partial clearing of the air pocket, as shown in Fig. (3.29).

(4) In the case of a sharp bend R'/D = 0.5, in particular, an intense swirl is generated, usually alternating in direction. This may reach the tunnel roof and plunge back down into the main body of the flow, entraining considerable quantities of air and leading again to partial clearing of the pocket from the bend.

A theoretical model has not been attempted for the clearing of air pockets from a bend, in view of the utter complexity of the situation. Instead, resort will be made to an empirical relationship for clearing, based on experimental data later in this thesis.

3.7 THEORETICAL MODEL FOR STRAIGHT PIPES INCLINED ABOVE THE HORIZONTAL

This model is intended to investigate the rising velocity of air pockets in continuous straight pipes inclined upwards above the horizontal, where the air pockets move in the same direction as the flowing water with a velocity higher than that of the flowing water, as already outlined in chapter (2). An air pocket rising in a straight pipe inclined above horizontal is shown in Fig. (3.30),

where the air pocket is moving with a speed V_r. In order to obtain a model for such air pockets, the following assumptions will be made:

1 - An observer will be moving with the front nose of the air pocket to reduce the problem to the steady state. This means that relative velocities will be applied to the region considered between section (1) and (3), as shown in Fig. (3.30).

2 - For the above case the front nose of the pocket at point B will be a stagnation point with a zero velocity.

3 - The shape of the front nose of the air pocket will be considered as a parabola[14,24].

4 - Losses between points A and B are negligible, with all the losses concentrated between A and the tail of the air pocket.

5 - The air pocket pressure is constant = P_{air}.

6 - The angle the front nose of the air pcket forms with the pipe wall Φ will be taken equal to 60°[14,24].

7 - In this model both energy and force-momentum balance will be used to obtain the air pocket rising velocities.

Applying Bernoulli's equation between points B and C:

$$\frac{P_B}{\rho g} + \frac{V_B^2}{2g} = \frac{P_C}{\rho g} + \frac{V_C^2}{2g} + L_2 \mathrm{Sin}\theta + \lambda \frac{L_2}{D} \frac{V_C^2}{2g} \qquad (3.91)$$

where $V_B = 0$, $P_B = P_{air}$ and $V_C = V_r - V_o$, the relative velocity at point C. Substituting for V_B and V_C and rearranging:

$$\frac{(V_r - V_o)^2}{2g} = \frac{P_{air}}{\rho g} - \frac{P_C}{\rho g} - L_2 \mathrm{Sin}\theta - \lambda \frac{L_2}{D} \frac{(V_r - V_o)^2}{2g} \qquad (3.92)$$

Applying continuity between sections (1) and (3):

$$(V_r - V_1)\, A_1 = (V_r - V_o)\, A_p \qquad (3.93)$$

Applying force-momentum balance between sections (1) and (3) the following is obtained:

(Pressure + Momentum flux) at section (1) - (Pressure + momentum flux) at section (3) - (weight of water between (1) and (2)) - (weight of water between (2) and (3)) - (Resistance between (1) and (2)) - (Resistance between (2) and (3)) = 0 (3.94)

The resistance between sections (1) and (2) will be ignored as it is known to have negligible effect on the final result[14]. The weight of water between sections (1) and (2) is calculated on a linear change of water level between these two sections. This is not the case, as the free surface takes up a parabolic shape but the errors engendered are negligible. Equation (3.94) can be written in the following form:

$$P_{air}A_p + \rho g\frac{D}{2}\mathrm{Cos}\theta\left(A_1\mathrm{Cos}a_1 + \frac{2}{3}\frac{D^2}{4}\mathrm{Sin}^3 a_1\right) + \rho(V_r-V_1)^2A_1 - P_cA_p$$

$$- \rho g\frac{D}{2}\mathrm{Cos}\theta A_p - \rho(V_r-V_o)^2A_p - \rho g L_2 \mathrm{Sin}\theta A_p - \rho g L_1 \mathrm{Sin}\theta$$

$$\left(\frac{A_p + A_1}{2}\right) - \rho g A_p \lambda \frac{L_2}{D}\frac{(V_r - V_o)}{2g} = 0 \qquad (3.95)$$

Dividing equation (3.95) by $\rho g A_p$, substituting equations (3.92) and (3.93) and rearranging, the following is obtained for the air pocket rise velocity:

$$V_r = \{[\cos\theta(1-\frac{A_1}{A_p}\cos a_1 - \frac{2}{3\pi}\sin^3 a_1) + \frac{L_1}{D}\sin\theta(1+\frac{A_1}{A_p})]$$

$$x \frac{gD}{(\frac{2A_p}{A_1} - 1)}\}^{1/2} + V_o \qquad (3.96)$$

In order to solve equation (3.96), L_1 is defined according to Bacopolous[14], where the shape AB at the air pocket nose is assumed to be a parabola of the form shown in Fig. (3.31):

$$y = A' x^2 \qquad (3.97)$$

where the parabola vortex is at point A, and for $x = L_1$, $y = H$, hence $A' = H/L_1^2$. Differentiating (3.97) the following is obtained:

$$\frac{dy}{dx} = 2 A' x \qquad (3.98)$$

where the slope dy/dx at point B is given by $\tan\phi$. Substituting for dy/dx and A' in equation (3.94) the following is obtained:

$$L_1 = \frac{2 H}{\tan\phi} \qquad (3.99)$$

Substituting equation (3.99) into equation (3.96), the rising velocity for the air pockets is obtained in terms of the maximum depth of the air pocket (H), the conduit slope (θ), and the water velocity (V_o), as follows:

$$V_r = \{[\cos\theta(1 - \frac{A_1}{A_p}\cos a_1 - \frac{2}{3\pi}\sin^3 a_1) + \frac{2}{D}\frac{H}{\tan\phi}\sin\theta\ (1 + \frac{A_1}{A_p})]$$

$$x \frac{gD}{(\frac{2A_p}{A_1} - 1)}\}^{1/2} + V_o \qquad (3.100)$$

Equation (3.100) is plotted in Fig. (3.32) for an angle of +1.5° with horizontal for different values of H/D, assuming $\Phi = 60°$. It is not clear at this stage if equation (3.100) can be applied to all conduit slopes from 0° to 90° as the angle of the air pocket nose Φ appears to vary with conduit slope θ.

However, equation (3.100) has been derived for a single air pocket in a pipe with mean water velocity V_o. In practice, such air pockets usually move one behind the other giving a constant air supply Q_A. This means that the average water velocity for a continuous supply of air pockets should be $V_o(1+\beta)$, where β is the ratio of air/water, and hence equation (3.100) takes the form:

$$V_r = K\sqrt{gD} + V_o(1+\beta) \qquad (3.100a)$$

for a constant conduit slope θ, constant air pocket nose angle Φ, and constant air pocket depth H, A_1. The effect of β is shown in Fig. (3.33) for H/D = 0.2, showing a steepening of the lines for increasing β values.

Wallis[177] points out that in practice, continuous air pockets may move even faster than that predicted in equation (3.100a) due to the wake effect "pulling-along" air pockets coming behind.

3.8 THEORETICAL MODELS FOR STRAIGHT PIPES INCLINED BELOW THE HORIZONTAL

Air pockets in straight pipes inclined downwards below the horizontal can either blow-back up the pipe, or clear downstream along the pipe, depending on the water velocity. For the case of air pockets blowing-back the same procedure of relative velocities in section (3.7) will be used. For the clearing air pockets downstream the criteria of the air pocket at the point of blow-back will be used to find the water velocity at that point, whereupon any increase above that water velocity will clear the air pocket downstream. Both models are shown in Fig. (3.34).

3.8.1 Air Pockets Blowing Back

Referring to Fig. (3.34) and applying Bernoulli's equation between points A and B:

$$\frac{P_A}{\rho g} + \frac{V_A^2}{2g} + L_1 \mathrm{Sin}\theta = \frac{P_B}{\rho g} + \frac{V_B^2}{2g} + \lambda \frac{L_1}{D} \frac{V_A^2}{2g} \qquad (3.101)$$

where $P_B = P_{air}$, $V_B = 0$ and $V_A = V_r + V_o$. Substituting for P_B and V_A and rearranging:

$$\frac{(V_r + V_o)^2}{2g} = \frac{P_{air}}{\rho g} - \frac{P_A}{\rho g} - L_1 \mathrm{Sin}\theta + \lambda \frac{L_1}{D} \frac{(V_r + V_o)^2}{2g} \qquad (3.102)$$

Applying continuity between sections (1) and (3):

$$(V_r + V_o)\, A_p = (V_r + V_3)\, A_3 \qquad (3.103)$$

Applying force-momentum balance between sections (1) and (3) the following is obtained, assuming that losses between section (2) and (3) can be neglected:

$$P_A A_p + \rho g \frac{D}{2} \mathrm{Cos}\theta A_p + \rho (V_r + V_o)^2 A_p - P_{air} A_p - \rho g \frac{D}{2} \mathrm{Cos}\theta$$

$$(A_3 \mathrm{Cos}a_3 + \frac{2}{3} \frac{D^2}{4} \mathrm{Sin}^3 a_3) - \rho (V_r + V_3)^2 A_3 + \rho g L_1 \mathrm{Sin}\theta A_p$$

$$+ \rho g L_2 \mathrm{Sin}\theta \left(\frac{A_p + A_3}{2}\right) - \rho g A_p \lambda \frac{L_1}{D} \frac{(V_r + V_o)^2}{2g} = 0 \qquad (3.104)$$

Dividing equation (3.104) $\rho g A_p$, substituting equations (3.102) and (3.103) and rearranging, the following is obtained:

$$V_r = \{[\cos\theta(1 - \frac{A_3}{A_p}\cos a_3 - \frac{2}{3\pi}\sin^3 a_3) + \frac{2}{D\tan\phi}\frac{H}{}\sin\theta(1+\frac{A_3}{A_p})]$$

$$x \frac{gD}{(\frac{2A_p}{A_3} - 1)}\}^{1/2} - V_o \qquad (3.105)$$

Considering the case of a downward sloping angle of -1.5°, equation (3.105) is plotted in Fig. (3.35) for different values of H/D. In this case the rise velocity V_r is in the opposite direction to the water flow. It can be noted from Fig. (3.35) that the air pockets can blow-back up to a certain flow velocity, after which the air pockets will move downstream and clear from the tunnel. In any case, equation (3.105) may be used to predict the blow-back air pocket velocity at any conduit angle θ, provided the relationship between θ and the nose angle φ is known.

3.8.2 Air Pockets Clearing

To obtain the velocity required to clear air pockets downstream in a downward sloping pipe, the criteria of the air pockets at the point of blow-back will be used. Using the same assumptions as in sections (3.7) and (3.8.1), it appears that the velocity of water at the point of blow-back can be obtained from equation (3.105) by substituting for V_r as zero, hence, the non-dimensional water velocity to prevent the air pocket from blowing back will be:

$$\frac{V_o}{\sqrt{gD}} = \left[\frac{\cos\theta(1 - \frac{A_3}{A_p}\cos a_3 - \frac{2}{3\pi}\sin^3 a_3) + \frac{2}{D\tan\phi}\frac{H}{}\sin\theta(1 + \frac{A_3}{A_p})}{(2\frac{A_p}{A_3} - 1)}\right]^{1/2} \qquad (3.106)$$

This means that for any value of air pocket depth H/D, and angle of tunnel θ, there is only one value of Froude Number to prevent

the air pocket from blowing back. Above this value of Froude Number the air pocket will clear along the pipe. Equation (3.106) is plotted in Fig. (3.36) for different values of H/D and angles of inclination Θ with the assumption that $\phi = 40°$ which is within the range found in this work. Although equation (3.106) is plotted for different angles of inclinations, it may not be completely correct because the shape of the air pocket changes with the angle of inclination as well as the angle ϕ, the angle the nose of the air pocket forms with the pipe wall. In fact, in vertical shafts the air pocket may not be attached to the pipe wall, as outlined earlier in chapter (2).

3.9 CONCLUSIONS

The behaviour of air pockets at the junction of dropshaft/tunnel bend is complex, two-phase, chaotic and often unsteady, and depends on many parameters which makes it difficult to obtain a single simplified theoretical model for its behaviour. Different models have been proposed for each assumed regime of air pocket behaviour, although the case of air pocket clearing from the bend needs more development. These models will be compared with the experimental results of this work in Chapter (7) in order to determine their accuracy or otherwise.

Also, the theoretical models for straight pipes will be compared with results of this work in Chapter (7). The models derived in this chapter are simple theoretical models and may need modification after doing detailed experimental work for the complex flow at the bend to obtain exact velocity profiles, pressure distribution in order to find the exact correction factors to be applied to the flow around the bend. Also, a detailed study must be done for the secondary currents and swirl at the bend which affect the behaviour of the air pockets.

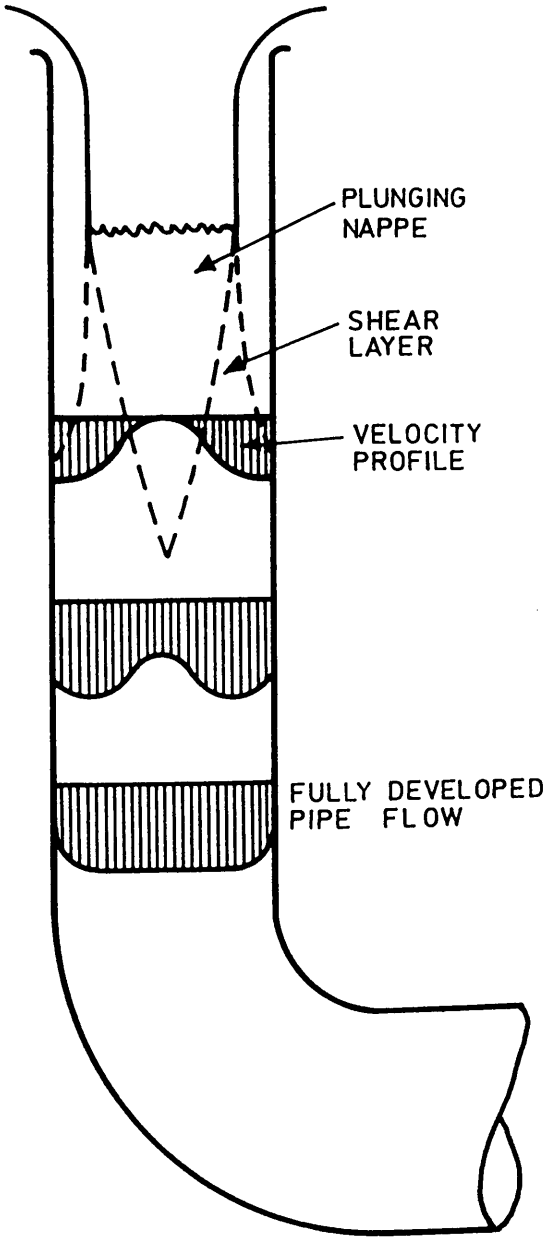

FIG. (3.1) FLOW DESCENDING THE DROPSHAFT AND GENERATING THE SHEAR LAYERS

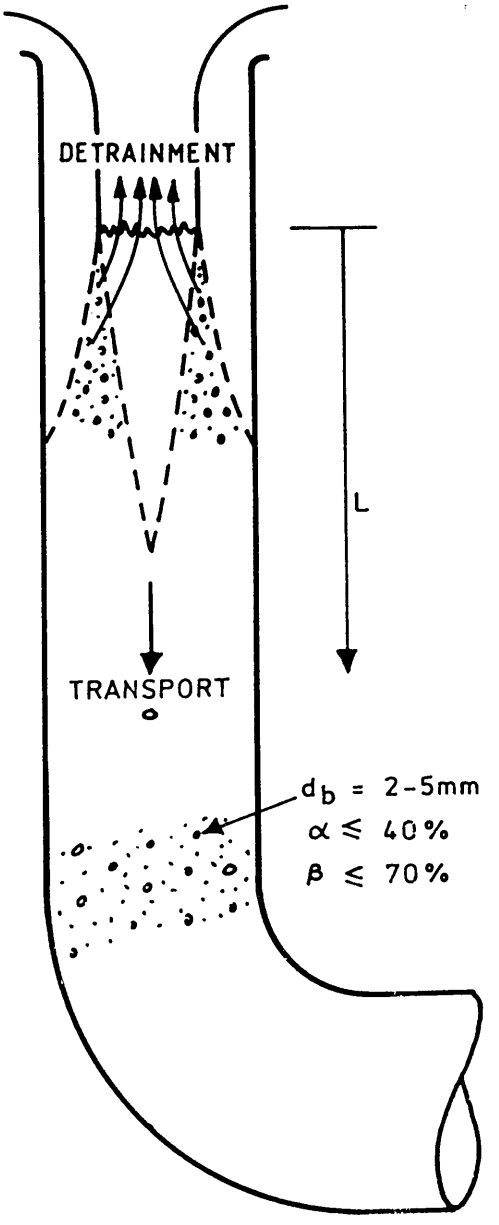

FIG. (3.2) THE UNIFORM DISTRIBUTION OF AIR BUBBLES APPROACHING THE BEND

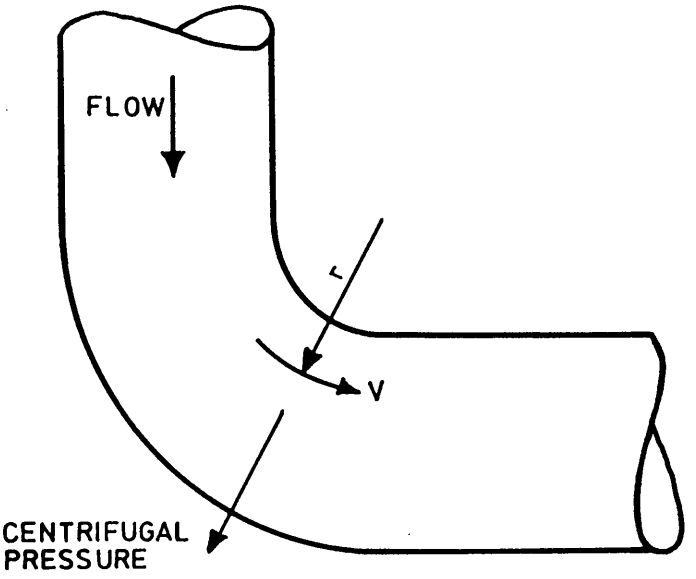

FIG. (3.3) THE CURVED FLOW AT THE BEND

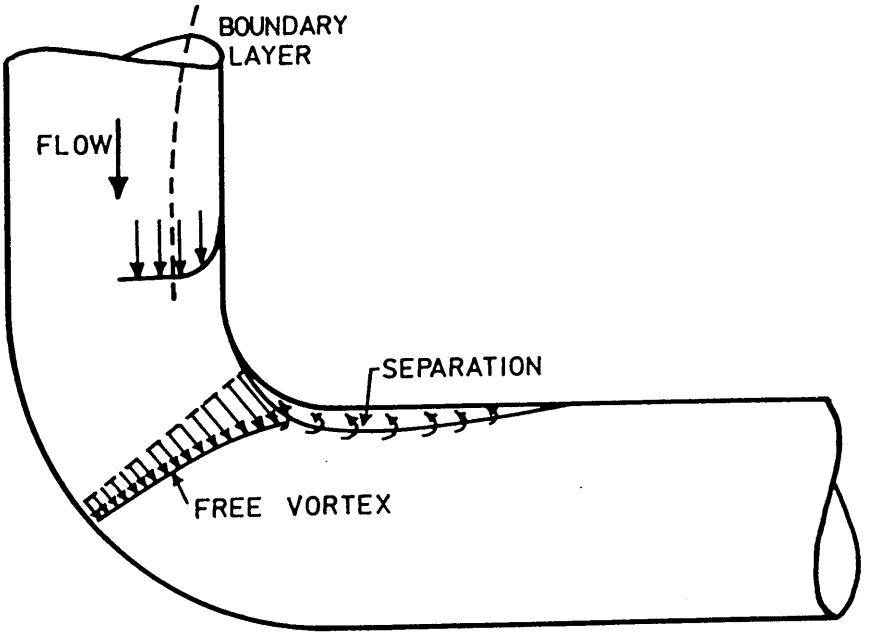

FIG. (3.4) SEPARATION AT THE INNER BEND

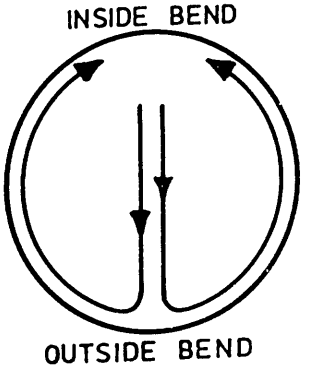

FIG. (3.5) SECONDARY CURRENTS IN THE FORM OF A DOUBLE SPIRAL

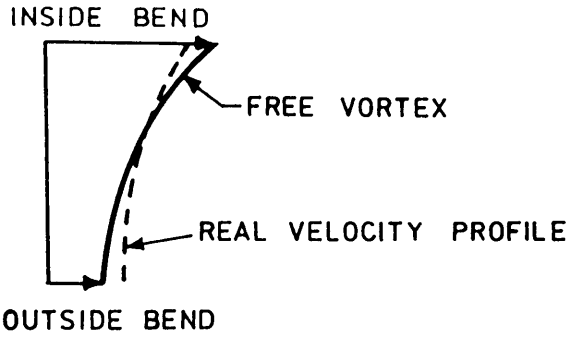

FIG. (3.6) THE DISTORTION OF THE FREE VORTEX VELOCITY PROFILE

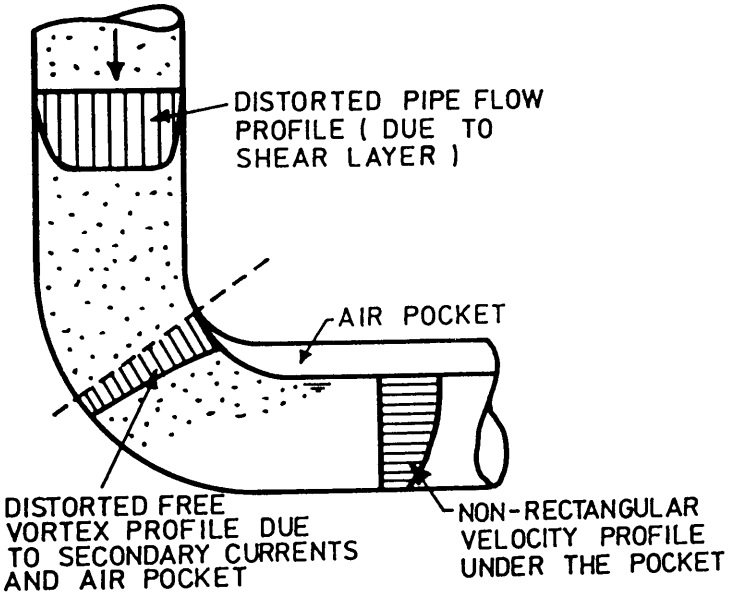

(a) VELOCITY PROFILES

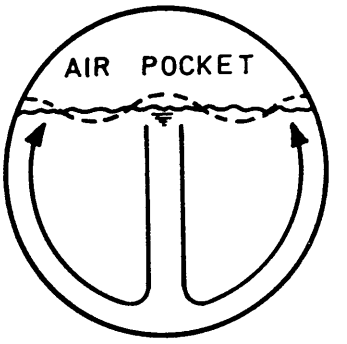

(b) SECONDARY CURRENTS UNDER THE AIR POCKET

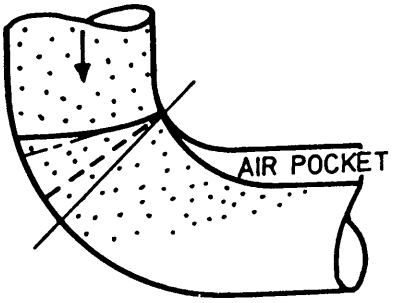

——— REAL PRESSURE ALLOWING FOR AIR BUBBLE AND CENTRIFUGAL PRESSURE

—·— HYDROSTATIC (WATER ONLY)

– – – HYDROSTATIC ALLOWING FOR AIR BUBBLES

(c) PRESSURE DISTRIBUTION AT THE BEND

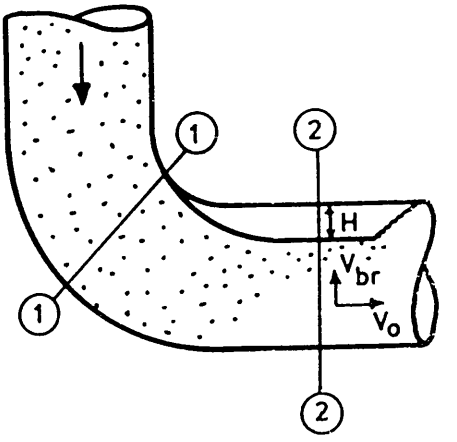

(d) PATH OF AIR BUBBLE TRAVEL

FIG. (3.7) THE PARAMETERS AFFECTED BY THE AIR POCKET FORMATION AT THE BEND

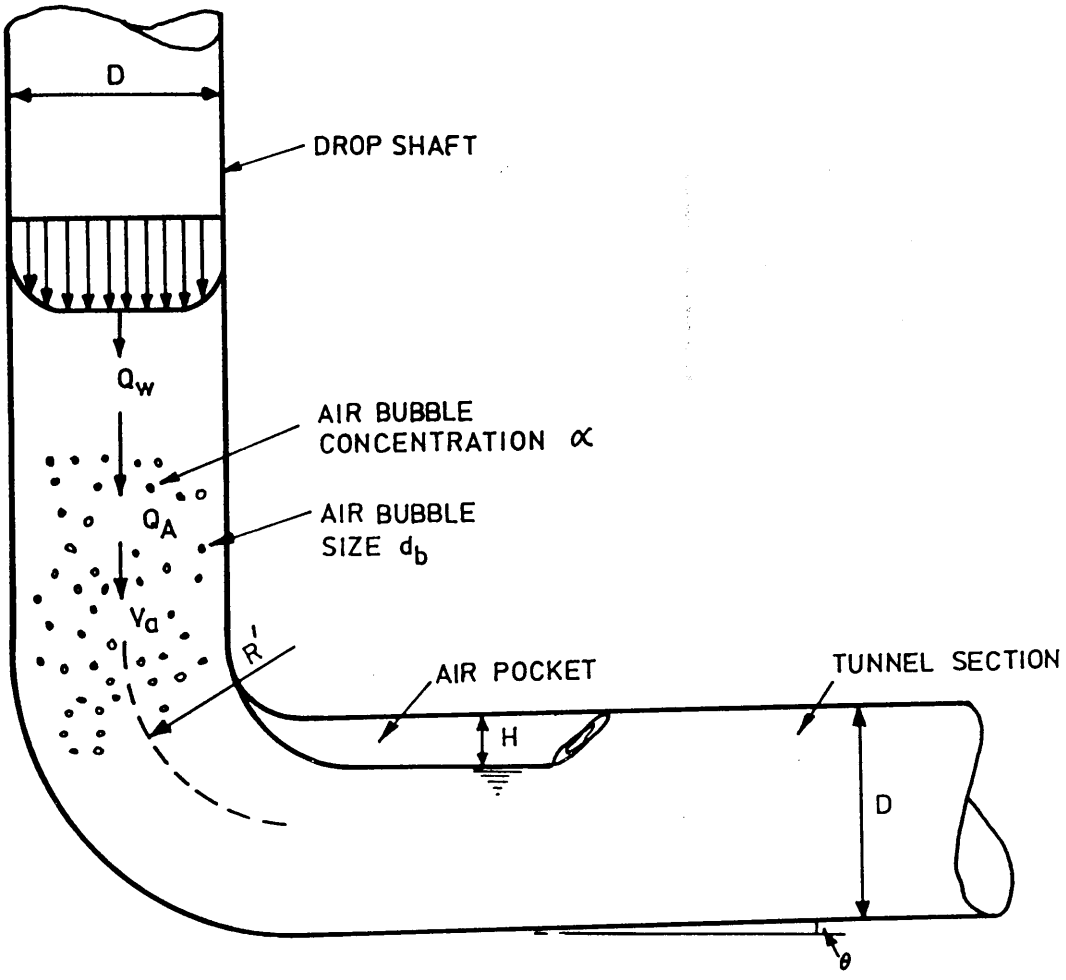

FIG. (3.8) FLOW AND GEOMETRIC PARAMETERS FOR THE DIMENSIONAL ANALYSIS OF AIR POCKET FORMATION

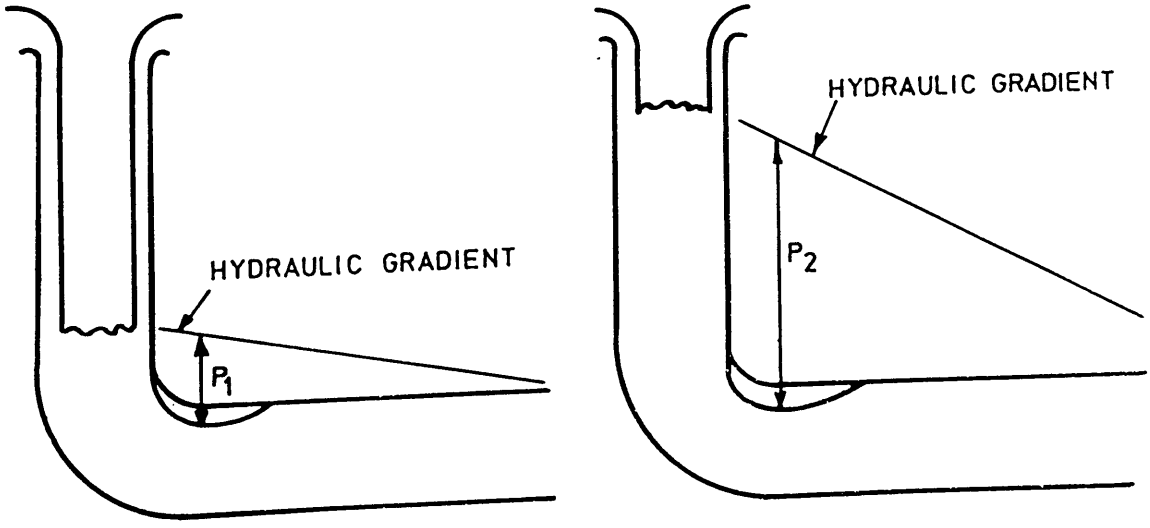

FIG. (3.9) THE EFFECT OF HYDRAULIC GRADIENT ON THE PRESSURE AT BEND

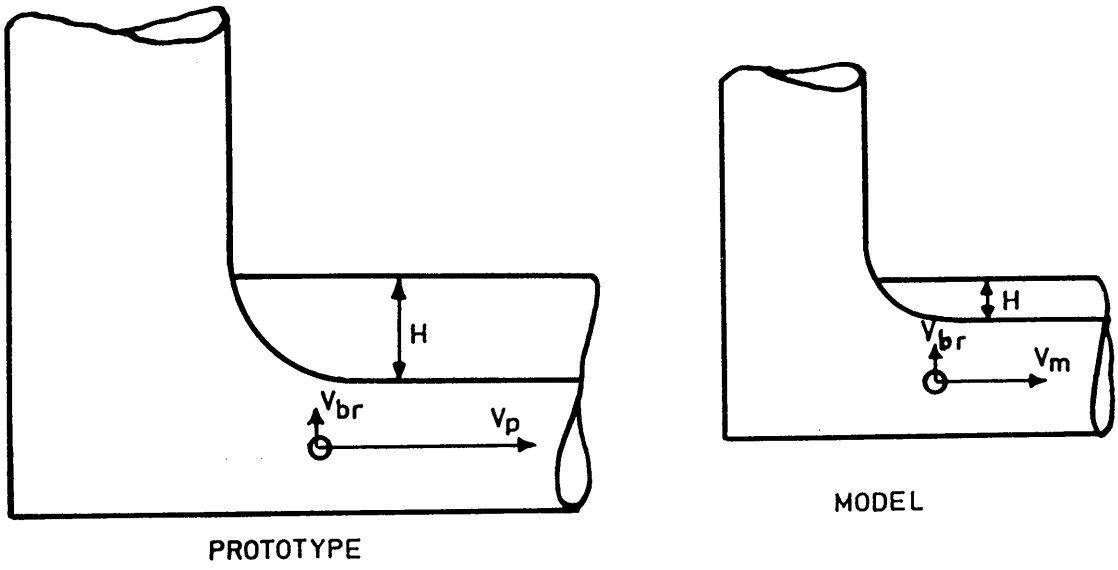

FIG. (3.10) VELOCITY VECTORS FOR AIR BUBBLES APPROACHING THE AIR POCKET IN MODEL AND PROTOTYPE

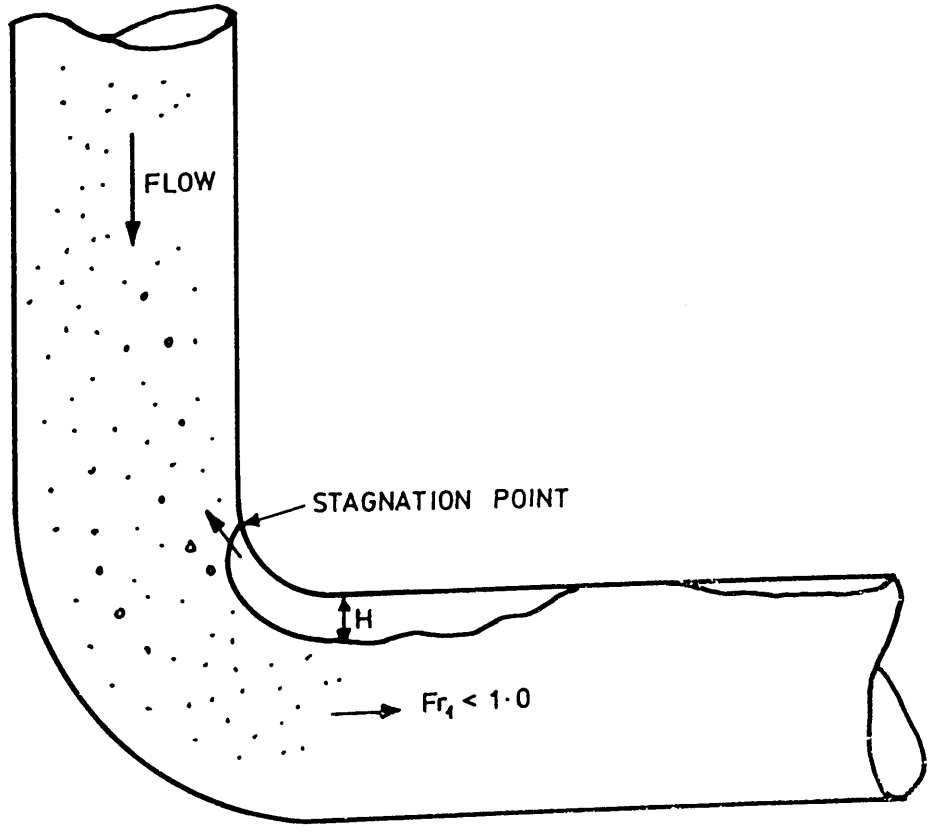

FIG. (3.11) MODEL TYPE 1, FOR VENTING OR BLOWING BACK UP THE VERTICAL SHAFT

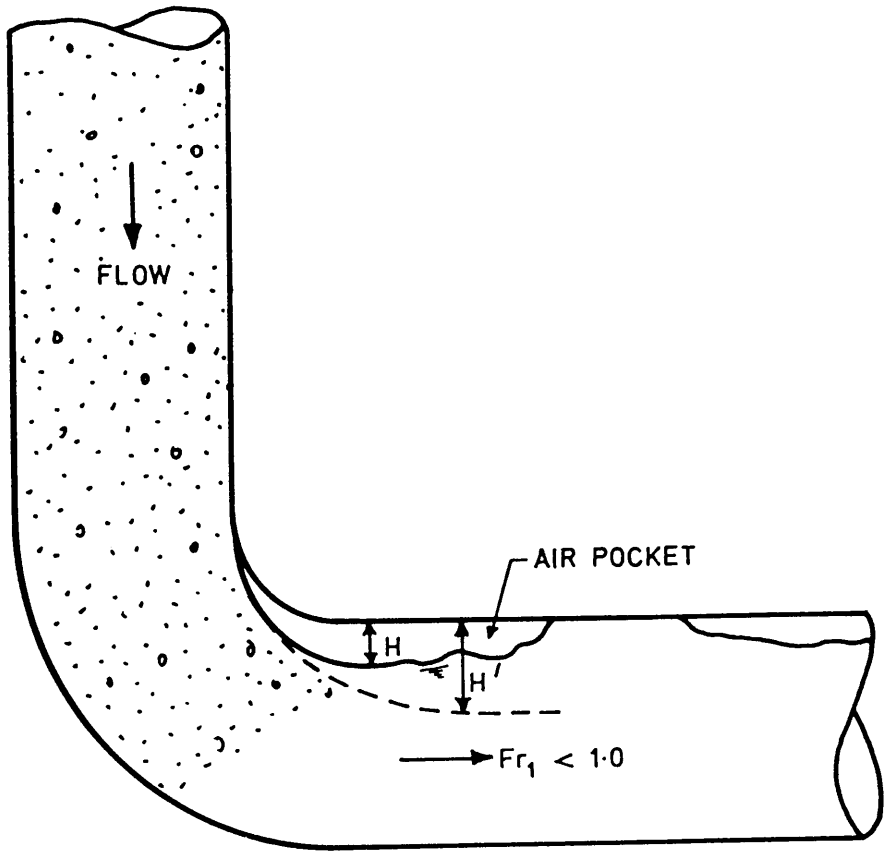

FIG. (3.12) MODEL TYPE 2, THE DROWNED HYDRAULIC JUMP

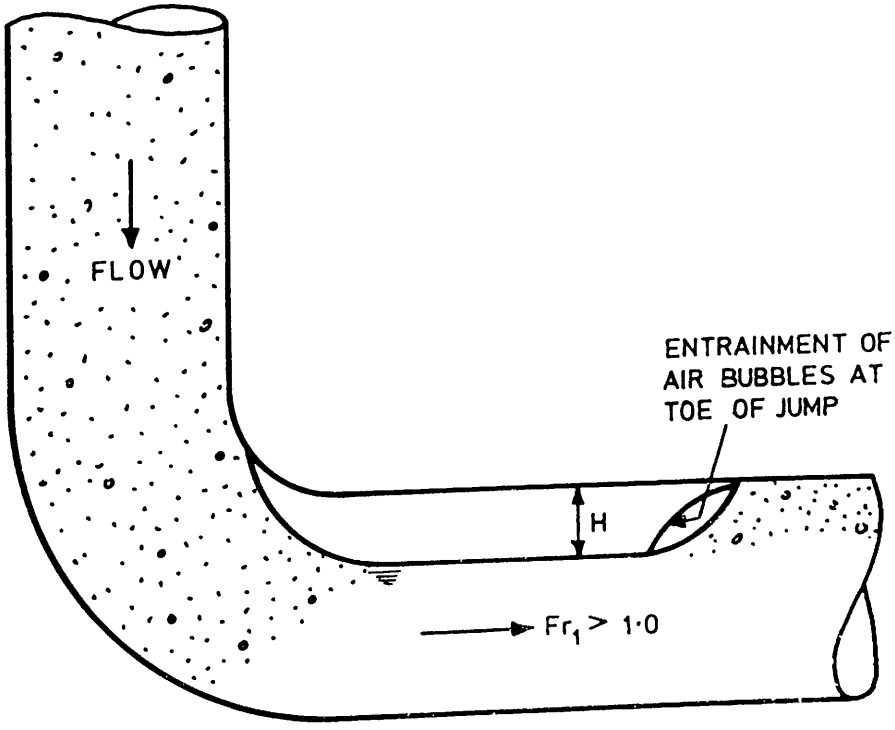

FIG. (3.13) MODEL TYPE 3, THE AIR POCKET WITH A STABLE HYDRAULIC JUMP AT ITS END

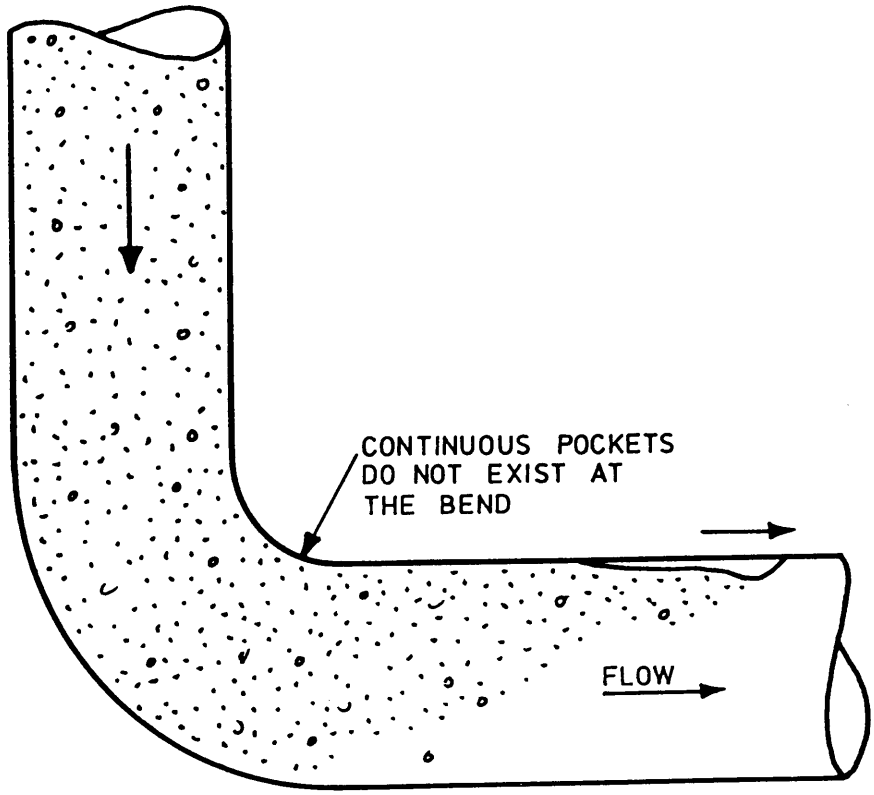

FIG. (3.14) MODEL TYPE 4, AIR POCKET CLEARING

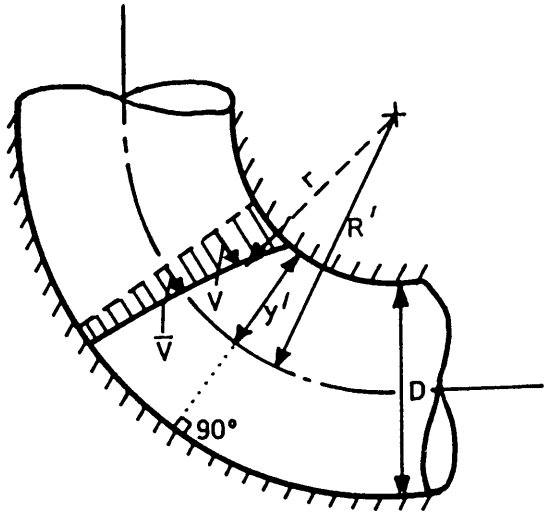

FIG. (3.15) THE BEND OF A CIRCULAR PIPE

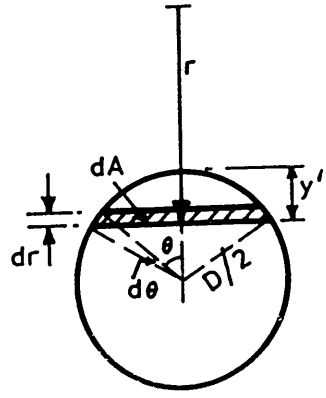

FIG. (3.16) CROSS-SECTION OF OF THE PIPE SHOWING ELEMENTS OF THE INTEGRATION

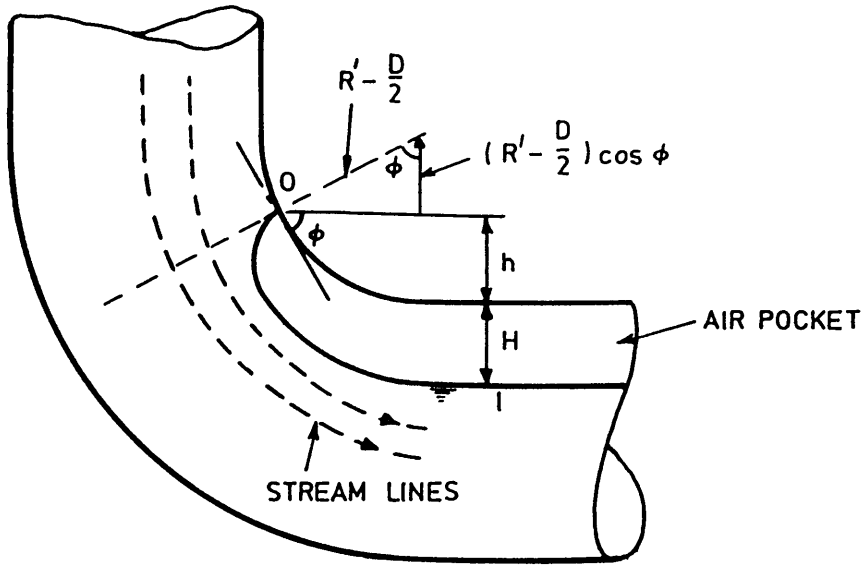

FIG. (3.17) MODEL TYPE 1, SHOWING THE GEOMETRIC CONFIGURATION OF AN AIR POCKET BLOWING BACK

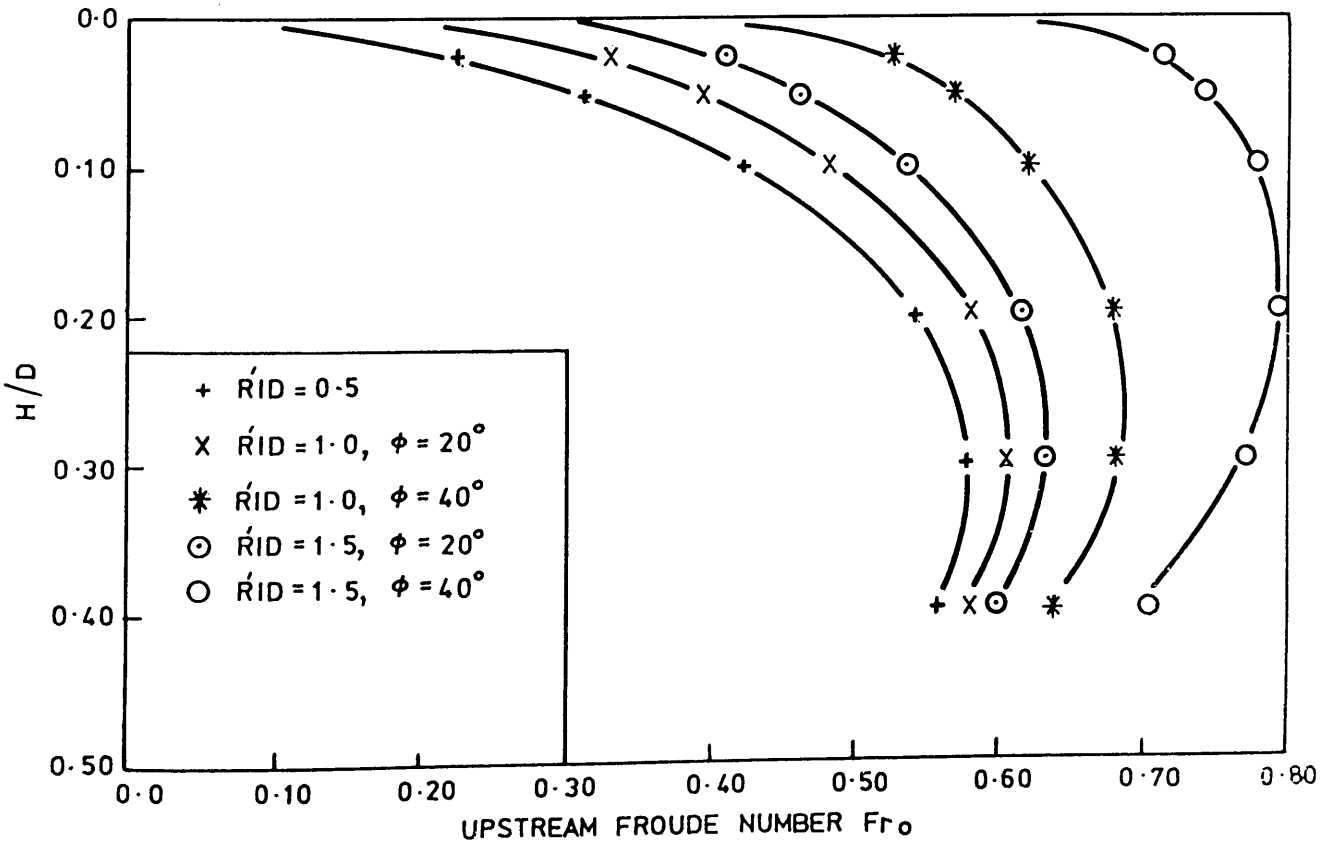

FIG. (3.18) RELATION BETWEEN Fr_o AND H/D FOR MODEL TYPE 1 ACCORDING TO EQUATION (3.56)

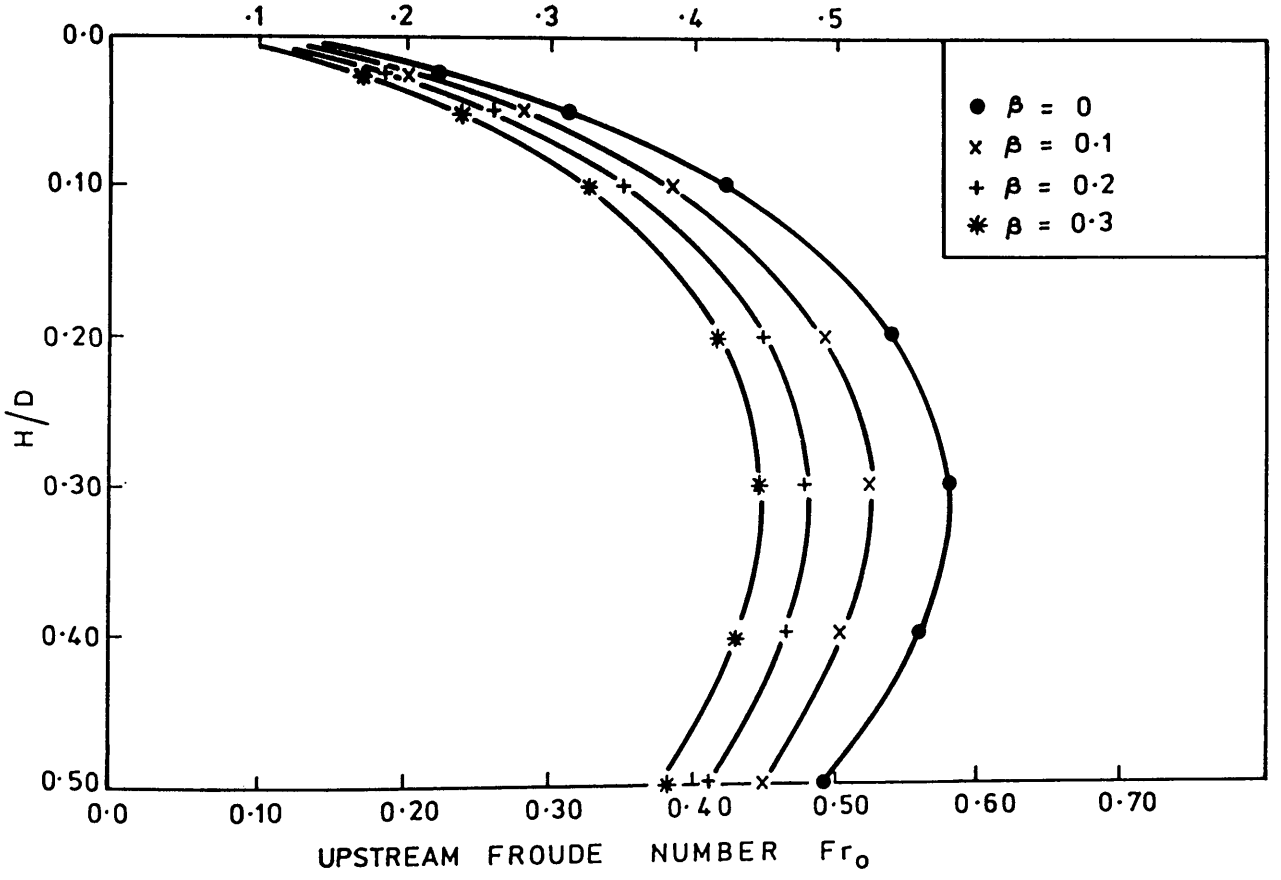

FIG. (3.19) THE EFFECT OF AIR/WATER RATIO ON AIR POCKET DEPTH FOR MODEL TYPE 1 FOR A BEND RADIUS R'/D = 0.5.

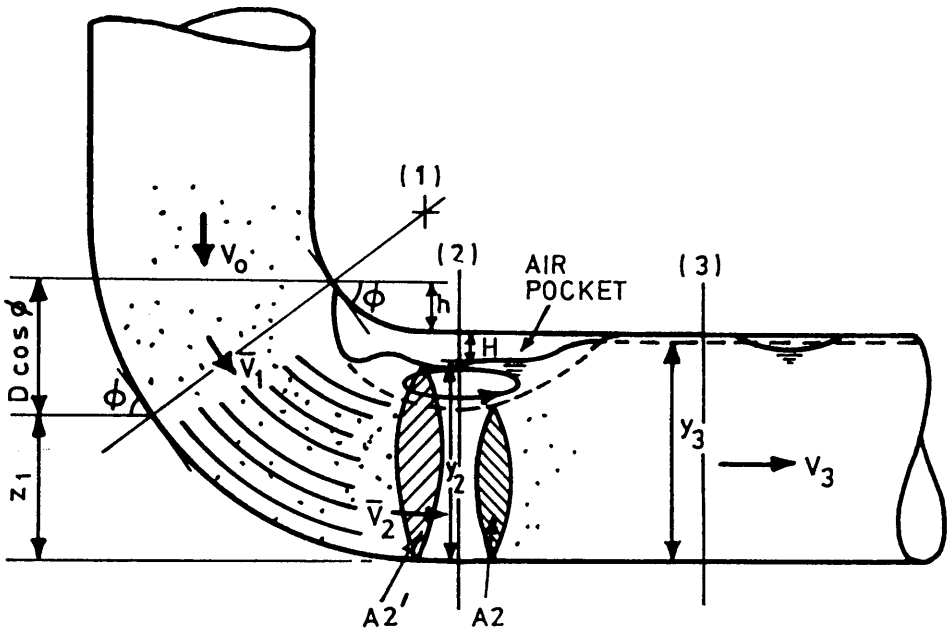

FIG. (3.20) MODEL TYPE 2, SHOWING THE DROWNED JUMP

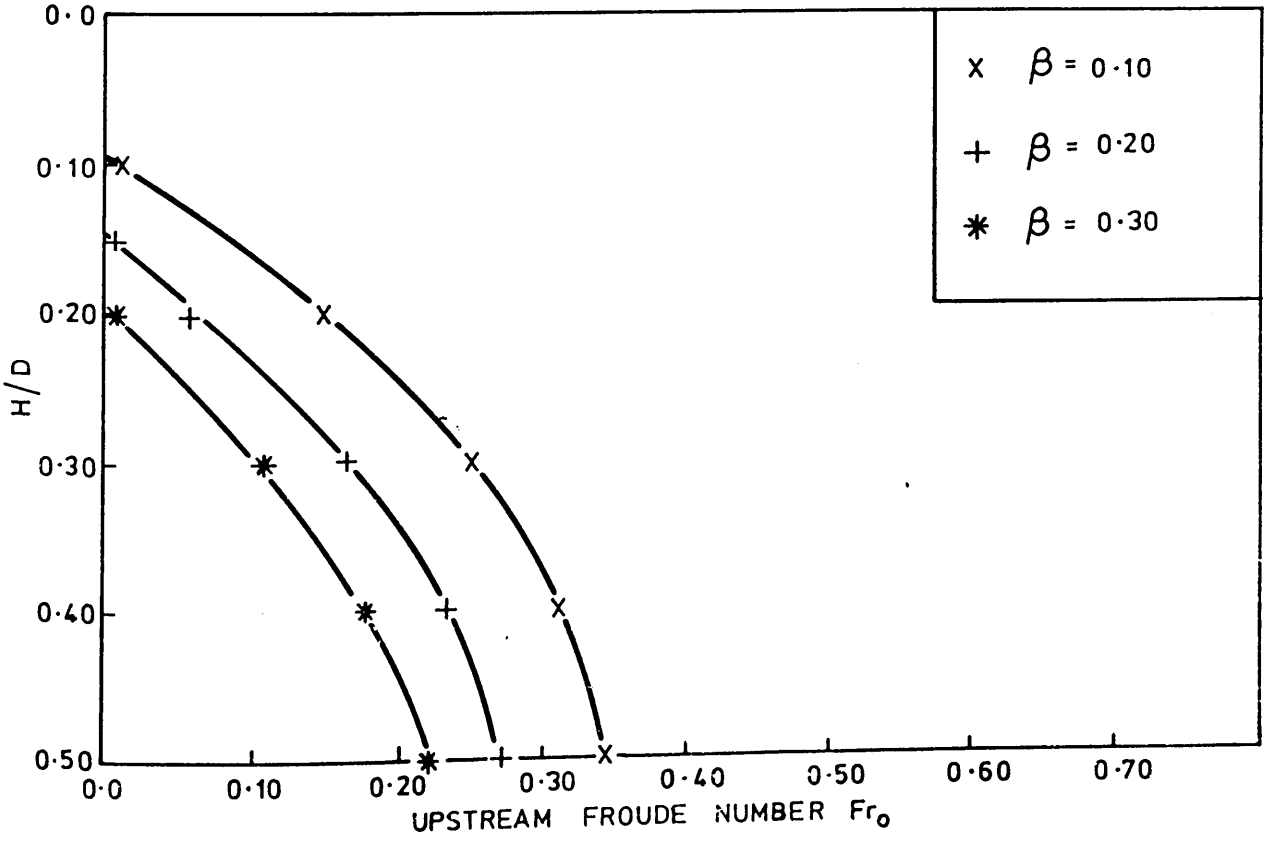

FIG. (3.21) THE RELATION BETWEEN Fr_o AND H/D FOR MODEL TYPE 2

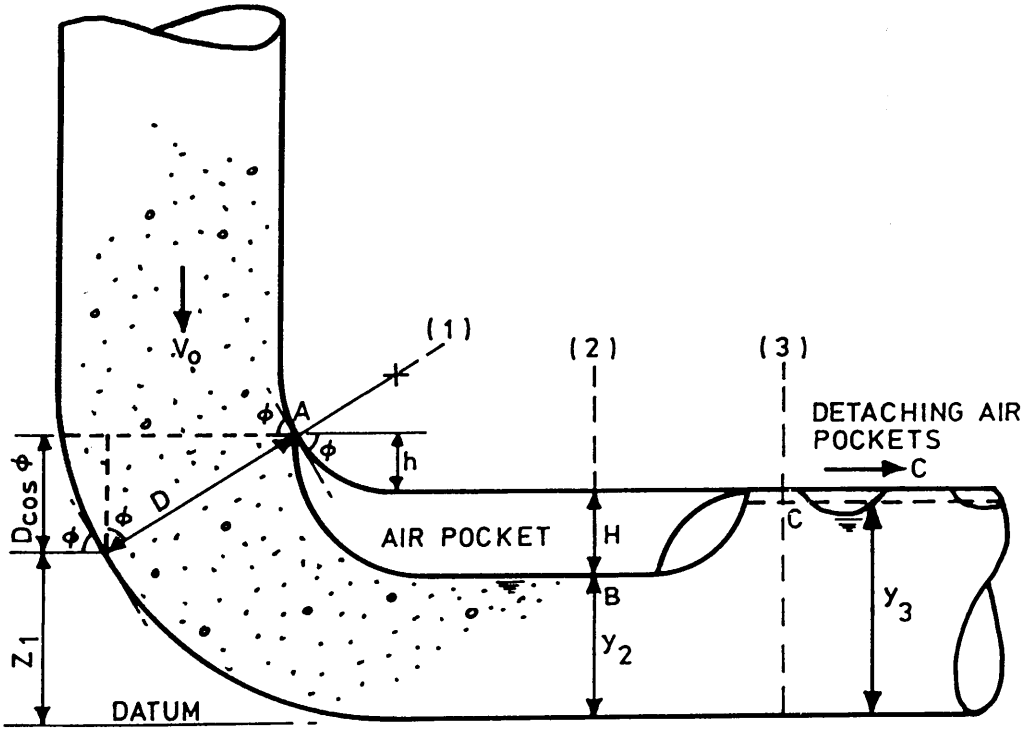

FIG. (3.22) MODEL TYPE 3, THE STABLE HYDRAULIC JUMP

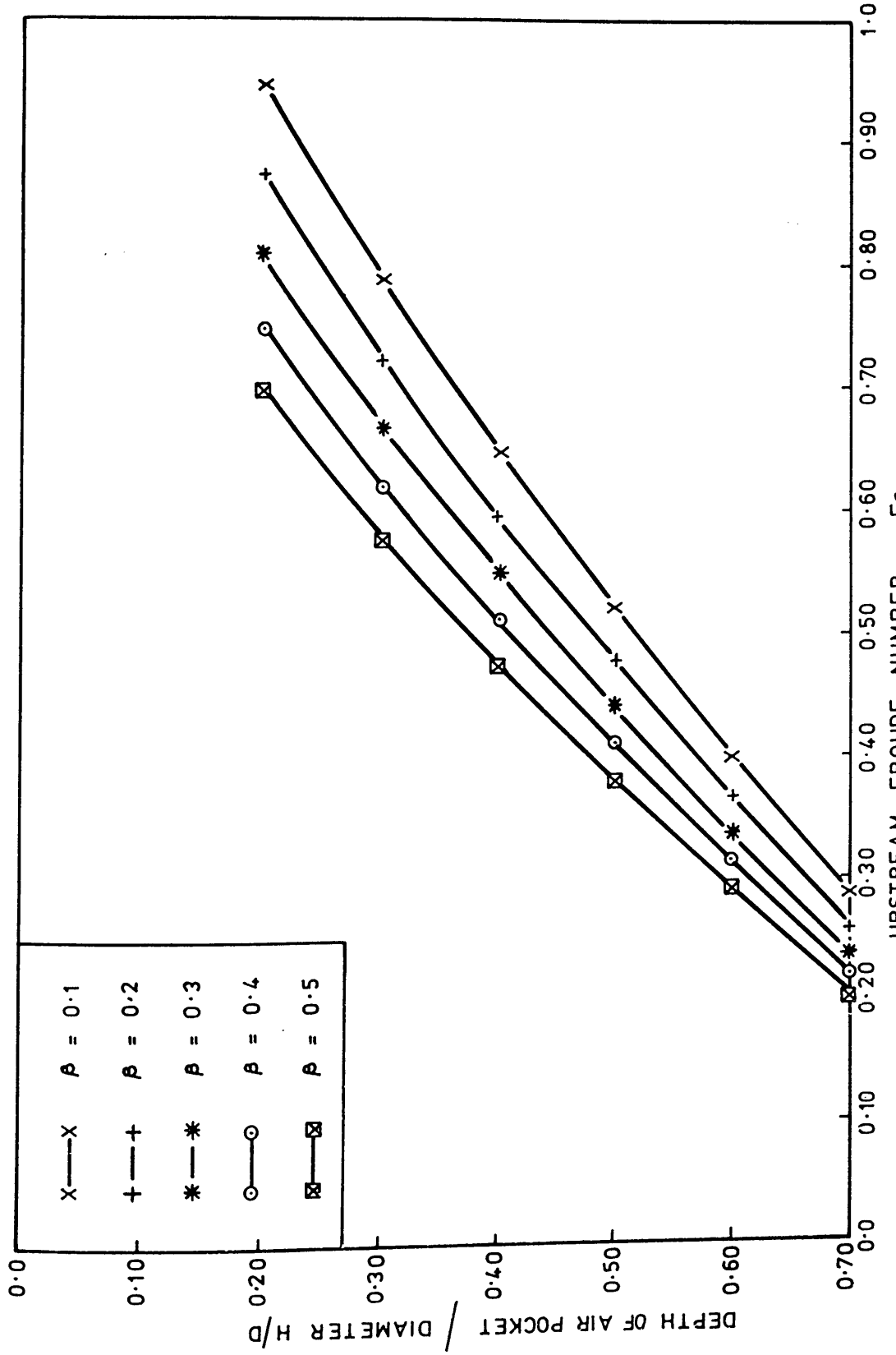

FIG. (3.23) THE STABLE HYDRAULIC JUMP FROM EQUATION (3.74) FOR THE SHARP BEND

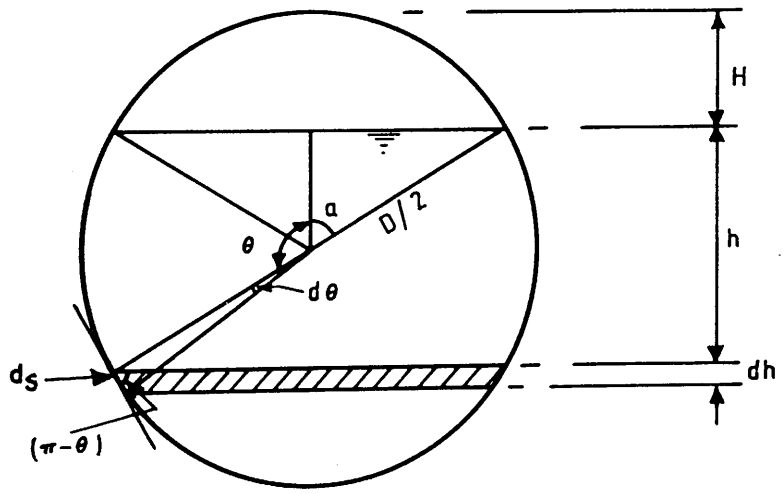

FIG. (3.24) ELEMENTS OF INTEGRATION FOR THE PRESSURE FORCE IN A CIRCULAR SECTION

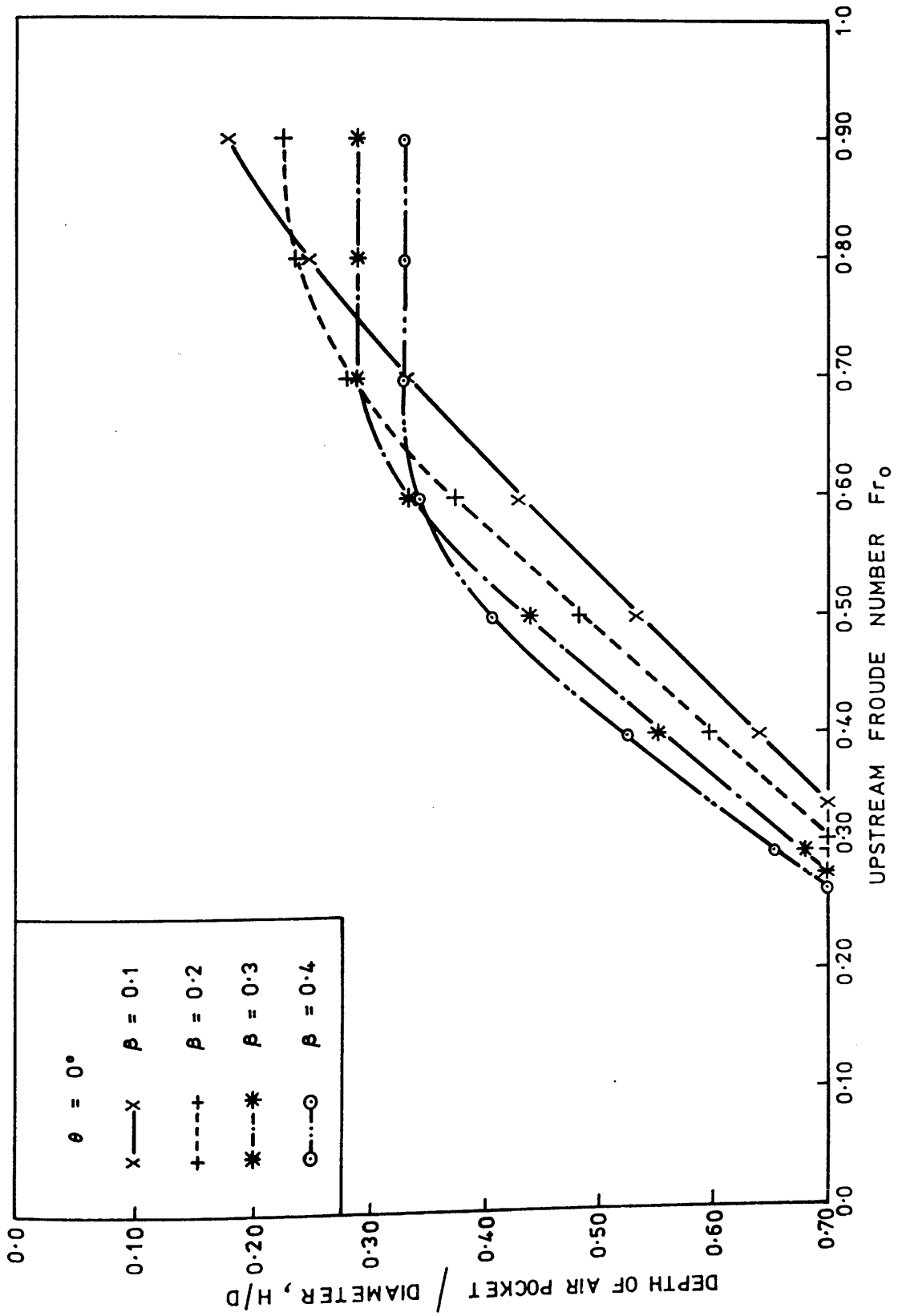

FIG. (3.25) THE STABLE HYDRAULIC JUMP FROM EQUATION (3.87) FOR HORIZONTAL TUNNEL

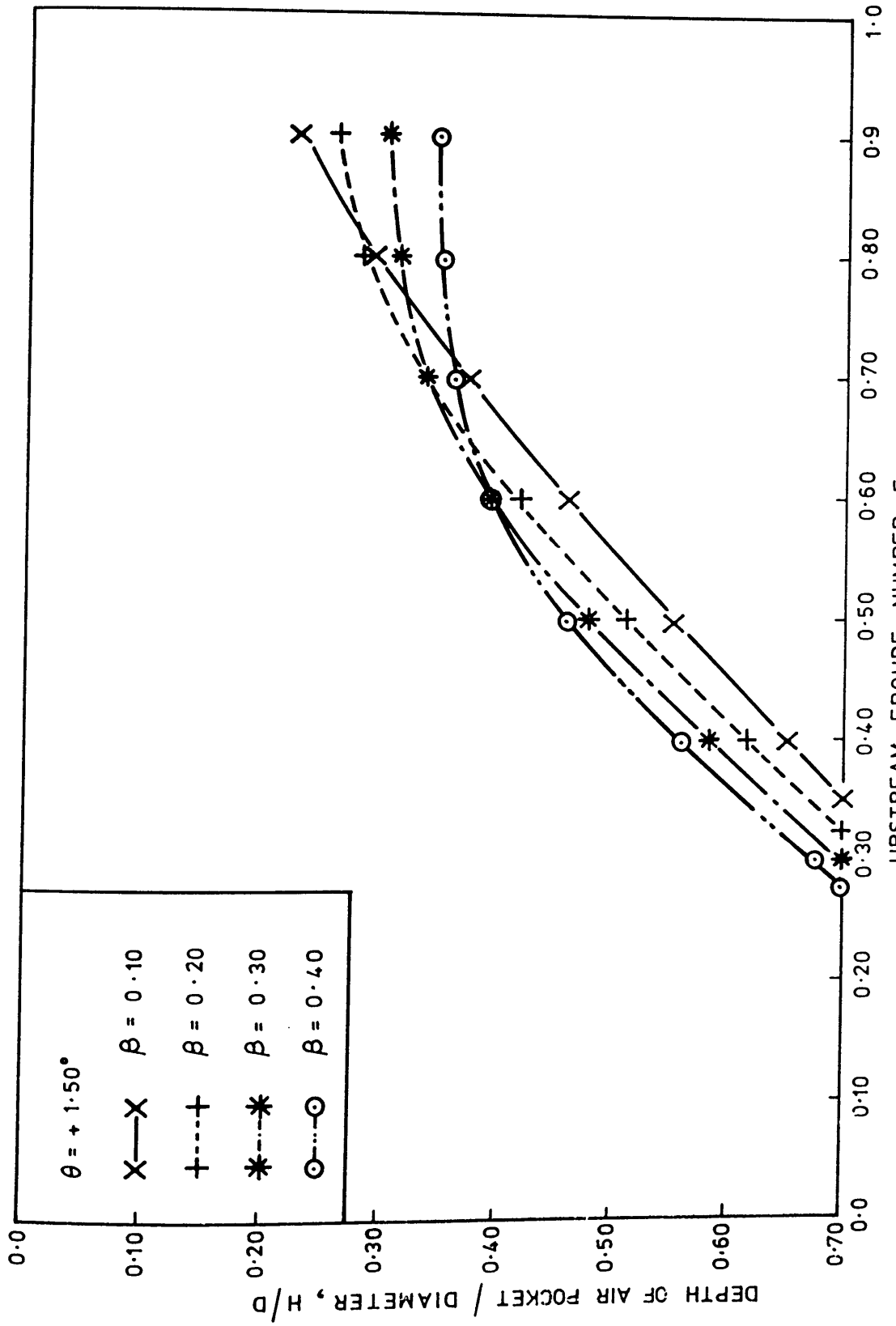

FIG. (3.26) THE STABLE HYDRAULIC JUMP FROM EQUATION (3.87) FOR AN UPWARD SLOPING TUNNEL AT AN ANGLE OF +1.5° WITH HORIZONTAL

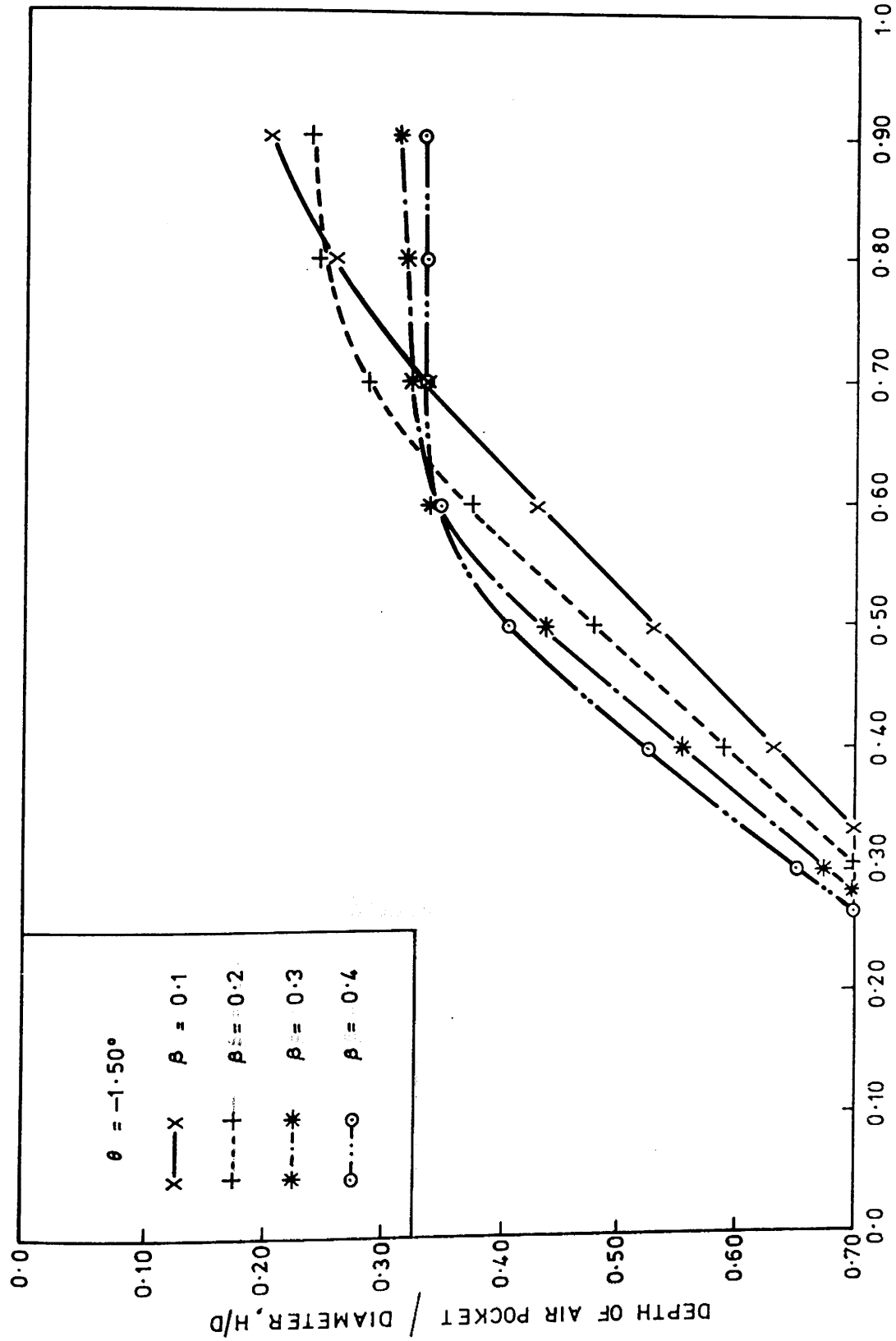

FIG. (3.27) THE STABLE HYDRAULIC JUMP FROM EQUATION (3.87) FOR A DOWNWARD SLOPING TUNNEL WITH AN ANGLE OF −1.5° WITH HORIZONTAL

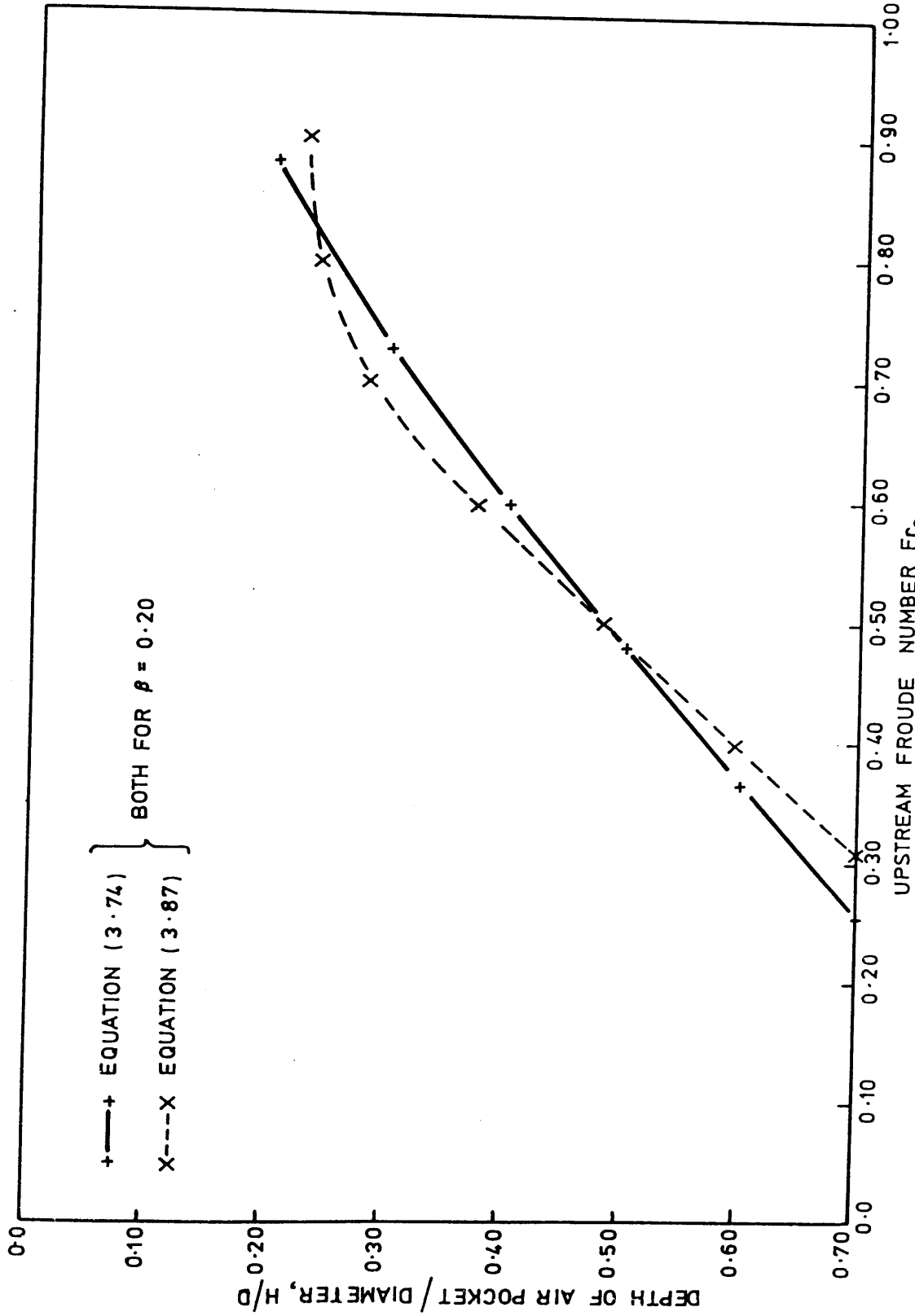

FIG. (3.28) COMPARISON BETWEEN ENERGY EQUATION AND FORCE MOMENTUM BALANCE FOR A STABLE HYDRAULIC JUMP IN A HORIZONTAL TUNNEL

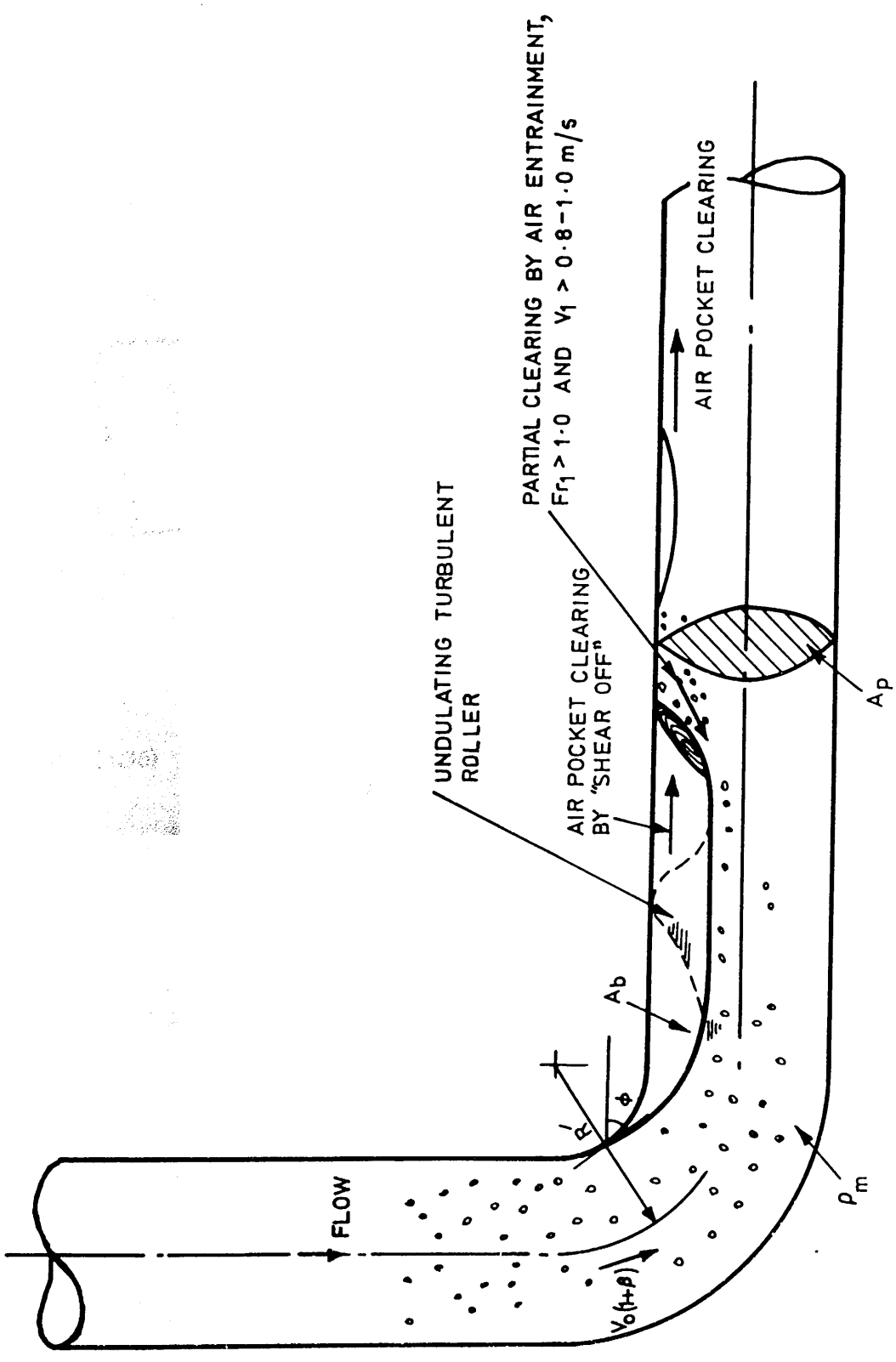

FIG. (3.29) THE DIFFERENT COMPONENTS OF CLEARING FOR MODEL TYPE 4

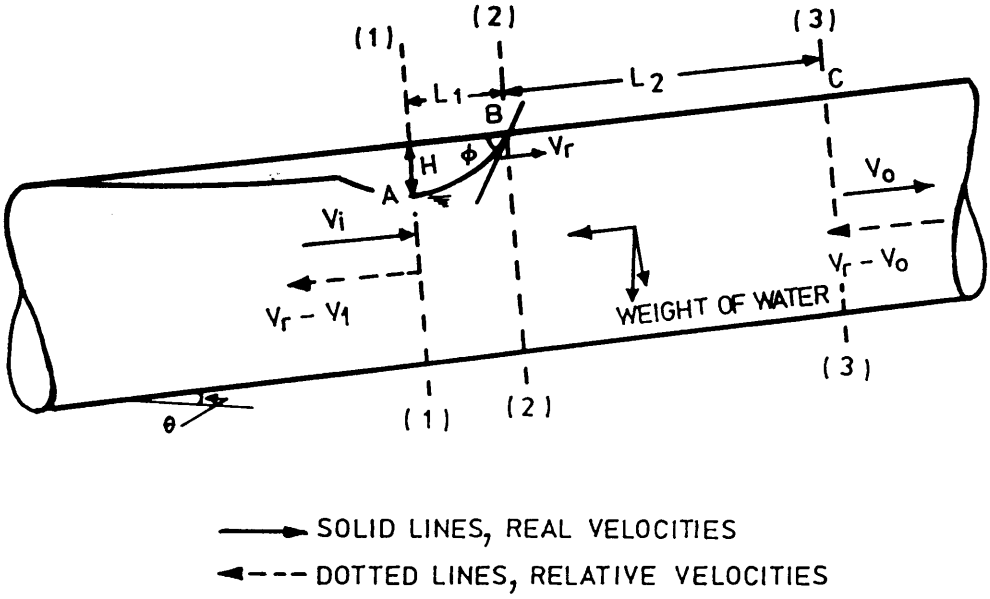

FIG. (3.30) THE MODEL FOR AIR POCKETS RISING IN A STRAIGHT PIPE FOR INCLINED ABOVE HORIZONTAL

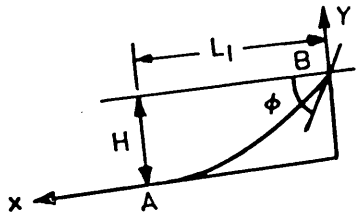

FIG. (3.31) THE PARABOLIC SHAPE OF THE AIR POCKET AT THE NOSE REGION

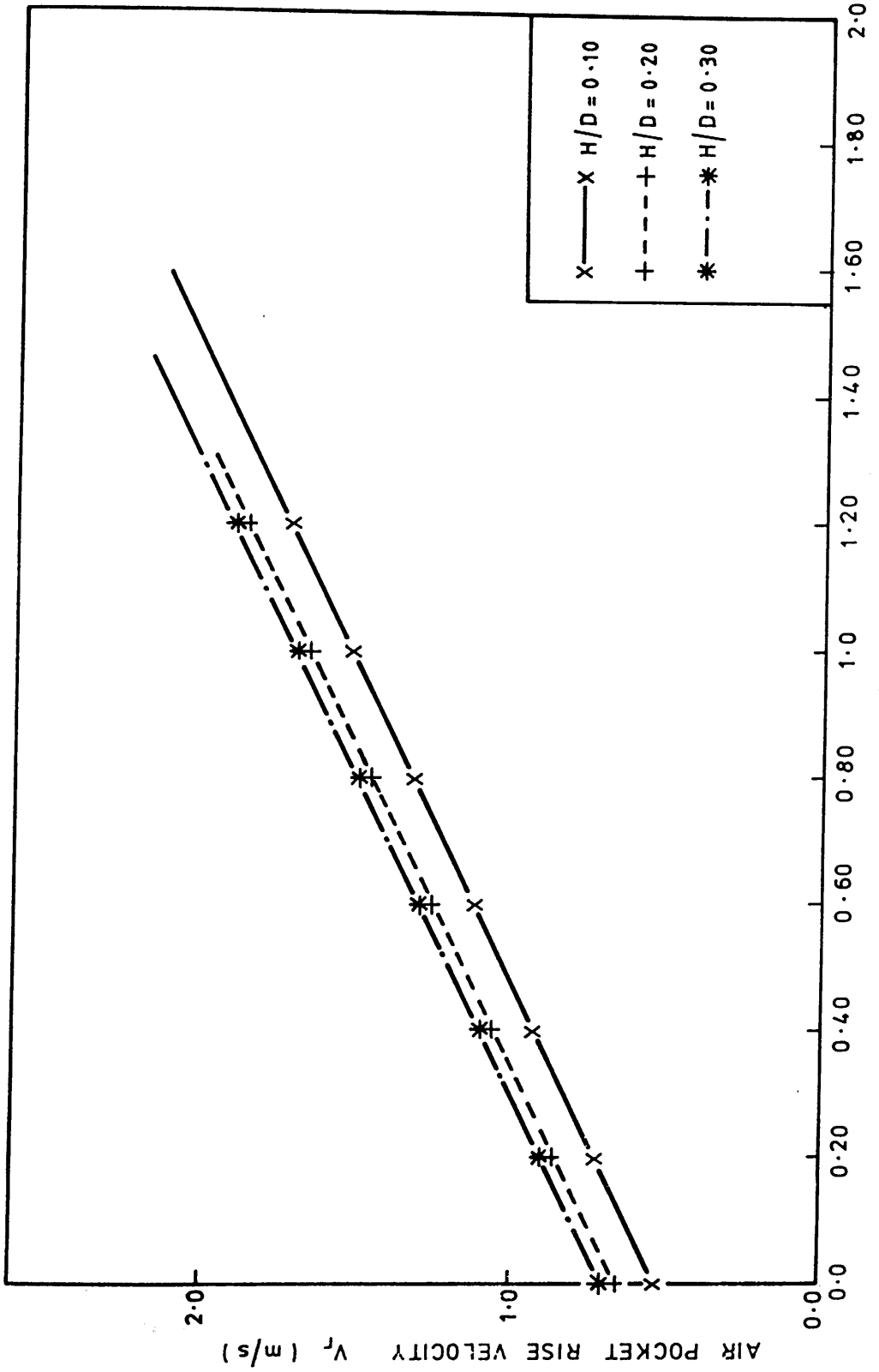

FIG. (3.32) THE RISING VELOCITY OF AIR POCKETS IN A STRAIGHT PIPE LAID AT AN ANGLE OF +1.5° WITH HORIZONTAL FOR DIFFERENT VALUES OF H/D

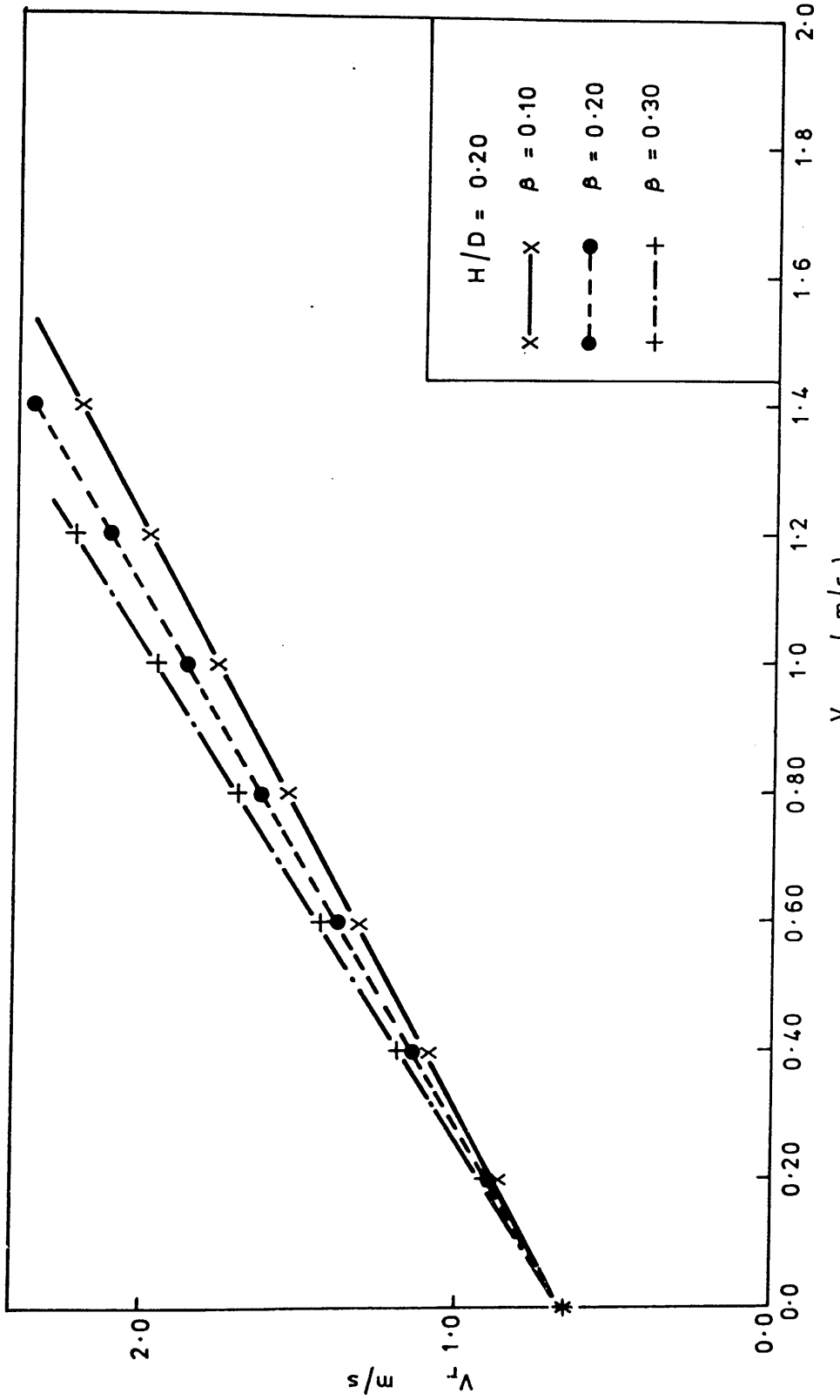

FIG. (3.33) THE RISING VELOCITY OF AIR POCKETS IN A STRAIGHT PIPE LAID AT AN ANGLE OF +1.5° WITH HORIZONTAL FOR DIFFERENT AIR/WATER RATIOS

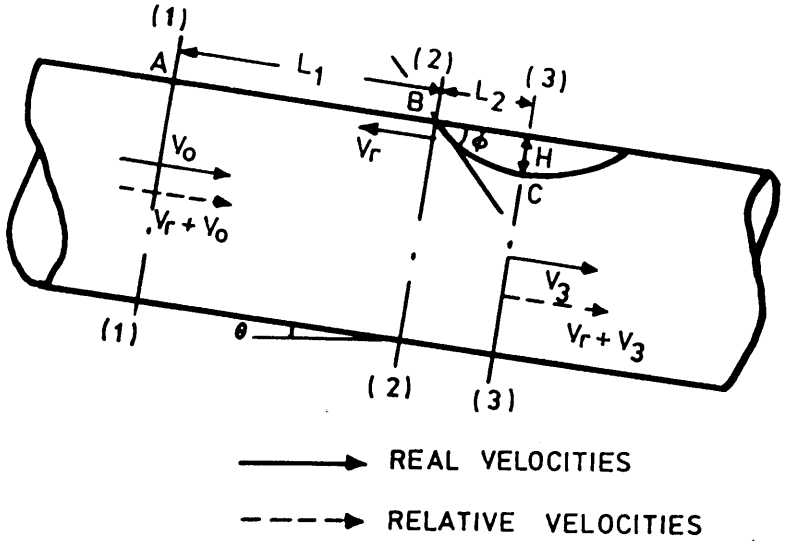

FIG. (3.34) THE MODEL FOR AIR POCKETS BLOWING BACK OR CLEARING IN A STRAIGHT PIPE INCLINED BELOW HORIZONTAL

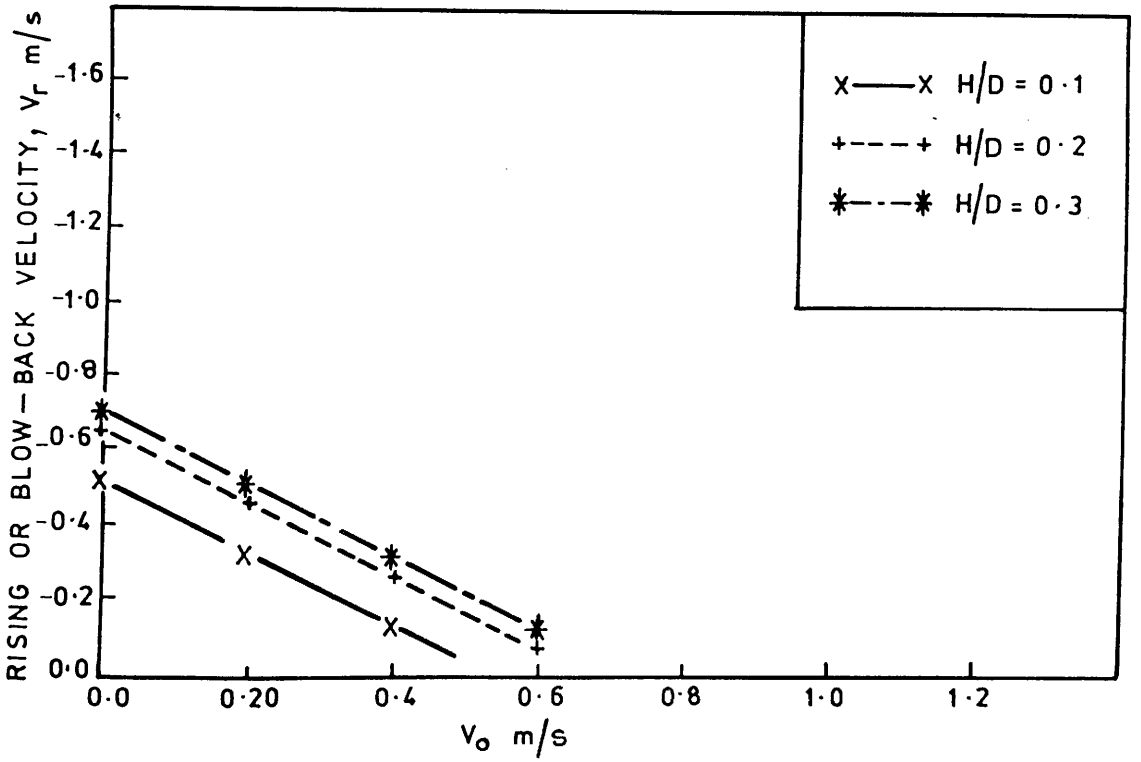

FIG. (3.35) THE RISING VELOCITY OF AIR POCKETS IN A STRAIGHT PIPE LAID AT AN ANGLE OF -1.5° BELOW HORIZONTAL, i.e. THE VELOCITY OF AIR POCKETS BLOWING BACK

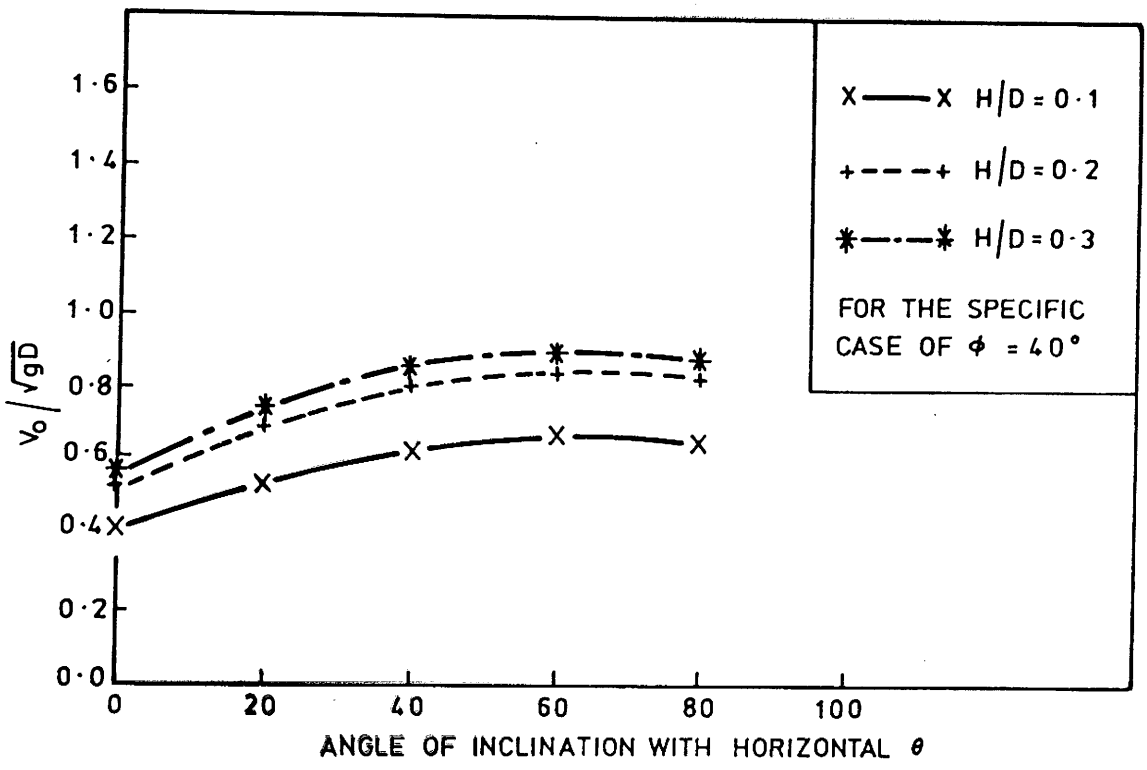

FIG. (3.36) NON-DIMENSIONAL WATER VELOCITY REQUIRED TO CLEAR AIR POCKETS IN STRAIGHT PIPES LAID BELOW HORIZONTAL

Chapter Four

DESIGN AND CONSTRUCTION OF EXPERIMENTAL APPARATUS

4.1 INTRODUCTION

The aims of this work can be summarised in the following three broad categories:

I To investigate the behaviour of air pockets forming at a dropshaft/tunnel junction

II To investigate blowback and clearing of air pockets in a straight pipe inclined slightly downwards

III To investigate air pocket movement in a straight pipe inclined slightly upward

Part I is by far the main thrust of the work, but nevertheless, it was intended to construct a physical model capable of covering all three areas. This was achieved in part by incorporating a facility which would allow the straight tunnel section, shown in Figs. (4.1) and (4.2), to incline upwards to an angle of 1.5° above the horizontal, to incline downwards to an angle of 1.5° below the horizontal, and also to be laid on the horizontal. By using this technique, Parts II and III could be investigated as well as Part I, albeit at a limited range of pipe slopes. The range of tunnel slopes, however, is generally within the range used in Engineering practice downstream of dropshafts.

It became obvious at the early stages of this work that physical modelling, combined with the development of simple

theoretical models, was the best way to investigate this phenomenon. The only available theoretical models dealing with air pocket behaviour generally were those developed by Benjamin[24] and Bacopolous[14], and in both cases concerned air pockets in straight pipes, in stationary water and inclined at small angles to the horizontal. Other more complex problems such as air pocket formation at a high point in a pipe line, downstream of a hydraulic jump or at dropshaft/tunnel junctions, have been treated by previous authors in the form of empirical correlations of experimental data. This approach has not been successful, producing a range of empirical correlations giving widely different answers to a particular physical situation. It was thus decided to pursue the physical model/theoretical model combination, with an awareness of possible scale effects in the physical model data[53].

4.1.1 Modelling Air Pockets at the Dropshaft/Tunnel Junction

Physical modelling of air pocket formation at a dropshaft/tunnel junction is dependent on an awareness of the cause of this pheomenon. High up in the dropshaft structure, water flows over a weir and commences to plunge down the dropshaft structure in the form of a nappe or jet. At some point in the dropshaft, the falling nappe impinges on the shaft full conditon, entraining small air bubbles, generally 1-8 mm diameter. If the upward air bubble buoyancy is overcome by downward drag forces from the flowing water, the air bubbles will descend the dropshaft and may be transported to the dropshaft/tunnel bend. On reaching the bend, the sudden change in direction (90°) usually gives rise to a flow separation at the upper side of the bend which may entrap air bubbles descending the shaft. The gradual entrapment of bubbles, due to this separation region and the natural bubble rise velocity to the roof of the tunnel, may often give rise to air pocket formation. Such air pockets usually extend in length and depth along the initial tunnel section and may remain trapped, blowback up the shaft, or be transported

along the tunnel section.

The depth of the air pocket forming at the bend is dependent on a range of geometrical and flow parameters as outlined in section (3.3.), and shown in Fig. (4.3), namely:

$$\frac{H}{D} = f(Fr_o, \beta, \frac{R'}{D}, \theta, \frac{V_{br}}{V_o}, Re, We) \qquad (4.1)$$

The latter three terms in equation (4.1) are scale effect terms. According to past research[192] the viscous and surface tension effects can be overcome in air pocket modelling if the pipe diameter is greater than about 150 mm. Thus our first criterion in the choice of physical model dimensions was that the dropshaft/tunnel diameter be greater than 150 mm. In this case, equation (4.1) effectively reduces to:

$$\frac{H}{D} = f(Fr_o, \beta, \frac{R'}{D}, \theta, \frac{V_{br}}{V_o}) \qquad (4.2)$$

Consider each of these parameters in turn. First, if the air pocket at the bend is considered a free surface flow, then we can conclude that the air pocket depth scales primarily on the Froude Number of the flow. That is, for a given β, V_{br}/V_o, angle of inclination and geometry. Thus the physical model in this work can be considered as a Froude Scale model. Secondly, the value of β is the ratio of air flow to water flow and of necessity is not scaled properly in a Froude model[53]. Thus it was decided that air injection into the system would be carried out independently of the water flow, thus allowing a range of air/water ratios to be investigated up to and beyond the typical prototype range. This implies further, that natural air entrainment by the plunging nappe would not be allowed because of the lack of control of the air/water

ratio approaching the bend. Thus a system would be devised whereby the water flow would enter the dropshaft (but not by plunging nappes) and that air flow would be injected independently, in air bubble sizes found in nature. This was achieved in practice (Fig. 4.2) by allowing the water to enter the dropshaft via a 45° angle piece under pipe-full conditions. Air was injected just upstream of the 45° entry piece and the air bubbles were subsequently broken down into their proper sizes by intense turbulent mixing at the junction of the dropshaft and the 45° inlet pipe. In this manner the value of air/water ratio approaching the bend could be controlled independently.

The non-dimensional bend radius R'/D was thought to be an important geometrical factor in determining air pocket behaviour at the dropshaft/tunnel bend. It had already been noted by Goldring[65] that the value of R'/D had a significant effect on, (a) the degree of separation at the upper part of the bend, (b) the development of secondary currents at the bend, (c) the degree of swirl in the flow under the air pocket, (d) the position of the upstream nose of the air pocket at the bend, (e) the velocity and pressure distribution at the bend, and (f) the flow conditions determining both blowback and clearing of the air pocket. It was thus decided to investigate three values of R'/D ranging from 0.5 (a completely sharp 90° bend) to 1.5, which is the R'/D value installed at Hunterston 'B' Power Station. An intermediate case of R'/D of 1.0 is also to be investigated.

The inclination of the tunnel section downstream of the bend (θ) was also thought to be influential in determining air pocket behaviour at the bend. It would seem logical that a tunnel section sloping in the downward direction after the bend, as the case of Hunterston 'B' Power STation, would produce a tendency for air pockets to blowback and greater difficulty in transporting air pockets along the tunnel section to the outlet. Conversely, a tunnel section sloping slightly in the upward direction may produce air pockets with

less tendency to blowback up the dropshaft and greater tendency to be transported downstream along the tunnel section. It was decided to investigate three tunnel inclinations to the horizontal, (I) an upward slope of +1.5°, (II) completely horizontal $\theta = 0°$, and (III) a tunnel section sloping downwards at -1.5° to the horizontal. It was thought that this range of conduit slopes would adequately cover typical inclinations found in practice, such as Kielder Transfer works[44] where $\theta = +0.117°$, and Hunterston 'B' Power Station[112,165] where $\theta = -0.286°$.

Modelling the parameter V_{br}/V_o in equation (4.2) is a much more difficult proposition. This parameter is the ratio of the air bubble rise velocity to the water velocity and can only be scaled properly using "scaled-down" bubble sizes, which is not feasible. The other alternative is to investigate behaviour at the bend using models at different scales. This would mean that V_{br}/V_o could be varied independently of Fr_o , β , $\acute{R}/D$, and θ. However, at least three model scales would be required, and this would mean considerable extra experimental work to cover the other model scales. This course of action was not adopted. Instead, in view of the amount of experimental work to be carried out, only one model scale was used and estimates of the influence of V_{br}/V_o could be obtained from other research data and the limited amount of prototype data available. V_{br}/V_o is a useful parameter, as it is a measure of the proportion of air approaching the bend which is trapped in the bend air pocket and also what proportion of air bubbles by-pass the air pocket by transport under the air pocket.

In summary, the following general requirements would be needed for physical modelling of air pockets at the dropshaft/tunnel junction:

(I) The dropshaft and tunnel should be of diameter greater than 150 mm to avoid substantial viscous and surface tension effects.

(II) Independent air injection is required to cover a wide range of air/water ratio (β), independently of the water flow.

(III) Geometrical parameters of the bend radius ($\acute{R}/D$) and tunnel slope (θ) should be varied over a range of at least three values respectively.

(IV) The air pocket depth (H) and the air pocket length (L) should be measured for every single test. This, in fact, necessitated the use of special water depth probes at the bend to be described in (4.3.2).

(V) In theory, the most complete picture of this phenomenon would be obtained by testing various model scales. This objective was not pursued.

(VI) Given the pipe diameter it was considered necessary to provide a large water discharge 50-60 ℓ/s, to produce a wide range of velocities (V_o), and pipe full Froude Numbers (Fr_o). The upper limit pipe full velocity was of the order 2.5 m/s and the upper limit pipe Froude Number around 2.05.

4.1.2 Modelling Air Pocket Behaviour in Straight Tunnel Sections

It has been mentioned in section (4.1) that two ther aspects of air bubble behaviour have been chosen for investigation in this thesis. (a) Air pocket behaviour in the flowing water conditions for a pipe inclined slightly upward, and (b) blowback and clearing in a straight pipe inclined slightly downwards. Both of these cases have received some experimental consideration in the past but, as yet, neither has been the subject of theoretical investigations. It was decided thus to obtain some experimental data to compare with

theoretical models. The following general model requirements were considered necessary:

(I) The pipe again should be greater than 150 mm diameter to avoid viscous and surface tension effects.

(II) The straight tunnel section should be as long as possible. This was governed by the space available in the laboratory and a final straight length of 8.33 m was used.

(III) At least two special air pocket depth probes would be required to measure air pocket speeds between any two points along the tunnel, to measure the maximum depth of a passing air pocket H, and to record the exact shape of a passing air pocket.

(IV) Other considerations, such as independent air injection and different model scales, were also thought to be an advantage, although different model scales were not used.

(V) Again, water discharges up to about 50ℓ/s were considered necessary to provide pipe full velocities up to 2.50 m/s and pipe full Froude Numbers up to 2.05.

(VI) The independent air injection system would also require air flow capacities up to 20-30 ℓ/s to give an air/water ratio of 0.50 at maximum water discharge values.

4.2 DESIGN AND CONSTRUCTION OF EXPERIMENTAL APPARATUS

The experimental model is a recirculating system where the

water is pumped from the sump tanks to the inlet to the vertical shaft through P.V.C. pipes of 152 mm inside diameter. This is shown in plan view in Fig. (4.1). A 152 mm diameter butterfly valve is connected before the pump as a safety device in case of any leakage and to isolate the pump for repair and maintenance work. A gate valve is connected after the pump to control the water discharge from the pump. Plate (4.1) shows the connection between the butterfly valve, the pump and the gate valve. Downstream from the gate valve at a distance of about 3750 mm, the orifice plate meter is connected to measure the water discharge. The main part of the model is the vertical dropshaft and tunnel system which was built using perspex pipes because visual measurement is required as well as instrumentation measurements. This is shown in Fig. (4.2). The inlet to the vertical shaft is a 45° perspex piece which is connected to the main pipe from the pump by a flexible piece of pipe to avoid the strain on the perspex flanges which can be caused by not having an exact alignment for the two pieces of pipes. At the end of the tunnel section another 152 mm butterfly valve is connected for safety and control of the water level in the vertical dropshaft. The outlet tank has a side weir to allow water to return again to the sump tanks to obtain a complete circulation for the model. Figures (4.1) and (4.2) show a plan and a section through the model. The upper limit of water discharge through the system is around 50 ℓ/s (0.05 m^3/s).

4.2.1 Tunnel and Shaft Construction

The tunnel and the dropshaft were constructed using perspex pipes of 152 mm inside diameter. Each section of pipe is 3000 mm long with an outside diameter of 164 mm. The inside and outside diameters were checked for each pipe section used, to obtain an accurate mean value of both the inside and the outside diameter. The vertical dropshaft was constructed using five pieces of perspex pipes, as shown in Fig. (4.2), with a total height of 2225 mm. The fifth piece at the bottom of the shaft is a part of the bend

connecting the vertical dropshaft to the tunnel. The central piece is a part of the 45° Y-piece manufactured to allow the water to flow into the vertical dropshaft. Details and dimensions of the Y-piece inlet are shown in Fig. (4.4).

The tunnel was constructed using three equal lengths of the perspex pipe, each 2400 mm long. Two extra pieces of the perspex pipe each 150 mm long were also connected to the tunnel, where each piece was manufactured so that a probe, connected to the wave monitor, can be inserted through the top of that piece to measure the water depth at the centre of the pipe. Each 150 mm long piece can be connected at the end of any of the three 2400 mm long pipes forming the tunnel. This enabled air pocket measurements at various locations along the tunnel. At the end of the perspex tunnel a flexible pipe is used to connect the tunnel to the outlet butterfly valve. This enabled the inclination of the tunnel section to be changed from +1.5° to -1.5°. The butterfly valve at the end of the tunnel is used as a safety device and if necessary to act as a control for the water level in the vertical dropshaft. Plate (4.2) shows the connection of the perspex tunnel to the outlet tank. The total length of the tunnel section was about 8415mm.

At each end of each length of perspex pipe, a flange was placed and glued in position. Each flange was manufactured in the laboratory by using 12 mm thick perspex sheets with 153 mm and 210 mm inside and outside diameters respectively. Sixteen holes were drilled through each flange, each hole is of 7 mm diameter on 190 cm PCD. Figure (4.5) shows a typical design and dimensions of a perspex flange. To ensure that all the connections were watertight, rubber gaskets were cut to the same dimensions as the perspex flanges and placed between the flanges before screwing them together. Great care was taken to ensure smooth inside edges to the flange connections so that air pockets will not be disturbed when moving past these sections.

A measuring tape was fixed along the entire tunnel length to measure the length of the air pocket which forms at the bend junction, and indeed to measure air pocket lengths at any point along the tunnel section.

Air pocket depths were measured using a combination of air pocket probes (to be described in section 4.3.2) and also measuring tapes placed around the pipe/tunnel perimeter at various locations along the tunnel length. To achieve accurate positioning and calibration of the measuring tapes, each length of pipe was sub-divided into quadrants by marking tangent lines at the top, bottom and centre-line of the pipe. This measuring scale was designed to get a visual measurement of the water depth at any section of the tunnel. The outside pipe diameter was used to get the length of the perimeter for the measuring tape, then the equivalent length for each millimeter of air pocket depth was marked on the tape. This procedure was done for the whole depth along the outside diameter until a complete measuring scale was developed. Calculations were done to allow for the pipe wall thickness and hence a direct measurement technique was developed for air pocket or water depths. A typical measuring tape is illustrated in Plate (4.3).

4.2.2 Design and Construction of the Dropshaft/Tunnel Bends

Referring to the work carried out by Goldring[65], as already discussed in section (4.1), the bend radius has an effect on the flow depth under the air pocket forming at the bend and also on the process of air pockets venting back up the shaft and clearing along the tunnel section. Hence it was decided to investigate the effect of three different bend radii of R'/D = 0.50, 1.00 and 1.50. D is the inside pipe diameter and R' is the radius of curvature of the bend measured to the centre line of the pipe. In practical terms, only two radiused bends were used of R'/D=1.0 and 1.5 and one mitre bend.

The bends were manufactured using the same perspex pipe used

for constructing the dropshaft and the tunnel. The first bend manufactured is with a radius $\acute{R}/D = 0.5$, which is a single mitre sharp edge bend, as shown in Fig. (4.6) and Plate (4.3). This bend consists of two pieces of perspex pipe, each piece cut to form a 45° with one side of the pipe and a 135° with the other side of the pipe. Then the two pieces are glued together forming a smooth surface inside the bend to reduce the turbulence which may form due to irregularities at the pipe walls. A perspex flange was glued to the inlet and outlet of the bend for easy connection to the dropshaft and tunnel sections.

The second bend has an $\acute{R}/D$ value of 1.0, where $\acute{R}$ is the length of the radius forming the bend which extends from the centroid of a circle to the centre line of the pipe. The main part of the bend was manufactured by using six identical segments of the perspex pipe. This is shown in Fig. (4.7) and Plate (4.4). The 90° angle between the dropshaft and tunnel section was divided into six segments, which means that a 15° angle must form between the two sides of each segment at the centroid of the bend radius. The radius for the bend of $\acute{R}/D = 1.0$ was $\acute{R} = 152$ mm, which implies that every segment will have an 18 mm inside width and 62 mm outside width. The six pieces were cut to the above sizes and glued together to form the bend. Then an extra two perspex pieces with a flange at one end were glued to the two sides of the bend thus forming the connection with the dropshaft and tunnel sections.

The third bend is with $\acute{R}/D = 1.50$, where the radius $\acute{R}$ is 228mm. This was chosen to give the same configuration as the Hunterston 'B' Power Station. This was also manufactured by using six identical segments of perspex pipe each forming a 15° angle between the sides at the centroid of the bend. In this case the width of each segment was 38 mm at the inside bend and 82 mm at the outside bend. Again two extra pieces of perspex pipe were fitted at the end of each side of the bend to place it in position between the dropshaft and tunnel sections. Figure (4.8) and Plate (4.5) show

details and dimensions of the third bend with R/D = 1.50.

It must be mentioned that the accuracy in manufacturing these 90° bends was within ± 30'. At this stage it was debated as to whether a further six bends would have to be manufactured, three for the upward sloping tunnel angle +1.5° and three for the downward sloping tunnel angle -1.5°. This course of action was rejected in favour of simply inserting a small tapered piece of perspex for tunnel angles other than horizontal. Hence it was decided to use the same three bends for the other two angles of tunnel. This method will be outlined in section (4.2.9) with the reasons for using it and to what extent it can affect the experimental results.

4.2.3 Sump Tanks

Two galvanised steel tanks were used as sump tanks with a total capacity of 4.54 m^3. These are shown in plan in Fig. (4.1). The size of each tank is 1.86 m x 1.22 m x 1.0 m. A connecting hole of 400 mm diameter was cut into each tank, flanged on either side of the hole and the two tanks were thus connected together at this orifice with a rubber gasket placed between the flanges for water-tightness. The tanks were positioned, as shown in Fig. (4.1), and a further hole of 150 mm diameter was cut into one of the tanks to take the pipe connection from sump tanks to the pump. A butterfly valve was fitted to the 150 mm diameter connection for the purpose of isolating the sump tanks from the pump during maintenance. A small length of pipe about 1 m long was used as the connection between the butterfly valve and the pump. The general arrangement for this part is shown in Plate (4.1) and Plate (4.8).

4.2.4 Pump

It was decided to use a pump with an effective upper limit

flow capacity of 60 ℓ/s (0.06 m^3/S). To select a suitable pump the head losses through the system were estimated. Consideration was given to all the losses through the pipe bends, sudden expansion, orifice plate meter, gate valve, butterfly valves, entrance and exit losses and the frictional losses through the pipes. The head loss was approximately 4.5 m at discharge 45 ℓ/s. The static head required by the pump was taken as 0.5 metres. The most suitable available pump was chosen as MYSON MSK 150-4210 centrifugal pump, and its characteristics are shown in Fig. (4.9).

The chosen pump operates at a constant speed, thus a control device for the discharge had to be introduced after the pump. Also the chosen pump had to be operated under a positive upstream head. This was considered in the design of the sump tanks, where the water level in the sump tanks was not allowed to drop to less than 150 mm above the crown of outlet pipe to the pump. This was necessary to avoid vortices at the intake which will entrain air into the pump and reduce its efficiency.

4.2.5 Gate Valve

It was noted in the previous section that the chosen pump operates at one speed only, and hence a control device is required downstream of the pump. A 150 mm gate valve was connected to the downstream side of the pump, which allows it to control the discharge through the system. The gate valve is shown in Plate (4.1).

A 150 mm diameter P.V.C. pipe of 3.50 m length was connected to the downstream end of the gate valve. It incorporates an orifice plate at a distance of 3.75 m downstream the gate valve. The orifice plate was used to measure the total water discharge and its design is given in section (4.2.7).

4.2.6 Outlet Tank and the Side Weir

To provide a complete recirculation of water, the downstream end of the tunnel system is connected into an outlet tank which in turn is provided with a side weir to allow the water discharge to overflow back into the sump tanks. The size of the galvanised outlet tank is 1.230 x 1.230 x 1.230 m with an opening in its side of 700 x 300 mm for the side weir. This is shown in plan in Fig. (4.1) and in elevation in Fig. (4.2). The tank was placed in position on two I-beams of 210 mm height to allow tilting of the tunnel section without changing the height of tank. The details of the outlet tank and its connection with the tunnel are shown in Plate (4.2) and Plate (4.7). A 25 mm diameter connection was made in one side of the outlet tank and fitted with a vertical perspex tube to allow accurate measurement of the tank water level. A graduated scale was provided on this tube.

The length of the side weir was determined after carrying out initial calculations for the height of water over the weir for different weir lengths. The weir used is a sharp crested weir where the following equation was used to determine height of water for different weir lengths:

$$Q_w = C_d L h^{3/2} \qquad (4.3)$$

where Q_w = water discharge, m^3/s

L = length of weir, m

h = depth of water in the tank above the weir, m

and C_d = coefficient of discharge

The maximum discharge expected in the experimental work was 50 ℓ/s. Initially a value of C_d of 1.8 was chosen for calculations of the most suitable weir length. Table (4.1) contains the results for the depth of water over the weir for different weir lengths.

Table (4.1): Depth of water over the weir for different weir lengths

Q_w	h (m)					
m^3/s	L=0.50m	L=0.60m	L=0.70m	L=0.80m	L=0.90m	L=1.00m
0.005	0.0313	0.0277	0.0250	0.0229	0.0212	0.0197
0.01	0.0497	0.0440	0.0397	0.0363	0.0336	0.0313
0.015	0.0651	0.0577	0.0520	0.0476	0.0440	0.0410
0.020	0.0789	0.0699	0.0631	0.0577	0.0533	0.0497
0.025	0.0916	0.0811	0.0732	0.0669	0.0619	0.0577
0.030	0.1034	0.0916	0.0826	0.0756	0.0699	0.0651
0.035	0.1147	0.1015	0.0916	0.0838	0.0774	0.0722
0.040	0.1253	0.1110	0.1001	0.0916	0.0847	0.0789
0.045	0.1356	0.1200	0.1083	0.0991	0.0916	0.0854
0.050	0.1454	0.1288	0.1162	0.1063	0.0983	0.0916

From Table (4.1) a weir length of 700 mm was chosen. The weir was manufactured using a 6 mm thick aluminium plate which was cut to the size 700 mm long and 300 mm deep. The bottom of the weir was hinged to the opening cut into the tank, and its top edge was connected to a screwed rod connected to the top of the outlet tank. This rod had a revolving wheel to allow raising and lowering of the weir according to the required water level in the dropshaft. An aluminium apron was

fixed to the tank opening to provide a watertight fit at the weir edges when tilting the weir. Fig. (4.10) shows experimental data for the actual stage-discharge curve for the 700 mm weir after instalation. The relationship is given approximately by $Q_w = 2.09L\ h^{3/2}$.

4.2.7 Orifice Meter

To measure the water discharge efficiently and accurately, it was decided to use one of the devices outlined in BS1042:Part 1, 1964. It was found that the simplest device to fit was the orifice plate meter with pressure tappings at a distance of D and D/2 upstream and downstream from the orifice plate, where D is the inside diameter of the pipe.

The orifice plate is essentially a circular disc with a hole of known diameter at its centre. The orifice plate is inserted into the pipeline acting as a contraction to the flow, and producing an energy or head loss after the flow passes through the throat of the orifice plate. This energy loss can be conveniently measured on a manometer by measuring the pressure difference between the two pressure tappings upstream and downstream of the orifice plate. According to BS1042, Part 1, 1964:

$$Q = 0.01252\ CZ\epsilon Ed^2 \sqrt{\frac{h}{\rho_w}} \qquad (4.4)$$

where Q = the discharge through the orifice in m^3/hr

C = basic correction coefficient

Z = Reynolds Number correction factor

ϵ = the expansibility factor which for incompressible flow can be taken as 1.0

E = velocity of approach factor

h = the difference in pressure (in mm water) between the upstream and downstream pressure tappings at the orifice plate

ρ_w = the density of water, and

d = the diameter of the orifice throat

The following values for each parameter are given below after calculating their values using the methods specified in BS1042, Part 1, 1964:

ρ_w = 998 Kg/m^3
C = 0.6064
Z = 1.02
E = 1.206
d = 114 mm
ϵ = 1.0

The orifice plate details are shown in Fig. (4.11) and Plate (4.8). The orifice plate throat diameter was taken as 114 mm as it was considered important to obtain a reasonable head difference h over a wide range of discharge. If the water manometer was used to measure discharges in excess of 40 ℓ/s, then the expected value of h would be around 2000-3000 mm. It was therefore decided to utilise two manometers, one containing water for the measurement of low discharges, and the other containing mercury for measuring high discharges. Both manometers are shown in Plate (4.9).

An important point of consideration in the design of the orifice plate is the required distances upstream and downstream from the orifice plate to another device such as a pipe bend or a gate

valve. The minimum distance required downstream from the orifice plate is 7 pipe diameters, which is equivalent to 1.02 m. This requirement was satisfied. However, the minimum distance required upstream depends on the gate valve opening. When the gate valve is 3/4 closed the required distance to the gate valve from the orifice plate is 60 pipe diameters, which is equivalent to 9.06 m. When the gate valve is fully open the required distance is 27 pipe diameter or 4.05 m. Unfortunately neither requirement could be satisfied since the maximum available distance between the gate valve and the orifice was 3.75 m. It was decided to overlook this problem and take extra care in the calibration check on the orifice plate in its final position.

Calibration of the orifice plate was carried out by measuring the volume of water drawn from the 4.5 m^3 sump tanks in a given time. This time was short enough to prevent any water from recirculating through the system and back into the sump tanks. The levels in the manometers were read and the discharge measured from the drawdown in the sump tanks. The results of a number of such tests are shown in Fig. (4.12) and it can be clearly seen that for a wide range of discharges the orifice plate prediction of the discharge (equation 4.4) compares very well with the measured discharge. On the basis of these results, the orifice plate was considered a satisfactory flow measurement device in the system.

4.2.8 Design of Air Inlets

It has been noted in section (4.1) the importance of providing an air injection system independently of the water flow. This allows substantial control of the ratio of air flow to water flow (β) descending the dropshaft towards the bend. It is also important that the air enters the water flow generating small bubbles of dimensions found in nature, say, of the order 2-5 mm.

Air is injected into the system using an air blower. From the outlet of the air blower air flows through the air flow rotameters for measurement of air flow and then to an air chamber. The air chamber is used to achieve a uniform distribution of air to all sixteen air inlets before entering the water flow. The air chamber was manufactured using a piece of the perspex pipe used for building the dropshaft/tunnel system. Two blank flanges were fitted to the two ends of this piece, and a hole of (25.4 mm) diameter was cut through the top for the air coming from the air flow rotameters. Through the bottom flange sixteen holes each of 5 mm diameter were cut, to which sixteen 5 mm plastic tubes were connected at one end, and at the other end were connected to the injection points into the system. This is shown on Plate (4.10). The injection points were sixteen holes each 5 mm diameter drilled through a flange manufactured using a 24 mm perspex sheet. These holes were distributed uniformly around the perimeter of the flange. The main reasons for using the 5 mm injection points around the flange is to obtain even distribution of air at the water inlet. Also the use of 5 mm injection points means that the resulting injected air bubbles were of a size suitable for this type of work. Just downstream of the air injection point, the air bubbles were broken down by turbulent mixing into sizes 2-5 mm found in nature. This process occurred at the 45° Y-piece already discussed in section (4.2.1).

4.2.9 Tilting the Tunnel

The tunnel was supported along its length using six wooden supports, two at each end of pipe length used in constructing the tunnel. It was decided to use simple supports which could be manufactured by cutting wood to the required height of tunnel for each angle of tunnel tested. The first angle of tunnel was the horizontal, and the height of the supports was 390 mm to the pipe centre line. The longitudinal elevation along the tunnel was

checked by using a level and a staff. To change the angle of tunnel to +1.5° and -1.5°, it was required to adjust the height of supports and also to change the bend at the junction of the dropshaft/tunnel system. The bend was modified to incorporate the upward and downward sloping tunnel sections by the simple expedient of inserting a tapered perspex flange having the same angle as that required for the tunnel. The flange was fitted just before the bend which means that the dropshaft will stay in the vertical position and only the tunnel supports will require adjustment. Also the same flange can be used for getting an upward and downward tunnel slope by turning the tapered flange through 180°. The flange was manufactured using a 24 mm perspex sheet, cut to the same dimensions as the other pipe flanges, and then tapered along one surface in one direction to an angle of 1.50°. Bolt holes were drilled in the perspex flange and it was placed in position between the dropshaft and the bend. The angle of the tunnel then was checked using a level and staff as before to ensure that the required angle was obtained along the whole tunnel length. Details of the horizontal tunnel and the upward and downward slopes of tunnel are shown in Plates (4.11), (4.12) and (4.13) respectively. It can be noted that changing the tunnel angle was done at the upstream end of the tunnel not at the outlet tank end.

4.2.10 Inserting the Air Pocket Probes

At the outset of the experimental work it became apparent that reliable data was required for the air pocket depth, length and shape, both of the dropshaft/tunnel bend and also for the movement of the air pockets along the tunnel section. Research of the market revealed that the cheapest and most efficient way of achieving this was the use of Churchill Wave Monitor Probes connected to chart recorders. These probes essentially give an instantaneous reading of water level in an open channel or pipe. For instance, a probe could be inserted at the dropshaft/tunnel bend to give an

instantaneous reading of air pocket depth, and could also be used further along the tunnel section giving an accurate trace of the shape of a passing air pocket.

The probes consist of a pair of stainless steel wires, 1.5 mm diameter and spaced 12.5 mm apart. Details of the probe will be given in section (4.3.2), while here the method of inserting the probes will be given. Since the tests are done using closed conduit, a proper insertion of the probes is required because the system will be operating under high head of water which can cause the probes to blow out of position. It is thus necessary to get a water and airtight insertion of the probes to prevent leakage of water from the tunnel and to prevent extra air entering the system. The other point to be considered is that the position of the probes can be changed as required for each type of test. It was decided to insert each probe in a separate piece of perspex pipe which can be placed at any position along the tunnel. This piece is 150 mm long with two flanges at both ends to connect it to the tunnel section, as shown on PLate (4.14). A hole of 50 mm diameter was cut at the top of this 150 mm long section and a small perspex pipe with a small flange at one end was glued to this hole through which the probe will be inserted. A rubber bung was used to seal the hole and to insert the probe. The rubber bung was cut into two halves and two slots were cut on each half for placing the probe wires. The two halves of the bung were glued together for sealing after choosing the exact depth of immersion for the probe in the conduit. Then the rubber bung was forcedin position through the small pipe and a further flange cut into two pieces was screwed to the existing flange to ensure water and air tightness. The arrangement was quite good and allowed removal of the probes whenever required to check the calibration of the probes. For experiments on air pockets at the bend, one probe was placed at the bend to measure the water depth or air pocket depth and the second one was placed at the end of the first length of tunnel. For subsequent experiments on air pocket behaviour along the tunnel section, the

first probe was placed at the outlet tank end in order to measure the speed of air pockets along the tunnel, as well as an instantaneous trace of the shape and size of air pockets moving along the tunnel section. Plate (4.14) shows the details for insertion of the probes.

4.2.11 Air Blower

As mentioned already in section (4.1), an independent air supply is required in order to achieve the same air/water ratio as that in typical prototype structures. It was decided to use an air blower in order to introduce air at a pressure equal to or higher than the atmospheric pressure. Although the air injection point was at a relatively high point in the system, it was calculated that heads of up to 1 m might exist at that point and hence an air blower (Model P180-104-J803) was chosen which can supply air in excess of 20 ℓ/s. This value is sufficient to supply an air/water ratio (β) up to 50% at maximum water discharge, which is adequate for comparison with natural air entrainment in prototype structures. The relation between the air flow and the pressure for the chosen air blower is shown in Fig. (4.13). The outlet from the air blower was connected to a plastic pipe extending to the air flow rotameters where it is connected to a steel pipe with two branches, one for each air flow rotameter, with a valve to control the air going through the system. Plates (4.15) and (4.16) show the air blower and the connection to the air flow rotameters.

4.3 INSTRUMENTATION

It was mentioned earlier that several instruments were used to accomplish the experimental work. These include: the air flow rotameters used for measuring the air going into and out of the

system, the probes and their connection to the wave monitor and chart recorder and, in addition, the visual measurement of water and the scale designed to get this measurement. Details of each of the above mentioned instruments will be given in the following sections.

4.3.1 Air Flow Rotameters

Two arrangements of air flow rotameters were used. The first arrangement, used for the horizontal tunnel ($\theta = 0°$) and the upward sloping tunnel ($\theta = +1.5°$), consisted of two air flow rotameters at the air inlet section, each operating over the range 0.83 ℓ/s to 8.3 ℓ/s, and a further two rotameters for air outflow from the top of the shaft. The latter two rotameters were required as not all the air injected into the system was transported along the tunnel but substantial air volumes also escaped to the top of the shaft. The air flow rotameters were of the range 0.083 ℓ/s to 0.83 ℓ/s and 0.83 ℓ/s to 8.3ℓ/s respectively. The air outlet at the top of the shaft is shown in Plate (4.17).

The second arrangement, used for the tunnel sloping downwards at ($\theta = -1.5°$), consisted of two rotameters at the inlet, one of the range 0.083 ℓ/s to 0.83 ℓ/s and the other 0.83 ℓ/s to 8.3ℓ/s, plus only one rotameter at the outlet from the shaft.

The air flow rotameters, shown in Plate (4.18), were connected to the scaffolding supporting the dropshaft and secured in position using the end plates welded to the back of each rotameter. The metering tube is held in a simple quick release fixing sealed with interal '0' rings in nitrile rubber. The flow scales are fixed on enamelled plates which are pivoted to allow access to metering tube and accessories. The front of the rotameter is protected by a perspex cover.

The air flow rotameters measure the air flow rate in litres/minute at 15°C to get accurate measurements. This was achieved by allowing cool air to enter the air blower and also by allowing the air blower itself to cool before starting a new series of tests. The total capacity of the large two air flow rotameters can give an air flow ratio of up to 50% for the maximum water flow through the system for a horizontal tunnel and a tunnel at +1.50° with horizontal. Plate (4.18) shows one arrangement of the air flow rotameters.

4.3.2 The Probes and the Wave Monitor

The probes, as outlined in section (4.2.10), are used to measure rapidly changing water levels in hydraulic models. They operate on the principle of measuring the current flowing between the two parallel stainless steel wires forming the probes. The probe is energised with a high frequency square wave voltage to avoid polarisation effects at the wire surfaces. The wires dip into the water and the current that flows between them is proportional to the depth of immersion. The current is sensed by an electronic circuit which provides an output voltage proportional to the instantaneous depth of immersion. This can be plotted continuously on a chart recorder.

The probes consisted of a pair of stainless steel wires, 1.5 mm in diameter and spaced 12.5 mm apart with a length of 300 mm. The output voltage was calibrated in terms of water depth by varying the depth of immersion of the probe in stationary water by a measured amount, and recording the change in output signal. The probes were connected to the wave monitor at the red sockets on the front panel, as shown in Plate (4.19). To obtain a high degree of linearity of measurements for a wide range of probe conductivity, the resistance

of the connected cable was compensated. This was achieved by disconnecting the probe cable at the probe end and inserting the plug into the blue test sockets on the front panel. The switch was depressed to the test position and the Set Ouput Control was turned to its full clockwise position. The Set Datum Control was adjusted until the pointer of the balance meter was in its central position. Then the push button was depressed and the compensator control was rotated with a screw driver to restore the pointer to its balance position. Correct compensation was achieved when pressing and releasing of the push button resulted in no change in position of the meter pointer. Then the plugs were removed from the test socket and reconnected to the probe.

Subsequently it was required to set the output signal to zero for the initial depth of probe immersion, this will allow a maximum full scale output for water just reaching the bottom of the probe in their troughs. To set the Datum the probe was fixed in position to the required depth of immersion in stationary water. The switch on the front panel was set to Operate position, the Set Output Control was turned to its fully clockwise position, and then the Set Datum Control was rotated to bring the indicating meter to its central position. It is important to note here that for the available depth of immersion in the tunnel used, a central position for the datum was not achieved. After checking with the manufacturer a resistor was connected to the probes. The resistor did not affect the circuit of the wave monitor but it means that a new calibration must be carried out for the probe with the resistor connected to it. The wave monitor has two channels to which the two probes used can be connected. Also the chart recorder has two pens to record the signal obtained from the wave monitors simultaneously. In order to have a full range of the output from the two probes, the Set Output Control on the wave monitor can be set to any value of voltage between zero and 10 volts. This can be done provided the datum has been adjusted,

as described earlier. To do so the control was set to the required output and locked, but it was always set to its maximum value before carrying out any test to restore the sensitivity of the adjusted datum and cable resistance.

The calibration of the probe was done by noting the change in the output signal when the probe was raised or lowered by multiples of 10 mm in stationary water. The calibration of the probe was checked twice every week, but the datum was set before and after every test to ensure that there is no changes during any test. The change in the temperature can also affect the calibration of the probe, so it was decided to measure the water temperature through some tests and it was found that the temperature over a period of about three hours changed by 1°C. This is not very significant.

The probes were always kept clean, because any accumulation on the wires affects the sensitivity of the probes. This was done by rubbing the probe wires with very fine emery cloth.

4.3.3 The Chart Recorder

The chart recorder used was the Washington 400 MD Series which has two channels to record the output signal from the wave monitor. Plate (4.20) shows the chart recorder where it can be seen that it has two pens to record the output signals. At the two edges there is a time marker which records the time in seconds or minutes, depending on the chart speed, and an event marker to mark the events as pulses when depressing the event marker button.

The calibration of the chart recorder was checked by switching the power supply on and switching the Facility Coupler signal switch to the "OFF" position. The amplifier attenuator

control was set to position 0.02 and a slow chart speed was selected. The motor function switch and the record function switch were depressed. The pen zero control was adjusted to a central zero line on the chart, and the calibration button marked 20 mV was depressed and released. This provides a square wave on the write-out with a level of 10 mm.

The input current was also set to zero by setting the attenuator to 0.01 and operating the ON/OFF switch on the Coupler. There should be no pen movement. For any visible pen movement the pre-set was adjusted with the coupler switch on ON, so that the pen moves to the same position as that when the switch is OFF. This was repeated more than once to obtain the best results.

The linearity of pen deflection was also checked by returning the attenuator to 0.02 and depressing the Calibrate switch on the Coupler. When the pen is adjusted to a centre reference point, the deflection is 10 mm. Then the pen was adjusted 15 mm above the reference point and the Calibration Switch was depressed, and the deflection should be 10 mm, if not the pre-set was adjusted until 10 mm deflection was obtained. This was repeated for a pen at 25 mm below the reference point where a deflection of 10 mm must be obtained. This was repeated several times to get the best results and ensure linearity of pen deflection.

The chart recorder can be adjusted to the required speed by pressing the button for that speed. It has six different speeds ranging from 0.25 to 50 mm/sec. The event marker button was mainly used to mark the nose of an air pocket passing the first probe in the tunnel section, and when it reaches the second probe. This can be used to find the speed of air pockets along the tunnel.

4.3.4 Visual Measurement of Water Depth

To obtain measurements of the depth of water below a long air pocket or the depth of the air pocket itself along the tunnel, it was decided that visual measurements would be a useful addition to measurements from the probes. This has been discussed in section (4.3.1) with the description of accurately calibrated measuring tapes around the tunnel perimeter. This will allow three readings of air pocket depth at the same section; one at the centre of pipe using the probe and two on both sides of the pipe. Since there were only two probes available, visual measurement gave greater detail of depths of longer air pockets extending along the tunnel. It is important to emphasize that great care was taken in producing an accurate scale for the air pocket measurement.

As outlined in section (4.3.1), the measuring scales were placed around the outside perimeter of the tunnel, and the equivalent length along the perimeter for each millimeter depth of air pocket was marked. Several measuring tapes were produced in the same way and fixed on both sides of tunnel at the probe section and also at other sections along the tunnel. Also extra scales were produced which can be used at any time for taking extra readings at any section, if required.

Water depth measured by the probes at the pipe centre line were generally slightly less than the visual measurements at the pipe walls. This was thought to be due to water splashing on both sides of pipe, especially in the section near the dropshaft/tunnel bend. The average value of the three depths obtained at any section was used in analysing the results. For sections far away from the bend along the tunnel, the depths measured were almost identical using either probes or visual measurements. Extra depth readings were taken for the case of air pockets at the bend extending partly along the tunnel length, but not extending far enough to reach the second probe.

4.4 EXPERIMENTAL PROCEDURE AND FLOW CHART

The aim of the experimental work, as already outlined in section (4.1), is (i) to investigate air pocket behaviour at the dropshaft/tunnel bend, (ii) to investigate air pocket speeds in a pipe inclined slightly upwards, and (iii) to investigate blow back and clearing phenomena in a pipe inclined slightly downwards. It was decided to obtain as much information as possible, although some parameters were not recorded, such as detailed velocity profiles and detailed pressure measurements especially in the region of the bend.

In broad terms, three tunnel angles were employed, and for each tunnel angle, 3 different bend radii were investigated. This gives a total of 9 basic geometrical configurations, shown in Table (4.2).

Table (4.2): The nine geometrical configurations tested

Tunnel horizontal	$R'/D = 0.5$	$R'/D = 1.0$	$R'/D = 1.5$
$\theta = +1.5°$	$R'/D = 0.5$	$R'/D = 1.0$	$R'/D = 1.5$
$\theta = -1.5°$	$R'/D = 0.5$	$R'/D = 1.0$	$R'/D = 1.5$

For each of the nine geometries above, the air flow rate and water flow rate were varied independently over a wide range, producing a range of experimental observations for each test run, including:

(a) air pocket depth (H) and length at the bend

(b) regime of air pocket behaviour at the bend, including back

venting, stable air pocket, hydraulic jump formation, air pocket extending to the outlet tank, and air pocket clearing.

(c) air pocket speeds along the tunnel section, especially for the upward sloping pipe

(d) clearing and blowback phenomena in the downward sloping tunnel.

A total number of approximately 232 test runs were carried out, providing a good deal of experimental data for comparison with theoretical models and past research work.

Consider, thus, a detailed procedure for a single test run for the case of the air pockets forming at the dropshaft/tunnel junction.

1. Starting the pump and allowing a water discharge to flow through the system, measure Q_w.

2. Starting the air blower, measuring and supplying a known air flow rate into the system. To measure the air escaping from the top of the shaft, and hence calculating the net air flow through the system.

3. Recording all the information required for the specified water and air flow rates. This includes remarks on the behaviour of the supplied air bubbles such as venting back, forming an air pocket at the bend, the behaviour of the pocket and clearing the pocket from the bend.

4. Measuring the depth of air pocket at the bend and other suitable locations along the tunnel. Measuring air pocket lengths.

5. For a given air flow rate the water discharge is increased and all the information and measurements are recorded again. The water discharge is continuously changed until the air pocket at the bend has cleared completely. For every air flow rate there is a number of water flow rates starting from a small rate up to the flow which clears the air pocket from the bend.

6. For some runs at a given air flow rate, the water flow rate was decreased to investigate any hysteresis effects.

7. The above procedure was done for a wide range of air flow rates to find the effect of air/water ratio on air pocket behaviour.

A generalised flow chart is shown in Fig. (4.14) for the study of air pockets at the bend.

Experiments were also carried out for the speed of air pockets along the tunnel. This was done by choosing a water flow rate and an air flow rate and recording the speed of the rising air pockets between two specified sections along the tunnel using the probes, wave monitor and the chart recorder. Also the depth and length of the rising air pockets were recorded and some photographs were taken for the rising air pockets to specify their shape and the angle at the air pocket nose. This was done in great detail for the upward slope of the tunnel. For the downward slope, the range for these air pockets was small and they mainly tend to move back up the tunnel. They can form at any section along the tunnel for this slope so their speed was recorded by using a stopwatch and measuring the distance they tend to travel. A total number of approximately 100 test runs were carried out for air pockets in the straight section of the tunnel.

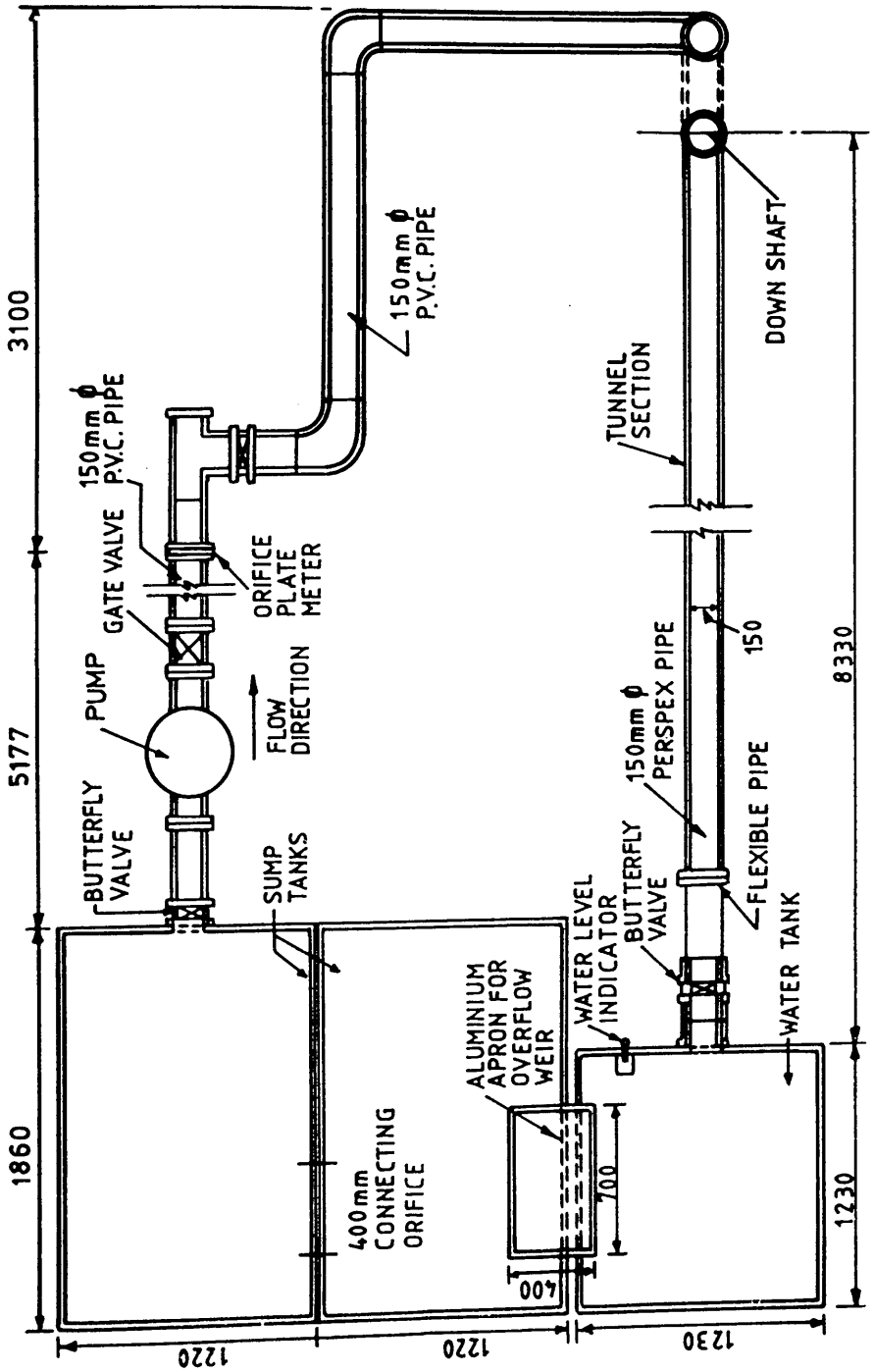

FIG. (4.1) PLAN OF THE EXPERIMENTAL MODEL

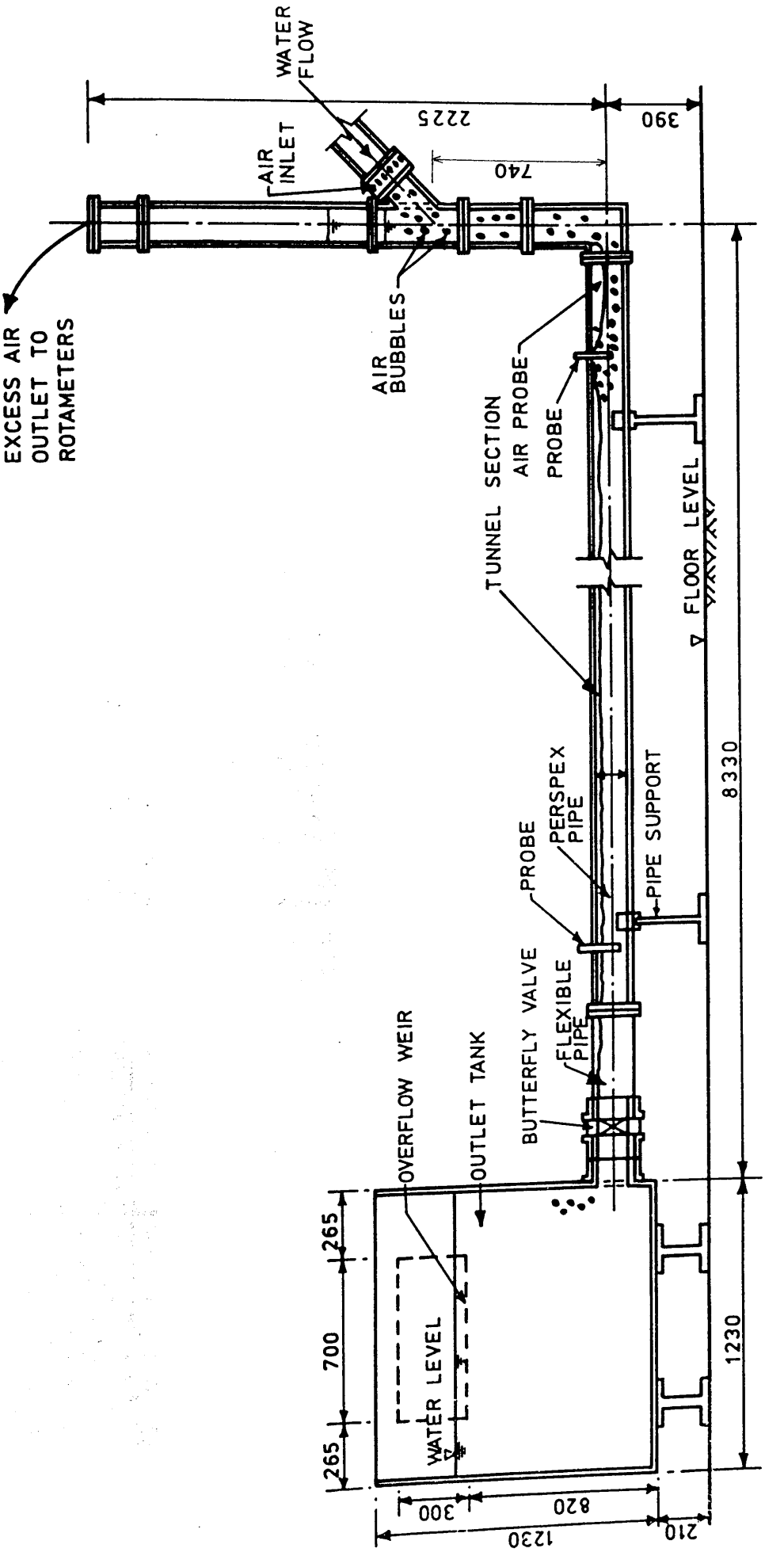

FIG. (4.2) SECTION THROUGH THE EXPERIMENTAL MODEL (HORIZONTAL CASE)
(All dimensions are in mm)

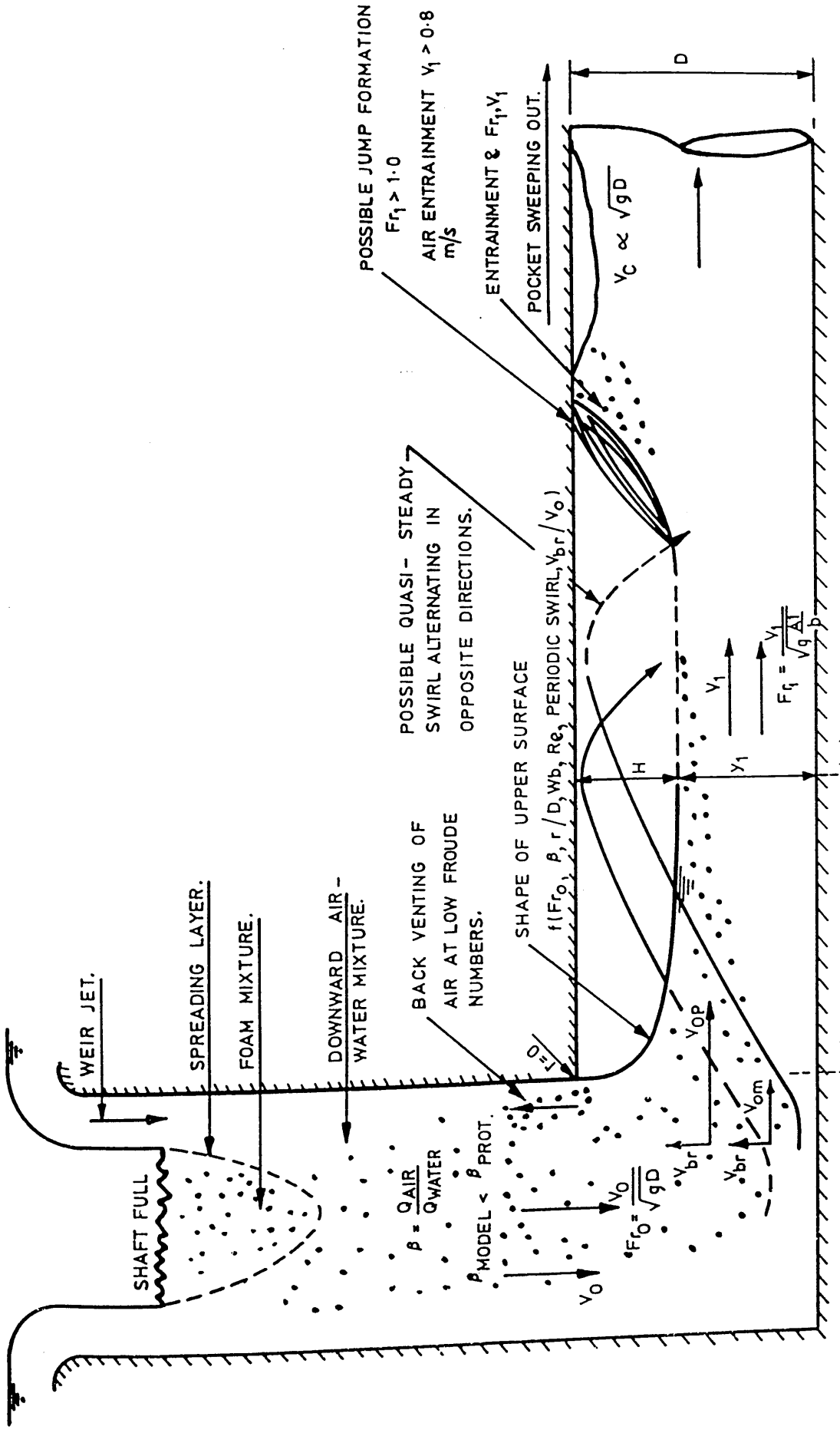

FIG. (4.3) ILLUSTRATION OF THE PARAMETERS AFFECTING THE DEPTH OF AIR POCKET AT THE BEND

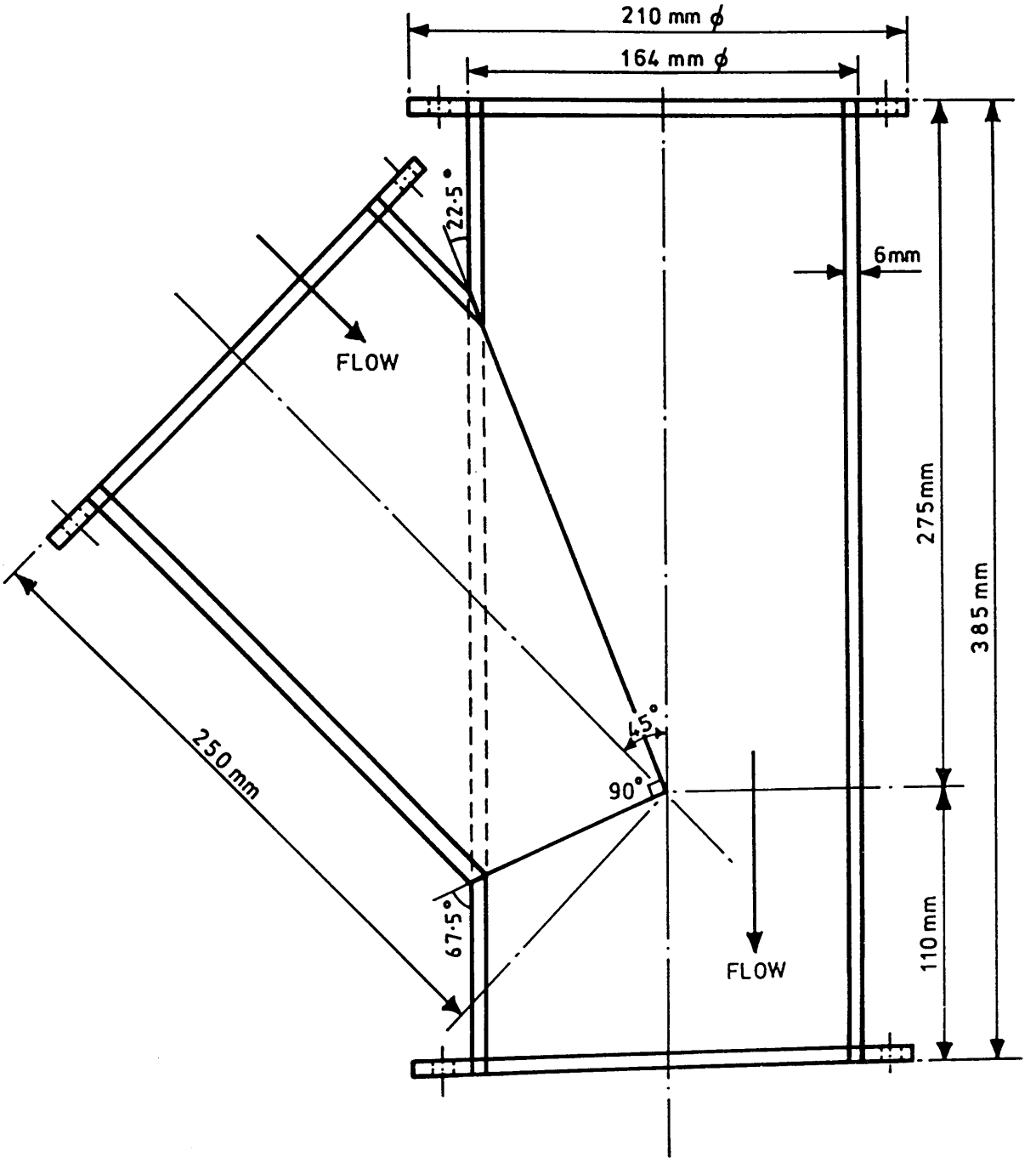

FIG. (4.4) DETAILS AND DIMENSIONS OF THE 45° Y-PIECE FOR THE WATER INLET

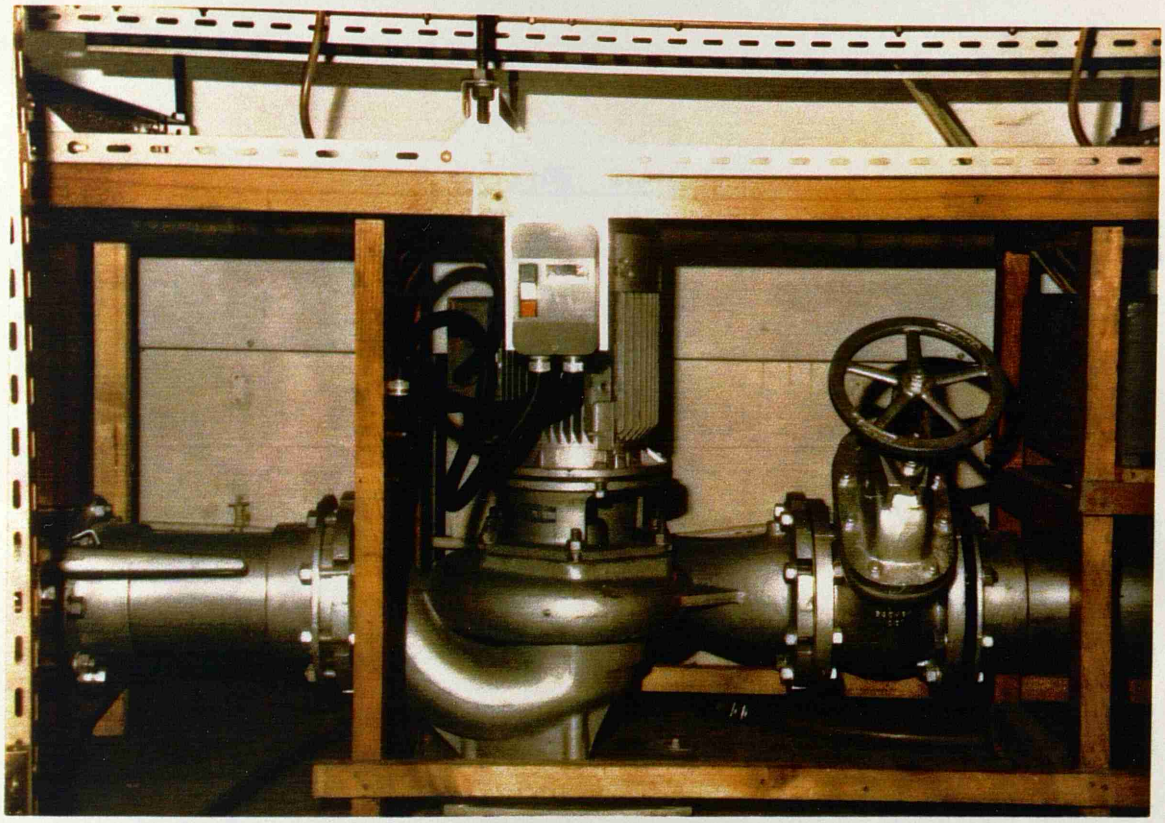

PLATE (4.1) ARRANGEMENTS FOR THE BUTTERFLY VALVE, PUMP AND GATE VALVE

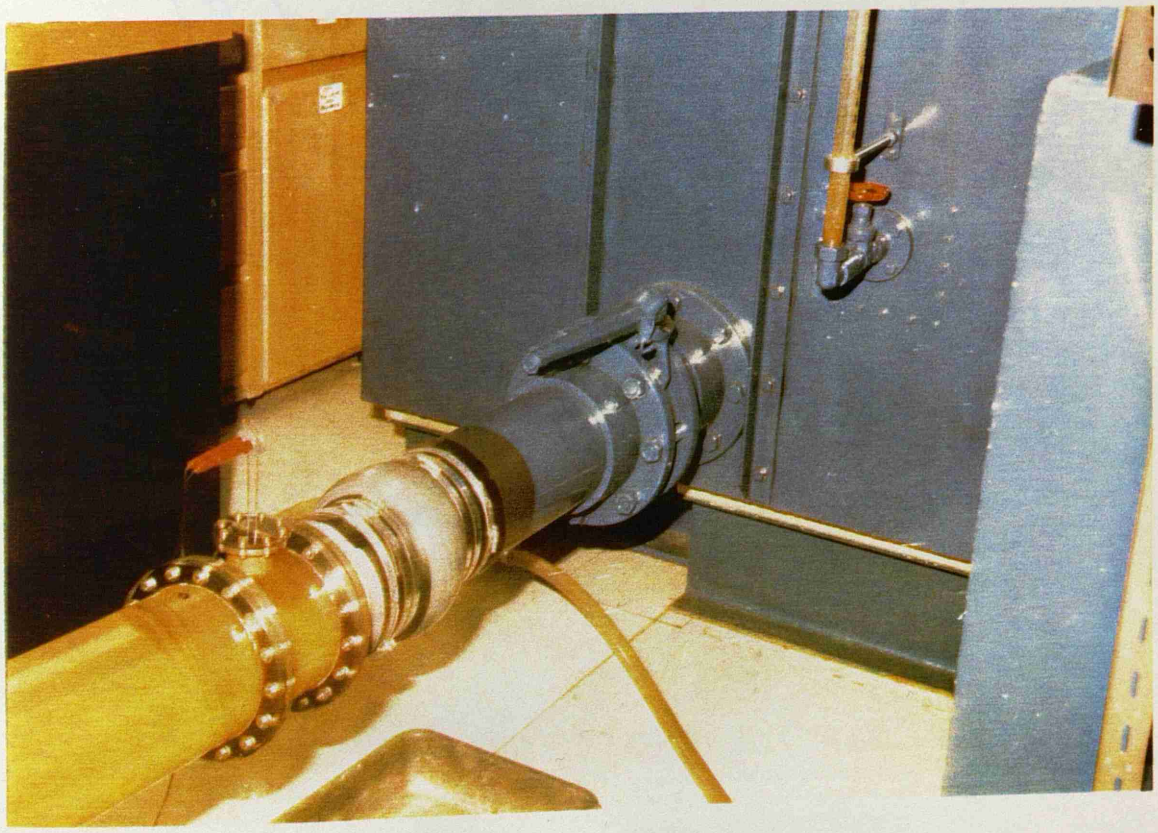

PLATE (4.2) THE CONNECTION AT THE OUTLET TANK

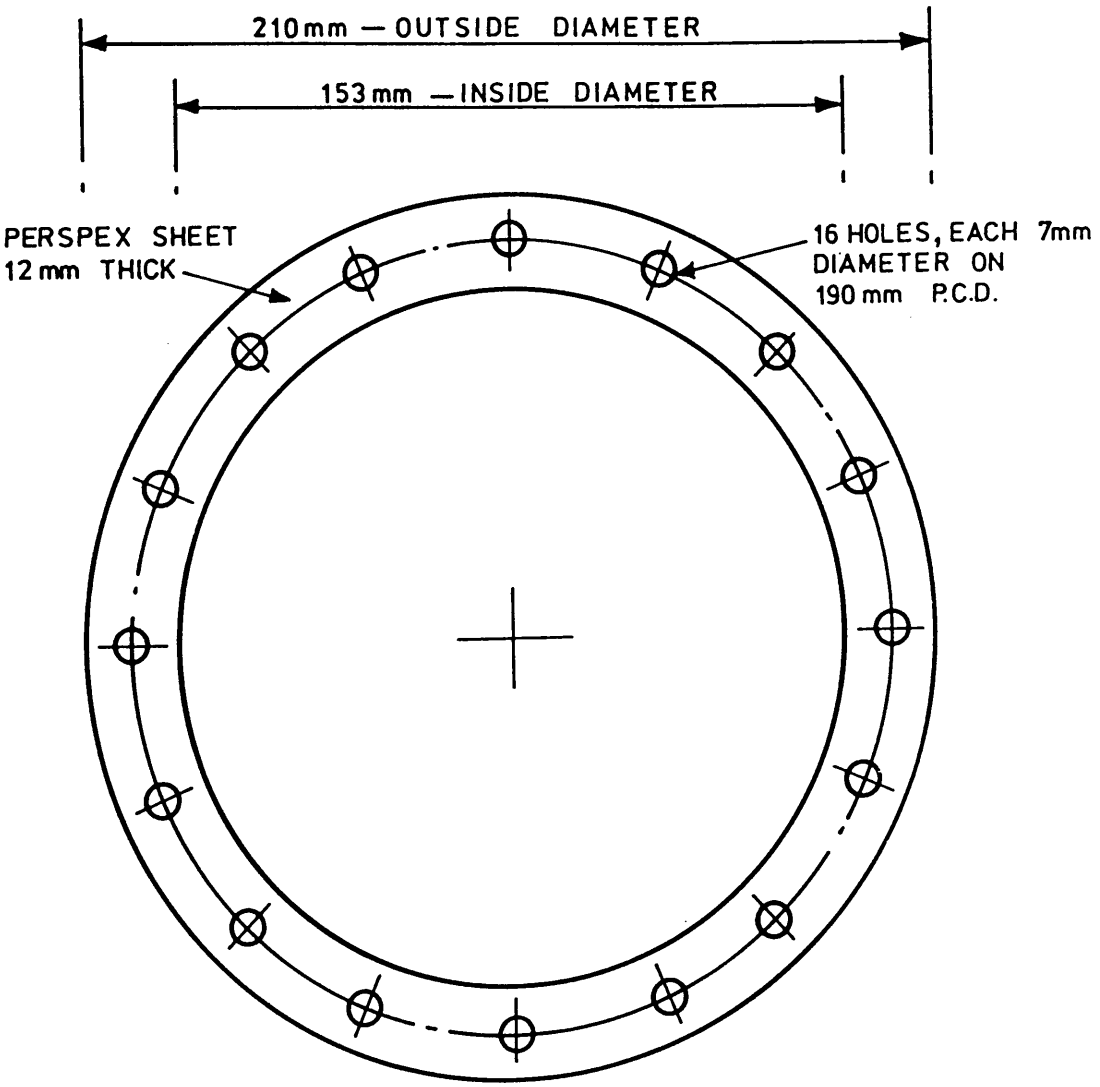

FIG. (4.5) DETAILS AND DIMENSIONS OF THE PERSPEX FLANGE

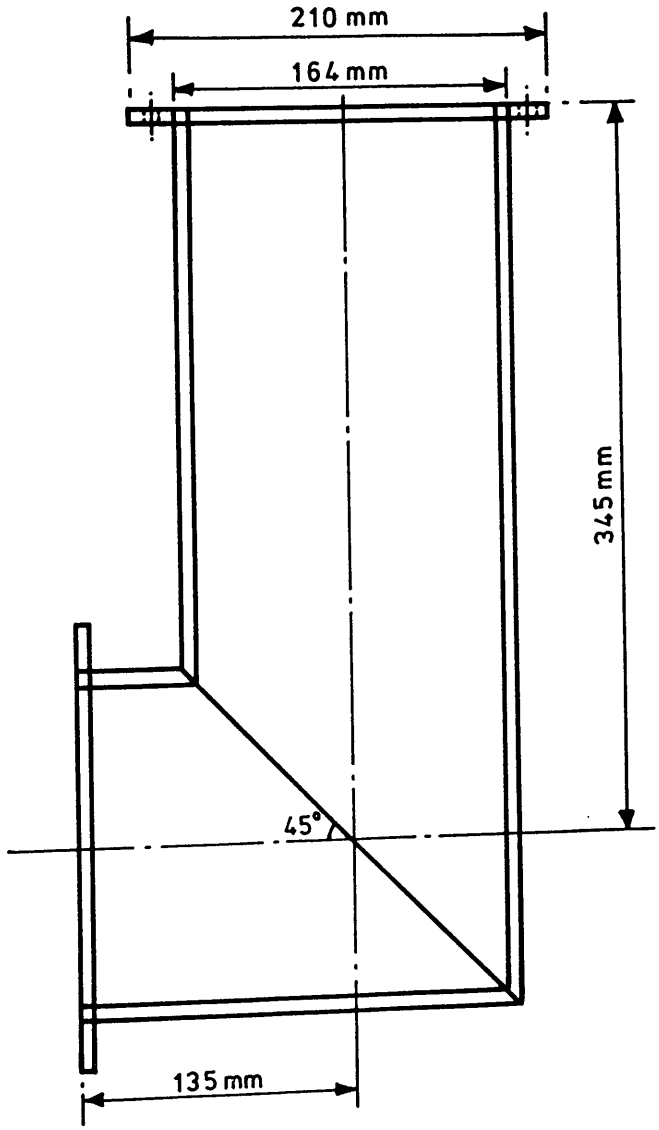

FIG. (4.6) DETAILS OF THE SHARP BEND WITH R'/D = 0.50

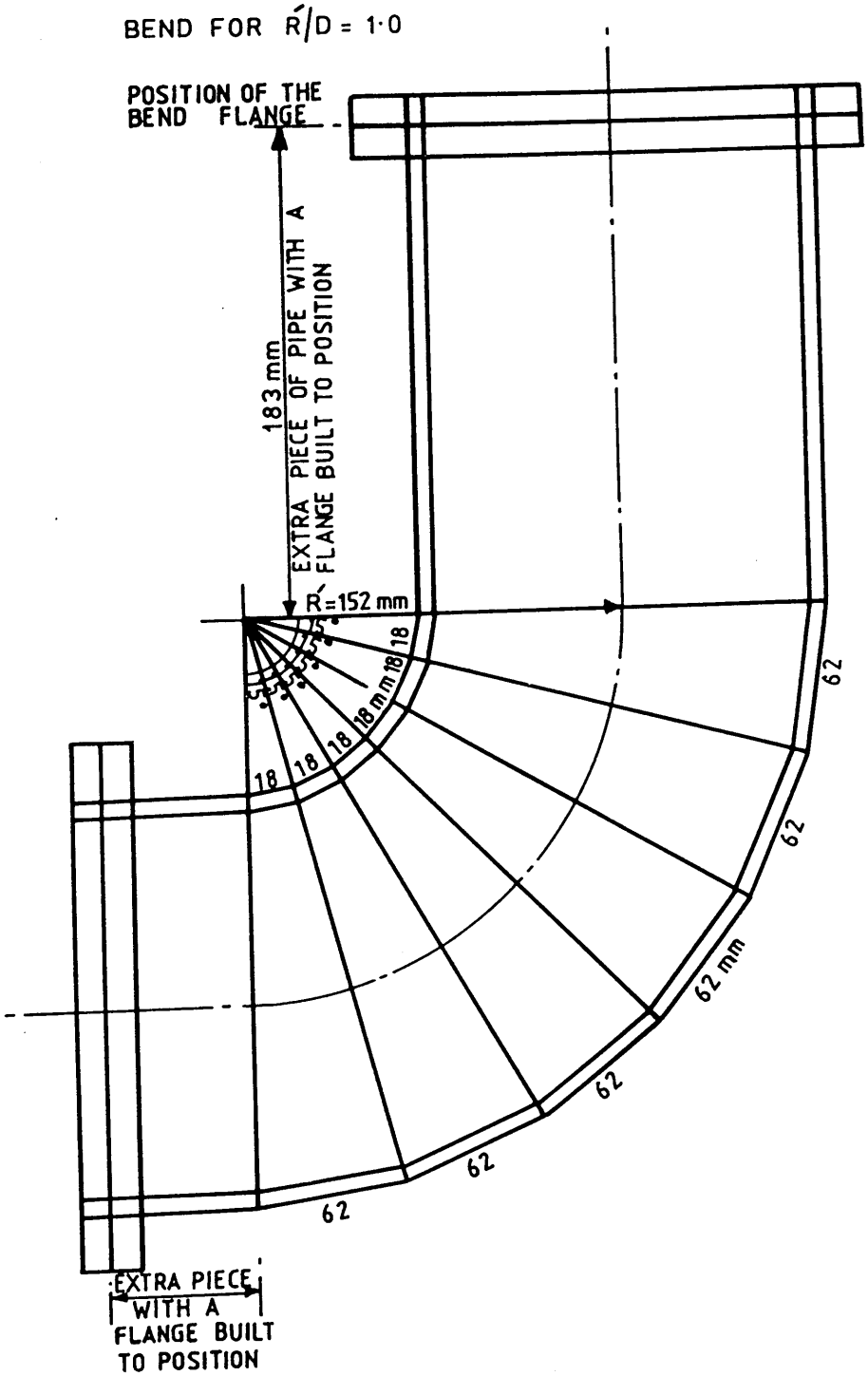

FIG. (4.7) DETAILS OF THE BEND WITH R'/D = 1.0

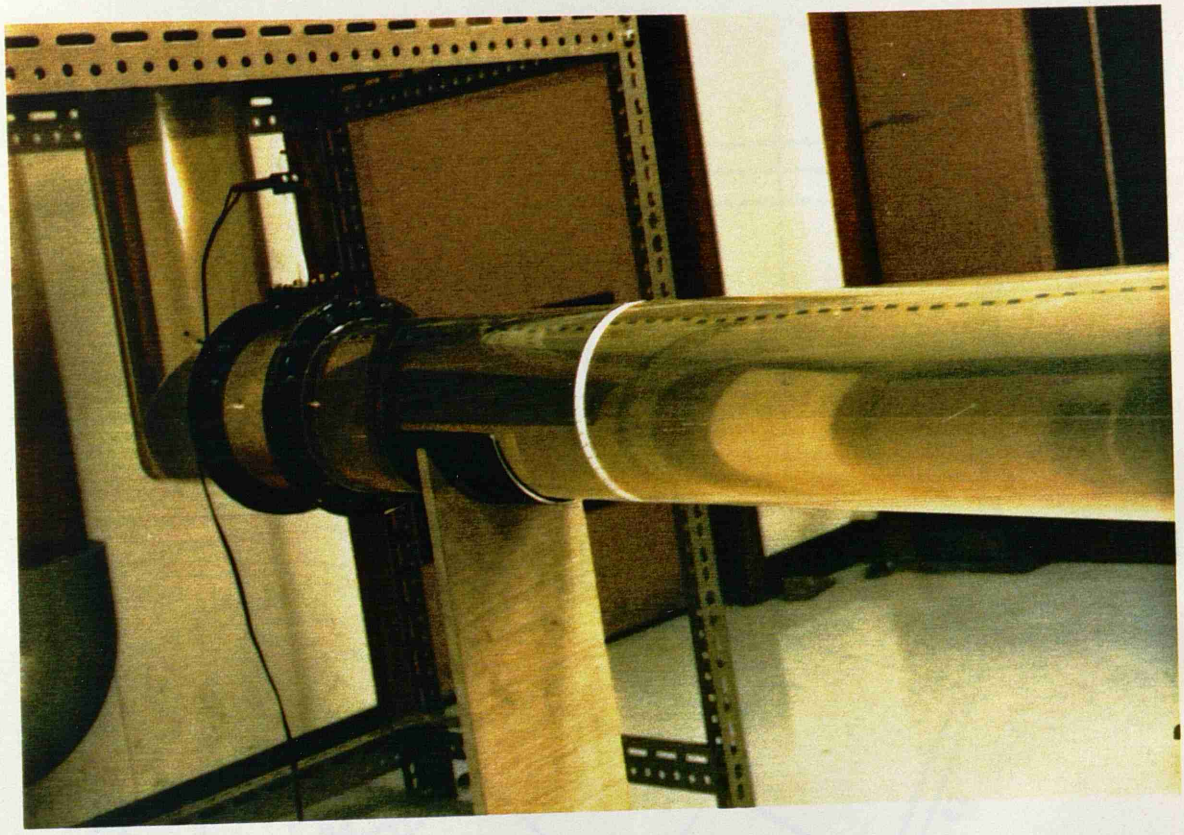

PLATE (4.3) THE SHARP BEND AT THE JUNCTION OF THE DROPSHAFT/TUNNEL SYSTEM

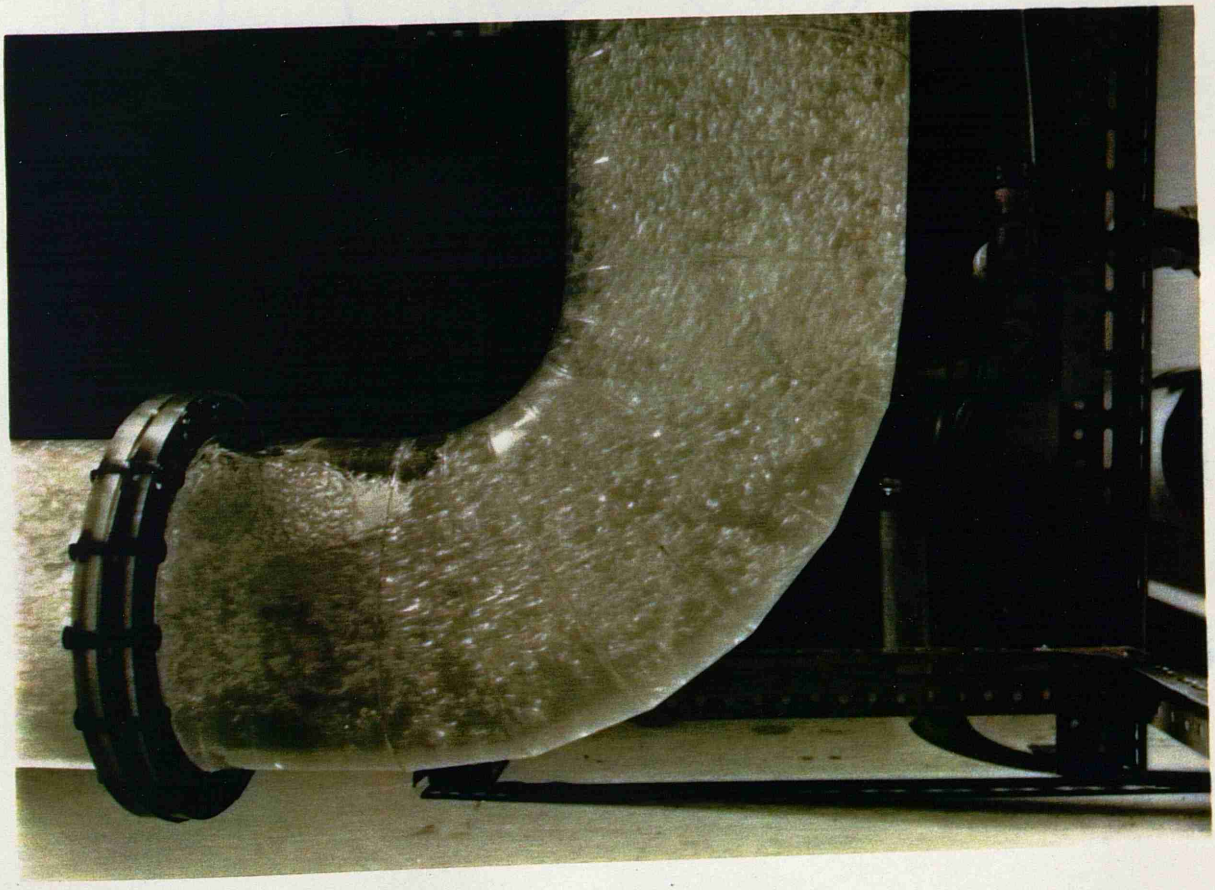

PLATE (4.4) THE BEND WITH R'/D = 1.0

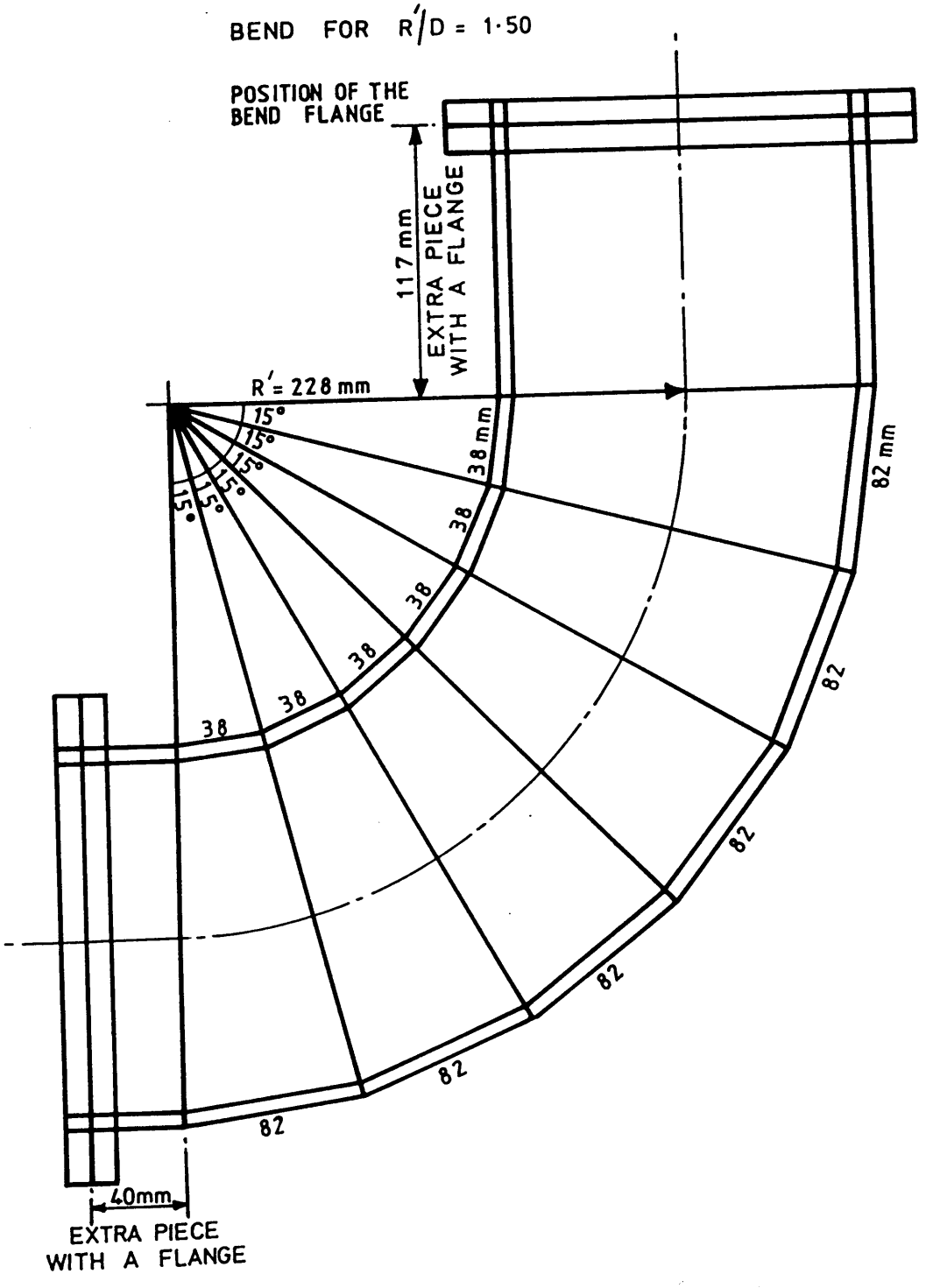

FIG. (4.8) DETAILS OF THE BEND WITH R'/D = 1.5

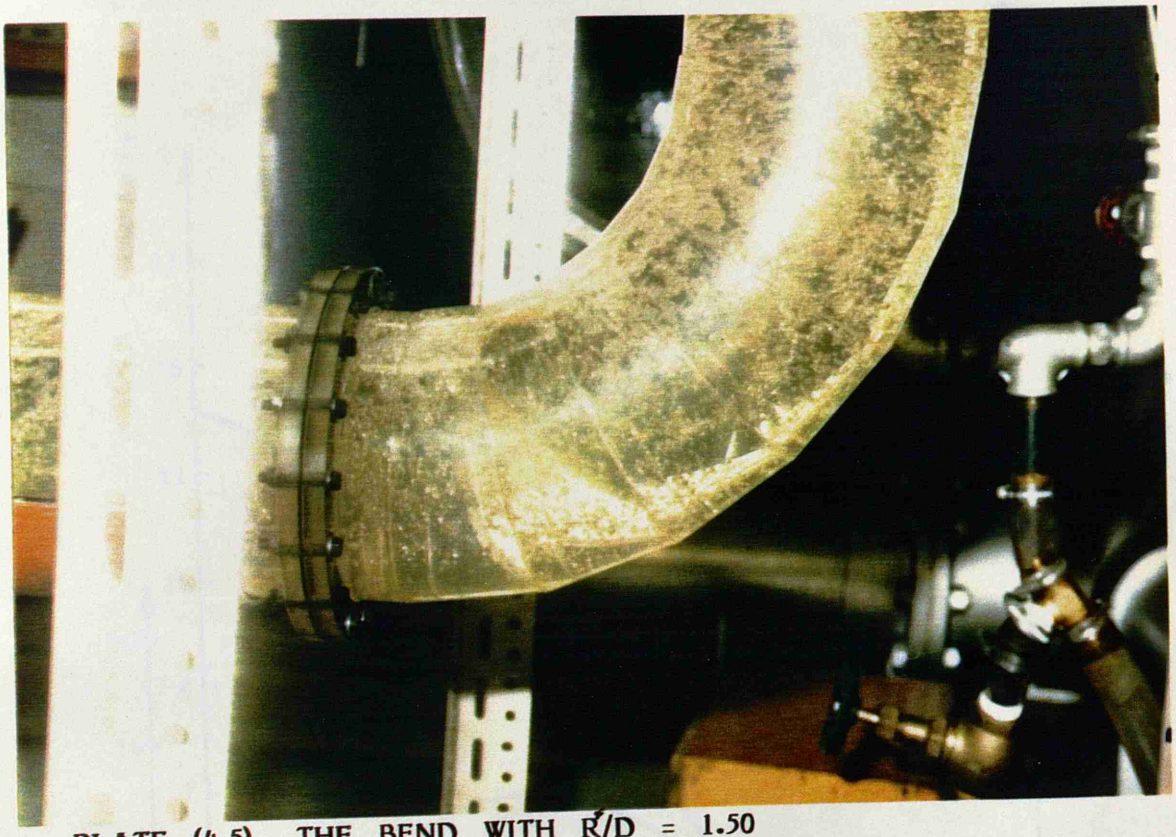

PLATE (4.5) THE BEND WITH R/D = 1.50

PLATE (4.6) THE CONNECTION OF THE BUTTERFLY VALVE TO THE SUMP TANK

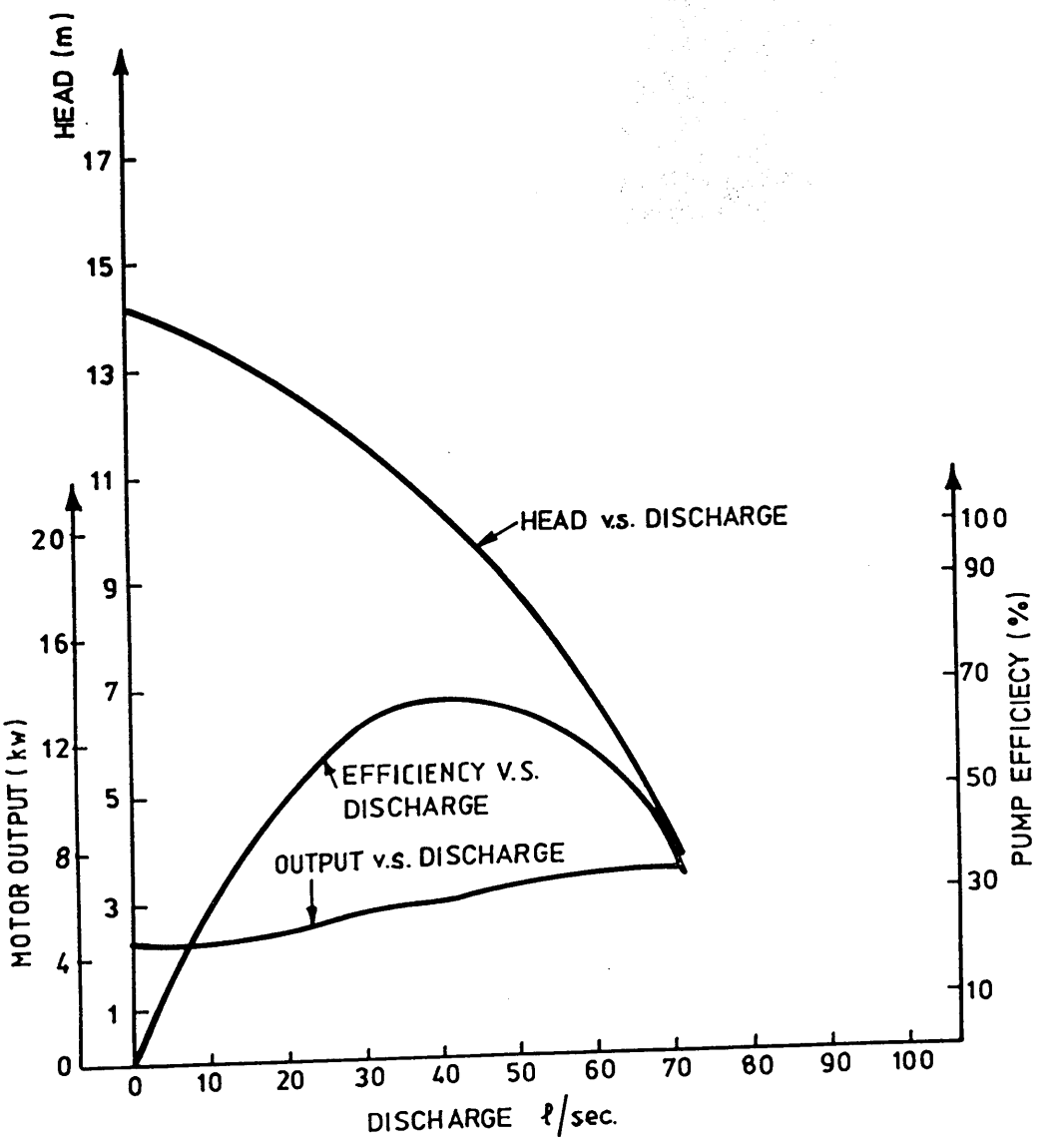

FIG. (4.9) CHARACTERISTICS OF CENTRIFUGAL PUMP TYPE MYSON MSK 150-4210

PLATE (4.7) OUTLET TANK WITH THE SIDE WEIR AND THE PIPE USED TO MEASURE HEIGHT OF WATER IN THE TANK

PLATE (4.8) THE ORIFICE PLATE METER

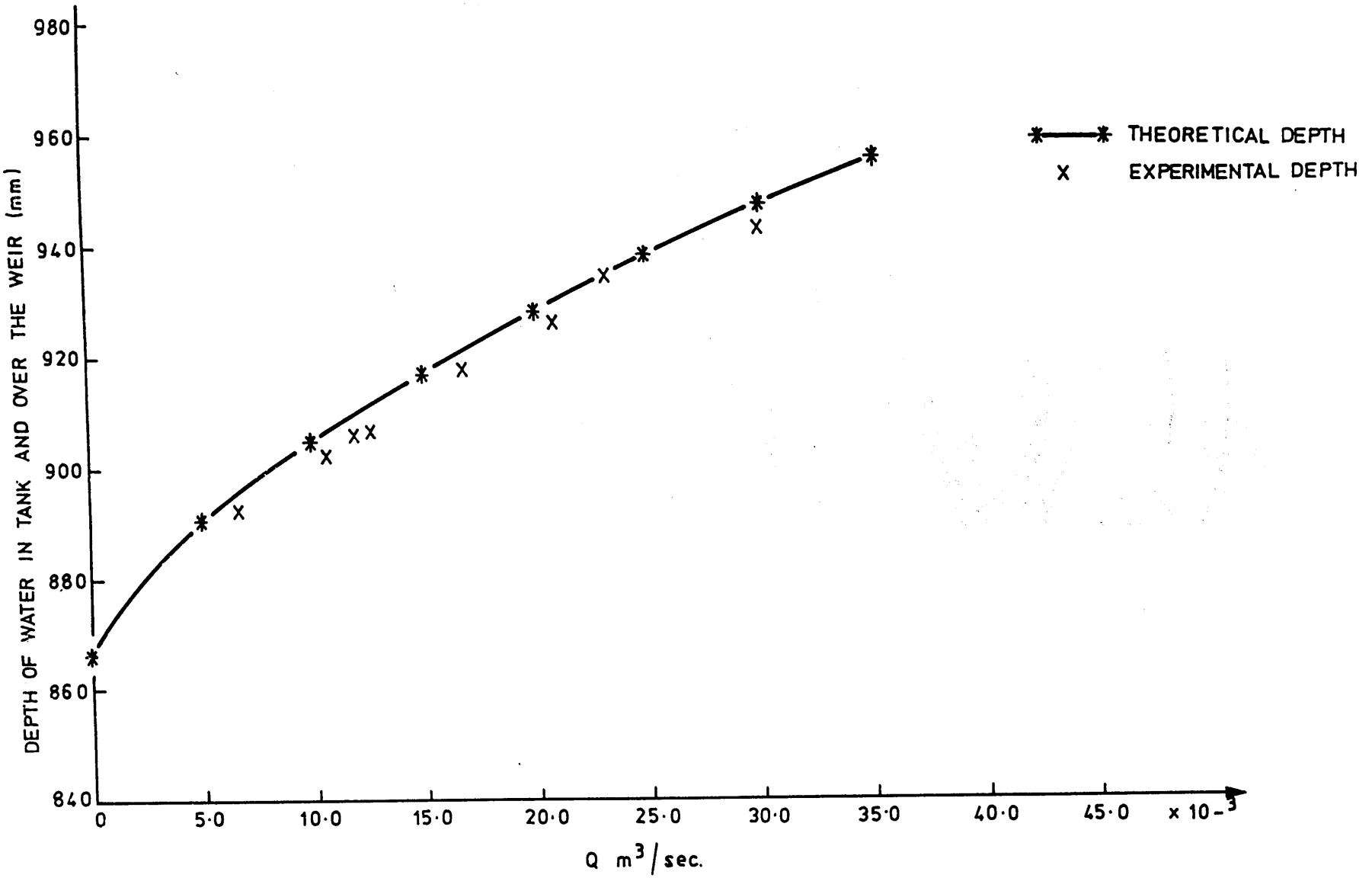

FIG. (4.10) THEORETICAL AND EXPERIMENTAL DATA FOR DEPTH OF WATER INTO THE TANK AND OVER THE WEIR

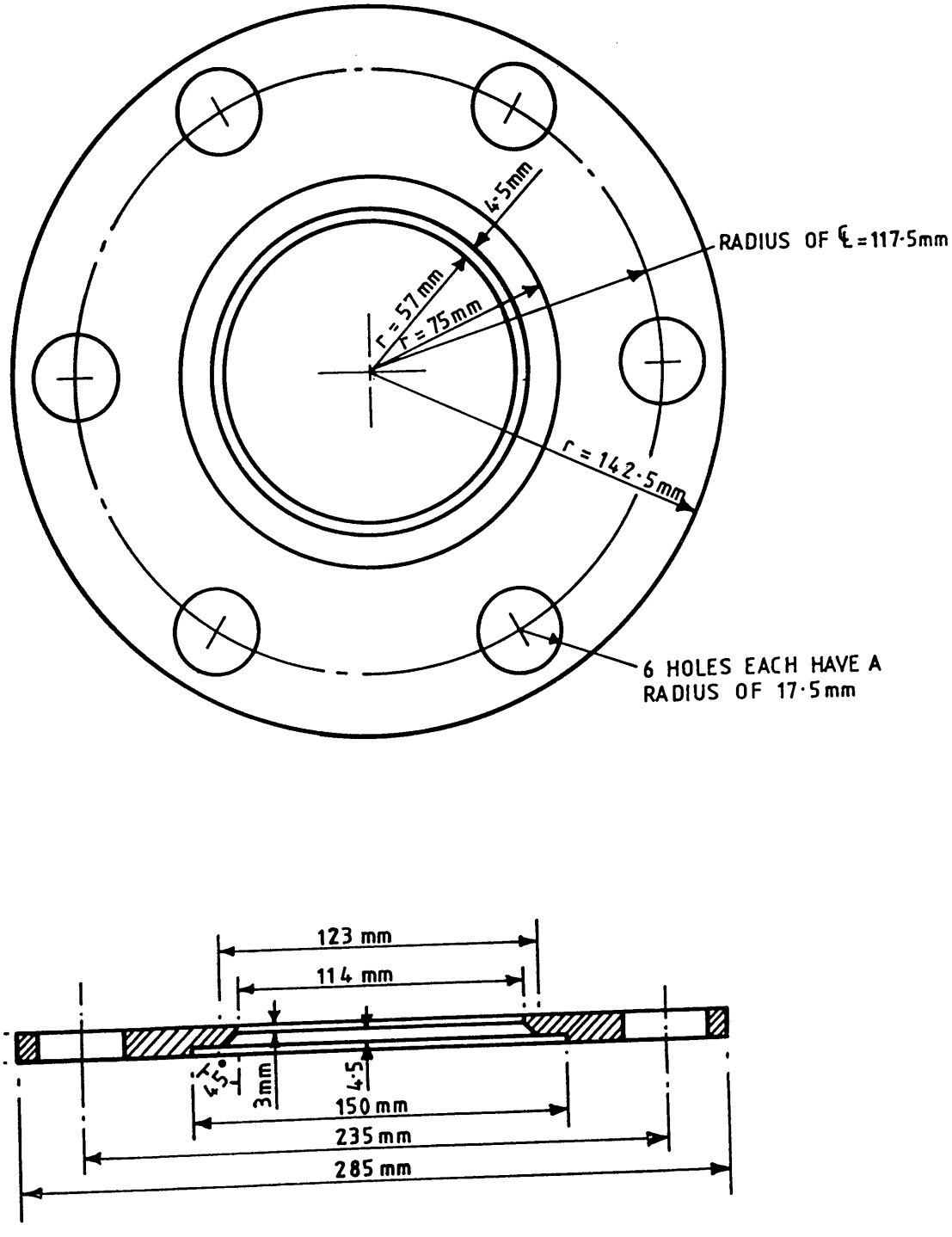

FIG. (4.11) ORIFICE PLATE METER DESIGN

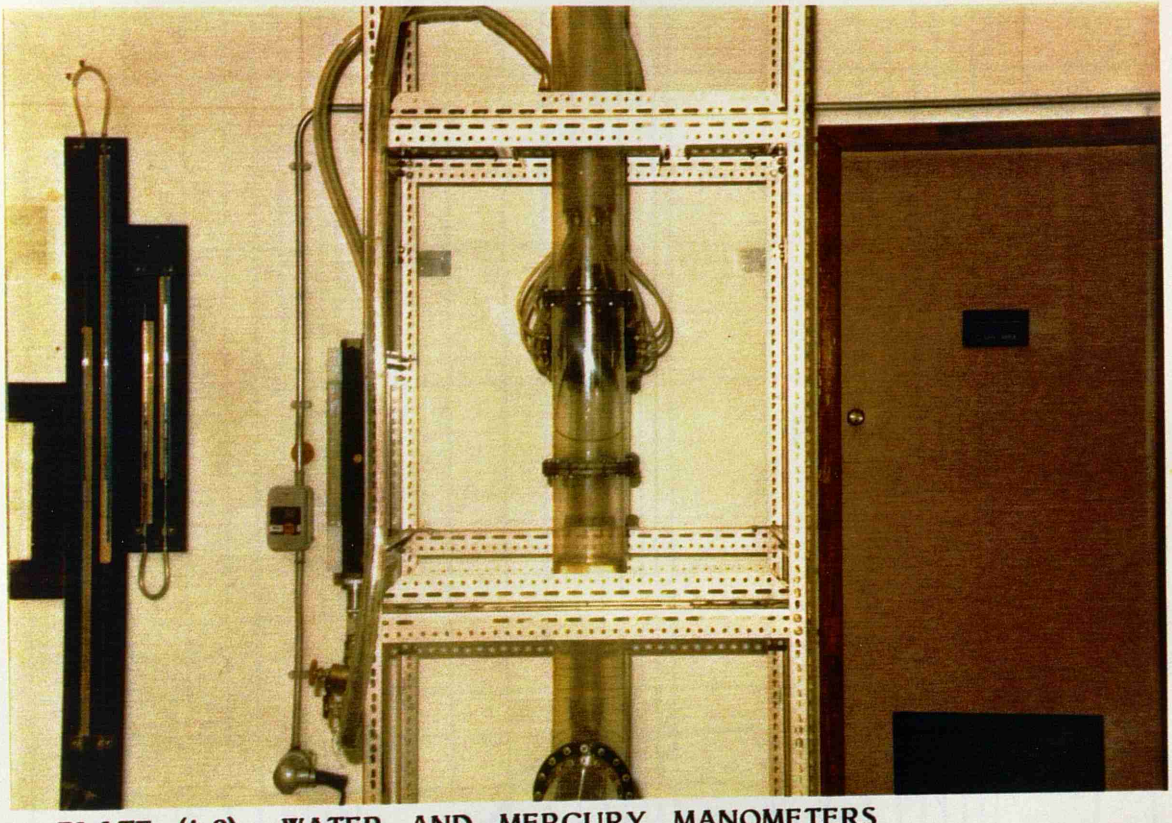

PLATE (4.9) WATER AND MERCURY MANOMETERS

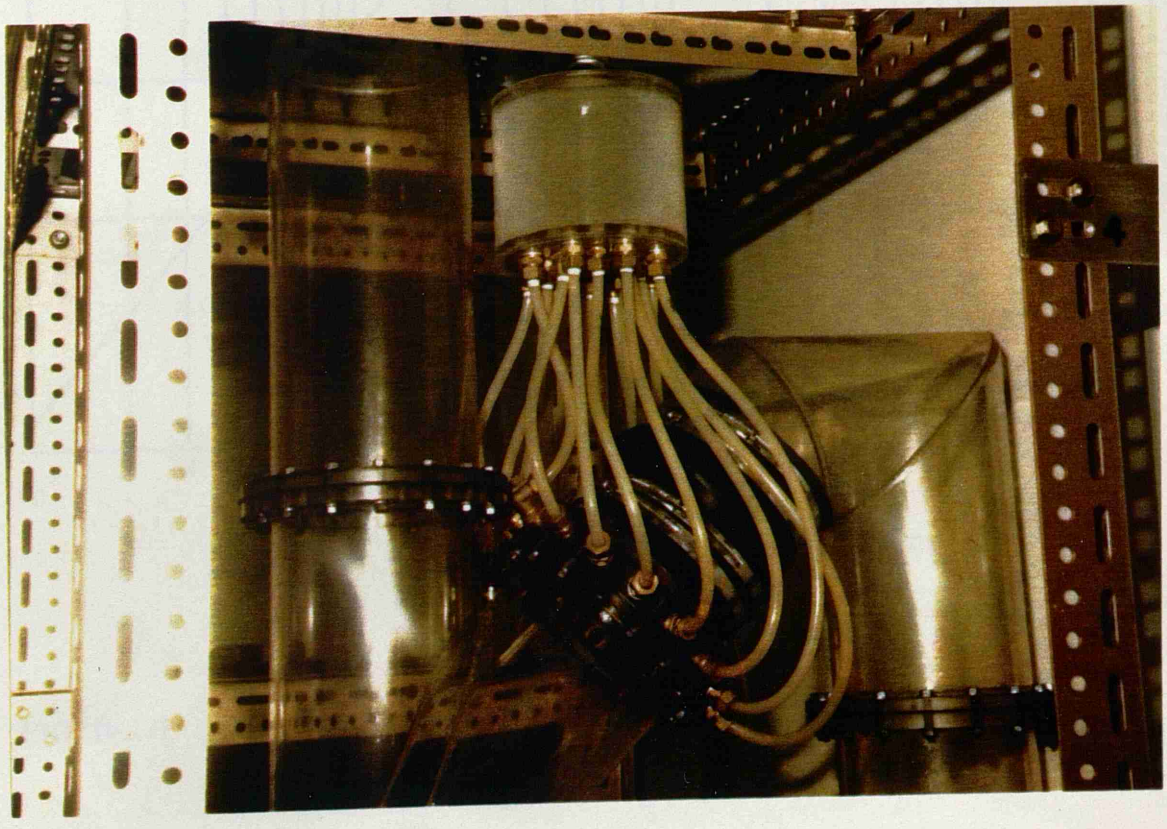

PLATE (4.10) DETAILS OF THE AIR CHAMBER AND THE AIR INLETS

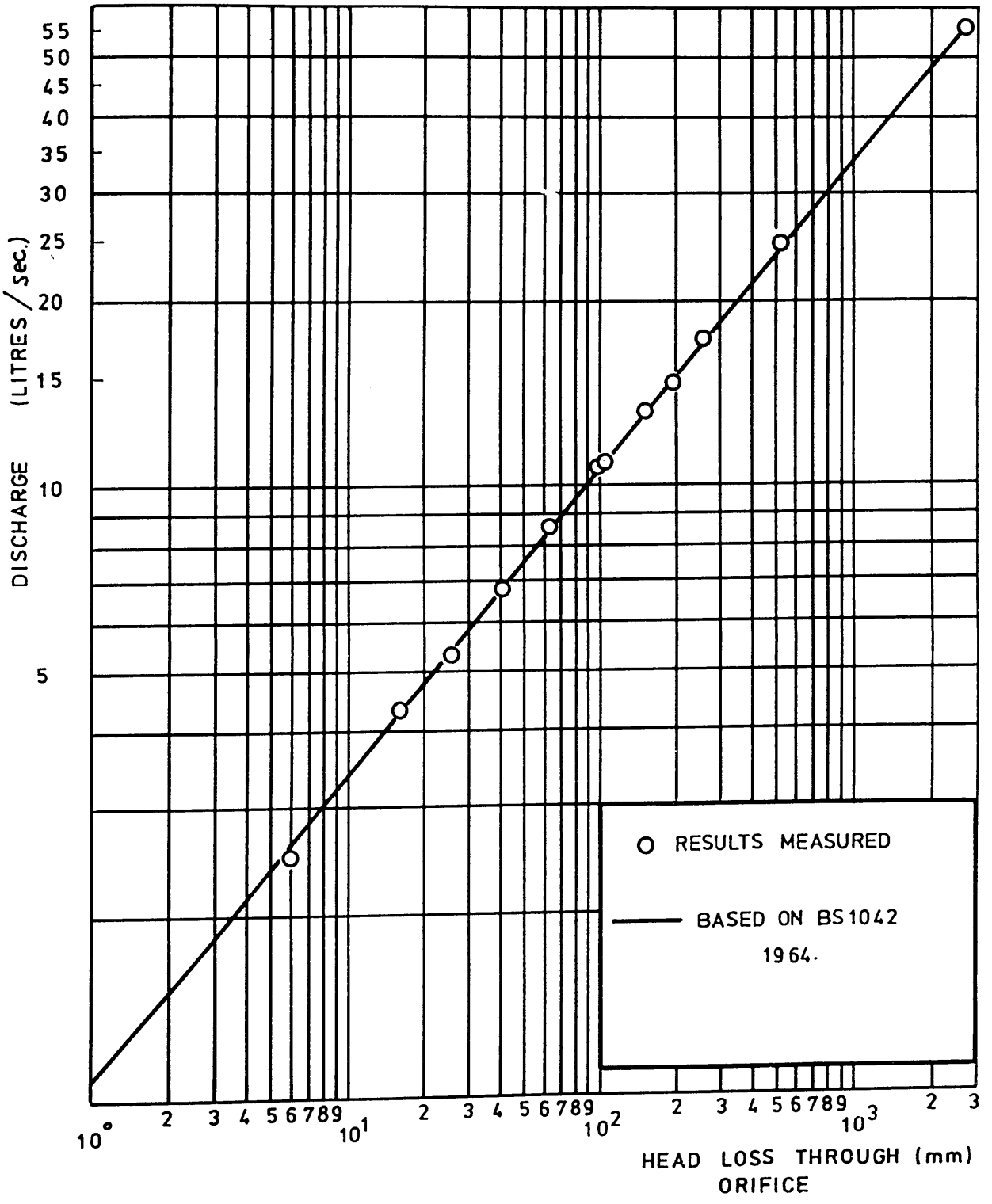

FIG. (4.12) RELATIONSHIP BETWEEN MEASURED DISCHARGE AND ORIFICE READING

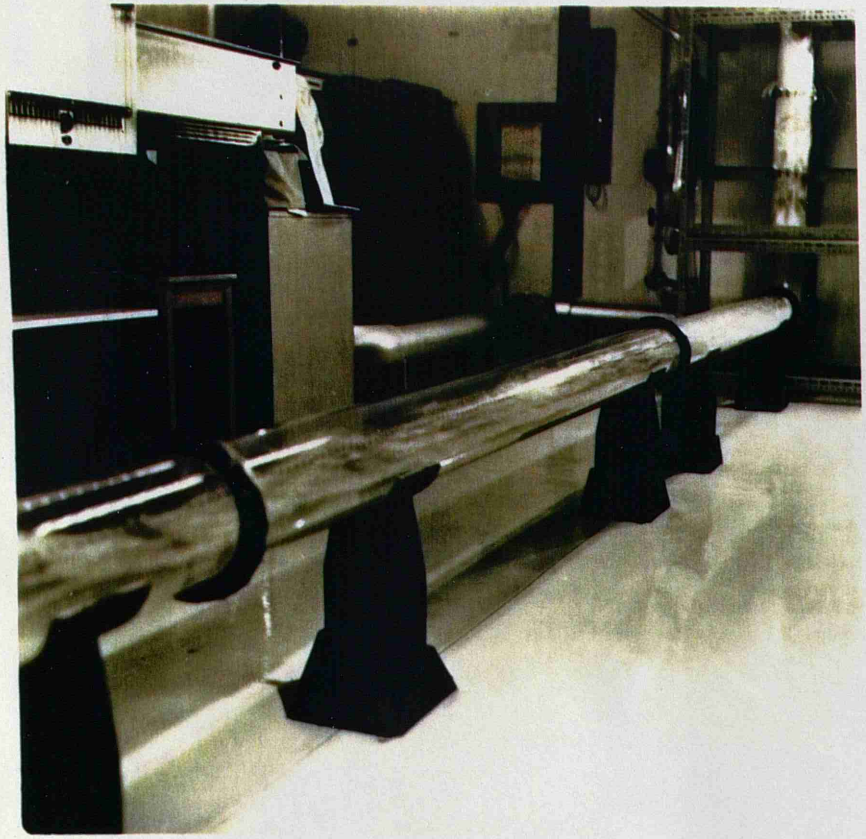

PLATE (4.11) THE HORIZONTAL TUNNEL

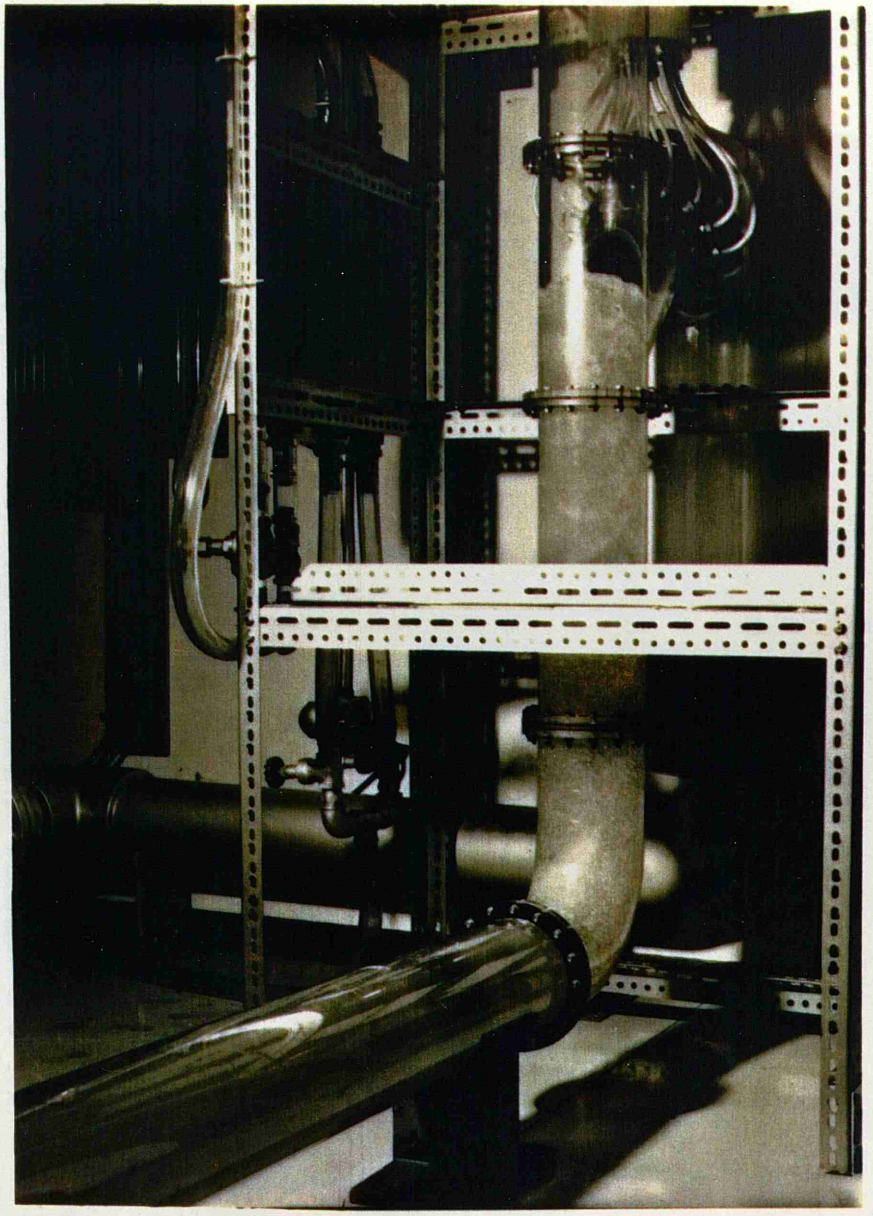

PLATE (4.12) THE UPWARD SLOPING TUNNEL $O = +1.50^{o}$

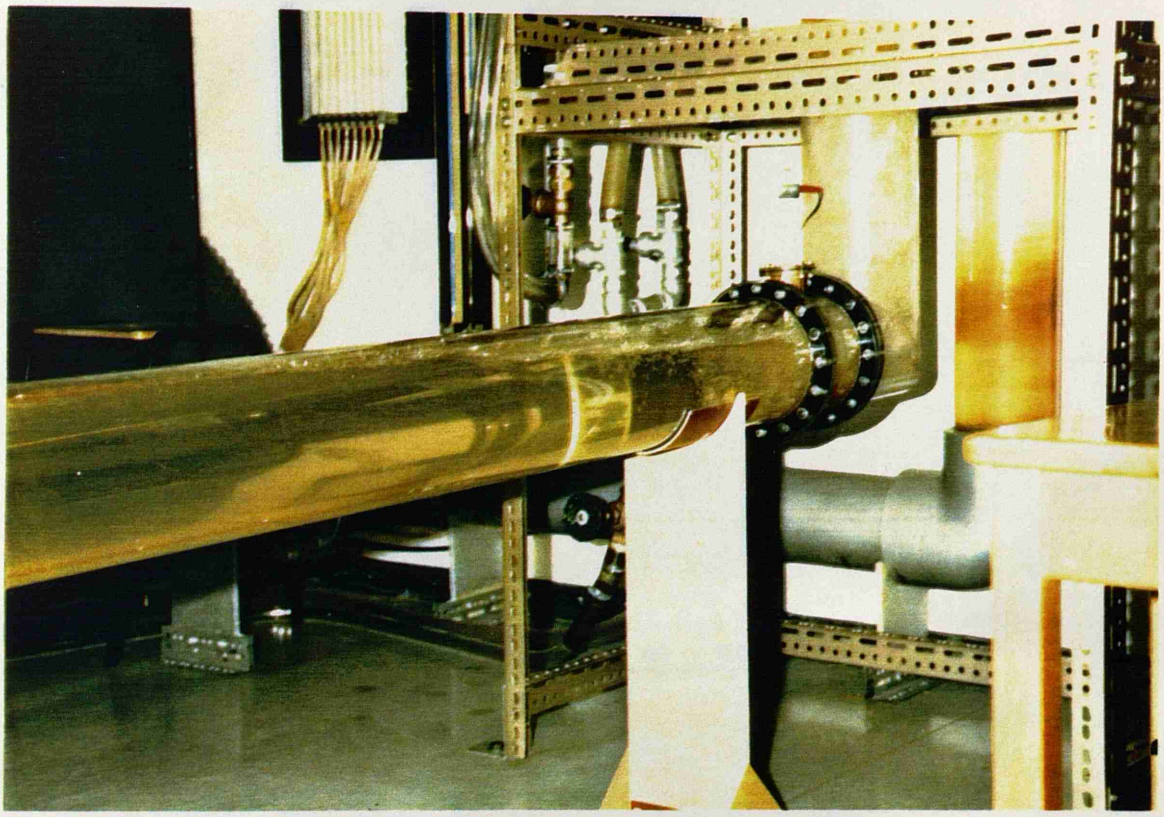

PLATE (4.13) THE DOWNWARD SLOPING TUNNEL O = -1.50°

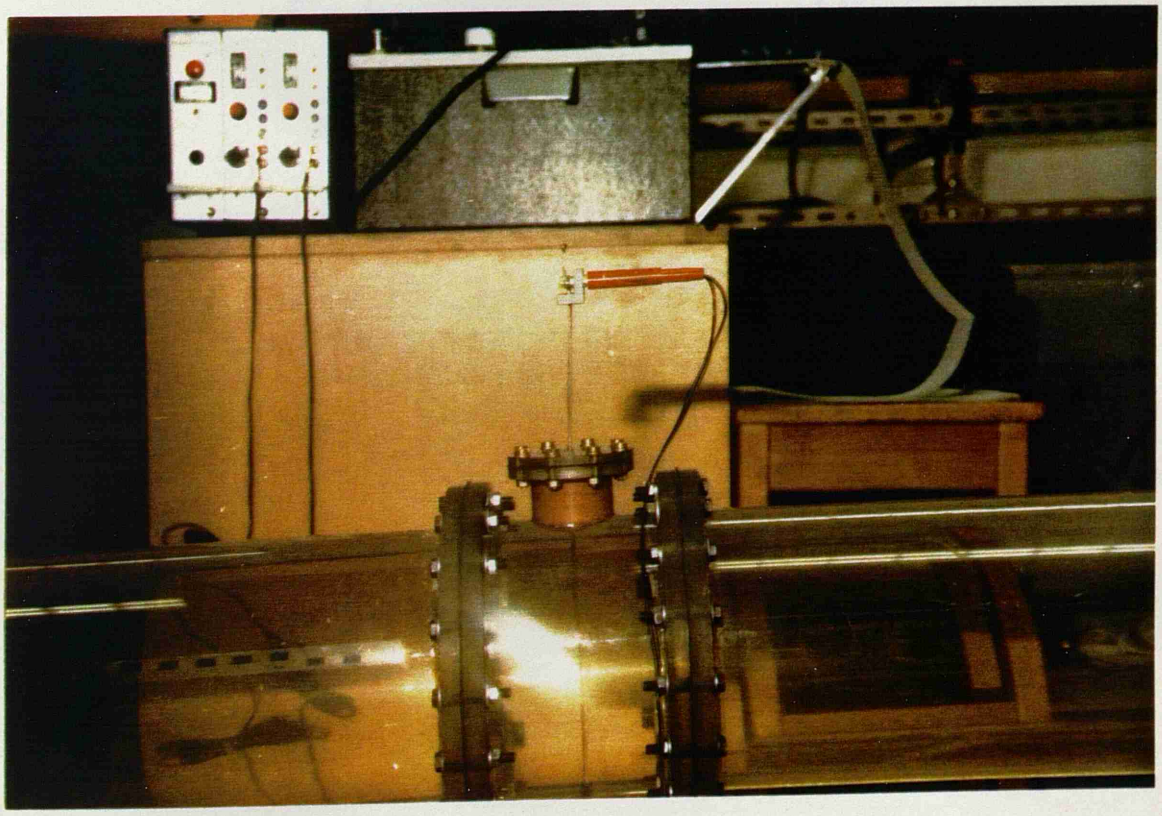

PLATE (4.14) DETAILS FOR INSERTING THE PROBE

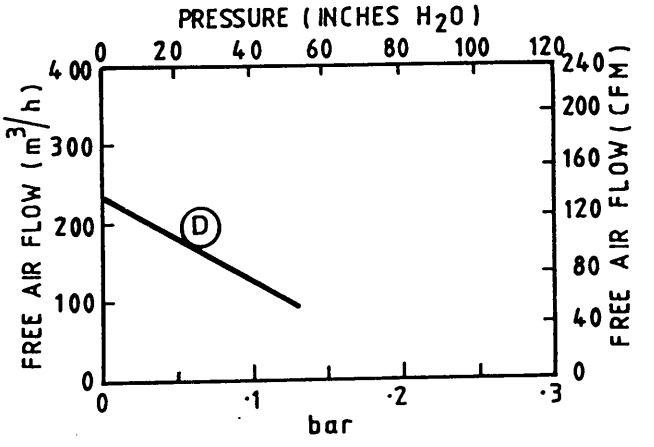

FIG. (4.13) THE RELATION BETWEEN AIR FLOW AND PRESSURE FOR THE AIR BLOWER

PLATE (4.15) THE AIR BLOWER

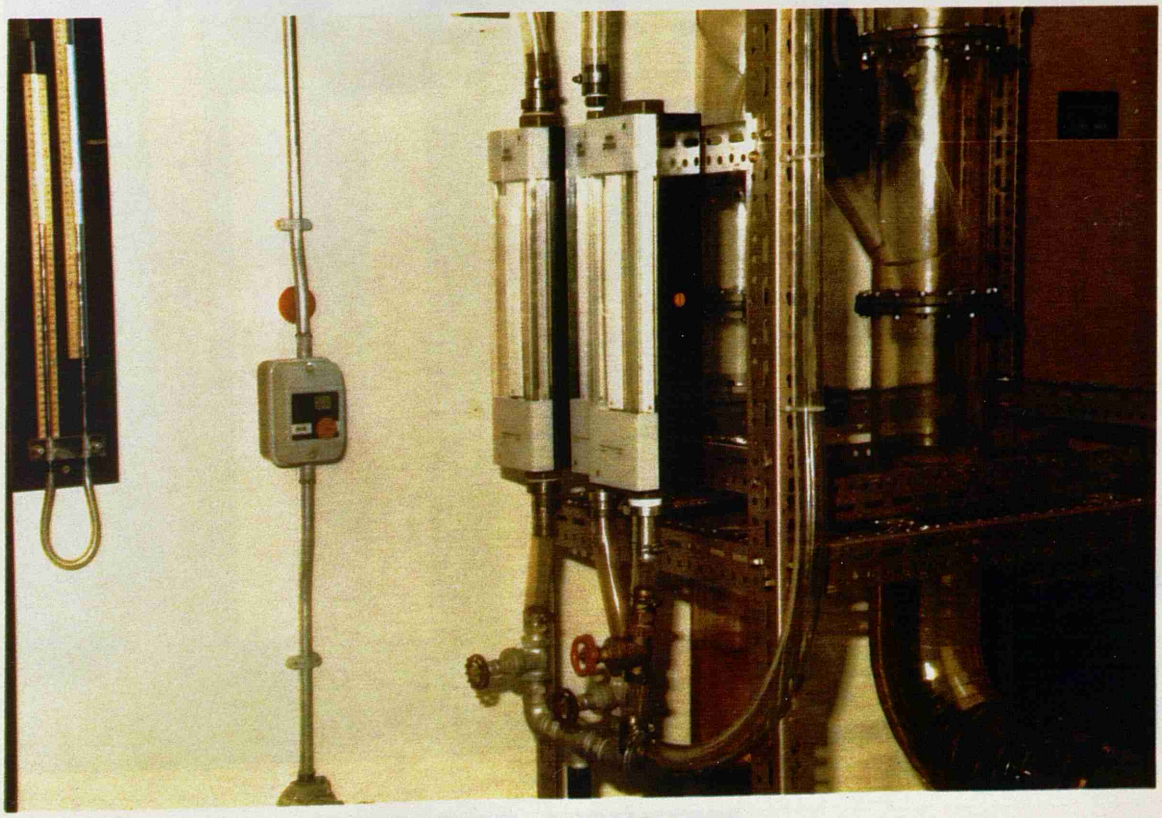

PLATE (4.16) THE CONNECTION TO THE AIR FLOW ROTAMETERS

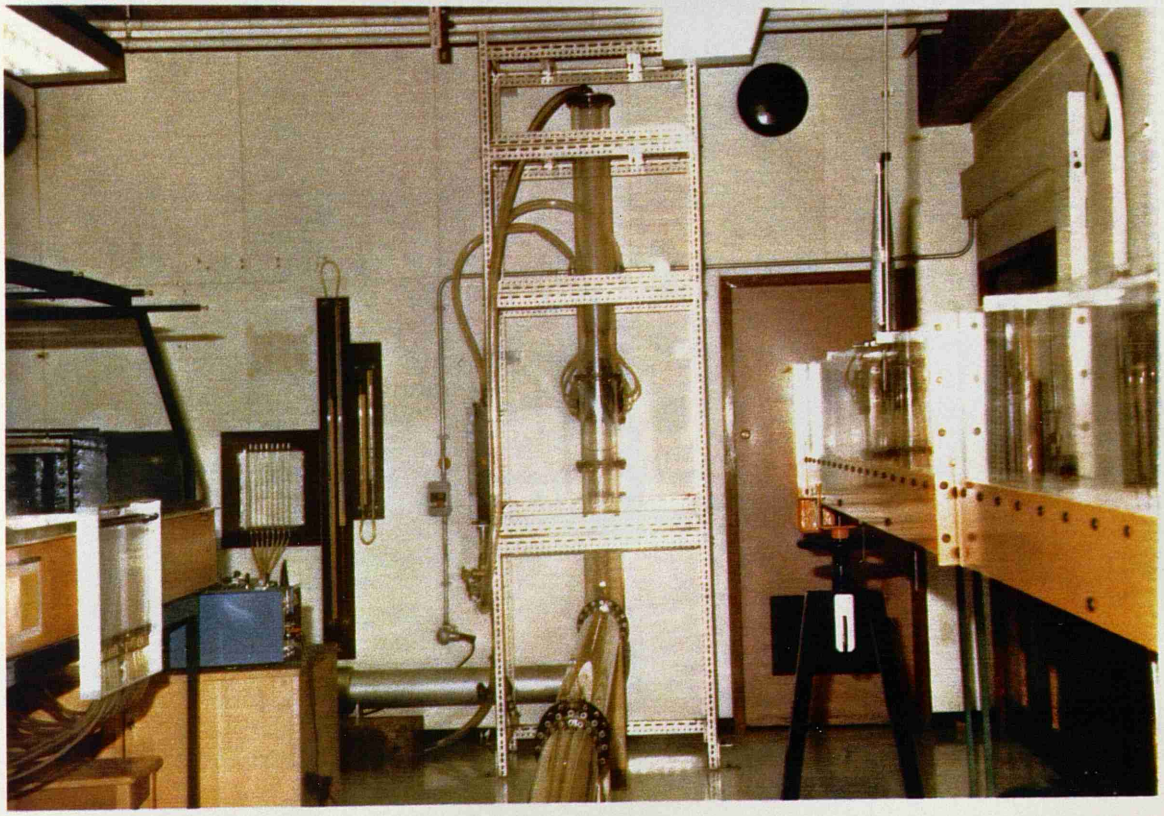

PLATE (4.17) THE AIR OUTLET AT THE TOP OF THE DROPSHAFT

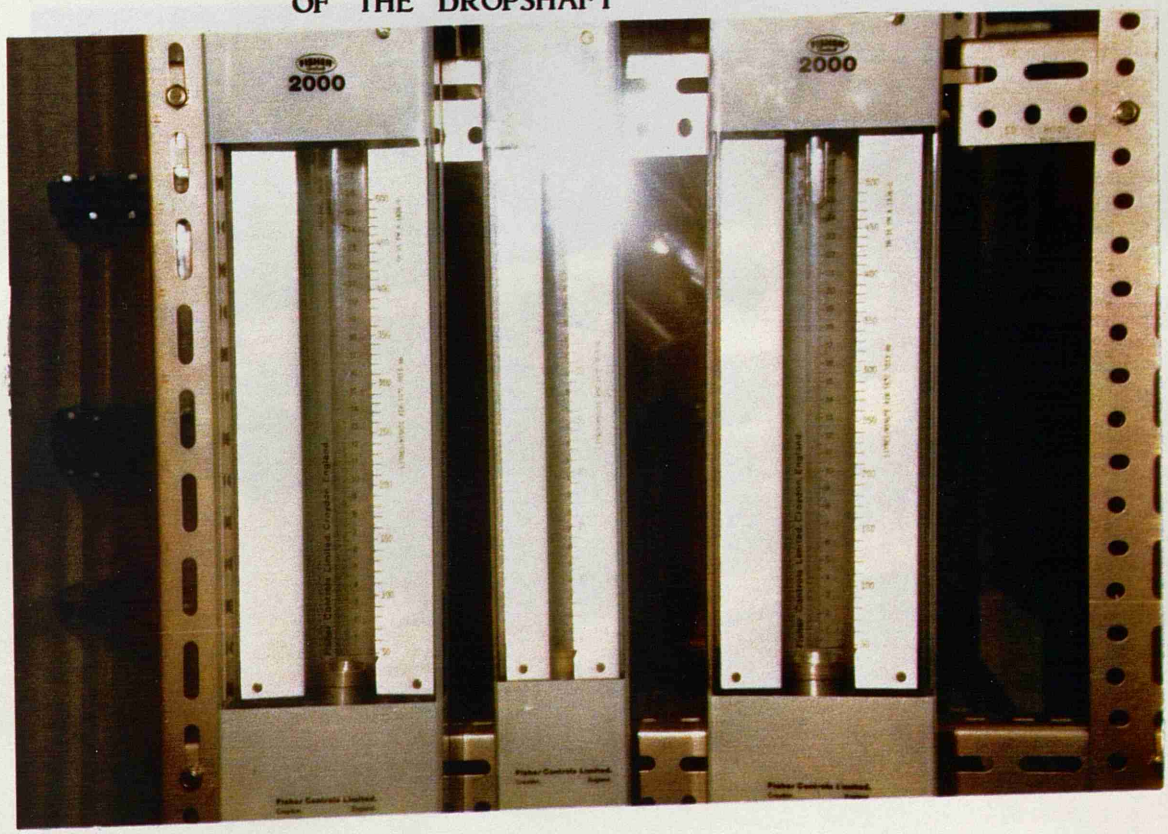

PLATE (4.18) THE AIR FLOW ROTAMETERS

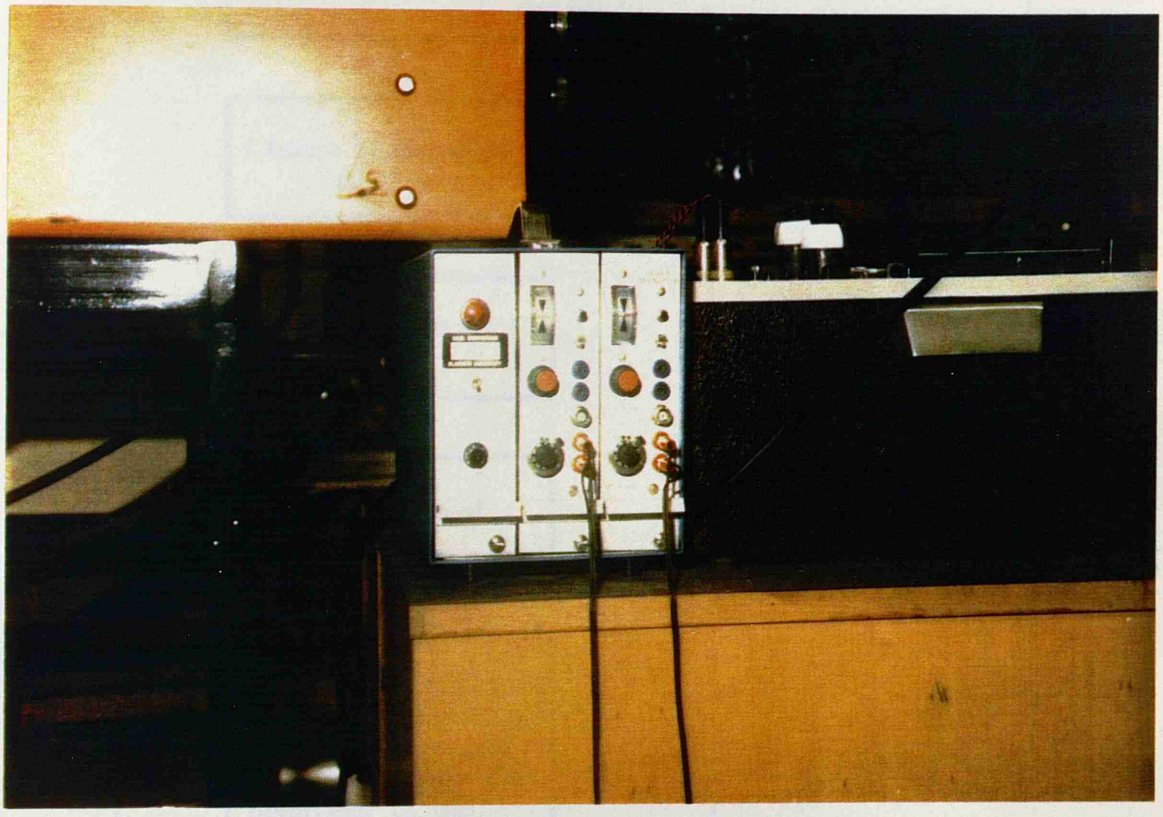

PLATE (4.19) THE WAVE MONITOR

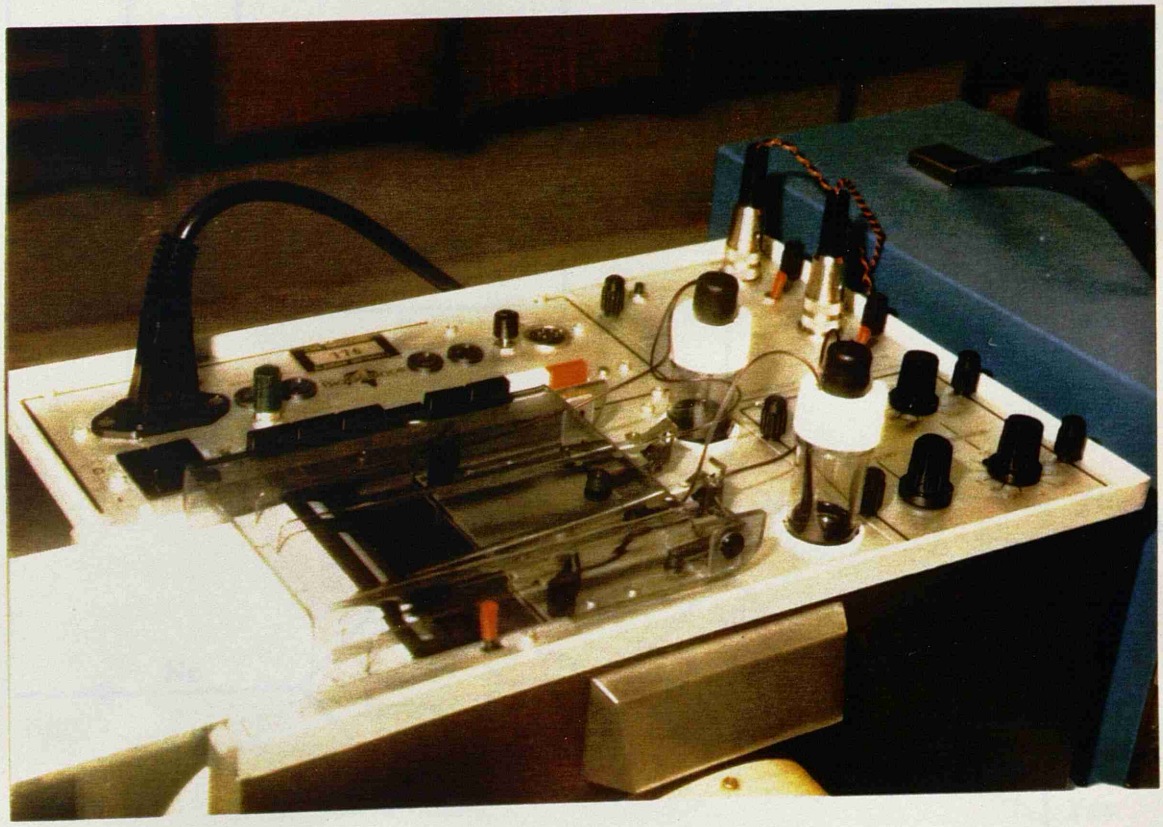

PLATE (4.20) THE CHART RECORDER

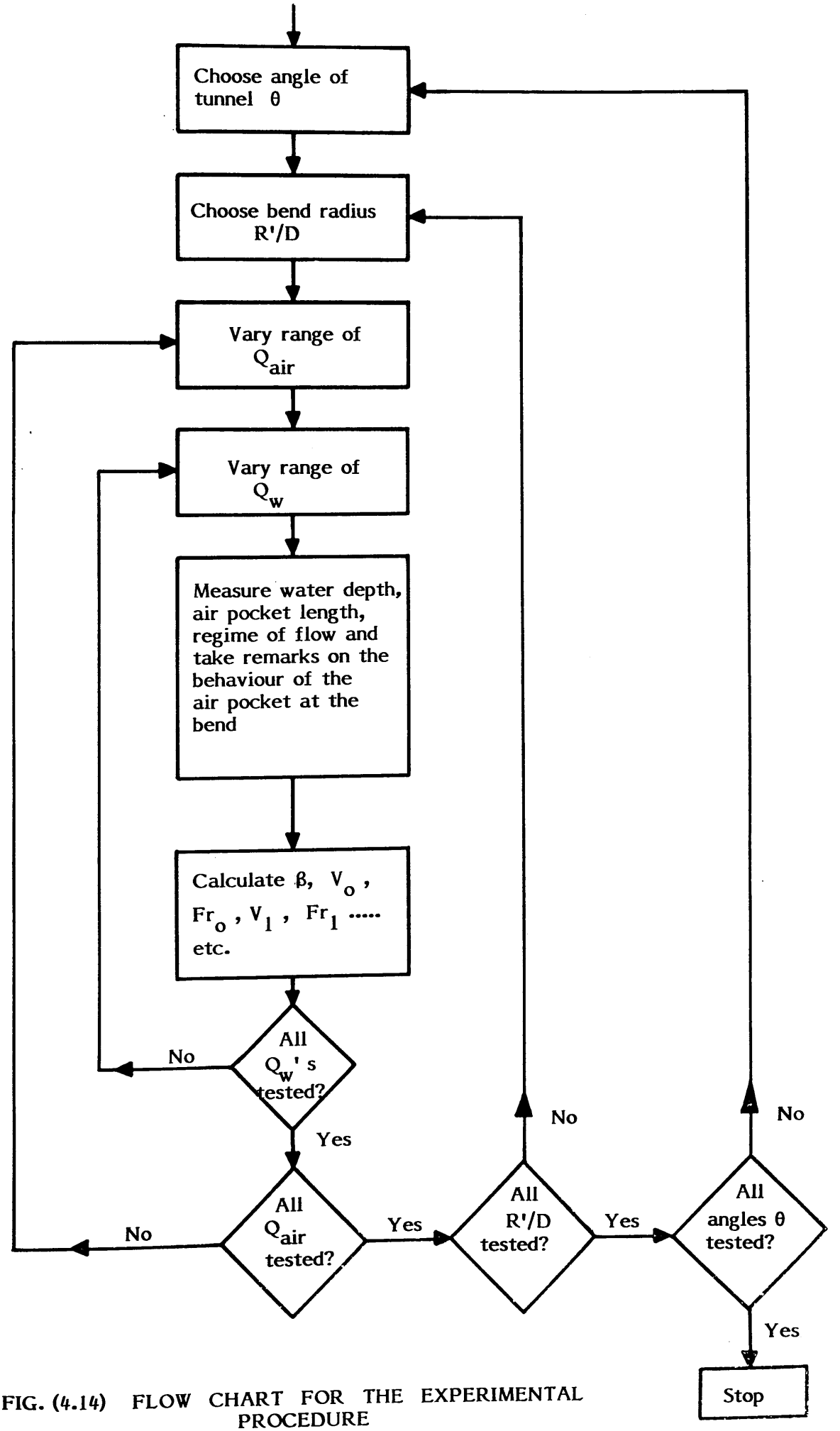

FIG. (4.14) FLOW CHART FOR THE EXPERIMENTAL PROCEDURE

Chapter Five

EXPERIMENTAL RESULTS FOR AIR POCKET BEHAVIOUR AT THE DROPSHAFT/TUNNEL JUNCTION

5.1 INTRODUCTION

In this chapter experimental data for air pocket behaviour at the junction of the vertical dropshaft/tunnel model will be presented, while the analysis of the results and the comparison with the theoretical models will be carried out in Chapter (7). As mentioned earlier in Chapter (4), this will be carried out for the three angles of inclination of the tunnel tested ($\theta = 0°$, $+1.5°$ and $-1.5°$) and for each value of θ, the results of the three bend radii ($R'/D = 0.5$, 1.0 and 1.5) will be presented. A total of nine bend geometries are investigated. A schematic representation of the flow regimes found in the experimental work will be shown for each of the nine geometries tested. Photographs of the general flow regimes occurring for air pockets at the junction of the vertical dropshaft/tunnel system will be shown in Plates (5.1) to (5.13). For each angle of tunnel inclination and bend tested, the general conditons affecting the behaviour of the air pockets will be outlined.

The experimental work was carried out by setting up "steady state" conditions in the system with a constant air flow rate and water discharge rate. Over a range of experiments, the air flow rate remained constant and the water flow rate was increased, thereby decreasing the air/water ratios. In some tests the effect of decreasing water flow rate was also investigated. Additional tests were carried out to determine the minimum water velocity required to

transport the introduced air bubbles down the dropshaft to the bend in order to form the air pocket in the first place.

5.2 GENERAL FLOW REGIMES FOR AIR POCKETS AT THE DROPSHAFT/TUNNEL JUNCTION

For the nine geometries tested, there were four general stable flow regimes occurring at the junction of the vertical dropshaft/tunnel system, although in many cases the transitions between the four stable regimes, involved unsteady and unstable air pocket behaviour. These regimes can be summarised as follows:

(1) Flow regime 1, the blowback region, which features air bubbles, air pockets or a combination of both, venting or blowing back up the vertical dropshaft. This region mainly occurs at low upstream Froude numbers and it can be sub-divided as follows:

a - air bubbles venting back up the shaft with long shallow air pocket extending downstream of the bend, as shown in Plate (5.1).

b - air pockets blowing back up the shaft with the Froude number below the pocket $Fr_1 < 1.0$, as shown in Plate (5.2a and b).

c - air pockets blowing back up the shaft with the Froude number below the air pocket $Fr_1 > 1.0$, as shown in Plate (5.3). This occurred mainly in downward sloping tunnel at $\theta = -1.5°$.

The blowback and venting back phenomenon often caused water level to rise in the vertical shaft and in some cases caused oscillation in the system, as shown in Plate (5.4a and b).

(2) Flow regime 2, featuring a stable air pocket forming at the bend with a Froude number below the pocket $Fr_1 < 1.0$. This air

pocket can either be short or long, depending on the flow parameters, the angle of inclination of the tunnel, as well as the bend radius. This flow regime is shown in Plates (5.5) and (5.6) for two angles of inclination (θ = 0° and +1.5°). It was noted from the experimental work that this flow regime rarely occurred for the downward sloping tunnel (θ = -1.5°). This will be shown in Section (5.5).

(3) Flow regime 3, featuring a stable air pocket at the bend with a hydraulic jump at its downstream end. In all cases flow under the air pocket is supercritical, $Fr_1 > 1.0$, and in most cases the water velocity under the pocket was in excess of 1.0 m/s, ensuring both entrainment and transport of air bubbles at the toe of the jump. An air pocket with an hydraulic jump is shown in Plate (5.7a and b) and an air pocket with air entrainment at its end is shown in Plate (5.8). In some cases the air pocket extended in length to the outlet tank, when it is generally referred to as stratified flow, as shown in Plate (5.9). This condition is "artificial" in the sense that a longer tunnel section would eventually produce a hydraulic jump at the point of equal specific forces. For the shorter length of tunnel in this experiment, the force-momentum flux from the supercritical flow under the air pocket is greater than that acting backwards from the outlet tank, thus producing stratified flow.

Before discussing Flow regime 4, for air pockets clearing from the bend, there is a transition region between Flow regime 3 and Flow regime 4, which is worthy of some discussion. The following events often occurred:

a - The air pocket starts to reduce in size due to air entrainment at its toe, combined with sections of the air pocket sheared off. In this case the amount of air transported at the end of the jump exceeded the amount of air introduced at the bend. This is shown in Plate

(5.10).

This phenomenon occurred mainly for the case of low ratios of air to water (β).

b - Waves start to form on the surface of the air pocket. These waves grow in amplitude, often sealing the top of the pipe. The pocket formed between the wave crest and the jump is transported and a new air pocket forms at the bend. The new pocket will grow in size and the same procedure will be repeated. Any increase in the water flow rate will cause this new air pocket to be transported. This transition region is shown in Plate (5.11).

c - A combination of waves sealing the pipe and an alternating swirl mechanism, especially at the mitre bend ($R'/D = 0.5$), will cause the air pocket at the bend to clear. This is shown in Plate (5.12).

(4) Flow regime 4, features air pockets clearing from the bend and being transported continuously downstream. In this region only air bubbles will be flowing around the bend, as shown in Plate (5.13) with air pockets forming some distance along the tunnel. It must be noted that for the mitre bend ($R'/D = 0.5$) there will still be a small separation region at the bend, even if all the air bubbles introduced are transported along the tunnel.

Each of the above flow regimes will be clarified for each of the nine geometries tested and presented in schematic form preceding each set of experimental data.

5.3 EXPERIMENTAL DATA FOR THE CASE OF THE VERTICAL DROPSHAFT AND HORIZONTAL TUNNEL, $\theta = 0°$

In this section the behaviour of bend air pockets will be considered for each bend radius separately. The experimental

results will be presented mainly in two forms, the first showing the flow regimes experienced for each bend where the air/water ratio β is plotted against the upstream non-dimensional water velocity ($V_o/\sqrt{gD}$), and the second form, showing the non-dimensional depth of flow below the air pocket (Y1/D) plotted against the upstream non-dimensional water velocity ($V_o/\sqrt{gD}$), for different air/water ratios β. Additional data will be presented (for each bend radius) representing the upper limits of flow conditions for blowback and back venting to occur (Flow regime 1), as well as data for the flow conditions necessary for clearing air pockets from the bend (Flow regime 4) just to occur. Finally, a comparison between the three bend radii (for $\theta = 0°$) will be given.

5.3.1 Air Pockets at the Bend of R'/D = 0.5

The first bend tested was the mitre bend for a horizontal tunnel, where the air flow rate was varied between 0.334 ℓ/s up to 10.5 ℓ/s, and for each air flow rate, the water flow rate was varied from 2.0 ℓ/s up to the water flow rate required to cover all four regimes of flow and beyond. In most cases, even after air pocket had cleared from the bend, the water flow rate was further increased to ensure that no other regimes of flow were in evidence. The four flow regimes outlined in section (5.2) occurred for the mitre bend and are shown in Fig. (5.1), and described below.

(1) Flow regime 1, where air bubbles and air pockets were venting or blowing back, as shown in Fig. (5.1a and b). For a given value of air flow rate Q_A, air bubbles were mainly venting back up the shaft with a long shallow air pocket extending along the roof of the tunnel. This occurred with smaller values of water flow rate, Q_W. For a further increase in Q_W, small air pockets formed at the bend and blew back up the shaft. The venting and blowing back phenomenon was noted to exist up to an upstream non-dimensional water velocity $V_o/\sqrt{gD}$ of 0.28.

(2) Flow regime 2, where a stable air pocket formed at the bend for $V_o/\sqrt{gD} > 0.28$. The air pocket length was greater than 150 mm with a Froude number below the pocket less than 1.0, as shown in Fig. (5.1c). This regime did not occur with larger ratios of air/water, β.

(3) Flow regime 3, where an air pocket with a hydraulic jump formed at the bend and sometimes extended in length to the outlet tank, as shown in Fig. (5.1d and e). The Froude number below the air pocket was supercritical $Fr_1 > 1.0$, and often the water velocity $V_1 > 1.0$ m/s, which ensured air entrainment and transport at the end of the air pocket.

(4) Flow regime 4, with no air pocket at the bend occurred with higher Froude numbers ($V_o/\sqrt{gD}$), and after the transition had taken place between an air pocket at the bend (Regime 3) and no air pocket at the bend. The transition and flow regime 4 are shown in Fig. (5.1f and g). To specify the onset of flow regime 4, the points at which the transition occurred were selected from the experimental data and a line was fitted through these points using the Least Square Method. The experimental results are shown in Fig. (5.2), where the air/water ratio is plotted against the non-dimensional water velocity indicating the four flow regimes which occurred for the sharp bend (R'/D = 0.5) and the horizontal tunnel. It can be noted that the effect of air/water ratio on the extent of the blowback region is almost negligible, while it has a significant effect on the clearing of air pockets from the bend. The effect of increasing water velocity or the Froude number ($V_o/\sqrt{gD}$) for a constant value of air/water ratio is, in effect, to change the flow regime from the blowback region to stable air pocket with the Froude number below the pocket $Fr_1 < 1.0$ or $Fr_1 > 1.0$, and then on to clearing from the bend.

In Fig. (5.3) the relation between the non-dimensional water depth below the air pocket Y_1/D and $V_o/\sqrt{gD}$ for different values of

air/water ratios β is shown. This, in effect, is a plot of air pocket depth as $H/D = 1 - Y_1/D$. For any specific value of β it can be noted from Fig. (5.3) that the depth of air pocket increases with increasing Fr_o until a stable air pocket with a hydraulic jump forms. Further increases in Froude number produces a decreasing air pocket depth until the whole air pocket is cleared and the value of Y_1/D returns to unity. This effect is seen more clearly in Fig. (5.3) where three selected values of β have been chosen, with tentative curves drawn through each β value, indicating the nature of the change of air pocket depth with increasing Froude number . At the unstable clearing point the curves are vertical.

From experimental observations it was realised that although the depth of pocket was decreasing with increasing Fr_o, the length of the pocket was increasing and often reaching the outlet tank forming stratified flow. Hence when a comparison is carried out in Chapter (7) between the theoretical model for air pockets with a hydraulic jump and the experimental data for such air pockets, the stratified flow data will be excluded because the force balance is unknown for this case.

The experimental points up to which blowback occurred, and at which clearing of air pockets started, are shown in Figs. (5.4), (5.5) and (5.6), where the air/water ratio β is plotted against Froude number $(V_o/\sqrt{gD})$, velocity under the pocket (V_1) and the Froude number below the air pocket $(V_1/\sqrt{gA_1/b})$ respectively. The best fit line for clearing shown in Fig. (5.4) is obtained by linear regression. It can be noted from Figs. (5.5) and (5.6) that air pocket clearing (at least for lower values of β) occurred with $Fr_1 < 1.0$ and $V_1 < 1.0$ m/s, implying that the clearing mechanism was not by air entrainment at the toe of the jump but more by large waves on the free surface under the air pocket and by an alternating swirl mechanism peculiar to the sharp bend.

5.3.2 Air Pockets at the Bend of R'/D = 1.0

For the horizontal tunnel with a bend radius R'/D = 1.0 similar flow regimes to the sharp bend, as outlined in Section (5.3.1), occurred. These are shown in Fig. (5.7). Flow regime 1 occurred up to an upstream Froude number Fr_o = 0.41, where some of the back venting air pockets had a Froude number below the air pocket $Fr_1 > 1.0$, although this occurred at high values of β. Flow regime 2 occurred only over a small range, as can be seen in Fig. (5.8), where it also can be noted that most of the air pockets between blowback and clearing extended to the outlet tank forming a large region of stratified flow. The clearing line was again fitted by regression analysis.

Figure (5.9) shows the relation between Y_1/D and $V_o/\sqrt{gD}$ for different values of β, where again the same pattern as for the sharp bend R'/D = 0.5, occurs. For the purposes of clarity three values of β were selected and tentative curves drawn through each β value. It can be noted that in comparison with the sharp bend, for a given Froude number and β values, the air pocket depth is greater for R'/D = 1.0. As well as this, we find significantly that clearing of air pockets downstream is more difficult in the R'/D = 1.0 bend.

The points up to which blowback took place, and at which clearing started, are shown in Figs. (5.10), (5.11) and (5.12), where β is plotted against $V_o/\sqrt{gD}$, V_1 and Fr_1 as before. It can be noted from Figs. (5.11) and (5.12) that the successive air pockets clearing from the bend required a velocity $V_1 > 1.0$ m/s and also supercritical flow under the pocket, $Fr_1 > 1.0$. It was observed that clearing was more influenced by entrainment of air bubbles at the jump, compared with the sharp bend, although waves sealing the top of the pipe were also a significant influence.

5.3.3 Air Pockets at the Bend of R'/D = 1.5

Flow regimes for the horizontal tunnel and bend radius R'/D = 1.5 are shown in Fig. (5.13) again producing similar patterns of flow to the bends R'/D = 0.5 and 1.0. The regimes of flow are illustrated in Fig. (5.14), with the blowback regime extending up to Froude numbers ($V_o/\sqrt{gD}$) of 0.6, although this value decreased rapidly for larger values of air/water ratio. Regime 2 with a stable pocket and subcritical flow under the pocket did not exist for R'/D = 1.5. In fact stratified flow appeared to be the major regime for this bend, especially for moderate values of Fr_o and air/water ratio. For a longer experimental tunnel section this type of flow would likely produce an hydraulic jump at the point of equal specific forces. The air pocket clearing line in Fig. (5.14) revealed a greater difficulty in air pocket clearing relative to the previous two bends.

Figure (5.15) is a plot of Y_1/D or (1-H/D) against $V_o/\sqrt{gD}$, and reveals a similar pattern to the previous bends. At lower Froude numbers the air pocket depth increases with Froude number until the stable hydraulic jump region is reached, when subsequent increases in Froude number decreases the pocket depth and eventually leads to clearing completely from the bend. This pattern is seen more clearly from the tentative curves plotted for three selected values of air/water ratio in Fig. (5.15). One point of note is that stratified flow air pockets are generally deeper than shorter pockets with hydraulic jump, hence the reason for the separation of experimental data into two different ranges of Y_1/D, as shown in Fig. (5.15).

The experimental data for blowback and clearing limits are given in Figs. (5.16), (5.17) and (5.18). Figure (5.16) in particular reveals that clearing for the R'/D = 1.5 bend occurs at higher Froude numbers than the other two bends R'/D = 0.5 and 1.0, and blowback is also more likely. This is a surprising development

indicating that the sharp bend R'/D = 0.5 is the most efficient with regard to air pocket behaviour even though it will undoubtedly generate the highest head loss. Figure (5.18) reveals that blowback can occur in the R'/D = 1.5 bend even with supercritical flows under the pocket, and at the opposite end of the spectrum, clearing of the pocket can occur for subcritical flows under the pocket. This reveals again that clearing by hydraulic jump entrainment may not be the primary mechanism, but bodily sweeping and surface wave formation may be more significant.

5.3.4 Comparison between the Three Bends Used for the Horizontal Tunnel Case

The experimental results have shown that the bend radius has a significant effect on the behaviour of air pockets at the junction of the vertical dropshaft and horizontal tunnel. The effect of air/water ratio (β) and water flow rate (Q_w) on the flow regimes has already been shown, where, for a given bend radius, increasing β will increase the size of the air pocket, and increasing Fr_o (or Q_w) will at first increase the air pocket size, then decrease it until the clearing point.

To clarify the effect of the bend radius, the points up to which blowback took place, and after which air pockets cleared from the bend, are plotted in Fig. (5.19) for the three bend radii R'/D = 0.5, 1.0 and 1.5. It can be noted that increasing the bend radius increases the Froude number up to which blowback occurred and also makes it more difficult to clear any air pocket formed at the bend. For the case of the sharp bend, small air bubbles were venting back in flow regime 1, while for the other two bends, air pockets were blowing back. This is due to the fact that the nose of the air pocket in the bends R'/D = 1.0 and 1.5, is attached to the upper end of the bend which allows the buoyancy to act and causes the air pocket to blowback if the downward water drag force is less than the buoyancy force of the air pocket. For the sharp bend, air bubbles

mainly fill the separation zone at the bend which means that the nose of the pocket is exactly at the centre of the bend, hence there is no buoyancy acting. If the water velocity in the sharp bend is not sufficient to form a stable air pocket at the bend, the separation zone will be unstable and air bubbles will vent back up the vertical shaft. It was also found that stratified flow occurs more easily in the radiused bends (R'/D = 1.0 and 1.5).

Clearing the air pockets in the three bends depended on the flow conditions at the bend such as the waves sealing the bend, secondary currents, the flow conditions below the air pocket, and the amount of sweeping force in the flow. It can be noted from Fig. (5.19) that clearing the air pockets occurred at higher Froude numbers for the larger radiused bends showing that clearing is not only dependent on the flow parameters, but also on the geometry of the bend.

The first tentative conclusion would be that for the case of a horizontal tunnel outlet, the sharp bend R'/D = 0.5 is least likely to produce blowback effects and most likely to produce continuous clearing of air pockets from the bend. The largest radiused bend R'/D = 1.5 produces the greatest blowback potential and the least clearing potential.

5.4 EXPERIMENTAL DATA FOR THE CASE OF THE VERTICAL DROPSHAFT AND THE UPWARD SLOPING TUNNEL, θ = +1.5°

In this section experimental data on the behaviour of air pockets at the junction of the vertical dropshaft and the tunnel with an upward slope of +1.5° with horizontal will be presented. Separate results are presented for each bend radius, R'/D = 0.5, 1.0 and 1.5, in a similar manner to section (5.3), with emphasis on the extent of each regime of flow in terms of Froude number (Fr_o) and air/water ratio (β), the variation of air pocket depth, the limiting

state for blowback potential and clearing of air pockets downstream, as well as an overview comparison between behaviour at the three bend radii, and the two tunnel inclinations (θ), tested so far. It was felt intuitively that changing the tunnel slope from horizontal to an upward slope of +1.5° would reduce the likelihood of air pocket blowback, and increase the chances of air pocket clearing downstream. This was based on the premise that the upward sloping tunnel would provide pockets (forming just downstream of the bend) with a buoyancy component acting in the outlet direction. One complication in this argument is the effect of an upward sloping tunnel on the force-momentum balance. Certainly flow under an air pocket at the bend might be considered as open channel flow on an adverse slope. This will produce an additional backward weight force in the force momentum balance and should lead to a larger range of regime 2, the drowned jump condition and generally shorter air pockets than either the horizontal tunnel case or the downward sloping tunnel case. In this sense, stratified flow should also be more difficult to achieve, because the additional backward force will mean that a larger upstream flow will be required to push the hydraulic jump condition to the outlet tank (stratified flow), and hence the air pocket is likely to have cleared by that flow rate anyway because of the upward slope of the tunnel.

5.4.1 Air Pockets at the Bend R'/D = 0.5

For the tunnel at an angle of +1.5° with horizontal and a bend radius R'/D = 0.5 the four flow regimes outlined in Section (5.2) occurred again, but with significant differences. For Flow regime 1 there were air pockets blowing-back with a Froude number below the air pocket, Fr_1, either less or greater than 1.0, as shown in Fig. (5.20). Flow regime 2, consisting of air pockets with subcritical flow under the pocket, occurred much more frequently than in the case of the horizontal tunnel outlet, while Flow regime 3, for the case of air pockets with a hydraulic jump, was again significant but very few regime 3 pockets extended to the outlet tank to form

stratified flow. Hence, stratified flow is not shown in Fig. (5.20) because it is not an important regime for this bend. Air pocket clearing again took place by waves sealing the bend at higher water flow rates and the bend pocket being bodily swept out.

Experimental results are shown in Fig. (5.21) where β is plotted against $V_o/\sqrt{gD}$ and the various regimes of flow are illustrated. It was found that air pockets at the bend were blowing back up to an upstream Froude number Fr_o = 0.245, which is less than that for a horizontal tunnel. Comparison of Figs. (5.21) and (5.2) for the horizontal tunnel case, reveals a much larger range of regime 2 (stable subcritical pocket) in the upward sloping pipe,as well as a smaller range of hydraulic jump and stratified flow, regime 3. It is also noted from Fig. (5.21) that air pocket clearing occurred over a narrower range of Froude number 0.5-0.7. It was observed that for low values of β, clearing was taking place by air entrainment at the end of the air pocket, while for higher values of β, surface waves forming at high water flow rates on the interface between water and air were sealing the tunnel roof at the bend, forming a succession of clearing air pockets. Any increase above this flow rate caused the air pocket at the bend to clear completely. Air bubbles flowing around the bend formed air pockets a short distance from the bend which were transported along the tunnel (in succession), the instant they were formed. This is the general mode of regime 4.

Experimental data for the air pocket depth against the upstream Froude number is shown in Fig. (5.22), where tentative curves are plotted for selected values of β. For lower flow ranges the air pocket depth increases with increasing Froude number and air/water ratio. Once supercritical regime 3 is reached the air pocket depth decreases in size until the clearing process occurs. One notable exception, as seen in Fig. (5.22), is for the case of $\beta < 0.1$, where downstream clearing of the air pocket occurs before regime 3 occurs at all.

The points for blowback and clearing are shown in Figs. (5.23), (5.24) and (5.25) where β is plotted against $V_o/\sqrt{gD}$, V_1 and Fr_1 respectively. It can be noted from the last two figures that most points of clearing had a velocity and Froude number below the air pockets greater than 1.0.

It is informative to compare blowback and clearing data for this case and the horizontal tunnel case, shown in Figs. (5.4), (5.5) and (5.6). If we consider for the meantime only β values less than 0.4, then comparing Figs. (5.4) and (5.23) directly it is seen that the average upstream Froude number ($V_o/\sqrt{gD}$) to cause clearing is approximately the same in each case, around 0.6. Comparing the clearing velocity and Froude number under the air pocket for the two cases shows that most of the clearing air pockets for the horizontal tunnel have $V_1 < 1.0$ m/s and $Fr_1 < 1.0$, while for the upward sloping tunnel mostly $V_1 > 1.0$ m/s and $Fr_1 > 1.0$. This shows that for the upward sloping tunnel the air entrainment at the toe of the jump aided in clearing the air pocket, while for the horizontal tunnel the clearing mechanism was mainly by the surface waves and the alternating swirl at the bend.

5.4.2 Air Pockets at the Bend of R'/D = 1.0

For the tunnel at an upward slope of +1.5° with horizontal and a bend radius R'/D = 1.0 the four general flow regimes outlined in Section (5.2) occured, as shown in Fig. (5.26). Flow regime 1 included air pockets blowing back with under-pocket Froude number Fr_1, both smaller and greater than 1.0. Regime 1(B) in Fig. (5.26) occurred generally with larger air/water ratios, $\beta > 0.3$, whereas regime 1(A) was confined to $\beta < 0.3$. Flow regime 2 with a stable air pocket and subcritical flow under the pocket was again a significant regime, although less so than the case of R'/D = 0.5 in Section (5.4.1). Flow regime 3 included a wide range of stable hydraulic jump behaviour as well as a large number of stratified flow conditions where the jump extended to the outlet tank. It was noted

that for the sharp bend (R'/D = 0.5) stratified flow was practically non existent. Its existence for the radiused bends leads to the inevitable conclusion that the effect of the larger bend radius is to produce a flow under the pocket with a greater force-momentum flux so that the jump can be transported more easily to the outlet tank. Experimental data points for these various regimes of flow are shown in Fig. (5.27) for the case of β against the pipe full Froude number ($V_o/\sqrt{gD}$). It is notable from Fig. (5.27) that blowback potential occurred up to $Fr_o \simeq 0.4$. This is significantly greater than for the sharp bend shown in Fig. (5.21), but similar to R'/D = 1.0 and horizontal tunnel. Of course the larger radiused bends allow the upstream nose of the air pocket to drift closer to the dropshaft and hence producing a greater backward buoyancy. Figure (5.27) also reveals that clearing of air pockets occurs at larger Froude numbers than the sharp bend case, for a given value of β. Comparison with Fig. (5.8) for R'/D = 1.0, but the horizontal tunnel case reveals that clearing occurs at marginally larger Froude numbers in the upward sloping pipe. This is surprising in view of the additional buoyancy assistance in the upward sloping pipe.

The values of the bend air pocket depth, in the form Y_1/D are shown plotted against Froude number in Fig. (5.28), where tentative curves are fitted for selected values of β. It is clear from Fig. (5.28) that air pocket depth increases with Froude number and β until a stable jump or stratified flow is reached, thereafter the air pocket decreases in depth until successive clearing occurs. Figure (5.28) reveals the definite split in regime 3 flows between the hydraulic jump data (upper points) and the stratified flow data (lower points). Figure (5.28) shows a significant feature for values of $\beta < 0.1$. In the Froude number range 0.4-0.6, air pocket depth decrease, as if to clear before reaching supercritical flow regime 3. Clearing in fact does not occur at this point, pockets reach regime 3, and clear as indicated at Froude numbers in excess of 0.7.

Blowback and clearing limits are shown in Figs. (5.29), (5.30) and (5.31), where β is plotted against Fr_o, V_1 and Fr_1 respectively. Two observations are worthy of note:

(1) Although blowback occurs up to Froude number (pipe full) of 0.4 over a wide range of β values, it can be noted from Figs. (5.30) and (5.31), that for β values in excess of 0.25, the flow under the pocket becomes highly supercritical or, in other words, the air pocket depth increases dramatically over a small variation in air/water ratio from 0.2 to 0.3. This is reflected in Fig. (5.28) where an increase in β of this order can effectively produce two different regimes of flow. This phenomenon occurred in a similar fashion for the case of the horizontal tunnel and R'/D = 1.5, as shown in Fig. (5.15). It should be noted from Fig. (5.28) that this phenomenon is likely to give rise to significant flow instability at low Froude numbers, 0.1-0.4, and at moderate air/water ratios, 20-30%, as the air pocket depth can suddenly change from almost zero to 80% of the pipe diameter. An explanation for this phenomenon will be attempted later.

(2) The clearing points all had the characteristic of $V_1 > 1.0$ m/s and $Fr_1 > 1.0$.

5.4.3 Air Pockets at the Bend of R'/D = 1.5

The flow regimes for the case of the upward sloping tunnel ($\theta = +1.5°$) and the largest R'/D value tested (1.5) are shown in Fig. (5.32). The behaviour is similar to the last bend but exhibiting a greater tendency towards blowback, especially regime 1(B), a greater tendency to by-pass regime 2 completely, the stable subcritical air pocket, a greater tendency towards stratified flow, regime 3(E), and clearing of air pockets often occurring by the bodily sweeping mechanism after large waves had appeared on the free surface under

the air pocket.

The experimental data is shown in Fig. (5.33), revealing a blowback potential up to Froude numbers of 0.45 and clearing limit very similar to the R'/D = 1.0 bend for the upward sloping tunnel. A comparison with the horizontal tunnel case in Fig. (5.14) reveals a reduced likelihood of blowback and greater difficulty in clearing in the upward sloping tunnel.

Data for the air pocket depth is given in Fig. (5.34), with tentative curves for selected values of β. Figure (5.34) reveals a great propensity towards two completely separate data sets, one for β < 20% and the other for β > 20%, the latter producing much greater depths of air pocket, much shallower depths of flow under the air pocket, and greater tendency towards stratification.

Details of blowback and clearing limits are shown in Figs. (5.35), (5.36) and (5.37), where β is plotted against $V_o/\sqrt{gD}$, V_1 and Fr_1 respectively. Again blowback potential is confined to an almost constant value of Fr_o ($\simeq$ 0.45), but this masks the large variation in flow conditions under the air pocket (V_1 , Fr_1) with increasing β. Again, clearing data points all reveal V_1 > 1.0 m/s and Fr_1 > 1.0.

5.4.4 Comparison Between the Three Bends for the Upward Sloping Tunnel Case

A comparison of the blowback and clearing data for the three bends R'/D = 0.5, 1.0 and 1.5, is shown in Fig. (5.38). The effect of increasing the bend radius is to increase the tendency to blow back up the dropshaft. This is a result of the upstream nose of the bend air pocket creeping back towards the dropshaft at larger radius bends, hence giving extra blowback buoyancy.

The effect of increasing bend radius is to increase the

Froude number, or difficulty, of clearing air pockets from the bend, although from Fig. (5.38), clearing data for R'/D = 1.0 and 1.5 are very similar.

The effect of increasing bend radius is also seen in the change of flow regimes and air pocket depths. An increasing radius will reduce the possibility of stable regime 2, will increase the possibility of stratified flow, or at least the hydraulic jump moving downstream along the tunnel, and we may conclude again, as in the case of the horizontal tunnel outlet, that in every sense of the word except head loss, the sharp bend is the most efficient and trouble free from the view point of air pocket formation. The effect of the tunnel slope will be included in Section (5.6).

5.5 EXPERIMENTAL DATA FOR THE CASE OF THE VERTICAL DROPSHAFT AND THE DOWNWARD SLOPING TUNNEL , $\theta = -1.5°$

In this section the experimental results showing the behaviour of air pockets at the junction of the vertical dropshaft and the tunnel with a downward slope of -1.5° with horizontal will be presented. The results will be presented for each bend radius separately, then a comparison between the three bends will be carried out. The general flow regimes outlined in Section (5.2) also occurred for this downward slope, although the blowback regime extended to higher Froude numbers than both the horizontal tunnel and the upward sloping tunnel. The back-venting air pockets at first extended in length, sometimes reaching the outlet tank, and then suddenly blew-back up the dropshaft causing the water level to rise in the vertical dropshaft and sometimes overspill of water from the top of the shaft. This blowback phenomenon in the downward sloping tunnel caused considerable oscillation and vibration in the system. Also, it was found that increasing the air/water ratio (β) caused the flow to become stratified very quickly. That is, the hydraulic jump was pushed downstream to the outlet tank. For the above reasons it

was decided to use generally lower air/water ratios for this slope in order to investigate the exact behaviour of the air pockets at the bend under conditions of semi-stability. Flow regime 2 almost disappeared for the three bends except for a few air pockets for the sharp bend, with the tendency to move directly to flow regime 3, which was a mixture of hydraulic jump and stratified flow phenomenon. The downward sloping tunnel with its extra weight component (downstream) in the force-momentum equation, encourages an hydraulic jump to move downstream and hence will increase the likelihood of stratified flow with the jump removed to the downstream outlet tank.

The clearing of air pockets for the case of small values of air/water ratio was by air entrainment at the end of the air pocket, as shown earlier in Plate (5.10), where the size of the air pocket reduces until the air pocket is cleared. When the ratio of air to water is increased, the supercritical flow under the pocket is unable to transport air bubbles (by entrainment at the toe of the jump) to the required levels of incoming air/water ratio. In fact, a high incoming air/water ratio will have a tendency to push the hydraulic jump downstream, towards the condition of stratified flow. From this point on, the mode of air pocket clearing appeared to take the form of large surface waves on the free surface close to the bend, sealing the top of the pipe and travelling downstream carrying the air pocket along with it. The source of this instability is not immediately obvious.

5.5.1 Air Pockets at the Bend of R'/D = 0.5

In this section the behaviour of air pockets for the downward sloping tunnel with a bend radius of R'/D = 0.5 will be presented. The flow regimes for this bend are shown in Fig. (5.39) where the general four regimes outlined in Section (5.2) occurred. For flow regime 1 at low Froude numbers, air bubbles vented back up the dropshaft, which at slightly higher Froude numbers, air pockets were blowing back. The mechanism of blowback appeared to be that of

small air bubbles transported along the tunnel section, eventually forming air pockets. These air pockets gorw in size and start moving in opposite direction to the flowing water, i.e. blowing back along the tunnel section. These blowing back air pockets coalesced with any air pocket forming at the bend, and caused the whole pocket to blowback up the vertical shaft. This behaviour happened mainly for low values of air/water ratio, β, while for higher values of β the air pocket at the bend exhibited a mechanism of increasing and decreasing in length, and suddenly blowing back up the shaft causing vibration in the system and raising the water level in the vertical dropshaft.

Regime 2 in Fig. (5.39) with the stable pocket and sub-critical flow under the pocket proved to be virtually non-existent for the case of a downward sloping tunnel section. The flow patterns tended to migrate from blowback (regime 1) to hydraulic jump and stratified flow, regime 3. For the sharp bend, a stable hydraulic jump occurred at lower Froude numbers in regime 3 and quickly became stratified flow for any increase in water flow rate. In fact, stratified flow was the dominant mechanism even for small values of air/water ratio β. The regime in dominance appeared to be simply a function of the force-momentum balance acting.

Clearing of air pockets was by air entrainment at the toe of the air pocket formed at the bend, for low values of β, and by waves sealing the bend for high values of β.

Experimental data for the various regimes of flow are shown in Fig. (5.40) with β against $V_o/\sqrt{gD}$. The blowback regime was experienced for this bend and slope up to a Froude number of 0.3, which is not significantly greater than the case of the horizontal tunnel and upward sloping tunnel. Figure (5.40) reveals the dominance of the stratified flow regime, which in a longer tunnel section would probably consist of a long air pocket with hydraulic jump. The clearing data points fall into two distinct catagories. When β <

5%, clearing of the air pocket occurs by entrainment and transport at the toe of the jump. For β in the 10-20% range, clearing occurs by the surface wave, bodily sweeping mode.

Experimental data points for the depth of air pocket at the bend, plotted in the form of the depth of flow under the air pocket, are shown in Fig. (5.41). Most of the data falls into the regime 3 category, with a stable hydraulic jump or stratified flow. It can be seen that the influence of the air/water ratio (β) seems negligible for this case with a much reduced spread of data. Clearing begins at Froude numbers around 0.7 to 0.8 which is significantly greater than the case of horizontal or upward sloping tunnels with a sharp bend.

Figures (5.42), (5.43) and (5.44) show detailed data points for both blowback and clearing in the downward sloping case, where β is plotted against $V_o/\sqrt{gD}$, V_1 and Fr_1 respectively. It is apparent that the ratio of air to water (β) has little effect on either process in this case, thus the correlation line of clearing must remain vague. The upstream Froude number required for clearing is approx- imately three times that of the upper limit for blowback occurrence. Most of the clearing data reveals $V_1 > 1.0$ m/s and $Fr_1 > 1.0$.

5.5.2 Air Pockets at the Bend of R'/D = 1.0

Flow regimes for the downward sloping tunnel and the bend radius R'/D = 1.0 are shown in Fig. (5.45) where the same regimes and behaviour outlined in Section (5.5.1) occurred here. For this bend there was a significant increase in regime 1(B) behaviour, which is a blowback regime with deep air pocket at the bend and supercritical flow under the air pocket. Also regime 2 all but disappeared with a tendency to move from the blowback regime 1, to either hydraulic jump or stratified flow in regime 3, when the water discharge rate was increased. Stratified flow tended to dominate the flow regimes for

this slope and bend radius. Clearing again took place by air entrainment at the toe of the existing air pocket at the bend and by waves sealing the bend.

Experimental results are shown in Fig. (5.46) for β against $V_o/\sqrt{gD}$, where it is noted that blowback for this bend occurred up to an upstream Froude number of about 0.56, although it was reduced for higher air/water ratios when stratified flow appeared instead. Stratified and hydraulic jump flows dominate this bend and tunnel slope, with ultimate clearing, from Fig. (5.46), not occurring until Froude numbers of the order 0.9 to 1.2. This is greater than the sharp bend and greater than any of the other bend radii for the horizontal tunnel and upward sloping tunnel, at least for the range of air/water ratio covered by the clearing data $\beta < 0.15$, in Fig. (5.46).

Figure (5.47) is a plot of Y_1/D against $V_o/\sqrt{gD}$ for different values of air/water ratios. The pattern of air pocket depth development is similar to before, although there are very few experimental data points in the low Froude number range, for β values higher than 0.1. It is again apparent that unstable air pocket behaviour is likely for Froude numbers less than about 0.4, where the pocket depth can vary very rapidly from say 10% to 80% of the pipe diameter. Figure (5.47) also indicates the dominance of regime 3, with air/water ratio having a greater influence than the sharp bend as evidenced by the spread of results.

Some experimental data points were taken for decreasing water flow rate and the results are shown in Fig. (5.48) for β against the non-dimensional water velocity $V_o/\sqrt{gD}$. Similar flow regimes existed as for increasing water flow rate. The air pocket depth results for these runs are also shown in Fig. (5.49) for Y_1/D against $V_o/\sqrt{gD}$, where the results had the same trend as the results for increasing water flow rate, although data was not obtained for $Fr_o < 0.2$.

The points up to which blowback occurred and at which clearing started for the runs with increasing water flow rate are shown in Figs (5.50), (5.51) and (5.52), for β against $V_o/\sqrt{gD}$. V_1 and Fr_1 respectively. It can be noted that the blowing air pockets were all with $Fr_1 > 1.0$ which means that the air pocket forming at the bend was with unstable hydraulic jump. The clearing data reveals that $V_1 > 1.0$ m/s and $Fr_1 > 1.0$, where some of the air pockets were clearing by air entrainment at the toe of the jump, the rest is clearing by surface waves sealing the bend.

5.5.3 Air Pockets at the Bend of R'/D = 1.5

The flow regimes of the downward sloping tunnel and the bend radius R'/D = 1.5 are shown in Fig. (5.53). Also, for this bend there was a significant increase in regime 1(B) behaviour, which is a blowback regime with deep air pocket at the bend and supercritical flow under the air pocket. The blowing air pocket caused vibration in the system. Also flow regime 2 disappeared for this bend, and stratified flow dominated flow regime 3. Clearing of air pockets also was either by air entrainment at the toe of the bend air pocket or by the surface waves sealing the bend and, in some cases, a combination of both.

The experimental results are shown in Fig. (5.54) for β against $V_o/\sqrt{gD}$, where it is noted that blowback for this bend occurred up to a Froude number of about 0.58, although it was reduced for higher air/water ratios when stratified flow appeared instead and was the dominant flow regime for this bend, with even fewer air pockets with a hydraulic jump.

Figure (5.55) is a plot of Y_1/D against $V_o/\sqrt{gD}$ for different values of air/water ratios. The pattern of air pocket depth development is similar to before, although there are few experimental data points in the low Froude number range for β values higher than 0.1. It is apparent that unstable air pocket behaviour occurs for

Froude numbers less than 0.5, where the air pocket depth can vary very rapidly as for the bend radius R'/D = 1.0. Figure (5.55) also indicates that the influence of air/water ratio is less than the bend radius R'/D = 1.0, and much less than the same bend radius for the other two tunnel inclinations.

Experimental data points were also taken for decreasing water flow rate and the results are shown in Fig. (5.56) and (5.57) for β against $V_o/\sqrt{gD}$ and Y_1/D against $V_o/\sqrt{gD}$ respectively. Similar flow regimes existed in Fig. (5.56) as for increasing water flow rate, and the results in Fig. (5.57) had the same trend as the results for increasing water flow rate, although data was not obtained for $Fr_o < 0.2$.

The points up to which blowback occurred and at which clearing started for the runs with increasing the water flow rate are shown in Figs. (5.58), (5.59) and (5.60) for β against $V_o/\sqrt{gD}$, V_1 and Fr_1 respectively. It can be noted that all the points of air pockets blowing back had a velocity $V_1 > 1.0$ m/s and Froude number under the pocket greater than 1.0, while the points for clearing all had $V_1 > 1.0$ m/s with some pockets with $Fr_1 < 1.0$.

In Figs. (5.61) and (5.62) the results for decreasing water flow rate for the bends of R'/D = 1.0 and 1.5 are presented as β against V_1 and Fr_1 respectively, where the points at which the air pocket started to form at the bend are used as the transport points, and the points at which blowback started as the points up to which blowback occurred. It can be seen that here also the blowback points had $Fr_1 > 1.0$.

5.5.4 Comparison between the Three Bends for the Downward Sloping Tunnel

A comparison of the blowback and clearing data for the three bends R'/D = 0.5, 1.0 and 1.5 is shown in Fig. (5.63). It can be

noted that the bend radius has a great effect on air pocket blowing back up the shaft, where the tendency to blow back is greater for the radiused bend. This is a result of the upstream nose of the air pocket at the bend creeping back towards the dropshaft at large radiused bends, which increases the blowback buoyancy.

The effect of increasing bend radius is also to increase the Froude number of clearing air pockets from the bend, although from Fig. (5.63), clearing data for R'/D = 1.0 and 1.5 are very similar. The same thing applies for the runs with decreasing water flow rate, shown in Fig. (5.64), for R'/D = 1.0 and 1.5, where clearing took place at higher values of Fr_o for R'/D = 1.5 than R'/D = 1.0. The effect of increasing bend radius is also seen in the change of flow regimes and air pocket depths. An increasing radius causes the stable regime 2 to disappear and transfers the flow from the blowback regime 1 to stratified flow regime 3. The increasing radius also increases the possibility of larger air pockets with higher Froude number below the pocket to blow back suddenly, which raises the water level in the dropshaft and causes vibration in the system. Hence, it can be concluded that the sharp bend is the most efficient bend from the viewpoint of air pocket formation.

5.6 COMPARISON BETWEEN THE THREE ANGLES OF INCLINATION OF THE OUTLET TUNNEL

From the results of air pockets blowing back and clearing at the junction of a vertical dropshaft and a tunnel which can be inclined either above or below horizontal or at horizontal, it was noticed that laying the tunnel below the horizontal increased the possibility of air pockets blowing back. Also, for this inclination it was more difficult to clear the air pockets from the bend. This was noticed for the three bends used for each angle of inclination. For the downward sloping tunnel large air pockets were forming and extending in length and then suddenly blowing back up the vertical shaft causing spillage from the top of the shaft and oscillation and

vibration to the whole system. This was exactly what happened in Hunterston "B" Power outfall system(165).

Increasing the bend radius for any tunnel inclination was found to have an effect on the blowback region, where the possibility of blowback increased with increasing the bend radius.

Some runs were carried out to find the minimum water velocity required to transport the introduced air bubbles to the bend for different air/water ratios. It was found that a water velocity between 0.1317 and 0.1559 m/s giving Froude numbers of 0.1078-0.1278 respectively was required to transport the air bubbles to the upstream end of the bend. The range was for different air flow rates introduced to the system, below these values air bubbles were circulating in the vertical shaft.

An attempt was made to measure the exact shape of an air pocket at the bend from visual measurement to find the angle of the nose of the air pocket at the bend in addition to some photographs taken for this purpose. The shape of such stable air pocket at the bend radius R'/D = 1.0 for the upward sloping tunnel is shown in Fig. (5.65), where the angle of the nose of the air pocket with horizontal Φ is 73°.

For flow regime 3 air pockets with hydraulic jump formed for the three angles of inclination with the stratified flow dominating the results for the downward sloping tunnel. The air/water ratio had a great influence on the behaviour of air pockets in the three tunnel inclination, although it was noticed that very small values of β can cause great changes in the downward sloping tunnel which limited the range of β at which tests were carried out.

The transport of air pockets was affected by the air/water ratio, although this effect was not significant in the downward sloping tunnel, where clearing was more difficult for high air/water

ratios. An empirical correlation for the clearing of air pockets will be given in Chapter (7), also comparison will be carried out between the experimental results, simple theoretical models and results from previous investigators.

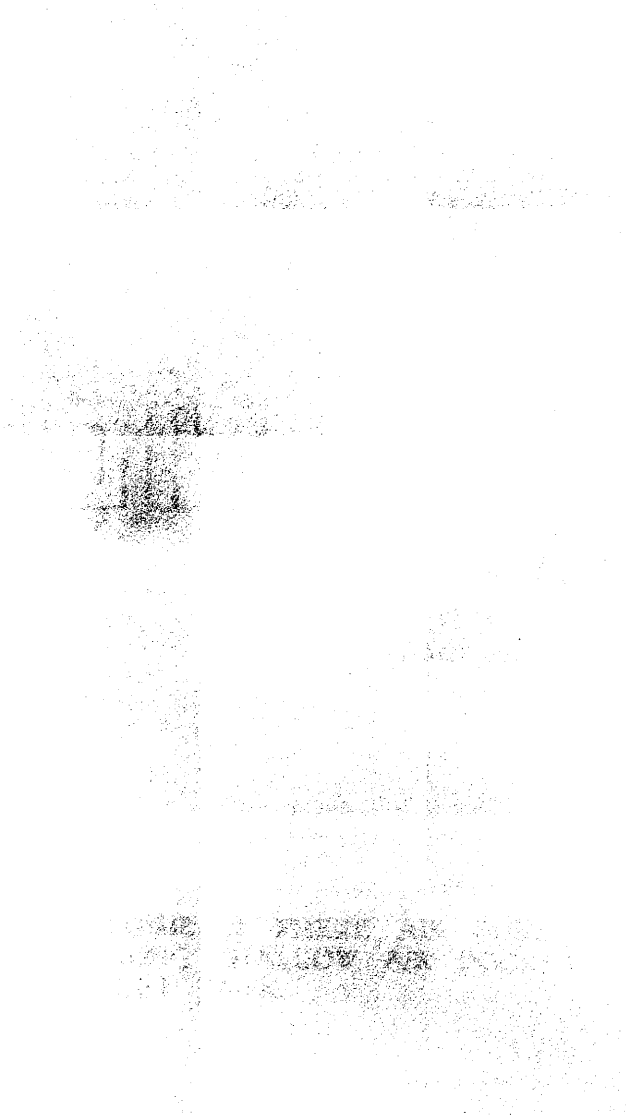

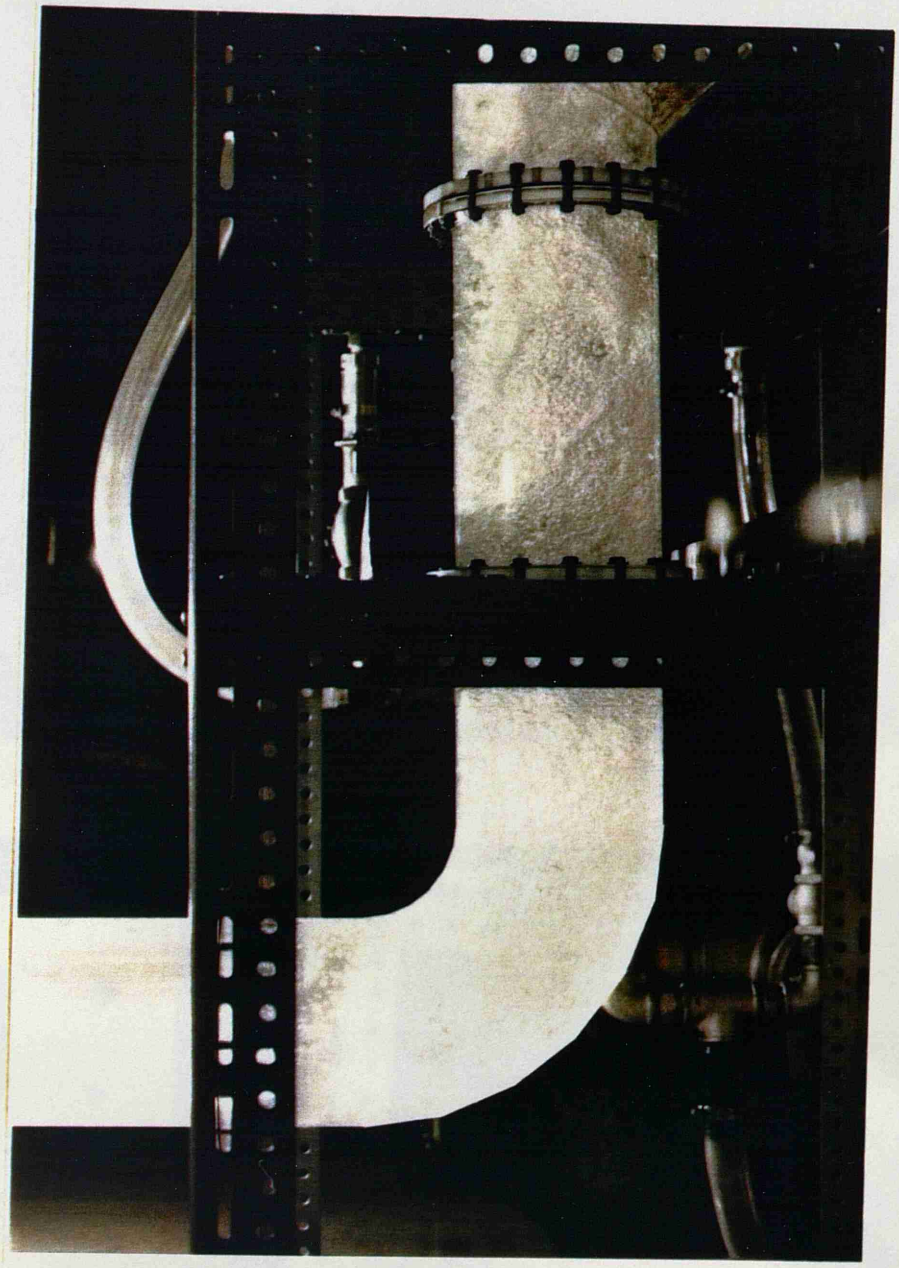

PLATE (5.1) FLOW REGIME (1) WHERE AIR BUBBLES BLOWBACK AND A LONG SHALLOW AIR POCKET EXTENDS TO THE OUTLET TANK

(a)

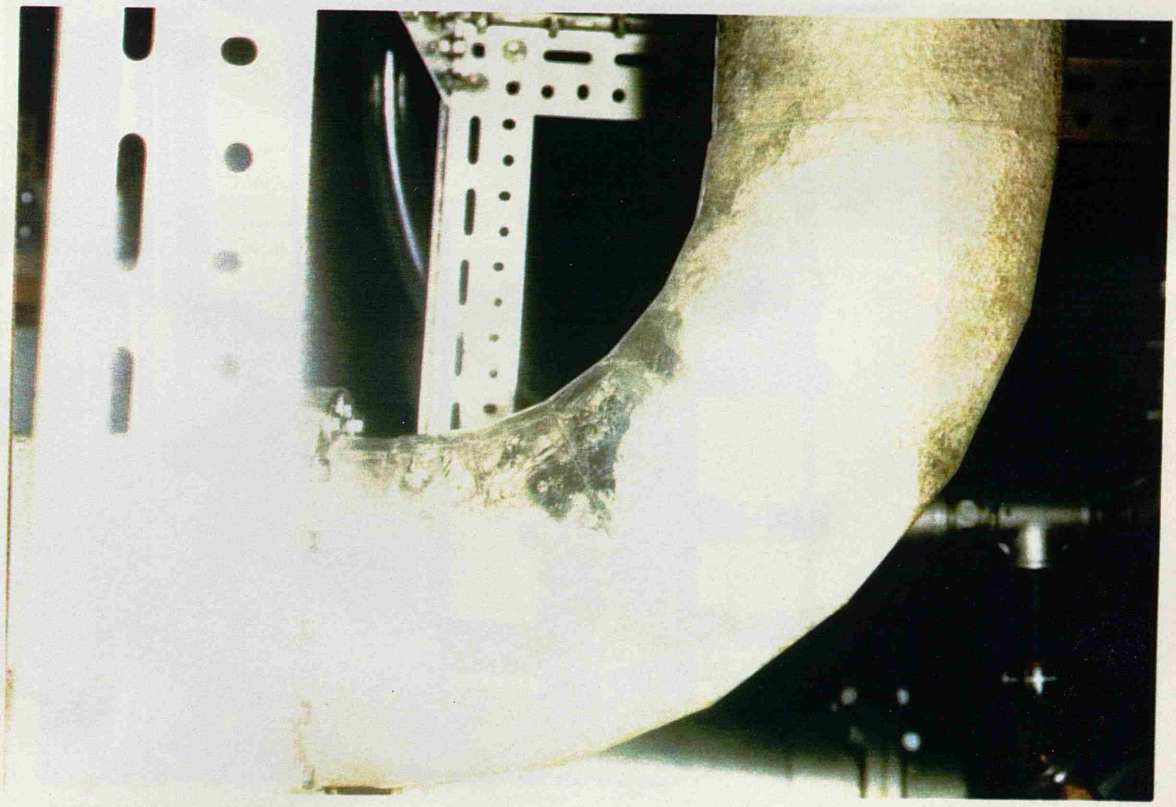

(b)

PLATE (5.2) FLOW REGIME (1) WHERE AN AIR POCKET FORMS AT THE BEND AND BLOW BACK UP THE VERTICAL SHAFT

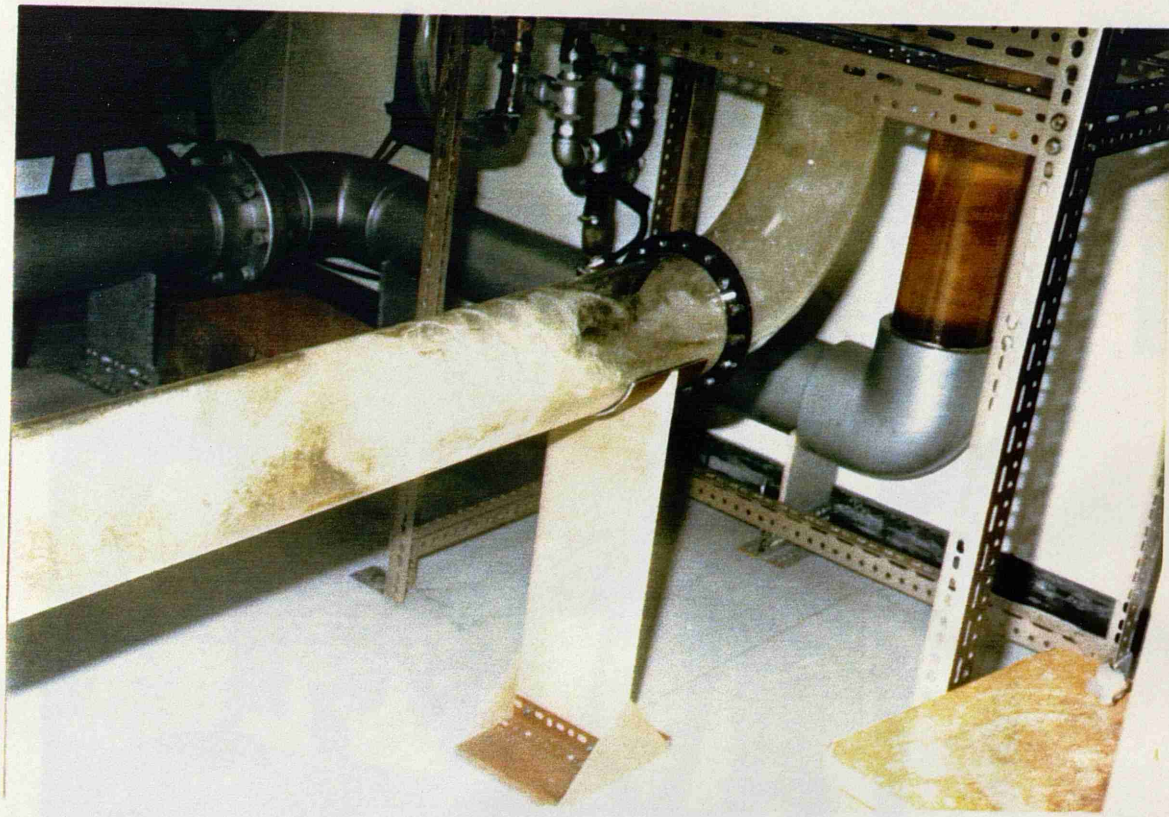

PLATE (5.3) FLOW REGIME (1) WHERE AN AIR POCKET AT THE BEND WITH $Fr_1 > 1.0$ IS BLOWING BACK UP THE SHAFT

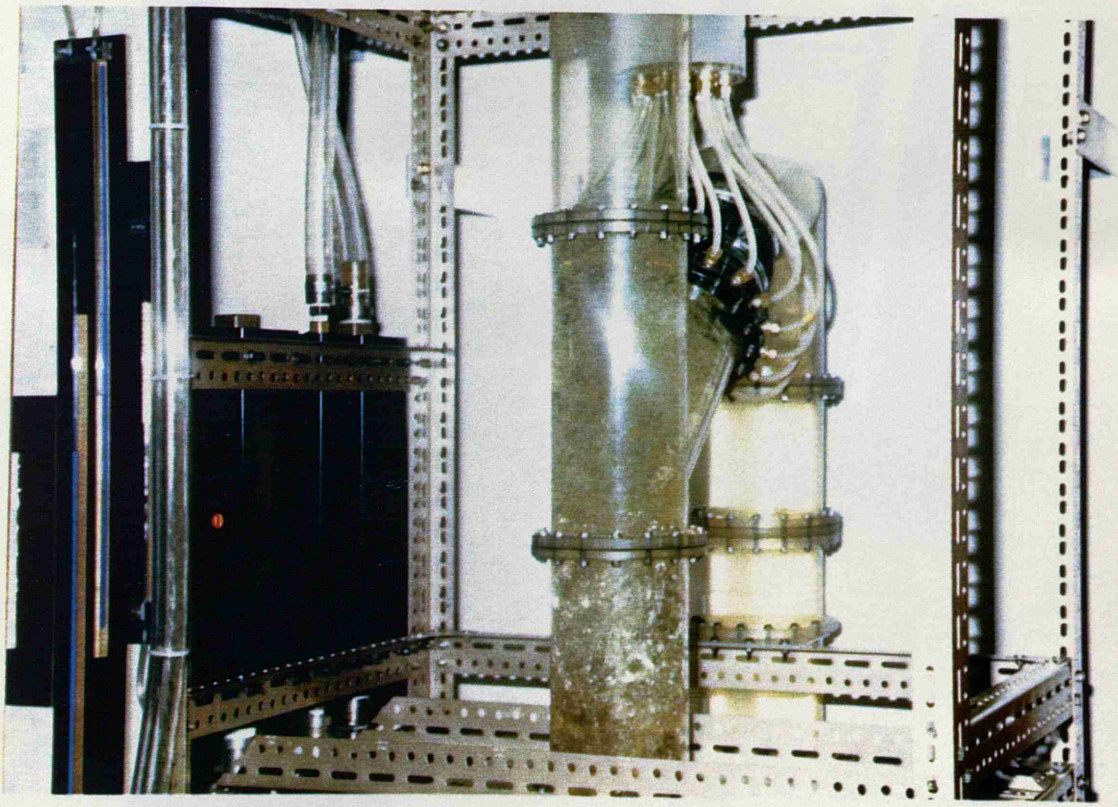

PLATE (5.4a) FLOW REGIME (1) WHERE THE BLOWING BACK AIR POCKET IS RISING UP THE SHAFT

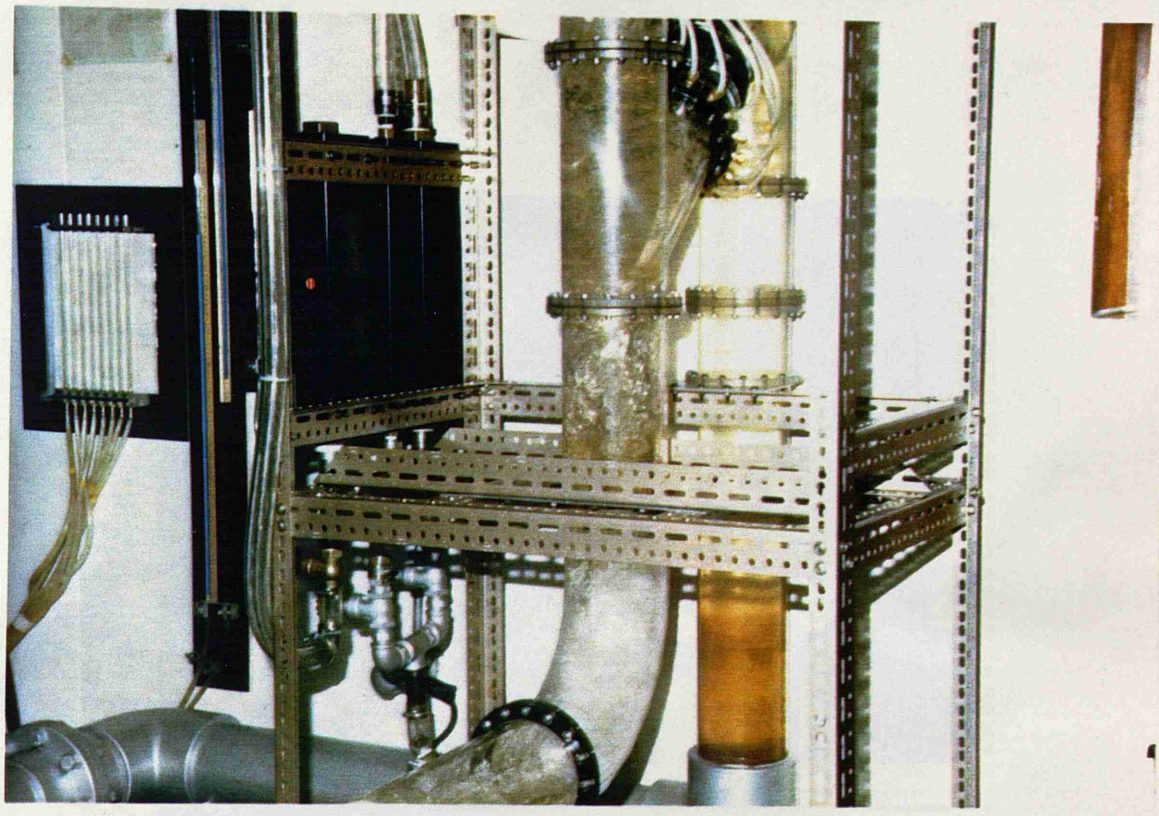

PLATE (5.4b) THE BLOWING BACK AIR POCKET RAISING THE SHAFT'S WATER LEVEL AND CAUSING OSCILLATION IN THE SYSTEM

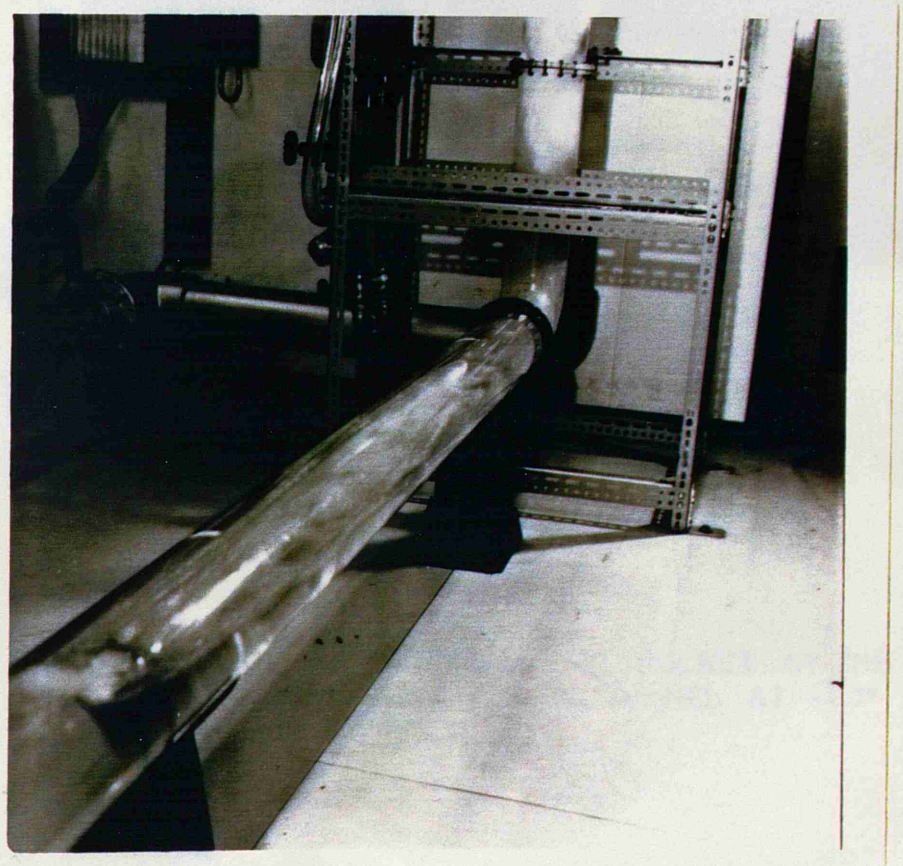

PLATE (5.5) FLOW REGIME (2) STABLE AIR POCKET AT THE BEND WITH $Fr_1 < 1.0$ FOR A HORIZONTAL TUNNEL

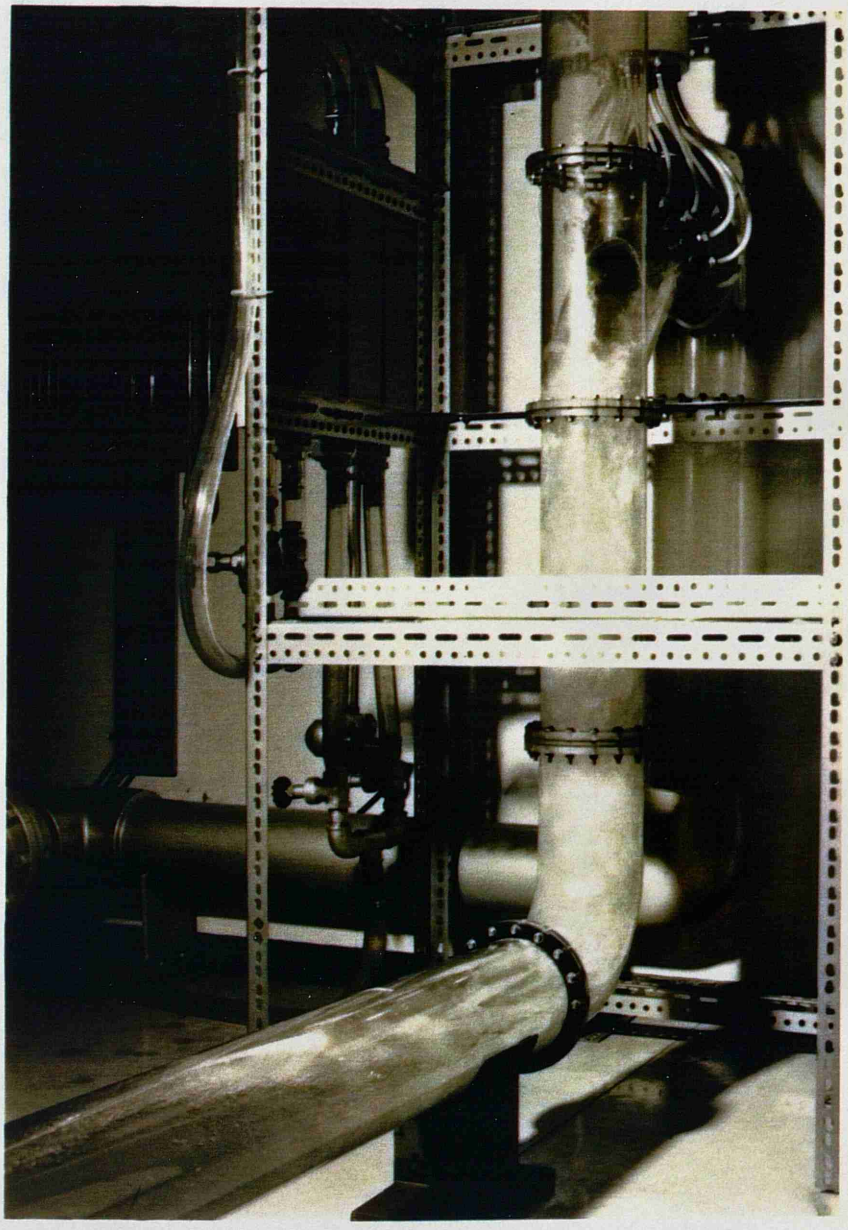

PLATE (5.6) FLOW REGIME (2) STABLE AIR POCKET AT THE BEND WITH $Fr_1 < 1.0$ FOR A TUNNEL AT +1.5° WITH HORIZONTAL

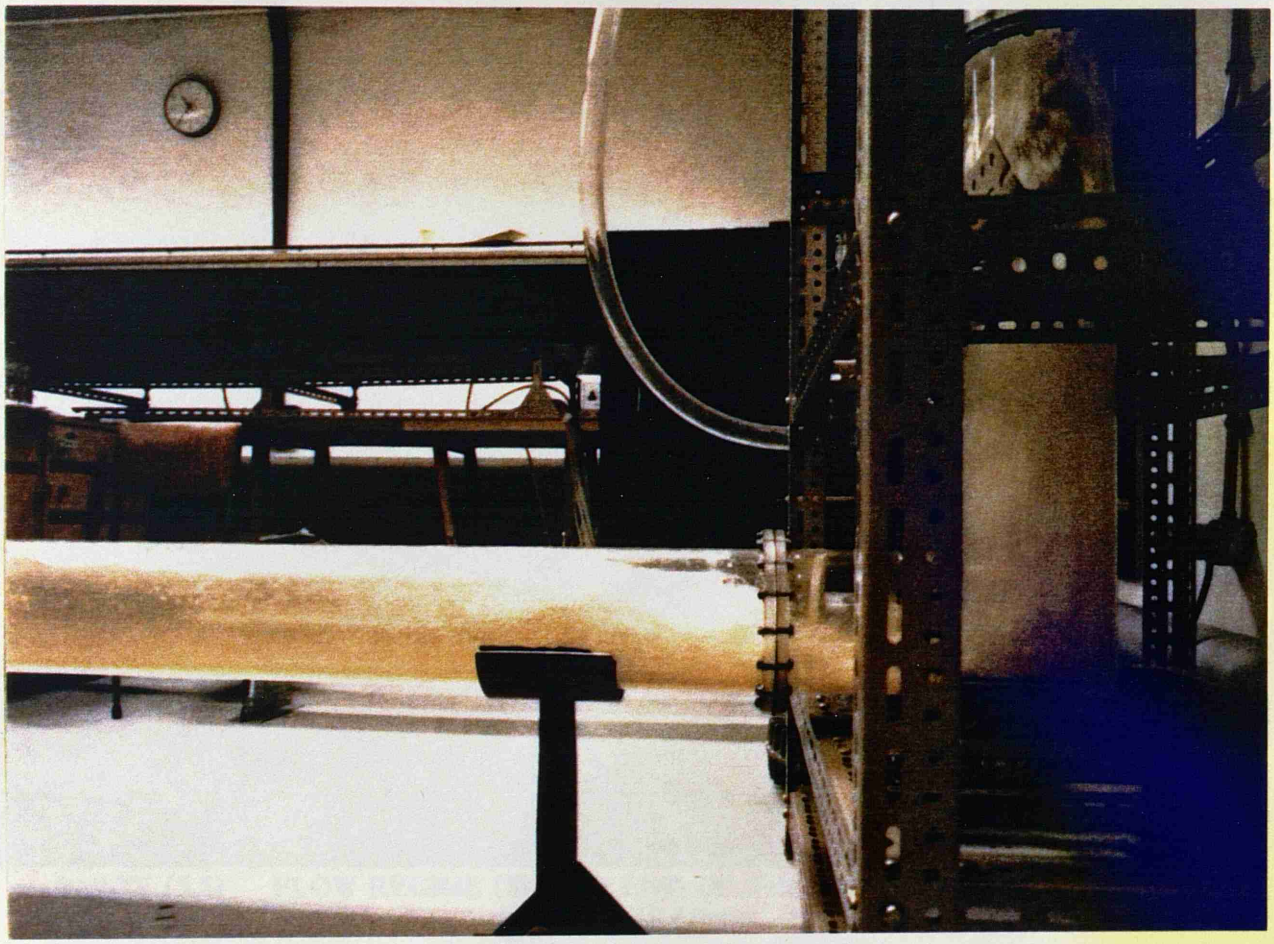

(a)

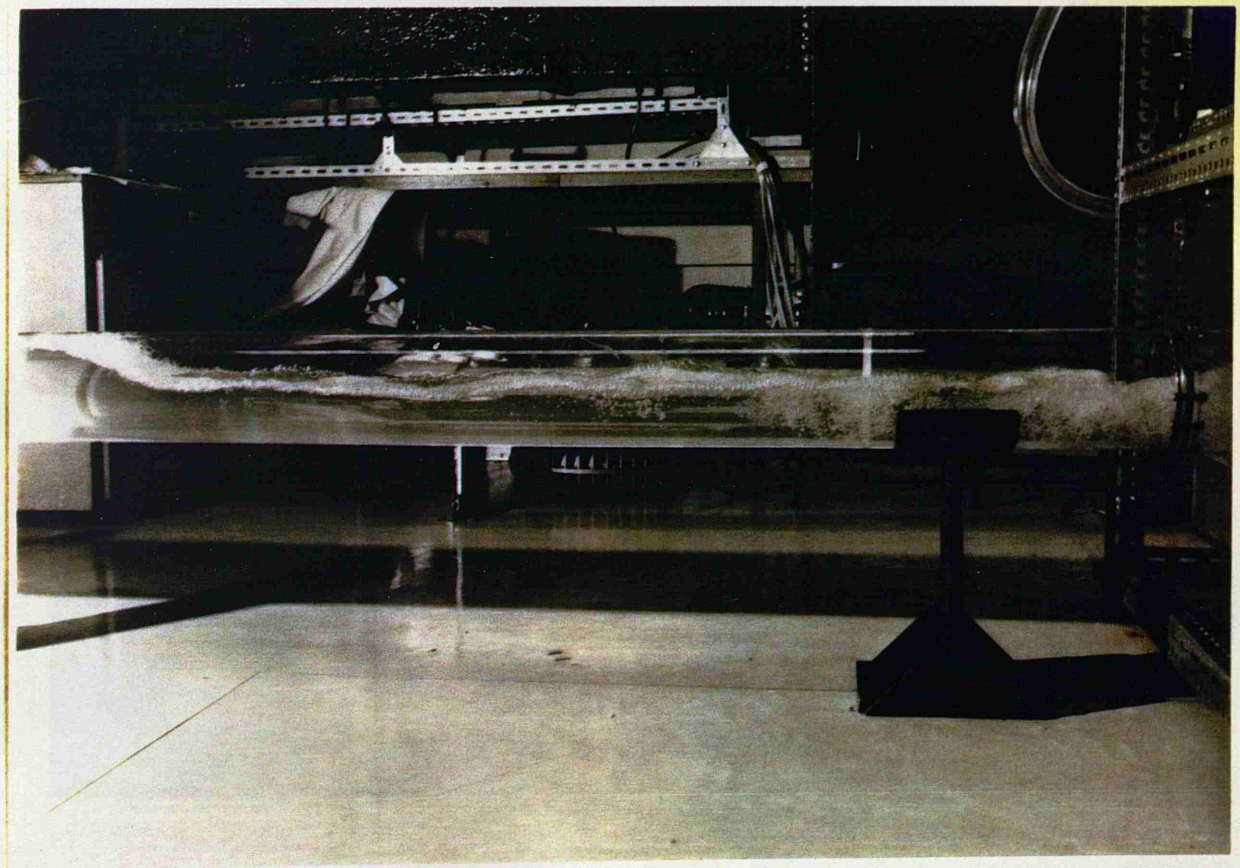

(b)

PLATE (5.7) FLOW REGIME (3) AN AIR POCKET AT THE BEND WITH A HYDRAULIC JUMP AT ITS END

PLATE (5.8) FLOW REGIME (3) THE END OF THE AIR POCKET WHERE THE JUMP IS ENTRAINING AIR DOWNSTREAM

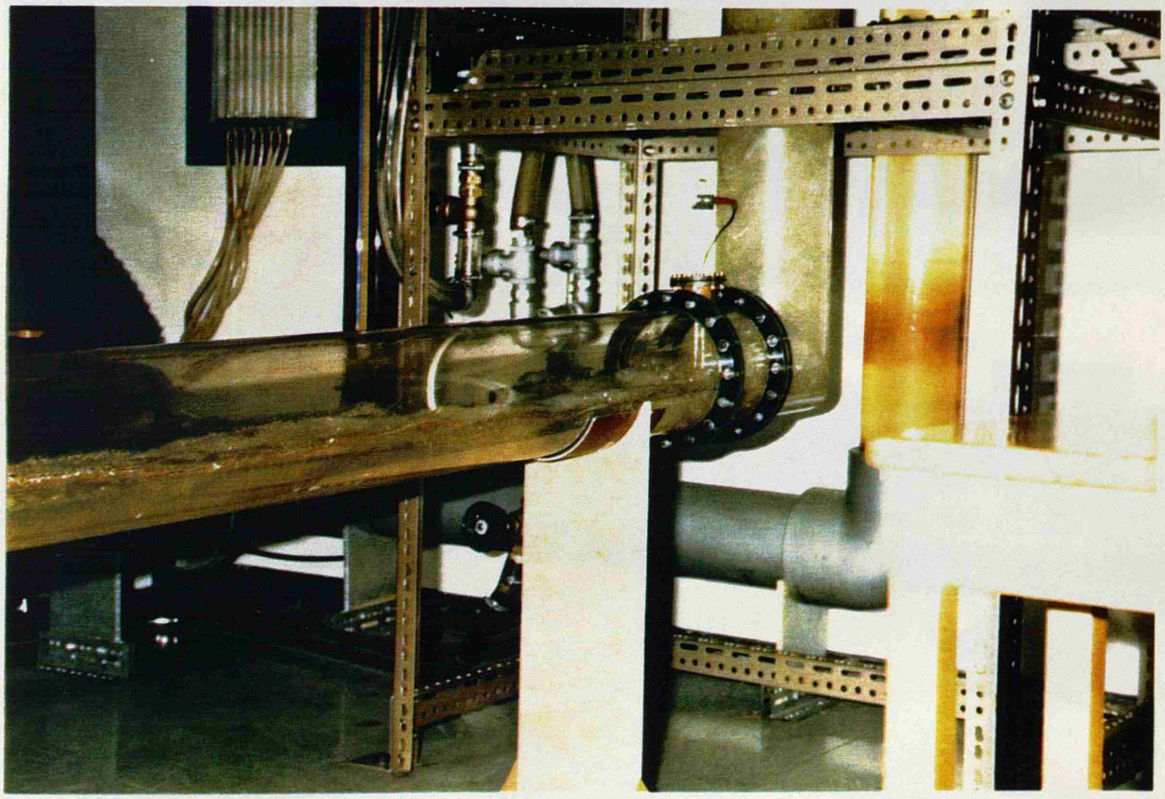

PLATE (5.9) FLOW REGIME (3) STRATIFIED FLOW WHERE THE AIR POCKET EXTENDS TO THE OUTLET TANK

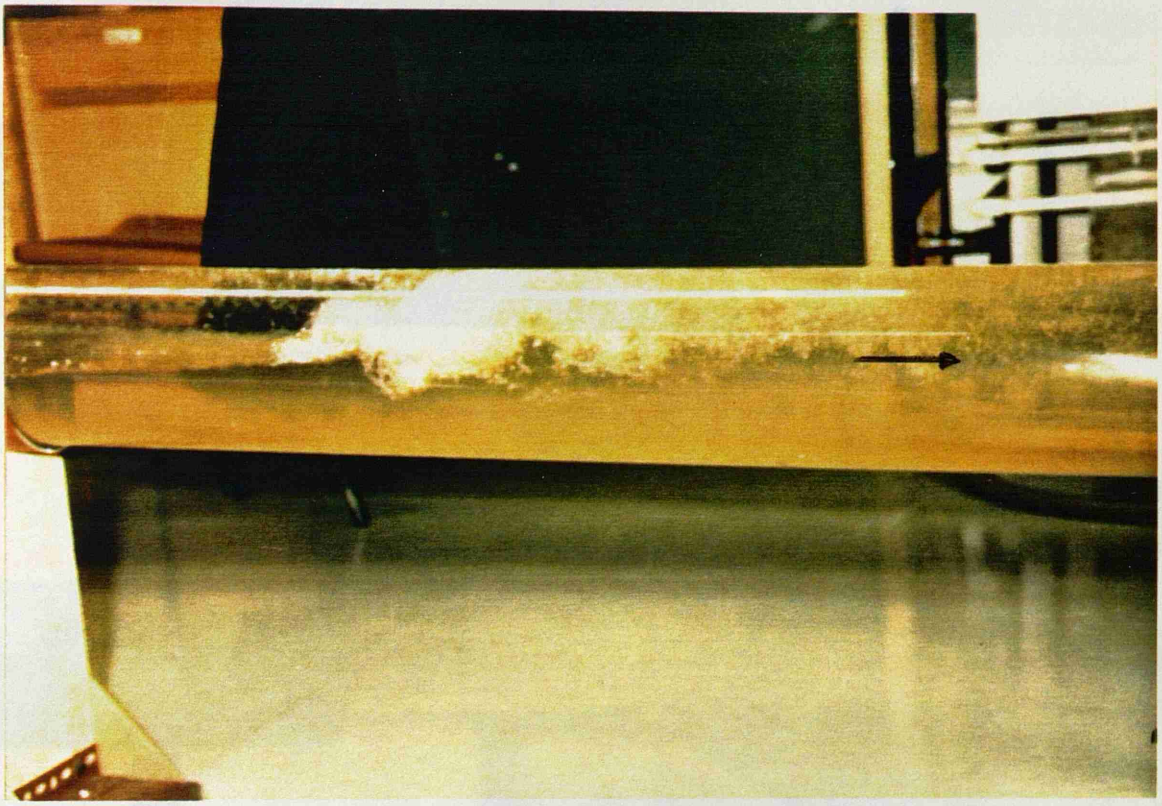

PLATE (5.10) TRANSITION FROM FLOW REGIME (3) TO (4) WHERE THE AIR POCKET IS REDUCED IN SIZE DUE TO AIR ENTRAINMENT AT ITS END

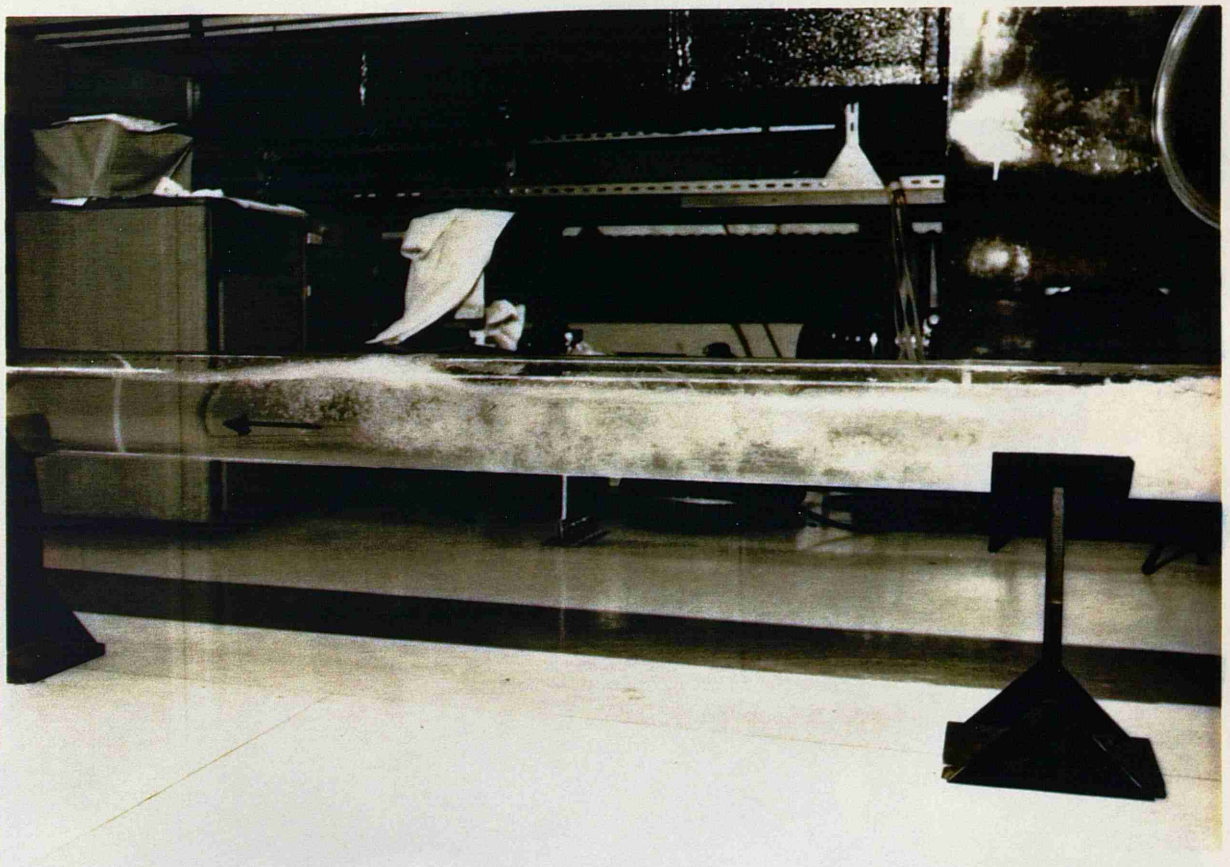

PLATE (5.11) TRANSITION FROM FLOW REGIME (3) TO (4) WHERE THE WAVES ARE SEALING THE PIPE AND FORMING A NEW POCKET AT THE BEND AND TRANSPORTING THE PREVIOUS ONE DOWNSTREAM

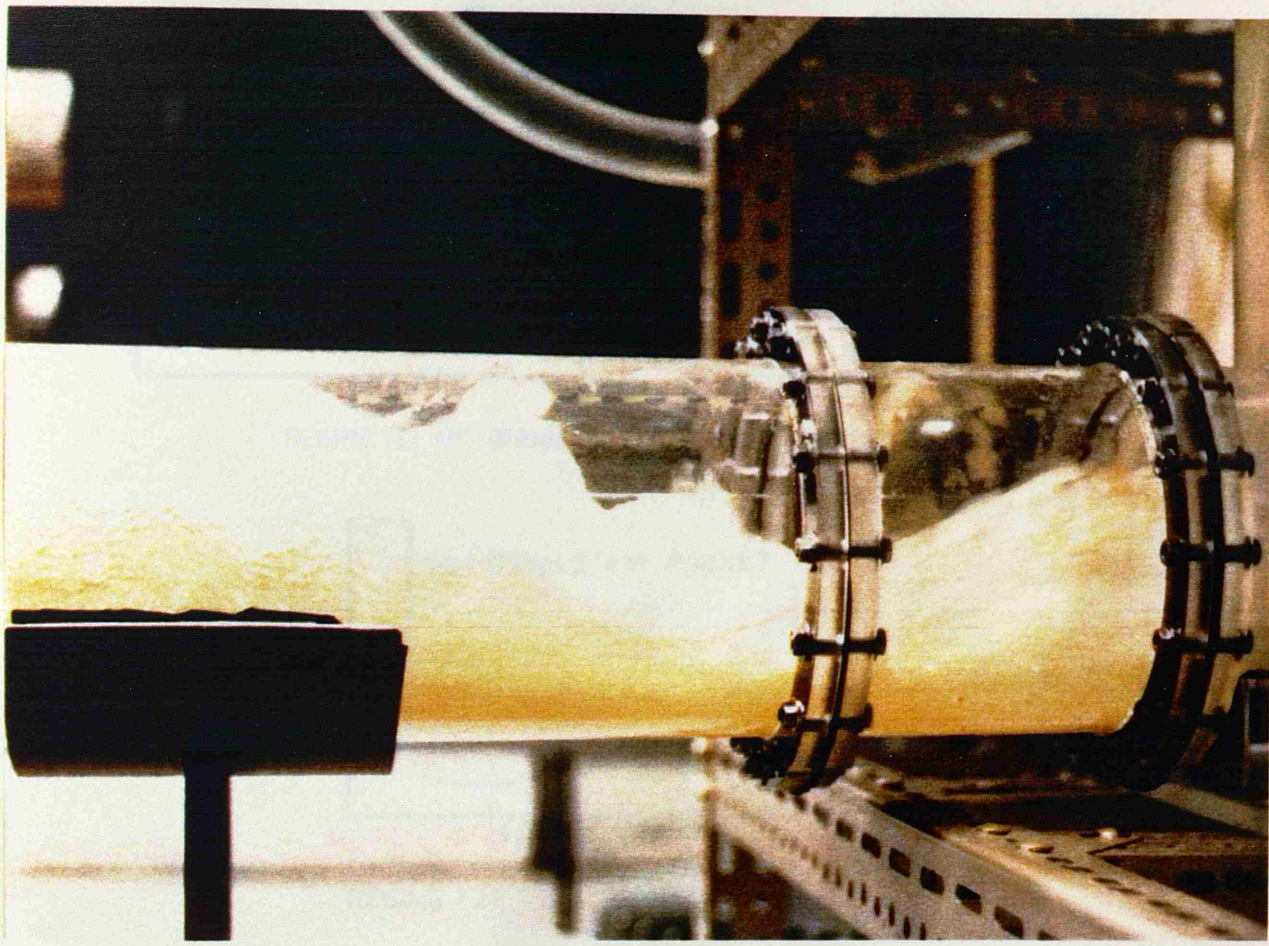

PLATE (5.12) TRANSITION FROM FLOW REGIME (3) TO (4) WHERE IN THE CASE THE WAVES AND THE ALTERNATING SWIRL AT THE BEND SEAL THE PIPE

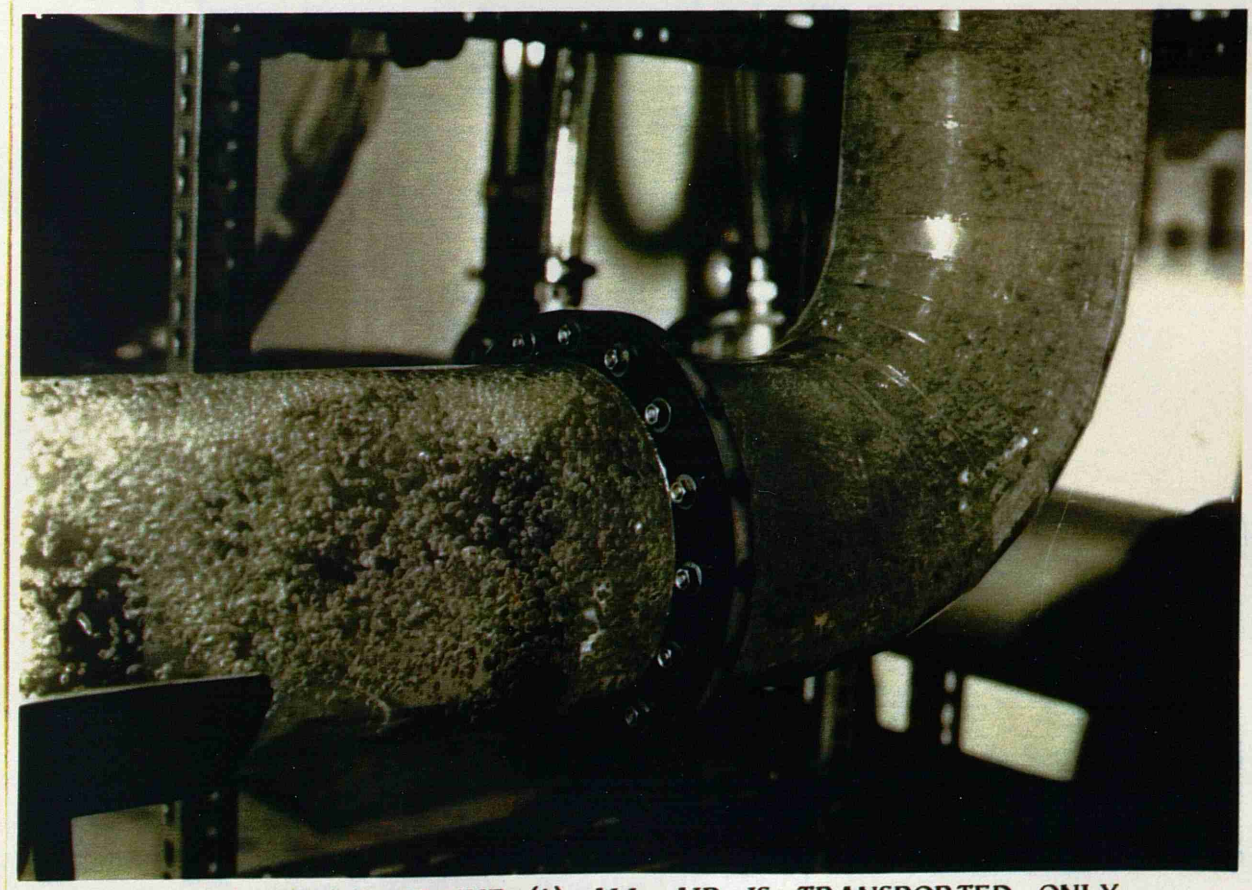

PLATE (5.13) FLOW REGIME (4) ALL AIR IS TRANSPORTED ONLY AIR BUBBLES ARE FLOWING AROUND THE BEND

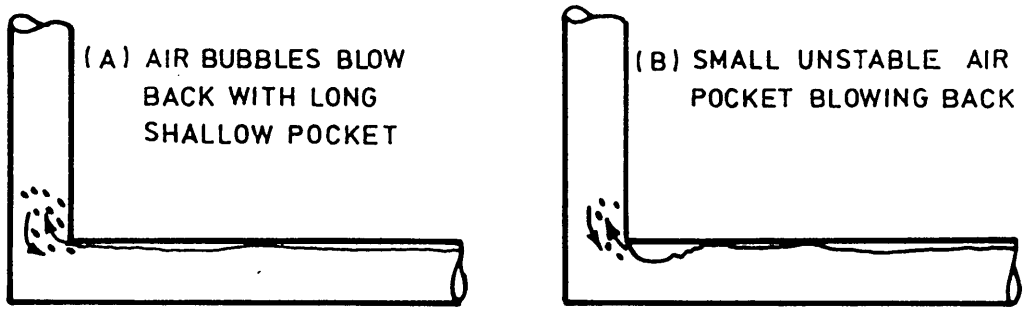

REGIME (1) AIR BUBBLES AND POCKETS BLOWING BACK

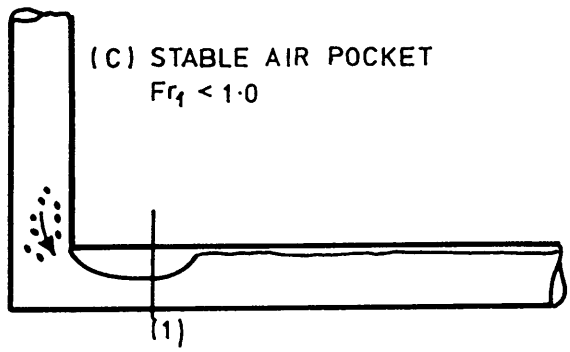

REGIME (2) STABLE AIR POCKET

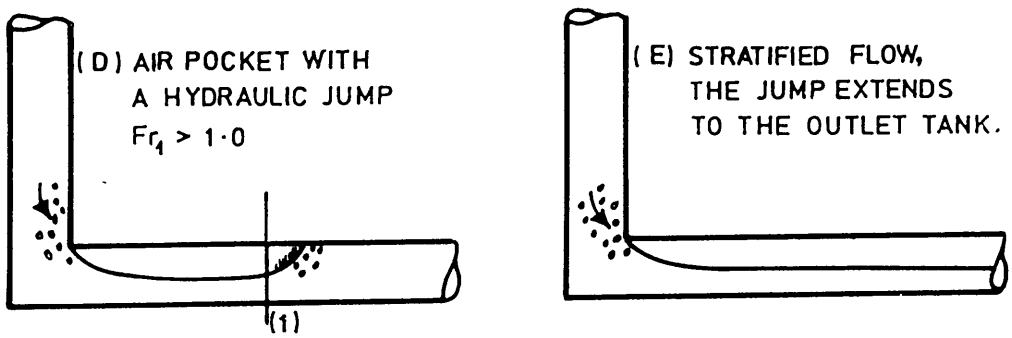

REGIME (3) AIR POCKET WITH A HYDRAULIC JUMP

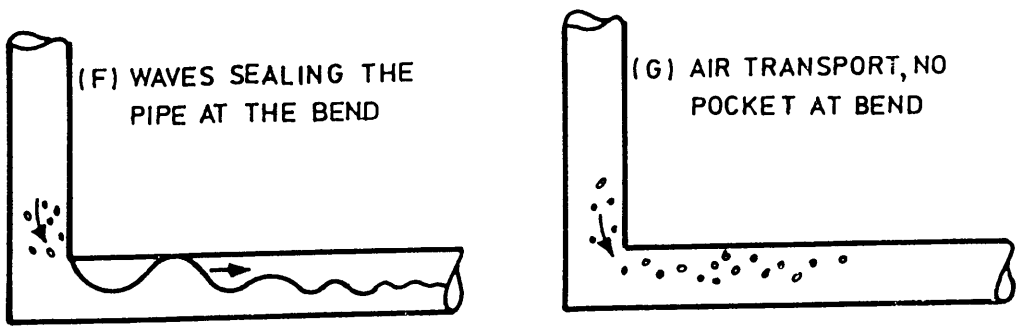

TRANSIT FROM REGIME (3) TO (4)

REGIME (4) NO POCKET AT BEND

FIG. (5.1) FLOW REGIMES WITH INCREASING UPSTREAM FROUDE NUMBER (Fr_o) FOR A HORIZONTAL TUNNEL WITH A BEND OF $R'/D = 0.50$ (SHARP BEND)

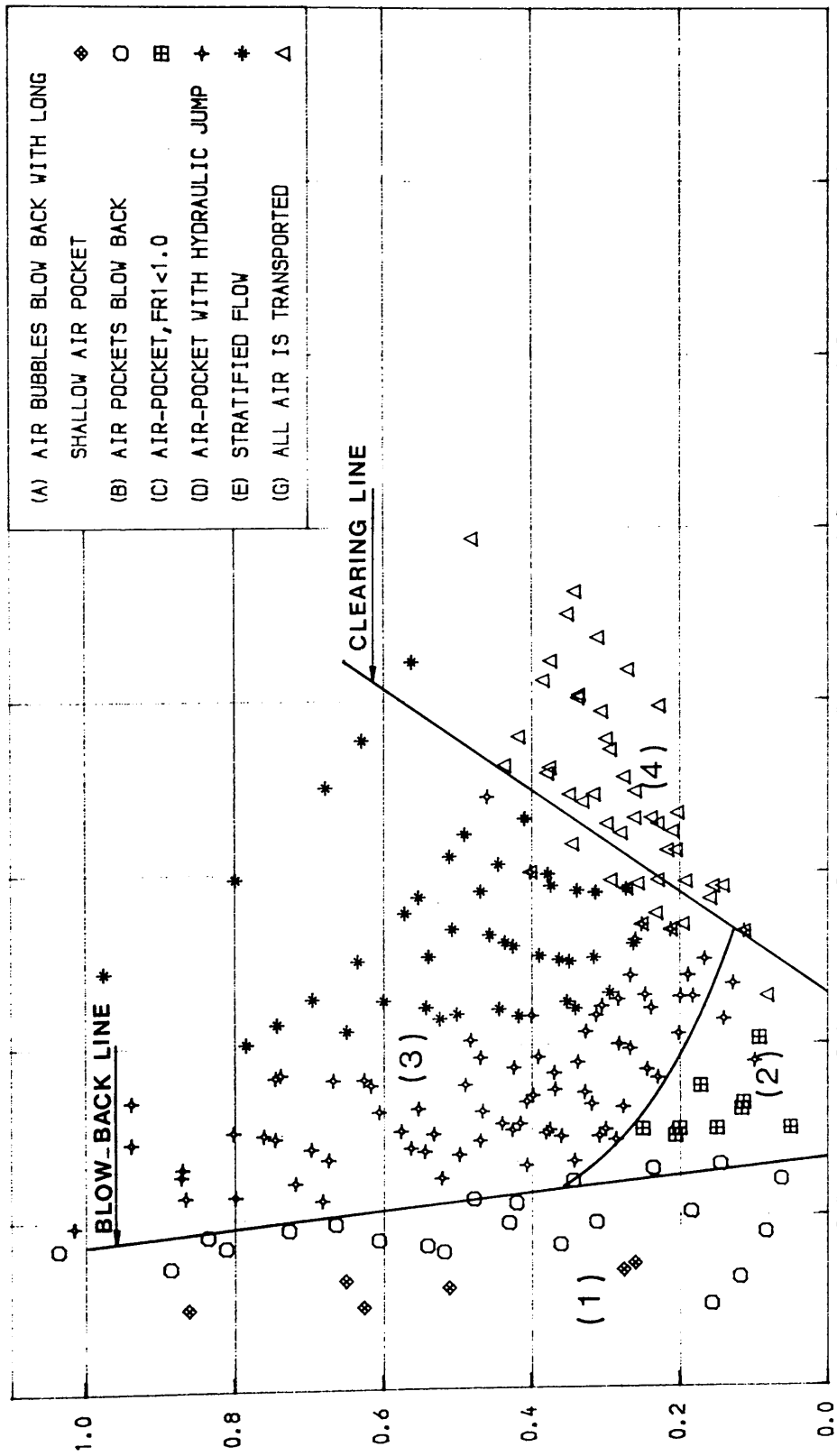

FIG. (5.2) RELATION BETWEEN UPSTREAM NON- DIMENSIONAL WATER VELOCITY & AIR-WATER RATIO FOR A HORIZONTAL TUNNEL WITH A BEND OF R'/D=0.5

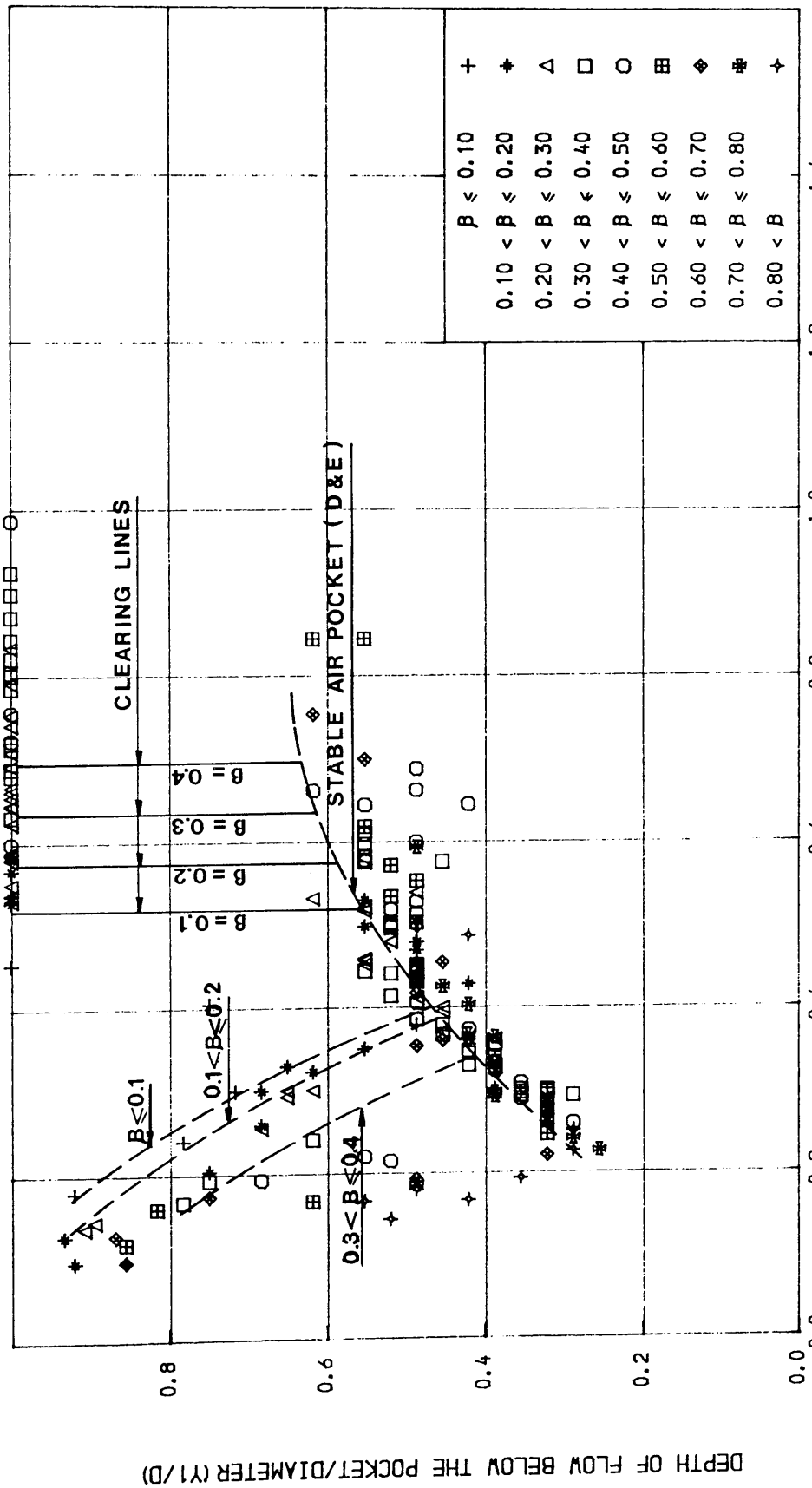

FIG. (5.3) RELATION BETWEEN UPSTREAM NON- DIMENSIONAL WATER VELOCITY & NON-DIMENSIONAL DEPTH OF FLOW BELOW THE POCKET FOR A HORIZONTAL TUNNEL WITH A BEND OF R/D=0.5

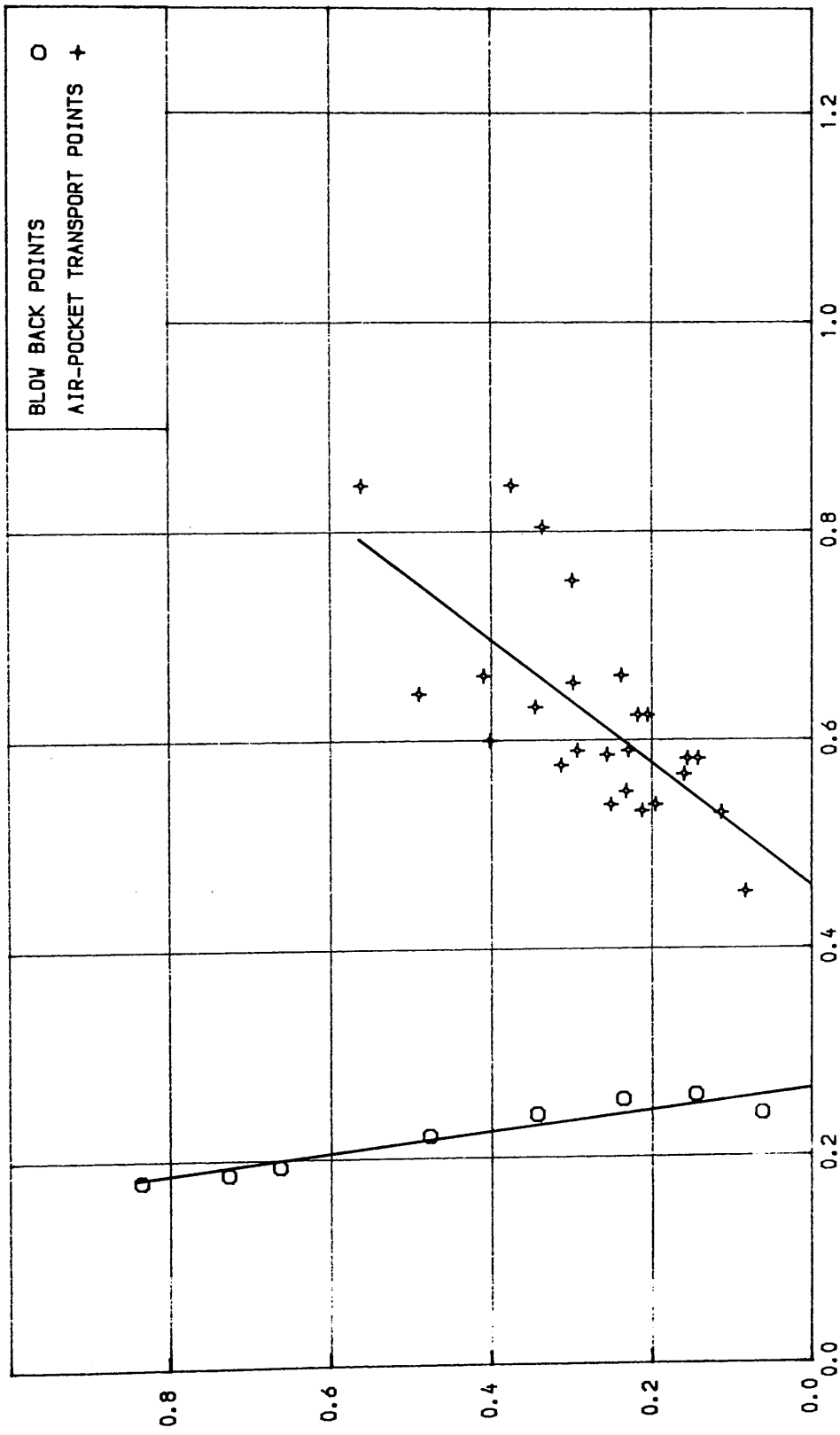

FIG. (5.4) RELATION BETWEEN UPSTREAM NON- DIMENSIONAL WATER VELOCITY & AIR WATER RATIO AT POINTS OF BLOWING BACK AND CLEARING FOR A HORIZONTAL TUNNEL WITH A BEND OF R/D=0.5

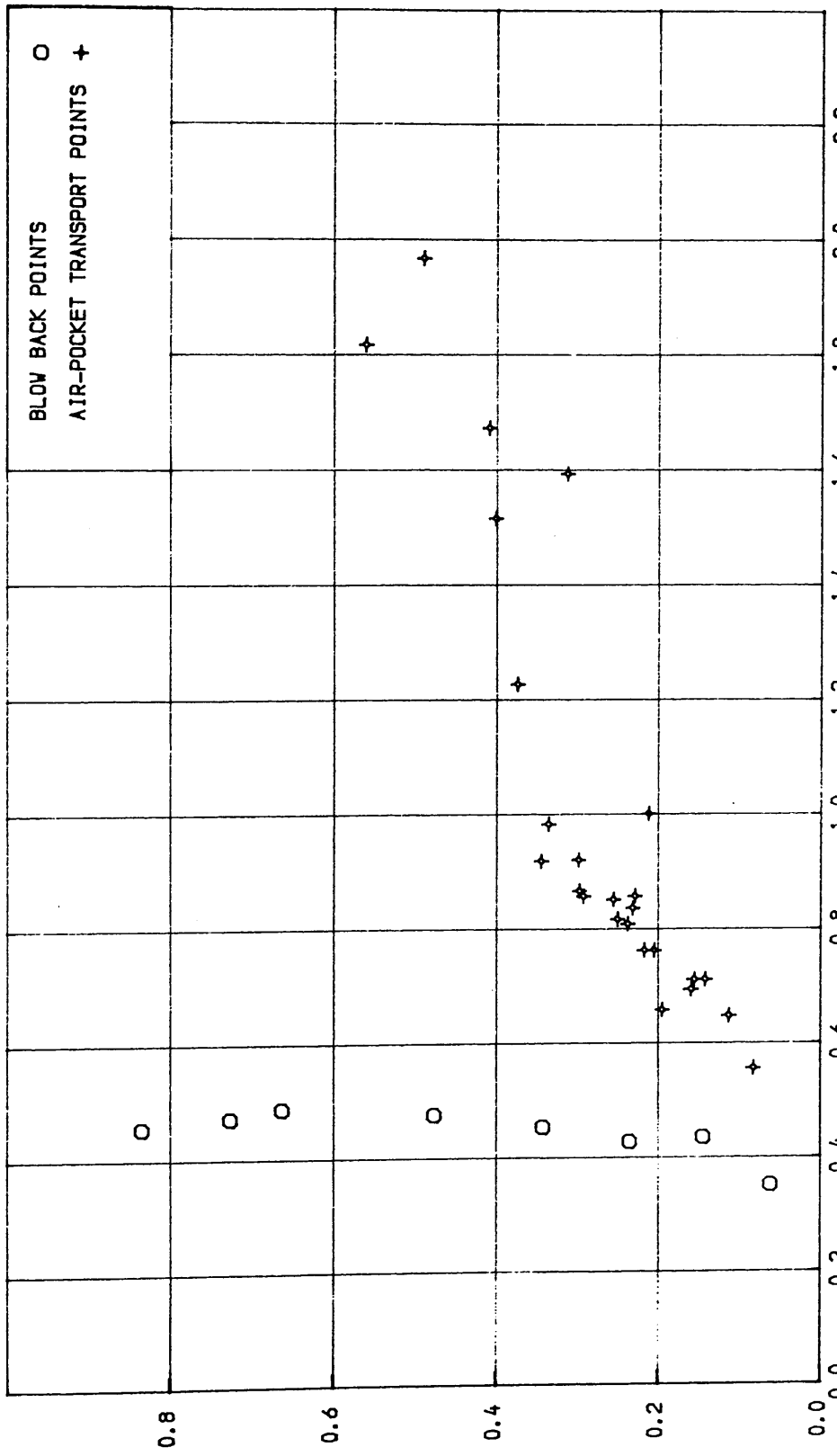

FIG. (5.5) RELATION BETWEEN WATER VELOCITY BELOW THE AIR POCKET & AIR WATER RATIO AT POINTS OF BLOWING BACK AND CLEARING FOR A HORIZONTAL TUNNEL WITH A BEND OF R/D=0.5

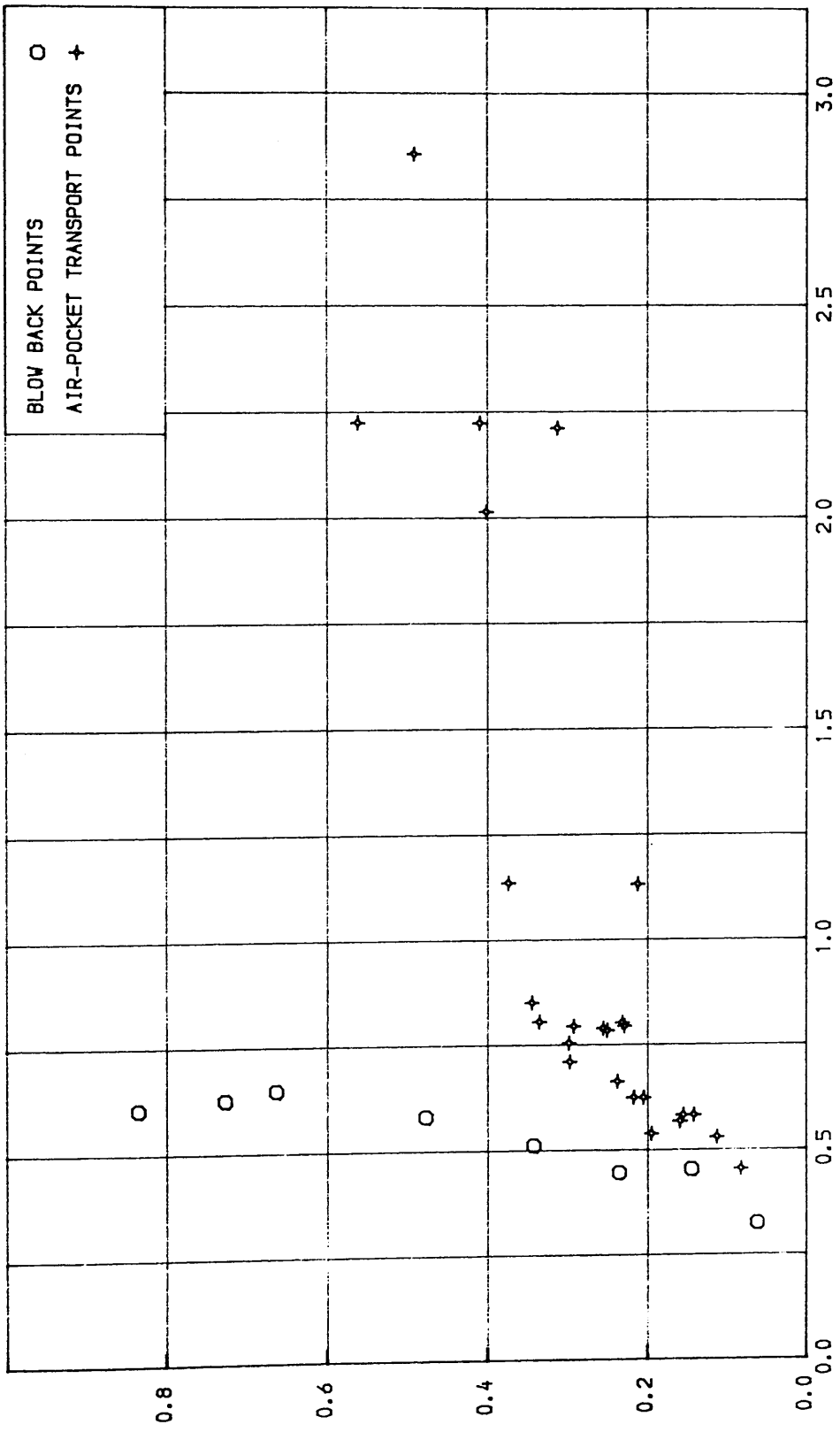

FIG. (5.6) RELATION BETWEEN THE FROUDE NUMBER BELOW THE AIR POCKET & AIR WATER RATIO AT POINTS OF BLOWING BACK AND CLEARING FOR A HORIZONTAL TUNNEL WITH A BEND OF R/D=0.5

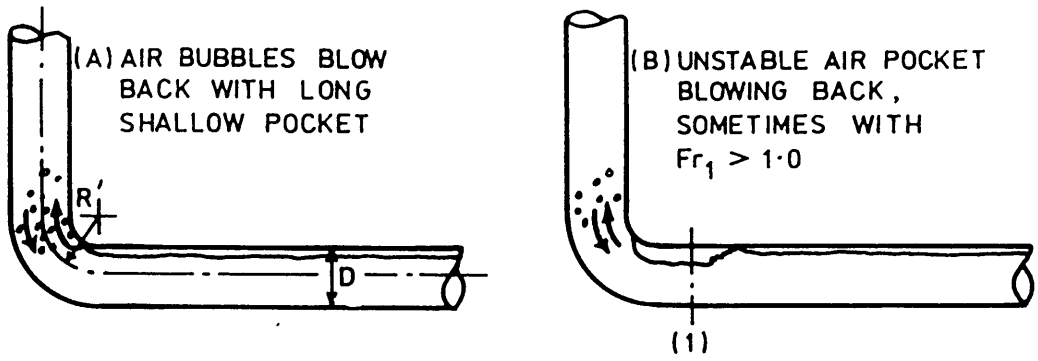

REGIME (1) AIR BUBBLES AND POCKETS BLOWING BACK

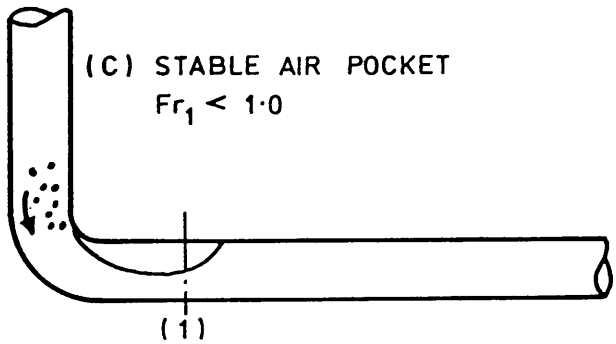

REGIME (2) STABLE AIR POCKET

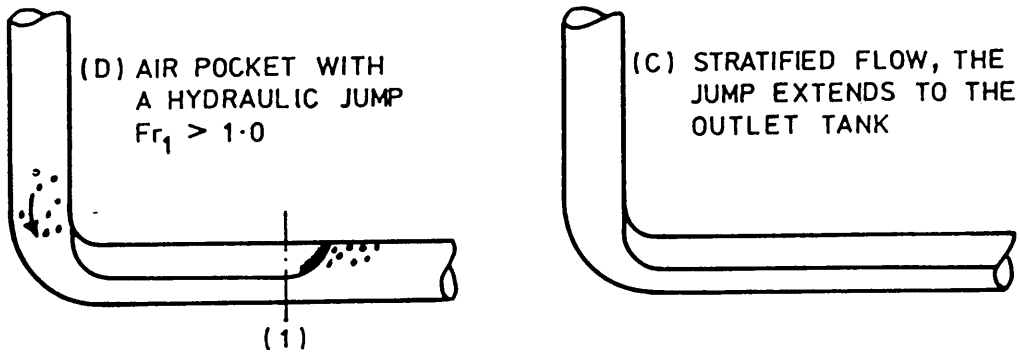

REGIME (3) AIR POCKET WITH A HYDRAULIC JUMP

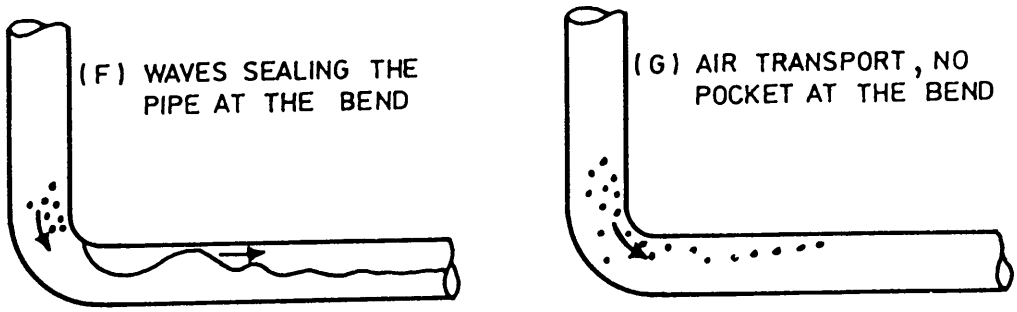

TRANSIT FROM REGIME (3) to (4)

REGIME (4) NO POCKET AT BEND

FIG. (5.7) FLOW REGIMES WITH INCREASING UPSTREAM FROUDE NUMBER (Fr_o) FOR A HORIZONTAL TUNNEL WITH A BEND OF $R'/D = 1.0$

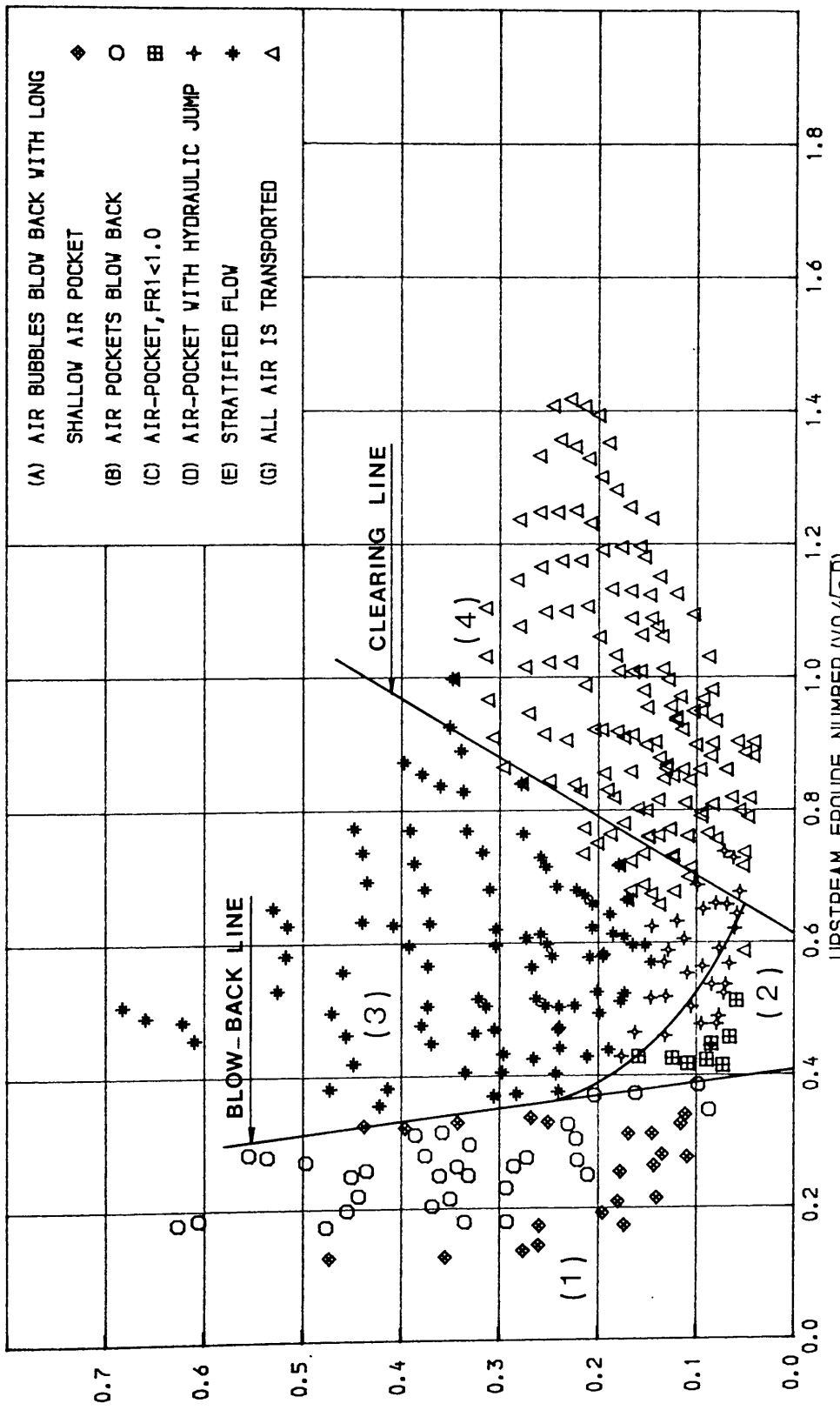

FIG. (5.8) RELATION BETWEEN UPSTREAM NON- DIMENSIONAL WATER VELOCITY & AIR-WATER RATIO FOR A HORIZONTAL TUNNEL WITH A BEND OF Ŕ/D=1.0

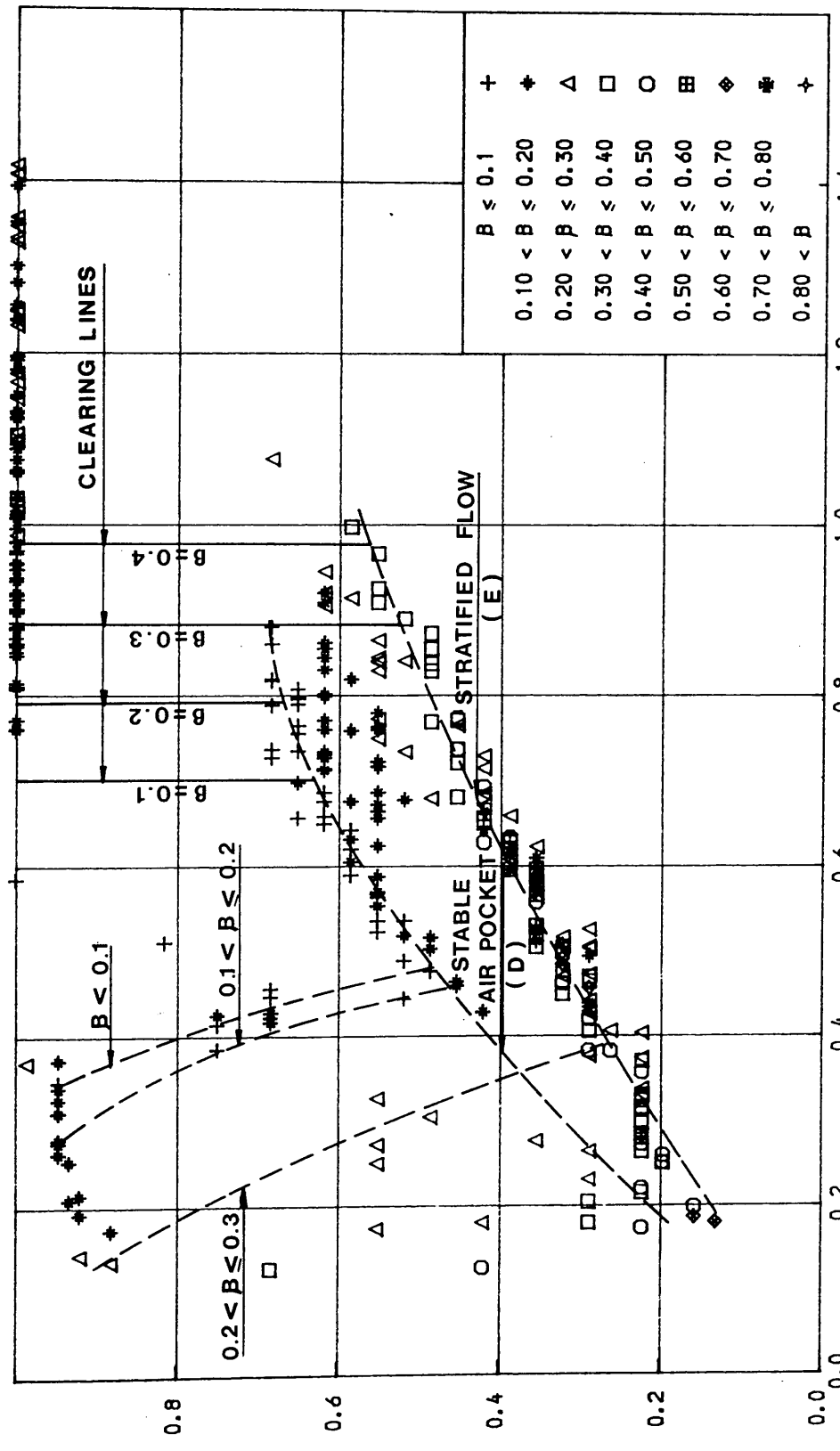

FIG. (5.9) RELATION BETWEEN UPSTREAM NON-D DIMENSIONAL WATER VELOCITY & NON-DIMENSIONAL DEPTH OF FLOW BELOW THE POCKET FOR A HORIZONTAL TUNNEL WITH A BEND OF R/D=1.0

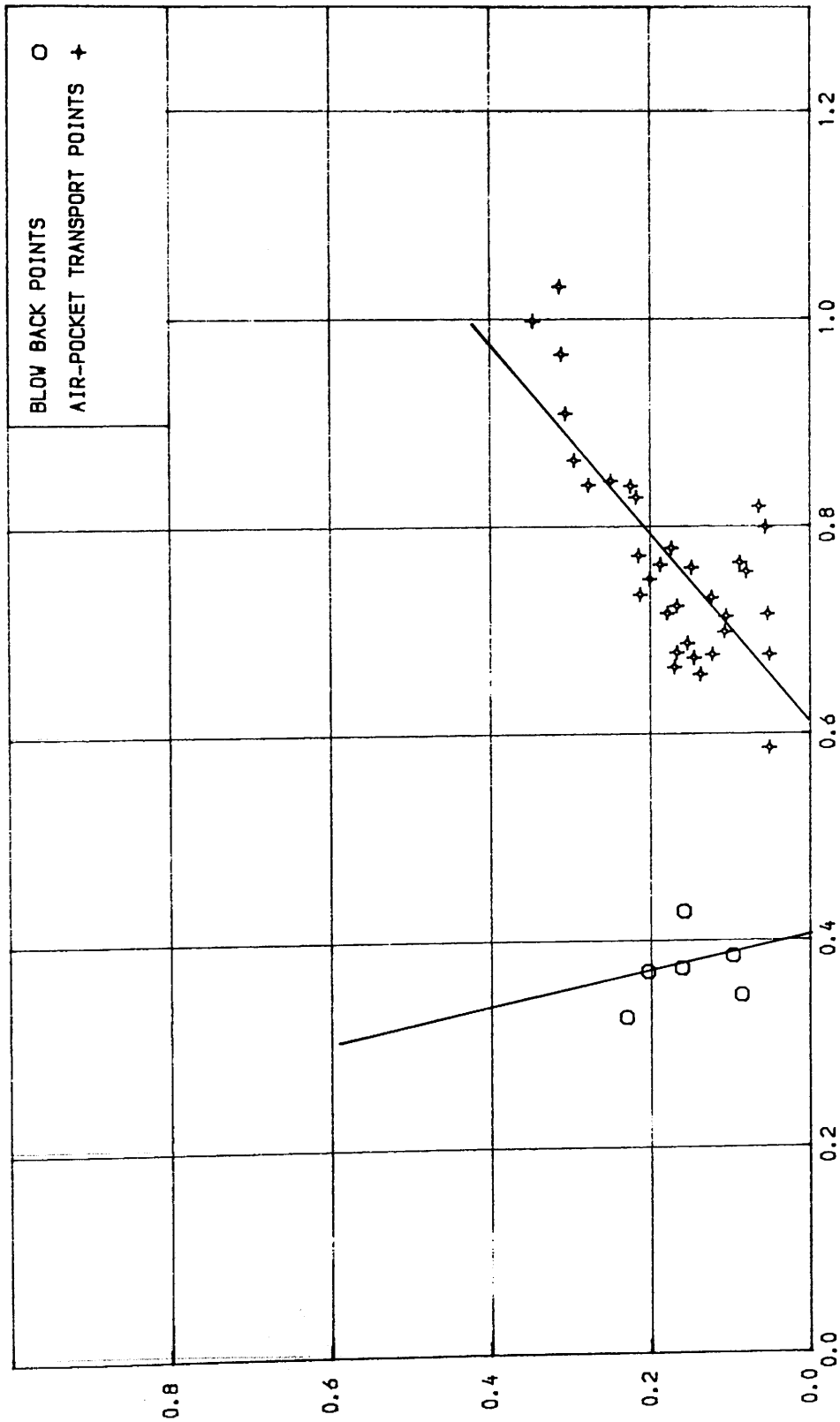

FIG. (5.10) RELATION BETWEEN UPSTREAM NON- DIMENSIONAL WATER VELOCITY & AIR WATER RATIO AT POINTS OF BLOWING BACK AND CLEARING FOR A HORIZONTAL TUNNEL WITH A BEND OF R′/D=1.0

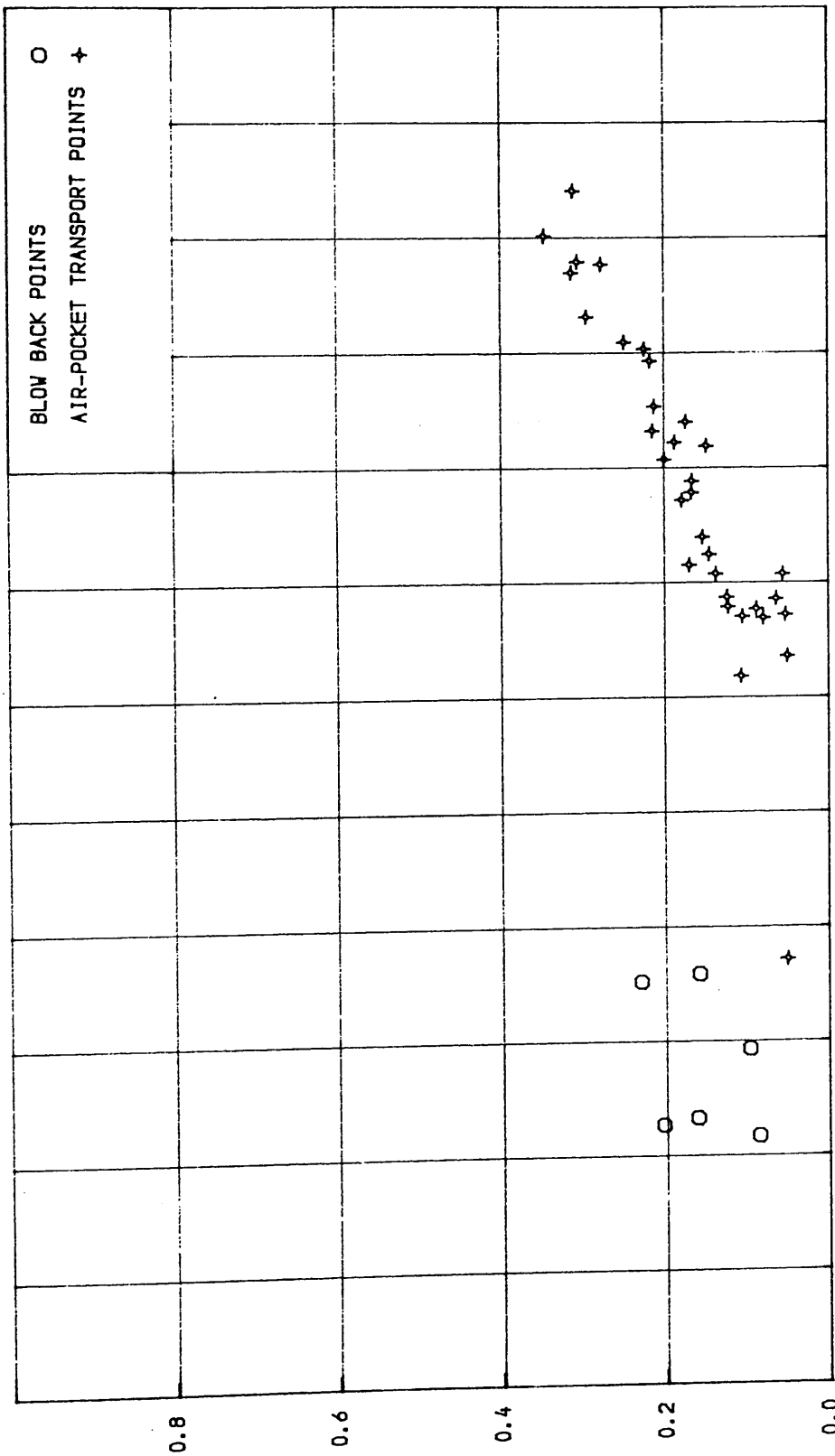

FIG. (5.11) RELATION BETWEEN WATER VELOCITY BELOW THE AIR POCKET & AIR WATER RATIO AT POINTS OF BLOWING BACK AND CLEARING FOR A HORIZONTAL TUNNEL WITH A BEND OF R/D=1.0

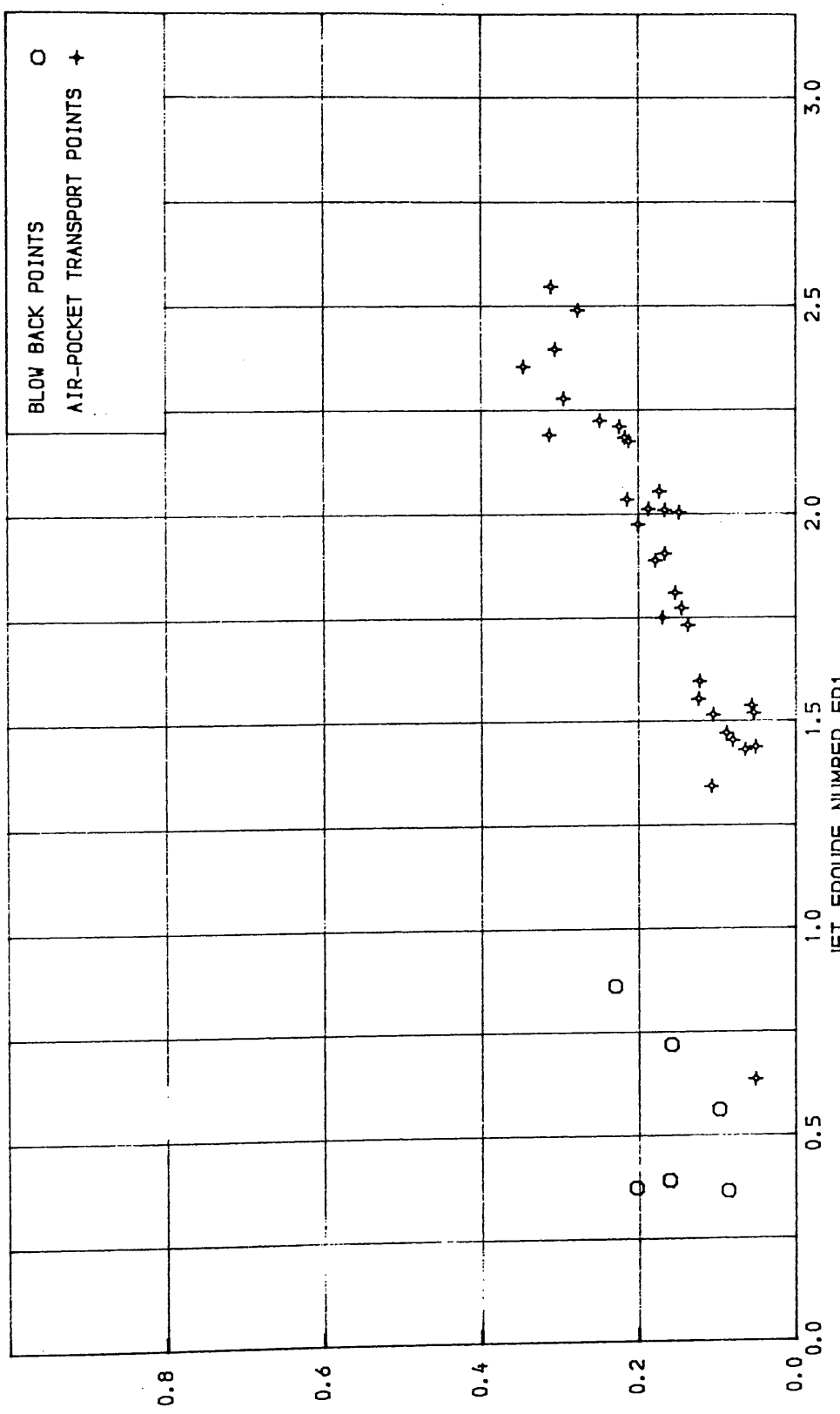

FIG. (5.12) RELATION BETWEEN THE FROUDE NUMBER BELOW THE AIR POCKET & AIR WATER RATIO AT POINTS OF BLOWING BACK AND CLEARING FOR A HORIZONTAL TUNNEL WITH A BEND OF R/D=1.0

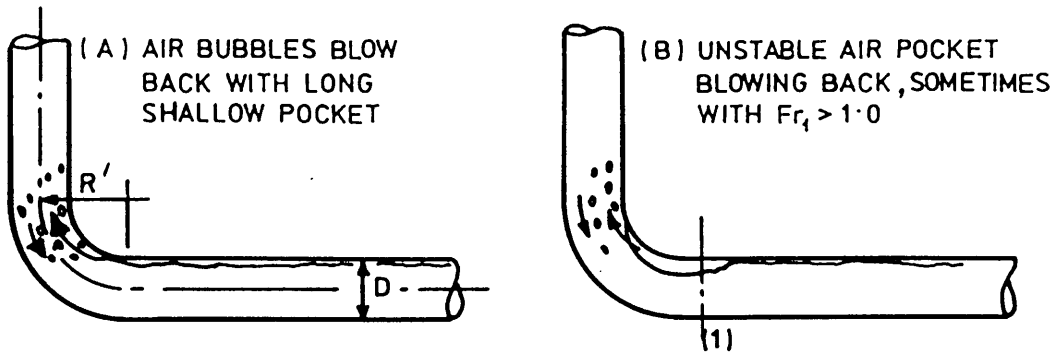

REGIME (1) AIR BUBBLES AND POCKETS BLOWING BACK

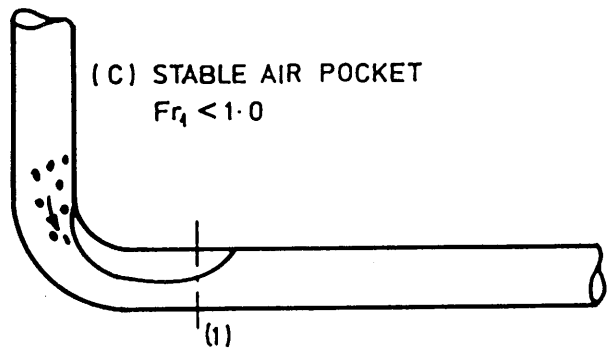

REGIME (2) STABLE AIR POCKET

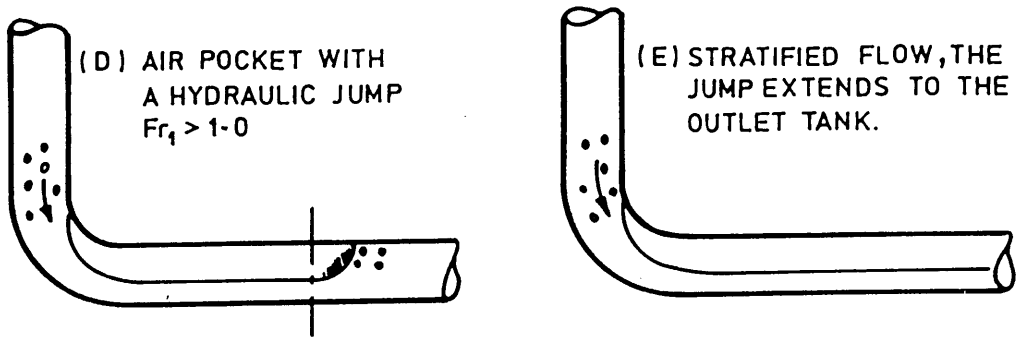

REGIME (3) AIR POCKET WITH A HYDRAULIC JUMP

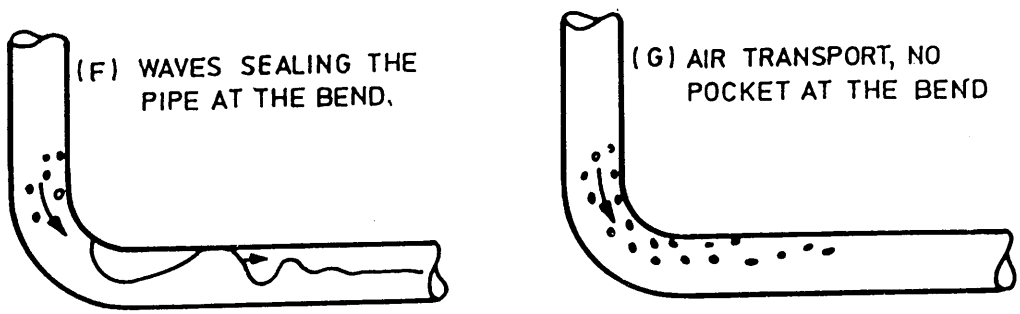

TRANSIT FROM REGIME (3) TO (4)

REGIME (4) NO POCKET AT BEND

FIG. (5.13) FLOW REGIMES WITH INCREASING UPSTREAM FROUDE NUMBER (Fr_o) FOR A HORIZONTAL TUNNEL WITH A BEND OF $R'/D = 1.50$

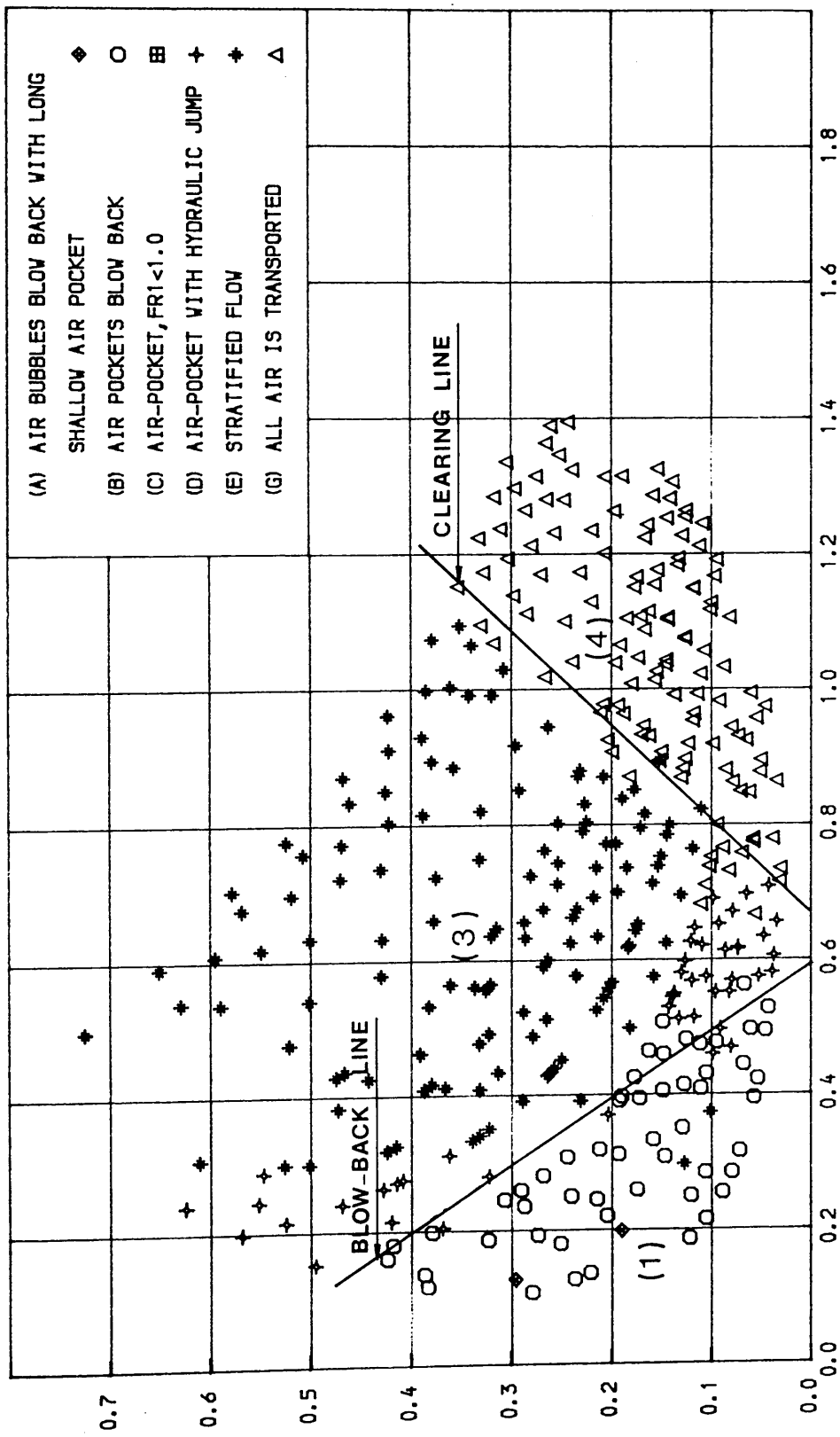

FIG. (5.14) RELATION BETWEEN UPSTREAM NON- DIMENSIONAL WATER VELOCITY & AIR-WATER RATIO FOR A HORIZONTAL TUNNEL WITH A BEND OF R/D=1.5

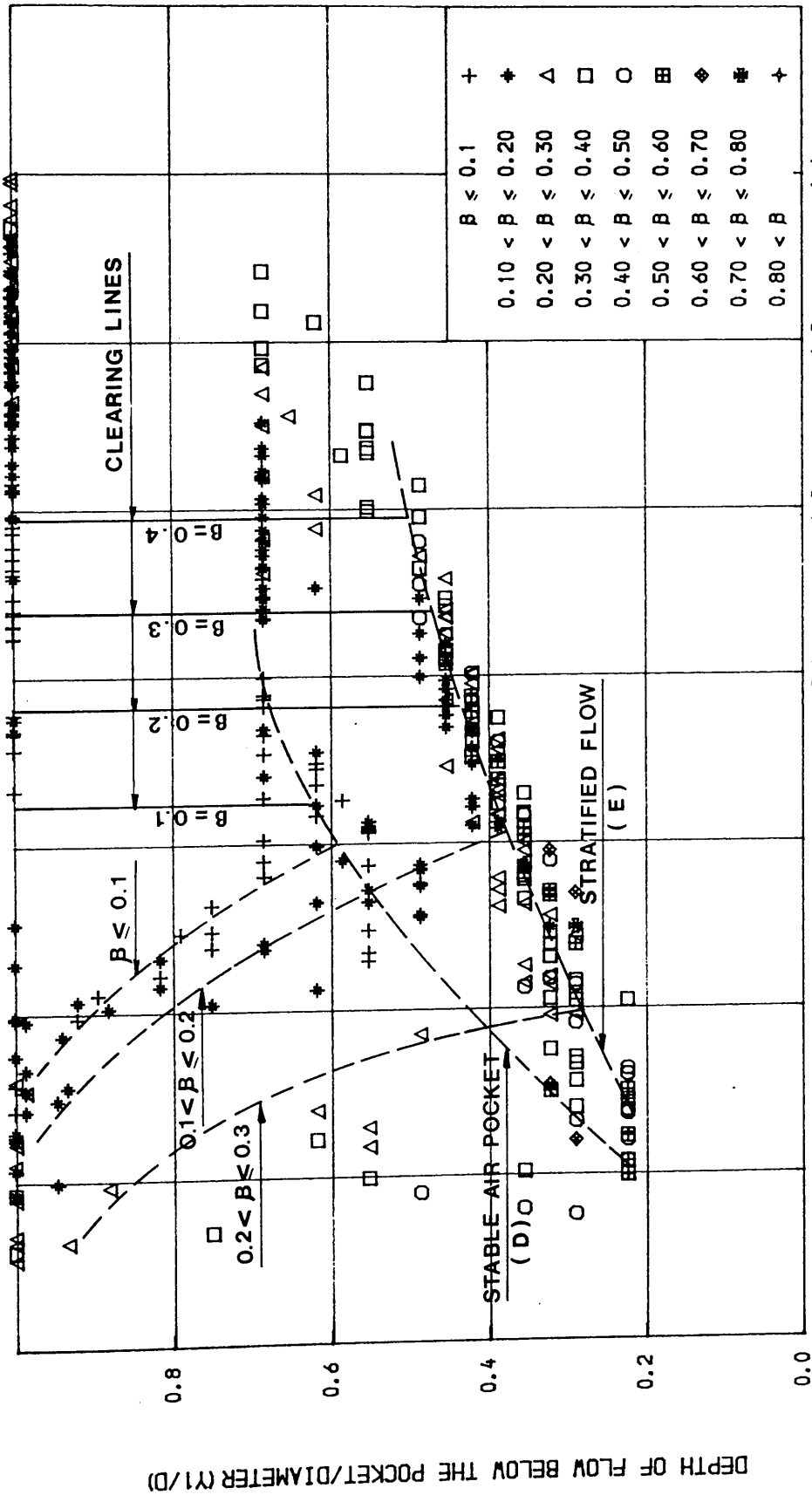

FIG. (5.15) RELATION BETWEEN UPSTREAM NON- DIMENSIONAL WATER VELOCITY & NON-DIMENSIONAL DEPTH OF FLOW BELOW THE POCKET FOR A HORIZONTAL TUNNEL WITH A BEND OF R/D=1.5

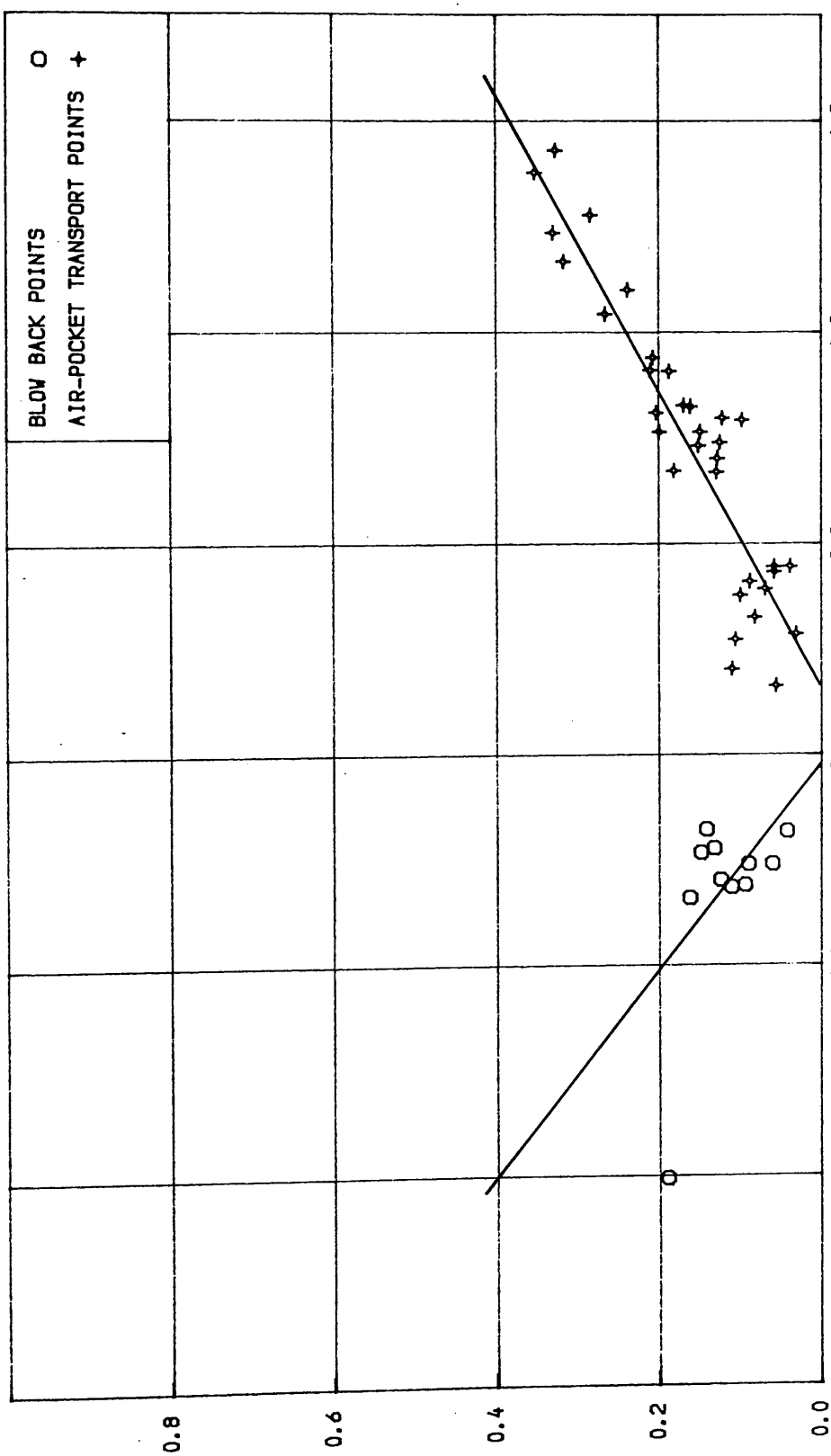

FIG. (5.16) RELATION BETWEEN UPSTREAM NON- DIMENSIONAL WATER VELOCITY & AIR WATER RATIO AT POINTS OF BLOWING BACK AND CLEARING FOR A HORIZONTAL TUNNEL WITH A BEND OF R/D=1.5

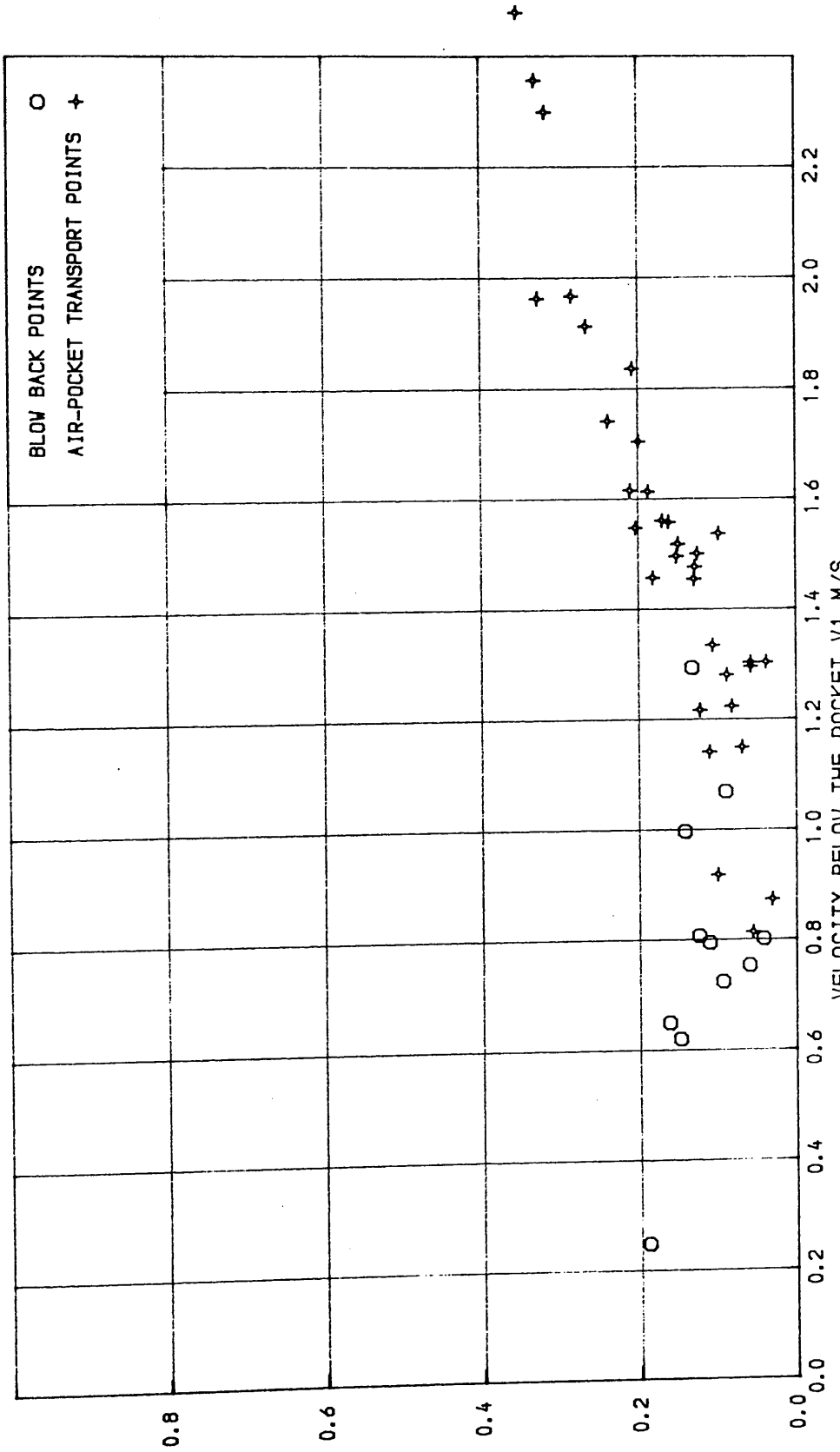

FIG. (5.17) RELATION BETWEEN WATER VELOCITY BELOW THE AIR POCKET & AIR WATER RATIO AT POINTS OF BLOWING BACK AND CLEARING FOR A HORIZONTAL TUNNEL WITH A BEND OF Ŕ/D=1.5

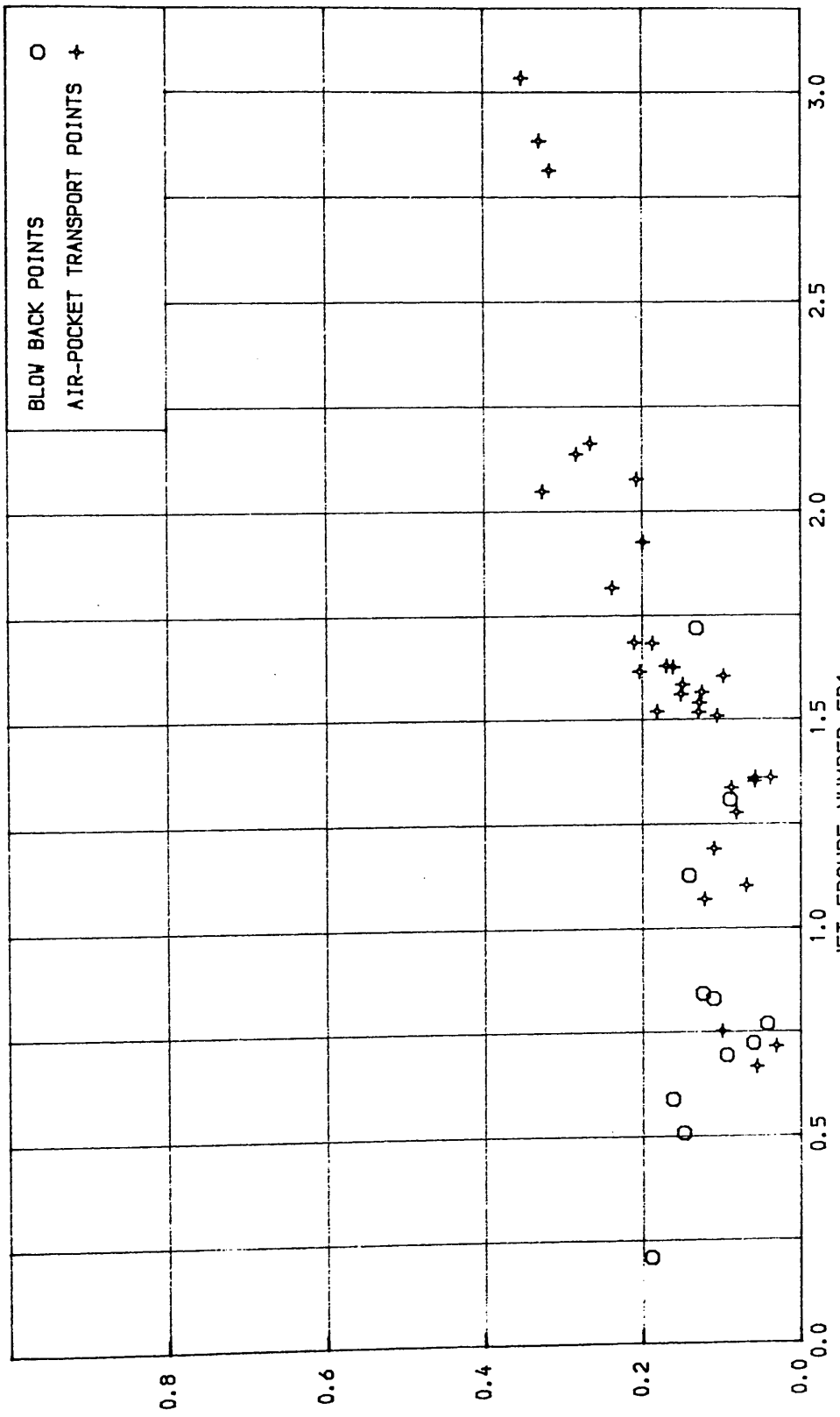

FIG. (5.18) RELATION BETWEEN THE FROUDE NUMBER BELOW THE AIR POCKET & AIR WATER RATIO AT POINTS OF BLOWING BACK AND CLEARING FOR A HORIZONTAL TUNNEL WITH A BEND OF R/D=1.5

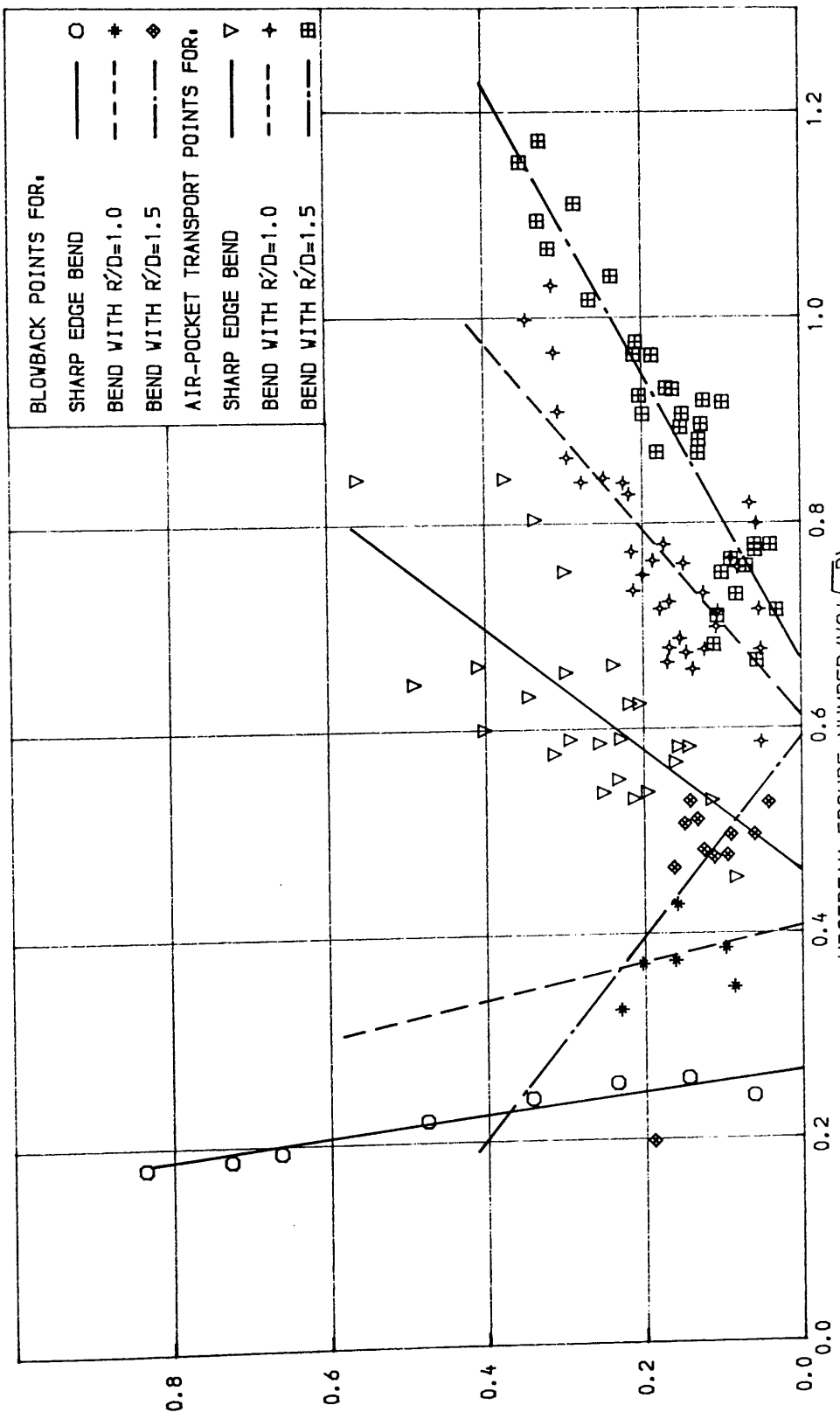

FIG. (5.19) RELATION BETWEEN UPSTREAM NON- DIMENSIONAL WATER VELOCITY & AIR-WATER RATIO AT POINTS OF BLOWING BACK AND CLEARING FOR A HORIZONTAL TUNNEL WITH THREE BENDS OF R/D=0.5, 1.0 &1.5

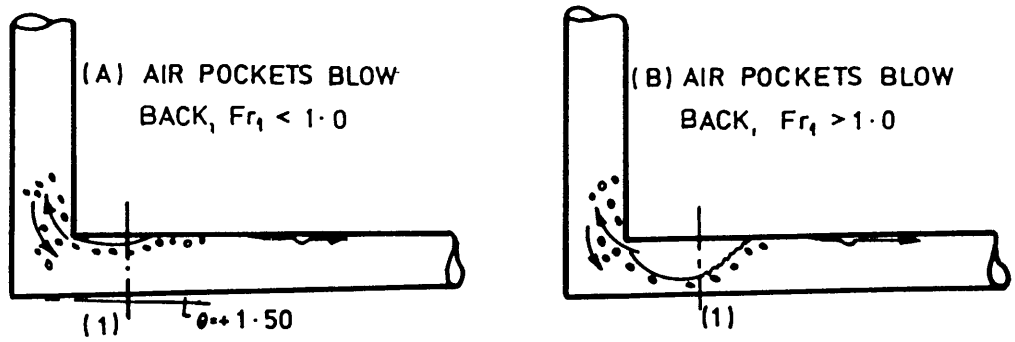

REGIME (1) AIR POCKETS BLOWING BACK

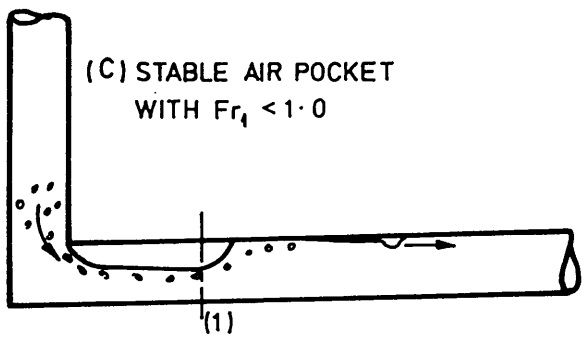

REGIME (2) STABLE AIR POCKET

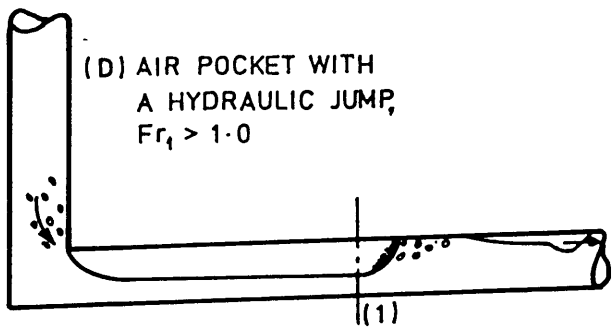

REGIME (3) AIR POCKET WITH A HYDRAULIC JUMP

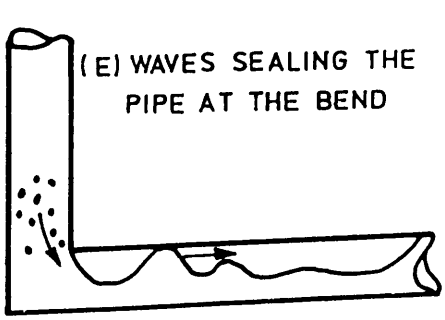

TRANSIT FROM REGIME (3) TO (4)

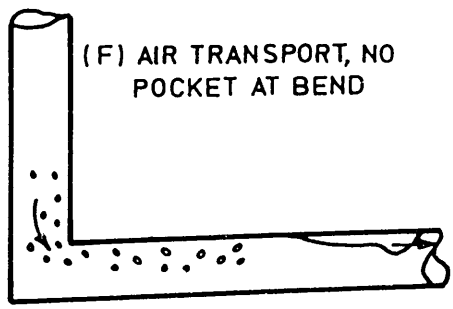

REGIME (4) NO POCKET AT BEND

FIG. (5.20) FLOW REGIMES WITH INCREASING UPSTREAM FROUDE NUMBER (Fr_o) FOR A TUNNEL AT +1.50° WITH HORIZONTAL AND A SHARP BEND, R'/D = 0.50

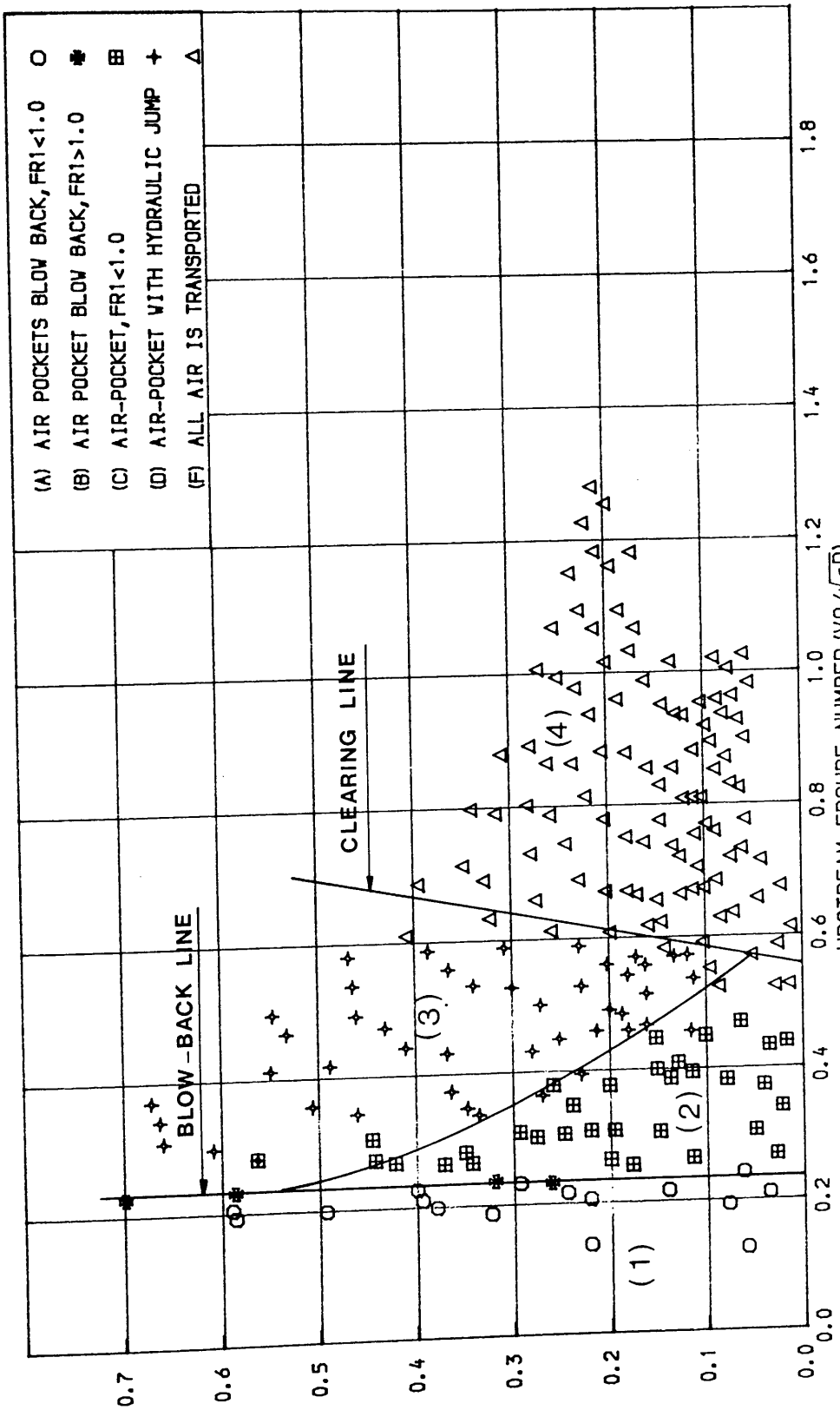

FIG. (5.21) RELATION BETWEEN UPSTREAM NON- DIMENSIONAL WATER VELOCITY & AIR-WATER RATIO FOR A TUNNEL AT +1.5 DEGREE WITH HORIZONTAL & A BEND OF R/D=0.5

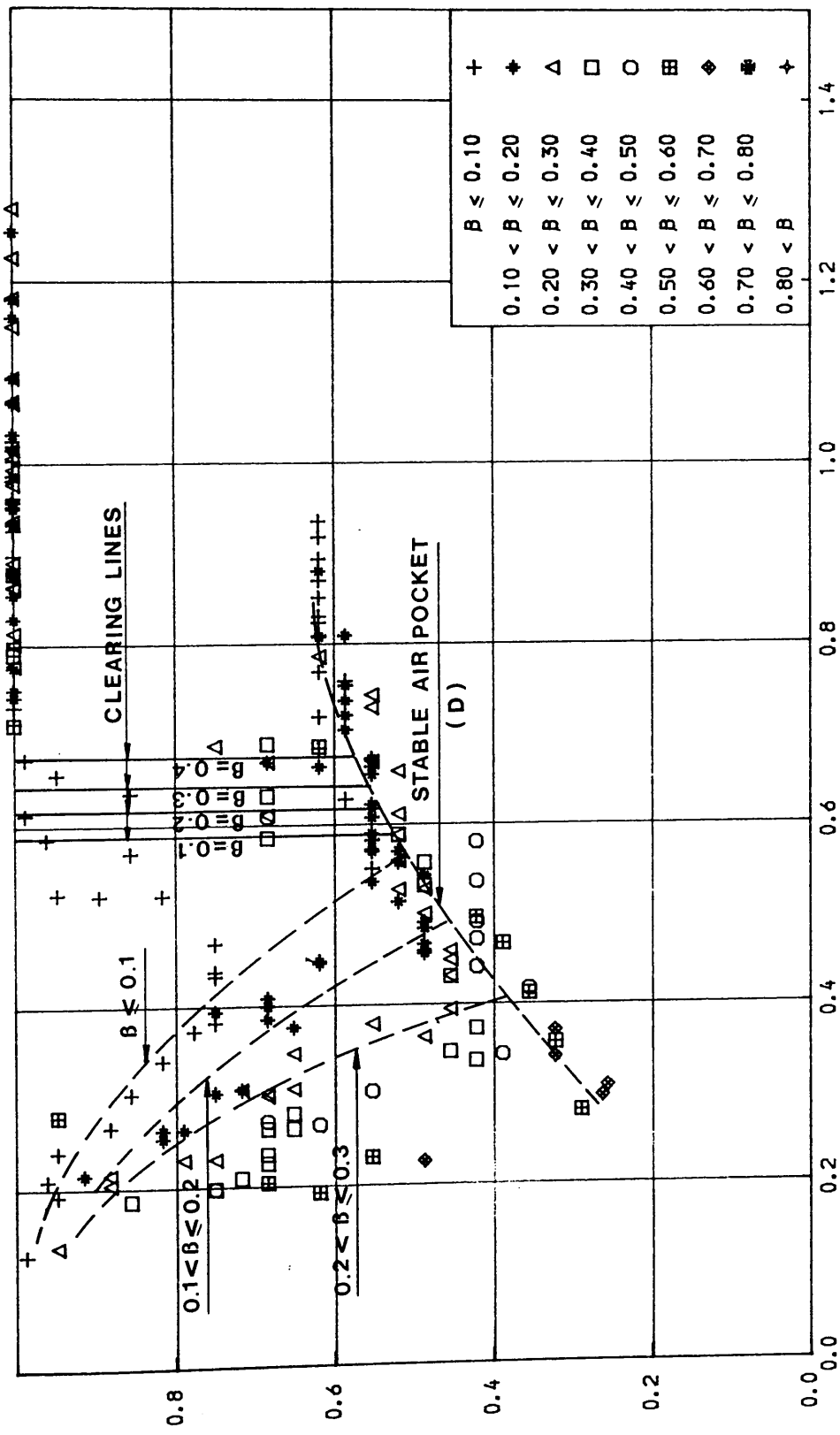

FIG. (5.22) RELATION BETWEEN UPSTREAM NON- DIMENSIONAL WATER VELOCITY & NON-DIMENSIONAL DEPTH OF FLOW BELOW THE POCKET FOR A TUNNEL AT +1.5 DEGREE WITH HORIZONTAL & A BEND OF R/D=0.5

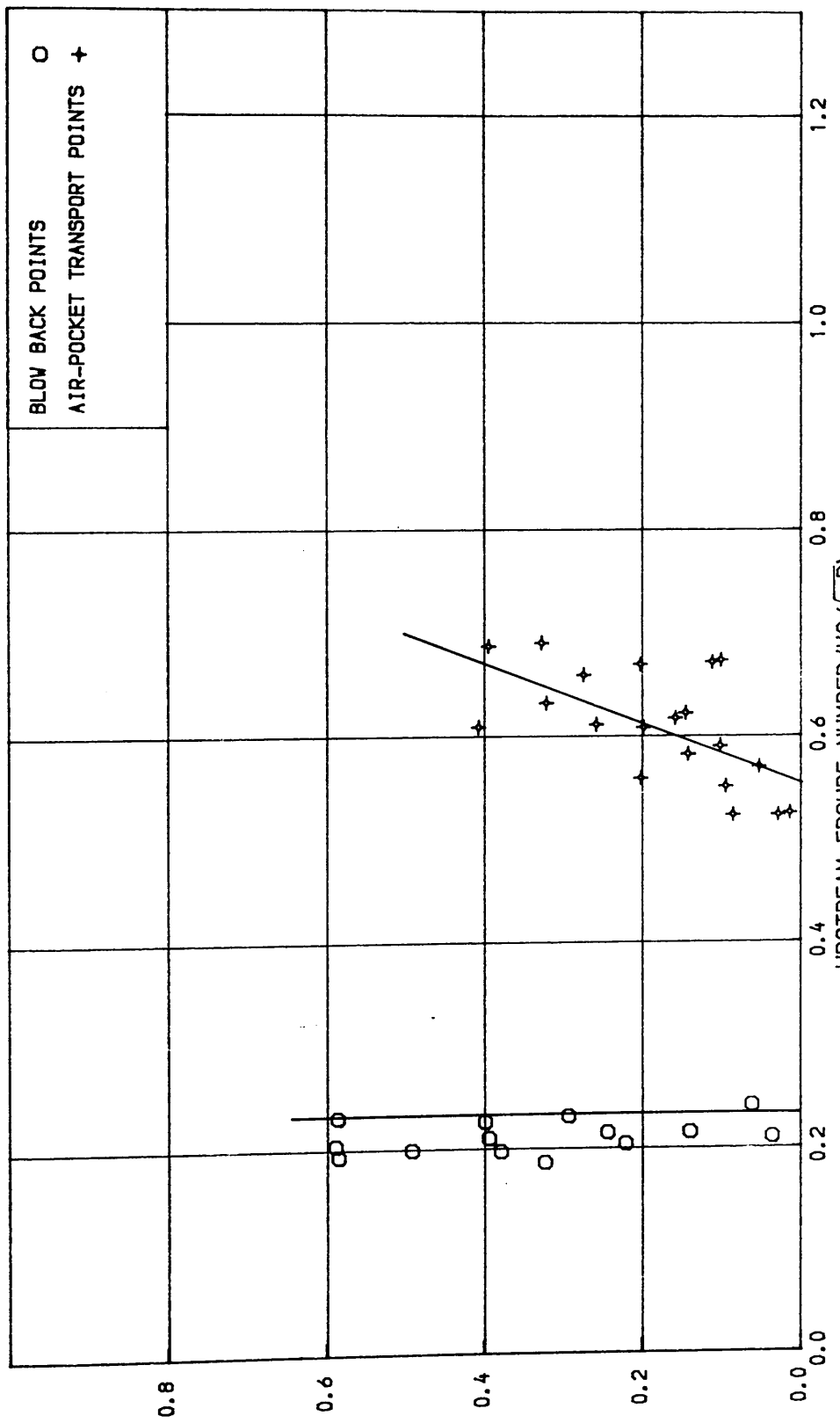

FIG. (5.23) RELATION BETWEEN UPSTREAM NON- DIMENSIONAL WATER VELOCITY & AIR WATER RATIO AT POINTS OF BLOWING BACK AND CLEARING FOR A TUNNEL AT +1.5 DEGREE WITH HORIZONTAL AND A BEND OF Ŕ/D=0.5

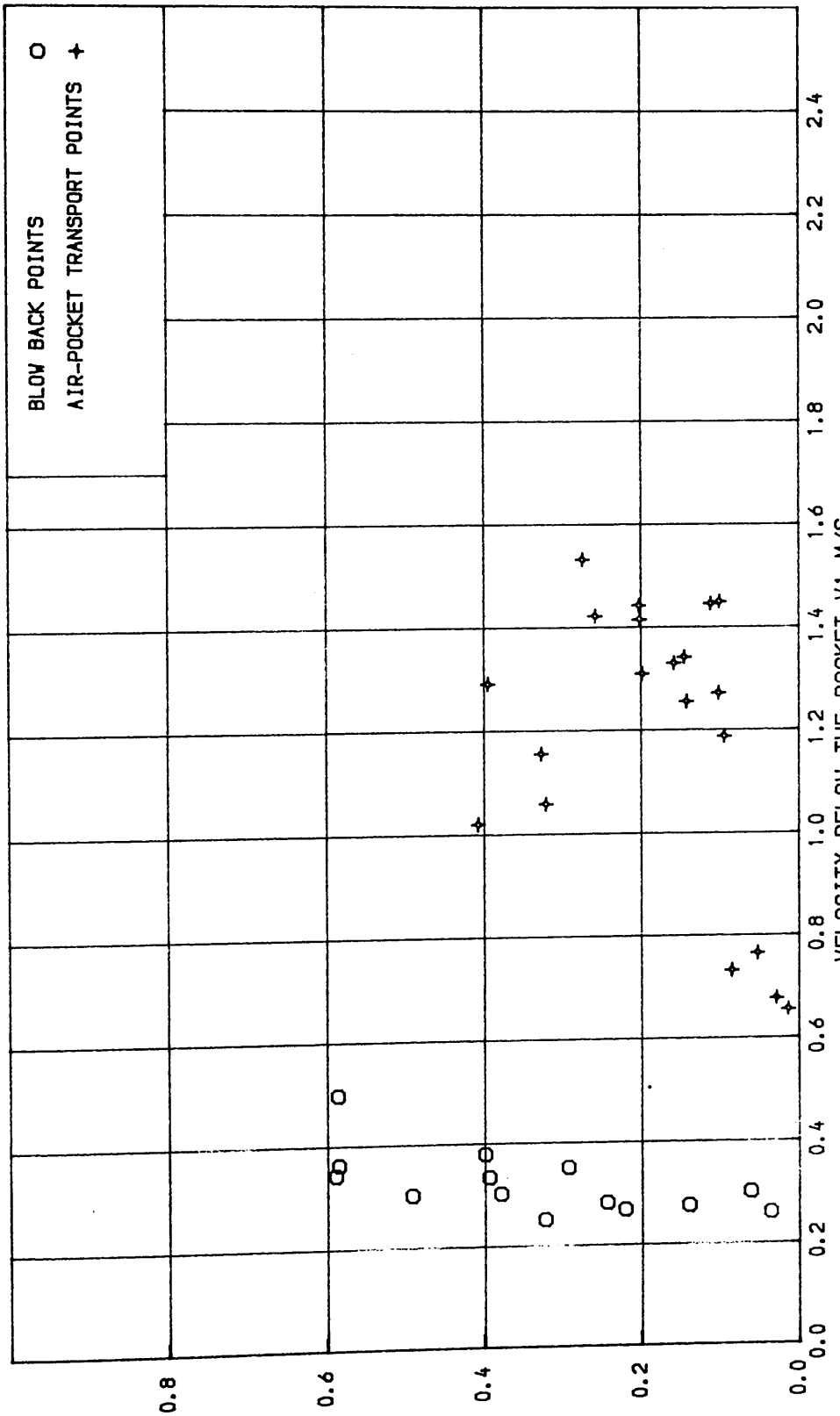

FIG. (5.24) RELATION BETWEEN WATER VELOCITY BELOW THE AIR POCKET & AIR WATER RATIO AT POINTS OF BLOWING BACK AND CLEARING FOR A TUNNEL AT +1.5 DEGREE WITH HORIZONTAL AND A BEND OF R/D=0.5

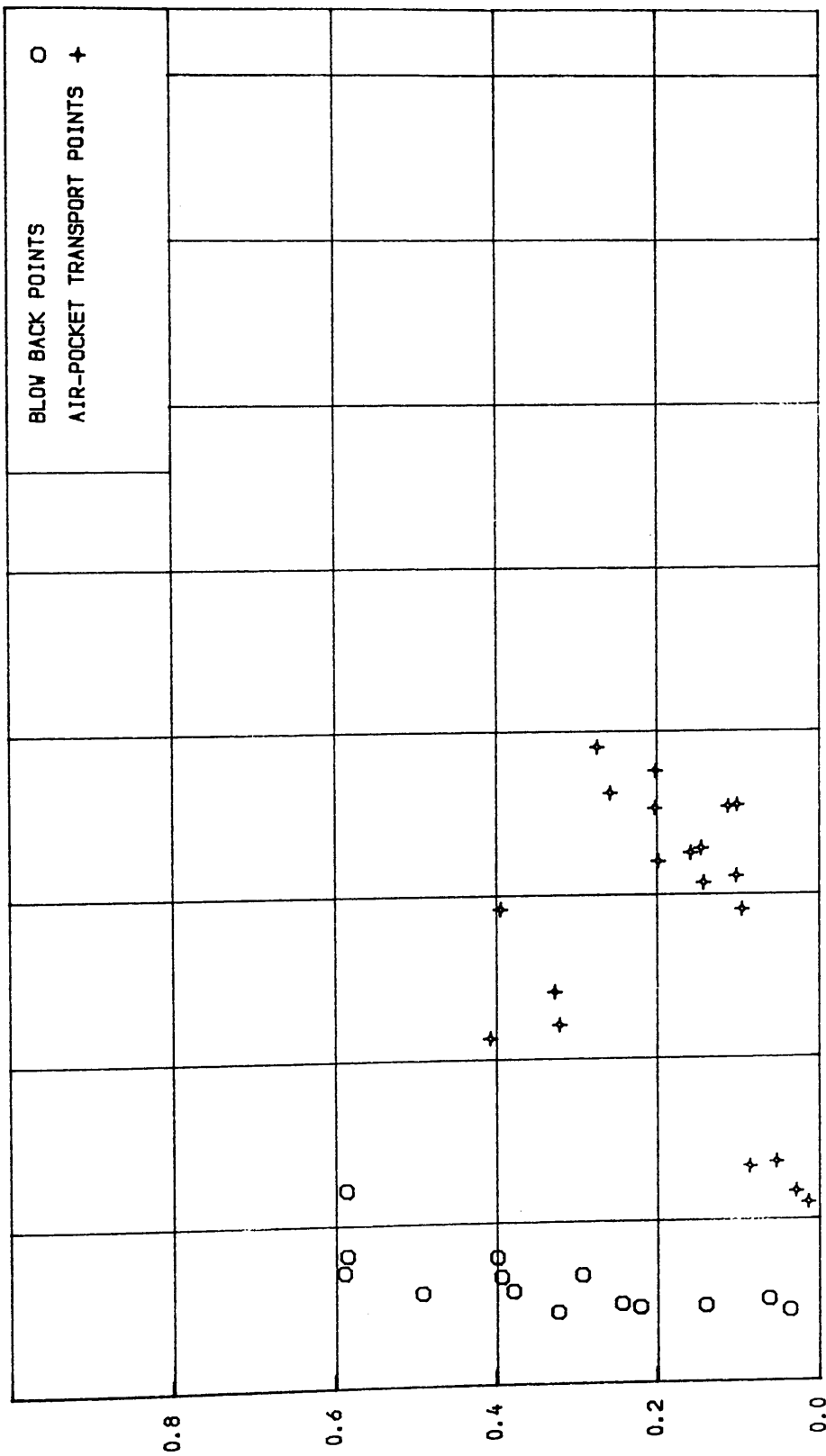

FIG. (5.25) RELATION BETWEEN THE FROUDE NUMBER BELOW THE AIR POCKET & AIR WATER RATIO AT POINTS OF BLOWING BACK AND CLEARING FOR A TUNNEL AT +1.5 DEGREE WITH HORIZONTAL AND A BEND OF R/D=0.5

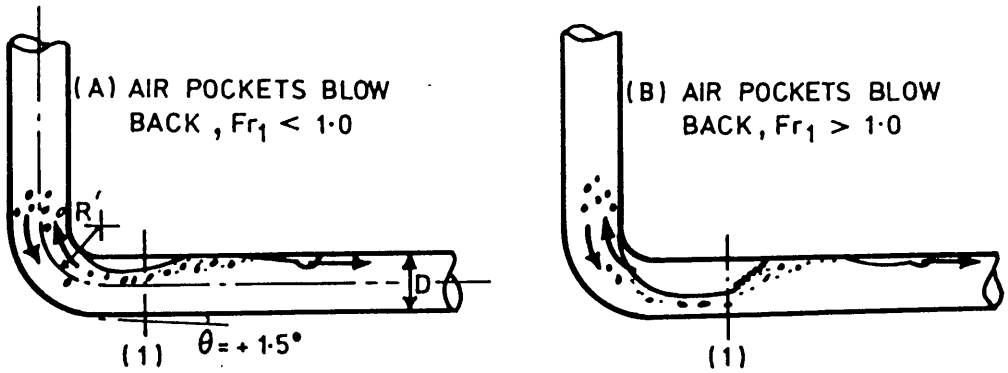

REGIME (1) AIR POCKETS BLOWING BACK

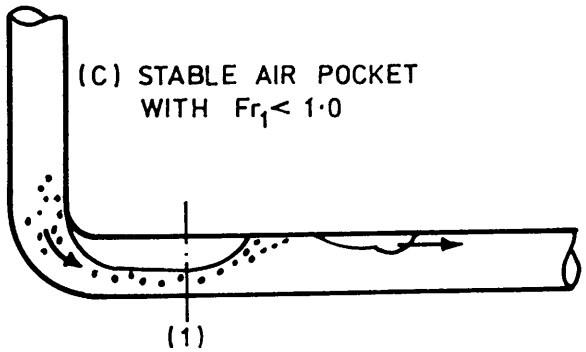

REGIME (2) STABLE AIR POCKET

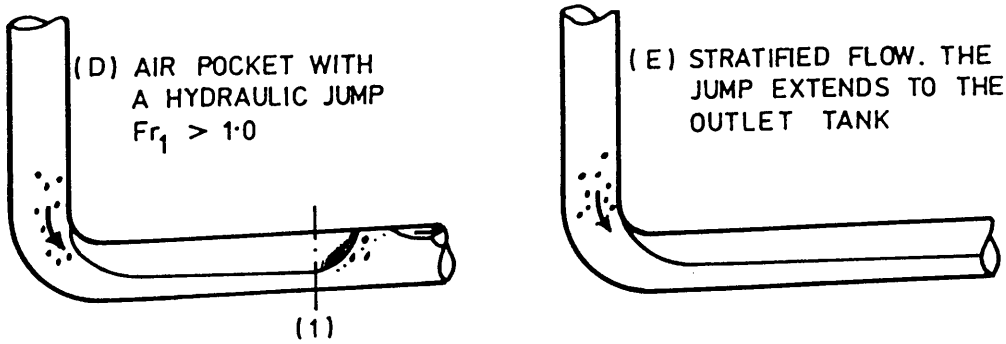

REGIME (3) AIR POCKET WITH A HYDRAULIC JUMP

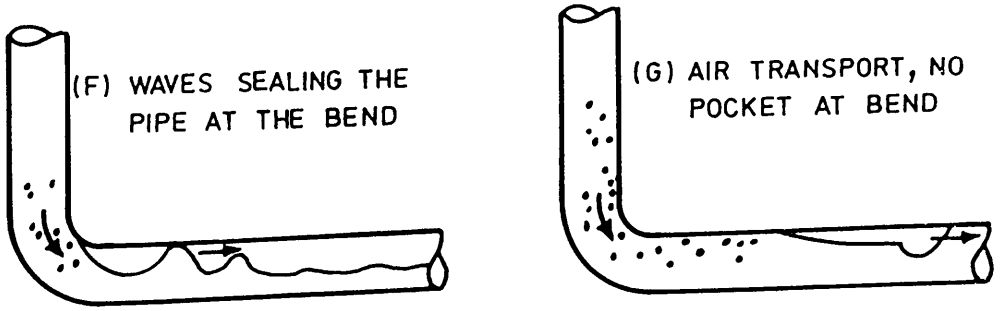

TRANSIT FROM REGIME (3) to (4)

REGIME (4) NO POCKET AT BEND

FIG. (5.26) FLOW REGIMES WITH INCREASING UPSTREAM FROUDE NUMBER (Fr_o) FOR A TUNNEL AT +1.50° WITH HORIZONTAL AND A BEND OF R'/D = 1.0

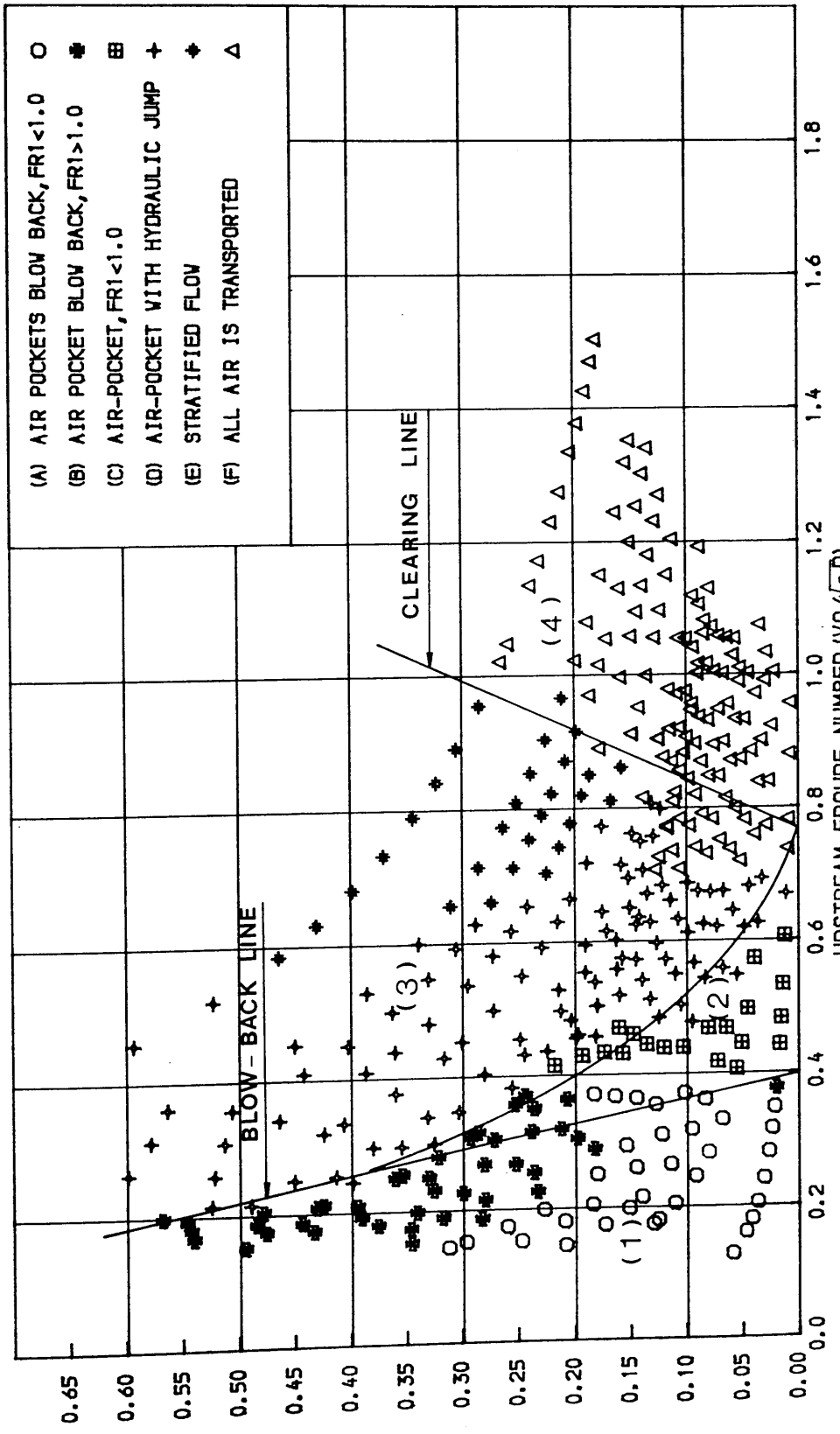

FIG. (5.27) RELATION BETWEEN UPSTREAM NON- DIMENSIONAL WATER VELOCITY & AIR-WATER RATIO

FOR A TUNNEL AT +1.5 DEGREE WITH HORIZONTAL AND A BEND OF Ŕ/D=1.0

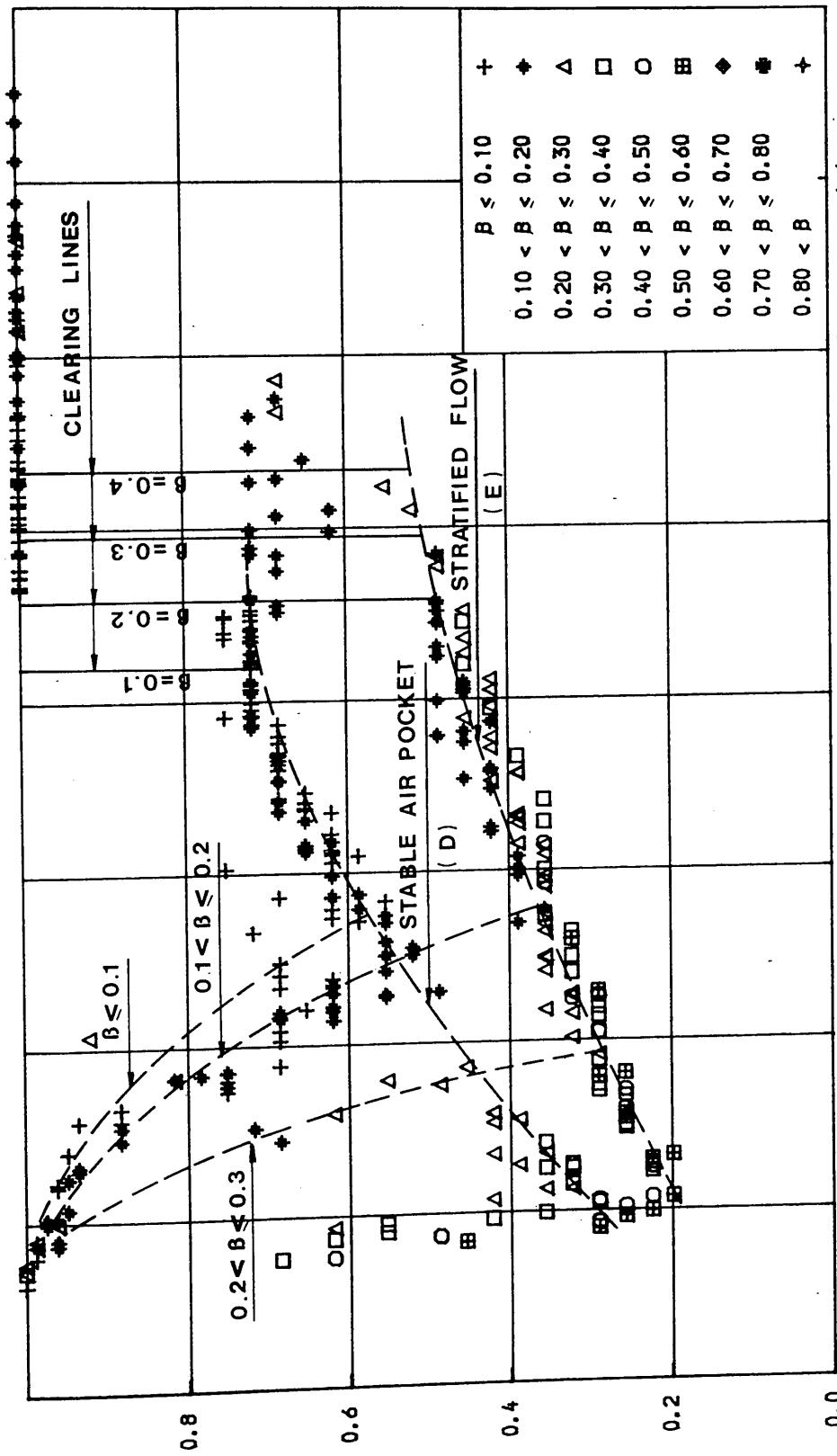

FIG. (5.28) RELATION BETWEEN UPSTREAM NON- DIMENSIONAL WATER VELOCITY & NON-DIMENSIONAL DEPTH OF FLOW BELOW THE POCKET FOR A TUNNEL AT +1.5 DEGREE WITH HORIZONTAL & A BEND OF R/D=1.0

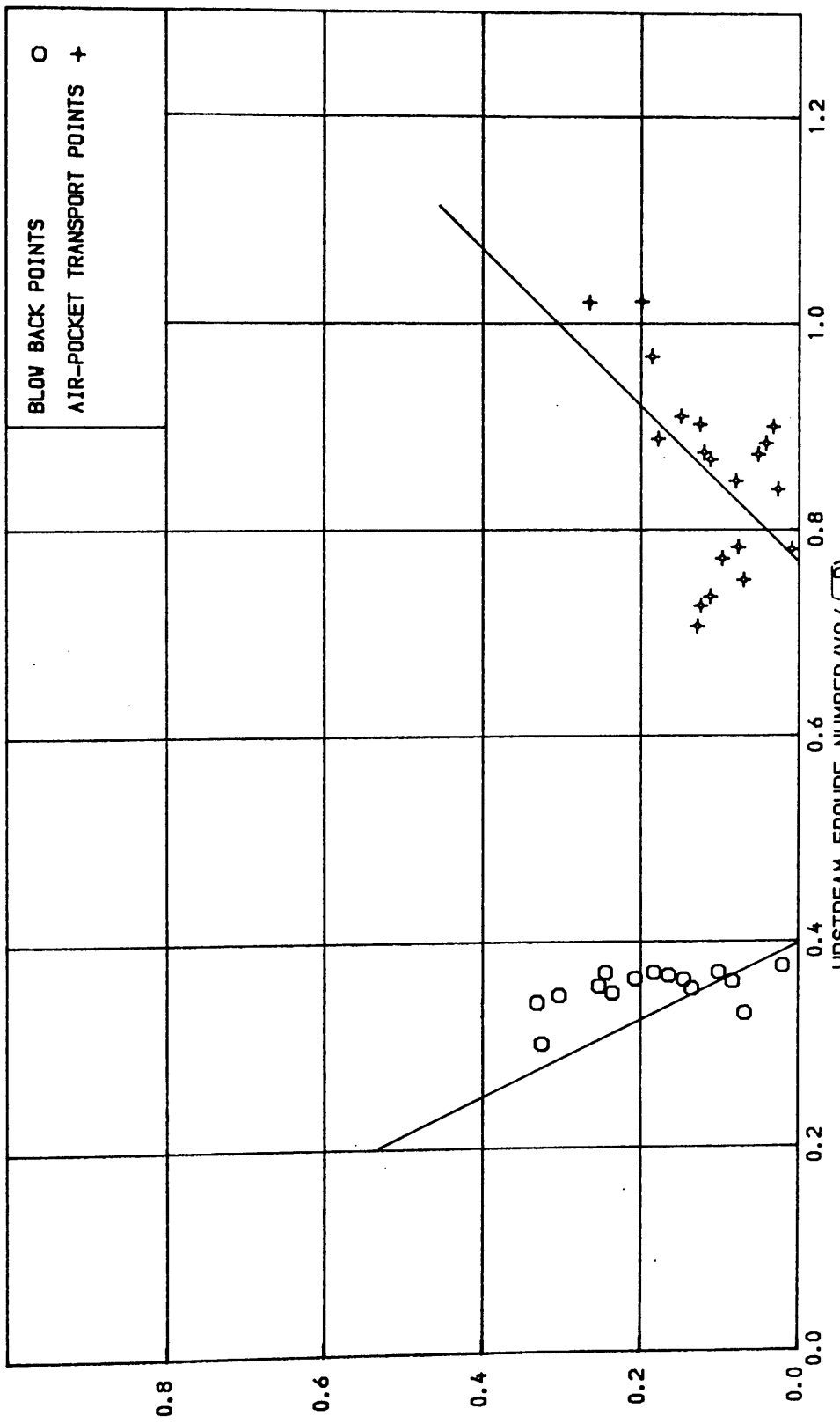

FIG. (5.29) RELATION BETWEEN UPSTREAM NON- DIMENSIONAL WATER VELOCITY & AIR WATER RATIO AT POINTS OF BLOWING BACK AND CLEARING FOR A TUNNEL AT +1.5 DEGREE WITH HORIZONTAL AND A BEND OF R/D=1.0

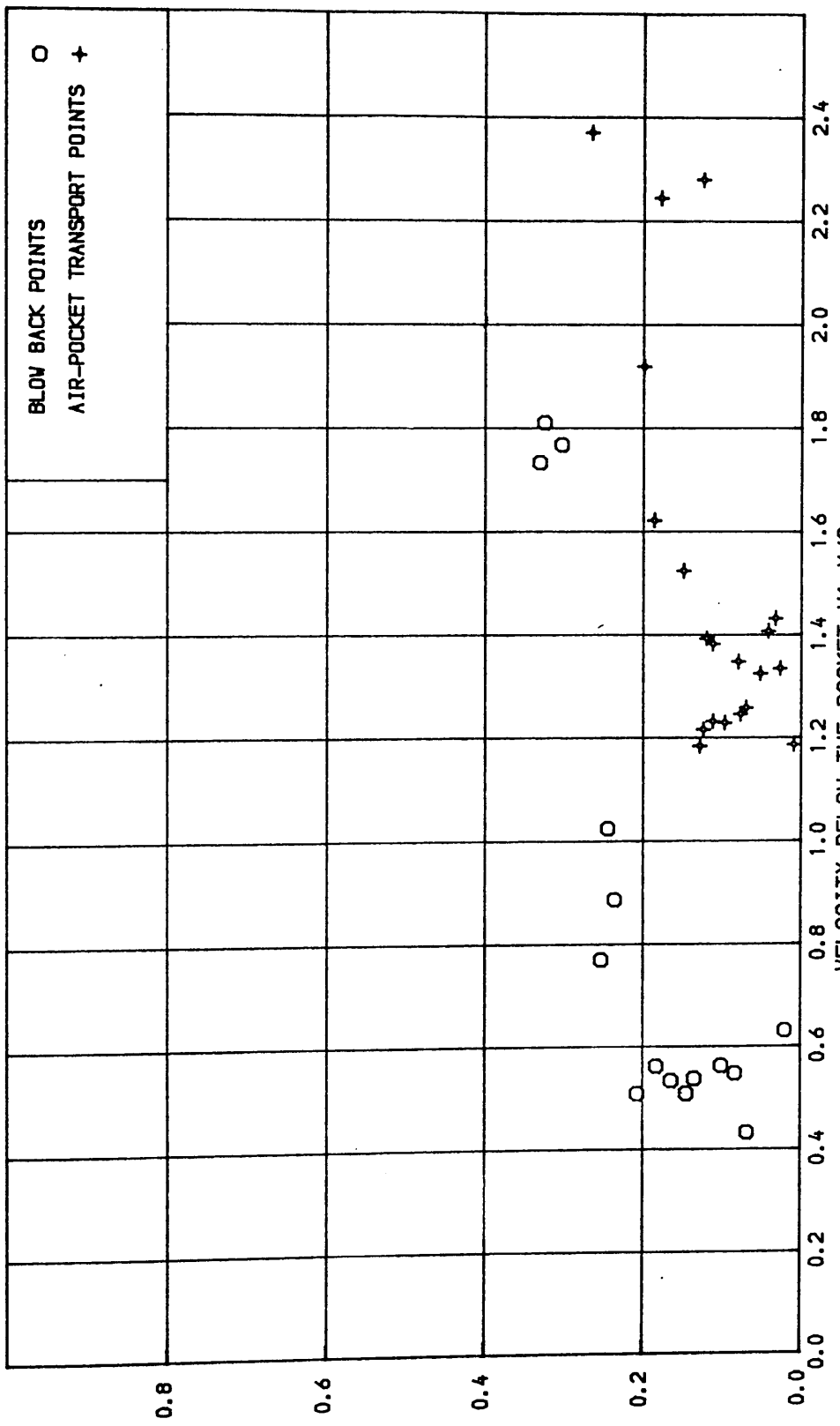

FIG. (5.30) RELATION BETWEEN THE WATER VELOCITY BELOW THE AIR POCKET & AIR WATER RATIO AT POINTS OF BLOWING BACK AND CLEARING FOR A TUNNEL AT +1.5 DEGREE WITH HORIZONTAL AND A BEND OF R/D=1.0

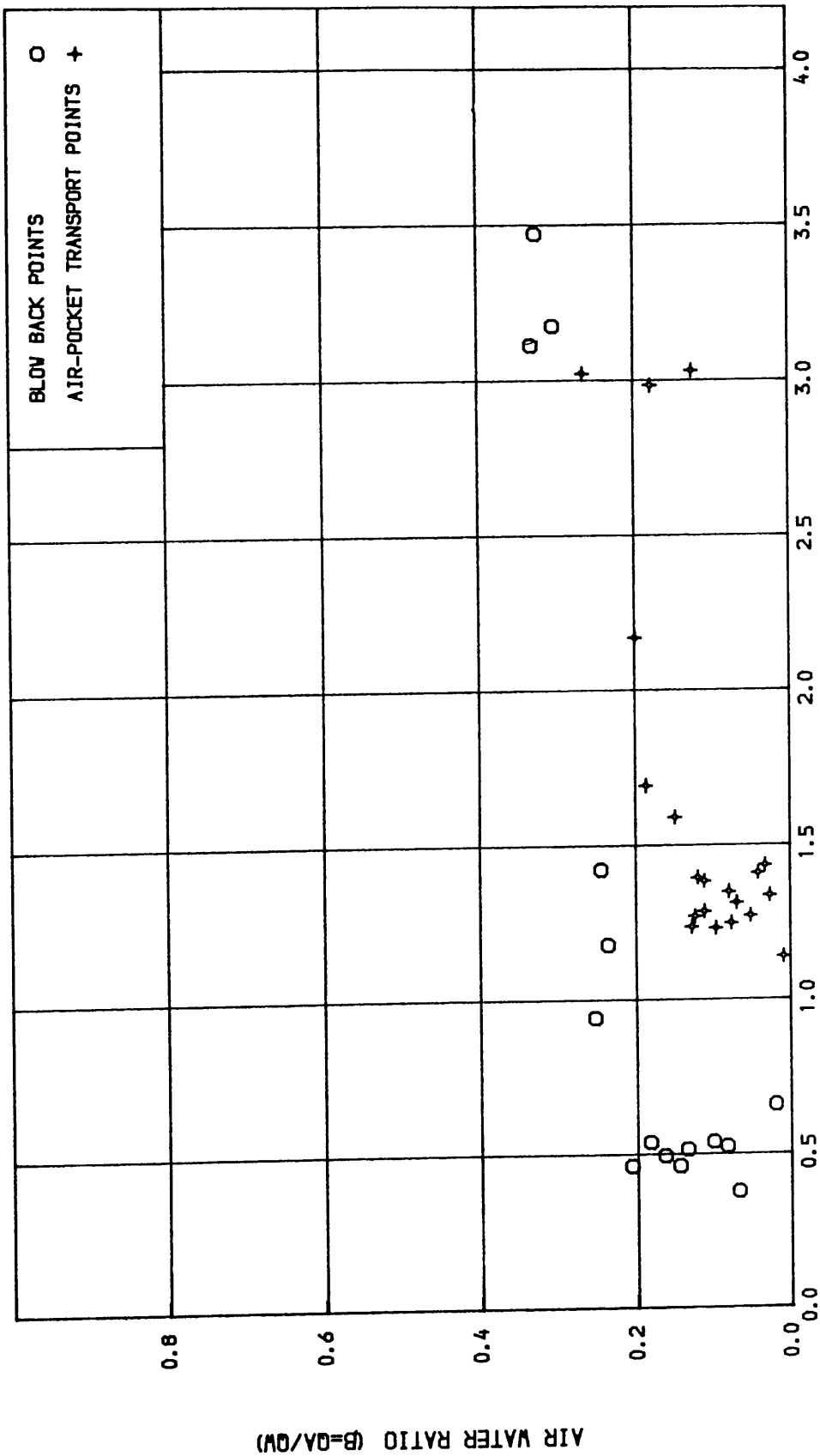

FIG. (5.31) RELATION BETWEEN THE FROUDE NUMBER BELOW THE AIR POCKET & AIR WATER RATIO AT POINTS OF BLOWING BACK AND CLEARING FOR A TUNNEL AT +1.5 DEGREE WITH HORIZONTAL AND A BEND OF R/D=1.0

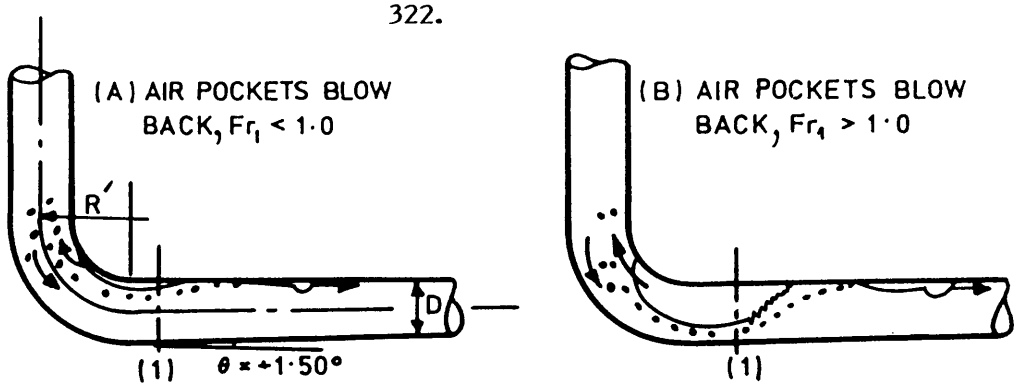

REGIME (1) AIR POCKETS BLOWING BACK

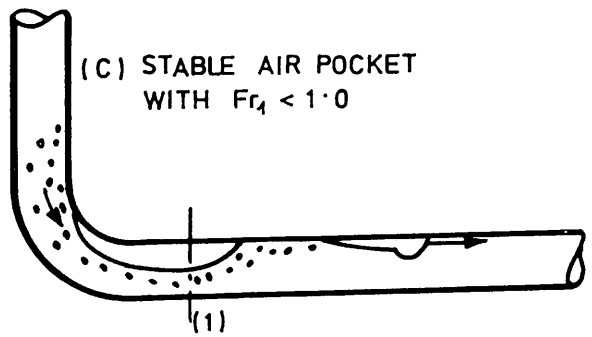

REGIME (2) STABLE AIR POCKET

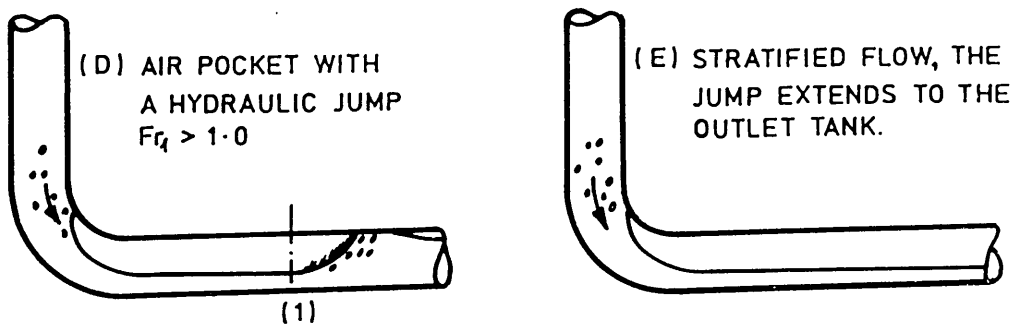

REGIME (3) AIR POCKET WITH A HYDRAULIC JUMP

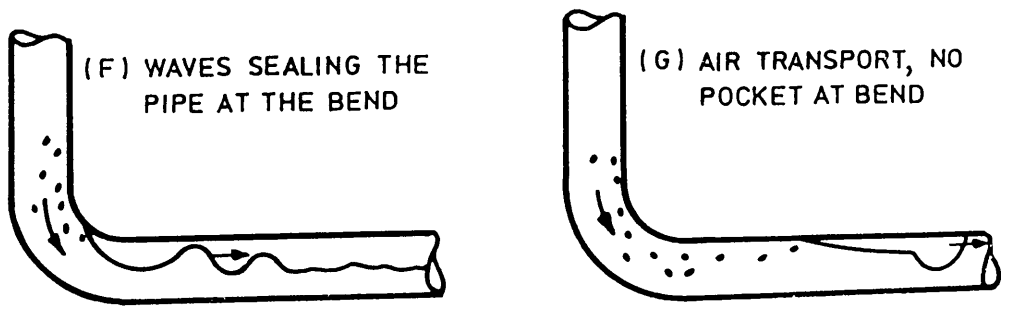

TRANSIT FROM REGIME (3) TO (4)

REGIME (4) NO POCKET AT BEND

FIG. (5.32) FLOW REGIMES WITH INCREASING UPSTREAM FROUDE NUMBER (Fr_o) FOR A TUNNEL AT +1.50° WITH HORIZONTAL AND A BEND OF R'/D = 1.50

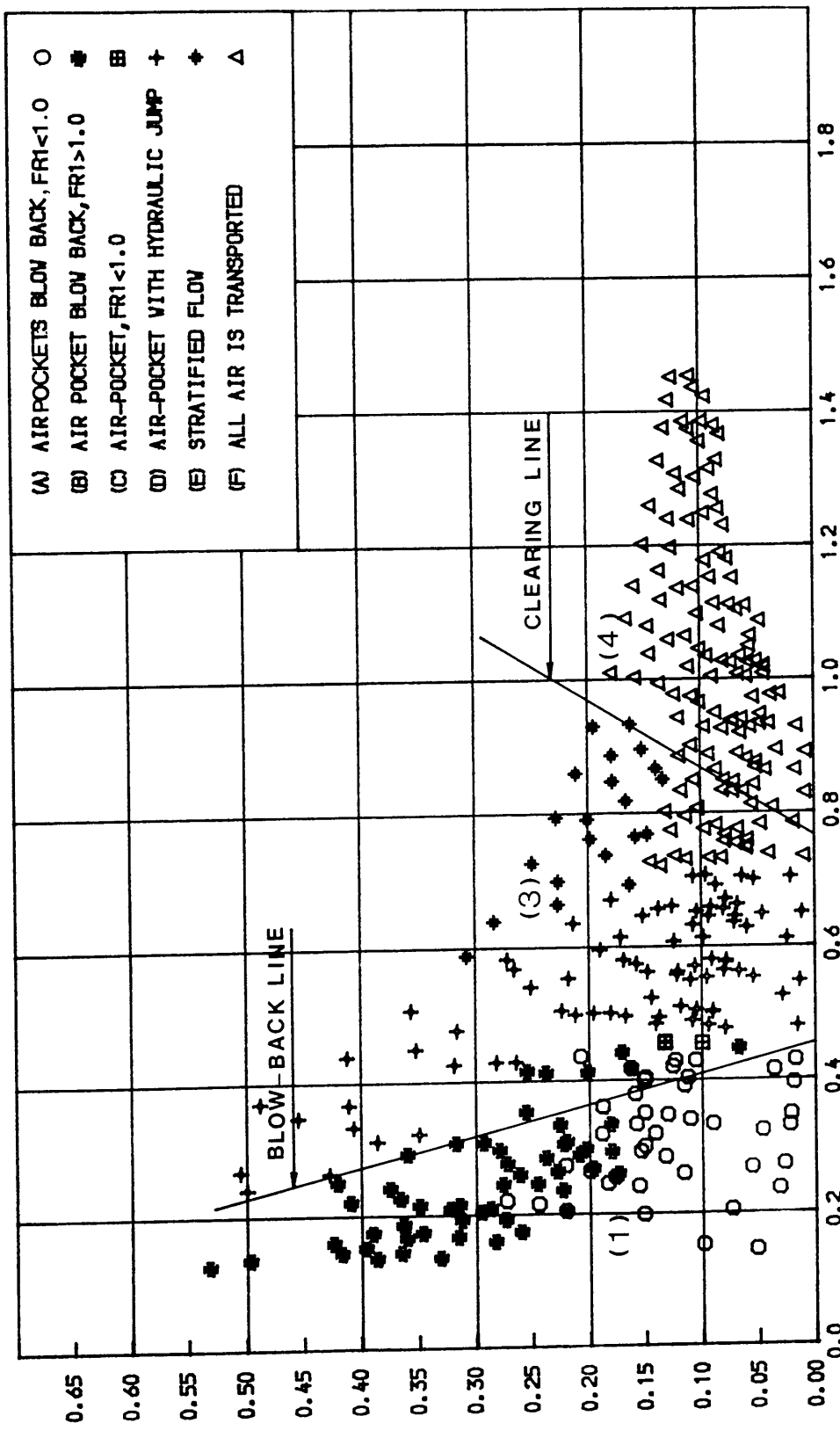

FIG. (5.33) RELATION BETWEEN UPSTREAM NON- DIMENSIONAL WATER VELOCITY & AIR-WATER RATIO

FOR A TUNNEL AT +1.5 DEGREE WITH HORIZONTAL AND A BEND OF R/D=1.5

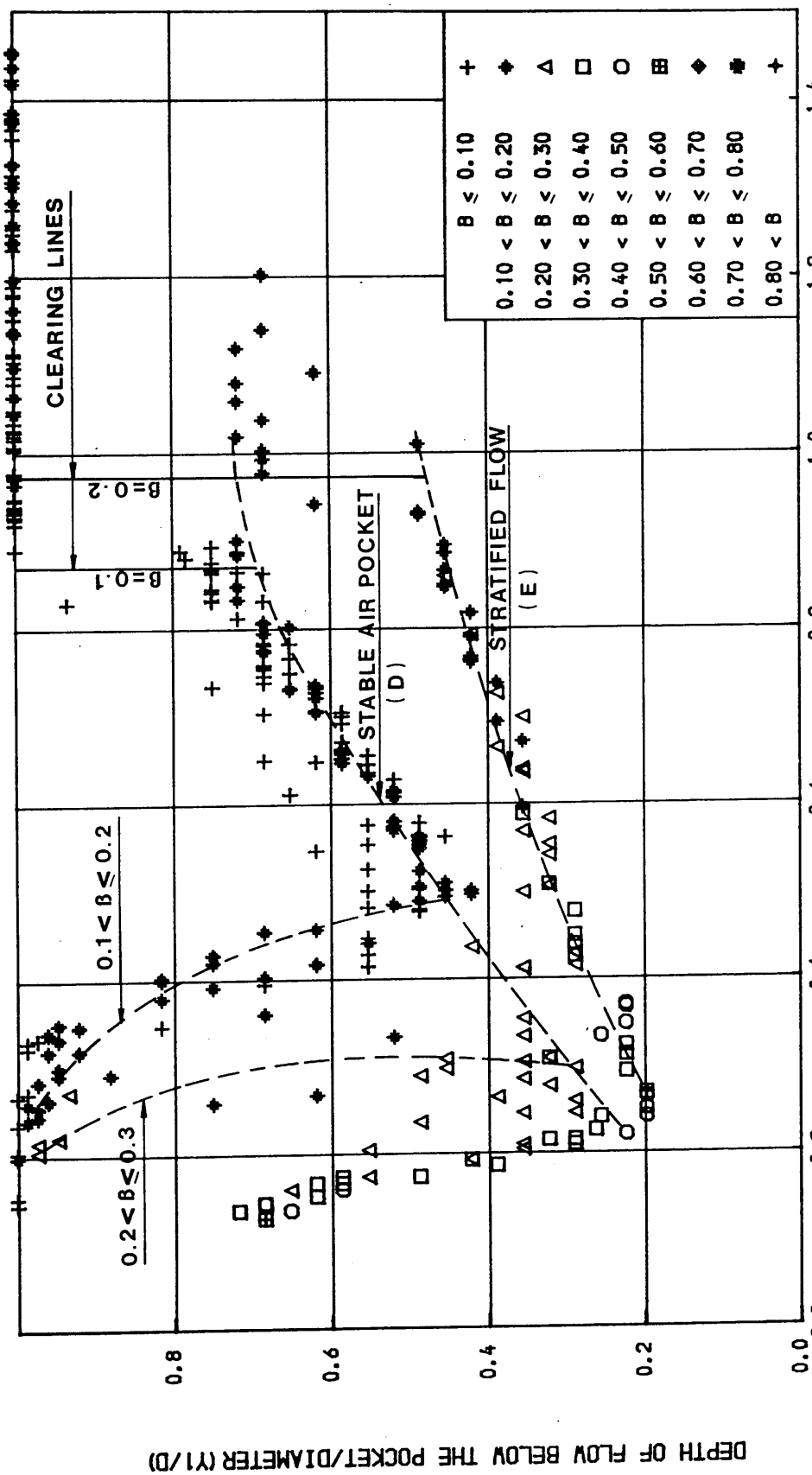

FIG. (5.34) RELATION BETWEEN UPSTREAM NON DIMENSIONAL WATER VELOCITY & NON-DIMENSIONAL DEPTH OF FLOW BELOW THE POCKET FOR A TUNNEL AT +1.5 DEGREE WITH HORIZONTAL & A BEND OF R/D=1.5

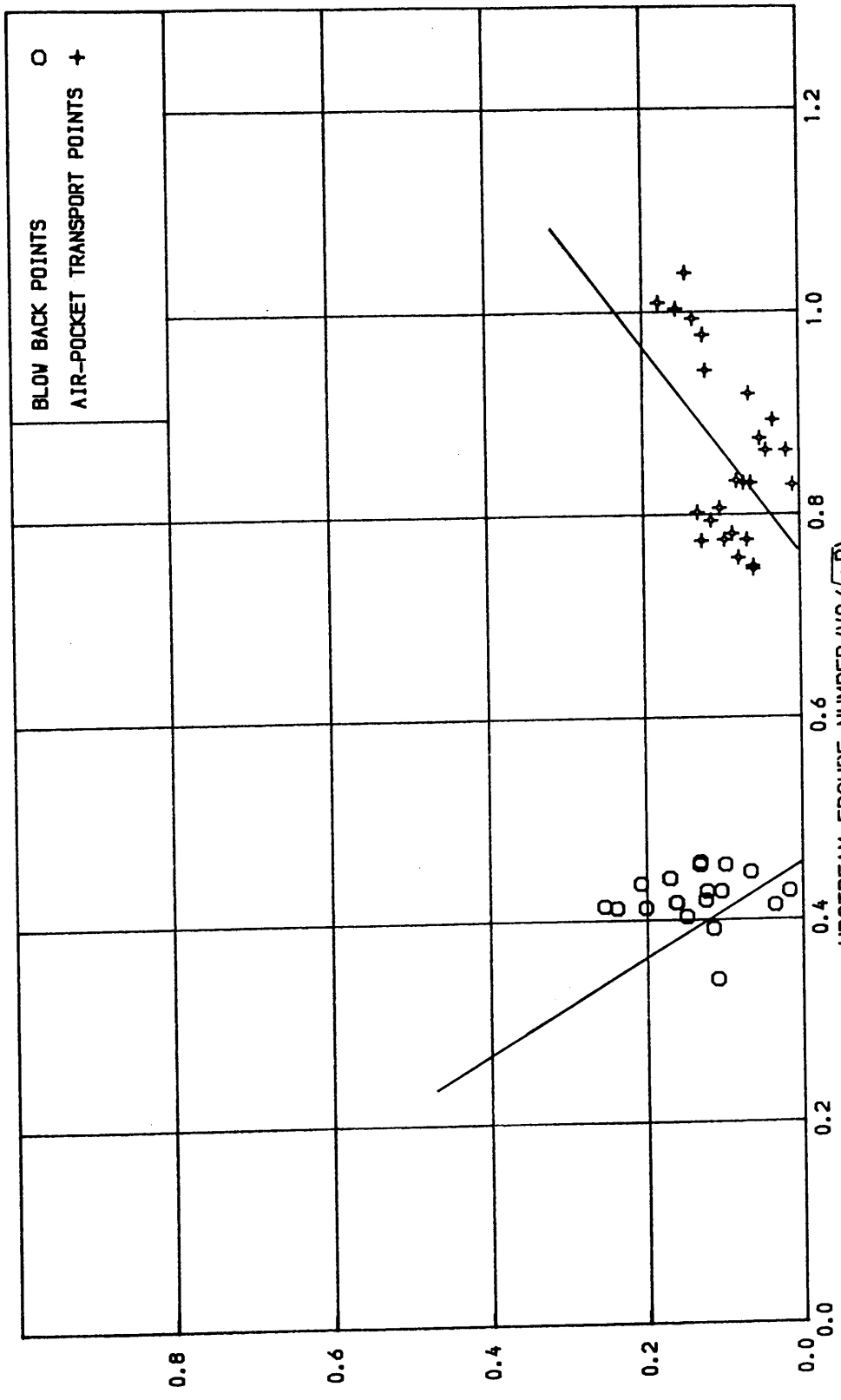

FIG. (5.35) RELATION BETWEEN UPSTREAM NON- DIMENSIONAL WATER VELOCITY & AIR WATER RATIO AT POINTS OF BLOWING BACK AND CLEARING FOR A TUNNEL AT +1.5 DEGREE WITH HORIZONTAL AND A BEND OF Ŕ/D=1.5

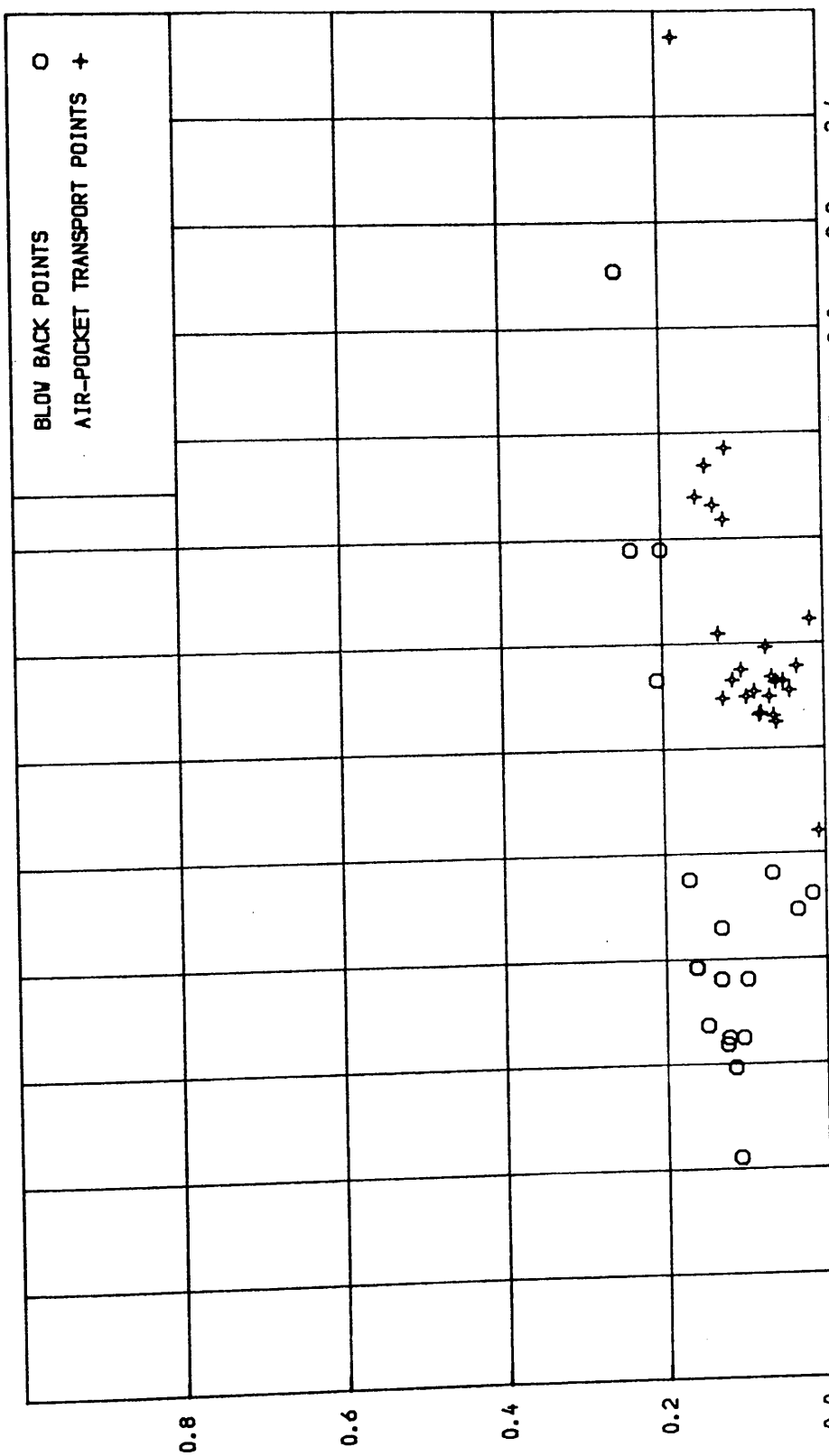

FIG. (5.36) RELATION BETWEEN THE WATER VELOCITY BELOW THE AIR POCKET & AIR WATER RATIO AT POINTS OF BLOWING BACK AND CLEARING FOR A TUNNEL AT +1.5 DEGREE WITH HORIZONTAL AND A BEND OF R/D=1.5

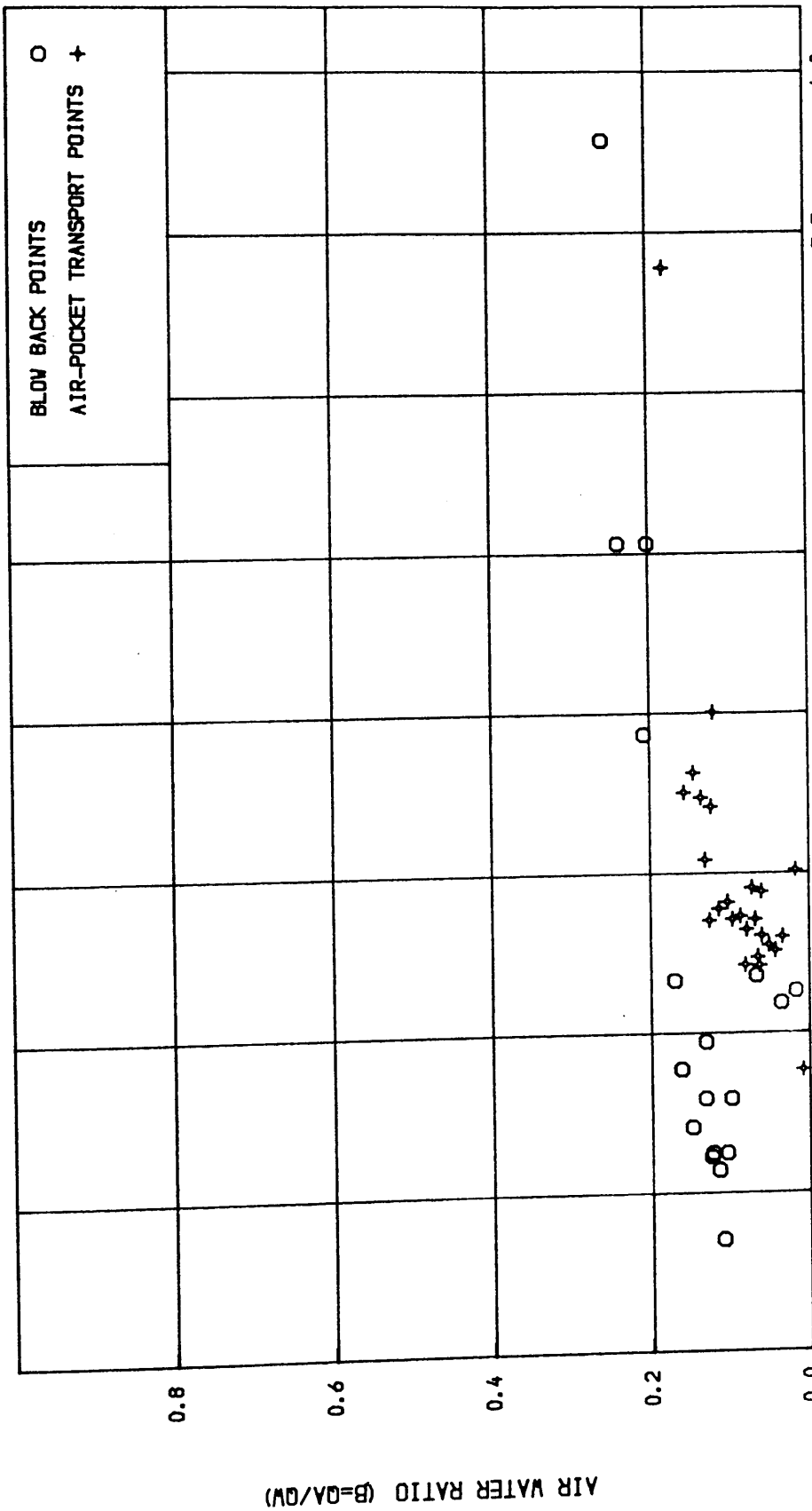

FIG. (5.37) RELATION BETWEEN THE FROUDE NUMBER BELOW THE AIR POCKET & AIR WATER RATIO AT POINTS OF BLOWING BACK AND CLEARING FOR A TUNNEL AT +1.5 DEGREE WITH HORIZONTAL AND A BEND OF R/D=1.5

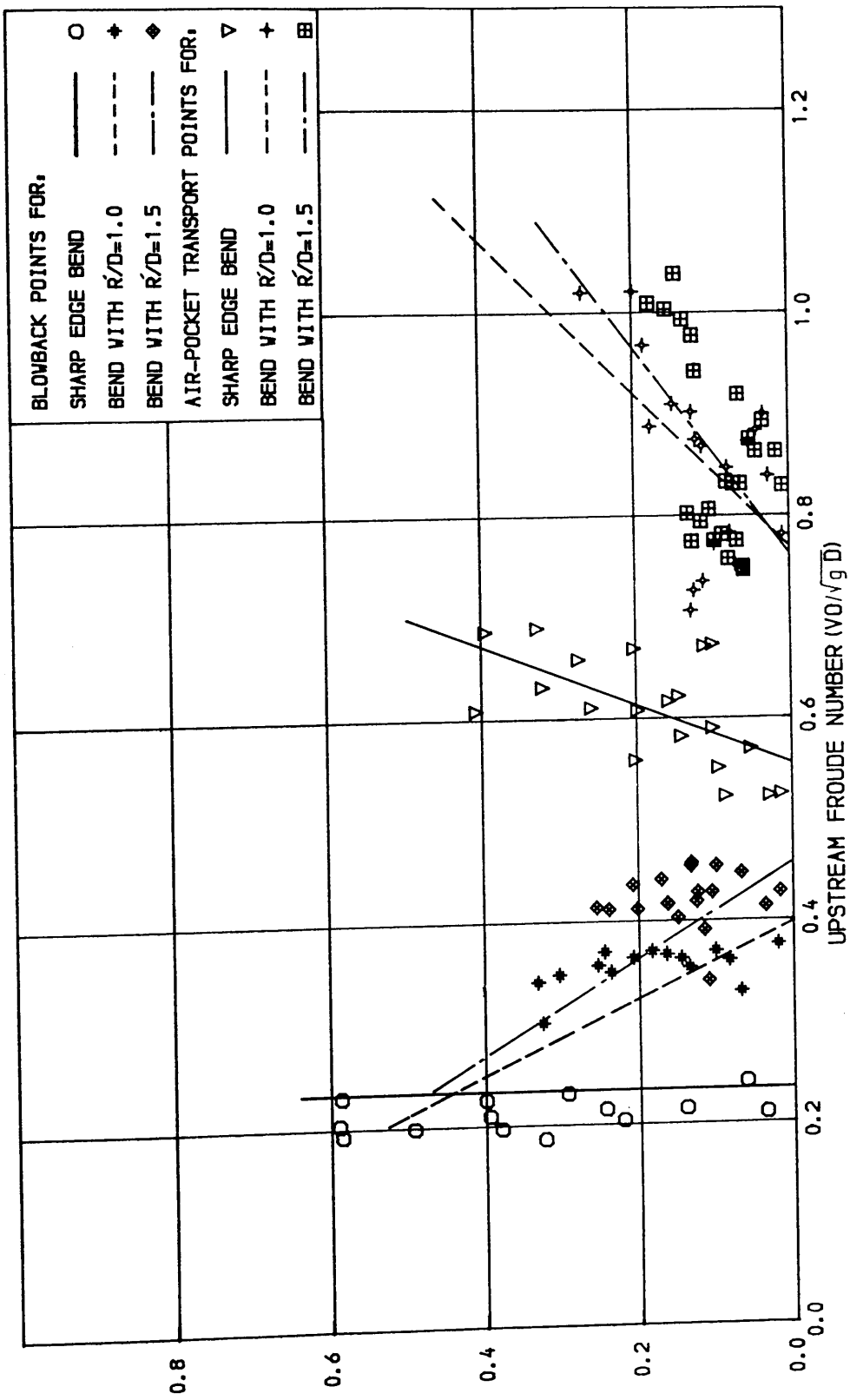

FIG. (5.38) RELATION BETWEEN UPSTREAM NON- DIMENSIONAL WATER VELOCITY & AIR-WATER RATIO AT POINTS OF BLOWING BACK AND CLEARING FOR A TUNNEL AT +1.5 DEGREE WITH HORIZONTAL & WITH THREE BENDS OF R/D=0.5, 1.0, & 1.5

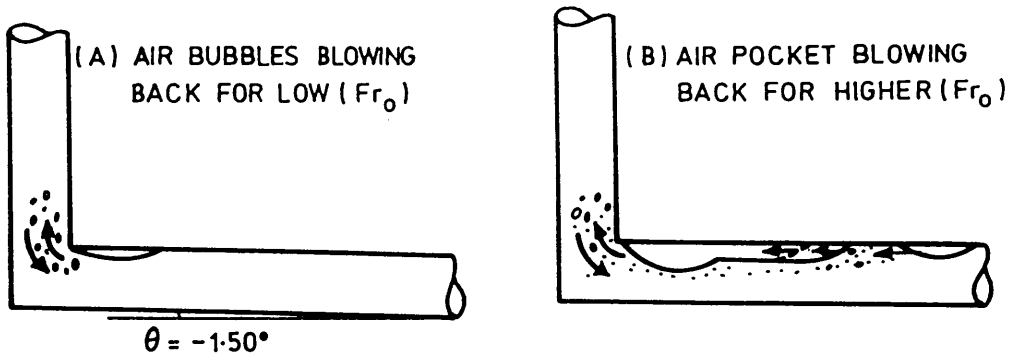

REGIME (1) AIR BUBBLES AND POCKETS BLOWING BACK

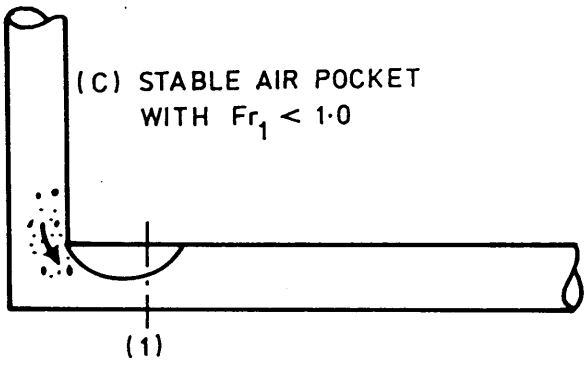

REGIME (2) STABLE AIR POCKET

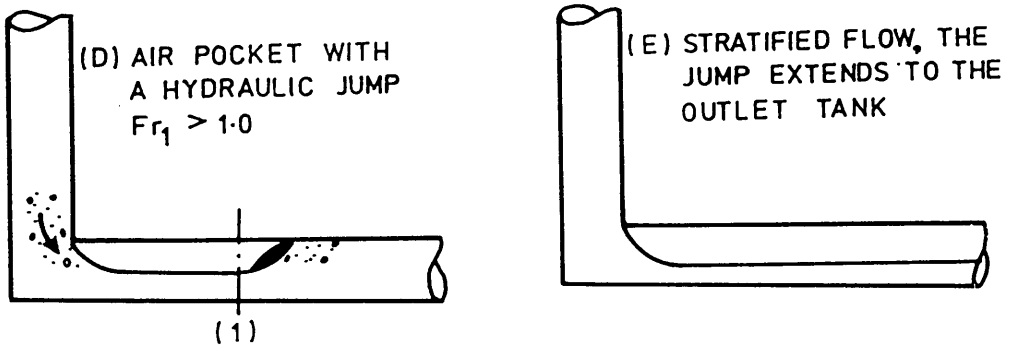

REGIME (3) AIR POCKET WITH A HYDRAULIC JUMP

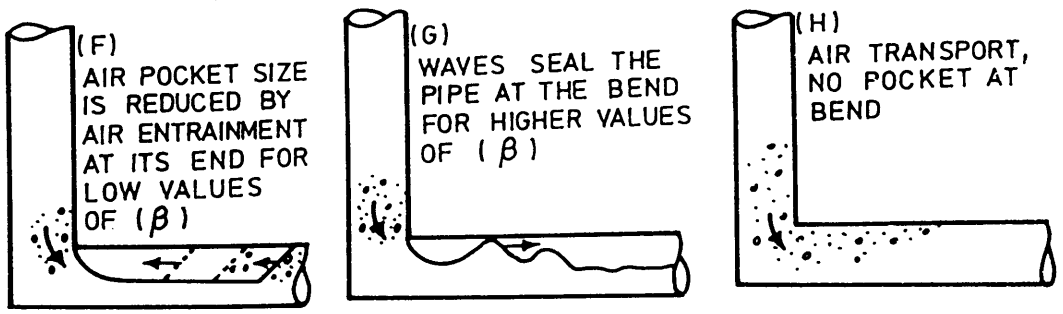

TRANSIT FROM REGIME (3) to (4)

REGIME (4) NO POCKET AT BEND

FIG. (5.39) FLOW REGIMES WITH INCREASING UPSTREAM FROUDE NUMBER (Fr_o) FOR A TUNNEL AT $-1.50°$ WITH HORIZONTAL AND A SHARP BEND OF $R'/D = 0.50$

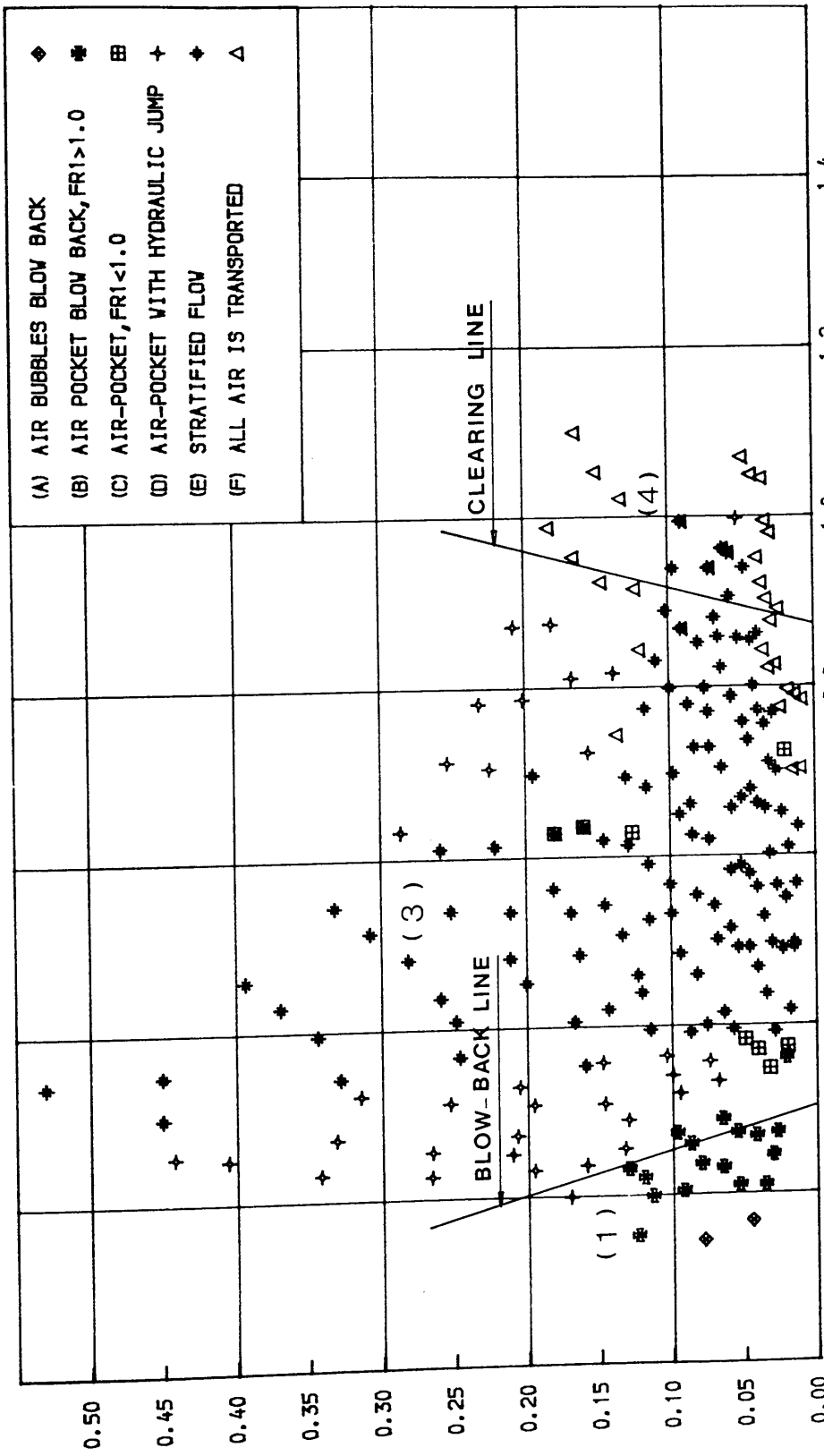

FIG. (5.40) RELATION BETWEEN UPSTREAM NON- DIMENSIONAL WATER VELOCITY & AIR WATER RATIO FOR A TUNNEL AT -1.5 DEGREE WITH HORIZONTAL & A BEND OF R′/D=0.5

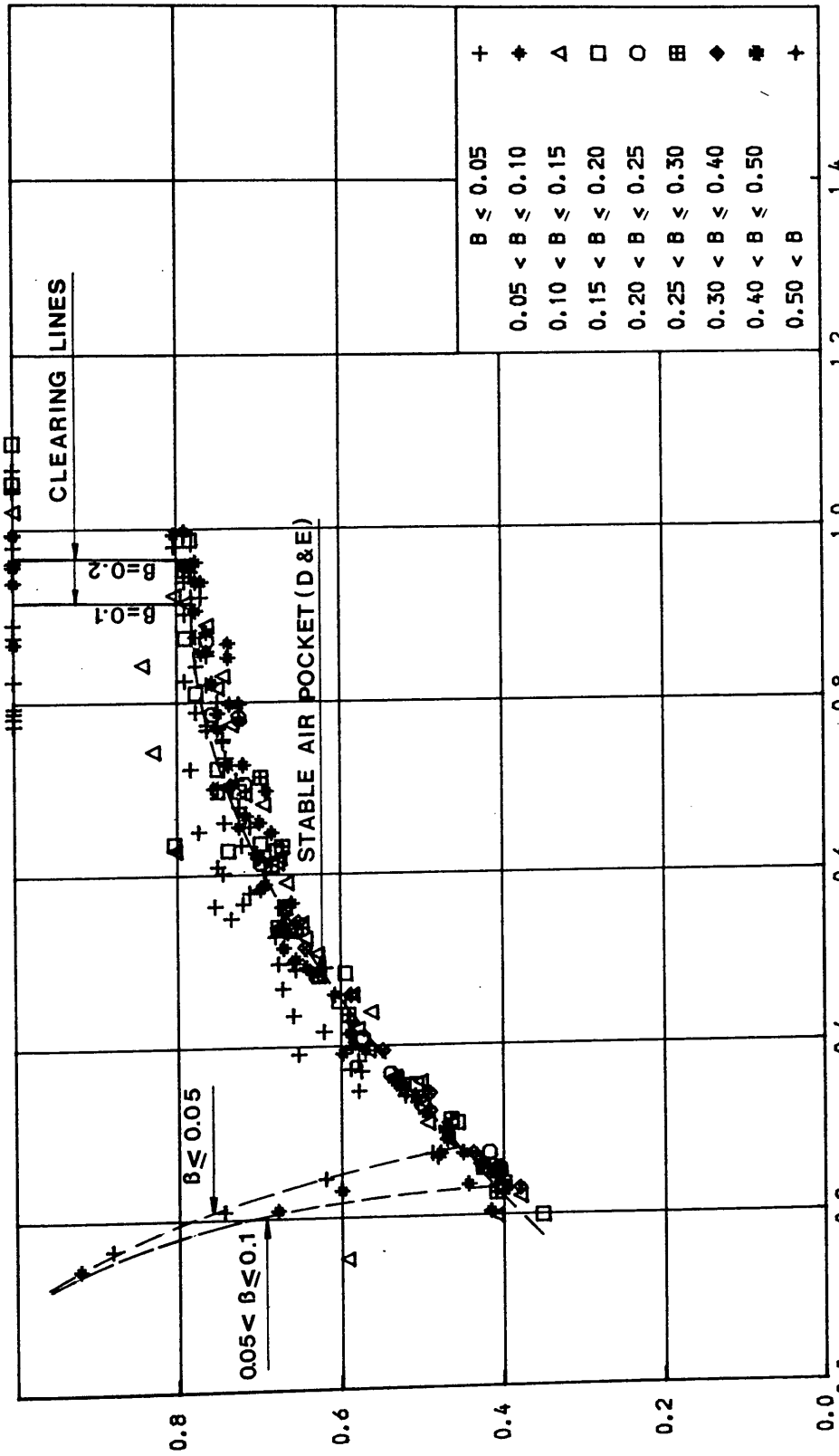

FIG. (5.41) RELATION BETWEEN UPSTREAM NON- DIMENSIONAL WATER VELOCITY & NON-DIMENSIONAL DEPTH OF FLOW BELOW THE POCKET FOR A TUNNEL AT -1.5 DEGREE WITH HORIZONTAL & A BEND OF R/D=0.5

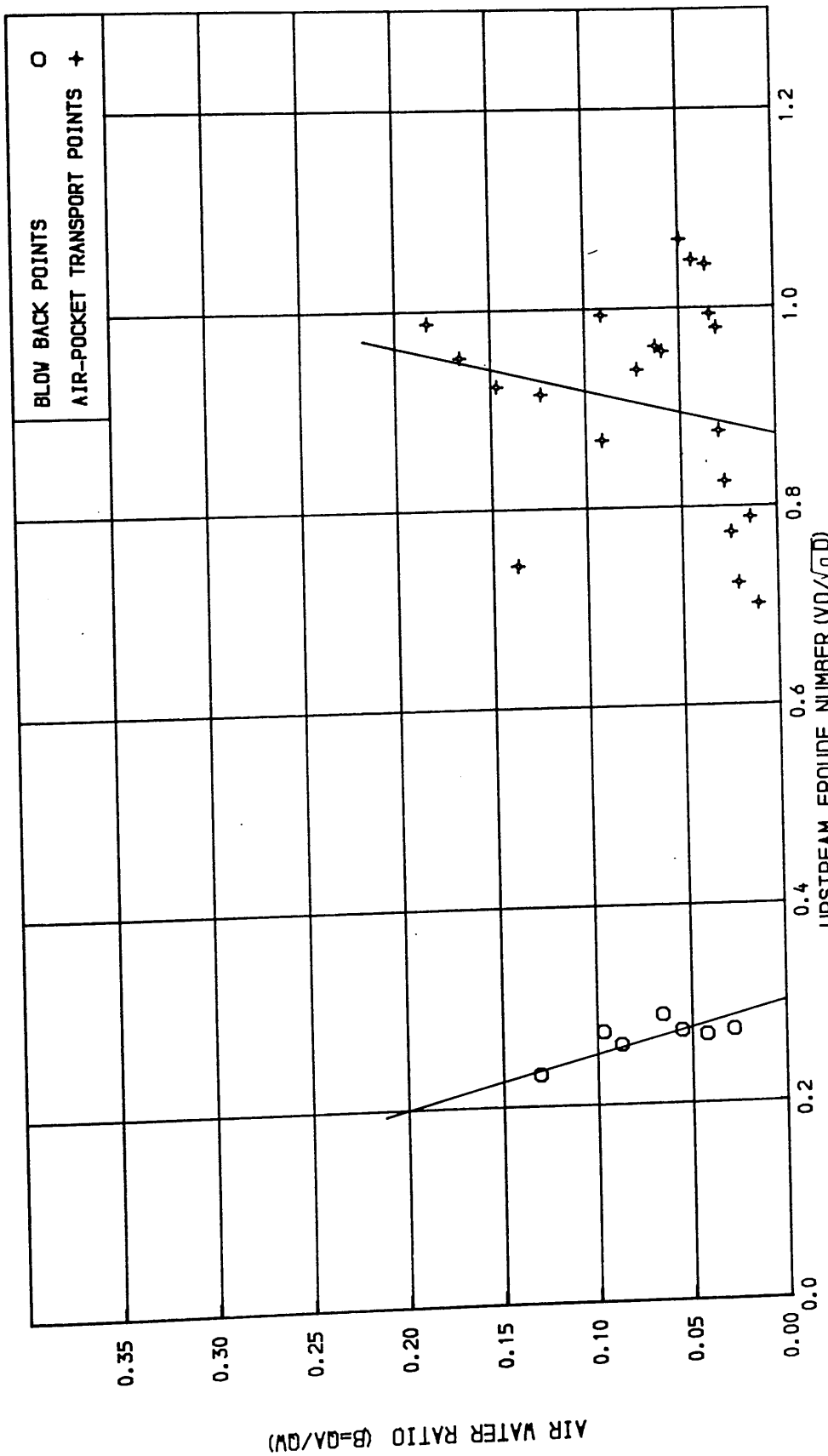

FIG. (5.42) RELATION BETWEEN UPSTREAM NON- DIMENSIONAL WATER VELOCITY & AIR WATER RATIO AT POINTS OF BLOWING BACK AND CLEARING FOR A TUNNEL AT -1.5 DEGREE WITH HORIZONTAL AND A BEND OF Ŕ/D=0.5

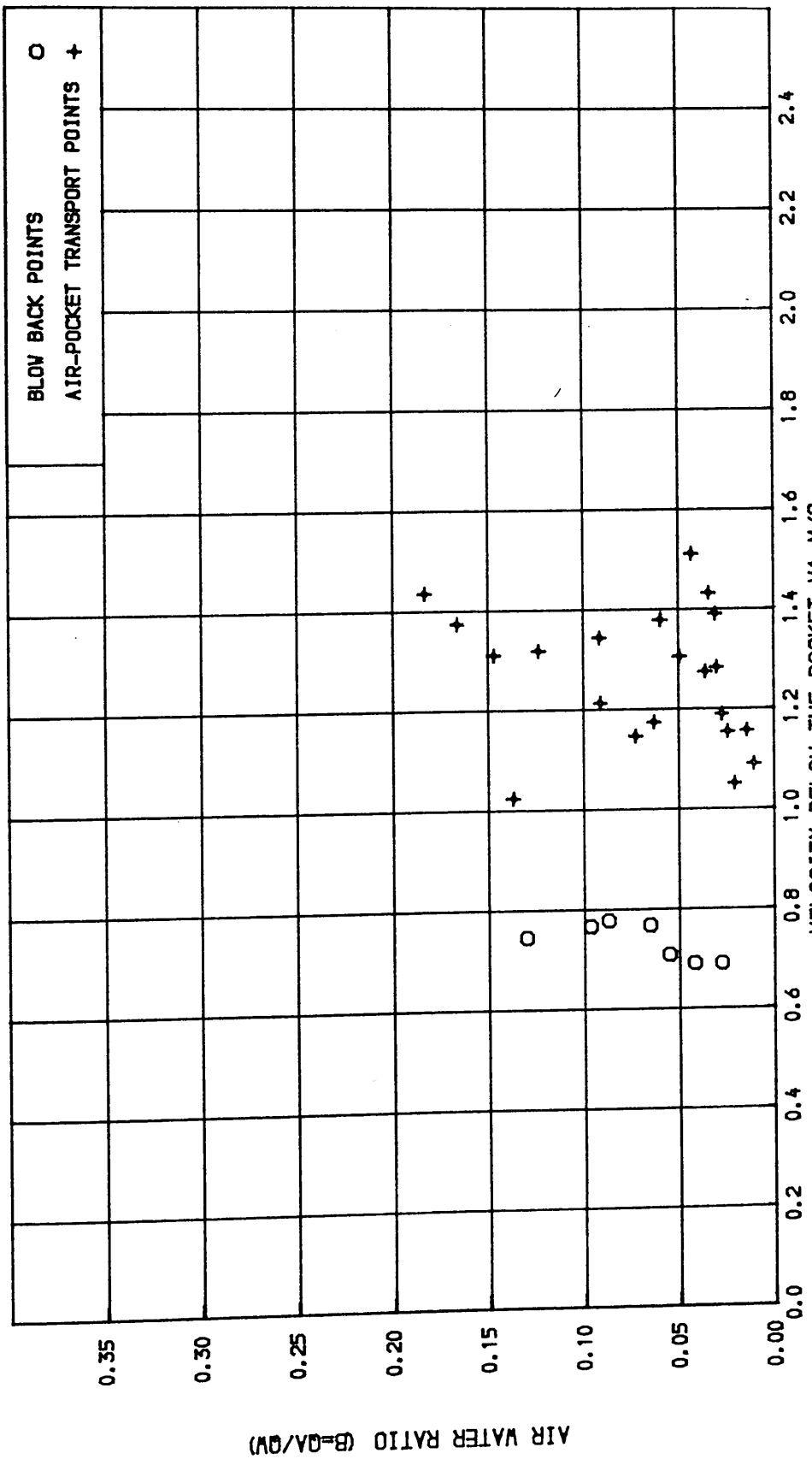

FIG. (5.43) RELATION BETWEEN THE WATER VELOCITY BELOW THE AIR-POCKET & AIR WATER RATIO AT POINTS OF BLOWING BACK AND CLEARING FOR A TUNNEL AT -1.5 DEGREE WITH HORIZONTAL AND A BEND OF R'/D=0.5

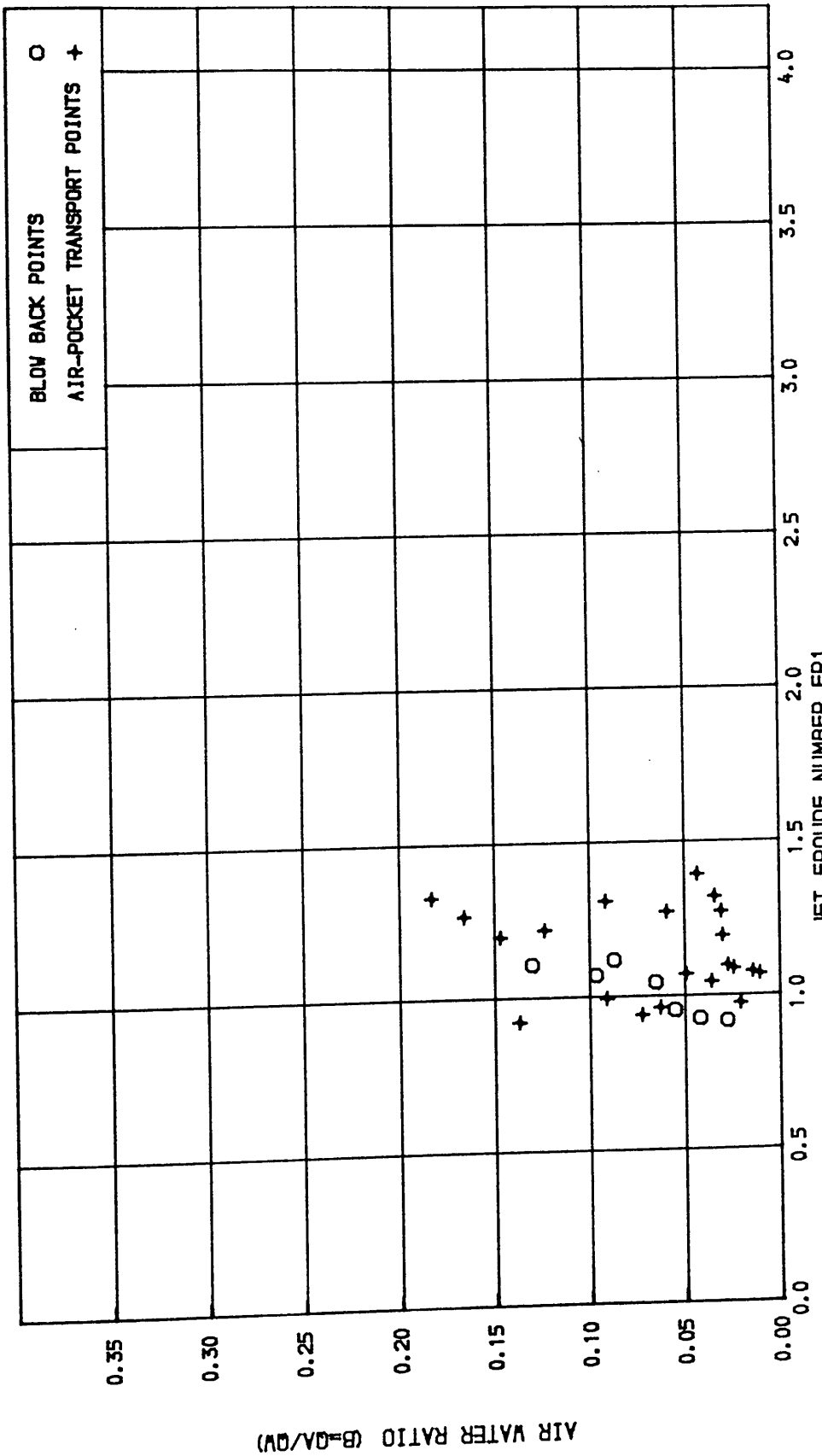

FIG. (5.44) RELATION BETWEEN THE FROUDE NUMBER BELOW THE AIR-POCKET & AIR WATER RATIO AT POINTS OF BLOWING BACK AND CLEARING FOR A TUNNEL AT -1.5 DEGREE WITH HORIZONTAL AND A BEND OF R/D=0.5

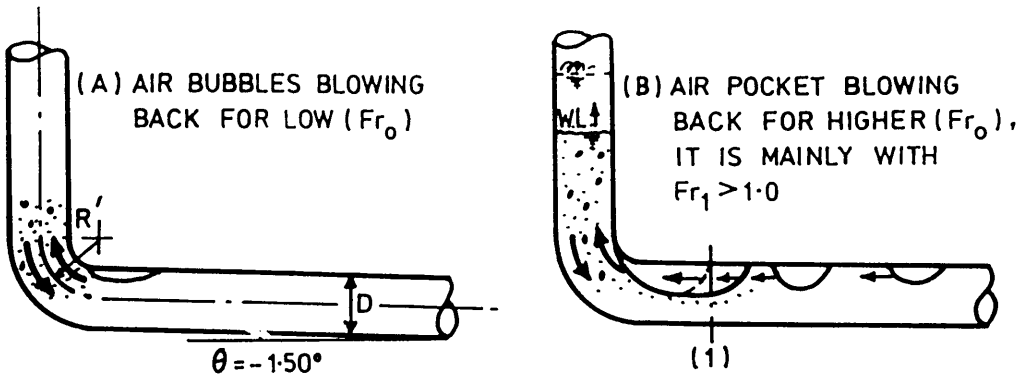

REGIME(1) AIR BUBBLES AND POCKETS BLOWING BACK

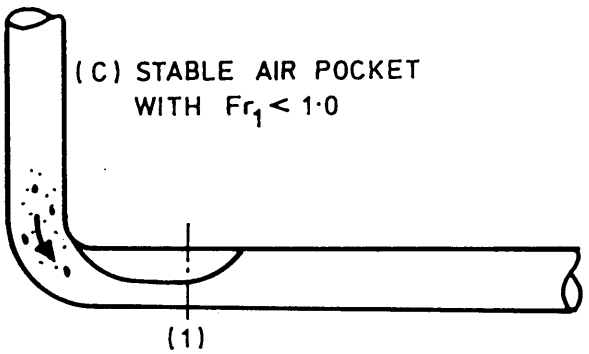

REGIME(2) STABLE AIR POCKET

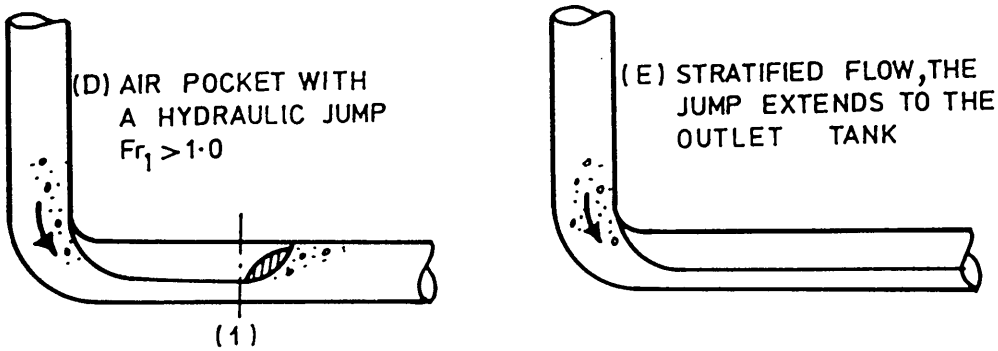

REGINE (3) AIR POCKET WITH A HYDRAULIC JUMP

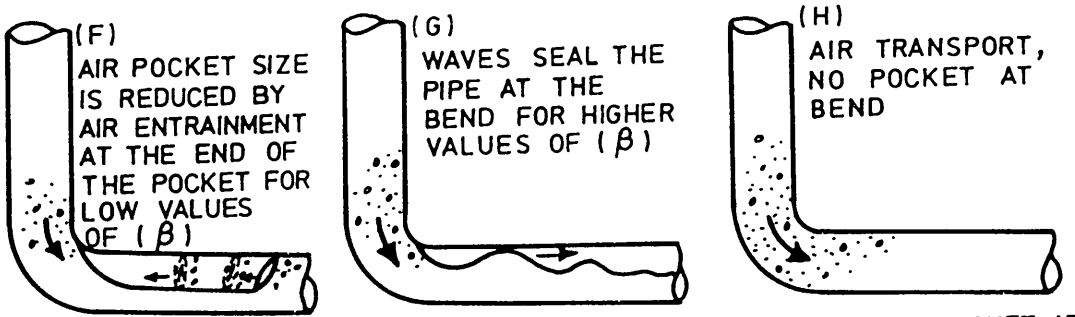

TRANSIT FROM REGIME (3) to (4)

REGIME (4) NO POCKET AT BEND

FIG. (5.45) FLOW REGIMES WITH INCREASING UPSTREAM FROUDE NUMBER (Fr_0) FOR A TUNNEL AT -1.50° WITH HORIZONTAL AND A BEND OF R'/D = 1.0

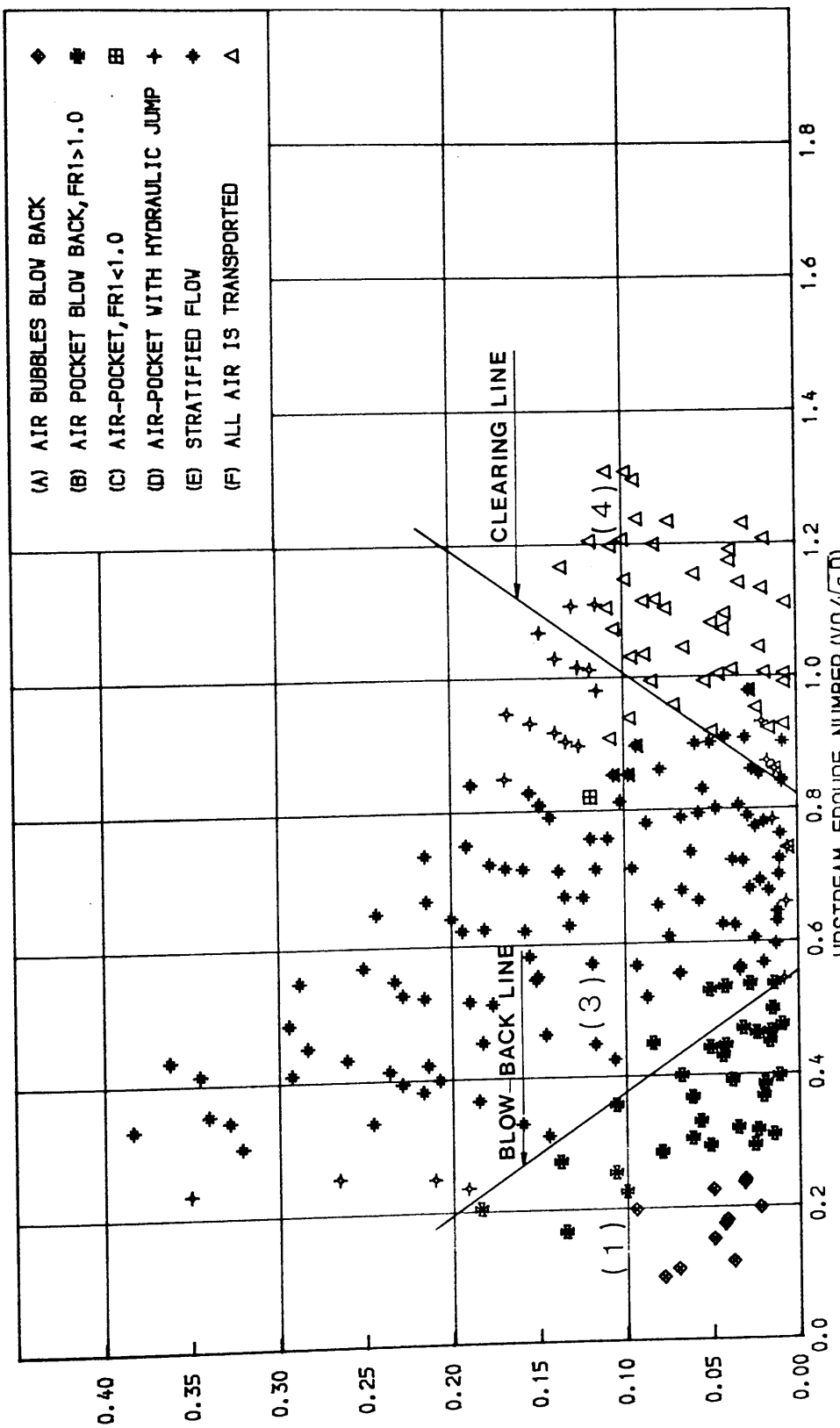

FIG. (5.46) RELATION BETWEEN UPSTREAM NON- DIMENSIONAL WATER VELOCITY & AIR-WATER RATIO FOR A TUNNEL AT -1.5 DEGREE WITH HORIZONTAL AND A BEND OF R/D=1.0

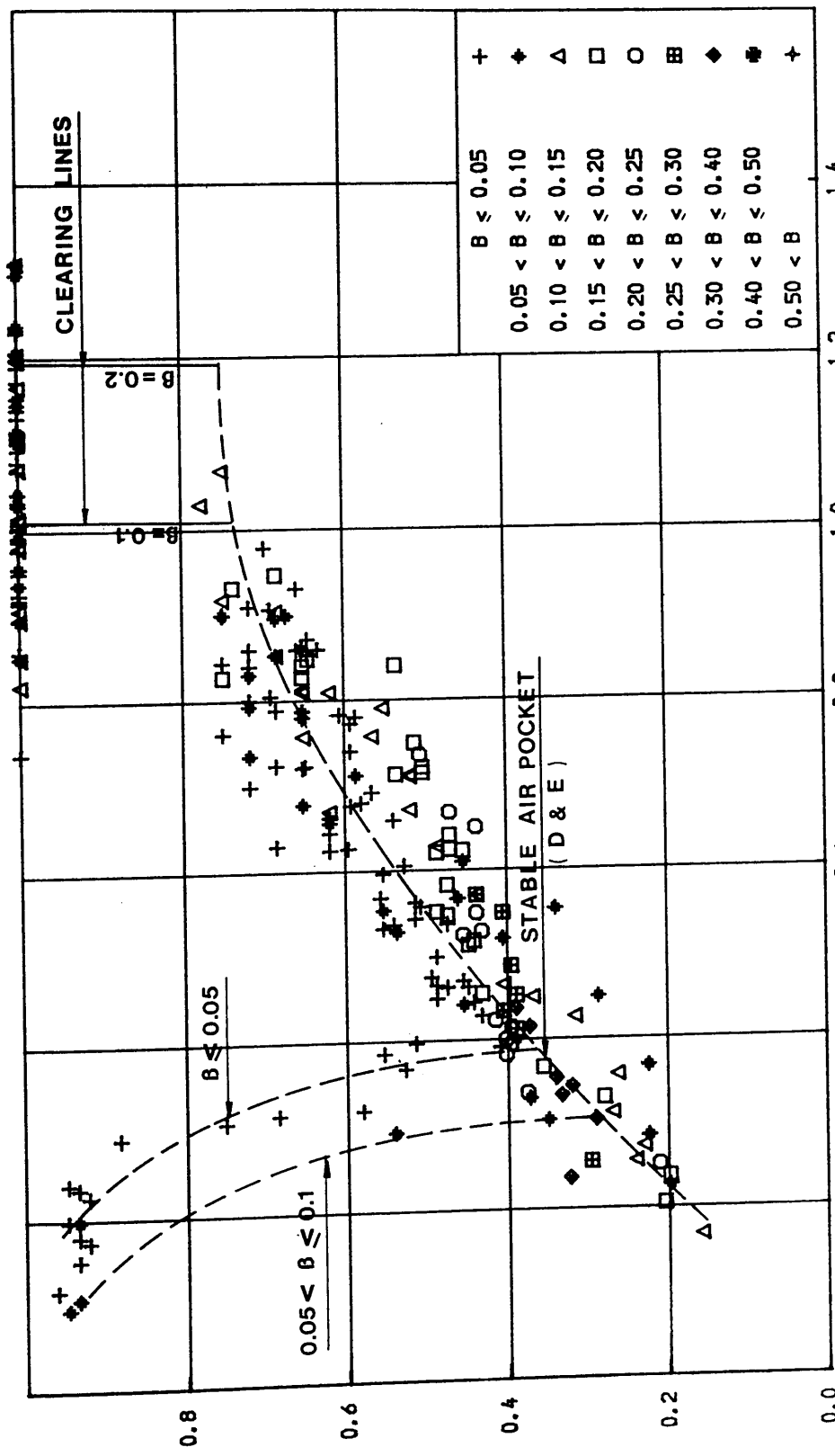

FIG. (5.47) RELATION BETWEEN UPSTREAM NON- DIMENSIONAL WATER VELOCITY & NON-DIMENSIONAL DEPTH OF FLOW BELOW THE POCKET FOR A TUNNEL AT -1.5 DEGREE WITH HORIZONTAL & A BEND OF R′/D=1.0

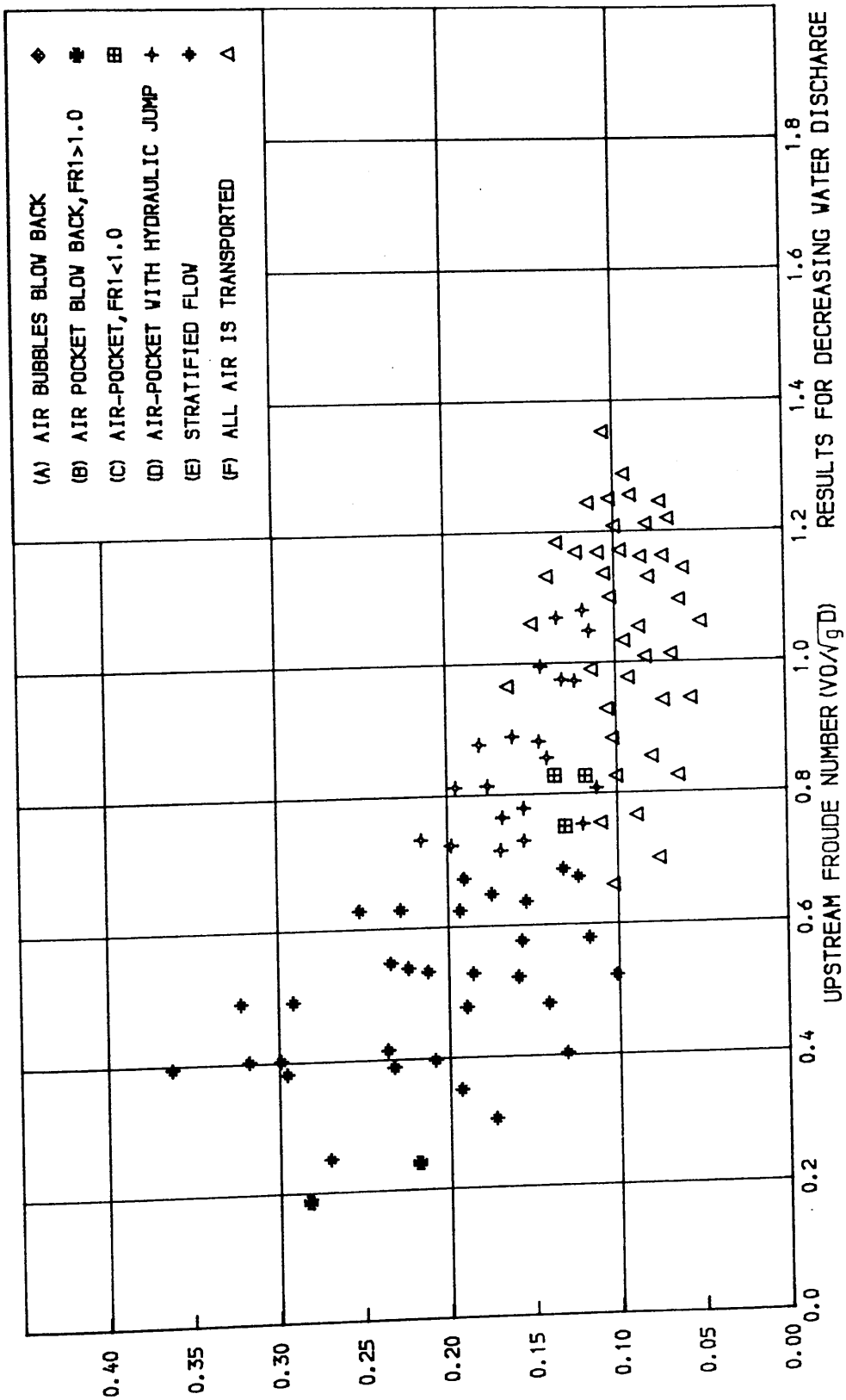

FIG. (5.48) RELATION BETWEEN UPSTREAM NON- DIMENSIONAL WATER VELOCITY & AIR-WATER RATIO FOR A TUNNEL AT -1.5 DEGREE WITH HORIZONTAL AND A BEND OF R/D=1.0

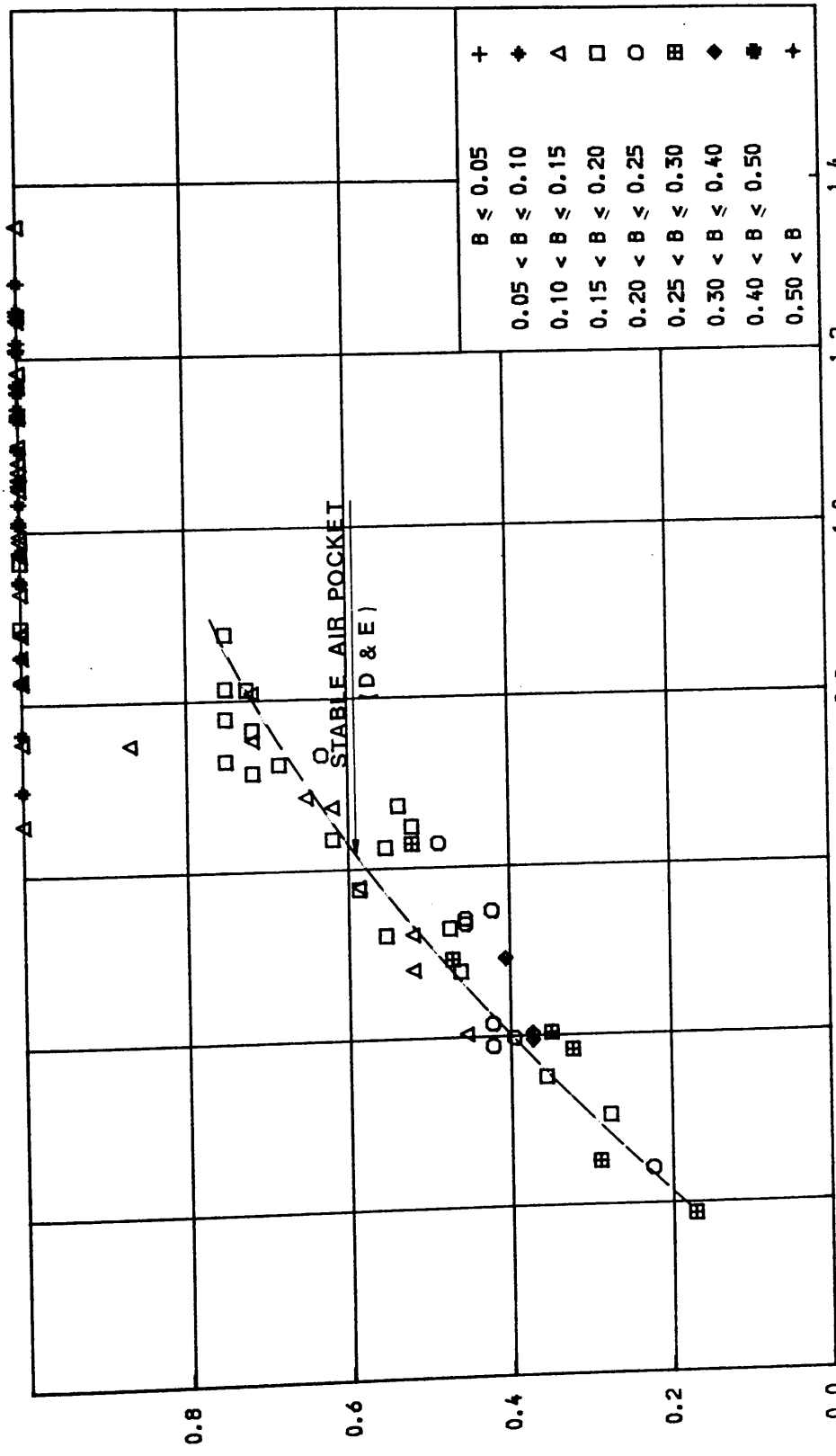

RESULTS FOR DECREASING WATER DISCHARGE

FIG. (5.49) RELATION BETWEEN UPSTREAM NON- DIMENSIONAL WATER VELOCITY & NON-DIMENSIONAL DEPTH OF FLOW BELOW THE POCKET FOR A TUNNEL AT -1.5 DEGREE WITH HORIZONTAL & A BEND OF R/D=1.0

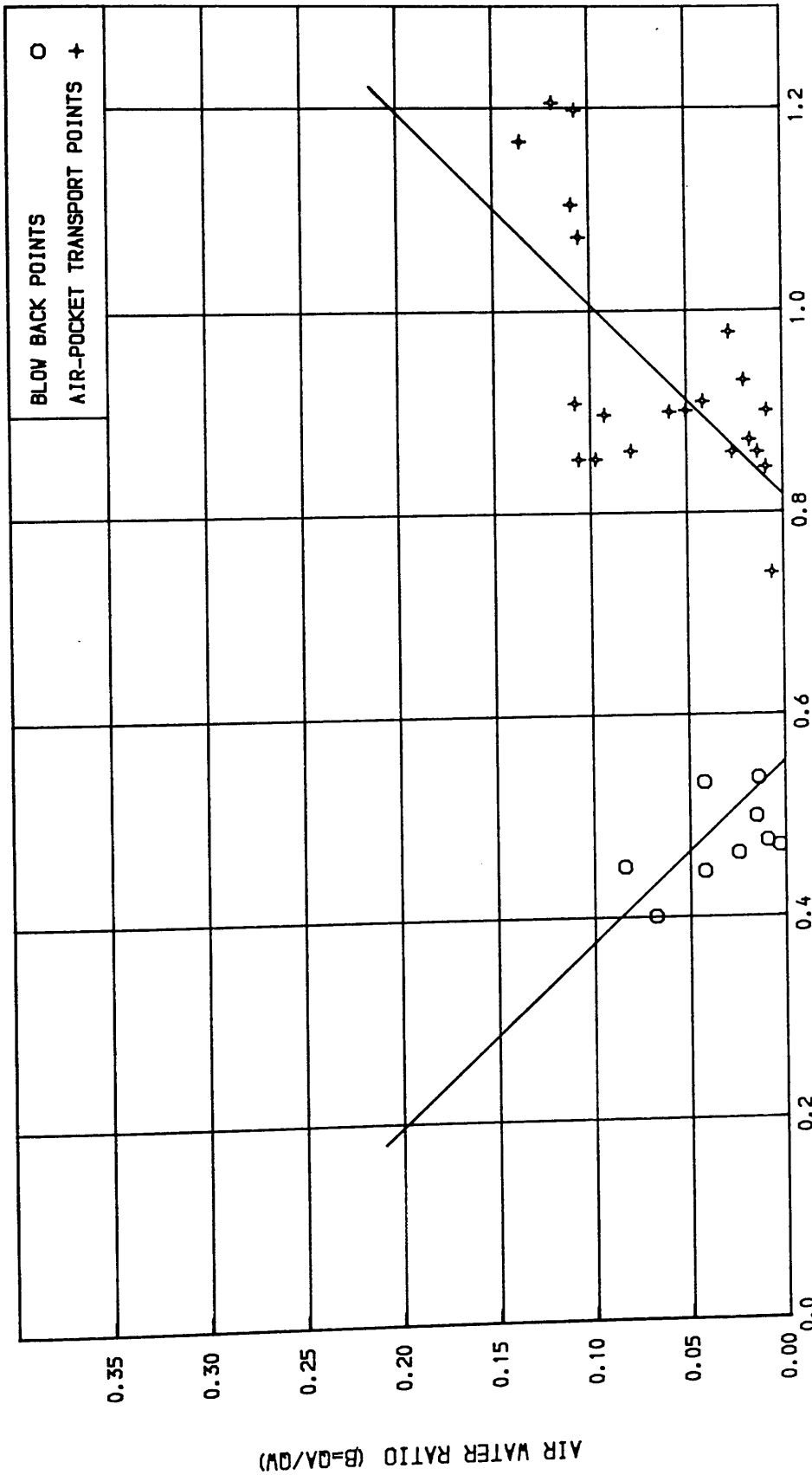

FIG. (5.50) RELATION BETWEEN UPSTREAM NON- DIMENSIONAL WATER VELOCITY & AIR WATER RATIO AT POINTS OF BLOWING BACK AND CLEARING FOR A TUNNEL AT -1.5 DEGREE WITH HORIZONTAL AND A BEND OF Ŕ/D=1.0

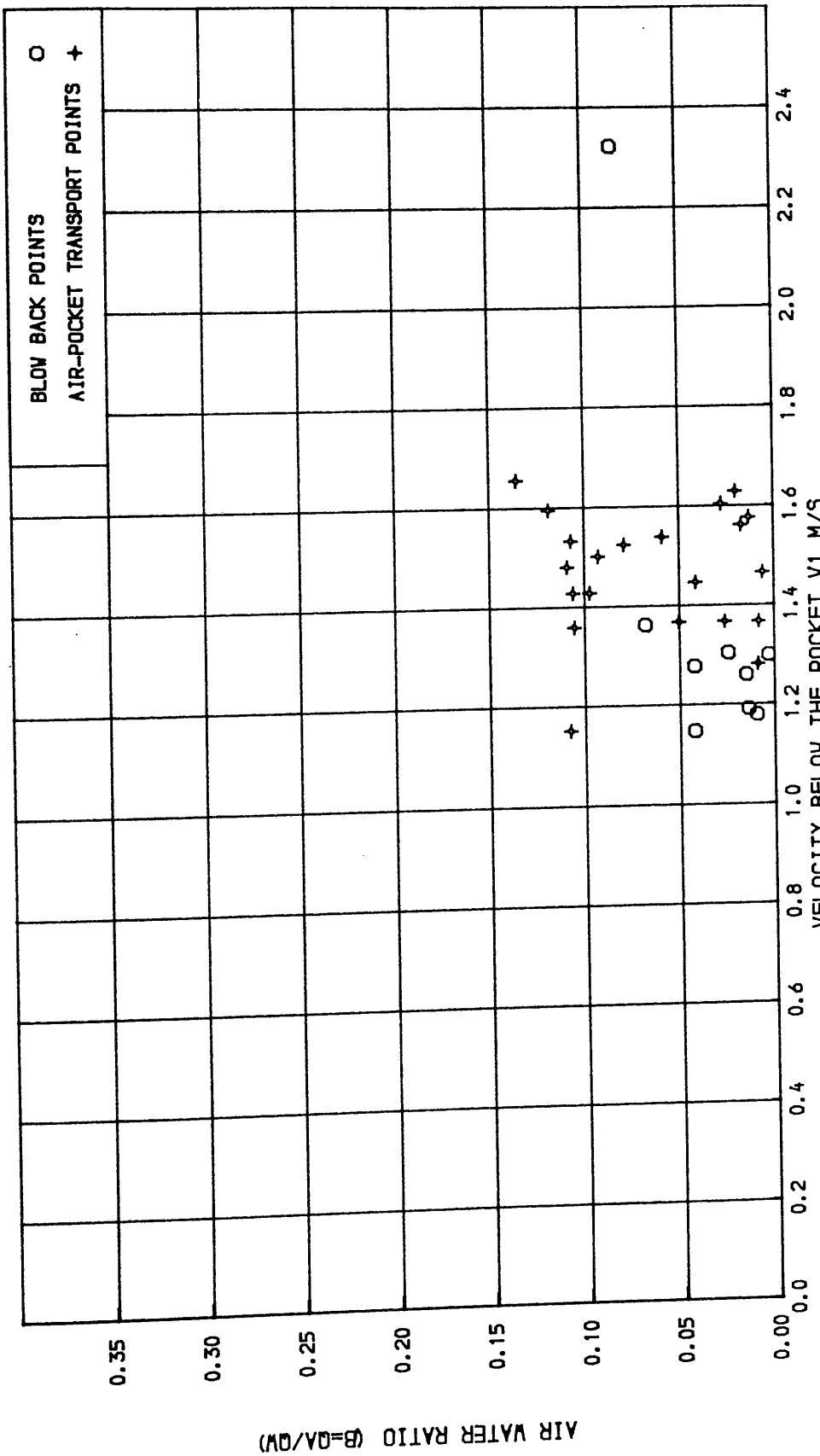

FIG. (5.51) RELATION BETWEEN THE WATER VELOCITY BELOW THE AIR-POCKET & AIR WATER RATIO AT POINTS OF BLOWING BACK AND CLEARING FOR A TUNNEL AT -1.5 DEGREE WITH HORIZONTAL AND A BEND OF R/D=1.0

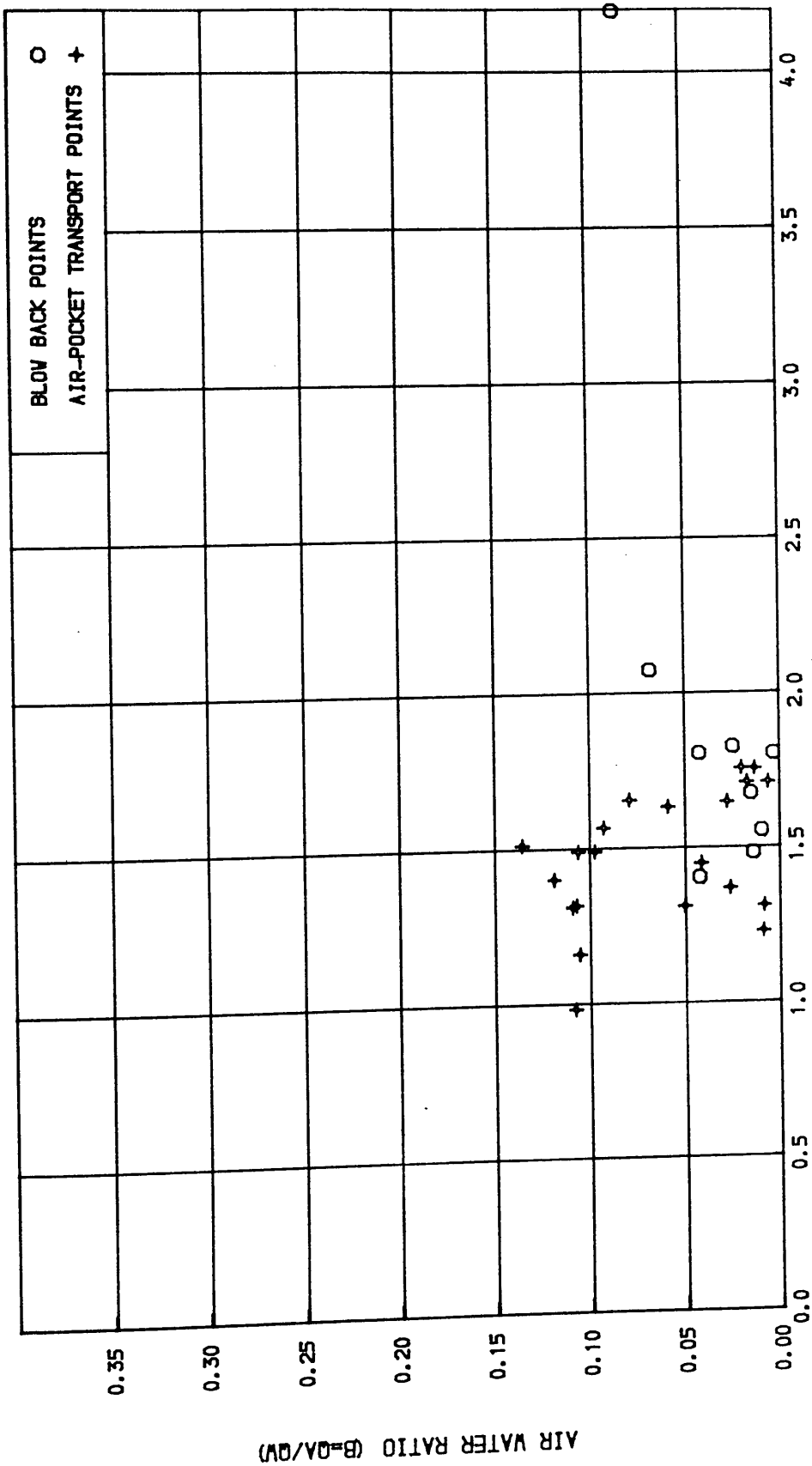

FIG. (5.52) RELATION BETWEEN THE FROUDE NUMBER BELOW THE AIR-POCKET & AIR WATER RATIO AT POINTS OF BLOWING BACK AND CLEARING FOR A TUNNEL AT -1.5 DEGREE WITH HORIZONTAL AND A BEND OF R/D=1.0

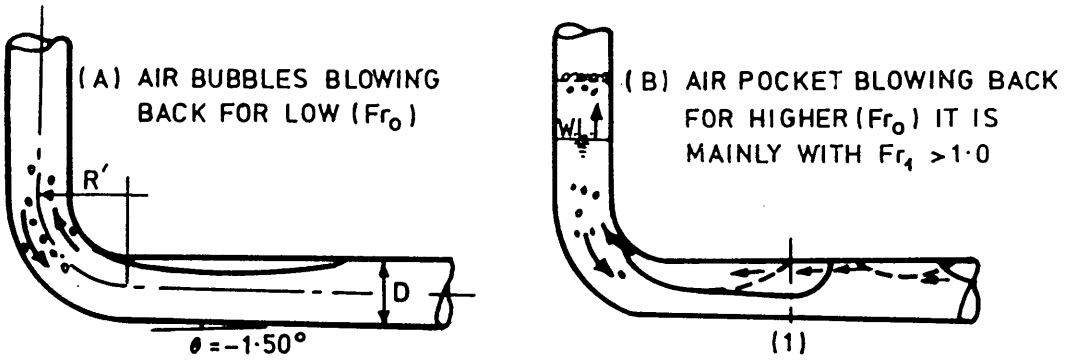

REGIME (1) AIR BUBBLES AND POCKETS BLOWING BACK

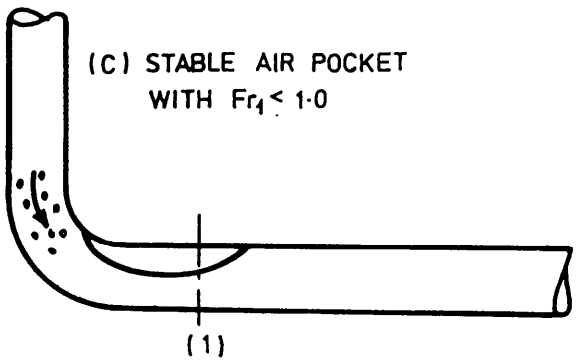

REGINE(2) STABLE AIR POCKET

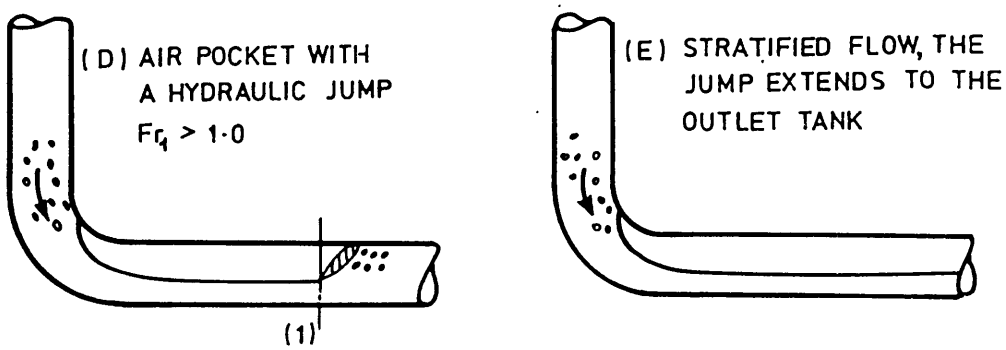

REGIME (3) AIR POCKET WITH A HYDRAULIC JUMP

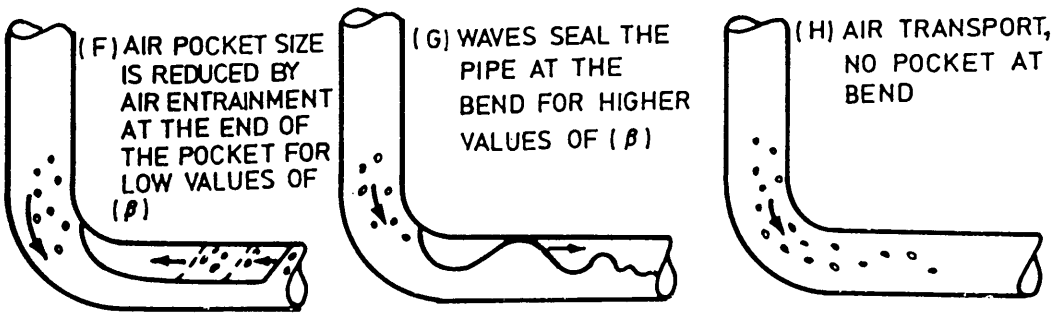

TRANSIT FROM REGIME (3) TO (4)

REGIME(4) NO POCKET AT BEND.

FIG. (5.53) FLOW REGIMES WITH INCREASING UPSTREAM FROUDE NUMBER (Fr_o) FOR A TUNNEL AT -1.50° WITH HORIZONTAL AND A BEND OF R'/D = 1.50

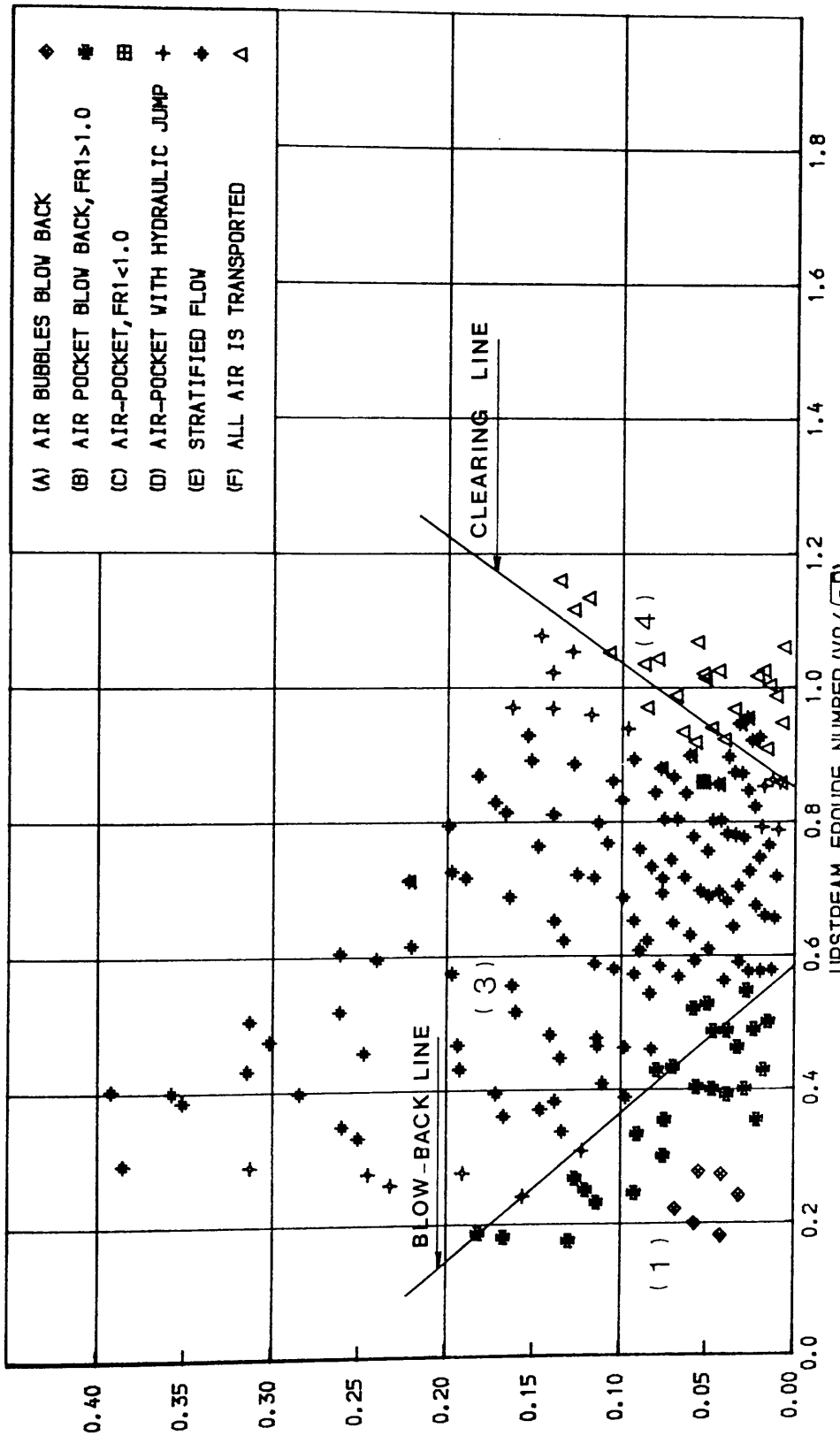

FIG. (5.54) RELATION BETWEEN UPSTREAM NON- DIMENSIONAL WATER VELOCITY & AIR-WATER RATIO FOR A TUNNEL AT -1.5 DEGREE WITH HORIZONTAL AND A BEND OF Ŕ/D=1.5

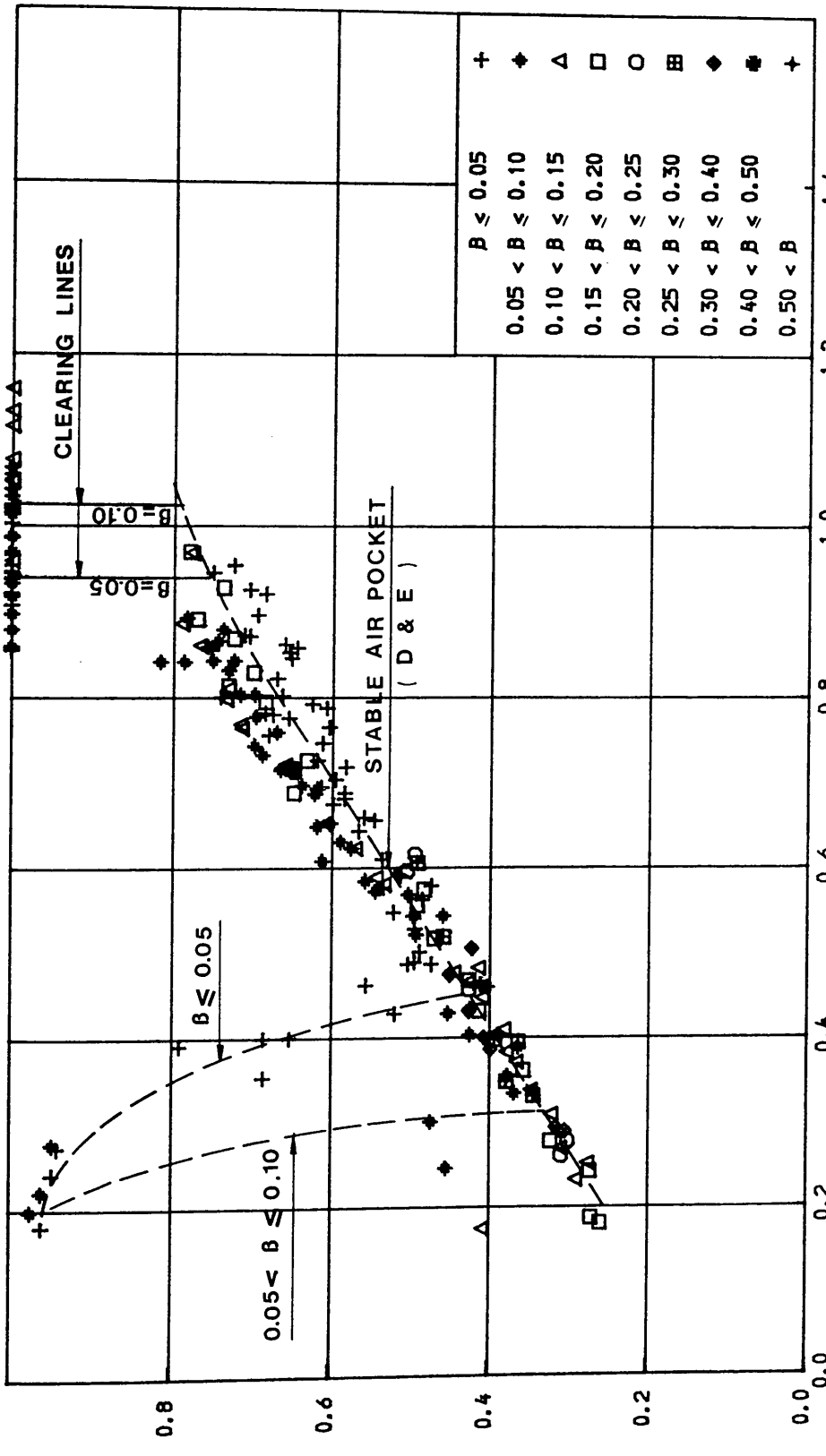

FIG. (5.55) RELATION BETWEEN UPSTREAM NON- DIMENSIONAL WATER VELOCITY & NON-DIMENSIONAL DEPTH OF FLOW BELOW THE POCKET FOR A TUNNEL AT -1.5 DEGREE WITH HORIZONTAL & A BEND OF R/D=1.5

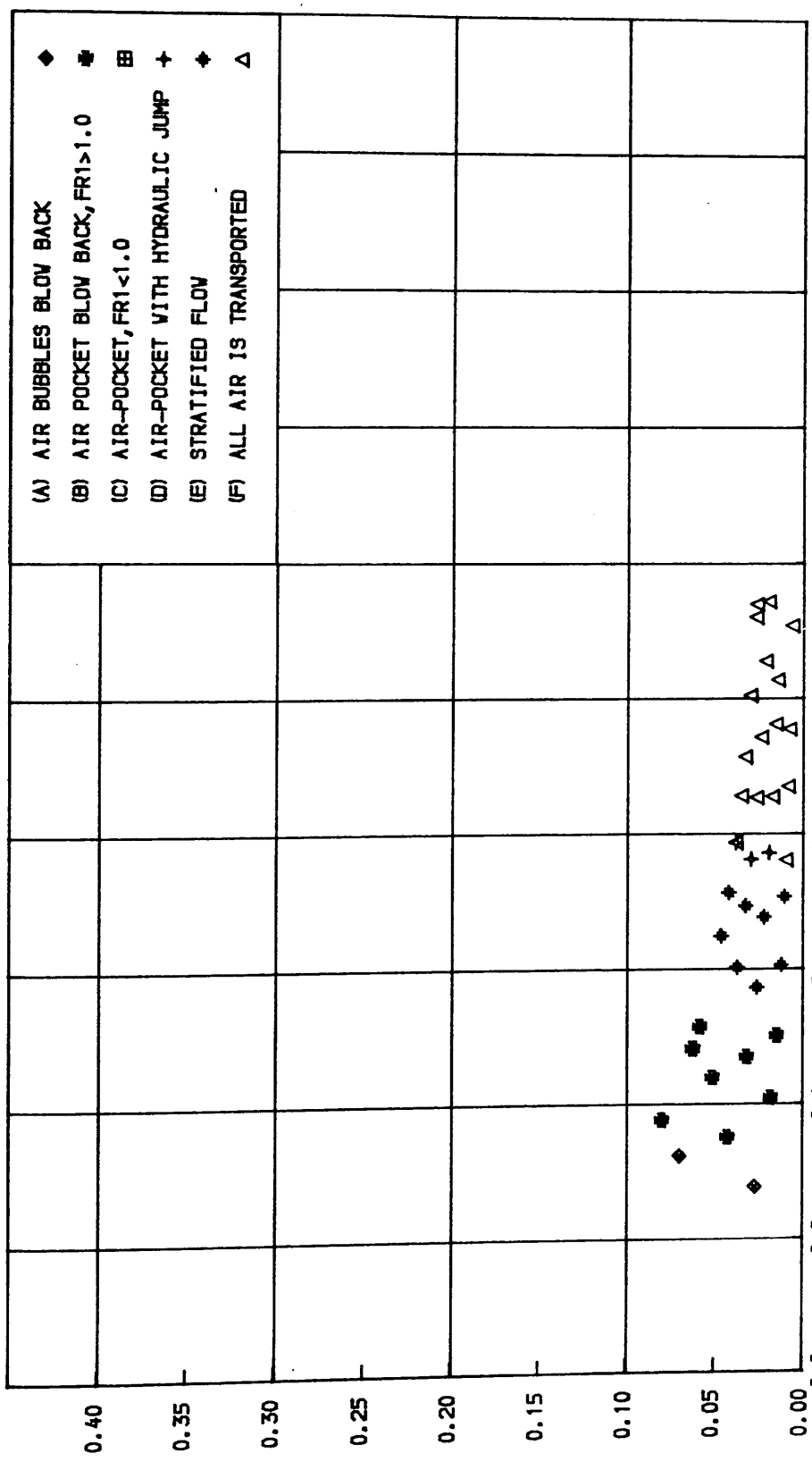

FIG. (5.56) RELATION BETWEEN UPSTREAM NON- DIMENSIONAL WATER VELOCITY & AIR-WATER RATIO FOR A TUNNEL AT -1.5 DEGREE WITH HORIZONTAL AND A BEND OF R/D=1.5

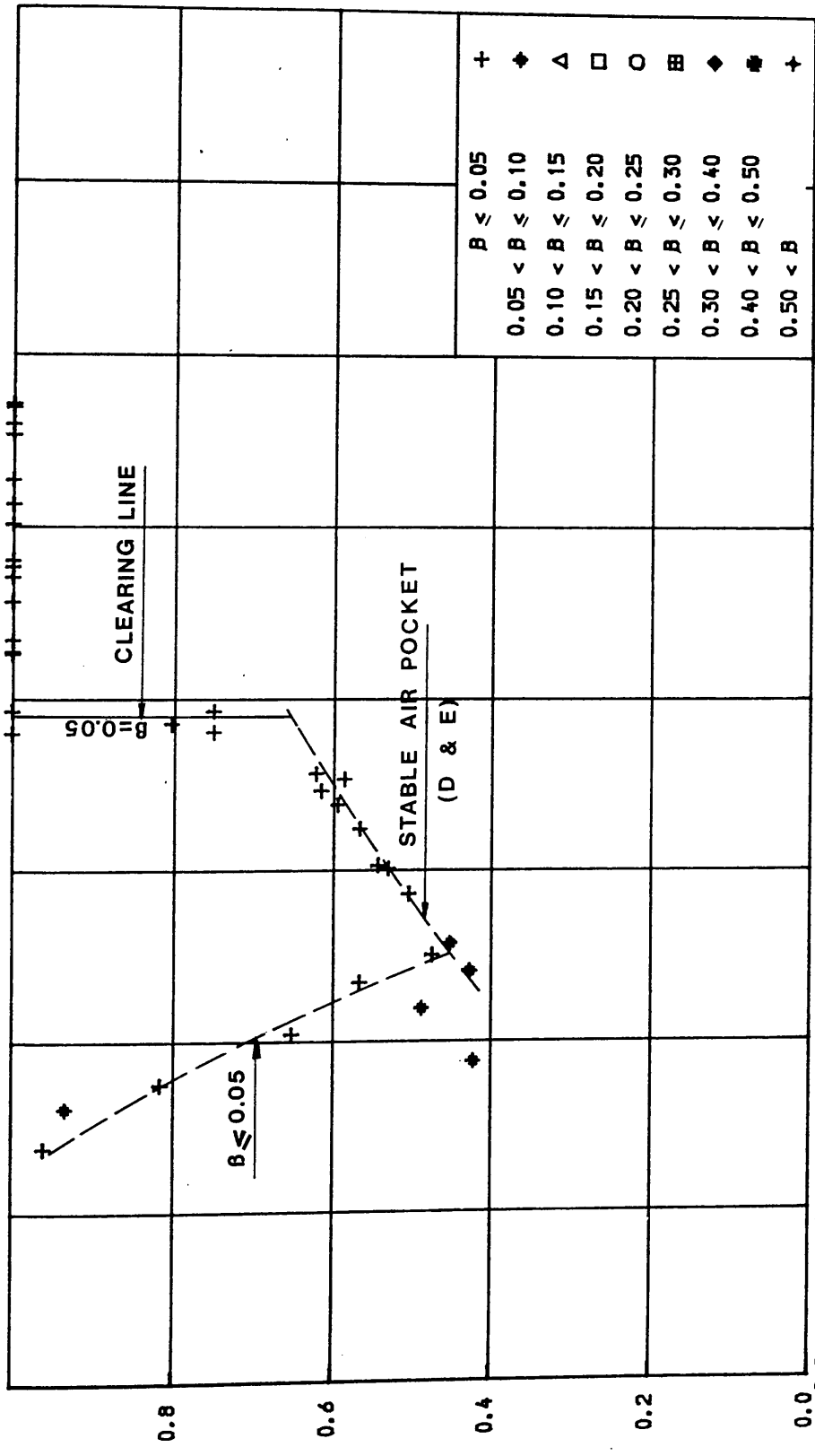

FIG. (5.57) RELATION BETWEEN UPSTREAM NON- DIMENSIONAL WATER VELOCITY & NON-DIMENSIONAL DEPTH OF FLOW BELOW THE POCKET FOR A TUNNEL AT -1.5 DEGREE WITH HORIZONTAL & A BEND OF R/D=1.5 RESULTS FOR DECREASING WATER DISCHARGE

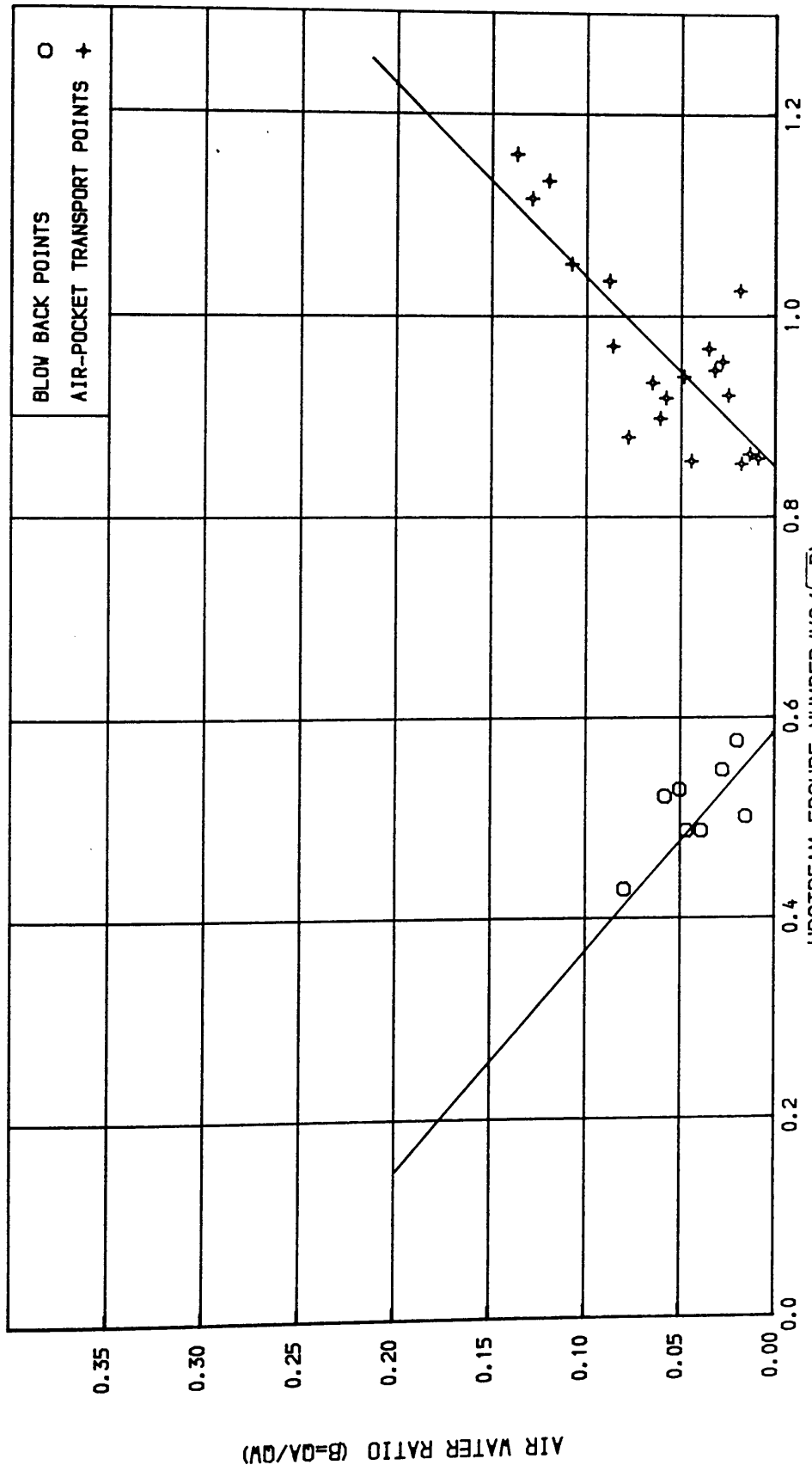

FIG. (5.58) RELATION BETWEEN UPSTREAM NON- DIMENSIONAL WATER VELOCITY & AIR WATER RATIO AT POINTS OF BLOWING BACK AND CLEARING FOR A TUNNEL AT -1.5 DEGREE WITH HORIZONTAL AND A BEND OF Ŕ/D=1.5

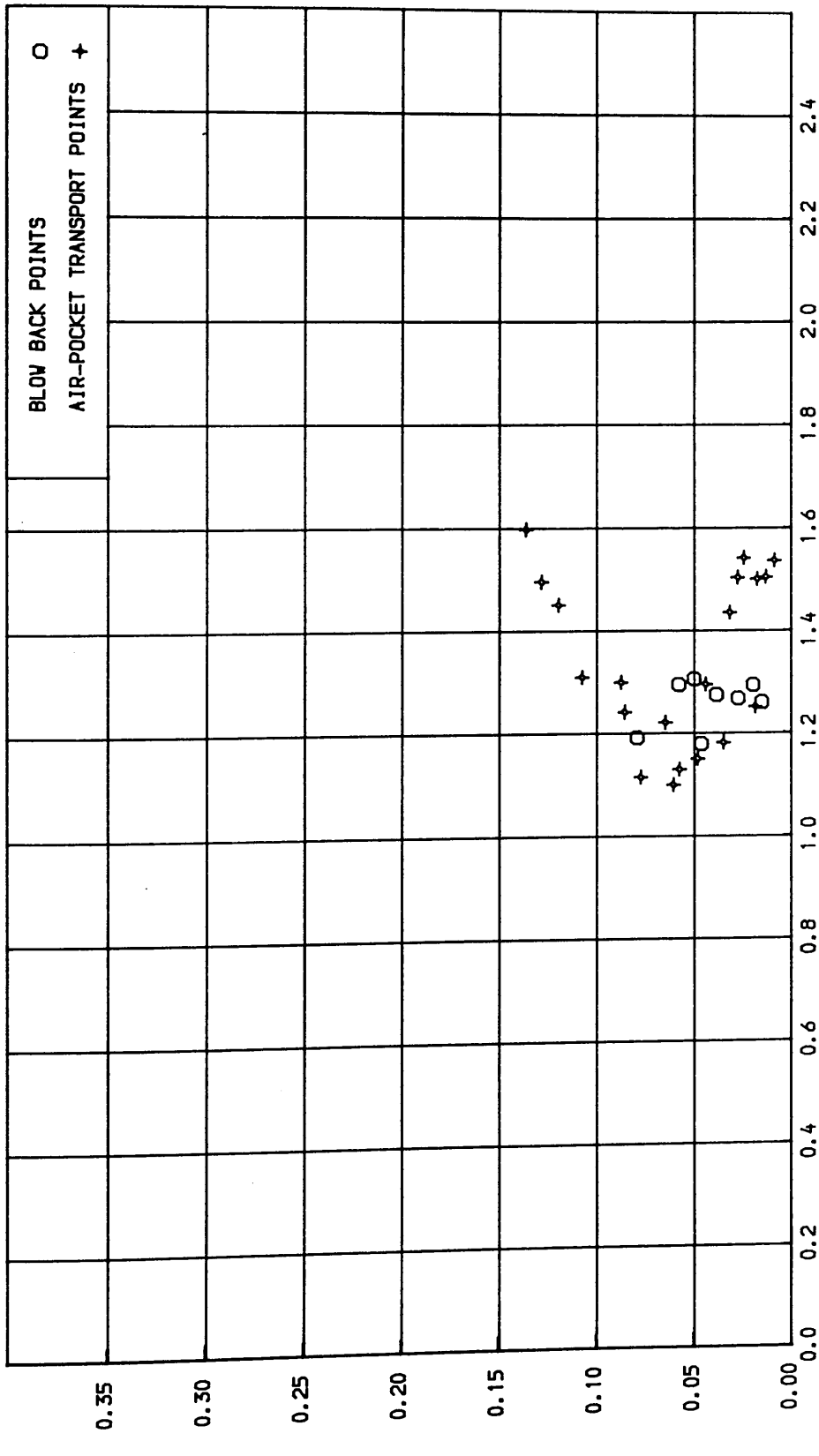

FIG. (5.59) RELATION BETWEEN THE WATER VELOCITY BELOW THE AIR-POCKET & AIR WATER RATIO AT POINTS OF BLOWING BACK AND CLEARING FOR A TUNNEL AT -1.5 DEGREE WITH HORIZONTAL AND A BEND OF R′/D=1.5

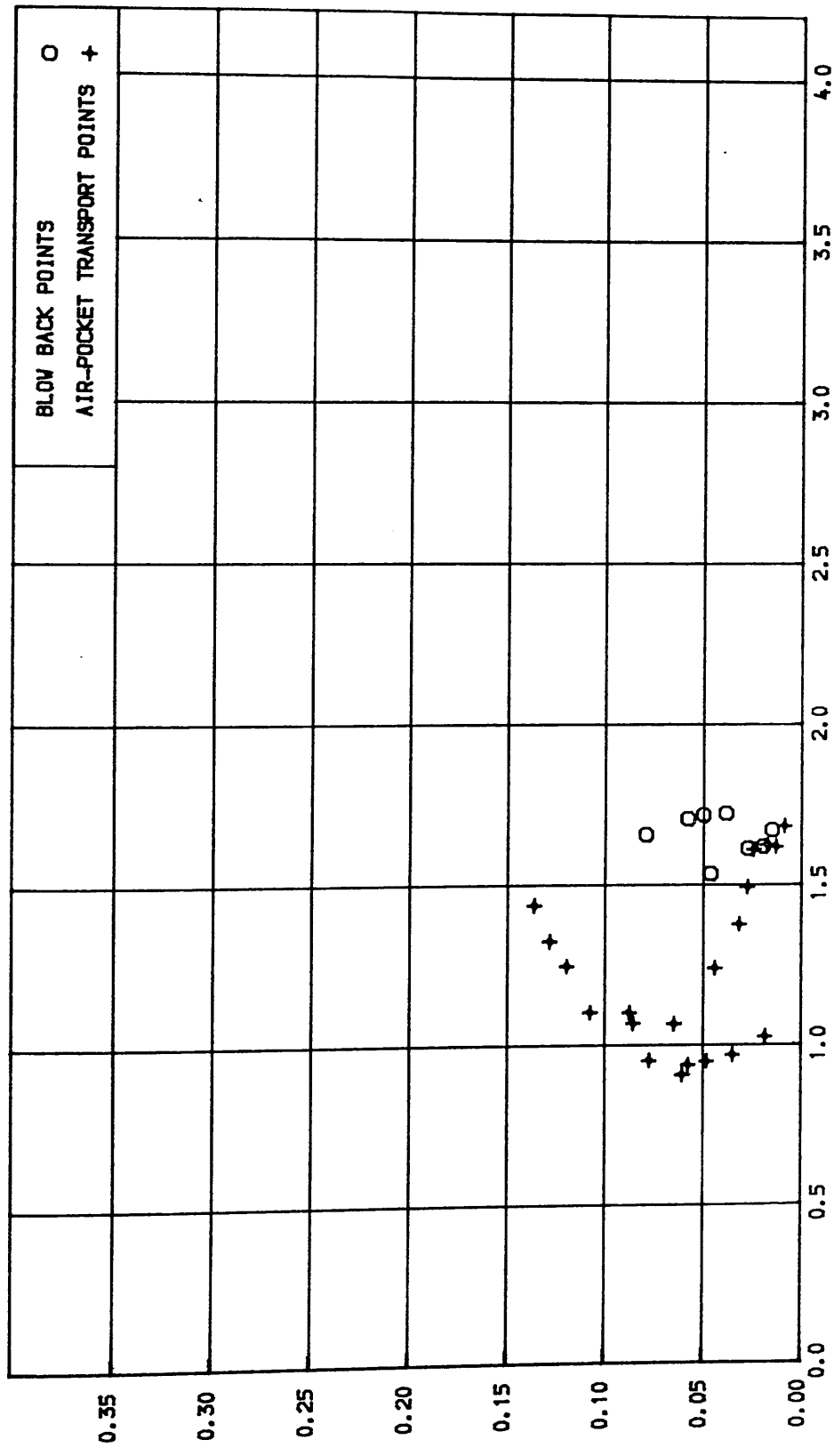

FIG. (5.60) RELATION BETWEEN THE FROUDE NUMBER BELOW THE AIR-POCKET & AIR WATER RATIO AT POINTS OF BLOWING BACK AND CLEARING FOR A TUNNEL AT -1.5 DEGREE WITH HORIZONTAL AND A BEND OF R/D=1.5

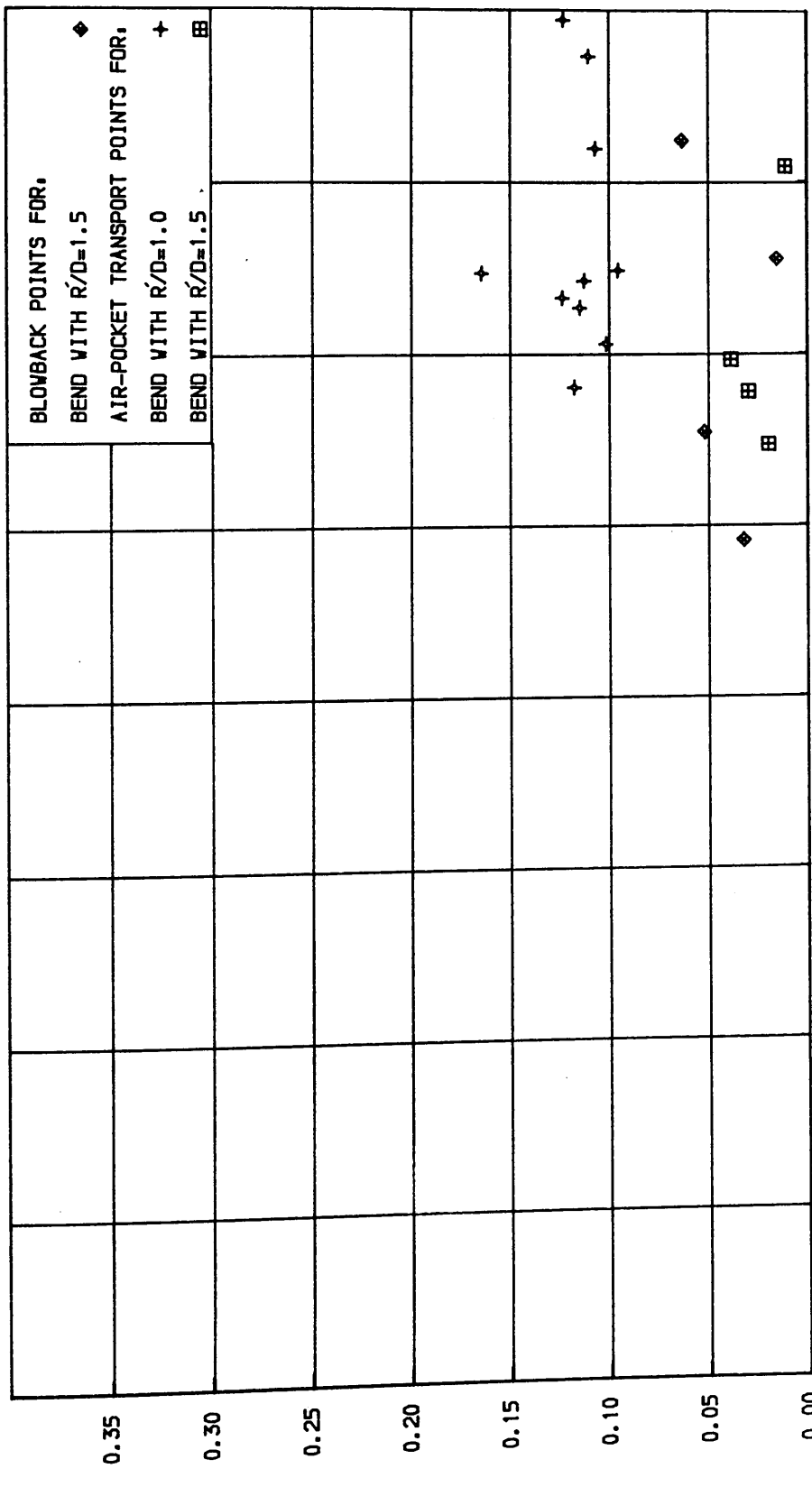

RESULTES FOR DECREASING WATER DISCHARGE

FIG. (5.61) RELATION BETWEEN THE WATER VELOCITY BELOW THE AIR-POCKET & AIR WATER RATIO AT POINTS OF BLOWING BACK AND CLEARING FOR A TUNNEL AT -1.5 DEGREE WITH HORIZONTAL AND TWO BENDS OF R/D=1.0 & 1.5

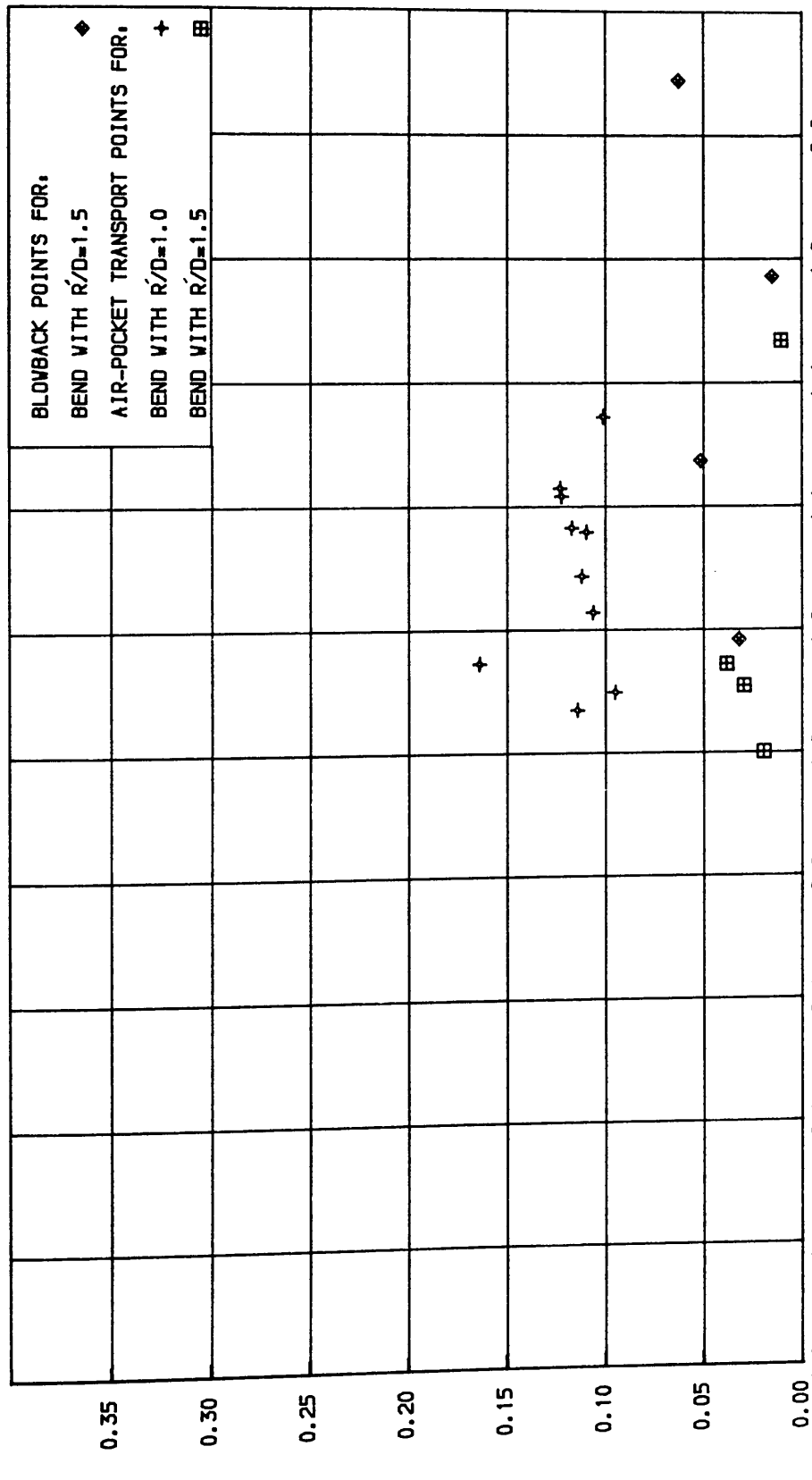

FIG. (5.62) RELATION BETWEEN THE FROUDE NUMBER BELOW THE AIR-POCKET & AIR WATER RATIO AT POINTS OF BLOWING BACK AND CLEARING FOR A TUNNEL AT -1.5 DEGREE WITH HORIZONTAL AND TWO BENDS OF R/D=1.0 & 1.5

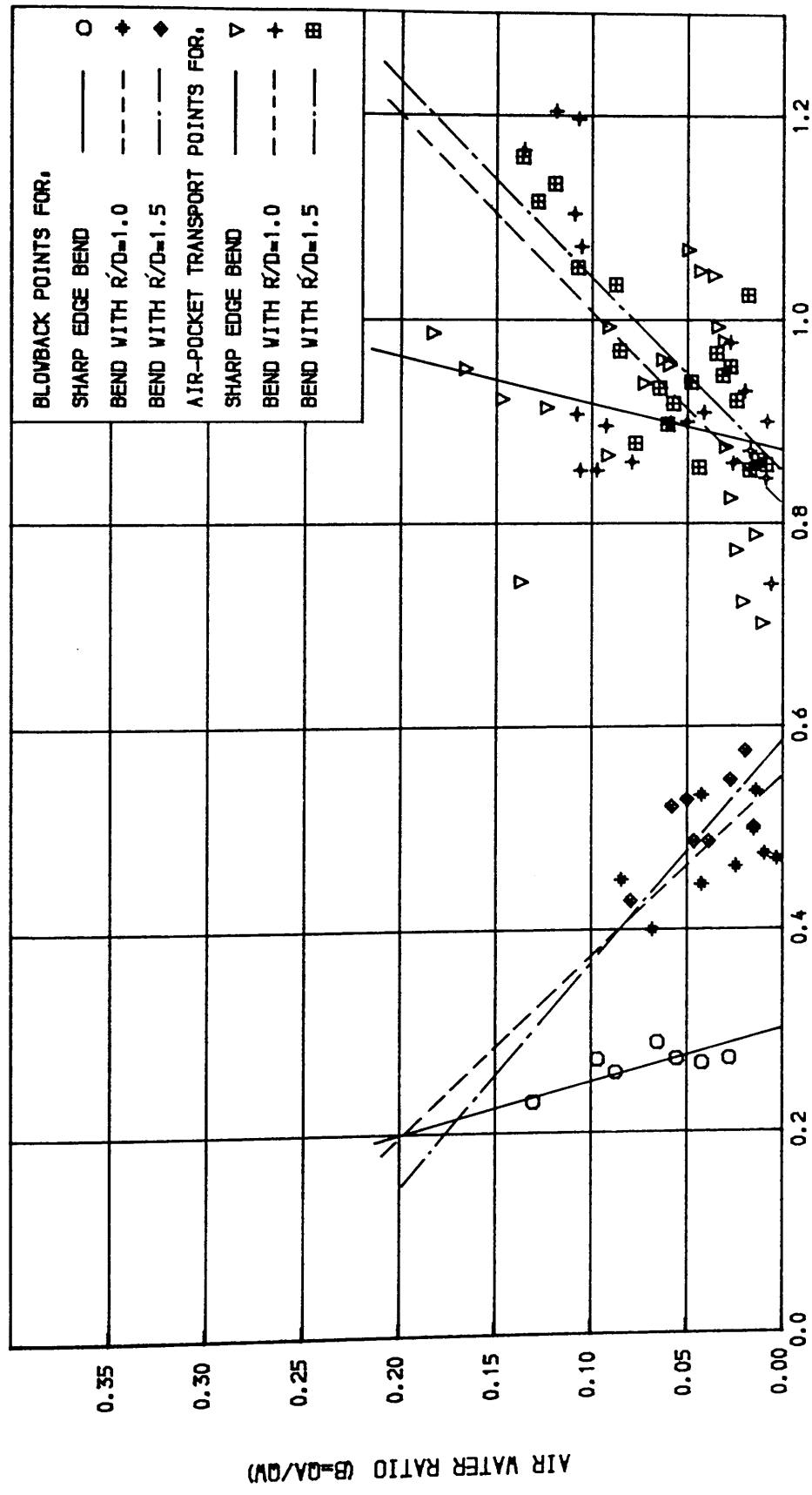

FIG. (5.63) RELATION BETWEEN UPSTREAM NON- DIMENSIONAL WATER VELOCITY & AIR-WATER RATIO AT POINTS OF BLOWING BACK AND CLEARING FOR A TUNNEL AT -1.5 DEGREE WITH HORIZONTAL & WITH THREE BENDS OF R/D=0.5, 1.0, & 1.5

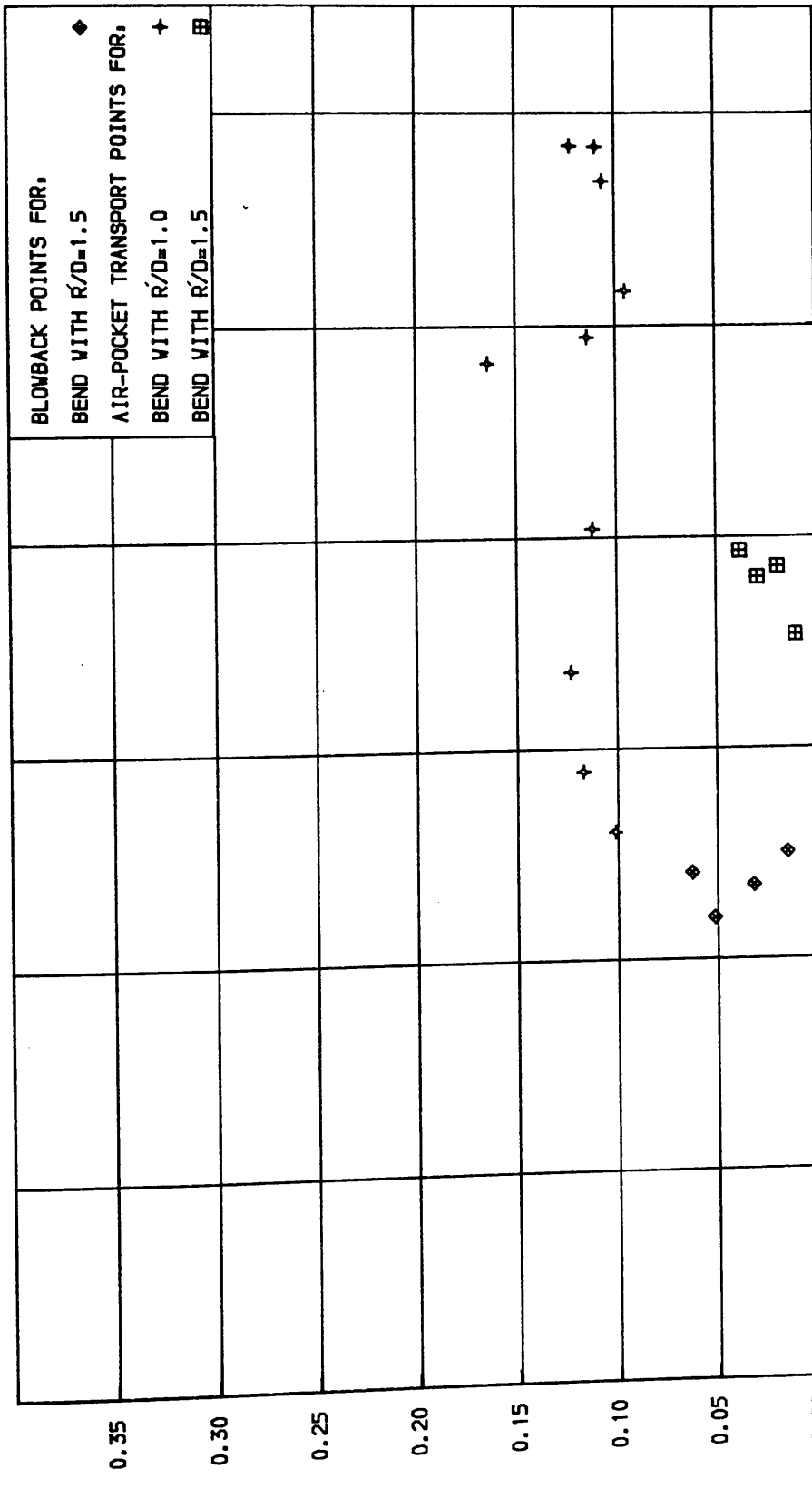

FIG. (5.64) RELATION BETWEEN UPSTREAM NON- DIMENSIONAL WATER VELOCITY & AIR-WATER RATIO AT POINTS OF BLOWING BACK AND CLEARING FOR A TUNNEL AT -1.5 DEGREE WITH HORIZONTAL & WITH TWO BENDS OF R/D=1.0 & 1.5

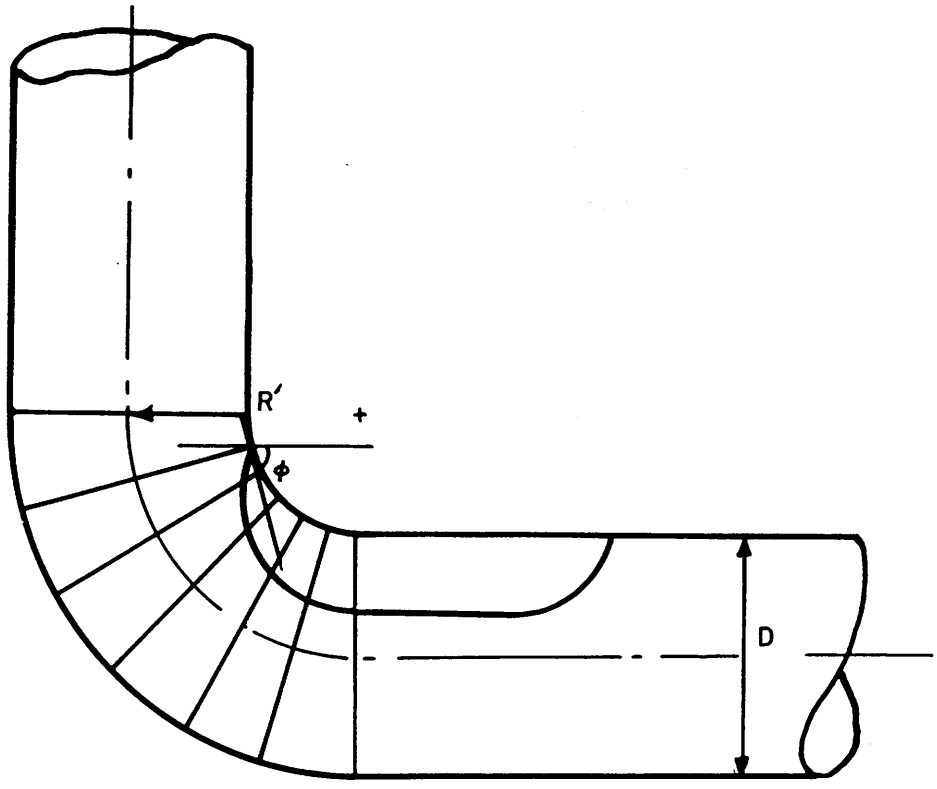

FIG. (5.65) A STABLE AIR POCKET WITH A HYDRAULIC JUMP AT ITS END FOR $Q_w = 10.56 \times 10^{-3}$ m^3/s AND Q_A FROM THE ENTRAINMENT OF THE PLUNGING JET, FOR AN UPWARD SLOPING TUNNEL AND R'/D = 1.0

Chapter Six

EXPERIMENTAL RESULTS FOR AIR POCKET BEHAVIOUR IN STRAIGHT PIPES INCLINED AT SHALLOW ANGLES ABOVE AND BELOW THE HORIZONTAL

6.1 INTRODUCTION

Air pockets in straight pipes inclined above the horizontal tend to rise in the same direction as the flowing water, due to their buoyancy effect and the drag force of the moving water. The shape of a typical air pocket is shown in Fig. (6.1a), and is similar to that given by Bacopoulous[14]. Air pockets in straight pipes inclined below the horizontal, with flowing water, can either blowback up the pipe, when buoyancy is greater than the water drag force, or clear downstream along the pipe, when the water drag force overcomes the buoyancy effect. The shape of a blowing back air pocket is shown in Fig. (6.1b). It is also possible to obtain a stationary air pocket when drag is balanced by buoyancy. Both air pocket shapes are based on experimental observations carried out on the straight tunnel section for an upward angle of +1.5° with horizontal, and a downward angle of -1.5° with horizontal. The experimental data presented in this chapter represent separate test runs to the dropshaft/tunnel results described in Chapter (5) and are confined to the straight 8.3m long tunnel section.

A wide range of results was achieved for the upward sloping tunnel, while only a few results were obtained for air pockets blowing back in the downward sloping tunnel. Description of each mode of behaviour will be given in the following sections, together with the experimental results obtained and their analysis.

Comparison of the experimental results with theoretical models, described in Chapter (3), will be carried out in Chapter (7).

6.2 AIR POCKETS IN A TUNNEL INCLINED AT +1.5° ABOVE HORIZONTAL

In this section the experimental results for air pocket rising up the inclined tunnel will be presented, together with photographs taken to show the shape of rising air pockets. An air pocket rises up an inclined pipe in stationary water due to its buoyancy, and the pocket velocity increases in flowing water where the rising velocity will have components due to buoyancy and water velocity. The method of forming air pockets in the tunnel system was the same as that of forming an air pocket at the dropshaft/tunnel bend. A mixture of air bubbles and water is transported down the dropshaft, an air pocket forms at the bend in any of the four stable regimes described in Section (5.2). Once the stable bend pocket forms, a continual supply of smaller pockets is shed off the end of the bend pocket, and these are the pockets under consideration in this section.

This procedure happens at any water flow rate and for any air flow rate allowing a wide range of experimental tests to be carried out. Around one hundred test runs were performed with different combinations of air and water flow rates, and for each run the experimental details of different air pockets were recorded. The number of air pockets for each run was between 10-25 to confirm the experimental results. The experimental data collected for each run included the water flow rate Q_W, and hence the pipe-full velocity V_O, the net air flow rate Q_A, and hence the air/water ratio β, the maximum depth of air pocket, giving H/D, the rise velocity of the air pocket V_r, and the detailed shape of a rising air pocket.

The velocity of the rising air pockets, their detailed centreline shape, and their maximum depth were obtained by using the

two wave monitor probes connected to the chart recorder, as explained in Chapter (4). The first probe was placed at the end of the first length of the tunnel section, about 2.9 m from the bend, and the second probe was placed at the end of the third tunnel section, giving a distance between the two probes of 4.677 m. To measure the speed of a rising air pocket, the event marker on the chart recorder was pressed when the air pocket reached probe 1 and then it was pressed again when the same air pocket reached probe 2. The chart recorder speed used was 10 mm/sec, which means that each 1-cm on the chart gives 1 second, as shown in Fig. (6.2). Hence, if the event is marked when the air pocket passes probes 1 and 2, and the time of travel is known, then since the distance between the two probes is fixed, the speed of the air pocket can be found. From the chart recorder the maximum depth of the rising air pocket is measured at both probes 1 and 2, and denoted in Fig. (6.2) as H_1 and H_2. The depth of the air pocket at probe 2 was in most cases greater than that at probe 1. The reason for this highlights the complexity involved in this study. Smaller air pockets, say $H/D \simeq 0.1$, propagate at a smaller speed than larger air pockets, say $H/D = 0.35$. If a smaller pocket is travelling along the pipe, followed by a larger one, the larger pocket overtakes the smaller one forming a single pocket. Thus progressing along the tunnel, air pockets have a tendency to enlarge due to coalescence phenomenon, implying that completely stable flow would only occur in a very long tunnel section where all the air pockets would have the same depth and be moving at the same speed.

Hence it was decided to use an average value of H_1 and H_2 to relate it to the average rising velocity of that pocket.

For a given water flow rate, increasing air flow rate causes the depth of the air pocket to increase and hence its speed also increases due to higher buoyancy force. Increasing the water flow rate for an increasing air flow rate also increases the speed of the rising air pocket. The effects of both are shown in Figs. (6.2),

(6.3), (6.4) and (6.5) recorded by the chart recorder, where the first two figures are for a fixed water flow rate and increasing air flow rate. Figures (6.4) and (6.5) show the effect of increasing both the water flow rate and the air flow rate for an almost constant air/water ratio β. In non-dimensional terms this is the effect of increasing pipe-full Froude number $V_o/\sqrt{gD}$ for almost constant β, showing, in comparing Figs. (6.4) and (6.5), that the air pocket depth and speed increases with larger values of Froude numbers.

A few results were obtained when the bend air pocket extended beyond probe 1, and air pocket speeds were obtained manually by using the tape measure attached to the tunnel section, together with a stopwatch to estimate velocities. In this case the average value of H/D is undefined as it could only be measured at probe 2, further along the tunnel section.

Different views of air pockets rising up the tunnel are shown in Plates (6.1), (6.2), (6.3) and (6.4), where it can be seen that different sizes of air pockets can be obtained and each air pocket can be divided into three zones as Bacopoulous[14] did. The first zone is the front nose of the air pocket which has a parabolic shape, where the tangent at the nose of the air pocket forms an angle Φ with the pipe wall, as shown in Fig. (6.1). This angle Φ was measured from different photographs taken for different air pockets rising up the pipe where its value varied between 36° and 65°. The second zone is a small hydraulic jump which is often undular in nature, or for deeper values of H/D, this may become a more defined jump with air entrainment and a definite energy loss. This can be seen most clearly in the lower two photographs of Plate (6.4). The third zone is the tail of the air pocket, and this region generally has an almost horizontal water surface extending in length until it reaches the pipe roof. Thus shallow conduit slopes tend to produce longer air pockets. These points are illustrated more clearly in Fig. (6.6), which is a trace of a typical passing air pocket taken from a photograph and expanded in depth and length for added clarity.

Such tracings confirm, to some extent, the assumptions in Chapter (3), theoretical models, that energy losses might be considered concentrated in the short hydraulic jump section, and the front nose section down to the point of maximum depth (H/D), might be reasonably considered as an energy conserving zone.

The experimental results of the air pocket rise velocity are shown in Fig. (6.7), plotted against the mixture velocity $(Q_A+Q_w)/A_p$, and split into bands of H/D, the maximum air pocket depth. It should be noted that each experimental data point in Fig. (6.7) represents the average data for a succession of air pockets formed under a given value of air flow and water flow rates. That is, the average rise velocity for a succession of air pockets, and, the average value of air pocket depth H/D, for the succession of pockets.

The form of Fig. (6.7) has already been discussed in Chapters (2) and (3), whereby the rise veloctiy of an air pocket is assumed to have two components, one due to the buoyancy of the air pocket and the other due to drag from the moving water. The buoyancy of the air pocket depends on the volume of the air pocket itself and can be related most effectively to its maximum depth[14,24] which means that the first component can be specified in terms of the depth of pocket or the non-dimensional depth of air pocket H/D. The second component has been shown to be a function of the mixture velocity <j> or $(Q_A+Q_w)/A_p$[107,177]. Thus the most appropriate framework for the rise velocity of air pockets in moving water[26,107,123] can be written in the form:

$$V_r = C_1\sqrt{gD} + C_o \langle j \rangle \qquad (6.1)$$

where in vertical pipes and for high Reynolds number the value of $C_o \triangleq 1.2$ and $C_1 = 0.35$[38,42,107,177]. The value of C_1 for shallow pipe slopes was expected to be slightly higher than the value for vertical pipes. The data in Fig. (6.7) was subjected to regression analysis to obtain the best fit lines through each band of H/D. The

slope of each line represents the value of C_o which in fact was less than 1.2, and generally is in the range 1.05-1.11. The intercept of each line represented the term $C_1\sqrt{gD}$, where D is the pipe diameter and equal to 0.152 m in this work. The value of C_1 was slightly higher than 0.35 as expected and appears to be dependent on H/D, for the tunnel angle of +1.5° tested in this work. The following are the rising velocities as represented by the straight lines shown in Fig. (6.7) for different values of H/D:

a - For $0.1 < H/D \leq 0.2$

$$V_r = 0.401 \sqrt{gD} + 1.10712 \langle j \rangle \qquad (6.2)$$

b - For $0.2 < H/D \leq 0.25$

$$V_r = 0.501 \sqrt{gD} + 1.0758 \langle j \rangle \qquad (6.3)$$

c - For $0.25 < H/D \leq 0.30$

$$V_r = 0.556 \sqrt{gD} + 1.0554 \langle j \rangle \qquad (6.4)$$

d - For $0.3 < H/D \leq 0.35$

$$V_r = 0.580 \sqrt{gD} + 1.098 \langle j \rangle \qquad (6.5)$$

where $\langle j \rangle = (Q_A+Q_W)/A_p$, the upstream mixture velocity. An attempt to represent the experimental results in one line without dividing the results into different bands of H/D resulted in the following equation for the rising velocity:

$$V_r = 0.432 \sqrt{gD} + 1.246 \langle j \rangle \qquad (6.6)$$

where C_1 is larger than 0.35 and $C_o \simeq 1.2$ as given by previous authors. This means that most previous research which was based on different air pocket depths without considering the depth of air pocket is a crude representation because the important parameter H/D has been omitted.

The importance of this discovery needs to be highlighted. Previous researchers working in the area of air pockets in moving water have produced relationships in the form of equation (6.6) giving one single value for C_1. This is now known to be inaccurate because C_1 varies with the air pocket depth (0.4 to 0.58 in this case) and may well vary with the conduit slope θ as well. Other researchers such as Benjamin[24] and Bacopoulous[14] have worked with air pockets moving in stationary water, which is equivalent to the intercept points $\langle j \rangle = 0$ in this work, and have found the air pocket speed, or the term C_1, to vary with H/D and θ. Thus Fig. (6.7) highlights that Benjamin's analysis of C_1 might now be applied to the moving water case. This will be analysed in some detail in Chapter (7).

The non-dimensional air pocket rising velocity $V_r/\sqrt{gD}$ is plotted in Fig. (6.8) against the non-dimensional mixture velocity $V_o(1+\beta)/\sqrt{gD}$, where again it can be noted that a linear relation can be applied between the non-dimensional rising velocity and mixture velocity. The effect of the air/water ratio β on the depth of the rising air pockets is shown in Fig. (6.9) where the upstream non-dimensional water velocity Fr_o is plotted against H/D for a range of β values. Tentative curves are drawn through each β value. It can be noted that increasing β increased the air pocket depth for a given value of Froude number $V_o/\sqrt{gD}$. It can also be noted that for a constant value of air/water ratio β, the air pocket depth increases with increasing Froude number.

6.3 AIR POCKETS IN A TUNNEL INCLINED AT -1.5° BELOW THE HORIZONTAL

Air pockets in a tunnel inclined below the horizontal can either blowback up the tunnel or clear downstream along the tunnel. For a downward sloping tunnel the buoyancy force of the air pocket is acting in the opposite direction to the flowing water. If the water drag force is less than the buoyant force the air pocket will blowback, and if it is greater than the buoyant force the air pocket will clear. The behaviour of blowing back or clearing air pockets will be discussed in the following two sections with some photographs to illustrate the air pocket shape and the angle the front nose of the air pocket forms with the tunnel roof.

6.3.1 Air Pockets Blowing Back

It was mentioned in Section (6.1) that only a few experimental data points were obtained for the case of air pockets blowing back up a downward sloping tunnel. This was due to the design of the apparatus which was primarily intended for studies of the air pocket behaviour at the bend.

In effect, to obtain air pockets blowing back along the tunnel section, it was necessary to form the pockets in the first place at the downstream end of the tunnel. In order to achieve that, air needed to be transported with the flow, down the dropshaft, along the tunnel, to coalesce at the end of the tunnel forming large enough pockets to produce the buoyancy to blow back against the oncoming water flow. It was found in the experiment that this could only be achieved by using low water velocities (or low Froude numbers), otherwise at higher water velocities, stratified flow occurred, where an air pocket forming at the bend extended along the full tunnel length to the outlet tank, thus rendering blowback studies impossible.

The limitation of this study is that only one conduit slope was tested for blowback, $\theta = -1.5°$, and, tests were carried out only over a small range of water velocity, actually 0.45 to 0.6 m/s. This is the equivalent of obtaining data in Fig. (6.7), for instance only over the mixture velocity range 0.45 to 0.6 m/s and hence great difficulty would be experienced in formulating generalised relationships.

Another important drawback regarding this set of data concerned the use of the wave monitor probes to determine the blowback air pocket speed, depth and shape. In practice these probes could not be used effectively for this section of the work because the air pocket formed at any arbitrary point along the tunnel, and travelling upstream did not necessarily pass both probes allowing an accurate picture to be formed. Resort was made to measure air pocket blowback speeds using a stopwatch and timing over a given distance, and air pocket depths were obtained using photography. It was not always possible to link the two, to give simultaneous readings of V_r, V_o and H/D.

The angle the front nose of the air pocket forms with the pipe roof was found from photographs to vary between 12° - 30°, and the angle the tail of the pocket forms with the pipe roof was between 19°-50°. The value of H/D varied between 0.05 - 0.27.

Plate (6.5) shows an air pocket blowing back and impacting with the downstream end of the air pocket at the bend. This occurred at $Fr_o = 0.486$ and the value of H/D is 0.213. In Plate (6.6) small successive air pockets are blowing back up the tunnel. The size of the air pockets increased with increasing air/water ratio and water flow rate, as shown in Plate (6.7).

The experimental results are shown in Fig. (6.10) where it can be seen that the limited range within which results were obtained is between $Fr_o = 0.375 - 0.50$. For a certain value of Fr_o the

rising velocity varied due to the variations in the maximum depth of air pocket H/D which unfortunately could not be recorded accurately at the same time as the speed of the air pocket. The data presented in Fig. (6.10) is almost meaningless until presented in a framework describing what is likely to occur at other Froude numbers. This is done in Fig. (6.11) presenting only the average air pocket velocities at each Froude number. The framework is argued below:

(a) When the mixture velocity is zero, $\langle j \rangle = 0$, the air pocket rise velocities for the upward sloping pipe must be equal to the blowback velocities in the downward sloping pipe, because the water is stationary in both cases and the tunnel slopes are exactly the same. Thus the data points only on the vertical axis must be a mirror image of each other, as shown in Fig. (6.11)

(b) The blowback photographs revealed that the air pocket depths varied from H/D = 0.05 to 0.27, with the front nose angle of the pocket θ varying from 12° to 30°. This information can be used in the blowback theoretical model presented in Section (3.8.1) to predict the range of behaviour over the full range of mixture velocity. These are indicated as solid lines on the lower part of Fig. (6.11). It can be seen that the theoretical range of behaviour fits the limited data range reasonably well.

(c) Kalinske and Robertson[94] carried out blowback experiments in a circular pipe, the same diameter used in this work, at conduit slopes up to 18° below the horizontal. They predicted the range of velocities below which blowback will occur and above which downstream clearing will occur. This must coincide with the horizontal axis in Fig. (6.11). It is seen from Fig. (6.11) that the range of Kalinske and Robertson fits well with the limited blowback experimental data and the theoretical predictions. Kalinske and

Robertson's range has been interpolated for a conduit slope of -1.5° from Fig(2.47) .

Although the experimental data points for blowback are limited in this work, it is now clear that the criterion determining whether blowback or clearing will occur in a downward sloping pipe must be related not only to the conduit slope as all the previous investigators have done, but also, and perhaps more importantly, the air pocket depth H/D, as well as the angle the front nose of the air pocket makes with the conduit Φ. This will be discussed in more detail in Chapter (7).

An important point worth mentioning here is the change of the angle of the front nose of the air pocket Φ with the depth of the air pocket. It was noticed from the experimental work and verified by photographs taken for air pockets rising in the upward sloping tunnel and blowing back in the downward sloping pipe, that the angle Φ increases with increasing the depth of air pocket H/D. This is shown in Fig. (6.12) for the two angles tested of +1.5° and -1.5° with horizontal. Although the data points are limited, a line is fitted visually for each range of data, where in both cases each line gives an indication of the increased value of the angle Φ with the depth of pocket H/D.

6.3.2 Air Pockets Clearing

Once the air pocket at the bend had cleared, the air bubbles flowing around the bend formed a long air pocket downstream of the bend, which started to reduce in size by air entrainment at its end. This process continued until the air pocket size reached a specific size where the water velocity was capable of clearing this air pocket. This occurred in a limited range of runs and the reduced air pocket was almost at the centre of the third length of tunnel, where suddenly it was cleared. The water velocities required to clear such air pocket were generally higher than that required to

clear the bend air pocket. The pipe-full water velocity and Froude number for clearing in the straight pipe section were in the range 1.1-1.29 m/s, 0.90-1.059 respectively, which are much higher than the theoretical model for clearing. This might be due to the fact that these air pockets are very large in depth and length and require higher water drag force to overcome their buoyancy and clear them along the tunnel. A clearing air pocket is shown in Plate (6.8). The angle of the nose of air pocket with the pipe roof in the direction of clearing was found to vary between 12°-27°. The available experimental data are shown in Fig. (6.13) together with the theoretical model for clearing air pockets given in equation (3.106) where the value of ϕ used is 15° which is within the range obtained from the photographs of air pockets clearing. It can be noted from Fig. (6.13) that the clearing data are much higher than the theoretical clearing for the angle of -1.5°, which gives an indication that the theoretical models can be applied to air pockets of moderate sizes, and for very large air pocket the model should be modified to include the volume of the air pocket not just H/D, because the length of the pocket from the nose of the pocket to the maximum depth is much longer than moderate sizes of air pockets and requires justification.

6.4 CONCLUSIONS

A good range of experimental data was obtained for the pipe sloping upwards at +1.5°. In all cases the air pocket velocity was greater than the water velocity. The air pocket shape, from the photographs and wave monitor readings, was very similar to that described by Bacopoulous[14], with almost parabolic nose, hydraulic jump and tail sections. The rising velocity of an air pocket in an upward sloping pipe is dependent on the pipe slope, the mixture velocity and the depth of air pocket. The depth of an air pocket increases with both air/water ratio β and the Froude number $V_o/\sqrt{gD}$. The angle of the front nose of the air pocket with the pipe wall was found to increase with increasing air pocket depth.

Great difficulty was experienced in obtaining a wide range of blowback data for the downward sloping pipe. Limited data, however, confirmed that blowback velocities, and the transition point between blowback and clearing downstream is heavily dependent on the pipe slope Θ, the depth of the pocket H/D, the mixture velocity $\langle j \rangle$, and the angle of the pocket nose ϕ. This is a departure from previous more simplified correlations. The angle of the nose of the air pocket ϕ was also found to increase with increased air pocket depth.

Very limited data was obtained for the water velocity required to clear an air pocket in the downward sloping pipe. Whereas no data was obtained for the speed of the clearing air pockets in the downward sloping pipe because of inadequacies of the experimental apparatus. It is clear from Fig. (6.13) that clearing is taking place at higher values than those predicted by the theoretical models, and that is due to the fact that the size of these clearing air pockets is beyond those used in deriving the models for clearing. Again, the clearing will still depend on the angle of the nose of pocket ϕ, the slope of conduit Θ and either H/D for moderate sizes of air pockets or the volume of pocket in the case of very large air pockets.

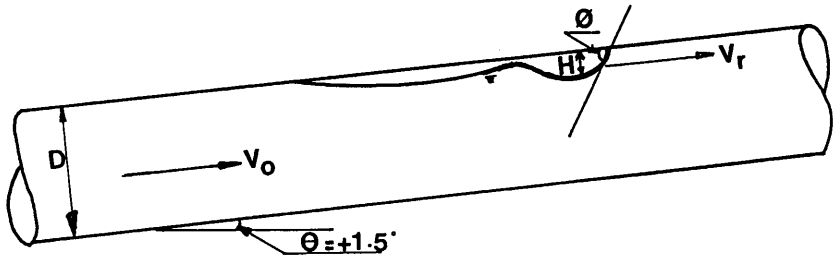

(a) AIR POCKET RISING IN AN UPWARD SLOPING TUNNEL

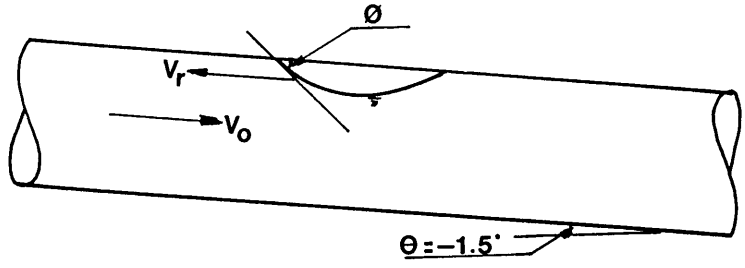

(b) AIR POCKET RISING IN A DOWNWARD SLOPING TUNNEL

FIG. (6.1) SHAPE OF AIR POCKETS IN AN UPWARD AND DOWNWARD SLOPING TUNNELS

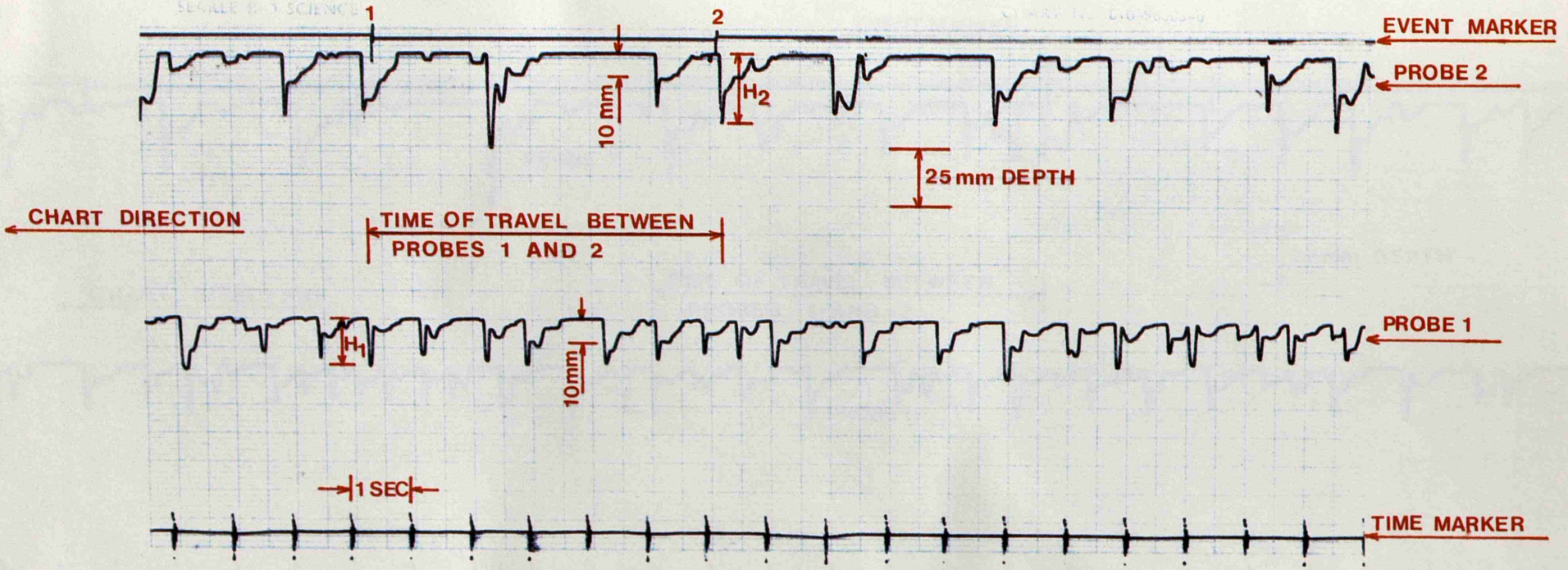

FIG. (6.2) THE RESULTS FROM THE CHART RECORDER FOR AIR POCKETS RISING IN A TUNNEL AT +1.5° WITH HORIZONTAL, FOR $Q_w = 4.27 \times 10^{-3}$ m^3/sec AND $Q_A = 0.333 \times 10^{-3}$ m^3/sec.

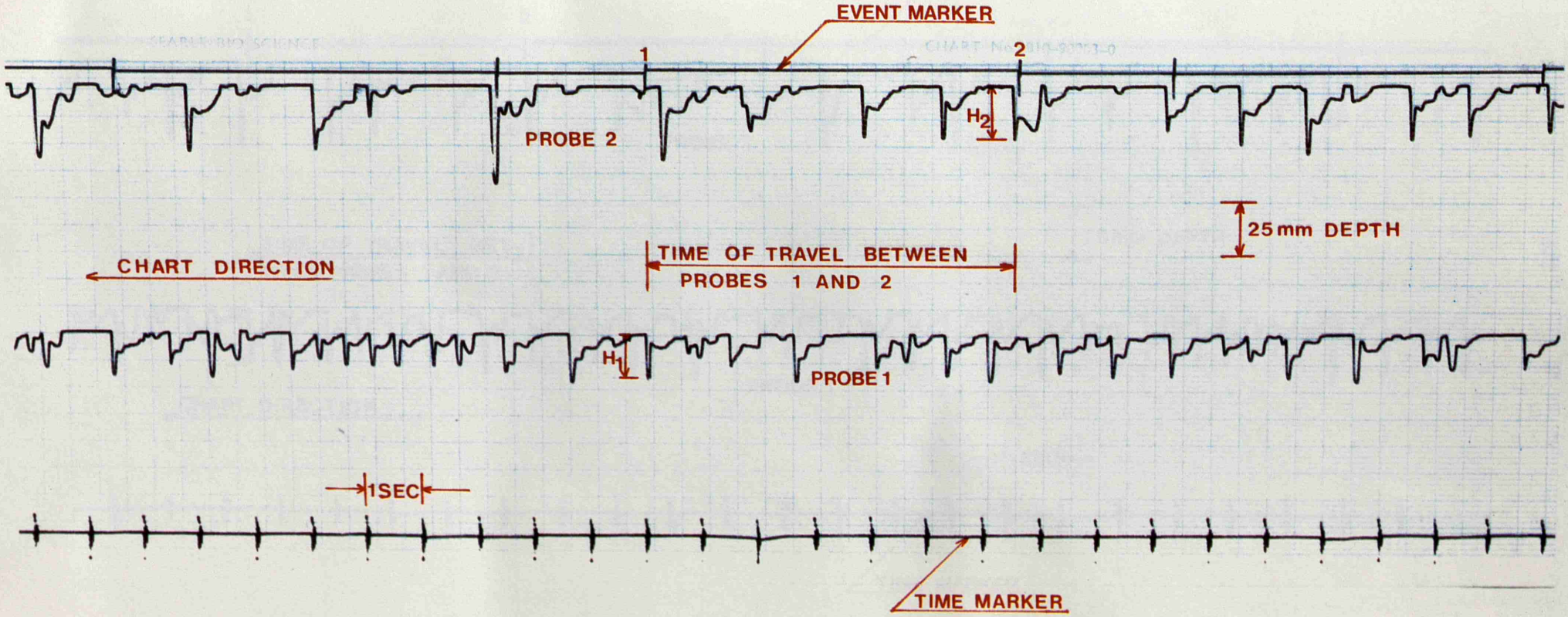

FIG. (6.3) THE RESULTS FOR AIR POCKET RISING UP THE TUNNEL, FOR $Q_w = 4.27 \times 10^{-3}$ m^3/s AND $Q_A = 0.5 \times 10^{-3}$ m^3/sec.

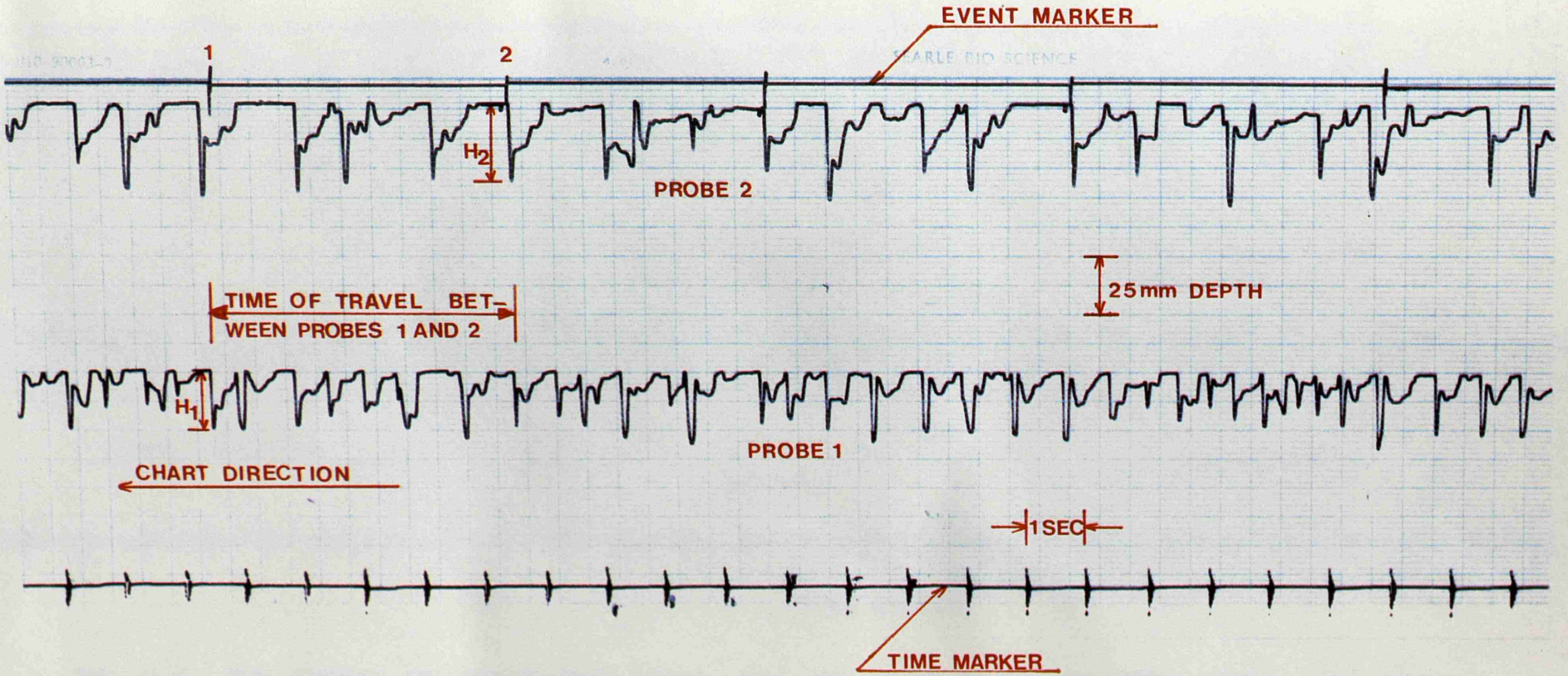

FIG. (6.4) THE EFFECT OF INCREASING THE MIXTURE VELOCITY ON THE SPEED OF AIR POCKETS UP A TUNNEL AT +1.5° WITH HORIZONTAL, FOR $Q_w = 6.49 \times 10^{-3}$ m^3/sec AND $Q_A = 0.667 \times 10^{-3}$ m^3/sec.

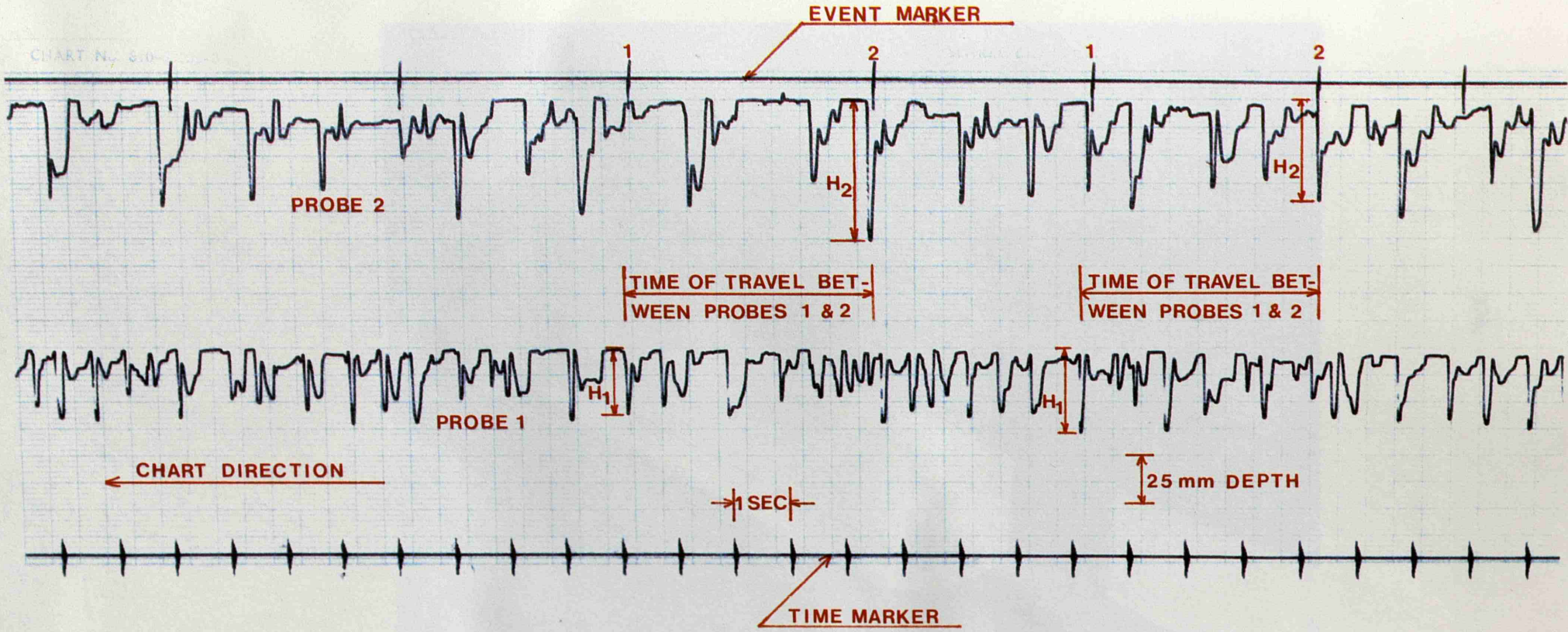

FIG. (6.5) THE EFFECT OF INCREASING WATER AND AIR FLOW RATES ON BOTH SPEED AND DEPTH OF AIR POCKETS FOR A TUNNEL AT +1.5° WITH HORIZONTAL, FOR $Q_w = 8.86 \times 10^{-3}$ m^3/sec AND $Q_A = 0.833 \times 10^{-3}$ m^3/sec.

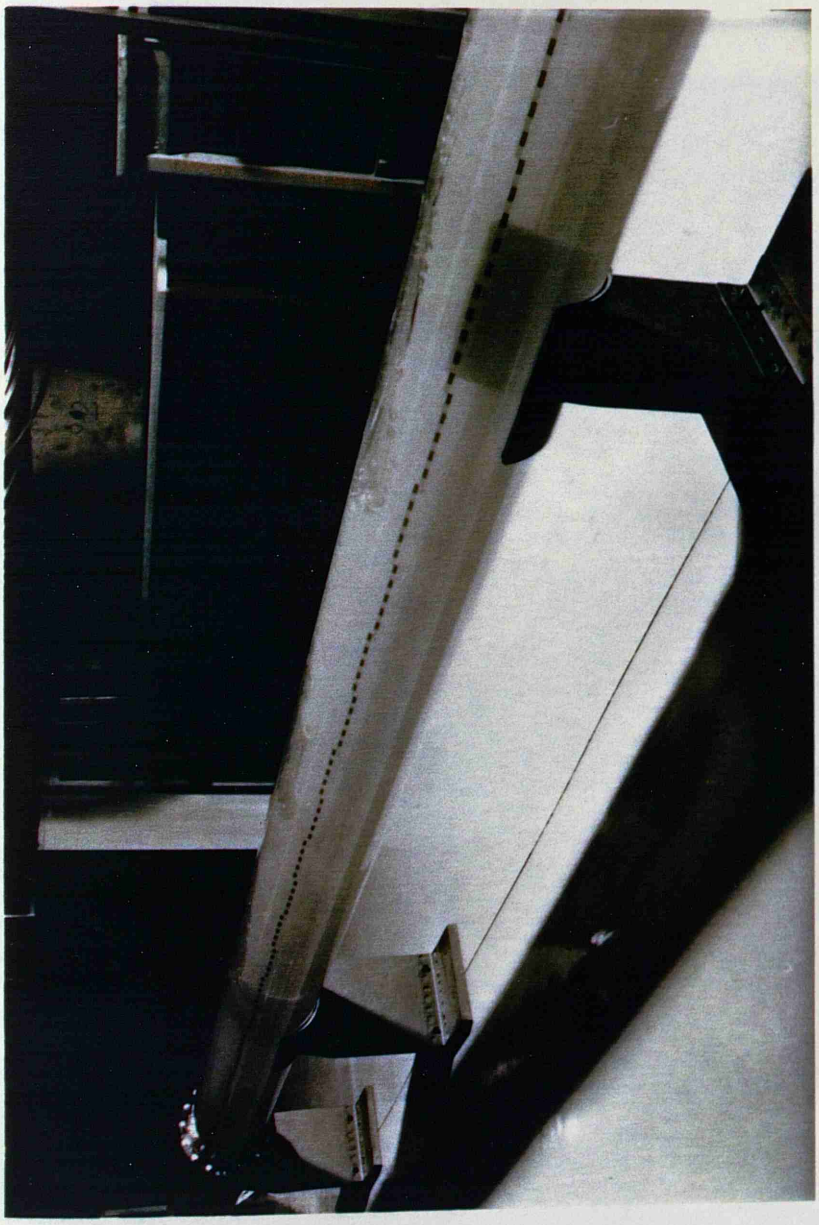

PLATE (6.1) AIR POCKETS RISING IN A TUNNEL AT +1.5° WITH HORIZONTAL

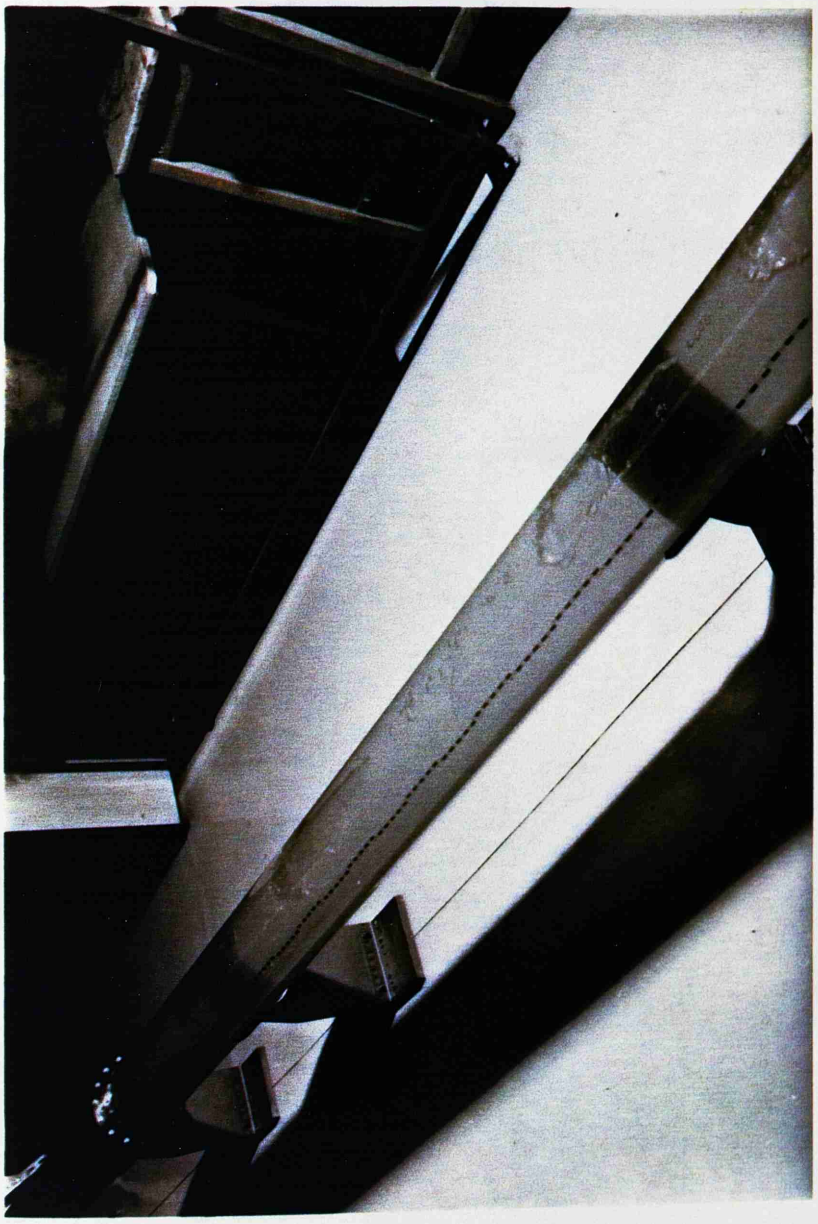

PLATE (6.2) SEPARATE AIR POCKETS RISING UP THE TUNNEL AT +1.5° WITH HORIZONTAL

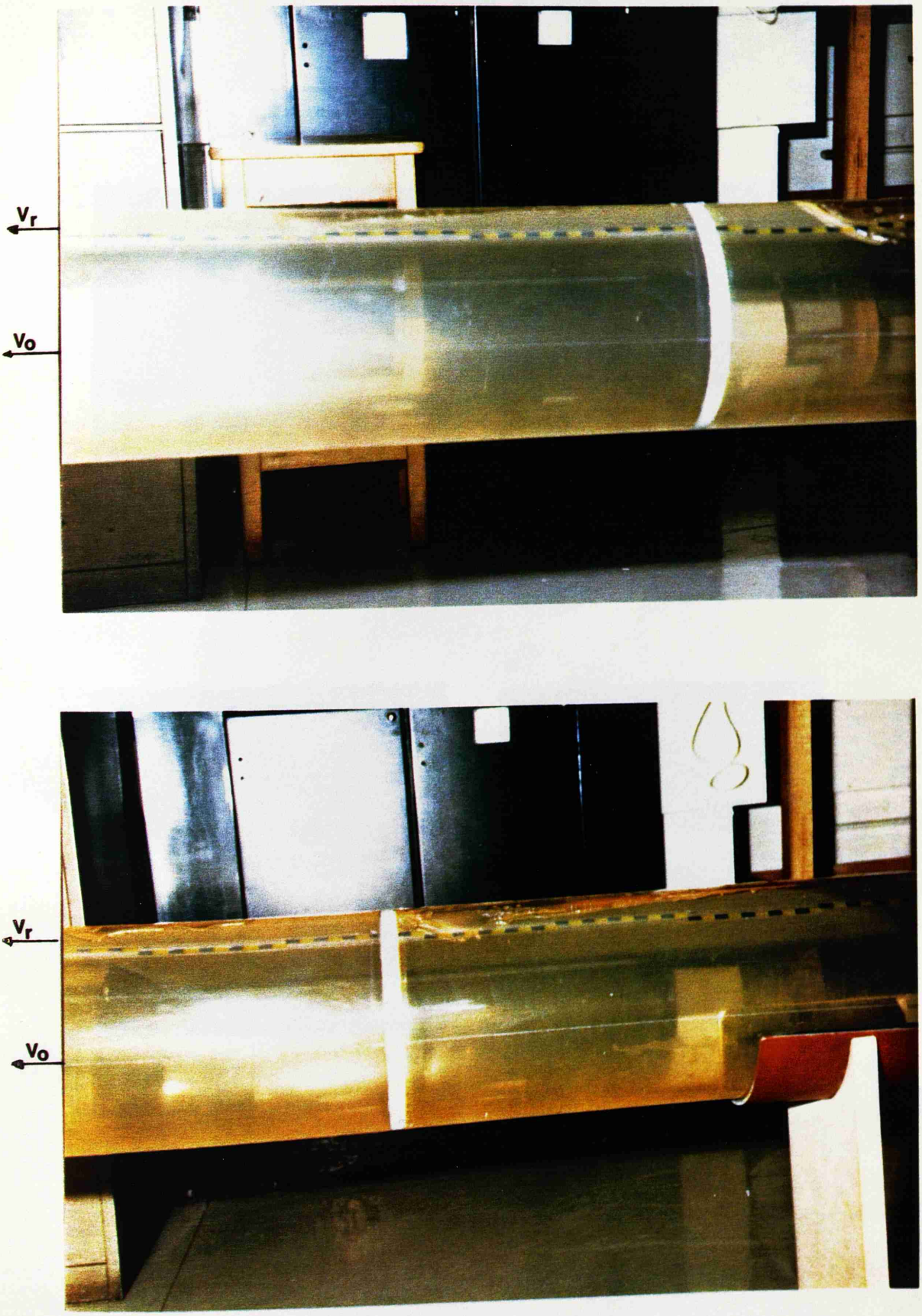

PLATE (6.3) SIDE VIEW OF AIR POCKETS RISING IN A TUNNEL AT +1.5° WITH HORIZONTAL

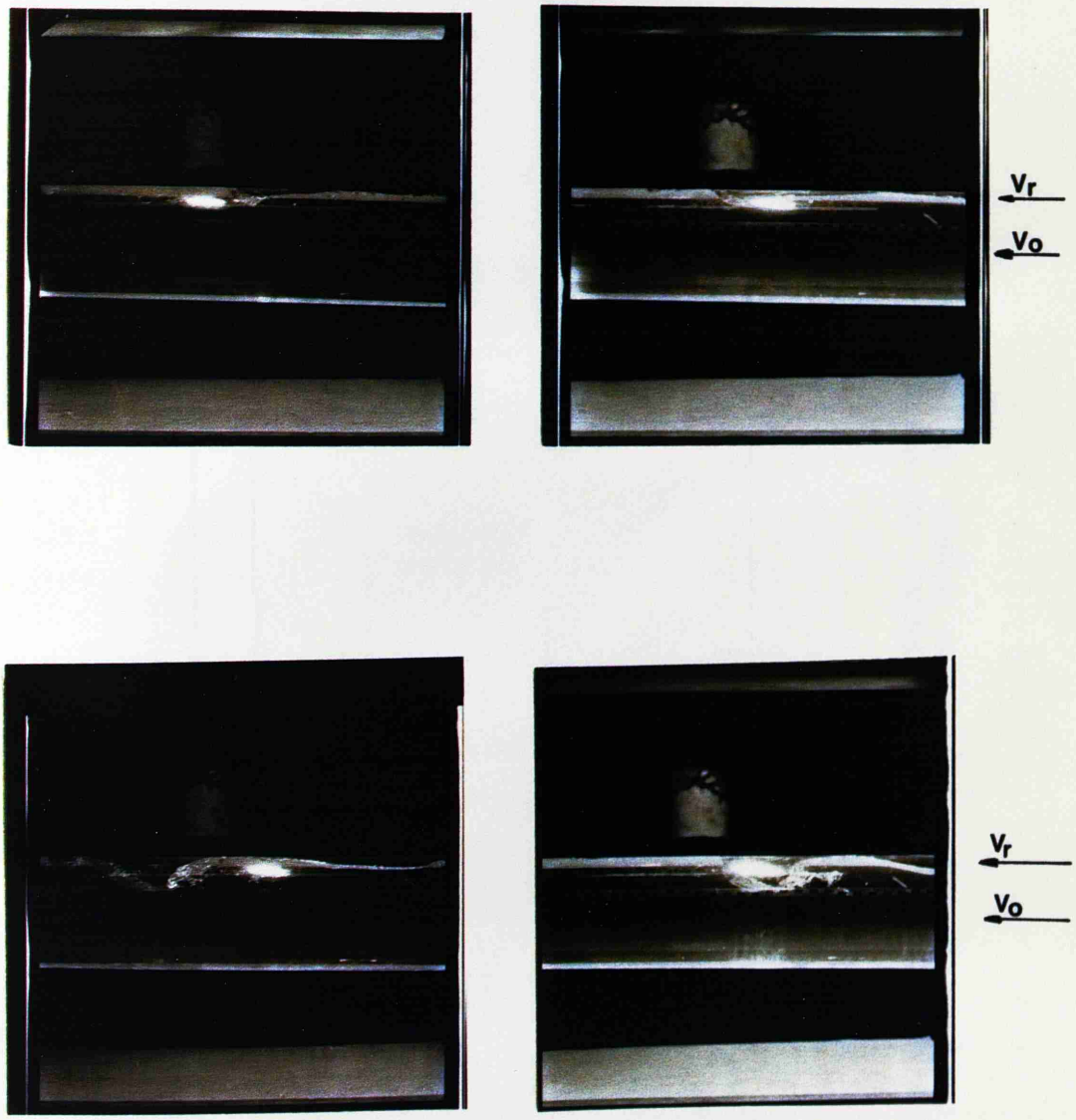

PLATE (6.4) DIFFERENT SIZES OF AIR POCKETS WITH DIFFERENT ANGLES AT THE NOSE OF THE AIR POCKET FOR A TUNNEL AT +1.5° WITH HORIZONTAL

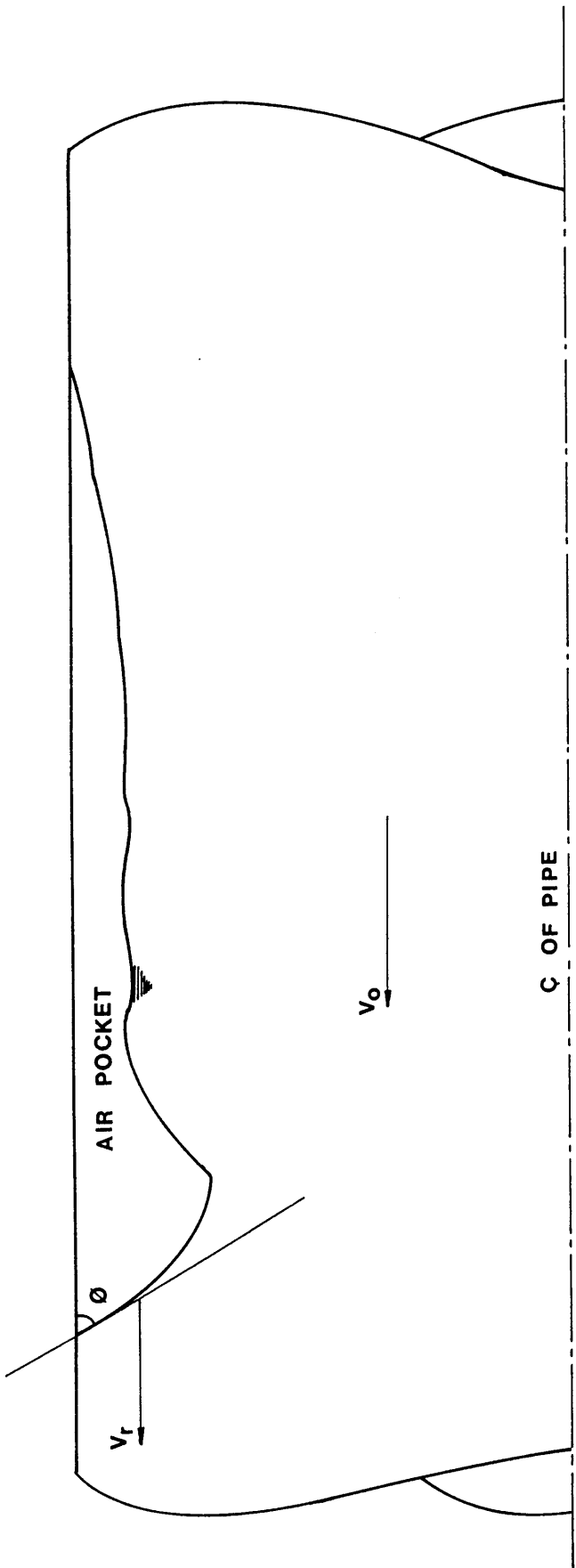

FIG. (6.6) EXPANDED VERSION OF A TYPICAL AIR POCKET TAKEN FROM A PHOTOGRAPH FOR AIR POCKET RISING IN A TUNNEL SLOPING AT +1.5° ABOVE THE HORIZONTAL

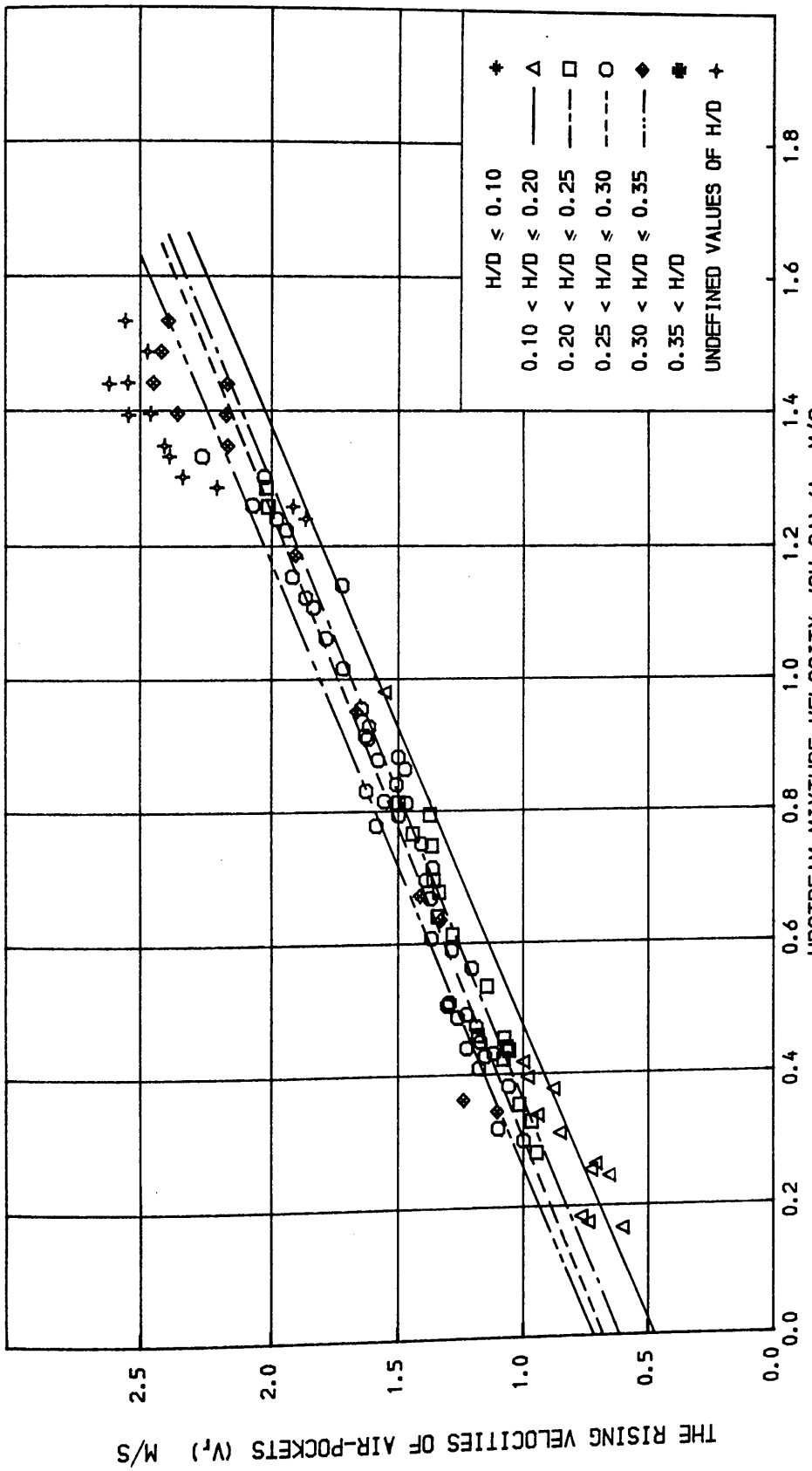

FIG(6.7) RELATION BETWEEN UPSTREAM MIXTURE VELOCITY AND THE RISING VELOCITY OF AIR-POCKETS IN A STRAIGHT PIPE LAID AT AN ANGLE OF +1.5 DEGREE WITH HORIZONTAL FOR AVERAGE VALUES OF H/D

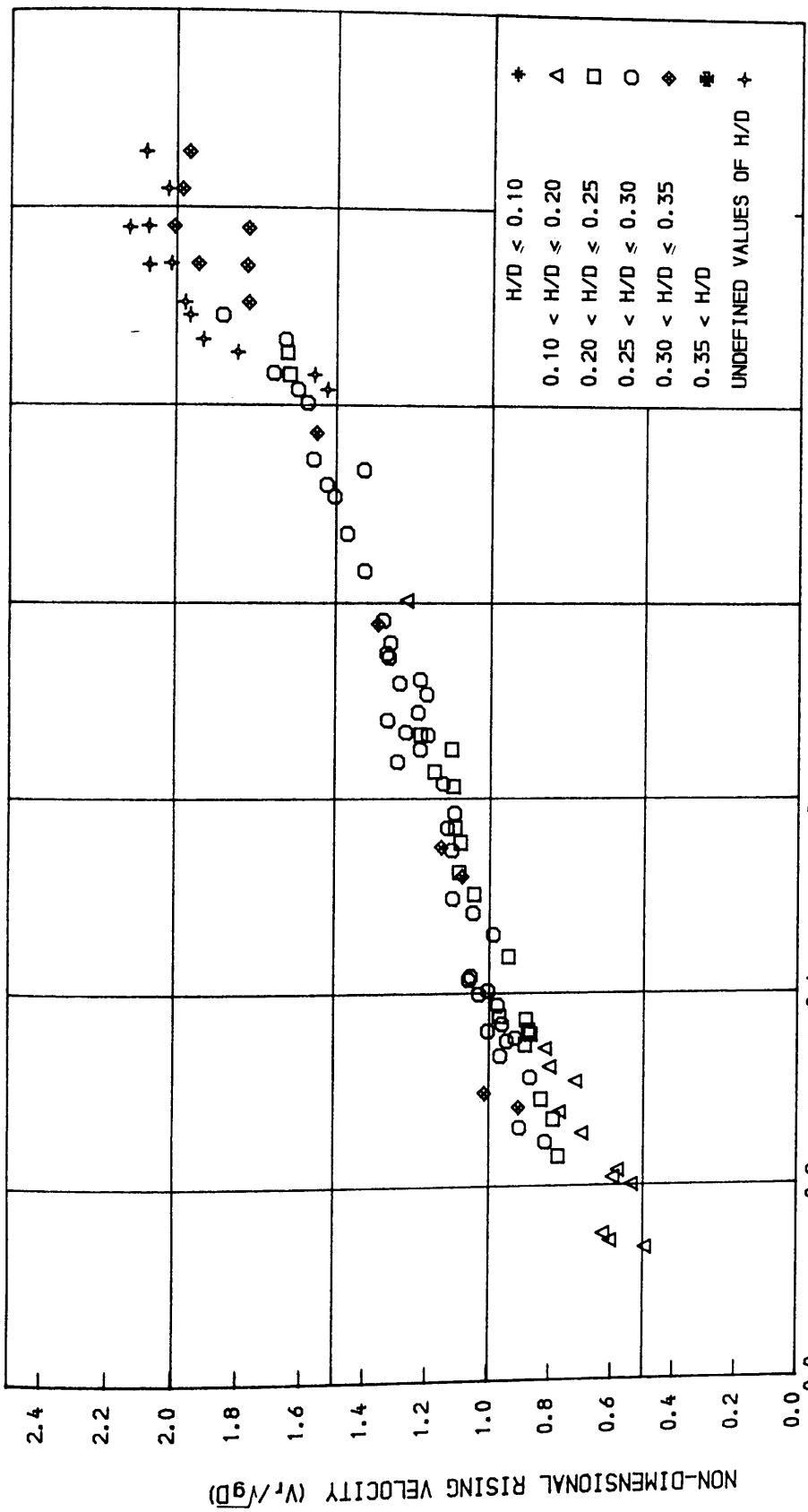

FIG (6.8) RELATION BETWEEN UPSTREAM NON- DIMENSIONAL MIXTURE VELOCITY AND NON-DIMENSIONAL RISING VELOCITY OF AIR-POCKETS IN A STRAIGHT PIPE LAID AT AN ANGLE OF +1.5 DEGREE WITH HORIZONTAL

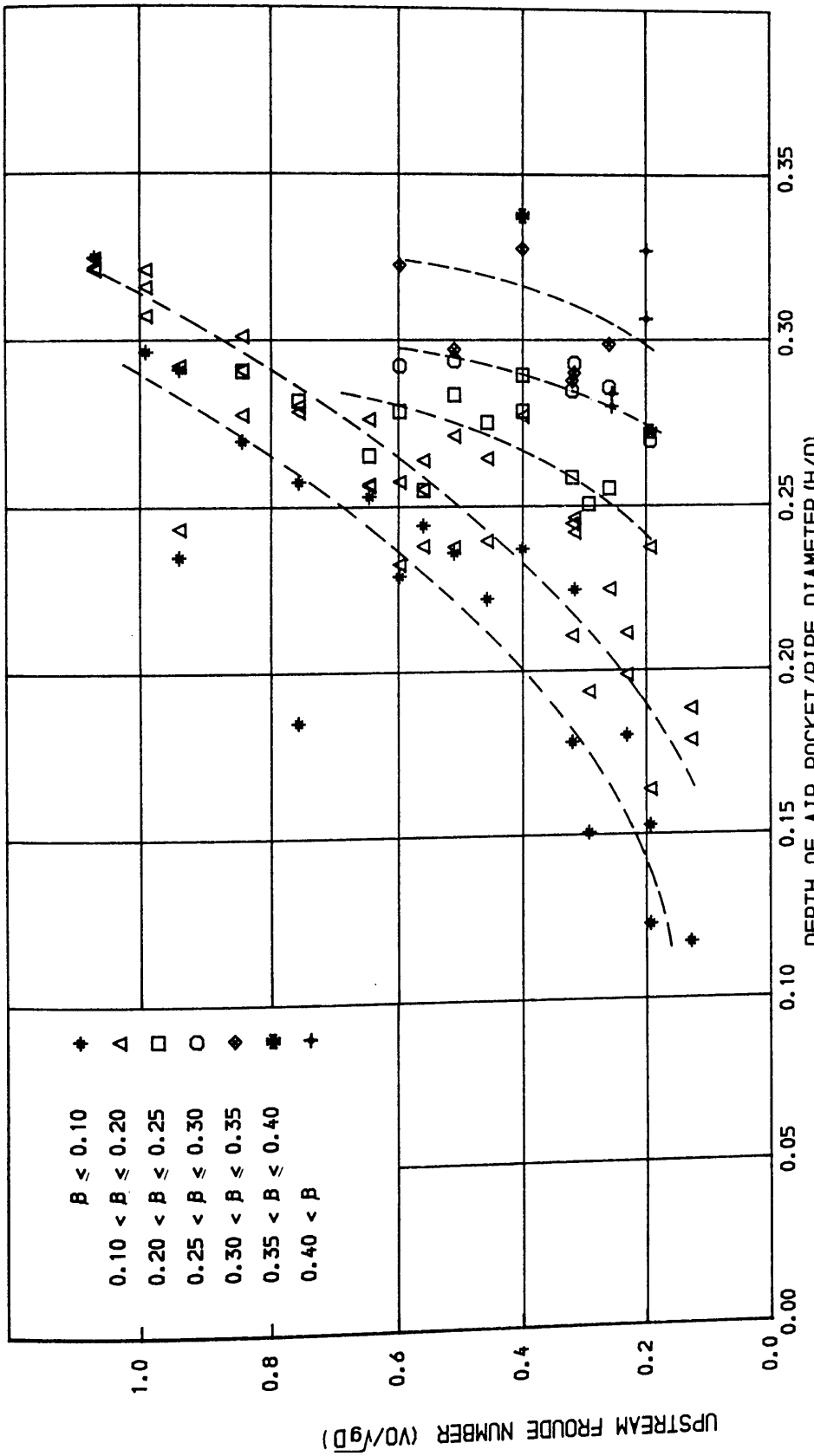

FIG (6.9) RELATION BETWEEN THE UPSTREAM NON- DIMENSIONAL WATER VELOCITY AND THE MAXIMUM DEPTH OF AIR-POCKET IN A STRAIGHT PIPE LAID AT AN ANGLE OF +1.5 DEGREE WITH HORIZONTAL

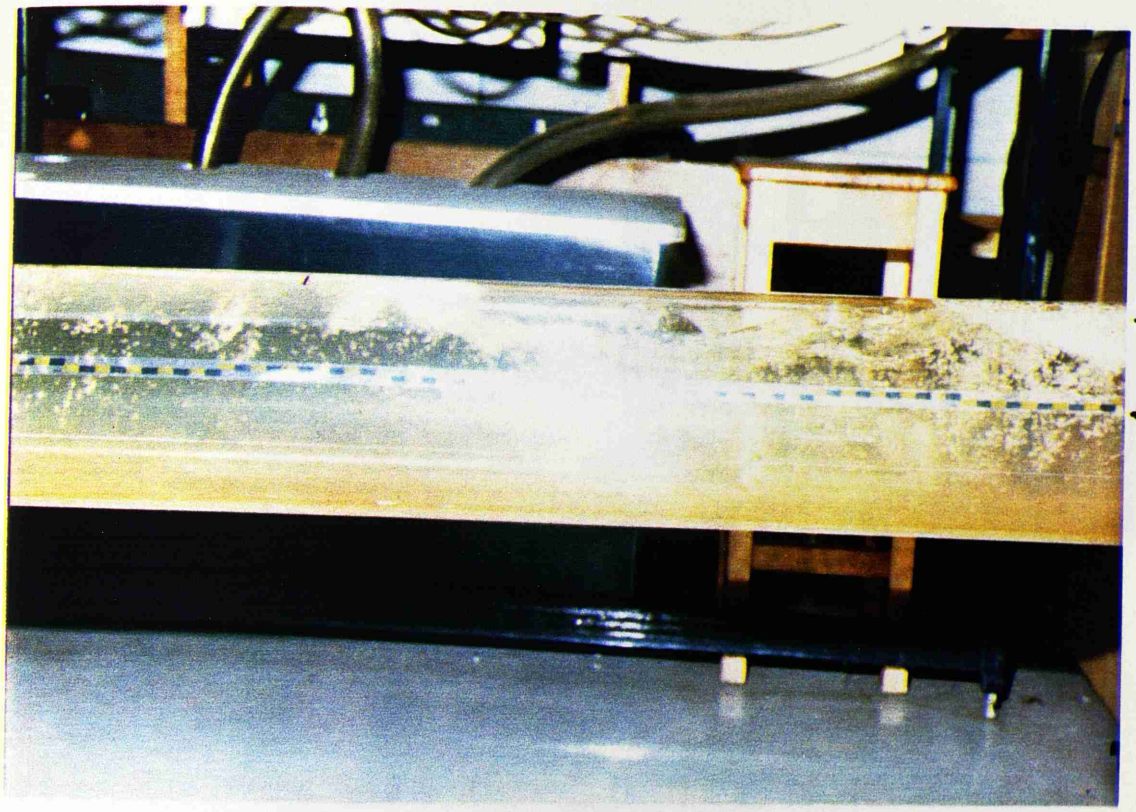

PLATE (6.5) AIR POCKET BLOWING BACK AND IMPACTING THE AIR POCKET AT THE BEND FOR A TUNNEL AT -1.5° WITH HORIZONTAL

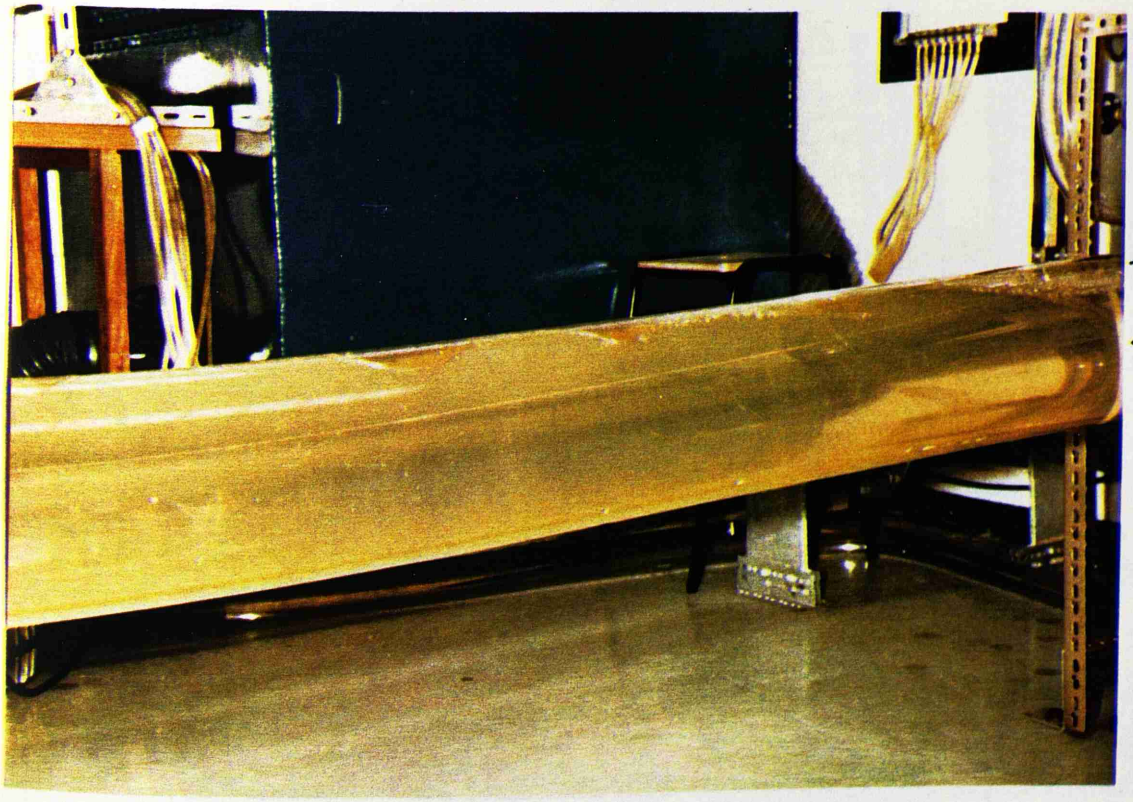

PLATE (6.6) SEPARATE AIR POCKET BLOWING BACK UP THE TUNNEL AT -1.5° WITH HORIZONTAL

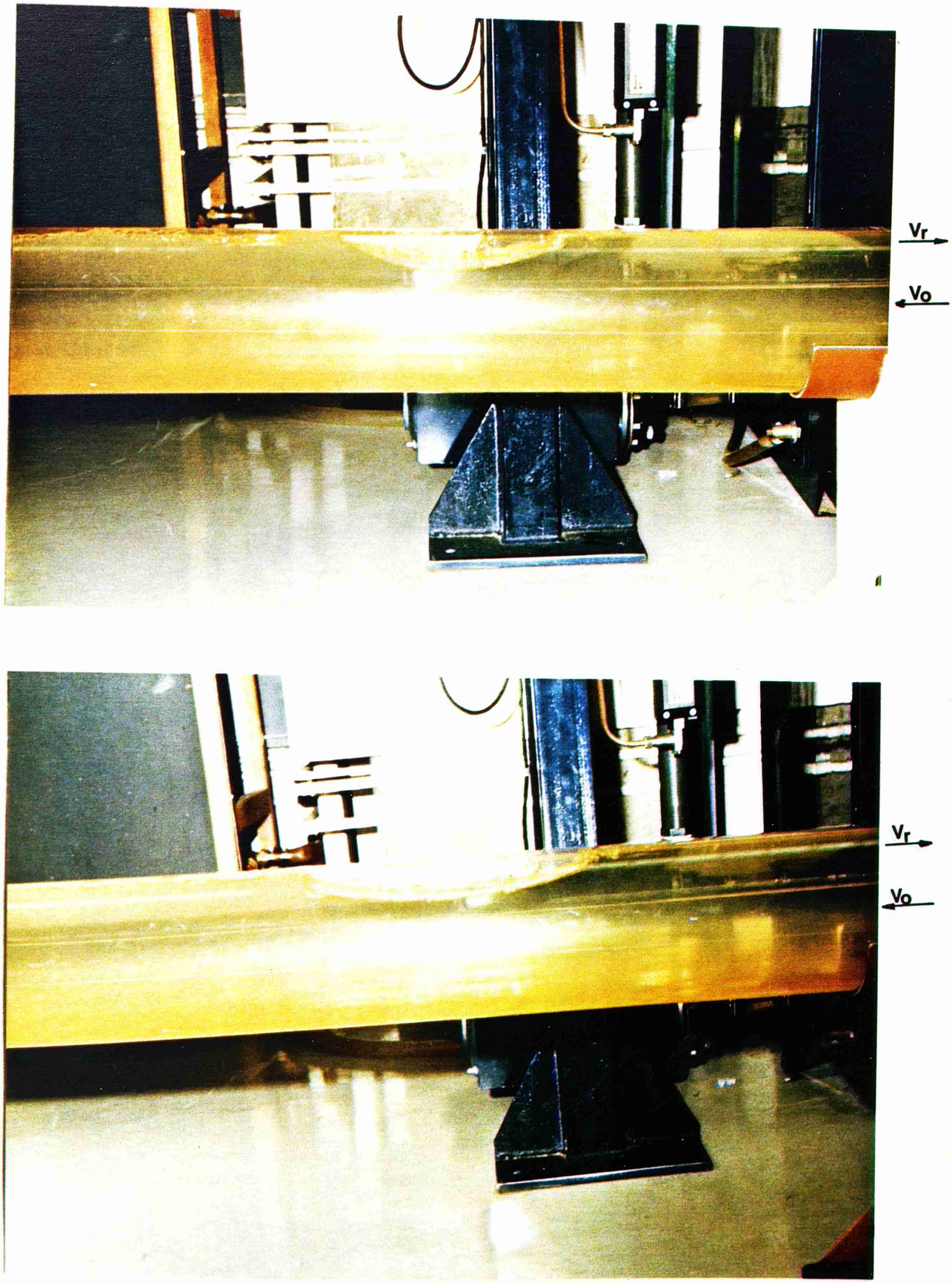

PLATE (6.7) LARGE AIR POCKETS BLOWING BACK UP THE TUNNEL AT -1.5° WITH HORIZONTAL

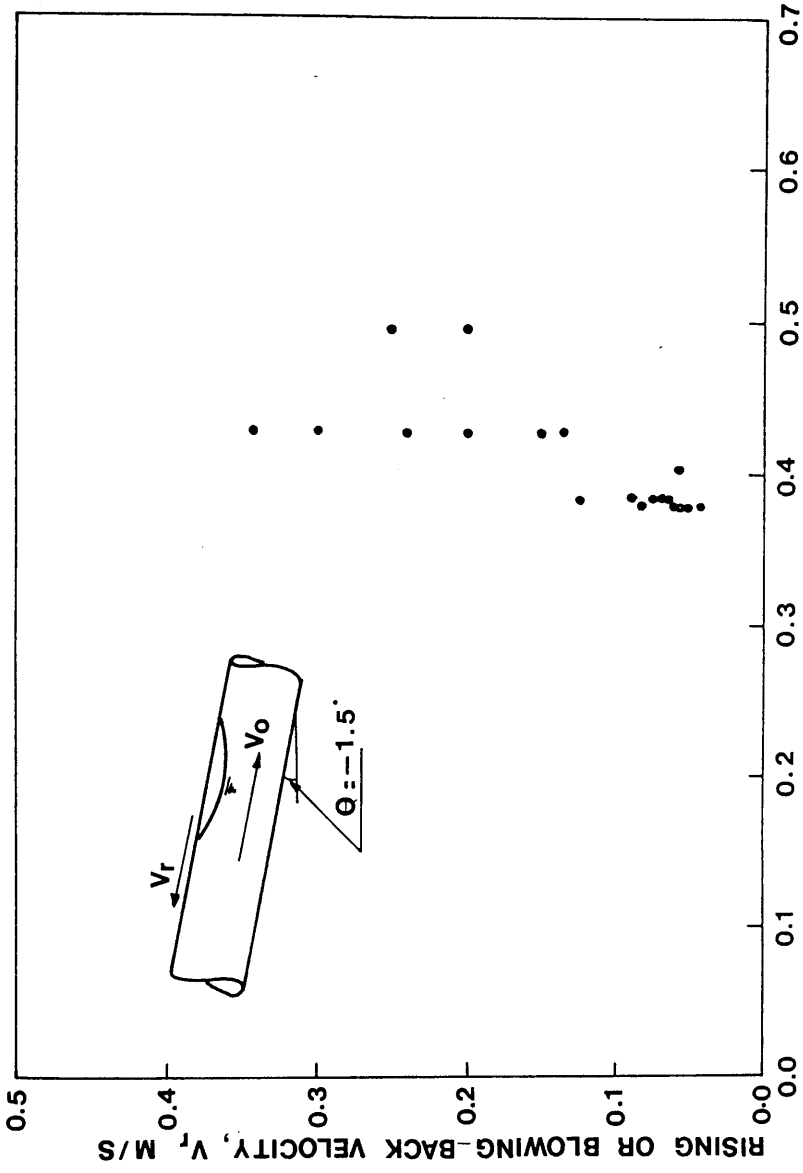

FIG. (6.10) RELATION BETWEEN THE RISING VELOCITY OF AIR POCKET AND THE FROUDE NUMBER FOR A TUNNEL LAID AT -1.5° WITH HORIZONTAL

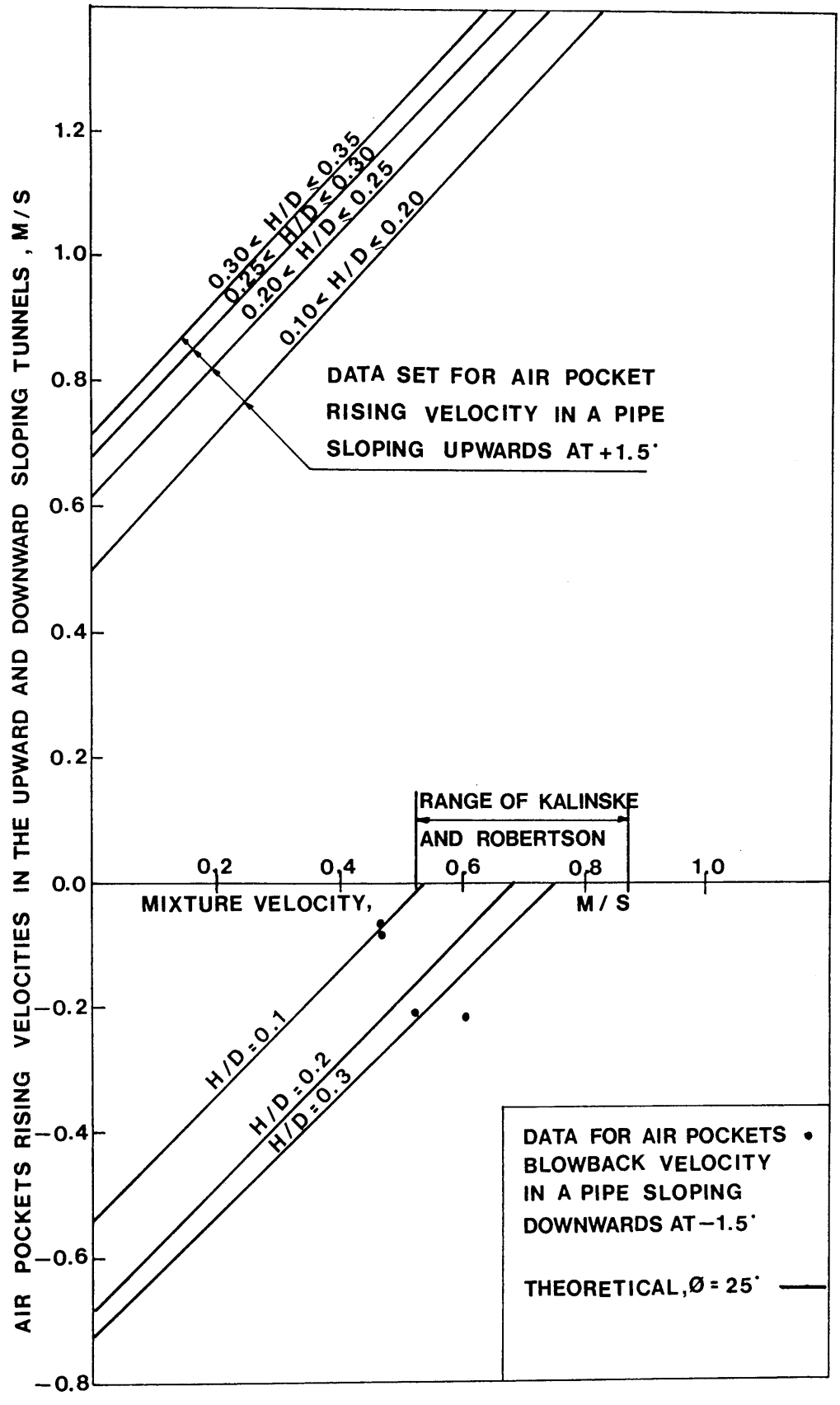

FIG. (6.11) THE RELATION BETWEEN AIR POCKET RISING VELOCITY AND MIXTURE VELOCITY FOR THE UPWARD AND DOWNWARD SLOPING TUNNEL FROM AUTHOR'S EXPERIMENTAL AND THEORETICAL DATA AND PREVIOUS RESEARCH

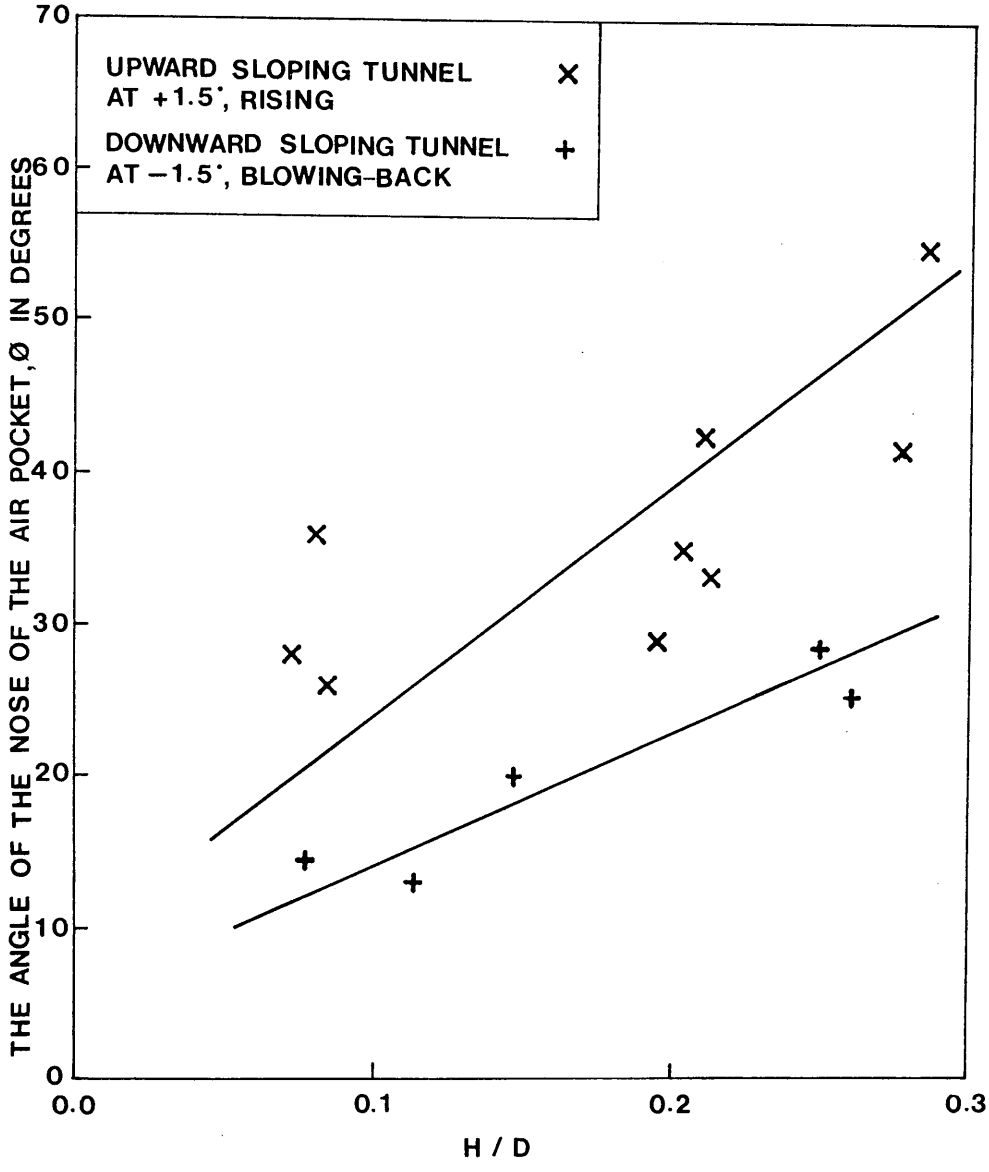

FIG. (6.12) THE ANGLE OF THE NOSE OF AIR POCKET WITH PIPE WALL FOR THE UPWARD AND DOWNWARD SLOPING TUNNEL

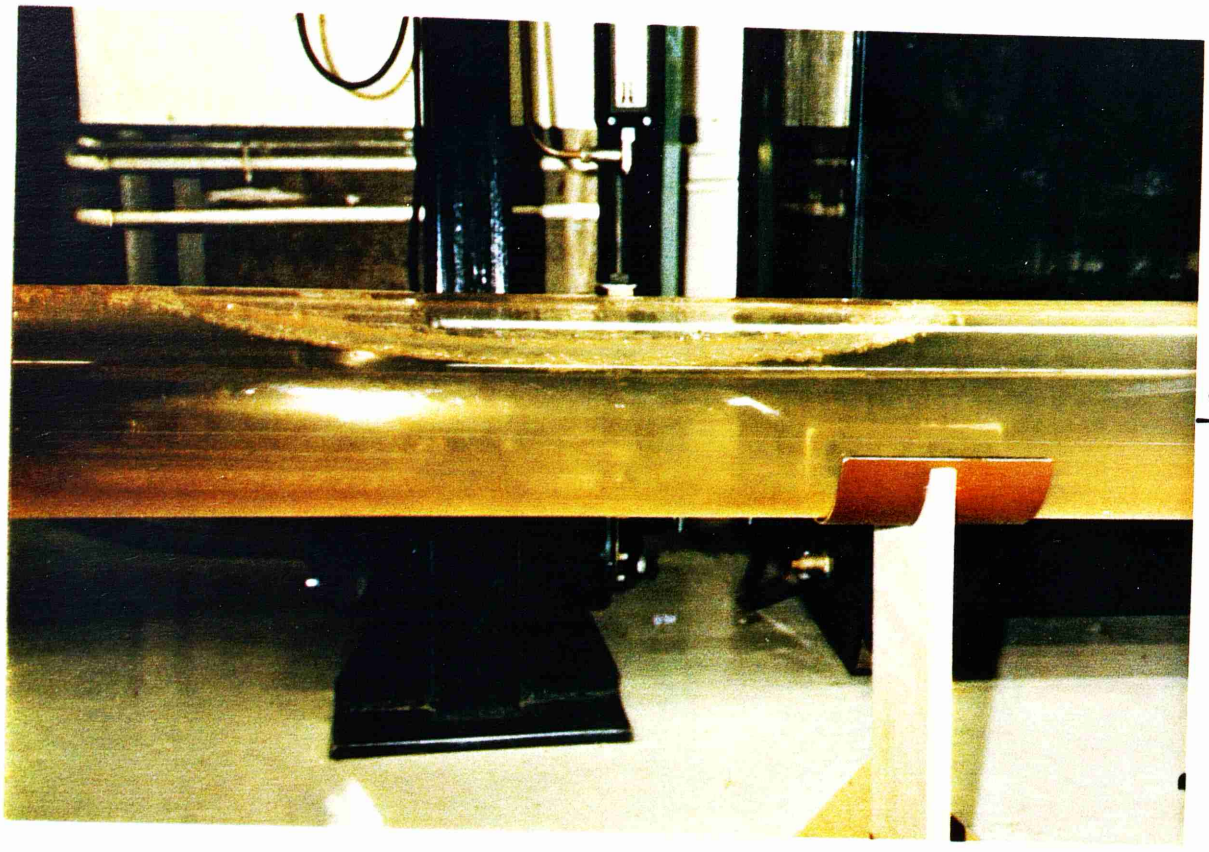

PLATE (6.8) AIR POCKET CLEARING ALONG THE TUNNEL AT -1.5° WITH HORIZONTAL

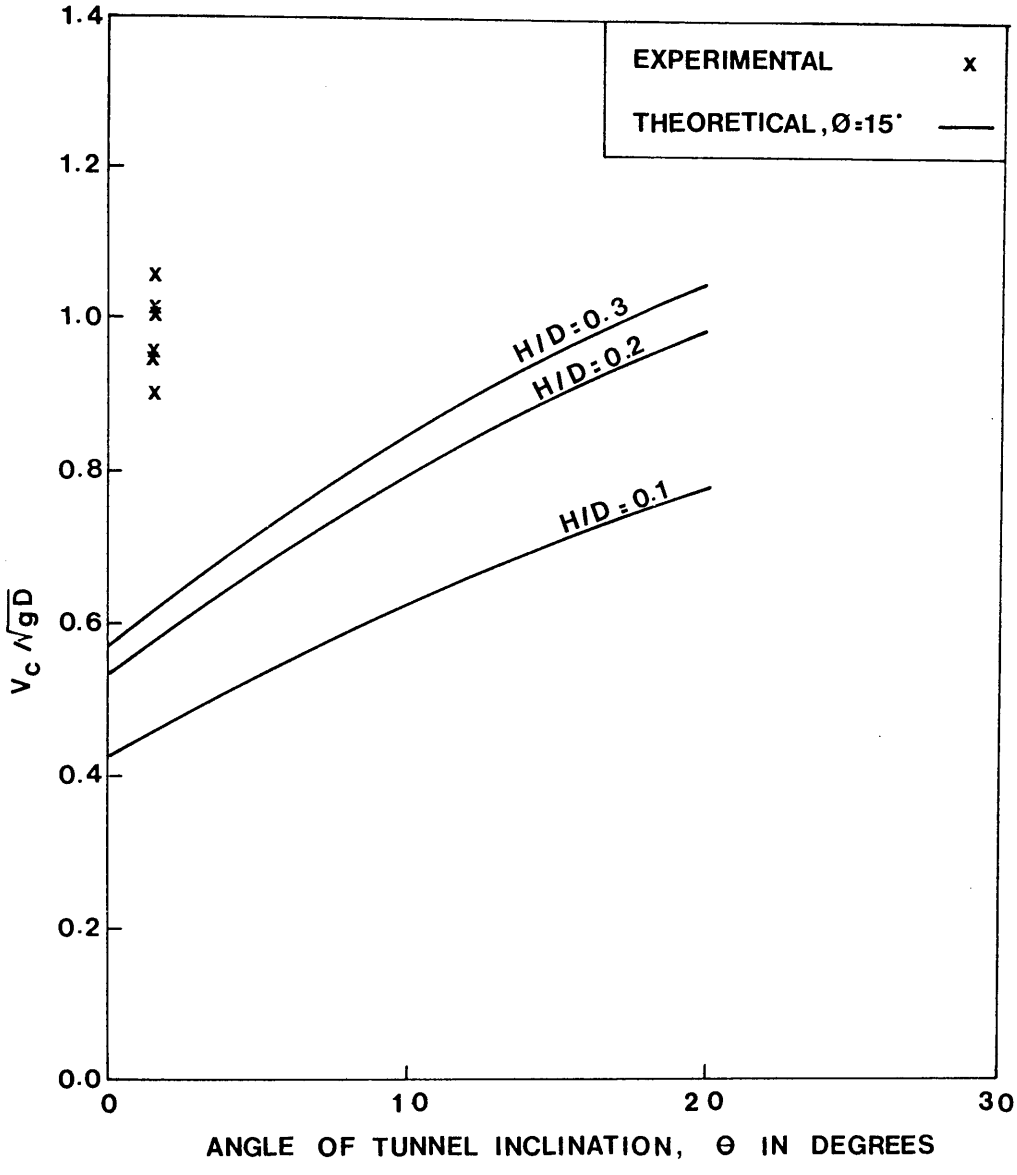

FIG. (6.13) RELATION BETWEEN THE CLEARING VELOCITY OF AIR POCKETS AND ANGLE OF INCLINATION BELOW THE HORIZONTAL

Chapter Seven

COMPARISON OF THE EXPERIMENTAL RESULTS WITH THEORETICAL MODELS AND PREVIOUS RESEARCH DATA

7.1 INTRODUCTION

In this chapter a comparison will be carried out between the experimental results and theoretical models for air pockets forming at the junction of the vertical dropshaft/tunnel system, for the nine geometries tested. This will include regime 1 with air bubbles and air pockets venting or blowing back up the vertical shaft, regime 2 with a stable air pocket and subcritical flow under the pocket, and regime 3 with a stable air pocket with a hydraulic jump at its end. An empirical equation, based on the experimental results, will be derived for regime 4 for air pockets clearing from the bend, as outlined in Section (3.6.4). A comparison will be carried out between the experimental results and theoretical models for air pockets in straight pipes with the pipe sloping upward and downward, and for air pockets clearing or blowing back. Finally, a comparison will be carried out between the experimental results and theoretical models with the results available from previous research.

7.2 COMPARISON OF THE EXPERIMENTAL RESULTS WITH THEORETICAL MODELS FOR AIR POCKETS AT THE BEND

It was outlined in Section (5.2) that four general stable flow regimes occurred for air pocket formation at the junction of the vertical dropshaft/tunnel system. This was based on extensive visual and photographic observations. In the following sections a comparison will be carried out between the experimental data and the

theoretical models for each flow regime, where the experimental data will be plotted together with the appropriate theoretical model to determine the extent, if any, to which each model can be applied. In the interests of brevity, the comparison will be carried out mainly for the experimental results of the horizontal tunnel, except for Model Type 3 where the effect of angle of tunnel inclination will be included in analysing the stable hydraulic jump behaviour. The comparison will include air pockets blowing back up the vertical shaft, air pockets with a drowned jump and air pockets with a hydraulic jump at their end, but will exclude stratified flow data.

7.2.1 Comparison with Model Type 1

Model Type 1 is for the air pockets venting or blowing back up the vertical shaft. Equation (3.56) has been derived in an attempt to represent this type of air pocket. It was found from the experimental data in Chapter (5) that air pockets can blowback up to a specific Froude number for each bend radius. Figure (5.19) for instance shows the pipe full Froude number $V_o/\sqrt{gD}$, up to which blowback is possible for each value of bend radius. It is noted that the Froude number decreases slightly with increasing value of air/water ratio. This is to be expected as the force exerted by the oncoming flow on the air pocket must be a function of ρV^2. As β is increased the density term ρ decreases, but the interstitial or average velocity V, increases. Thus the term V^2 increases more than ρ decreases allowing smaller blowback Froude numbers with increasing β.

It was decided that an empirical correlation of the blowback Froude number related to the value of R'/D, β and tunnel angle θ, may not be of great practical benefit, and in any case would not be able to predict the air pocket depth, H/D, at the bend. It was decided instead to compare the experimental data in this region with equation (3.56) to define its applicability to air pockets blowing back. The experimental results, together with equation (3.56), are shown in

Fig. (7.1) for three bend radii of R'/D = 0.5, 1.0 and 1.5 and for the horizontal tunnel. It should be noted from Fig. (7.1) that the experimental data points are for cases of air pockets blowing back, and only a few instances of this occurred for the sharp bend, R'/D = 0.5. Secondly, the theoretical curves from equation (3.56), are for the case of $\beta = 0$, and hence represent the upper limit of blowback Froude number. Figure (7.1) is thus a comparison between the theoretical upper limit and experimental data, and in that sense, the blowback model seems to give reasonable correlation with data, especially for larger radiused bends and at shallower pocket depths. Of course the experimental data points in Fig. (7.1) have a definite value of air/water ratio β, and hence a better comparison can be carried out with equation (3.57), the theoretical model incorporating the β value. This is shown in Fig. (7.2a) for the case of R'/D = 1.0 and Fig. (7.2b) for the case of R'/D = 1.5. It is noted that a good correlation exists for both radiused bends, giving some confidence in the simple blowback model proposed [equation (3.57)]. Returning to Fig. (7.1), it can be seen that some experimental data do not really fit the theoretical model. That is, in the range $Fr_o < 0.2$ and H/D = 0.05 to 0.15. The reason for this is not immediately clear, but most of those data points represent very short length pockets at the bend, which are also shallow in depth and appear often as a small separation region at the bend, and may not fit the gross assumptions of the blowback model outlined in Section (3.6.1).

Another important point from equations (3.56) and (3.57) is that none of the sharp bend experimental data (R'/D = 0.5) fitted the theoretical blowback model. This is illustrated in Fig. (7.3) where equation (3.57) is compared with all the sharp bend experimental data in the low Froude number range. It is clear that little correlation exists, and for a given Froude number of flow ($V_o/\sqrt{gD}$), and β value, the air pocket depth is greater than predicted from the blowback model. It should be noted that in a sharp bend, even at low Froude numbers, the flow separates at the sharp edge, implying that a

stagnation point is generally not the case, hence rendering equation (3.57) invalid.

Hence, the first conclusion regarding blowback model type 1, is that it gives reasonable correlation with experimental data in radiused bends R'/D = 1.0 and 1.5, it gives little or no correlation with sharp bends, it applies only to the region where air pockets can definitely blowback, and is dependent on a knowledge of the angle Φ [see Fig. (3.17)]. One drawback with equation (3.57) is that the angle Φ in fact changes with the Froude number, where Φ is defined in Fig. (3.17). At higher Froude numbers, even in the blowback zone, the air pocket gets pushed further towards the tunnel section and Φ is reduced. Typical values of Φ at the bend are 30^{o} to 70^{o} .

7.2.2 Comparison with Model Type 2

Model Type 2 is for stable air pockets with subcritical flow under the pocket. Visual and photographic evidence has revealed this regime to be similar to a drowned jump, as described in Section (3.6.2), and occurs usually as a prelude to the stable jump, regime 3. It should be noted that this regime 2 excludes all data points with a tendency to blowback, and is effectively concentrated in the sharp bend data with the tunnel sloping upwards or horizontal. Only a few data points exist for the radiused bends where the air pocket is not blowing back or forming a stable hydraulic jump.

A comparison between regime 2 data and the drowned jump theoretical model, equation (3.67), is given in Fig. (7.4) for the case of the horizontal tunnel. The experimental data points represent definite cases of the drowned jump where neither blowback nor a stable hydraulic jump occurred. The theoretical curves have been computed from equation (3.67) for the case of R'/D = 1.0 and varying β. An inspection of equation (3.67) will reveal the difficulty in computing this relationship for the sharp bend, R'/D = 0.5, in that the correction factors α_o and α' are theoretically

infinite for R'/D = 0.5, but have been calculated accurately for R'/D = 1.0 and 1.5. In fact, measurement of α_o and α' in the sharp bend would be virtually impossible because the quantities of air bubbles in the flow negate the use of pitot-static tube or laser doppler to determine the three-dimensional streamline pattern. However, it can be seen from Fig. (7.4) that equation (3.67) fits the experimental data reasonably well for all three values of R'/D and some confidence can be expressed in its use.

It does lead to the conclusion that air pockets forming at sharp bends fit the drowned jump model incorporating flow separation at the corner of the bend, and do not fit the blowback model with a stagnation point at the corner of the bend. Radiused bends in general have the opposite effect, fitting the blowback model more than the drowned jump model.

7.2.3 Comparison with Model Type 3

Model Type 3 is applicable to air pockets with a stable hydraulic jump at their end, where two approaches were used to achieve a relation between the Froude number of the flowing water and the maximum depth of the air pocket at the bend. The two solutions are represented by equations (3.74) and (3.87) using the energy principle and the force-momentum balance respectively. The former solution was derived for a horizontal tunnel, while the latter was derived with consideration for the angle of inclination of the tunnel with the horizontal.

In the experimental testing programme air pockets with a hydraulic jump at their downstream end formed in each of the nine geometries tested, and these constituted the bulk of the experimental data. These bend air pockets were stable but sometimes extended in length to the outlet tank forming stratified flow. Since it is not clear if the force-momentum balance can still be applied for such air pockets, the results for stratified flow will be excluded from the

comparison with the theoretical models. To get a clear idea of the applicability of the derived theoretical models for such stable hydraulic jump air pockets, a curve representing each value of air/water ratio β, and for each angle of tunnel inclination θ, will be plotted, together with the experimental results representing these two variables. The experimental results for the horizontal tunnel and the three bend radii tested are plotted in Figs. (7.5) to (7.8), together with the energy equation (3.74) and force-momentum equation (3.87), for air/water ratios β = 0.1 - 0.4 respectively. It can be noted that both solutions give a reasonable representation of the experimental results with the force-momentum equation proving the more accurate predictor. It is perhaps worth remembering here that the energy equation (3.74) computes H/D for the bend air pocket assuming conditions are known at the upstream nose of the pocket at the bend. The force-momentum equation is applied across the hydraulic jump and assumes known conditions downstream of the jump. This is much more simple to apply and probably more accurate, because downstream of the jump the pipe is straight and correction factors are closer to unity, whereas at the upstream air pocket nose at the bend the flow pattern is much more complex and difficult to assess. In fact, the energy equation (3.74) plotted in Figs. (7.5) to (7.8) is for the sharp bend only since applying it to other bend radii requires an accurate value of the angle of the nose of the air pocket with horizontal ϕ as well as other correction factors. An attempt to plot this equation for assumed values of the angle ϕ shifted the curve far to the right in Figs. (7.5) to (7.8), away from the experimental results. This means that the force-momentum balance is more reliable in representing the characteristics of flow below the air pocket, especially when the air pocket is reasonably long so that the effects of the complicated flow around the bend will cease near the toe of the hydraulic jump. It is noted in Figs (7.5) to (7.8) that a fair degree of experimental scatter occurs, especially in the β = 0.1 graph, but nevertheless, equation (3.87) seems a good predictor of the air pocket depth/Froude number relationship, for varying values of air/water ratio at the bend, and for the range of

bend radii tested.

The experimental results for the stable hydraulic jump for the other two angles of tunnel inclination tested are also compared with the theoretical model given in equation (3.87), where the effect of the angle of tunnel inclination has been introduced. The theoretical curve for each air/water ratio β and for each angle of inclination θ is also plotted on a separate graph, together with the experimental results for the three bend radii tested in the same range. These results are shown in Figs. (7.9) to (7.12) for the upward sloping tunnel with an angle of inclination $\theta = +1.5°$, and in Figs. (7.13) to (7.16) for the downward sloping tunnel with $\theta = -1.5°$. It can be noted from the above Figures that equation (3.87) gives a reasonable agreement with the experimental results, albeit with a slightly wider scatter of experimental data compared with the horizontal tunnel case. Fewer experimental results were available for the downward sloping tunnel which is due to the fact that stratified flow dominated the flow regimes for this slope, with air pockets extending to the outlet tunnel, when equation (3.87) could not be applied.

The effect of the angle of inclination on the theoretical model can be clearly seen in Figs. (7.5) to (7.16) where the upward sloping tunnel shifted the curve to the right of the horizontal one, while the downward sloping tunnel shifted the curve to the left. This was also clearly reflected in the trends of the experimental data, where in regime 3 behaviour excluding stratified flow, the upward sloping tunnel produced the deepest bend air pockets for a given Froude number and β value, whereas the downward sloping tunnel gave the shallowest pockets.

The effect of varying the air/water ratio β can also be clearly seen in Figs. (7.5) to (7.16) for regime 3 behaviour. In every case the curve moved to the left, implying shallower bend air pockets for increasing β. This is exactly the opposite of regimes 1

and 2, for blowback and drowned jump conditions, where an increasing air/water ratio increased the air pocket depth.

In broad terms, it can be said that equation (3.87) can be used to compute the bend air pocket depth (H/D) for a given value of upstream Froude number (Fr_o), tunnel inclination (θ), air/water ratio (β) and bend radius (R'/D), for the case of a stable hydraulic jump at the downstream end of the pocket. This appears to become more accurate for reasonably long air pockets where the effects of the flow at the bend can be neglected. At the same time equation (3.87) cannot be applied for the stratified flow points, because the force-momentum balance is unknown in the case of the air pocket extending to the outlet tank.

It is now apparent from Sections (7.2.1), (7.2.2) and (7.2.3) that the three theoretical models appear to give good predictions of the air pocket depth for the range of other parameters, at least for regimes 1, 2 and 3. This means that a "synthetic" or theoretical prediction can now be made for a wide range of conditions at the bend and this will be discussed in more detail in the discussion in Chapter (8). Regime 4 incorporating air pockets clearing from the bend was found to be not amenable to simplified theoretical analysis and hence resort was made to empirical equations.

7.3 EMPIRICAL EQUATIONS FOR AIR POCKETS CLEARING FROM THE BEND

It has already been noted in Section (3.6.4), for Model Type 4, that great difficulty was experienced in deriving a theoretical model for air pockets clearing completely from the bend. This is due to the fact that at least four different mechanisms were found to be responsible for clearing. (a) Partial clearing due to entrainment of air bubbles at the toe of the hydraulic jump at the

downstream end of the pocket, (b) the formation of large amplitude waves under the pocket, sealing the conduit roof and sweeping the air pocket out, (c) in the sharp bend an alternating swirl around the conduit roof partly cleared the pocket, and (d) the undulating roller of the hydraulic jump sheared-off downstream sections of the air pocket.

As a result, empirical equations have been formulated based on the β - Fr_o graphs in Chapter (5). This has been done for each angle of inclination and bend radius tested, where a line was obtained by regression analysis for the points at which clearing started. The equations are given in the form of the non-dimensional pipe-full water velocity ($Vo/\sqrt{gD}$) at which clearing commenced, and will be denoted at Fr_{oc}. It must be emphasised that the clearing velocity was dependent on a range of parameters including the velocity and the Froude number below the air pocket, the flow characteristics at the bend as well as the air/water ratio, and the angle of inclination of the tunnel. The following are the empirical equations for the clearing of air pockets:

1. The horizontal tunnel, $\theta = 0°$

(a) $R'/D = 0.5$

$$Fr_{oc} = 0.460911 + 0.593907\ Q_A/Q_w \qquad (7.1)$$

(b) $R'/D = 1.0$

$$Fr_{oc} = 0.613150 + 0.909964\ Q_A/Q_w \qquad (7.2)$$

(c) $R'/D = 1.5$

$$Fr_{oc} = 0.666464 + 1.40771\ Q_A/Q_w \qquad (7.3)$$

2. The upward sloping tunnel, $\theta = +1.5°$

(a) $R'/D = 0.5$

$$Fr_{oc} = 0.556249 + 0.289038\ Q_A/Q_w \qquad (7.4)$$

(b) $R'/D = 1.0$

$$Fr_{oc} = 0.770341 + 0.751368\ Q_A/Q_w \qquad (7.5)$$

(c) $R'/D = 1.5$

$$Fr_{oc} = 0.769054 + 1.005251\ Q_A/Q_w \qquad (7.6)$$

3. The downward sloping tunnel, $\theta = -1.5°$

(a) $R'/D = 0.5$

$$Fr_{oc} = 0.876167 + 0.450999\ Q_A/Q_w \qquad (7.7)$$

(b) $R'/D = 1.0$

$$Fr_{oc} = 0.82247 + 1.89107\ Q_A/Q_w \qquad (7.8)$$

(c) $R'/D = 1.5$

$$Fr_{oc} = 0.852092 + 1.866349\ Q_A/Q_w \qquad (7.9)$$

An alternative method of presenting equations (7.1) to (7.9) is in the form:

$$Fr_{oc} = A + B\ (Q_A/Q_w) \qquad (7.10)$$

where the values of A and B vary with bend radius R'/D and tunnel slope, θ. Values of A for the nine geometries are plotted in Fig. (7.17a), and the corresponding values of B in Fig. (7.17b). The values of A represent the pipe-full Froude number required to clear an air pocket from the bend, when the ratio of air to water is very small or tends towards zero. It can be seen from Fig. (7.17a) that this is almost constant for the downward sloping tunnel ($Fr_{oc} \simeq 0.85$), whereas in the horizontal and upward sloping tunnel, A increases with bend radius R'/D, although there is evidence of a levelling-off of the value of A at higher R'/D ratios. In fact, an infinite value of R'/D would correspond to a straight pipe and hence the $\theta = 0°$ and $+1.5°$ tunnels should theoretically give a zero value of A, as any flow above zero will produce clearing. It also appears from Fig. (7.17a) that the upward sloping tunnel requires larger Froude numbers for clearing. This is misleading because the values of B in Fig. (7.17b) also need to be taken into account.

Values of B represent the inverse of the clearing line slope on the β - Fr_o graphs in Chapter (5). A zero value of B would be a vertical clearing line and show no influence from the ratio of air to water, whereas a high value of B represents a shallow slope and a high influence of the ratio of air to water. It can be seen from Fig. (7.17b) that the value of B increases almost linearly with bend radius for the horizontal and upward sloping tunnels, and the value of B is higher in the horizontal tunnel compared with the upward sloping one. This means that for low values of air/water ratio, clearing is easier for $\theta = 0°$ than $\theta = +1.5°$, whereas for higher values of air/water ratio the opposite is the case.

It was hoped that a unified clearing equation might be possible incorporating the full range of β, R'/D and θ. This was not achieved due to the complexity of the clearing process.

One idea which did emerge, concerned the scale effects likely to be relevant to the clearing process. When clearing occurs

by the air entrainment process then substantial scale effects are to be expected[53,162], but when clearing occurs by the action of large amplitude waves sealing the conduit roof, as often happened in this experimental work, then in a reasonable sized model waves will scale on a Froude basis, and hence clearing should also be the same. Thus the values of A and B outlined above should be broadly aplicable to other larger model or prototype scales.

7.4 COMPARISON OF THE EXPERIMENTAL RESULTS WITH SIMPLE THEORETICAL MODELS FOR AIR POCKETS IN STRAIGHT PIPES

In this section a comparison will be carried out between the experimental data of the rising velocity of air pockets in the upward sloping tunnel and the theoretical model derived in Section (3.7) for air pockets rising in straight pipes. Also a comparison of the experimental results for the blowing back velocity of air pockets in the downward sloping tunnel will be carried out with the theoretical model derived in Section (3.8.1), albeit over a limited range of experimental data points as explained in Chapter (6). For air pockets clearing downstream in the downward sloping tunnel there is very limited experimental data to compare with the theoretical model derived in Section (3.8.2) and these air pockets, as outlined in Chapter (6), were very large in size and hence the theoretical model cannot be applied to them, so comparison of the theoretical model will be carried out in section (7.5) with the available experimental results of previous investigators.

7.4.1 Air Pockets Rising in the Upward Sloping Tunnel

The rising velocity of air pockets in the upward sloping tunnel with an angle of +1.5° with horizontal was, as expected, higher than the water velocity and depends on the size of the rising air pocket characterised by the parameter H/D, the maximum depth of the air pocket. The rise velocity is also dependent on the conduit slope θ, as seen in equation (3.100), but the conduit slope was not

varied in this section of the work. The experimental correlations obtained by regression analysis for the rising velocity of air pockets are given in Section (6.2), and are plotted again in Fig. (7.18), together with the theoretical model given in equation (3.100). Equation (3.100) is plotted using the mixture velocity $V_o(1+\beta)$, as given in equation (3.100a), in order to compare it with the experimental results.

It can be noted from Fig. (7.18) that the slope of the lines representing the experimental results are slightly steeper than those of the theoretical model, although the experimental lines are for a range of H/D values rather than one specific value of H/D as in the theoretical model. It should be noted from Fig. (7.18) that the intercept points, where $V_o(1+\beta) = 0$, gave a good comparison between the theoretical model, equations (3.100) and (3.100a), and the experimental data points. The theoretical value of the intercept corresponds to $V_o = 0$ in equation (3.100) and hence is dependent on A_1/Ap (or H/D), Θ and ϕ. A value of ϕ of 60° was used in these theoretical lines, and hence an even better correlation might have been obtained by varying ϕ. The only disagreement between theory and experiment in Fig. (7.18) is in fact the slope of the theoretical lines, which appear to be slightly less than that of the experimental lines. This can be explained with reference to equation (3.100a):

$$V_r = K\sqrt{gD} + V_o(1+\beta)$$

which gives a slope of unity in Fig. (7.18), Wallis[177] pointed out that the value of slope should be between 1.0 and 1.2, reflecting the "wake" effect of a succession of air pockets. Hence, an almost perfect correlation would have been obtained in this work with a factor of 1.1 to account for the wake effect.

Thus, an almost perfect correlation between theory and experiment for air pocket speed in a pipe sloping upwards at +1.5° is given by:

$$V_r = [\text{Cos}\theta(1 - \frac{A_1}{Ap}\text{Cosa}_1 - \frac{2}{3\pi}\text{Sin}^3 a_1) + \frac{2H}{D\text{tan}\phi}\text{Sin}\theta(1 + \frac{A_1}{Ap})]^{1/2} \times$$

$$[\frac{gD}{2Ap}]^{1/2} + 1.1\ V_o(1+\beta) \qquad (7.11)$$

$$(\frac{}{A_1} - 1)$$

7.4.2 Air Pockets Blowing Back in the Downward Sloping Tunnel

The blowback velocity of air pockets in the downward sloping tunnel with an angle of -1.5° with horizontal was recorded manually, which meant that simultaneous recording of the blowback velocity, depth H/D and air pocket nose angle ϕ was not possible. Instead, the blowback velocity was recorded and only a small range of data was possible because of the design of the apparatus, and hence recourse was made to photography to record air pocket depths H/D, and ϕ later. The values of ϕ were generally in the range 12° to 30° when H/D varied between 0.05 to 0.30, as shown in Fig. (6.12). The theoretical rising velocity given in equation (3.105) is shown in Fig. (7.19) with the limited range of experimental results. It can be noted that the range of the blowing back velocities is partly within the limit of the theoretical lines and partly higher than it. This shows the great effect of the size (H/D) of the blowing back air pocket on the rising velocity, although the theory does not appear to adequately cover the data. The theoretical lines in Fig. (6.19) were drawn with a constant ϕ value of 20° and better correlation with experimental results might be obtained if the full range of ϕ values had been drawn. The agreement between the experimental and theoretical rising velocities is reasonable although more work must be done to relate air pocket depth H/D, with the angle ϕ. Still, the theoretical model gives an indication of the expected blowing back velocity of such air pockets in a downward sloping tunnel.

7.5 COMPARISON OF THEORETICAL AND EXPERIMENTAL RESULTS WITH PREVIOUS RESEARCH

In this section a comparison will be carried out between the theoretical models and experimental results of this research and the previous theoretical and experimental research. This will be done for the air pockets at the junction of the vertical dropshaft/tunnel system and for air pockets in straight pipes sloping upward and downward. A lot of the previous research has been for air pockets in straight pipes with stationary water conditions. Very little systematic research has been reported on the case of air pockets trapped at the junction of the dropshaft/tunnel system, so it will appear as if most of the comparison is done for air pockets in straight pipes.

7.5.1 Air pockets at the Dropshaft/Tunnel Bend

The blowback and clearing limits of air pockets forming at the junction of a vertical dropshaft/tunnel system from the author's experimental results will be compared with the available results of similar research. So far the only direct comparative experimental results are those of Goldring[63] who had tested four bend radii (R'/D = 0.5, 0.75, 1.0 and 1.5) for a circular pipe of 140 mmΦ, and one bend radius for another three pipe diameters. Goldring's results for the pipe of 140 mmΦ will be compared with the present work although the range of air/water ratio, β, tested by Goldring was only up to 2% representing air bubbles coming out of solution in the outfall of the cooling water system of a nuclear power station. This ratio of 2% is very low compared to β values found in dropshaft/tunnel spillways.

The comparison of the lines representing the upper limit of blowback for the bends R'/D = 0.5, 1.0 and 1.5 are shown in Fig. (7.20a) for air/water ratio against the upstream non-dimensional water velocity. It can be noted that the author's blowback limits

are affected by the increase in air/water ratio β, where an increase in the value of β reduces the Froude number of the upper limit of the blowback phenomena. The blowback lines from Goldring's results are vertical and are not affected by the increase in the air/water ratio β although this might be due to small range of β values tested. This means that Goldring's empirical equation for blowback may not be satisfactory for higher values of air/water ratios. It also can be noted that Goldring's blowback lines are to the right of the blowback lines of this work for the similar bend radii.

The reason for this is not immediately clear. The most obvious reason is experimental error either on the part of the author, or Goldring, or both. Another possibility is that of scale effects. Goldring's lines plotted in Fig. (7.20a) are for a pipe diameter of 140 mm. It should be noted that when Goldring chose one radius value and tested four different pipe diameters from 0.072 m to 0.19 m, the blowback line remained constant at the same Froude number, implying that scale effects for blowback phenomenon are negligible. Unfortunately the only prototype data available for blowback from a dropshaft/tunnel bend is that of Hunterston 'B' Power Station, where it was noted that blowback occurred at 25% of maximum water discharge (Ref. 165) or a Froude number of 0.139. Unfortunately, a systematic prototype investigation was not carried out, and hence the upper limits of blowback in the 3.353 m diameter Hunterston system are not known.

In general, it is thought that the upper limit for blowback is not subject to significant scale effects. If the model and prototype have the same ratio of air to water reaching the bend at the same Froude number of flow, then the shape and size of the pocket should be scaled on a Froude basis, which in turn would imply that the same Froude number would be required to prevent blowback in both. The only problem is that it is not likely that model and prototype will have the same value of β at the same Froude number and hence differences may exist. This is compounded by the fact that for the

same Froude number the prototype will have larger velocities passing under the air pocket at the bend which will facilitate a faster removal of air reaching the bend, and hence make blowback less likely. Thus it could be postulated that the blowback lines in Fig. (7.20a) may be moved slightly to the left for a prototype structure but not significantly so.

The comparison of the clearing lines is shown in Fig. (7.20b) where it is noted that there is a big difference between the author's and Goldring's results, the author's lines for clearing being steeper. This is in fact due to low air/water ratio β used in Goldring's tests, where the effect of air concentration on the flow around the bend was negligible comapred to the present work. The high values of β increased the mixture velocity, the strength of the alternating flow at the bend, and formed waves which aided in removing the air pocket from the bend. For low air/water ratios the air pocket can stay stable for higher values of water discharge and starts to clear by air entrainment at the toe of the jump. In fact this was noticed in the downward sloping tunnel, where for low values of β the air pocket starts to reduce in size by air entrainment at its end. For slightly higher values of β the air pocket was cleared by a combination of waves sealing the bend and air entrainment at the toe of the jump. Increasing β more caused the air pocket to clear only by the waves sealing the bend. Thus in Goldring's work, with $\beta \leq 0.02$, the bend air pocket adjusted to form a Froude number under the pocket where all the air was removed by entrainment at the toe of the jump. This type of hydraulic jump at the bend can realistically only remove air/water ratios up to around 3%. For air/water ratios greater than this clearing occurs by a completely different mechanism, i.e. waves sealing the conduit roof, and hence the two sets of data in Fig. (7.20b) are comparing different mechanisms. In other words, Goldring's clearing lines are not relevant to higher ratios of air to water, β, and cannot be extended say beyond β of 0.03. The reason for the 3% limit is given by Kalinske and

Robertson's equation for air removal at an hydraulic jump:

$$\beta = 0.0066(Fr_1 - 1)^{1.4} \qquad (7.12)$$

It was found that Froude numbers under the pocket do not often exceed 4, and substitution into equation (7.12) gives $\beta \leq 0.03$.

7.5.2 Air Pockets in Straight Pipes

In this section the experimental and theoretical results of the author will be compared with previous research for air pockets rising, blowing back and clearing in straight pipes inclined above and below the horizontal, and for stationary and moving water.

If we consider first the case of air pocket speeds in a pipe inclined upwards at +1.5° as shown in Fig. (6.7) and Fig. (7.18). This work has been carried out for the case of moving water. Unfortunately, a great deal of the previous work on air pocket speeds has been carried out for the stationary water case, Bacopoulous[14], Benjamin[24] and Baines and Wilkinson[15], the latter two of which worked with rectangular section conduits. However, it is postulated, that if we take the extrapolated intercept points in Fig. (6.7) and (6.18) corresponding to a zero water velocity ($V_o = 0$) then the author's data could be considered as the equivalent stationary water case. This is shown in Fig. (7.21) with the air pocket rise velocity plotted against the air pocket depth, H/D, where the data is plotted for the rise velocity of air pockets in stationary water. It can be noted that the rising velocity increases with increasing depth of air pocket and is affected by the angle of tunnel inclination. The curves have the same trend and the author's results show good agreement with those of Bacopoulous remembering that these points were extrapolated from the experimental lines of the rising velocity of air pockets in moving water, when the lines intersect the vertical axis at $V_o = 0$. The results of Baines and Wilkinson using a potential flow model, are lower than those of

Bacopoulous and Benjamin where energy, momentum and continuity principles were used. It can be noted from Fig. (7.21) that the data and theory of Baines and Wilkinson, for a square conduit, is significantly lower than either Benjamin (continuous air cavity), Bacopoulous (single air cavities) and the author (extrapolated single air cavities). This may be a function of the conduit shape, square or circular, or the angle of inclination of the conduit above the horizontal, θ. In either case Fig. (7.21) highlights the variation of the air pocket speed with the maximum depth, H/D. Most authors quote this parameter as being much more important than the air pocket length, L/D, or the air pocket volume, $V/(\pi D^3/4)$. The other important feature of Fig. (7.21) is that force-momentum principles can now also be applied to the moving water case as evidenced by the close correlation between the author's data and Bacopoulous and Benjamin.

The author's equation for the rising velocity for air pockets in stationary water, $V_o = 0$ in equation (3.100), is also shown in Fig. (7.22) for the full range of conduit angles from 0° to 90°. Only two values of H/D are shown, with the angle of the cavity nose $\phi = 60°$ assumed in equation (3.100). The author's theoretical result is compared with experimental data of Gandenberger[59], Wisner et al[187], Zukoski[192] and Runge and Wallis[139]. It should be noted that these experimental data sets are simply correlations of the rise velocity in stationary water ($V_r/\sqrt{gD}$) with the conduit slope and with no reference to the air pocket depth H/D or the pocket nose angle ϕ. Hence proper comparison cannot be carried out. It is clear from Fig. (7.22) that equation (3.100) with $V_o = 0$ gives a very good correlation with these experimenters' data. It can be noted that their results lie in the range of the author's theoretical results. Gandenberger's and Wisner's results are very close to the curve of H/D = 0.1, while Zukoski's and Runge and Wallis's results are closer to the curve of H/D = 0.3. Although there is a disagreement for higher angles of inclination, this will be due to changes in the angle ϕ at higher conduit slopes. Figure (7.22)

shows that Zukoski and Runge and Wallis were probably dealing with larger air pockets, while Gandenberger and Wisner were probably dealing with smaller air pockets. In broad terms, it can be stated that the author's model for the rising velocity of air pockets when the water velocity, $V_o = 0$, can be used to anticipate the rising velocity of air pockets in stationary water, provided that accurate values of the angle Φ and H/D can be predicted for different angles of tunnel inclination. The relationship between H/D and Φ for air pockets rising in a conduit sloping upwards at +1.5° and blowing back in a conduit sloping downwards at - 1.5 ° has already been shown in Fig. (6.12) showing that the angle Φ increased with increasing air pocket depth H/D for both slopes.

The average rising velocity of air pockets in moving water obtained from the experimental results regardless of the value of H/D is plotted in Fig. (7.23) together with the experimental results of Parakh[125] for two different angles of inclination, but with pipe diameter of only 22 mm. It can be noted that the lines have almost the same slope, but the intercept where the mixture velocity is zero is much greater in the author's results. This is due to the fact that the author's line is for different sizes of air pockets with H/D in the range of 0.1 to 0.4, while Parakh did not quote any value for the depth of air pockets. Parakh's intercept for $\Theta = 5°$ is almost identical with that given in equation (6.2) for the range $0.1 < H/D \leq 0.2$, implying that Parakh may have been dealing with smaller air pockets. As well as this we have the distinct possibility of surface tension scale effects, as shown in Fig. (2.4). The comparison of the rise velocity between a pipe of 22 mm diameter and a pipe of 152 mm diameter at say a conduit angle $\Theta = 0°$ reveals a variation in $V_r/\sqrt{gD}$ from around 0.35 to 0.54 which is roughly in line with the variation in intercept points in Fig. (7.23).

It follows therefore that a definite prediction of air pocket speed can only be obtained when H/D, Φ and the physical scale of conduit are taken into account.

For the case of air pockets blowing back or clearing from a downward sloping pipe, the theoretical model, equation (3.106), will be used. In this model the air pocket is assumed to be held stationary and the water velocity required to achieve this is calculated. Below this value of water velocity the pocket will blow back, and above it the pocket will clear downstream. The author's model is plotted in Fig. (7.24) for H/D = 0.1 and 0.3, and for Φ = 30° and 40°, together with the experimental results of Gandenberger[59], Wisner et al[187], Kent[97] and Kalinske and Robertson[94]. Below the curves in Fig. (7.24) blowback occurs and above, clearing occurs. It can be noted that generally there is a good agreement between the author's curves and previous experimental research. The results of Kalinske and Robertson are close to the curves of H/D = 0.1 and 0.3 for Φ = 30°, Kent's range of results are also in agreement with the curve of H/D = 0.3 and Φ = 30°. The results of Gandenberger show agreement with part of the curve for H/D = 0.3 and Φ = 40°, while Wisner's range extends below and above the curve of H/D = 0.3 and Φ = 30°. It will be noted that the theoretical curves in Fig. (7.24) are calculated for Φ = 30° and 40° where, as in the case of the upward sloping pipe in Fig. (7.22), a value of Φ = 60° was used. This is because experimental observations described in Chapter (6) reveal the angle Φ for the upward sloping pipe is generally between 40° and 65° and hence Φ = 60° was chosen as a representative value, whereas for the downward sloping pipe, the nose angle Φ was approximately half that of the upward sloping pipe.

Figure (7.24) reveals the reason why no unifying criterion has yet been established for clearing and blowback in downward sloping pipes. The behaviour cannot be predicted accurately until H/D and Φ for the air pocket are known and this in turn will be a function of the upstream flow conditions, the air content in the flow, and the geometry of the structure. A lot of research is still required in this area, but the author's theoretical model does

provide some answers, especially on the choice of ϕ and H/D to give a reasonable prediction. The theoretical clearing velocity, again for a downward sloping pipe, is shown in Fig. (7.25), with the results of Veronese[174] and Wisner et al[187]. The experimental results here are for the limit air pocket , where the air pocket size is first reduced by air entrainment at the toe of the jump until it reaches a size where it will be swept bodily downstream along the tunnel. Their results are in the range of the theoretical curves of H/D = 0.1 - 0.2 and ϕ = 40° which means that the theoretical clearing velcoty in equation (3.106) can also be used to predict the bodily clearing of such limit air pockets from a downward sloping pipe.

7.6 CONCLUSIONS

The simple theoretical models outlined in Chapter (3) provided a reasonable agreement with the experimental results for air pocket behaviour at the junction of a vertical dropshaft/tunnel system. Model Type 1 represented the bend radii R'/D = 1.0 and 1.5 very well in the region of air pocket blowback at lower Froude numbers, while Model Type 2 represented the R'/D = 0.5 bend very well in the low Froude number range. Model Type 3, for a stable hydraulic jump formation under the air pocket, was in good agreement with all nine geometries tested, especially equation (3.87) derived using force-momentum balance. This appears more accurate than that using the energy principle, especially for longer stable air pockets at the bend where the effects of the flow at the bend had dissipated near the toe of the hydraulic jump.

The empirical equations for clearing air pockets from the bend show that clearing is dependent primarily on the bend radius, air/water ratio, and angle of tunnel inclination with the horizontal. For the three bend radii tested, the sharp bend (R'/D = 0.5) was most efficient in clearing the air pockets, and for the three tunnel

slopes tested, the downward slope was least efficient.

The theoretical model for the rise velocity of an air pocket in an upward sloping straight pipe gave good correlation with the experimental data, although the lack of experimental data for the downward sloping pipe made proper comparison incomplete. The work did show that the application of the force-momentum principle to air pocket behaviour, to the moving water case as well as the stationary water case, and to upward and downward sloping pipes is well justified. One area needing further investigation for the proper application of the force-momentum principle, is the relationship between the nose angle ϕ and air pocket depth H/D, and how these two parameters relate to the conduit slope, θ, and flow conditions, Fr_o, β, etc.

The theoretical models in Chapter (3) appear very promising when compared with previous researchers' work. For the first time fairly simplified models seem to be generally applicable at the dropshaft/tunnel junction, upward and downward sloping pipes, blowback and clearing. Until now only empirical correlations have existed. This is a step forward.

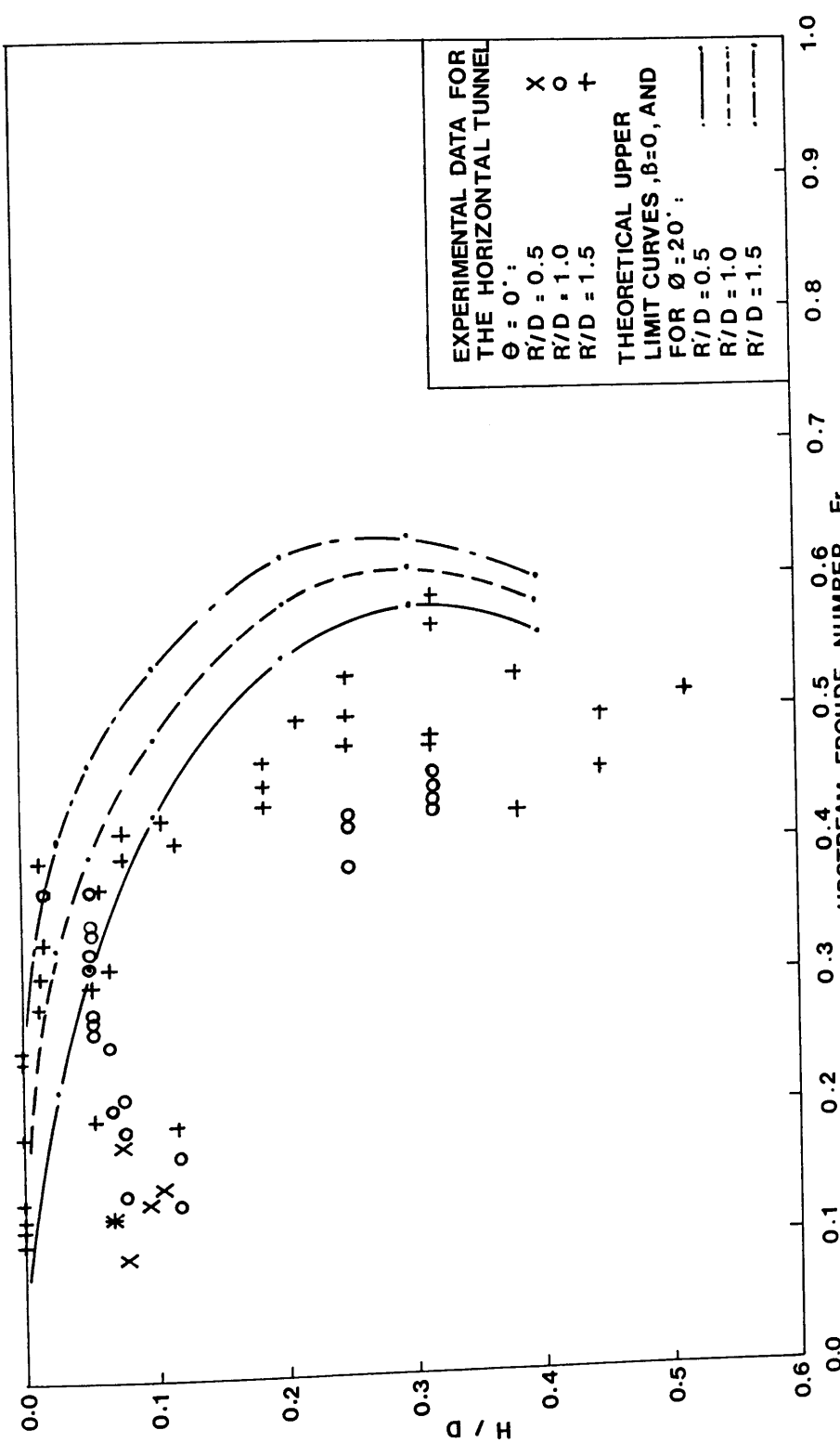

FIG. (7.1) COMPARISON BETWEEN EXPERIMENTAL RESULTS FOR AIR POCKETS BLOWING BACK AND MODEL TYPE 1 GIVEN IN EQUATION (3.56)

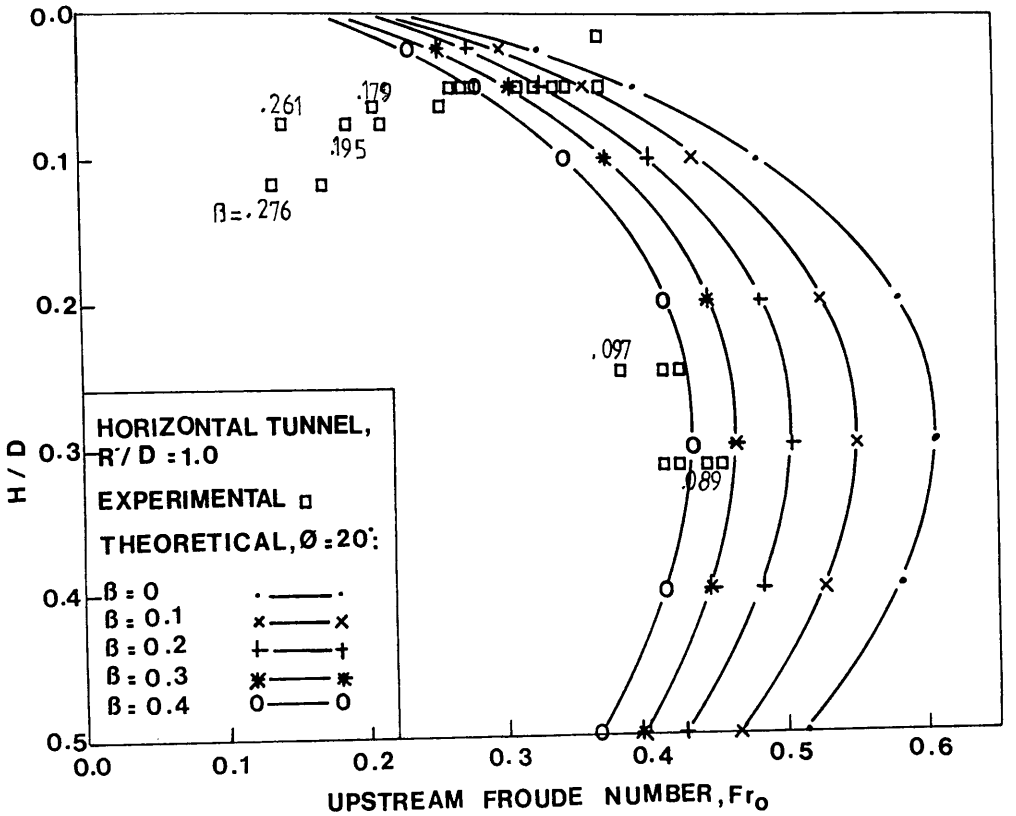

[a]

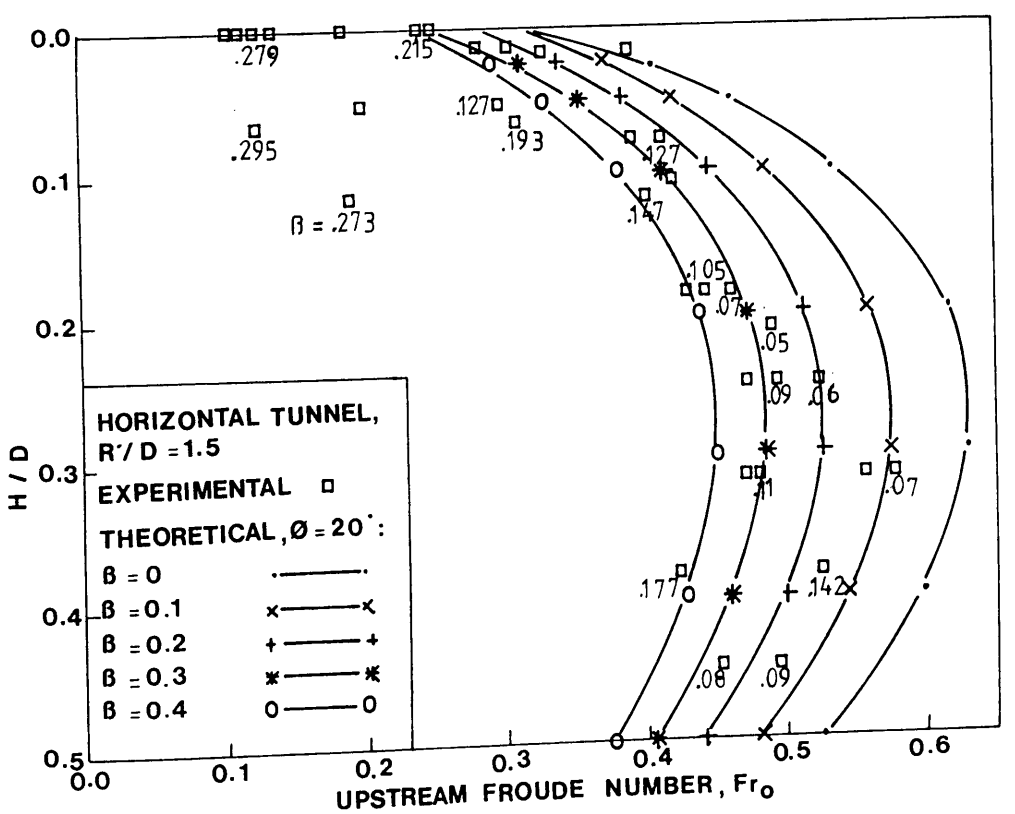

[b]

FIG. (7.2) COMPARISON BETWEEN EXPERIMENTAL RESULTS FOR AIR POCKETS BLOWING BACK AND MODEL TYPE 1 GIVEN IN EQUATION (3.57) FOR DIFFERENT VALUES OF β

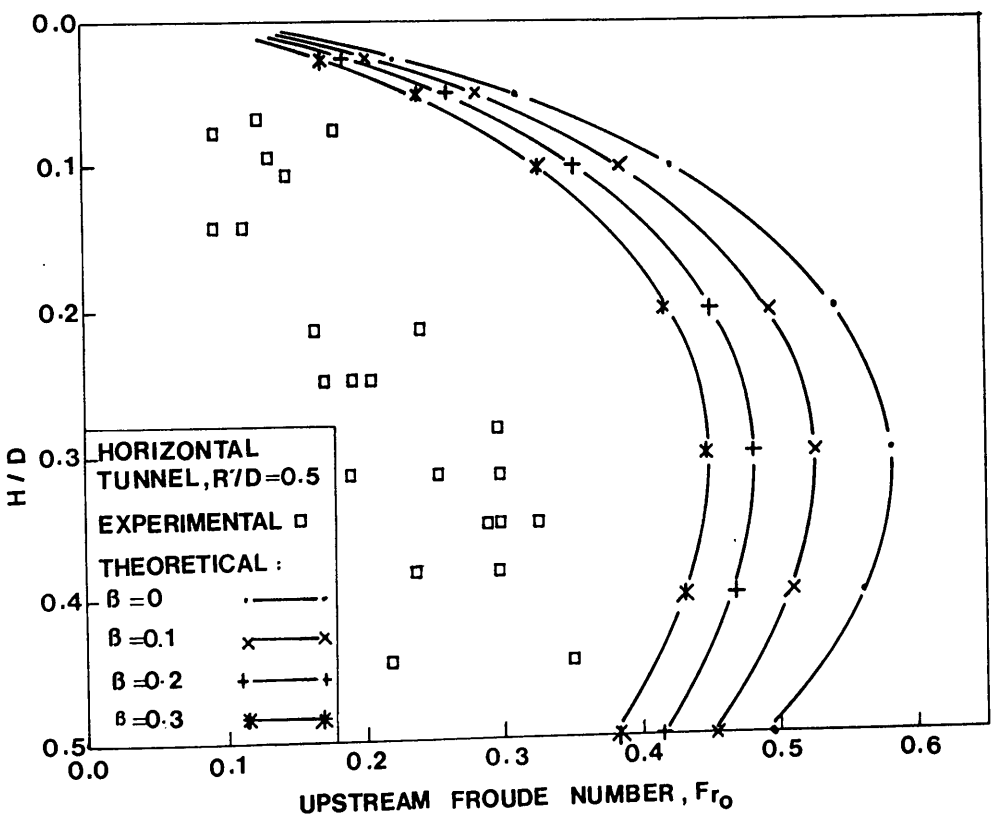

FIG. (7.3) COMPARISON BETWEEN EXPERIMENTAL RESULTS FOR NON HYDRAULIC JUMP POCKETS WITH LOW FROUDE NUMBER AND EQUATION (3.57) FOR DIFFERENT VALUES OF β

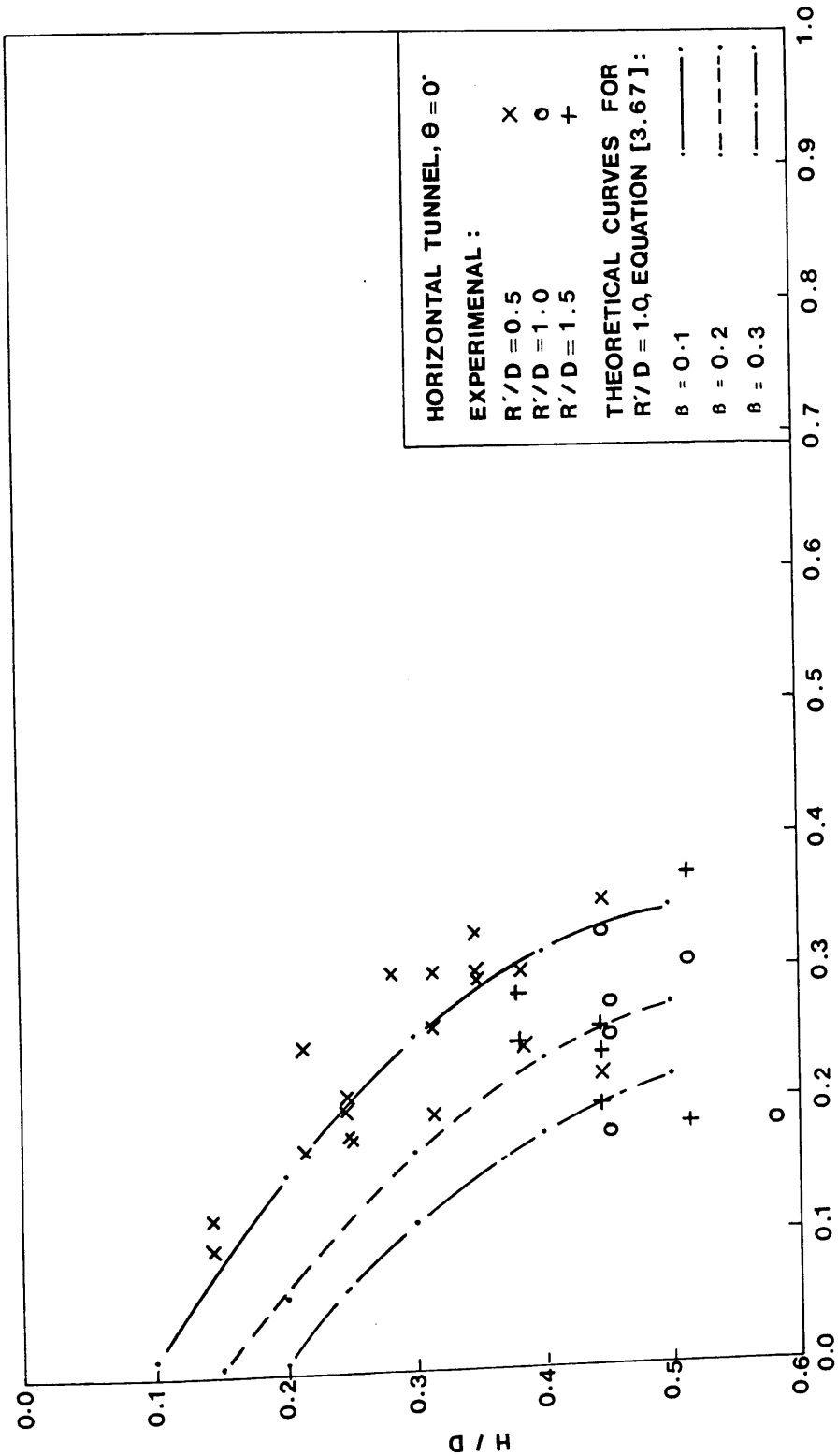

FIG. (7.4) COMPARISON BETWEEN EXPERIMENTAL RESULTS FOR THE AIR POCKET WITHOUT A HYDRAULIC JUMP AND MODEL TYPE (2) GIVEN IN EQUATION (3.67)

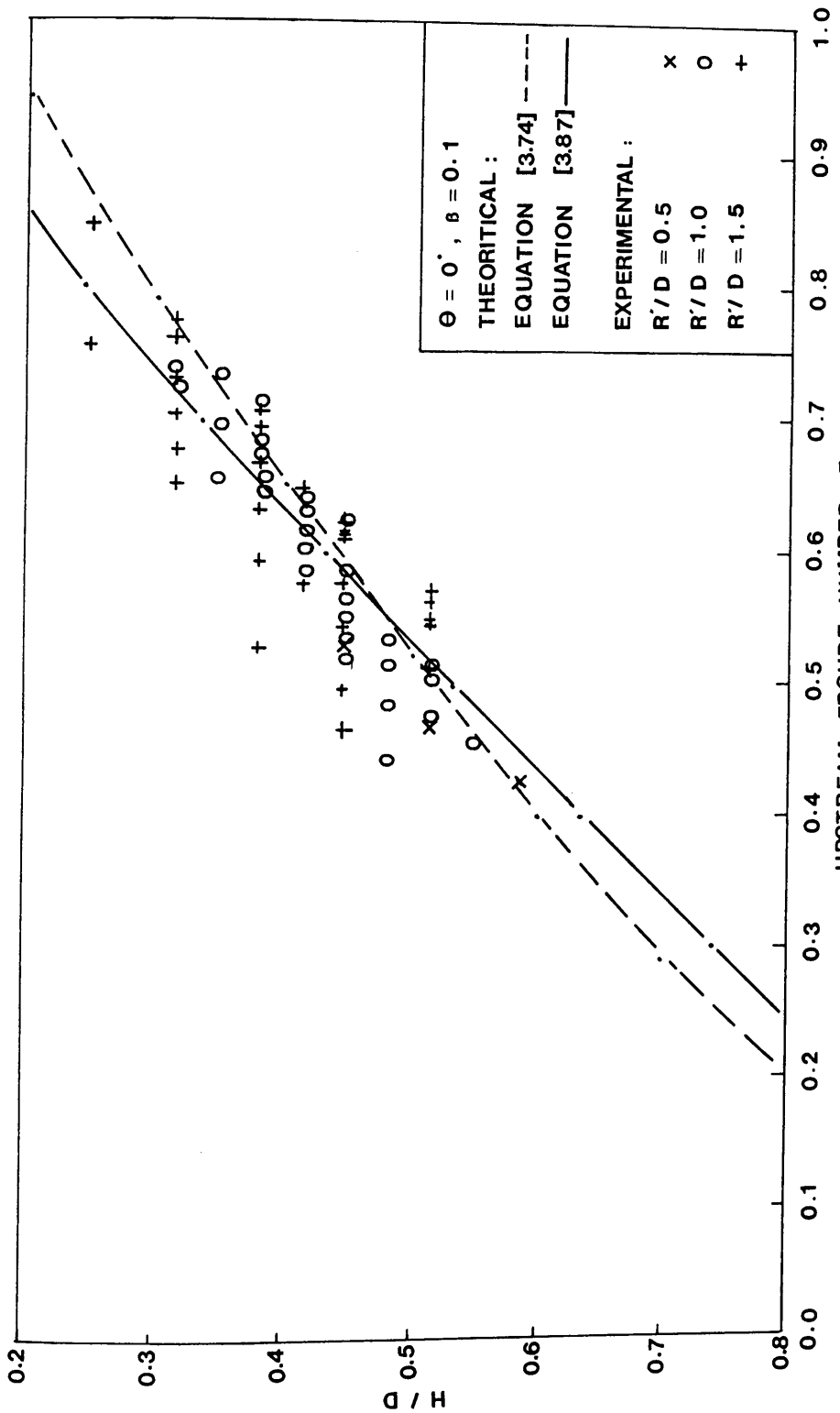

FIG. (7.5) COMPARISON BETWEEN EXPERIMENTAL RESULTS AND THEORETICAL MODELS FOR THE STABLE JUMP IN A HORIZONTAL TUNNEL

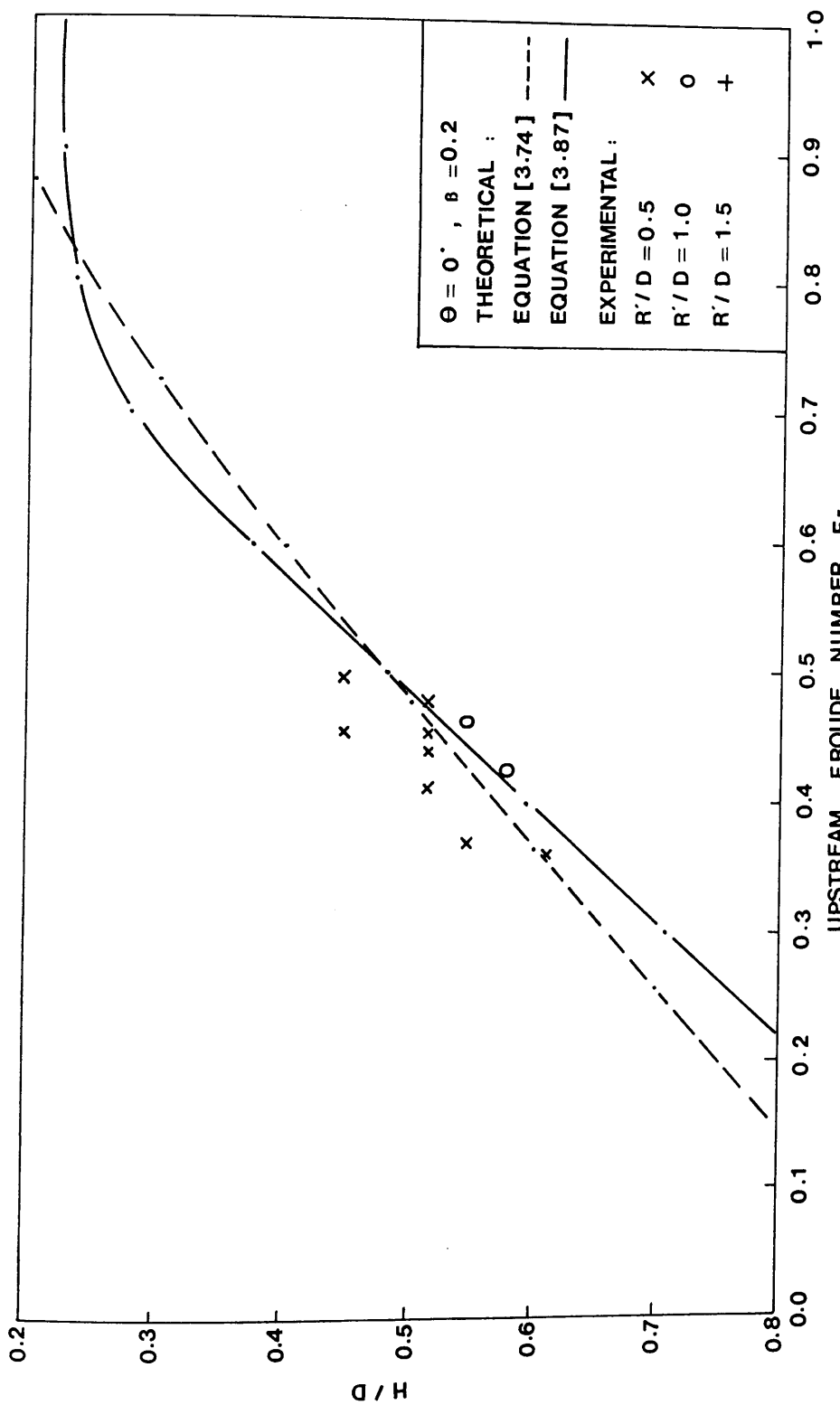

FIG. (7.6) COMPARISON BETWEEN EXPERIMENTAL RESULTS AND THEORETICAL MODELS FOR THE STABLE JUMP IN A HORIZONTAL TUNNEL

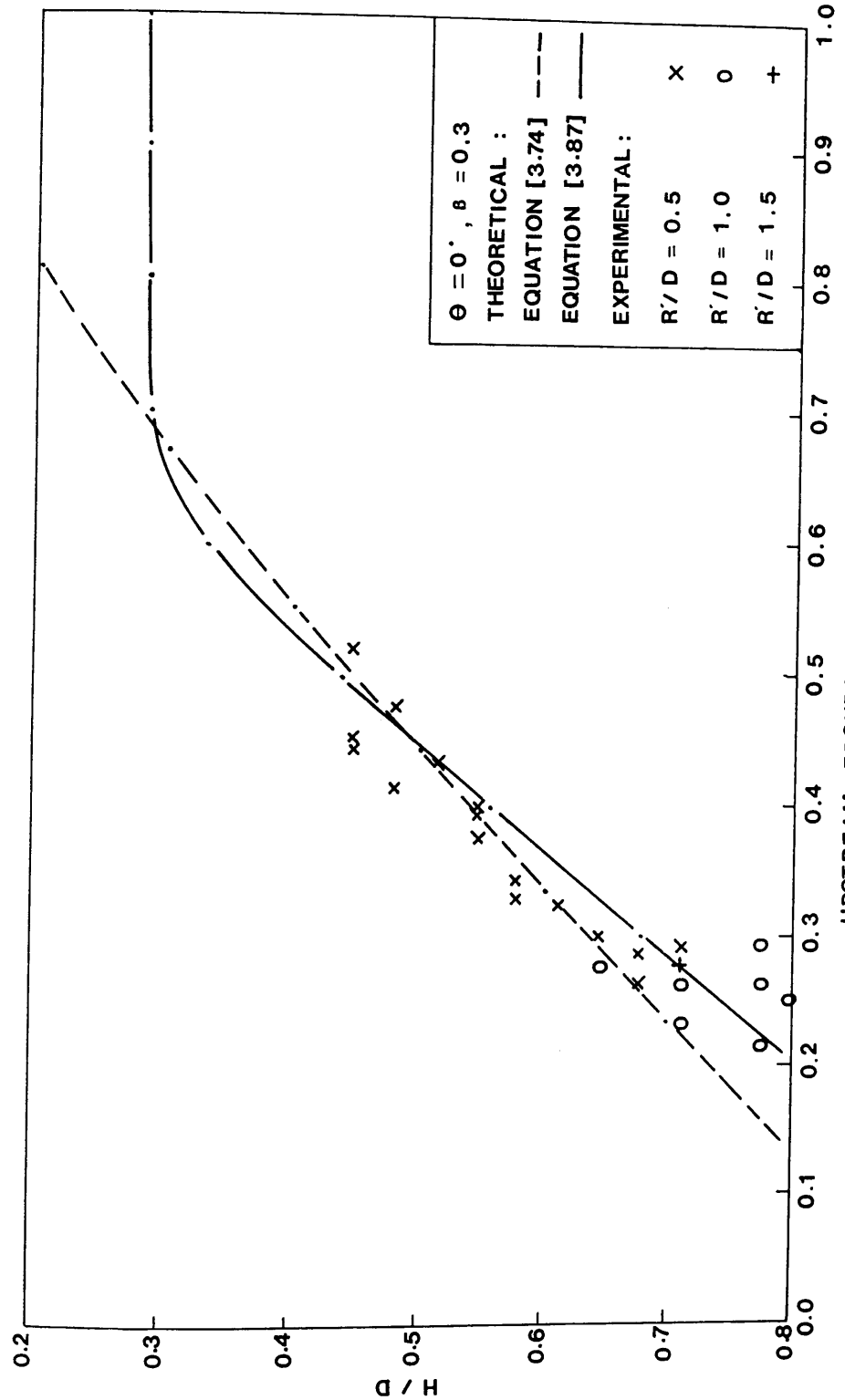

FIG. (7.7) COMPARISON BETWEEN EXPERIMENTAL RESULTS AND THEORETICAL MODELS FOR THE STABLE JUMP IN A HORIZONTAL TUNNEL

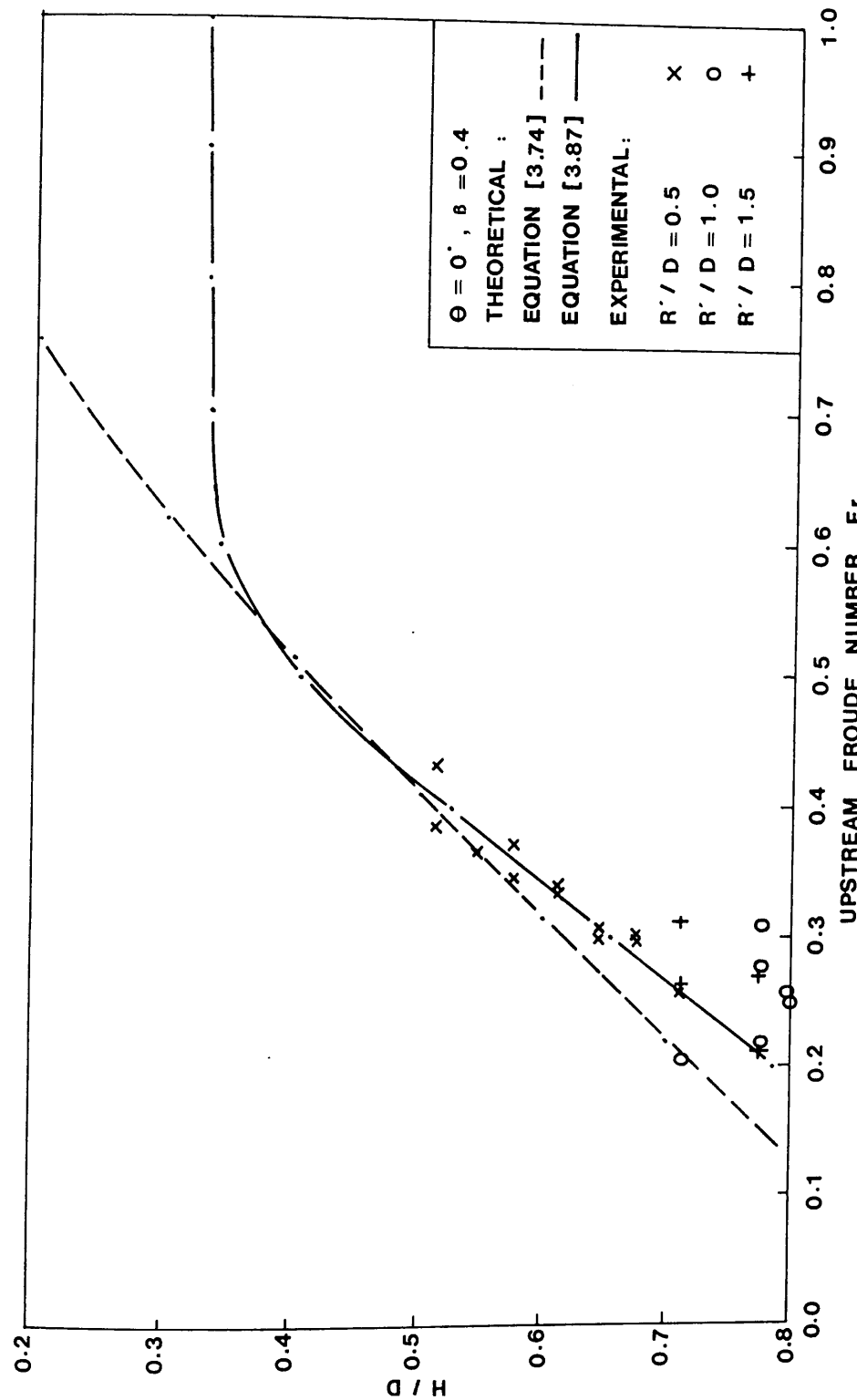

FIG. (7.8) COMPARISON BETWEEN EXPERIMENTAL RESULTS AND THEORETICAL MODELS FOR THE STABLE JUMP IN A HORIZONTAL TUNNEL

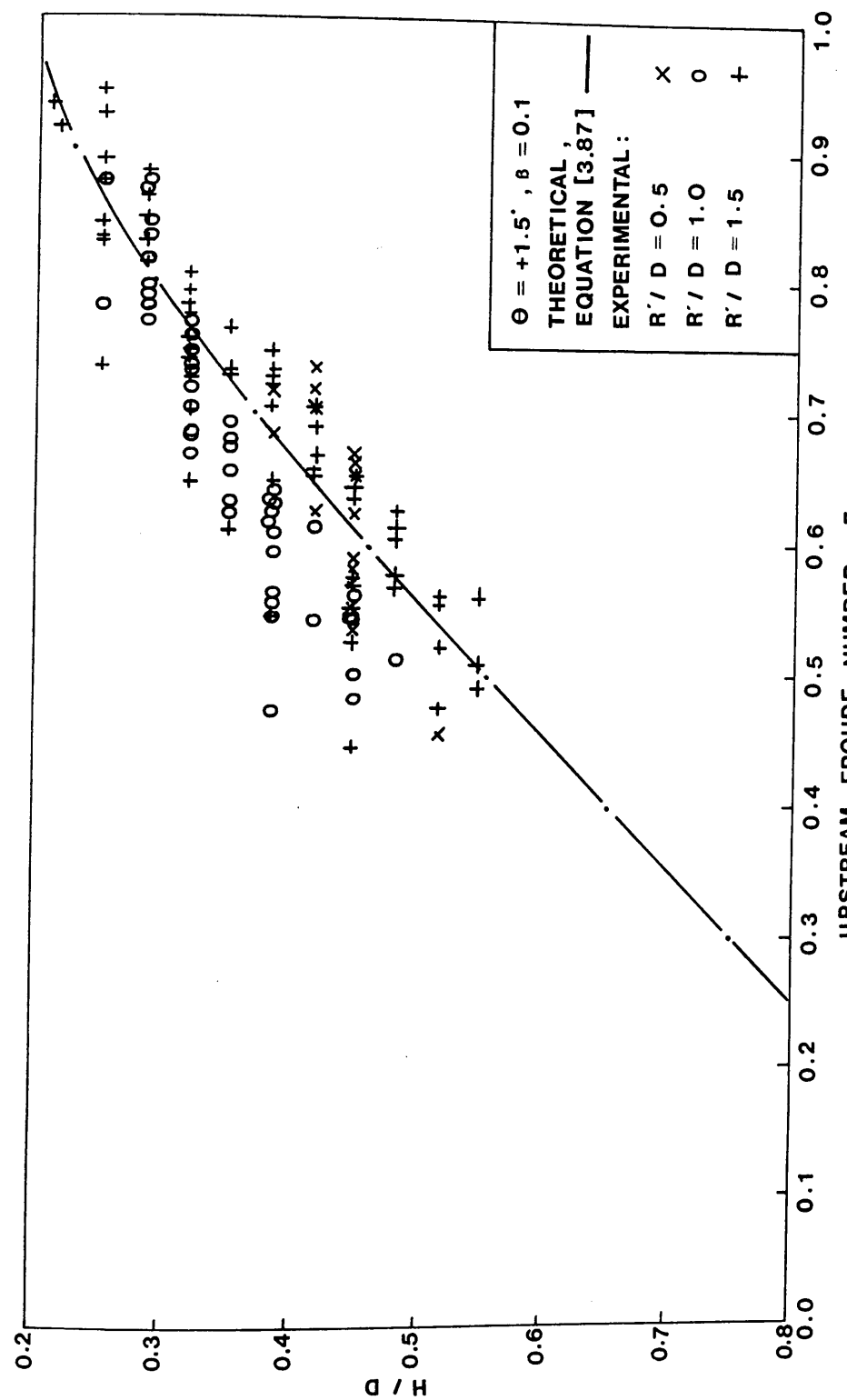

FIG. (7.9) COMPARISON BETWEEN EXPERIMENTAL RESULTS AND THEORETICAL MODELS FOR THE STABLE JUMP IN THE UPWARD SLOPING TUNNEL

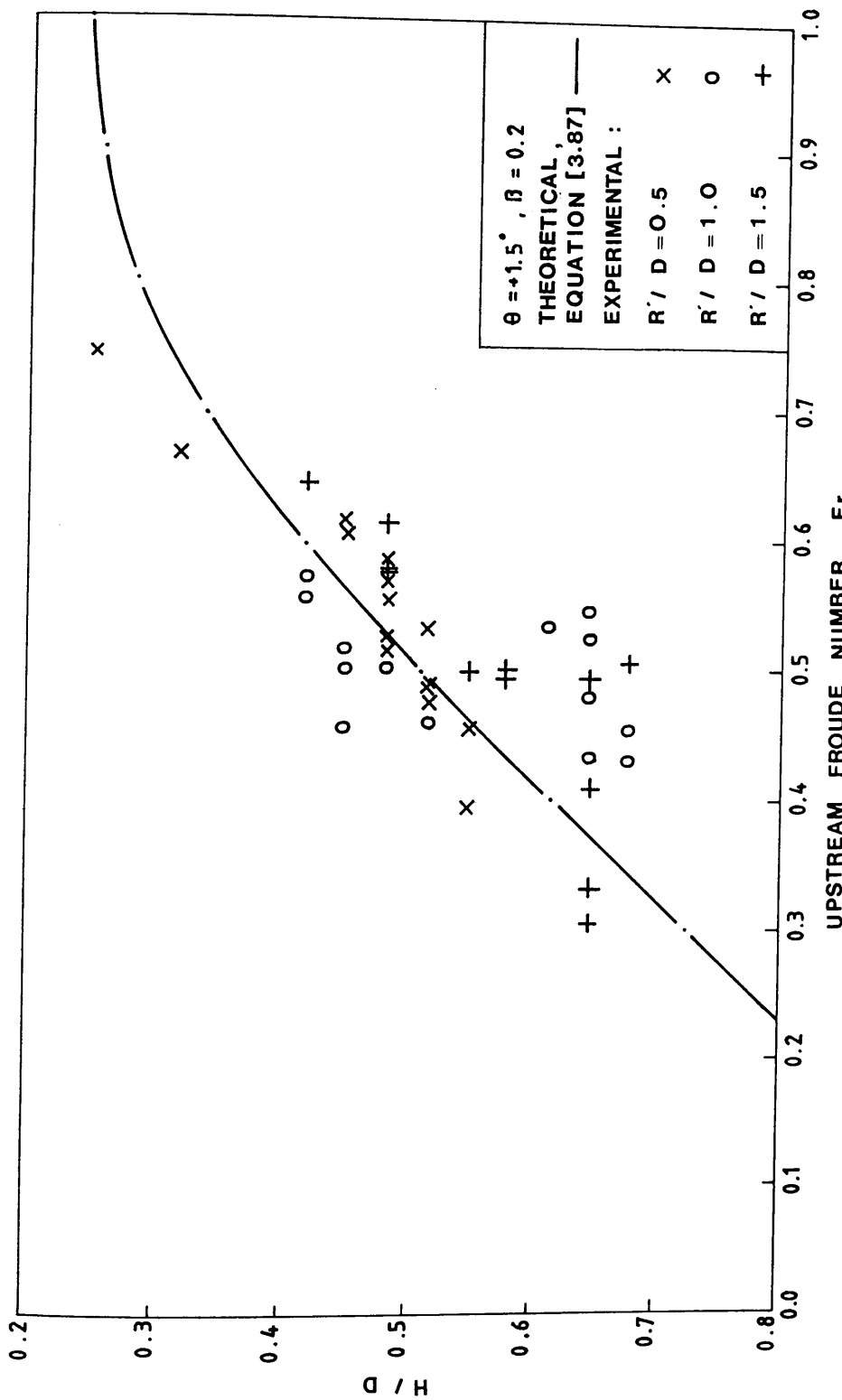

FIG. (7.10) COMPARISON BETWEEN EXPERIMENTAL RESULTS AND THEORETICAL MODELS FOR THE STABLE JUMP IN THE UPWARD SLOPING TUNNEL

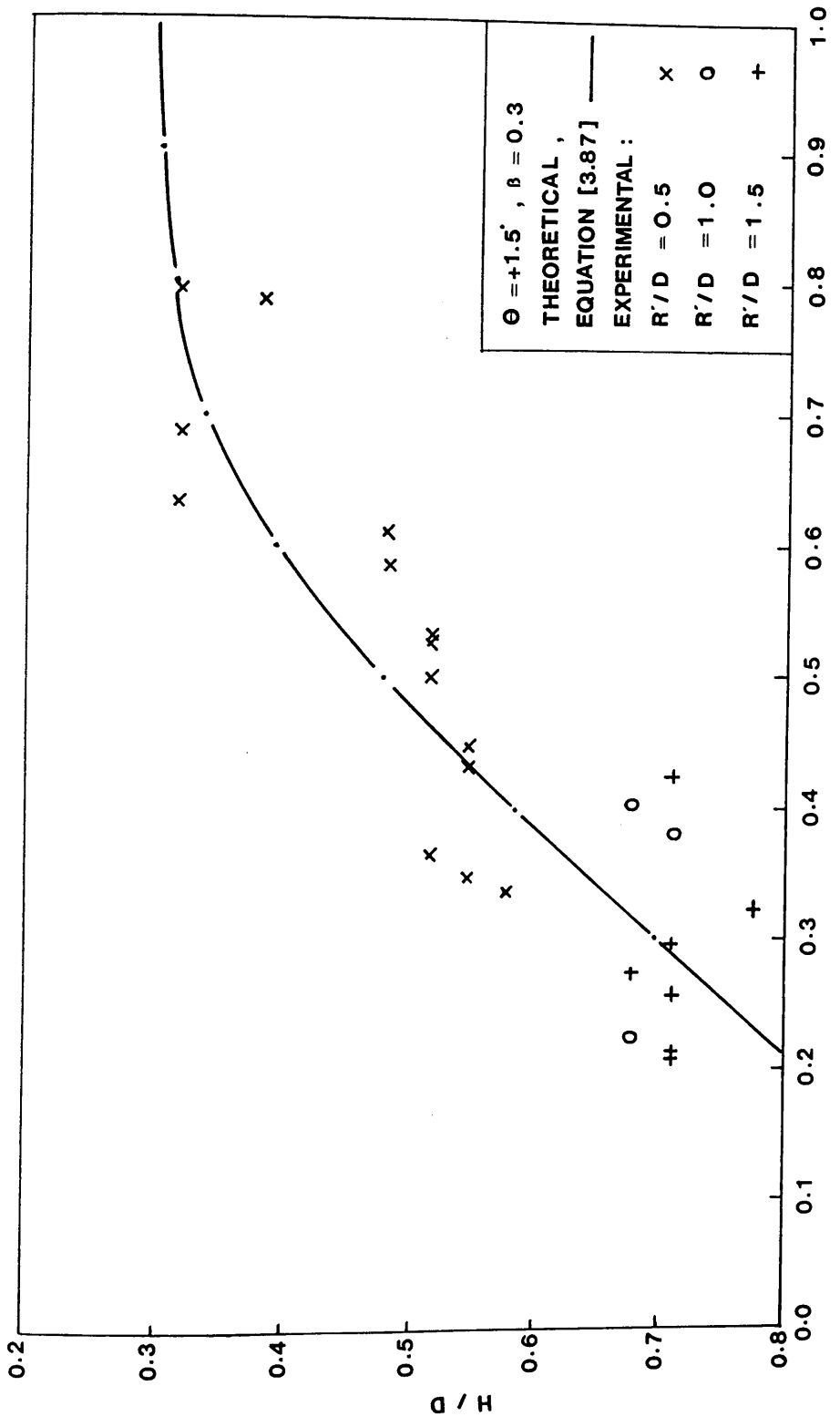

FIG. (7.11) COMPARISON BETWEEN EXPERIMENTAL RESULTS AND THEORETICAL MODEL FOR THE STABLE JUMP IN THE UPWARD SLOPING TUNNEL

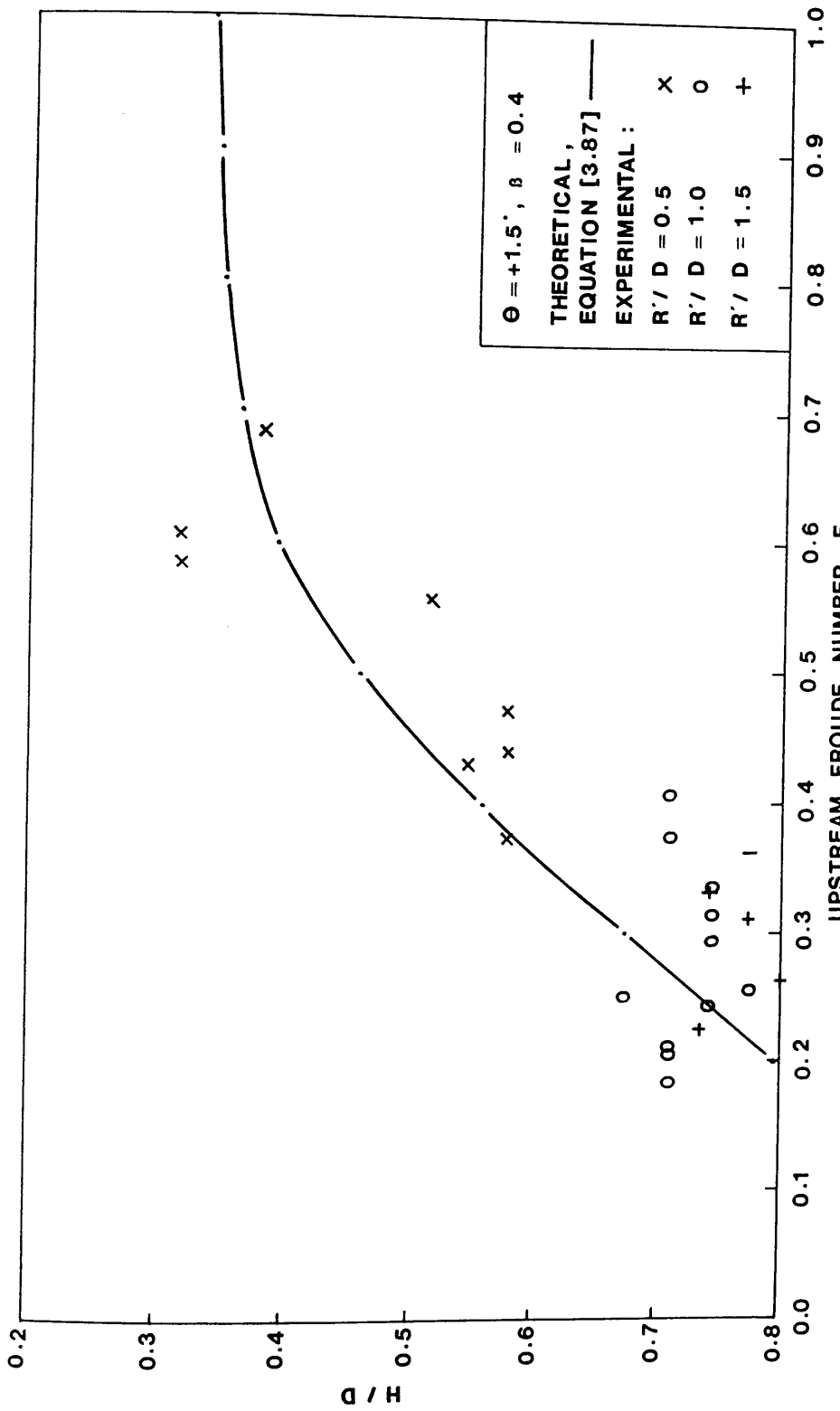

FIG. (7.12) COMPARISON BETWEEN EXPERIMENTAL RESULTS AND THEORETICAL MODEL FOR THE STABLE JUMP IN THE UPWARD SLOPING TUNNEL

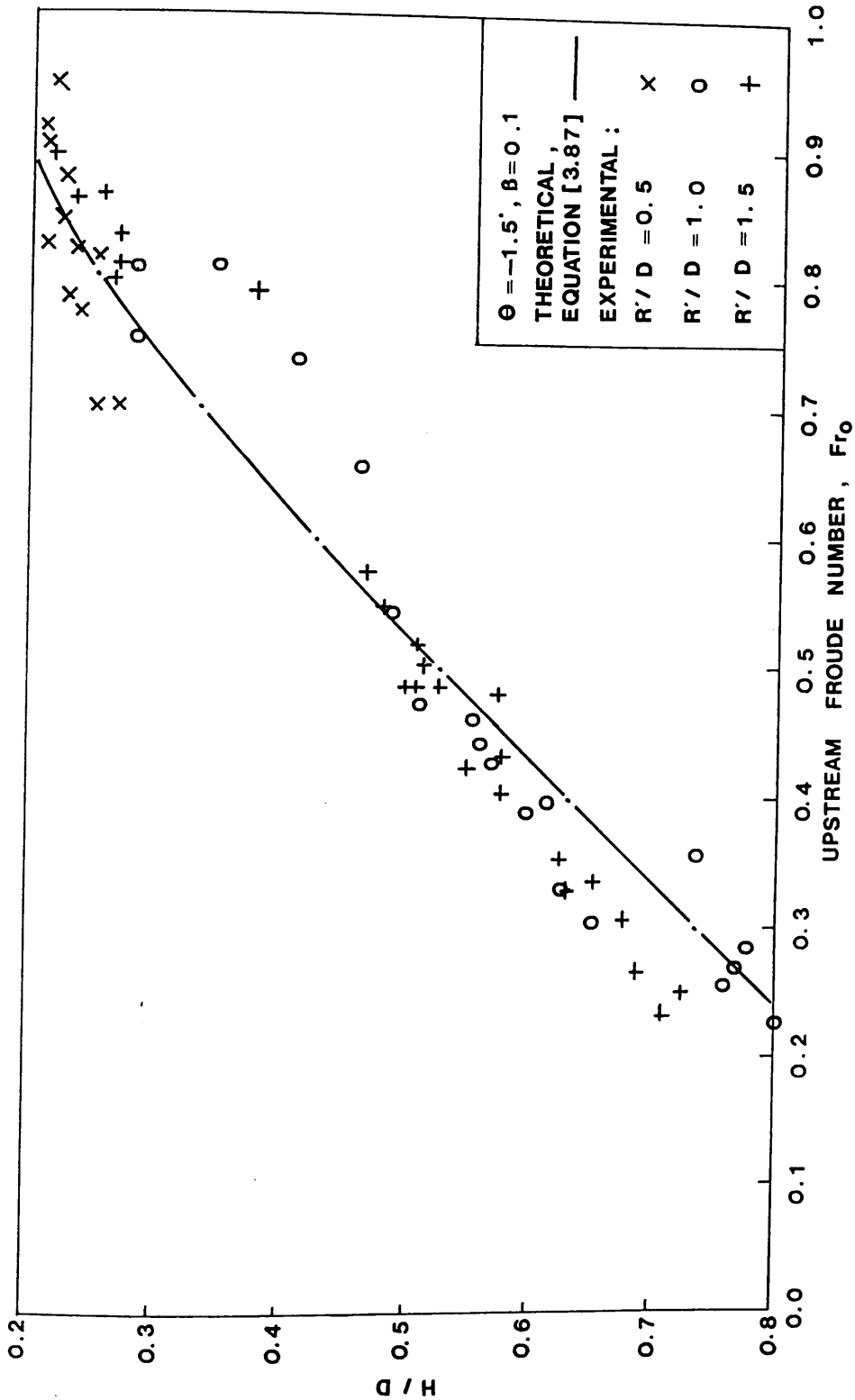

FIG. (7.13) COMPARISON BETWEEN EXPERIMENTAL RESULTS AND THEORETICAL MODEL FOR THE STABLE JUMP IN THE DOWNWARD SLOPING TUNNEL

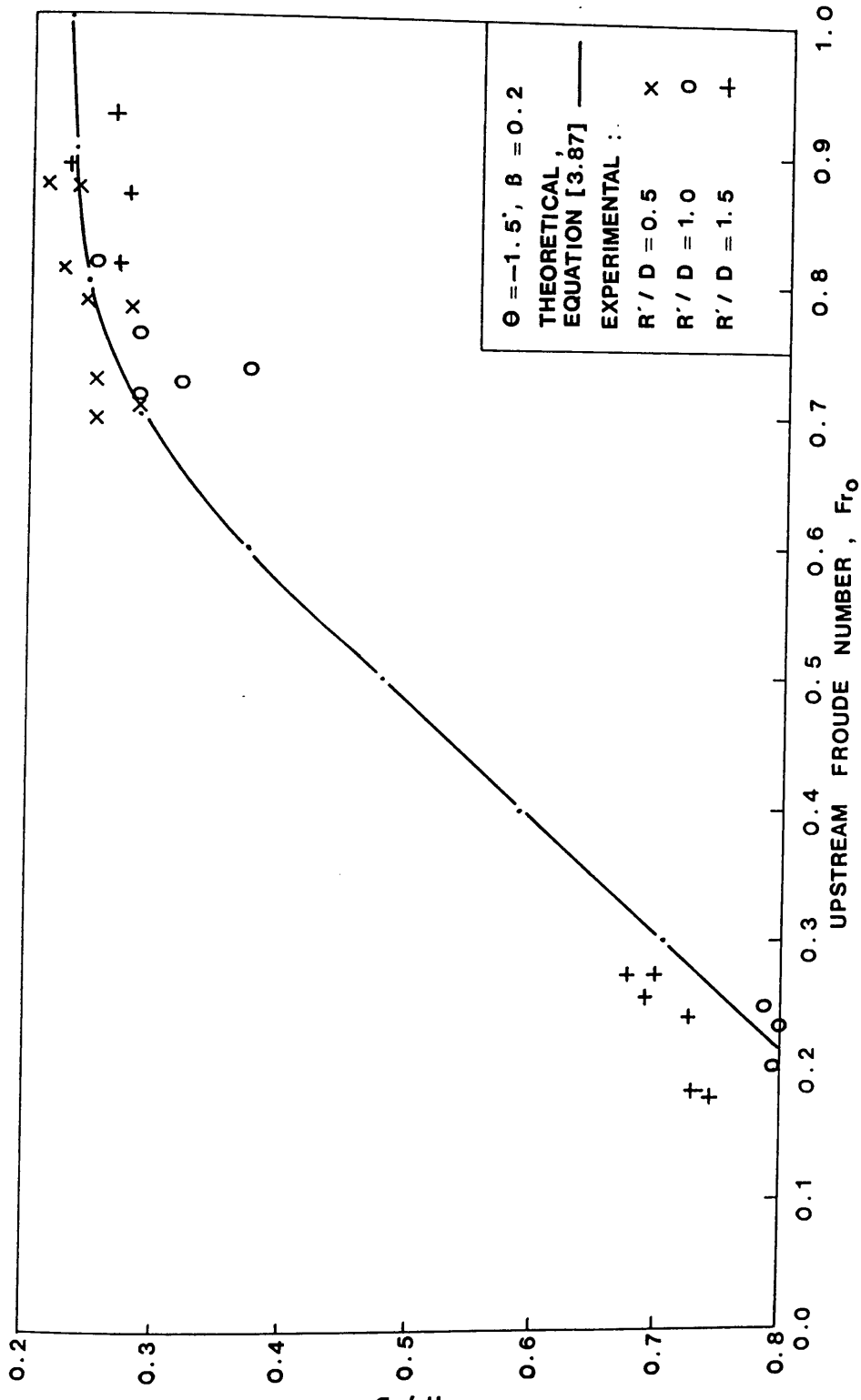

FIG. (7.14) COMPARISON BETWEEN EXPERIMENTAL RESULTS AND THEORETICAL MODEL FOR THE STABLE JUMP IN THE DOWNWARD SLOPING TUNNEL

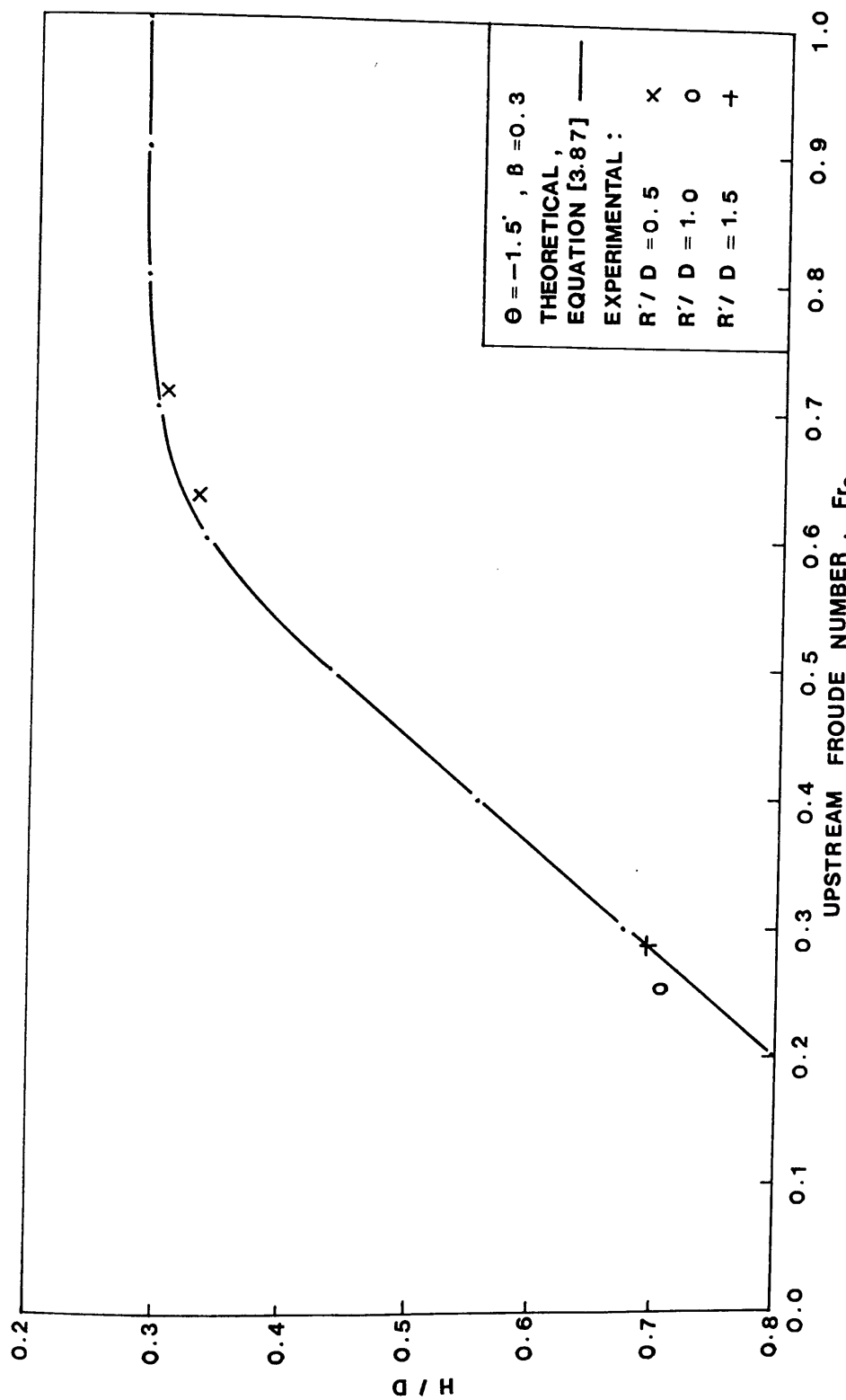

FIG. (7.15) COMPARISON BETWEEN EXPERIMENTAL RESULTS AND THEORETICAL MODEL FOR THE STABLE JUMP IN THE DOWNWARD SLOPING TUNNEL

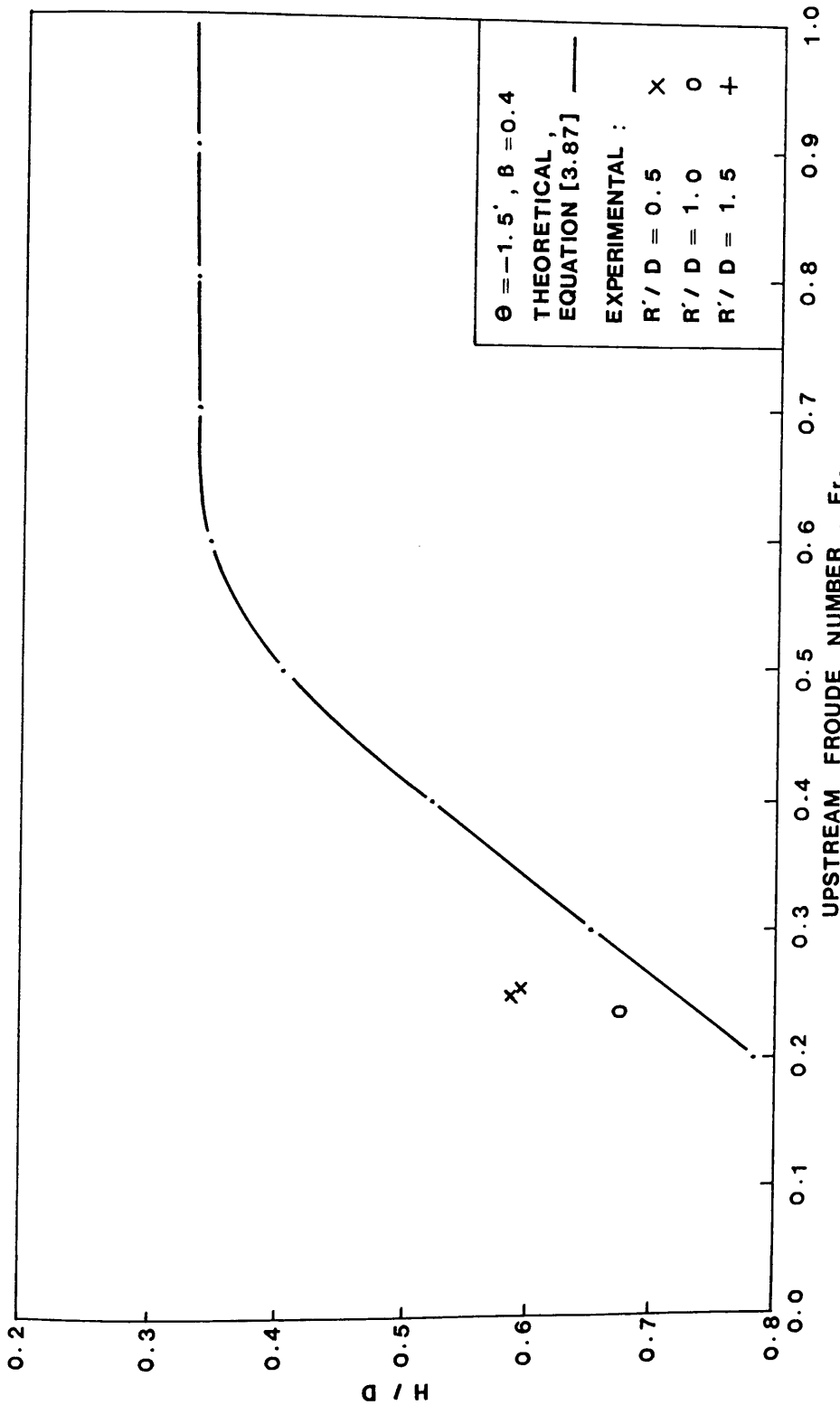

FIG. (7.16) COMPARISON BETWEEN EXPERIMENTAL RESULTS AND THEORETICAL MODEL FOR THE STABLE JUMP IN THE DOWNWARD SLOPING TUNNEL

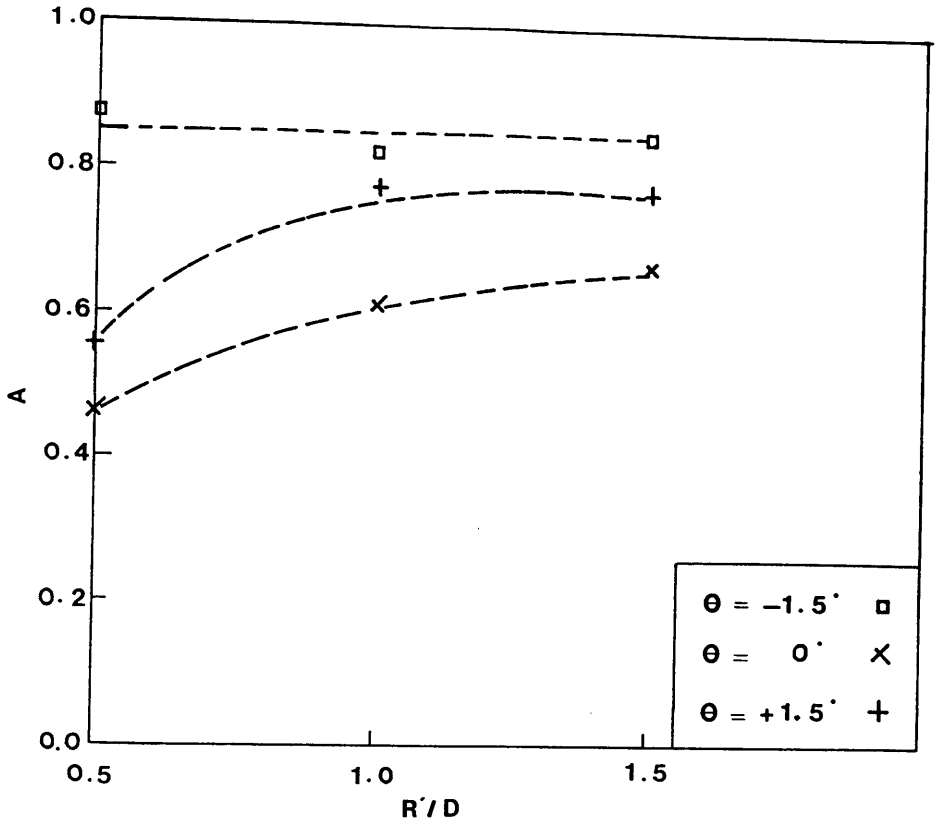

FIG. (7.17a) RELATION BETWEEN THE CONSTANT 'A' AND THE BEND RADIUS FOR DIFFERENT ANGLES OF TUNNEL INCLINATION, θ.

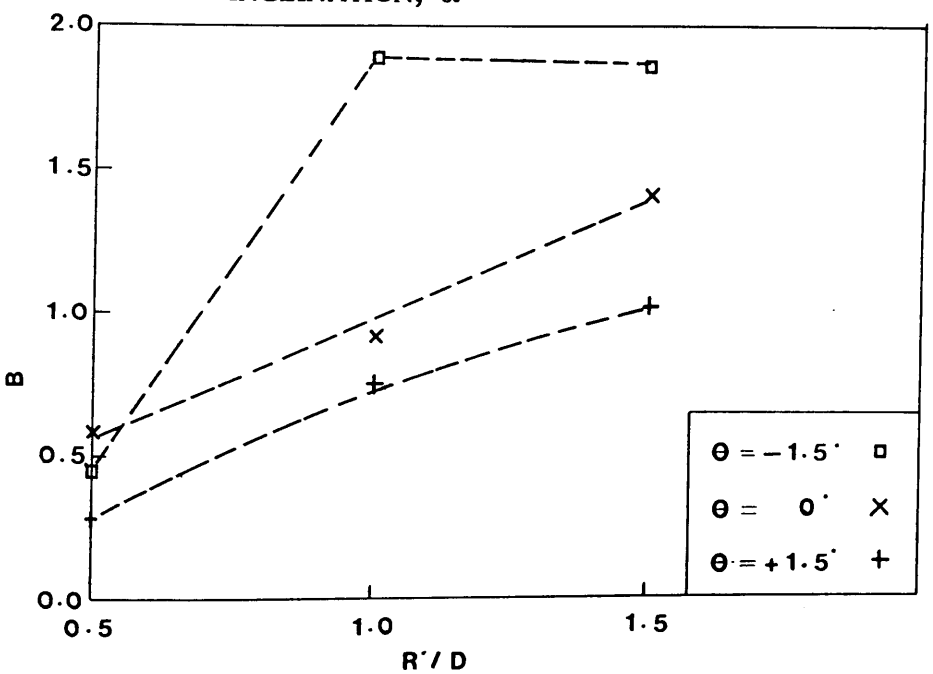

FIG (7.17b) RELATION BETWEEN THE CONSTANT 'B' AND THE BEND RADIUS FOR DIFFERRENT ANGLES OF TUNNEL INCLINATION, θ.

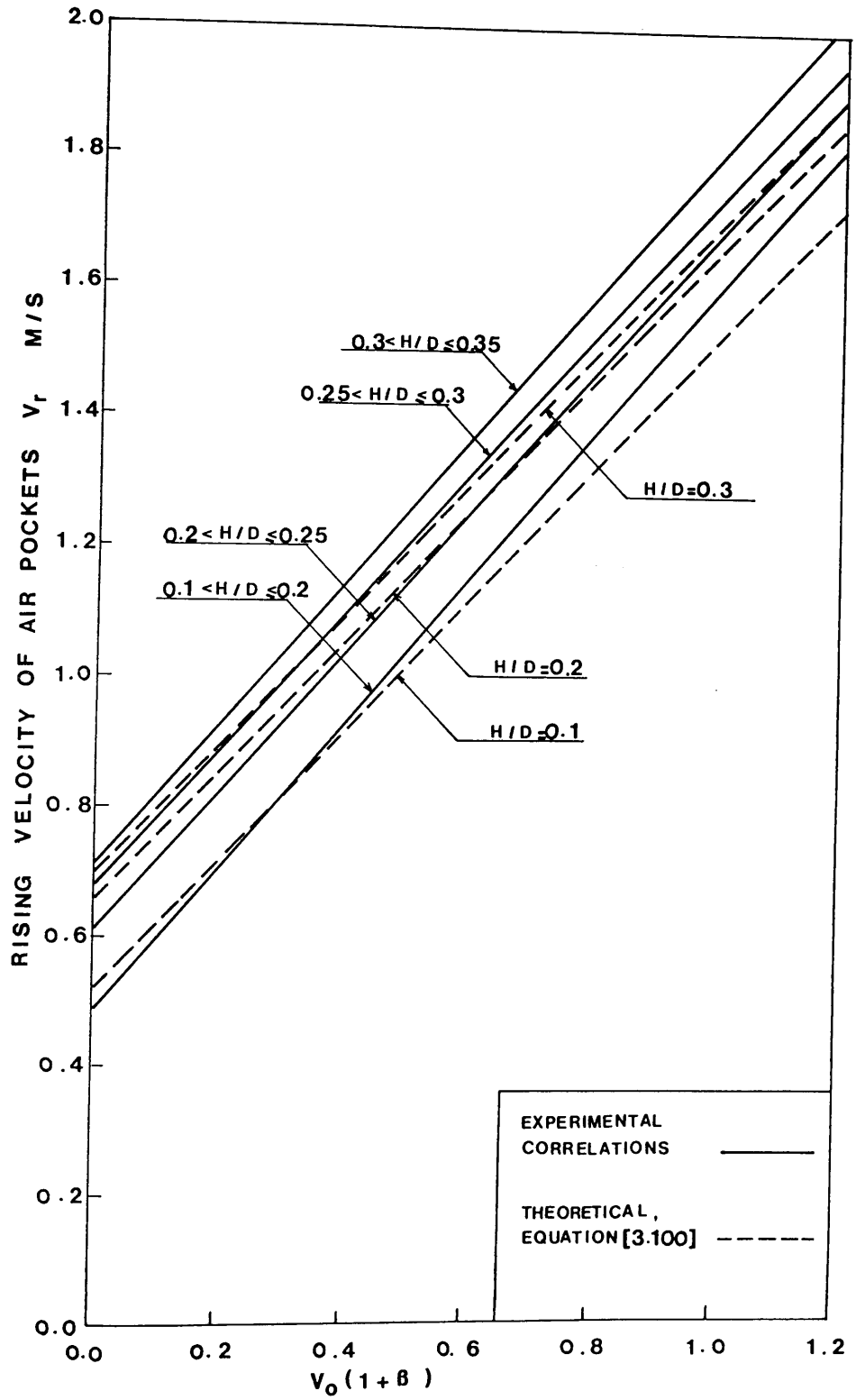

FIG. (7.18) COMPARISON BETWEEN EXPERIMENTAL RESULTS AND THEORETICAL MODEL FOR THE STABLE JUMP IN THE UPWARD SLOPING TUNNEL

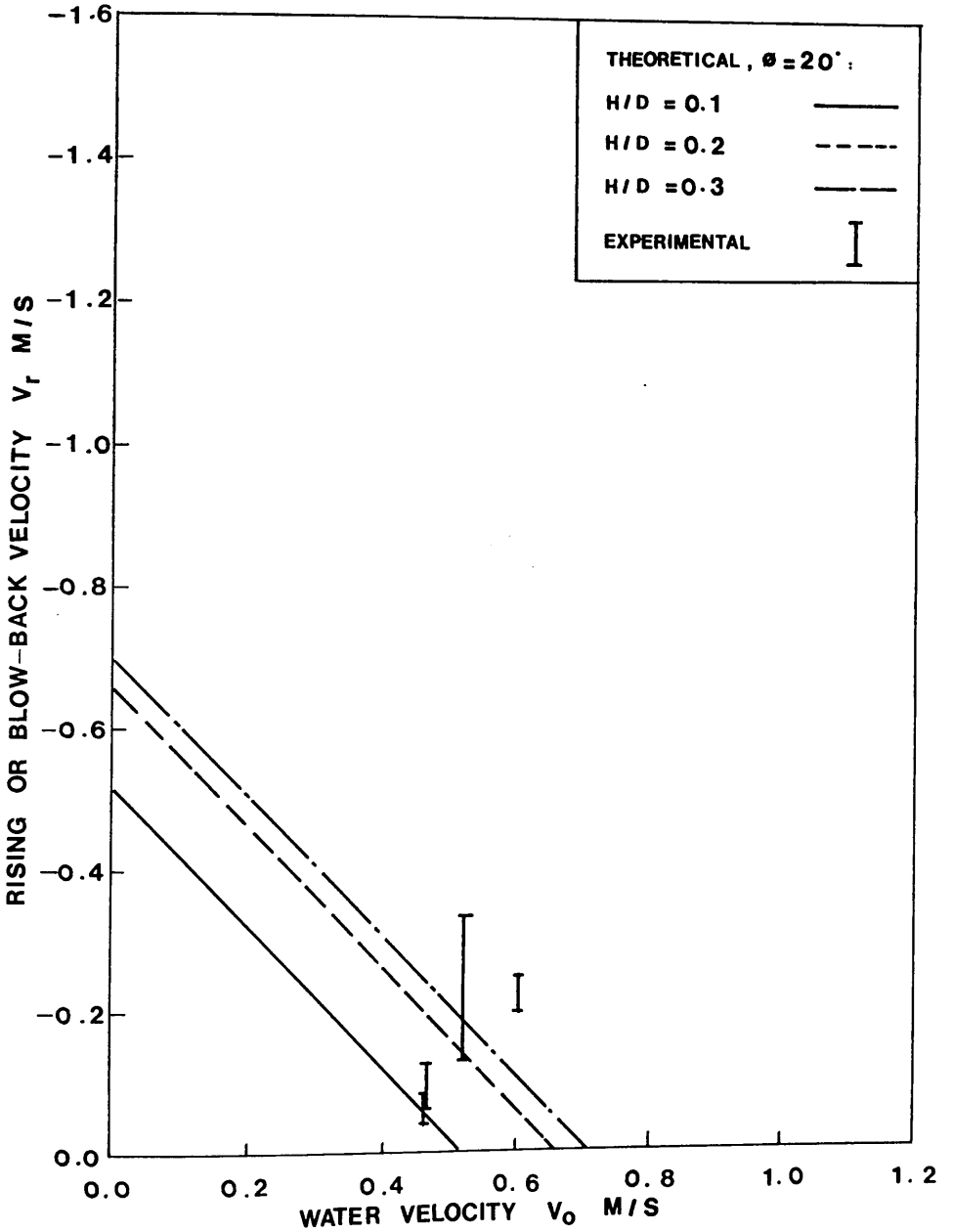

FIG. (7.19) COMPARISON BETWEEN EXPERIMENTAL AND THEORETICAL RISING VELOCITIES OF AIR POCKETS IN A DOWNWARD SLOPING TUNNEL

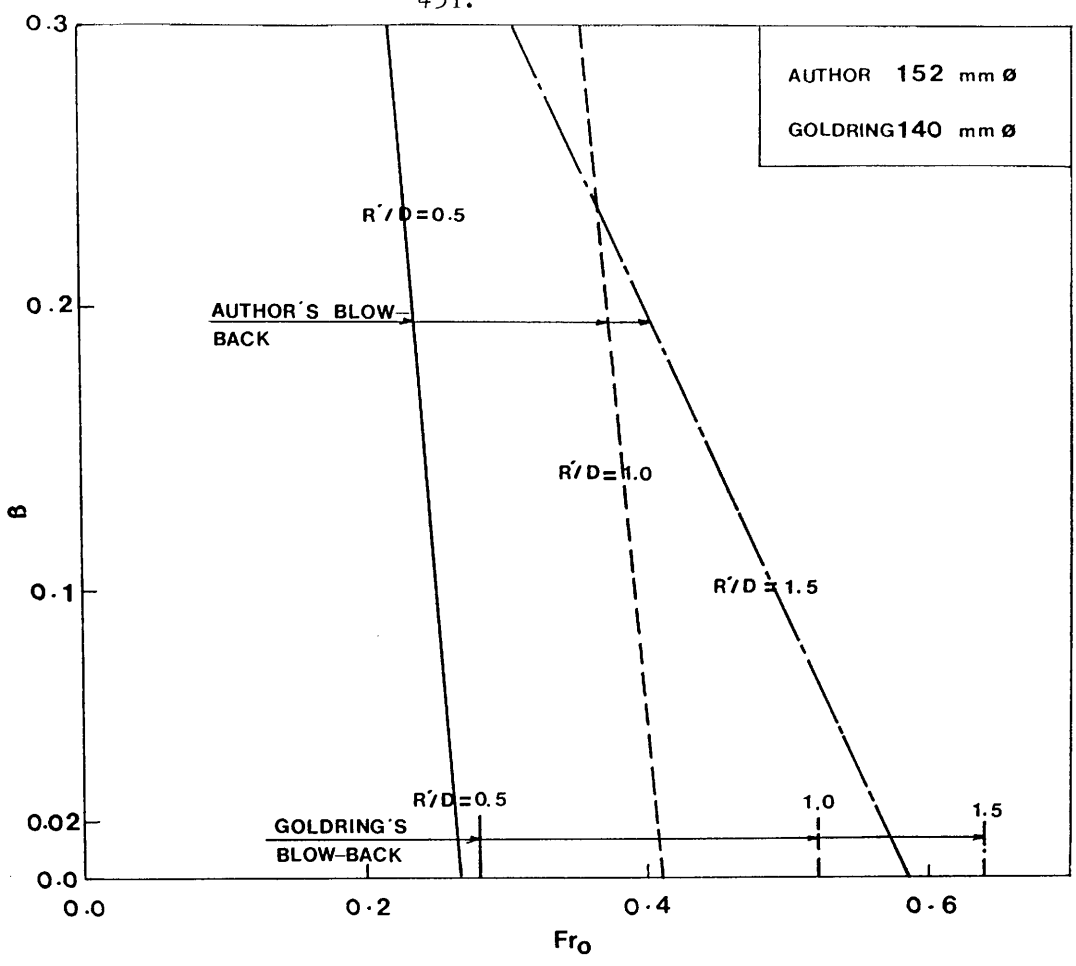

(a) BLOW-BACK UPPER LIMIT

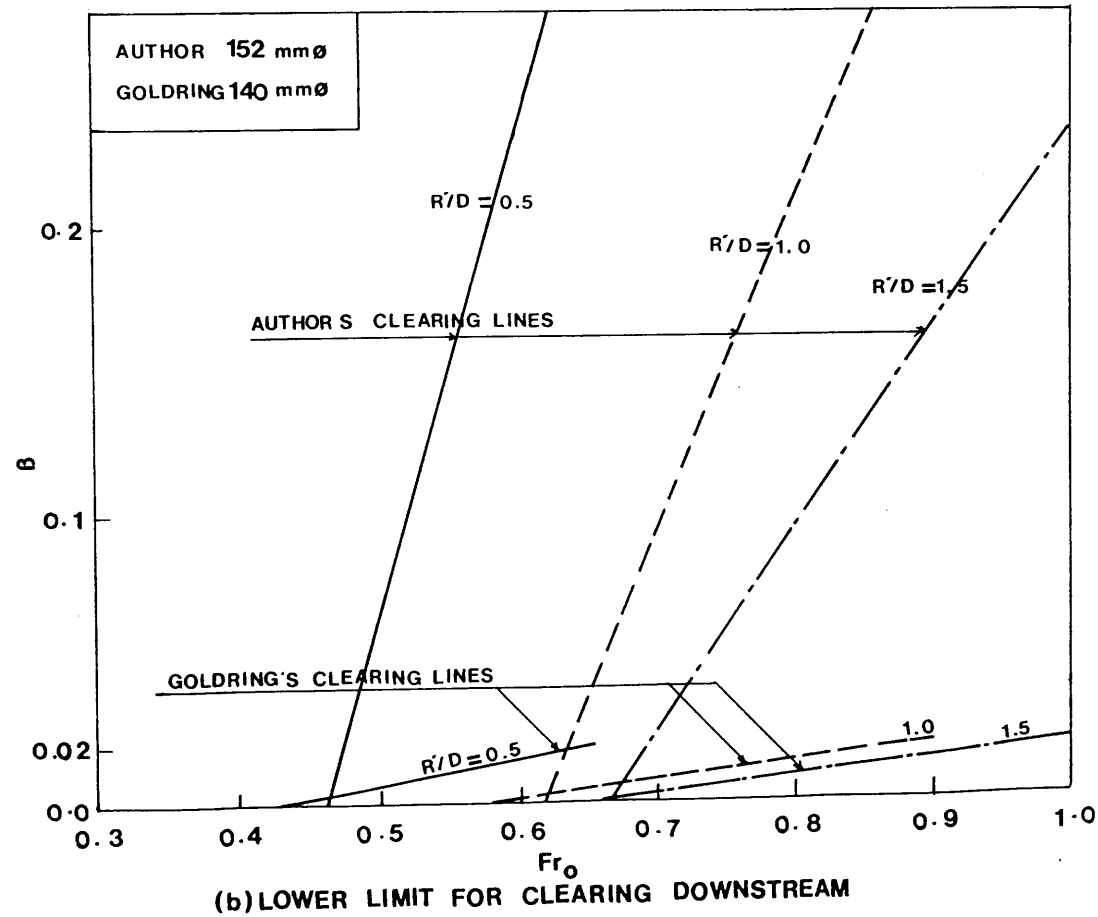

(b) LOWER LIMIT FOR CLEARING DOWNSTREAM

FIG. (7.20) COMPARISON BETWEEN AUTHOR'S EXPERIMENTAL RESULTS AND GOLDRING'S RESULTS FOR AIR POCKET AT THE JUNCTION OF A VERTICAL DROPSHAFT AND HORIZONTAL TUNNEL

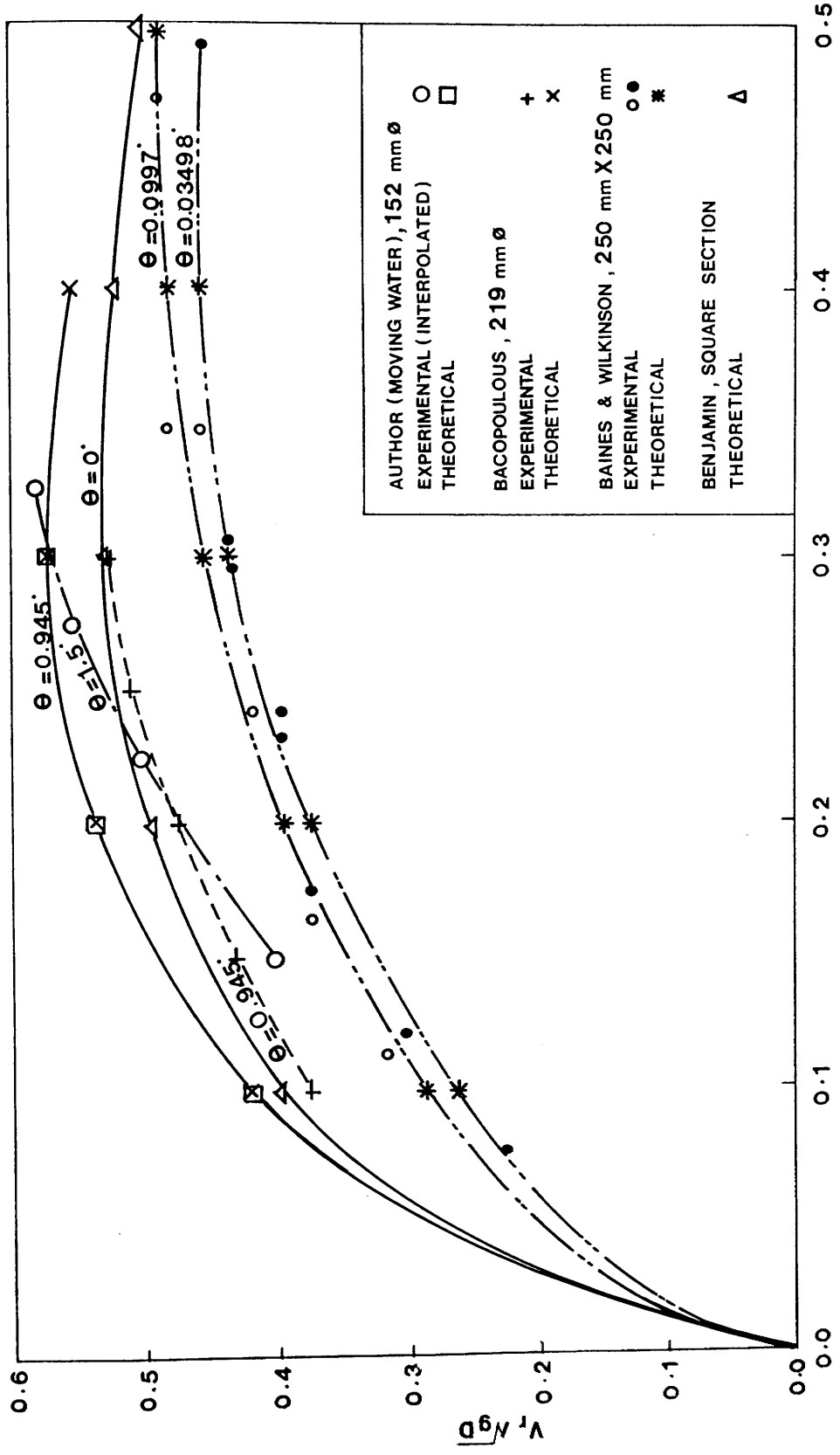

FIG. (7.21) COMPARISON BETWEEN AUTHOR'S AND PREVIOUS RESEARCH THEORETICAL AND EXPERIMENTAL RESULTS FOR THE RISING VELOCITIES OF AIR POCKETS IN UPWARD SLOPING TUNNEL IN STATIONARY WATER

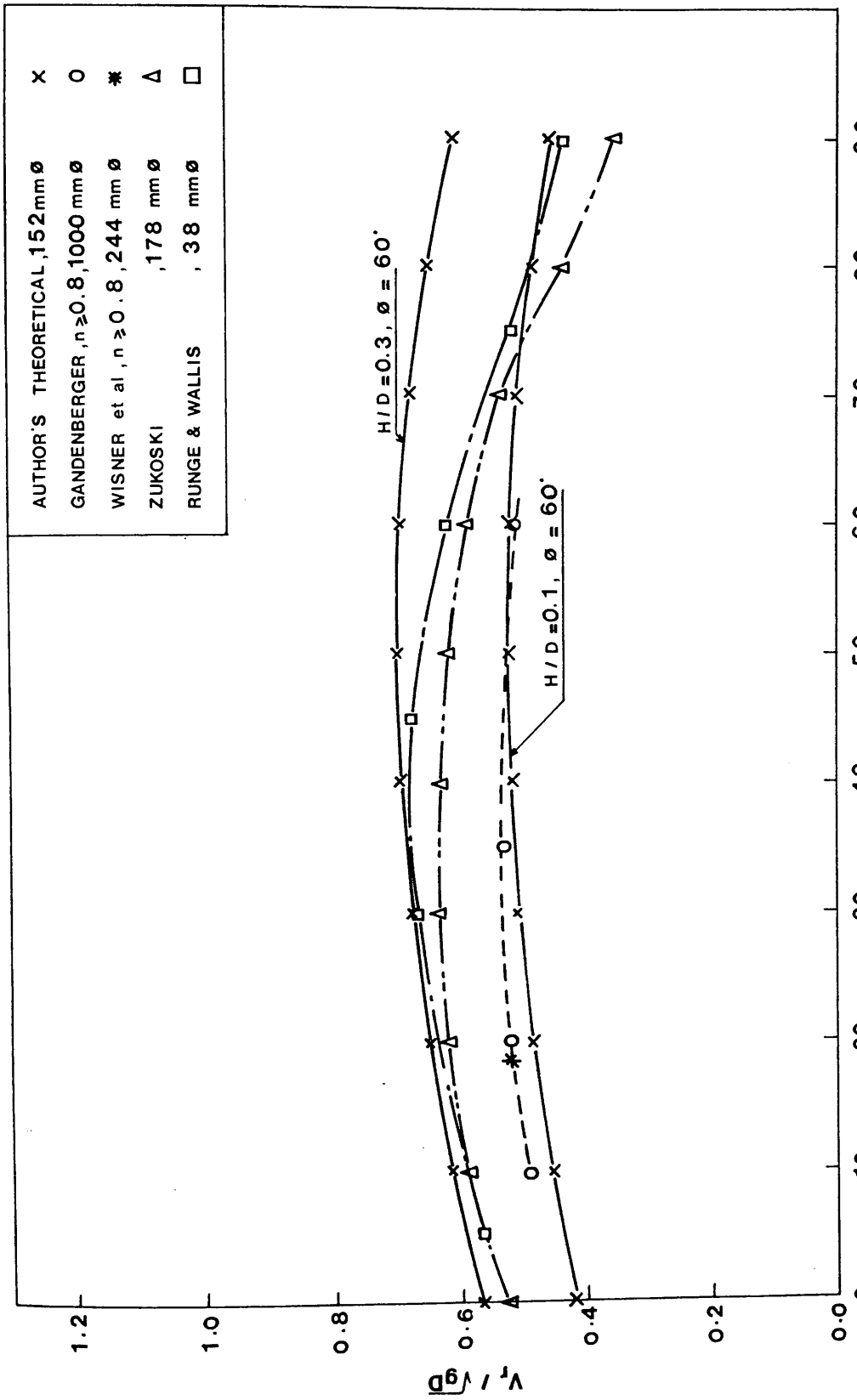

FIG. (7.22) COMPARISON BETWEEN THE AUTHOR'S THEORETICAL RISING VELOCITY FOR DIFFERENT ANGLES OF INCLINATIONS ABOVE HORIZONTAL AND EXPERIMENTAL RESULTS OF PREVIOUS INVESTIGATORS

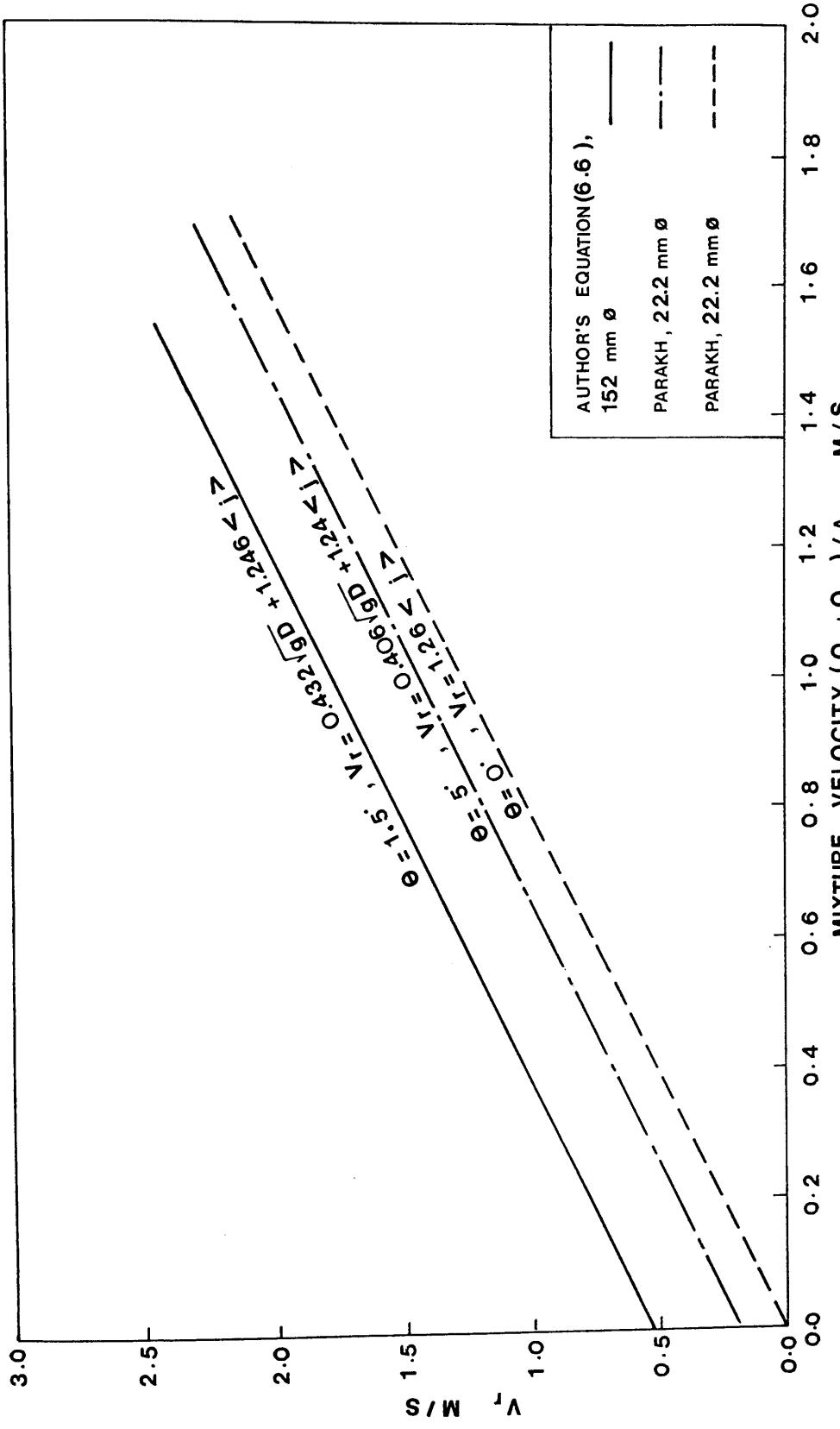

FIG. (7.23) COMPARISON BETWEEN AUTHOR'S EXPERIMENTAL RESULTS AND PARAK'S RESULTS FOR THE RISING VELOCITY OF AIR POCKETS IN UPWARD SLOPING TUNNELS WITH MOVING WATER

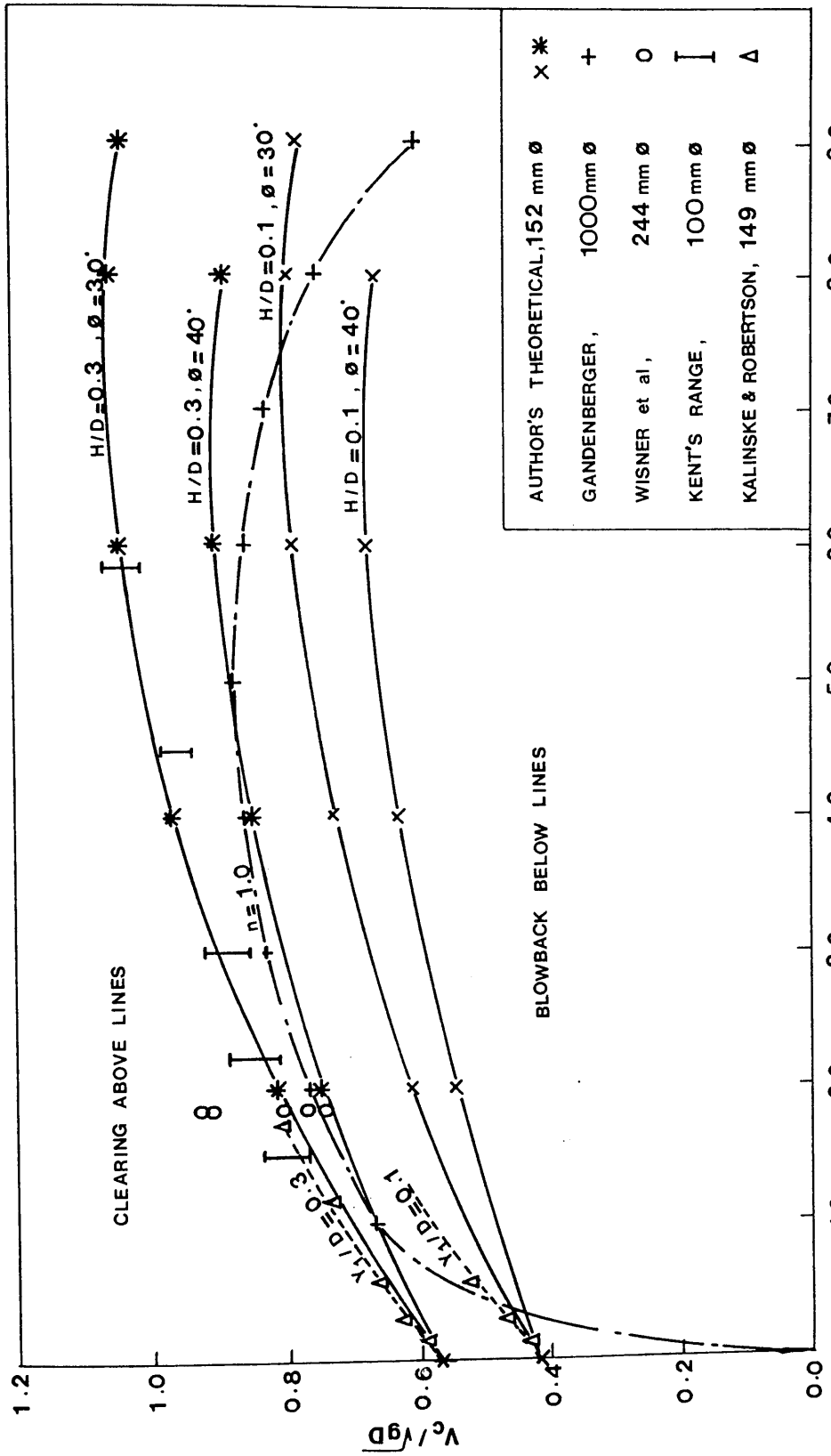

FIG. (7.24) COMPARISON BETWEEN AUTHOR'S THEORETICAL MODEL FOR BLOWING BACK AND CLEARING AIR POCKETS AND EXPERIMENTAL RESULTS OF PREVIOUS INVESTIGATORS FOR DOWNWARD SLOPING PIPE

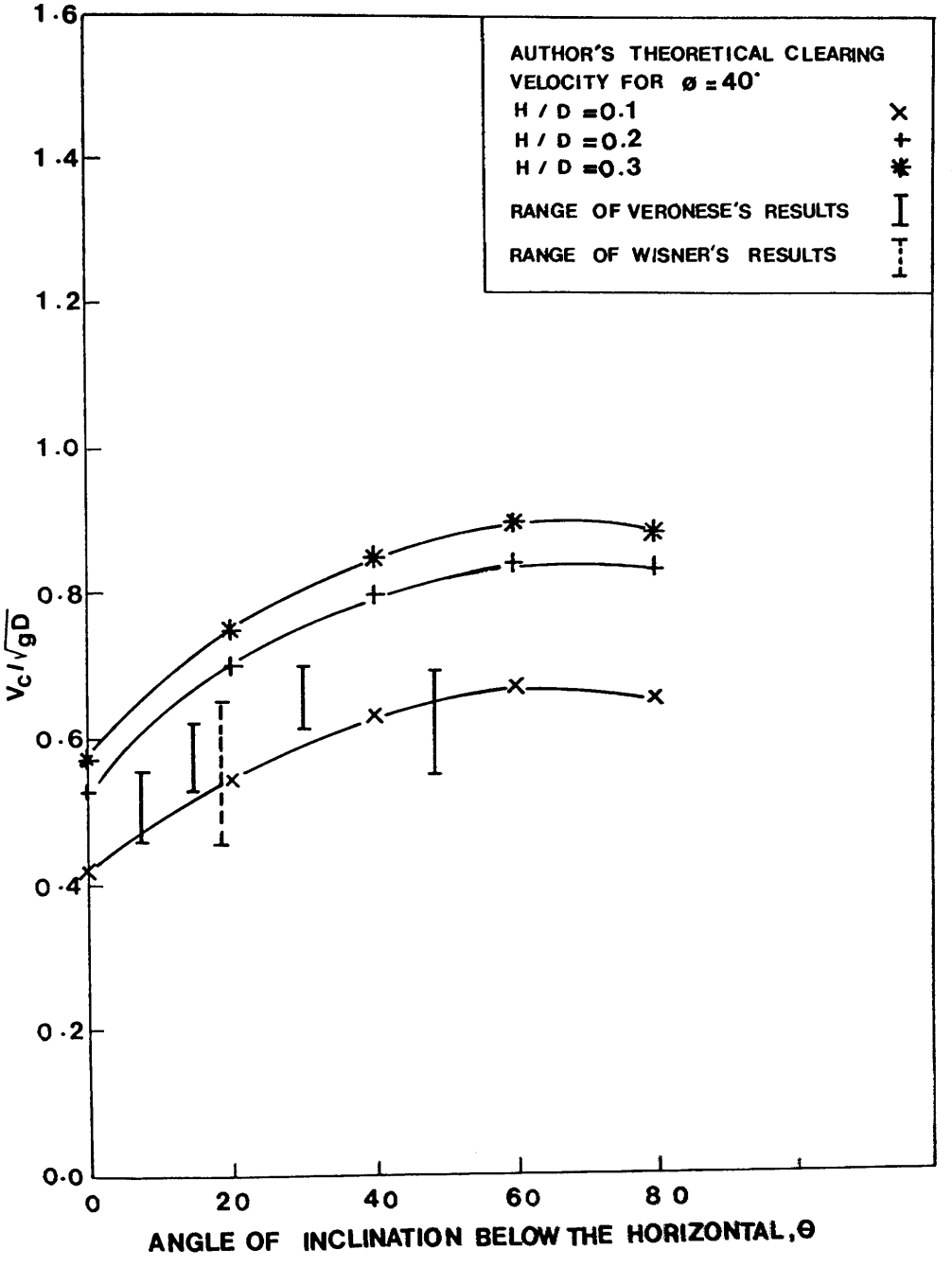

FIG. (7.25) COMPARISON BETWEEN THEORETICAL CLEARING VELOCITY OF AIR POCKETS IN A DOWNWARD SLOPING TUNNEL AND EXPERIMENTAL RESULTS OF PREVIOUS INVESTIGATORS FOR THE LIMIT AIR POCKET

Chapter Eight

DISCUSSION, CONCLUSIONS AND SUGGESTION FOR FUTURE RESEARCH

8.1 DISCUSSION

8.1.1 Introduction

The aims of this work were primarily as follows:

(a) to investigate air pocket behaviour at a dropshaft/tunnel bend.

(b) to investigate air pocket behaviour in straight pipes inclined upwards and downwards relative to the horizontal.

(c) to produce theoretical models for each of the above cases.

(d) to test the effectiveness of the theoretical models against the experimental data.

Secondary aims included:

(e) to produce a state-of-the-art study of air pocket behaviour in Civil Engineering hydraulic structures. This is attempted in the literature review in Chapter (2).

(f) to comment on the likely scale effects encountered in this kind of physical modelling.

(g) to produce design guidelines for designers of such hydraulic structures.

The effectiveness or otherwise of this work in achieving the aims listed above has depended to a large extent on the design of the experimental apparatus, the choice of instrumentation, the accuracy of the instrumentation, the range of physical parameters measured, the sophistication and accuracy of the theoretical models derived, as well as any empirical equations proposed, and the synthesis of experiment and theory to produce something meaningful for hydraulic designers. All these points require discussion, especially in the light of previous research work and any scale effects which may exist.

8.1.2 Apparatus and Instrumentation

The experimental apparatus was designed mainly for air pocket studies at the dropshaft/tunnel bend but was also designed to investigate air pocket behaviour in straight pipes. In the former case, the apparatus performed as it was designed, giving a comprehensive range of data for various bend radii, tunnel inclinations and ratios of air to water. In the latter case of the straight pipe, a good range of experimental data was obtained for the upward sloping pipe, but very little data was obtained for the downward sloping pipe. In the downward sloping pipe, it proved very difficult to introduce an air pocket from the upstream side, to have it remain stationary and then control the flow to investigate conditions necessary for blowback or clearing downstream. It was found generally that the straight tunnel section was too short for both sets of data in the straight pipe and the method of air introduction at the upstream end not suitable for the downward sloping pipe.

The method of air introduction at the upstream side proved effective. The concept of air injection rather than natural air

entrainment from plunging jets in the upper part of the dropshaft, meant that air flow to the bend could be controlled independently of the water flow. The method of achieving this using 16 air injection points each 5 mm diameter ensured a range of air bubble sizes comparable with nature. The method also overcome the scale effect problem of a model having a lower air/water ratio than the prototype structure, in that, any air/water ratio could be generated in this model independently of the scale of the model. One source of error in the air flow measurement was the neglect of measuring the air pressure at the rotameters, so that air volume could be corrected to atmospheric pressure. This was considered but not pursued, because having passed through the rotameters, the air entered the system at a relatively high point and descended the dropshaft to the bend where it increased in pressure again. Thus a measurement of air flow at the bend would have required a further pressure measurement at the bend for a further correction and the whole process was considered time consuming in the light of the knowledge that the head differences from atmosphere were not significantly large at either rotameters or dropshaft bend.

The method of measurement of the air pocket depth at the bend also proved reasonably effective, especially in view of the fact that the free water surface under the air pocket was often of a highly disturbed nature with a great deal of turbulence and swirl. Incidentally, great care was exercised in minimising the swirl phenomenon by an accurate alignment of the inlet flow, dropdshaft and outlet tunnel. The method of air pocket depth measurement at the bend was by a combination of wave monitor probe and calibrated scales on both sides of the pipe wall. Great care was taken with visual measurements from the calibrated scales, and these values were averaged with those of the wave monitor probe at the centre line of the pipe. It is difficult to see how else this depth measurement could have been taken apart from a battery of wave monitor probes which would have disturbed the flow and been expensive. The wave monitor probes proved very effective in measuring air pocket speeds

and sizes for the case of the upward sloping straight pipe.

8.1.3 Range of Parameters Tested

There is no doubt that the range of gross parameters tested in this work, apart from the diameter of the dropshaft/tunnel system, covered the range likely to be found in either model or prototype. This included the air/water ratio up to 100%, the pipe full Froude number up to 2, the ratios of bend radius R'/D from a sharp bend up to R'/D = 1.5, and the tunnel slope from +1.5° to -1.5°. There may be specific instances where the outlet tunnel slopes are greater than this range, but broadly speaking, such outlet tunnels are generally laid on the horizontal or sloping very slightly upwards.

There is, however, one major area which was not investigated in adequate detail in this experimental apparatus. That was, the measurement of point velocities in the water flow at the bend after the air pocket formed. A detailed knowledge of the point velocities and streamline patterns at the bend for each of the nine geometries tested would have produced accurate correction factors for the velocity and pressure heads at the front nose of the air pocket, α_o, β_o, α' and β'. This would have been very useful experimental information and would have produced much more accurate theoretical models, where resort was made to calculating theoretical correction factors.

The reason for the non-measurement of velocities around the bend was straightforward. It was extremely difficult and time consuming in the case of a two-phase flow. For instance, the laser doppler system in the laboratory could not be used for air concentrations greater than 2%. Insertion of a Pitot-Static tube at the bend meant that air bubbles reachaing the front nose of the Pitot-Static tube lodged there, giving completely spurious readings. It was thought that a miniature propeller meter might be suitable, but again it would require extensive calibration for two-phase flows

at different air bubble concentrations.

Another parameter which could have been developed more in this work was the measurement of ϕ, the angle of the front nose of the air pocket to the conduit roof in the case of straight pipes, and, the angle between the horizontal and a tangent to the front nose of the air pocket for the case of the bend air pocket. Some measurements were achieved of these angles during the course of the work, but in the hindsight of development of the theoretical models, accurate values of ϕ are essential.

8.1.4 Synthesis of Theory and Experiment

For air pocket formation at a dropshaft/tunnel bend, the experimental work has clearly shown that it is possible to simplify the flow patterns into four stable regimes. These have been outlined in Chapter (5). The experimental work has also revealed the extent of these regimes, especially the upper limits of blowback from the bend and the lower limits of clearing downstream from the bend, all for a wide range of bend radii R'/D, tunnel slope θ, and values of air/water ratio, β.

The theoretical models for the bend air pocket behaviour developed in Chapter (3) have been compared with experimental data in Chapter (7) clearly showing that it is possible to generate relatively simple models based on force-momentum and energy principles to give a good correlation with experiment, even in the face of the almost chaotic nature of the turbulent, two-phase flow at a vertical bend. One area which has not been amenable to theory so far, is that of an air pocket clearing downstream of a bend. This process is so complex that at least four separate mechanisms have been proposed in this thesis, as outlined in Chapter (7). In the absence of theory, empirical equations have been suggested for air pocket clearing, although these equations may be relevant only to the range of experimental parameters tested in this thesis.

An important question at the end of this work concerns the proposition of being able to accurately predict air pocket behaviour at a dropshaft/tunnel bend for any physical geometry without having to build a physical model of the system. One suggestion outlined below concerns the synthesis of the complete air pocket depth-Froude number graph for different values of air/water ratio. That is H/D versus Fr_o for different values of β, for a given geometrical configuration.

The first step in this process is to establish the pipe full Froude number at which an air pocket will just commence forming at the bend. Or, in other words, the Froude number required to transport air bubbles along the dropshaft to the bend. This process requires a definite downward velocity to counteract the upward bubble rise velocity. This process has been investigated by Ahmed and Ervine[4] who showed that air bubbles can be carried to the bend at velocities less than the bubble rise velocity ($\sim$ 0.25 m/s), because the bubbles are carried in vortices generated in the plunging jet shear layer. For shorter lengths from the jet impingement point to the bend, L/D < 20, air bubbles can be transported to the bend at velocities as small as 0.15 m/s. For longer dropshaft/lengths this velocity can increase to 0.25-0.3 m/s. Tests carried out in the experimental apparatus in this work have shown air bubbles to be carried to the bend at velocities as low as 0.13 to 0.15 m/s. It would be reasonable to assume the velocity to be around 0.15 m/s for air pockets to commence forming. This value is approximately constant for all model scales. Thus in this model, air pocket formation will commence at a Froude number $V_o/\sqrt{gD}$ of around 0.1 to 0.12, where as in the Hunterston 'B' Power Station prototype with D = 3.35 m, air pocket formation at the bend will commence at Froude numbers around 0.026. Hunterston 'B' is also considered a short droplength shaft as L/D =8.

The second step in the process is to estimate the ratio of air to water, β, which is likely to be reaching the bend for higher

water flow rates. Following the work of Ahmed this can now be done with some degree of accuracy. For closed cooling water systems with air coming out of solution, the value of β is unlikely to exceed 0.02, but for spillway dropshafts the value of β can reach 40-50% at the bend. For varying values of β with increasing Froude number of flow, the most satisfactory solution at present is to compute the range of behaviour with limits of $\beta = 0$ and $\beta = 0.5$.

From this point onwards, the equations presented in this thesis can be used to predict air pocket behaviour.

For the blowback regime 1, equation (3.57) is plotted corresponding to the bend radius R'/D and air/water ratio β. Equation (3.57) is relevant to any bend other than the sharp bend, where regime 2 behaviour is more applicable. Thus for the case of a sharp bend, R'/D = 0.5, equation (3.67) is applicable.

At higher Froude numbers, all bend radii and tunnel slopes, produce a stable hydraulic jump condition as outlined in equation (3.87). Finally, the air pocket will clear from the bend when the Froude number reaches the values predicted in equations (7.1) to (7.9). This is represented by a vertical line on the H/D - Fr_o graph. Tunnel slopes other than horizontal $\theta = 0^\circ$, or $\theta = +1.5^\circ$ or $\theta = -1.5^\circ$ will require interpolation of the values of A and B in Fig. (7.17) to produce a reasonably accurate clearing Froude number.

This process has been tentatively applied by the author to two practical situations and shown in Fig. (8.1):

(a) The Hunterston 'B' Power Station bend has an R'/D = 1.5, D = 3.35 m, $\theta = -0.286^\circ$ and $\beta = 0 \rightarrow 30\%$. The result is shown in Fig. (8.1a).

(b) The Kielder dropshaft at Letch House tank has an R'/D = 0.5, θ = +0.117°, D = 2.905 m and β = 0 → 40%. The result is shown in Fig. (8.1b).

8.1.5 Previous Research

The problem of comparing this work with previous research is that very little past work has been done in the area of air pockets forming at a dropshaft/tunnel bend which was the main thrust of this work, and a good deal has been done experimentally on straight pipes at various slopes, which is a minor part of this work.

Considering first the question of air pocket formation at the dropshaft/tunnel bend a comparison of the experimental data with that of Goldring[65] showed that there is some disagreement, especially for Froude numbers required for clearing downstream. This disagreement can be traced to the fact that air pockets clearing in this work were mainly by surface waves sealing the bend and bodily sweeping the air pocket, while for Goldring clearing was mainly by air entrainment at the toe of the jump. The difference is due to the fact that much higher air/water ratios were used in this work which affected the flow at the bend, while in Goldring's work, β values less than 0.02 only, were tested and air pockets cleared by air entrainment at the toe of the jump. The comparison of the upper blowback limits between this work and Goldring shows reasonable agreement, probably within the range of experimental error, and judgement as to what exactly constitutes blowback. Scale effects are not thought to be important in describing the blowback limits. The influence of β on the blowback limits was clearly shown in this work, but appear to have no effect on the data of Goldring. Again, it should be noted that Goldring tested only extremely small values of β.

The experimental results for air pockets rising in a straight pipe sloping upwards gave a good agreement both with

previous research and also the theoretical model derived in Chapter (3). Although more information is required on the relationship between the front nose of the air pocket ϕ and depth of pocket H/D, equation (3.100) now appears to give a very accurate estimate of the air pocket velocity in an upward sloping pipe for moving water conditions.

Very little experimental data was obtained for the case of blowback and clearing in a straight downward sloping pipe. The reasons for this are outlined in Chapter (6). However, the author's theoretical models for blowback and clearing in a straight pipe outlined in Chapter (3), gave an excellent comparison with past experimental data, as shown in Figs. (7.24) and (7.25). In the past, researchers have relied on experimental correlations for blowback and clearing and now the foundation has been set for producing a theoretical model which will be applicable in all situations.

8.1.6 Scale Effects

This aspect of the work has been discused in a paper by Ervine and Himmo[53] and also in Section (3.3) of this thesis.

Some care has been taken in the design of the experimental apparatus to minimise scale effects. The diameter of the dropshaft/tunnel system (D = 0.152 m) is known from the work of Zukoski shown in Fig. (2.4) and others, to produce almost negligible surface tension scale effects when modelling air pockets in closed conduit systems.

Furthermore, the air injection system allowed the air flow to be independent from the water flow which meant that air/water ratios were tested in the model which might normally only be present in a prototype situation. This potential scale effect was also avoided.

However, because only one scale of model was tested, two scale effects remain. The first is due to viscous effects and characterised by Reynolds number. In this context there is a growing recognition that for two-phase flows in general (air and water) that viscous effects are significant only up to a Reynolds number of around 10^5. This has been shown by Kobus[99] for bubbly two-phase flows and also Wisner et al[187] for larger air pocket two-phase flows. Using this criterion as a general guideline, a Reynolds number of 10^5 in the present work corresponds to a pipe-full velocity around 0.65 m/s and a pipe-full Froude number around 0.54. Approximately half the data would have been less than this Froude number value and hence subject to some viscous effects. The exact extent would not be known until the same experiments were carried out at other model scales, and even then could only be guessed at because the Weber number would also change, as would the ratio of air bubble diameter to pipe diameter which is perhaps the most significant scale effect in this type of modelling.

The most fundamental scale effect in two-phase flow modelling is the non-scaling of air bubble diameter, characterised by the ratio, d_b/D. This affects quantities of air descending the shaft, the relative movement of air bubbles under the pocket (V_{br}/V_1) and the rate of air transport out of the hydraulic jump when the flow is in regime 3. This in turn affects the air pocket clearing process which is partly governed by entrainment and transport of air bubbles at the toe of the hydraulic jump. Fortunately this mode of air pocket clearing is not as relevant for larger ratios of air to water β where the process is dominated by wave formation and bodily sweeping out of the pocket, the latter two phenomena hopefully essentially Froudian scaled. The most important outcome of non-scaling of air bubble sizes is that the clearing Froude numbers (Fr_{oc}) outlined in Chapter (6) are likely to be reduced in the prototype situation, although the exact extent would not be known until prototype data is available.

One method of overcoming the air bubble diameter scale effects is by the use of surfactants. This method was attempted by Townson[165] with little success. The air bubbles were scaled down to approximately the correct size, but the reduction in surface tension produced too many bubbles at the bend and led to air "hold-up" in the tunnel section because the tunnel water velocities were not adequate to remove such quantitites of air at the required rate.

The answer lies either in testing various model scales and comparing with prototype data, or, designing an air injection system where only smaller air bubbles exist but surface tension (σ) is not reduced.

It could be argued that scale effects were not significant in this model study. The main rationale for this argument is that the theoretical models derived in Chapter (3) are free of scale effects, but still gave good correspondence with most of the experimental data, as seen in Chapter (7). Unfortunately, the one exception to this rule was the process of clearing which is likely to be subject to some scale effects and no convincing theoretical model was derived for this phenomena.

8.2 CONCLUSIONS

1. Four general stable flow regimes were found to exist at the junction of the vertical dropshaft/tunnel system, namely:

   (a) Flow regime 1, with air bubbles and air pockets venting or blowing back up the vertical shaft.

   (b) Flow regime 2, with a stable air pocket at the bend and subcritical flow under the pocket.

(c) Flow regime 3, featuring a stable air pocket at he bend with a hydraulic jump at its downstream end. In some cases the pocket extended in length to the outlet tank, and is referred to as a stratified flow.

(d) Flow regime 4, featuring air pockets clearing downstream from the bend, where only air bubbles will be flowing around the bend.

2. The tunnel inclination with horizontal affected the flow regimes of the bend air pockets. The downward sloping tunnel increased the Froude number up to which blowback occurred compared to the horizontal and upward sloping tunnels, and also increased the Froude number at which clearing of air pockets commenced. The air pocket depth was generally shallower in the downward sloping tunnel compared with the upward sloping tunnel. Stratified flow appeared to be the dominant flow regime in the downward sloping tunnel, while more air pockets with subcritical flow (regime 2) occurred in the upward sloping tunnel.

3. For any tunnel inclination (θ), the value of bend radius showed an effect on the flow regimes of the bend air pocket. Increasing the bend radius from the sharp bend, $R'/D = 0.5$, to the more radiused bend, $R'/D = 1.5$, increased the possibility of air pockets blowing back and made it more difficult to clear the air pocket downstream. Also, increasing the bend radius increased the air pocket depth and stratified flow was more likely to occur. The sharp bend was found to be the most efficient for reducing blow-back effects and producing downstream clearing, although it is the bend which produces the largest head losses. In the sharp bend mainly smaller air bubbles vent back up the shaft, while in the radiused bends air pocket blowback occurs, which leads to oscillation and vibration in the system.

4. Increasing the air/water ratio reduced the Froude number at which air pockets blew back up the shaft and increased the Froude number required to clear an air pocket from the bend. Increasing the value of β increased the depth of the bend air pocket and often had the effect of changing the flow from blow back regime to stable air pocket.

5. For a fixed value of β, R'/D and θ increasing the Froude number of flow increased the air pocket depth until an air pocket with a stable hydraulic jump formed. At higher Froude numbers the depth of air pocket started reducing with increasing Fr_o until the whole pocket cleared. This is clearly seen in Figs. (5.3), (5.9) and (5.15) for Y_1/D against Fr_o.

6. Theoretical models were presented for flow regimes 1, 2 and 3, with a set of empirical correlations for clearing regime 4. The radiused bends R'/D = 1.0 and 1.5 fitted Models Type 1, 3 and 4, while the sharp bend R'/D = 0.5 fitted Model Types 2, 3 and 4. The comparison between theory and experiment revealed that Model Type 1 for blowing back is more applicable to radiused bends where the nose of the air pocket is considered a stagnation point, while Model Type 2 for the drowned jump is more applicable to the sharp bend where the nose of the pocket is considered a separation point. Equation (3.87) using force-momentum principles appeared to be more applicable to the air pockets with a hydraulic jump than equation (3.74), using a simplified energy method. The empirical equations for clearing air pockets from the bend show that clearing is dependent on tunnel inclination to horizontal, bend radius and air/water ratio. No satisfactory theoretical model was devised for air pockets clearing from the bend.

7. The rising velocities of air pockets in a straight upward sloping pipe is affected by the depth of air pocket H/D, angle of the pocket nose ϕ, air/water ratio β, water velocity V_o and

tunnel inclination θ. This is clearly seen in equations (6.2) to (6.5) and equation (3.100). Comparison between theory and experiment revealed good agreement and a perfect correlation was achieved in equation (7.11), where the factor 1.1 was applied to the term of the mixture velocity to account for the "wake" effect. Comparison of experimental data with previous research showed good agreement, particularly the case of previous research with stationary water which was compared with $V_o = 0$ in the author's moving water work, giving good agreement.

8. Blowback and clearing in a downward sloping pipe is also affected by air pocket depth H/D, angle of pocket nose ϕ, air water ratio β, water velocity V_o and tunnel inclination θ. The comparison of the theoretical model with experimental data was incomplete due to lack of data, but the author's theory showed a good agreement with previous research.

9. Comparison of the author's theoretical models with previous research showed a good agreement, especially for air pockets in straight pipes laid above and below the horizontal. The comparison for air pockets at the junction of a dropshaft/tunnel system was limited to only one piece of previous research, where the balue of β was limited to 0.02, which is much less than that used in this work. The results for air pockets blowing back were fairly comparable, while the results for air pockets clearing were in disagreement. This is due to two different mechanisms affecting the clearing of air pockets.

10. The surface tension effect was overcome by using a large pipe diameter (D = 0.152 m) as mentioned in previous research. To reach air/water ratios commonly found in prototype structures, a separate air injection system was used. Some viscous effects may have been affecting data with Froude numbers less than 0.54. This corresponds to the criterion of Reynolds number < 10^5. The air pockets clearing by air entrainment at the toe of the jump

are subject to scale effects, while air pockets clearing by surface waves can be Froudian scaled. It can be argued that scale effects were not significant in this study because the theoretical models derived in Chapter (3) are free of scale effects, and yet gave good agreement with experimental data.

8.3 SUGGESTIONS FOR FUTURE RESEARCH

1. A very useful extension of this work would be an investigation into methods of preventing the air pocket forming at the dropshaft/tunnel bend and efficient methods of air removal if the bend pocket is trapped. This should include studies of preventing air bubbles descending the dropshaft to the bend, a systematic study of the design of air vent pipes on the conduit roof just downstream of the bend, as well as an investigation into methods for inducing an intense swirl at the bend inhibiting the formation of a stable air pocket. This would be a very practical study with many changes of geometry required before optimum design is reached.

2. Another useful extension to this work would be a purpose built rig to investigate blowback and clearing of air pockets in downward sloping pipes. This would have design implications for long siphons, high points in pipelines and outlets of nuclear power stations. An important aspect of this work would be the development of the theoretical equations outlined in this thesis but with greater emphasis on the variation of the nose angle of the air pocket with H/D and conduit slope, θ.

3. An investigation could be carried out into the scale effects related to this type of physical situation. This might include, testing at different model scales, comparing with prototype data, using different fluids to look at the effect of viscosity, and using an air injection system with air bubbles scaled to the

proper ratio d_b/D. The use of surfactants may also be a useful addition.

4. A further study of air pocket formation at the bend might be carried out for a different range of geometrical parameters. This might involve a greater range of tunnel slopes, bend radii or even a range of dropshaft angles rather than simply vertical. One such application has been investigated by Dr. Ervine at the Hoover Dam in U.S.A. where the dropshaft was inclined and led to a horizontal outlet tunnel. Air pockets being cleared to the outlet had to pass through outlet valves before reaching the atmosphere. Problems of noise and vibration were encountered with air pockets escaping through the outlet valves.

5. Much more detailed work could be carried out for flow at the dropshaft/tunnel bend. This might include detalied point velocity measurements, pressure distribution and determination of the streamline pattern for the two-phase flow with an air pocket at the conduit roof. At the very least, this would provide valuable information on the correction factors required for the energy and momentum equations and would lead to more relaible predictions.

6. There is considerable scope for further development of the theoretical models outlined in Chapter (3) of this thesis. This might involve development of theoretical models for air pockets clearing from the bend, a more accurate assessment of the energy and momentum at a section at the front nose of the air pocket, and further work on the variation of the angle Φ with bend radius, tunnel slope and air/water ratio.

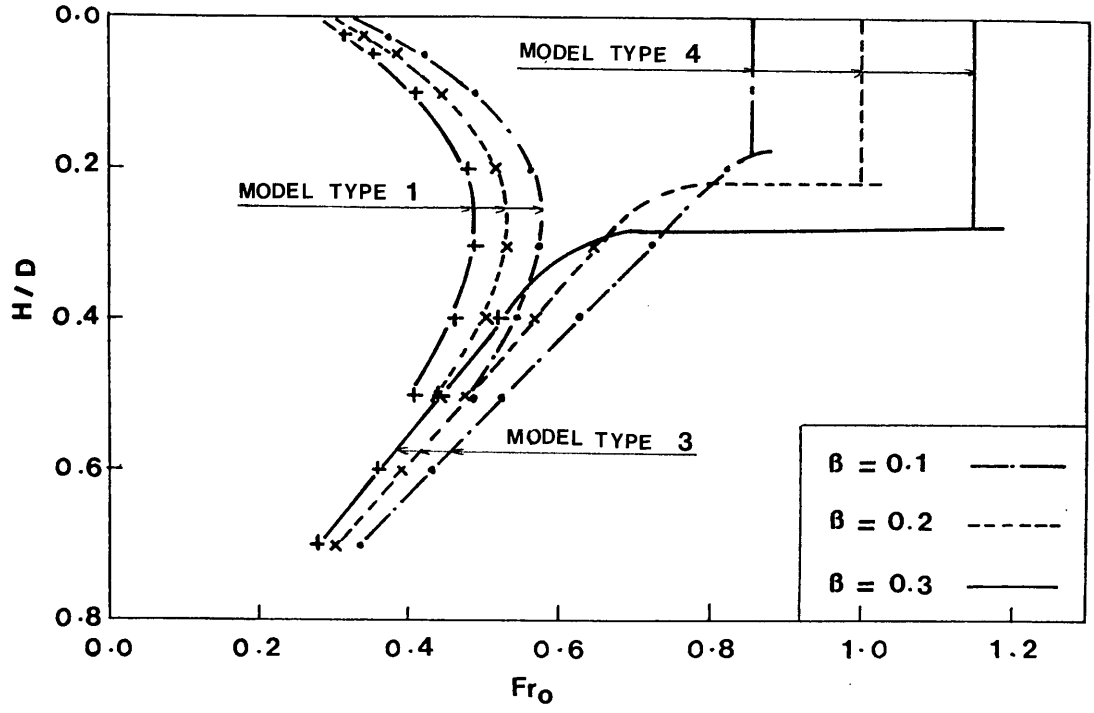

(a) HUNTERSTON "B" POWER STATION, WITH TUNNEL INCLINATION $\theta = -0.286^{\circ}$ AND BEND RADIUS $R'/D = 1.5$

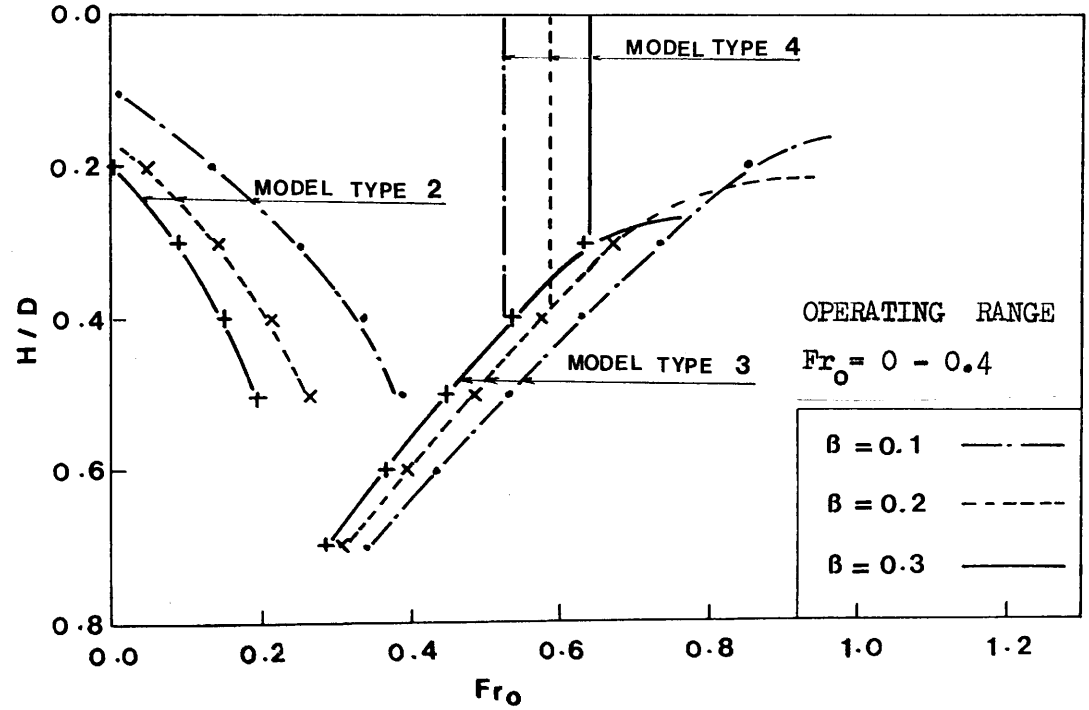

(b) THE KIELDER DROPSHAFT AT LETCH HOUSE TANK, WITH TUNNEL INCLINATION $\theta = +0.117^{\circ}$, AND BEND RADIUS $R'/D = 0.5$

FIG. (8.1) THE SYNTHESIS OF THE AIR POCKET IN PROTOTYPE STRUCTURES

LIST OF REFERENCES:

1. Addison, H. (1940). "Hydraulic Measurements", Chapman and Hall Ltd.

2. Advani, R.M. (1962). "A New Method For Hydraulic Jump In Circular Channels", Water Power, pp 349-350.

3. Agrawel, S.S., Gregory, G.A. and Govier, G.W. (1973). "An Analysis Of Horizontal Stratified Two-Phase Flow In Pipes", The Canadian Journal of Chemical Engineering, Vol. 51, pp 280-286.

4. Ahmed, A.A., Ervine, D.A. and McKeogh, E.J. (1984). "The Process Of Aeration In Closed Conduit Hydraulic Structures", Proc. Symp. of Scale Effects in Modelling Hydraulic Structures, Paper 4.13, Esslingen, Germany.

5. Albertson, M.L., Barton, J.R. and Simons, D.B. (1960). "Fluid Mechanics For Engineers", Prentice-Hall, Inc.

6. Ali, K.H.M. and Pateman, D. (1980). "Theoretical And Experimental Investigation Of Air-Regulated Siphons", Proc. Instn. Civ. Engrs., Part 2, Vol. 69, Paper 8309, pp 111-138.

7. Allen, D.N. de G. (1954). "Relaxation Methods In Engineering And Science", McGraw-Hill, New York, London.

8. Alves, G.E. (1954). Chemical Engineering Progress, Vol. 50, pp 449-456.

9. Amphlett, M.B. (1976). "Air-Entraining Vortices At A Horizontal Intake", Report No. OD7 of Water Resources and Irrigation.

10. Anderson, A. (1976). "Oscillation In A Cooling Water Outfall System, (Discussion)", Proc. Instn. Civ. Engrs., Part 2, Vol. 61, pp 499-506.

11. Anderson, A. (1984). "Surge Shaft Stability With Pumped Storage Schemes", A.S.C.E., Journal of Hydraulic Engineering, Vol. 110, No. 6, pp 687-706.

12. Anderson, A.H. (1961). "Model Studies Of Storm-Sewer Drop Shafts", St. Anthony Falls Hydraulic Laboratory, University of Minnesota, Technical Paper No. 35, Series B.

13. Babb, A.F., Schneider, J.P. and Thompson, K. (1973). "Air Flow In Combined Intake And Shaft Spillways", A.S.C.E., Journal of Hydraulic Division, Vol. 99, No. HY7, pp 1097-1108.

14. Bacopoulous, T. (1984). "The Motion Of Air Cavities In Large Water-Filled Conduits". A Thesis Submitted to The University of Strathclyde for the Degree of Doctor of Philosophy.

15. Baines, W.D. and Wilkinson, D.L. (1986). "The Motion Of Large Air Bubbles In Ducts Of Moderate Slope", Journal of Hydraulic Research, Vol. 25, No. 3, pp 157-170.

16. Baker, O. (1954). Oil Gas Journal, Vol. 53, No. 12, pp 185-190, 192.

17. Bakhmeteff, B.A. and Matzke, A.E. (1936). "The Hydraulic Jump In Terms Of Dynamic Similarity", Trans. A.S.C.E., Vol. 101, Paper No. 1935, pp 630-680.

18. Bakhmeteff, B.A. and Matzke, A.E. (1938). "The Hydraulic Jump In Sloped Channels", Trans. A.S.M.E., Vol. 60, pp 111-118.

19. Ball, J.W., Tullis, J.P. and Stripling, T. (1975). "Predicting Cavitation In Sudden Enlargements", A.S.C.E., Journal of Hydraulic Division, Vol. 101, No. HY7, pp 857-870.

20. Ball, J.W. (1976). "Cavitation From Surface Irregularities In High Velocity", A.S.C.E., Journal of Hydraulic Division, Vol. 102, No. HY9, pp 1283-1297.

21. Barr, D.I.H. (1965). "Economic Selection Of Pipeline And Tunnel Diameters", Water Power, pp 237-239.

22. Barr, D.I.H. (1969). "Method Of Synthesis - Basic Procedures For The New Approach To Similitude", Water Power, Vol. 21, 148-153, 183-188, April and May.

23. Beichley, G.L. and King, D.L. (1975). "Cavitation Control By Aeration Of High Velocity Jets", A.S.C.E., Journal of Hydraulic Division, Vol. 101, No. HY7, pp 829-846.

24. Benjamin, T.B. (1968). "Gravity Currents And Related Phenomena", Journal Of Fluid Mechanics, Vol. 31, Part 2, pp 209-248.

25. Binnie, A.M. (1962). "Experiments On The Swirling Flow Of Water In A Vertical Pipe And A Bend", Proc. of The Royal Soc., A270, pp 452-466.

26. Bonnecaze, R.H., Erskine, W., J.R. and Greskovich, E.J. (1971). "Holdup Pressure Drops For Two Phase Slug Flow In Inclined Pipelines", A.I.Ch.E. Journal, Vol. 17, No. 5, pp 1109-1113.

27. Bradley, J.N. (1956). "Prototype Behaviour", Trans. A.S.C.E., Vol. 121.

28. Bretherton, F.P. (1961). "The Motion Of Long Bubbles In Tubes", Journal of Fluid Mechanics, Vol. 10, pp 166-188.

29. Brook, H.N. and Blackmer, W.H. (1962). "Vortex Energy Dissipator For San Diego Ocean Outfall Laboratory Investigations". Final Report to Holmes and Narver Montgomery, Los Angeles, California.

30. Brown, R.A.S. and Govier, G.W. (1965). "The Mechanics Of Large Gas Bubbles In Tubes". The Canadian Journal of Chemical Engineering, pp 224-230.

31. Brown, R.A.S. (1965). "The Mechanics of Large Gas Bubbles In Tubes", The Canadian Journal of Chemical Engineering, pp 217-223.

32. Carver, M.B. (1984). "Numerical Computation Of Phase Separation In Two Fluid Flow", Trans. A.S.M.E., Journal of Fluid Engineering, Vol. 106, pp 147-153.

33. Caussade, B., George, J., Marodon, D. and Masbernat, L. (1982). "Mathematical Modelling Of Stratified Two-Phase Flow". Proc. of The Symp. (I.A.H.R.) Refined Modelling of Flows, Vol. 2, pp 657-669.

34. Chow, V.T. (1981). "Open Channel Hydraulics", McGraw-Hill International Book Company, Inc.

35. Colgate, D. (1966). "Hydraulic Model Studies Of The Flow Characteristics And Air-Entrainment In The Check Towers Of The Main Aqueduct, Canadian River Project, Texas", Report No. HYD 555, Denver, Colorado.

36. Collins, R. (1967). "The Effects Of A Containing Cylindrical Boundary On The Velocity Of A Large Gas Bubble In A Liquid", Journal of Fluid Mechanics, Vol. 28, Part 1, pp 97-112.

37. Collins, R., Moraes, F.F.D., Davidson, J.F. and Harrison, D. (1978). "The Motion Of A Large Gas Bubble Rising Through Liquid Flowing In A Tube", Journal of Fluid Mechanics, Vol. 89, Part 3, pp 497-514.

38. Davies, R.M. and Taylor, G.J. (1950). "The Mechanics Of Large Bubbles Rising Through Extended Liquids And Through Liquids In Tubes", Proc. of The Royal Soc. (London), Vol. 200, Ser. A, pp 375-390.

39. Denney, D.F. and Young, G.A.J. (1957). "The Prevention Of Vortices And Swirl At Intakes", The 7th Congress of I.A.H.R.

40. Diskin, M.H. (1961). "Hydraulic Jump In Trapizoidal Channels", Water Power, pp 12-17, 22.

41. Dukler, A.E. and Bergelin, O.P. (1952). "Characteristics Of Flow In Falling Liquid Film", Chemical Engineering Progress, Vol. 48, No. 11, pp 557-563.

42. Dumitrescu, D.T. (1943). Z. Angew Math. Mech., Vol. 23, No. 3, pp 139.

43. Edmunds, R.C. (1979). "Air Binding In Pipes", Journal of A.W.W.A., Water Technology Distribution, pp 272-277.

44. Ellis, J., Ervine D.A. and Balata, B.J. (1978). "Surge Protection Of The Kielder Water Scheme Transfer Works", Proc. Instn. Civ. Engrs., Part 1, Paper No. 8073, pp 227-246.

45. Enayet, M.M., Gibson, M.M., Taylor, A.M.K.P. and Yianneskis, M. (1982). "Laser-Doppler Measurements Of Laminar And Turbulent Flow In A Pipe Bend", Int. J.Heat and Fluid Flow, Vol. 3, No. 4, pp 213-219.

46. Ervine, D.A. (1976). "The Design And Modelling Of Air-Regulated Siphon Spillways", Proc. Instn. Civ. Engrs., Part 2, Vol. 61, pp 383-400.

47. Ervine D.A. and Kolkman, P.A. (1980). "Air Entrainment And Transport In Closed Conduit Hydraulic Structures", Internal Report S330, Delft Hydraulic Laboratories.

48. Ervine, D.A. (1980). "A Study Of Aeration And Air Venting In M'Dez Overflow Spillways, Morocco", Internal Report S370, Delft Hydraulic Laboratories.

49. Ervine, D.A. (1980). "Theoretical And Experimental Investigation Of Air-Regulated Siphons, (Discusion)", Proc. Instn. Civ. Engrs., Part 2, Paper No. 8309, pp 1059-1064.

50. Ervine, D.A., McKeogh, E. and Elsawy, E.M. (1980). "Effect of Turbulence Intensity On The Rate Of Air Entrainment By Plunging Water Jets", Proc. Instn. Civ. Engrs., Part 2, Vol. 69, Paper No. 8331, pp 425-445.

51. Ervine, D.A. and Oliver, G.C.S. (1980). "The Full Scale Behaviour Of Air-Regulated Siphon Spillway", Proc. Instn. Civ. Engrs., Part 2, Vol. 69, Paper No. 8351, pp 687-706.

52. Ervine, D.A. and Ahmed, A.A. (1982). "A Scaling Relationship For A Two-Dimensional Vertical Dropshaft", International Conference on The Hydraulic Modelling of Civil Engineering Structures, Coventry, England.

53. Ervine, D.A. and Himmo, S.K. (1984). "Modelling The Behaviour Of Air Pockets In Closed Conduit Hydraulic Systems", Symp. on Scale Effects in Modelling Hydraulic Structures, Paper 4.15, Esslingen, Germany.

54. Falvey, H.T. (1977). "Air Entrainment In High Speed Gated Conduits, (Discussion)", A.S.C.E., Journal of Hydraulic Division, Vol. 103, No. HY10, pp 1254-1255.

55. Falvey, H.T. (1980). "Air-Water Mixtures", U.S. Bureau of Reclamation Report, U.S. Dept. of Interior Water and Power Resources Service, Engineering Monograph No.41.

56. Falvey, H.T. (1982). "Predicting Cavitation In Tunnel Spillways", Water Power and Dam Construction, pp 13-15.

57. Foster, A.L. (1945). "Construction Of The Flow Net For Hydraulic Design", Trans A.S.C.E., Vol. 110, Paper No. 2255, pp 1237-1256.

58. Francis, J.R.D. and Minton, P. (1984). "Civil Engineering Hydraulics", Edward Arnold (Publishers) Ltd.

59. Gandenberger, W. (1957). "Uber Die Wirt Schaftliche Und Betriebssichere Gestaltung Von Fernwasserleitungen", R. Oldenbourg Verlag, Munich, Germany.

60. Gardner, G.C. and Crow, I.G. (1970). "The Motion Of Large Bubbles In Horizontal Channels", Journal of Fluid Mechanics, Vol. 43, Part 2, pp 247-255.

61. Gardner, G.C. and Adebiye, G.A. (1974). "The Liquid Film Left Behind By A Large Bubble In A Sloping Channel", Chemical Engineering Science, Vol. 29, pp 461-473.

62. Goldring, B.T. (1979). "The Use Of Small-Scale Siphon Models", Proc. Instn. Civ. Engrs., Part 2, Vol. 67, pp 929-942.

63. Goldring, B.T. Mawer, W.T. and Thomas, N. (1980). "Level Surges In The Circulating Water Dropshaft Of Large Generating Stations", Third International Conference on Pressure Surges, pp 279-299.

64. Goldring, B.T. (1981). "The Behaviour Of Entrained Air At Downshaft - Tunnel Bends", Central Electricity Generating Board, RL/L/N 155/80.

65. Goldring, B.T. (1983). "Air Voids At Downshaft-Tunnel Bends", A.S.C.E., Journal of Hydraulic Engineering, pp 189-198.

66. Goldring, B.T. (1984). "Blowbacks In Downward Sloping Pipes", Unpublished Report, Central Electricity Generating Board, Research Laboratory.

67. Goldsmith, H.L. and Mason, S.G. (1962). "The Movement Of Single Large Bubbles In Closed Vertical Tubes", Journal of Fluid Mechanics, Vol. 14, pp 42-58.

68. Gosline, J.E. (1935). "Experiments On The Vertical Flow Of Gas-Liquid Mixtures In Glass Pipes", Trans A.I.M.E., pp 56-70.

69. Govier, G.W. and Short, W.L. (1958). "The Upward Vertical Flow Of Air-Water Mixtures", The Canadian Journal of Chemical Engineering, pp 195-202.

70. Gregory, G.A. (1974). "Comments On The Prediction Of Liquid Holdup For Gas-Liquid Flow In Inclined Pipes", The Canadian Journal of Chemical Engineering, Vol. 52, pp 463-467.

71. Gregory, G.A. (1975). "Comparison Of Methods For The Prediction Of Liquid Holdup For Upward Gas-Liquid Flow In Inclined Pipes", The Canadian Journal of Chemical Engineering, Vol. 53, pp 384-388.

72. Greskovich, E.J. (1969). "True Gas Content For Horizontal Gas-Liquid Flow", Ind. Eng. Chem. Fundamentals, Vol. 8, No. 3, pp 591-593.

73. Greskovich, E.J. and Shrier, A.L. (1971). "Pressure Drop And Holdup In Horizontal Slug Flow", A.I.Ch.E. Journal, Vol. 17, No. 5, pp 1214-1219.

74. Greskovich, E.J. and Shrier, A.L. (1972). "Slug Frequency In Horizontal Gas-Liquid Slug Flow", Ind. Eng. Chem. Process Des. Develop., Vol. 11, No. 2, pp 319-320.

75. Greskovich, E.J. (1973). "Prediction of Gas-Liquid Holdup For Inclined Flows", A.I.Ch.E. Journal, Vol. 19, No. 5, pp 1060-1061.

76. Greskovich, E.J. and Cooper, W.T. (1975). "Correlation And Prediction Of Gas-Liquid Holdups In Inclined Upflows", A.I.Ch.E. Journal, Vol. 21, No. 6, pp 1189-1192.

77. Griffith, P. and Wallis, G.B. (1961). "Two-Phase Slug Flow", Trans. A.S.M.E., Journal of Heat Transfer, Series C, Vol. 83, pp 307-320.

78. Griffith, P. (1963). "The Prediction Of Low-Quality Boiling Voids", Trans. A.S.M.E., Journal of Heat Transfer, Paper No. 63-HT-20, pp 1-7.

79. Gutti, S.R. (1968). "Behaviour Of Small Gas Bubbles In Accelerated Liquid", A.S.C.E., Journal of Hydraulic Division, Vol. 94, No. HY4, pp 1073-1082.

80. Gutti, S.R. (1971). "Movement Of Smal Gas Bubbles In Smoothly Decelerating Liquid", A.S.C.E., Journal of Hydraulic Division, Vol. 97, No. HY7, pp 1117-1128.

81. Haberman, W.L. and Morton, R.K. (1956). "An Experimental Study Of Bubbles Moving In Liquids", Trans A.S.C.E., Vol. 121, pp 227-250.

82. Haindl, K. and Sotronik, V. (1957). "Quantity Of Air Drawn Into A Conduit By The Hydraulic Jump And Its Measurement By Gamma-Radiation". I.A.H.R., Seventh General Meeting, Transactions, Vol. 2, pp D31-1-D31-7, Lisbon.

83. Haindl, K. (1957). "Hydraulic Jump In Closed Conduits", I.A.H.R., Seventh General Meeting, Transactions, Vol. 2, pp D32-1-D32-12, Lisbon.

84. Haindl, K. (1969). "Zone Lengths Of Air Emulsion In Water Downstream Of The Ring Jump In Pipes", 13th Congress of the International Association for Hydrdaulic Research, August 31-Sept. 5, Vol. 2, pp 9-19, Kyoto, Japan.

85. Haindl, K. (1984). "Aeration At Hydraulic Structures". In "Development In Hydraulic Engineering - 2", Edited by Novak, P., Elsevier Applied Science Publishers.

86. Hall, L.S. (1944). "Conformity Between Model And Prototype (Discussion)", Trans A.S.C.E., Vol. 109, Paper 2207, pp 150-154.

87. Harmathy, T.Z. (1960). "Velocity Of Large Drops And Bubbles In Media Of Infinite Or Restricted Extent", A.I.Ch.E. Journal, Vol. 6, No. 2, pp 281-288.

88. Head, C.R. (1975). "Low Head Air-Regulated Siphons", A.S.C.E., Journal of Hydraulic Division, No. HY3, pp 329-345.

89. Henderson, F.M. (1966). "Open Channel Flow", MacMillan Publishing Co. Inc.

90. Hetsroni, G., Haber, S. and Wacholder, E. (1970). "The Flow Fields In And Around A Droplet Moving Axially Within A Tube", Journal of Fluid Mechanics, Vol. 41, Part 4, pp 689-705.

91. Inoue, M. (1978). "Estimation Of Head Loss Due To Air Pockets And Hydraulic Jump In A Downward Sloping Pipe", C.E.G.B., Translation Section No. C.E. 7752, 1981, Transactions Japan Society of Irrigation, Drainage and Reclamation Engineering, No. 77, pp 27-31.

92. Jenna, W.S. (1983). "Introduction To Fluid Mechanics", Brook/Cole Engineering Division.

93. Kalinske, A.A. and Bliss, P.H. (1943). "Removal Of Air From Pipelines By Flowing Water", A.S.C.E., Vol. 13, No. 10, pp 480-482.

94. Kalinske, A.A. and Robertson, J.M. (1943). "Closed Conduit Flow", Transactions, A.S.C.E., Vol. 108, pp 1435-1516. (Including The Discussion).

95. Kao, T.W. (1977). "Density Currents And Their Applications", A.S.C.E., Journal of Hydraulic Division, Vol. 103, No. HY5, pp 543-555.

96. Karman, T.V. (1940). "The Engineer Grapples With Non Linear Problems", Bull. Am. Math. Soc., Vol. 46, pp 615-683.

97. Kent, J.C. (1952). "The Entrainment Of Air By Water Flowing In Circular Conduits With Down-Grade Slopes", Thesis Presented to The University of California, at Berkeley, California, in Partial Fulfillment of the Requirements for the Degree of Doctor of Philosophy.

98. Kindsvator, C.E. (1937). "The Hydraulic Jump In Enclosed Conduits", A Thesis Submitted in Partial Fulfillment of the Requirements for the Degree of Master of Science in The Dept. of Mech. and Hydr., in The Graduate College of State, University of Iowa.

99. Kobus, H. (1984). "Local Air Entrainment And Detrainment", Proc. Symp. of Scale Effects in Modelling Hydraulic Structures, Paper 4.10, Esslingen, Germany.

100. Kobus, H.E. (1985). "An Introduction To Air-Water Flows In Hydraulics", Institut fur Wasserbau der Universitat Stuttgart, Heft Nr. 61.

101. Laird, A.D.K. and Chisholm, D. (1956). "Pressure And Forces Along Cylindrical Bubbles In A Vertical Tube", Industrial and Engineering Chemistry, Vol. 48, No. 8, pp 1361-1364.

102. Lara, C.D. (1955). "Degayage Natural Dans Les Pints Incline Relient Les A Ductions Secondaires Aux Galeries En Charge", Proc. of the 6th General Meeting, I.A.H.R., The Hague, Netherlands. (In French).

103. Leliavsky, S. (1965). "Design Textbook in Civil Engineering, Vol. 2, Irrigation Enginering: Syphons, Weirs and Locks", Chapman and Hall Ltd.

104. Li, W.H. and Walsh, J.P. (1964). "Pressure Generated By Cavitation In A Pipe", A.S.C.E., Journal of Engineering Mechanics Division, Vol. 90, No. EM6, pp 113-133.

105. Macagno, E.O. and Macagno, M.C. "Mixing Interfacial Hydraulic Jump", International Association for Hydraulic Research, C43, pp 373-381.

106. Martin, C.S. (1973). "Characteristics Of An Air-Water Mixture In A Vertical Shaft", A.S.C.E., Proc. Hydraulic Division Specialty Conference, Bozeman, Mont., August 15-17, pp 323-334.

107. Martin, C.S. (1976). "Vertically Downward Two-Phase Slug Flow", Trans. A.S.M.E., Journal of Fluid Engineering, Vol. 98, Series 1, No. 4, pp 715-721.

108. Massey, B.S. (1961). "Hydraulic Jump In Trapizoidal Channels", Water Power, pp 232-233, 237.

109. McConnachei, G.L. (1984). "Flocculation And Turbulence From Bubble Induced Mixing", Journal of the Institution of Water Engineers and Scientists, Vol. 38, No. 4, pp 337-347.

110. Mechler, W.A. (1966). "Factors Influencing Flow In Large Conduits", A.S.C.E., Journal of Hydraulic Division, Vol. 92, No. HY4, pp 203-218.

111. Mechler, W.A. (1976). "Removal Of Air From Water Lines By Hydraulic Means, (Discussion)", A.S.C.E., Journal of Hydraulic Division, Vol. 102, No. HY3, pp 420-421.

112. Miller, D.S. (1973). "Oscillation In A Circulating Water Outfall System Hunterston B Power Station", B.H.R.A., RR1196.

113. Miller, D.S. (1976). "Model Studies Of Kalan Power Station Outlets And Dropshaft", B.H.R.A., RR1350.

114. Mitsukiyo, M. et al (1977). "Flow Of Entrained Air In Centrifugal Pumps", Proc. I.A.H.R. 17th Congress, Baden-Baden, Paper B8, pp 71-79.

115. Mohsen, F.N. (1972). "Clearing Velocity Of Air Pockets In Water Lines", A Thesis Presented to the University of Waterloo at Waterloo, Ontario Canada, in Partial Fulfillment of the Requirements for the Degree of Master of Applied Science.

116. Moissis, R. and Griffith, P. (1962). "Entrance Effects In A Two-Phase Slug Flow", Trans. A.S.M.E., Journal of Heat Transfer, Series C, Vol. 84, No. 1, pp 29-39.

117. Mussalli, Y.G. (1978). "Size Determination Of Partly Full Conduits", A.S.C.E., Journal of Hydraulic Division, Vol. 104, No. HY7, pp 959-974.

118. Nelidov, I.M., Rajaratnam, N., Jones, L.E., Massey, B.A. and Advant, R.M. (1964). "Hydraulic Jump In All Shapes Of Horizontal Channels, (Discussion)", A.S.C.E., Journal of Hydraulic Division, No. HY4, pp 339-358.

119. Neville, A.M. and Kennedy, J.B. (1964). "Basic Statistical Methods For Engineers And Scientists", International Textbook Company.

120. Nguyen, V.T. and Spedding, P.L. (1977). "Holdup In Two-Phase Gas-Liquid Flow - 1", Chemical Engineering Science, Vol. 32, pp 1003-1014.

121. Nguyen, V.T. and Spedding, P.L. (1977). "Holdup In Two-Phase Gas-Liquid Flow-2", Chemical Engineering Science, Vol. 32, pp 1015-1021.

122. Nichols, B.D. and Hirt, C.W. (1971). "Improved Free Surface Boundary Conditions Of Numerical Incompressible Flow Calculations", Journal of Computational Physics, Vol. 8, pp 434-448.

123. Nicklin, D.J., Wilkes, J.O. and Davidson, J.F. (1962). "Two-Phase Flow In Vertical Tubes", Trans. Instn. Chem. Engrs., Vol. 40, pp 61-68.

124. Padmanabhan, M. (1984). "Air Ingestion Due To Free Surface Vortices", A.S.C.E., Journal of Hydraulic Engineering, Vol. 110, No. 12, pp 1855-1859.

125. Parakh, C. (1969). "Two-Phase Slug Flow In An Inclined Pipe", A Dissertation Submitted in Partial Fulfillment of the requirements for the Degree of Master of Engineering in Heat Power.

126. Peterka, A.J. (1954). "Performance Tests On Prototype And Models", Transactions, Proceedings, Separate No. 488, pp 385-409.

127. Pinto, N.L., Neidert, S.H. and Ota, J.J. (1982). "Aeration At High Velocity Flows", Water Power and Dam Construction, pp 34-38.

128. Quintala, A.C. (1980). "Flow Aeration To Prevent Cavitation Errosion", Water Power and Dam Construction, pp 17-22.

129. Rajaratnam, N. (1962). "Profile Equation For Hydraulic Jump:, Water Power, pp 324-327.

130. Rajaratnam, N. (1964). "The Forced Hydraulic Jump", Water Power, pp 14-19.

131. Rajaratnam, N. (1964). "The Forced Hydraulic Jump", Water Power, pp 61-65.

132. Rajaratnam, N. (1965). "Hydraulic Jump In Horizontal Conduits", Water Power, pp 80-83.

133. Rajaratnam, N. (1967). "Hydraulic Jumps", In "Advances In Hydroscience", Vol. 4, Edited by Chow, V.T., Academic Press, New York and London.

134. Rankine, W.J.M. (1871). "The Mathematical Theory Of Stream Lines", Philosophical Transactions, pp 267-306.

135. Resch, F.J., Leutheusser, H.J. and Alemu, S. (1974), "Bubbly Two-Phase Flow In Hydraulic Jump", A.S.C.E., Journal of Hydraulic Division, Vol. 100, No. HY1, pp 137-149.

136. Richards, R.T. (1957). "Air Binding In Large Pipelines Flowing Under Vacuum", A.S.C.E., Journal of Hydraulic Division, Vol. 83, No. HY6, pp 1454 (1-10).

137. Rockwell, D. and Knisely, C. (1979). "Unsteady Features Of Flow Past A Cavity", A.S.C.E., Journal of Hydraulic Division, Vol. 105, No. HY8, pp 969-979.

138. Rouse, H. (1964). "Engineering Hydraulics", John Wiley and Sons, Inc.

139. Runge, D.E. and Wallis, G.B. (1965). AEC Report NYO-3114-8, (Euraec - 1416).

140. Ryskin, G. and Leal, L.G. (1984). "Numerical Solution Of Free-Boundary Problems In Fluid Mechanics, Part 1, The Finite-Difference Technique", Journal of Fluid Mechanics, Vol. 148, pp 1-17.

141. Ryskin, G. and Leal, L.G. (1984). "Numerical Solution Of Free-Boundary Problems In Fluid Mechanics, Part 2, Buoyancy-Driven Motion Of A Gas-Bubble Through A Quiescent Liquid", Journal of Fluid Mechanics, Vol. 148, pp 19-35.

142. Ryskin, G. and Leal, L.G. (1984). "Numerical Solution Of Free-Boundary Problems In Fluid Mechanics, Part 3, Bubble Deformation In An Axi-symmetric Straining Flow", Journal of Fluid Mechanics, Vol. 148, pp 37-43.

143. Sailer, R.E. (1955). "San Diego Aqueduct, Air-Entrainment In Siphon Barrels", Civil Engineering, Vol. 25, No. 5, pp 268-271.

144. Salih, M.A. (1979). "Air Bubbles In A Convectively Accelerated Water Flow", Journal of Hydraulic Research, 17, No. 4, pp 315-327.

145. Sande, E.D. and Smith, J.M. (1973). "Surface Entrainment Of Air By High Velocity Water Jets", Chemical Engineering Science, Vol. 28, pp 1161-1168.

146. Sandover, J.A. and Holmes, P. (1962). "The Hydraulic Jump In Trapizoidal Channels", Water Power, pp 445-449.

147. Sharma, H.T. (1976). "Air Entrainment In High Head Gated Conduits", A.S.C.E., Journal of Hydraulic Division, Vol. 102, No. HY11, pp 1629-1646.

148. Silliman W.J. and Scriven, L.E. (1980). "Separating Flow Near A Static Contact Line: Slip At A Wall And Shape Of A Free Surface", Journal of Computational Physics, Vol. 34, pp 287-313.

149. Silvester, R. (1961). "Specific Energy And Force Equations In Open-Channel Flow", Water Power, pp 99-103.

150. Silvester, R. (1964). "Hydraulic Jump In All Shapes Of Horizontal Channels", A.S.C.E., Journal lof Hydraulic Division, No. HY1, pp 23-55.

151. Simpson, H.C., Rooney, D.H., Grattan, E. and Al-Samarrae, F.A.A. (1981). "Two-Phase Flow Studies In Large Diameter Horizontal Tubes", National Engineering Laboratory, Report No. 67,, Dept. of Industry.

152. Singh, G. and Griffith, P. (1970). "Determination of Pressure Drop Optimum Pipe Size For A Two-Phase Slug Flow In Inclined Pipe", Trans. A.S.M.E., Journal of Engineering for Industry, Vol. 92, pp 717-726.

153. Southwell, R.V. and Vaisey, G. (1946). "Relaxation Methods Applied To Engineering Problems - XII, Fluid Motions Characterised By 'Free' Stream Lines", Proc. Royal Soc., A240, pp 117-161.

154. Spedding, P.L. and Nguyen, V.T. (1978). "Bubble Rise And Liquid Content In Horizontal And Inclined Tubes", Chemical Engineering Science, Vol. 33, pp 987-994.

155. Stevens, J.C. (1933). "The Hydraulic Jump In Standard Conduits", A.S.C.E., Civil Engineering, Vol. 3, pp 565-567.

156. Street, R.L. (1964). "Two-Dimensional Jet And Cavity Flows", A.S.C.E., Journal of Hydraulic Division, Vol. 90, No. HY2, pp 141-161.

157. Taitel, Y. and Duler, A.E. (1976). "A Model For Predicting Flow Regime Transitions In Horizontal And Near Horizontal Gas-Liquid Flow", Journal of A.I. Ch.E., Vol. 22, No. 1, pp 47-55.

158. Task Force on The Flow in Large Conduits of The Committee on Hydraulic Structures, (1965). "Factors Influencing Flow In Large Conduits", A.S.C.E., Journal of Hydraulic Division, Vol. 91, No. HY6, pp 123-152.

159. Tekeli, S. and Maxwell, W.H.C. (1981). "Hot-Film Response And Digital Analysis In Bubbly Flow", A.S.C.E., Journal of Hydraulic Division, Vol. 108, No. HY2, pp 267-272.

160. Tekele, T. (1983). "Some Design Problems Related To Air-Entrainment And Absorption In Hydro-Power Systems With Secondary Dropshaft Intakes", International Association for Hydraulic Research.

161. Thiruvengadam, A. (1961). "Hydraulic Jump In Circular Channels", Water Power, pp 496-497.

162. Thomas, N.H. (1982). Air-Demand Distortion In Hydraulic Models", International Conference on Hydraulic Modelling of Civil Engineering Structures, Held at Coventry, England, 22-24 Sept.

163. Thomas, N.H., Auton, T.R., Sene, K. and Hunt, J.C.R. (1983). "Entrapment And Transport Of Bubbles By Transient Large Eddies In Multiphase Turbulent Shear Flows", International Conference on the Physical Modelling of Multiphase Flow, Held at Coventry, England, 19-21 April.

164. Thomas, W.J. and Portalski, S. (1958). "Counter-Current Flow In Wetted-Wall Columns", Industrial and Engineering Chemistry, Vol. 50, No. 7, pp 1081-1088.

165. Townson, J.M. (1975). "Oscillations In A Cooling Water Outfall System", Proc. Instn. Civ. Engrs., Part 2, Vol. 59, pp 837-847.

166. Townson, J.M. (1978). "Cooling Water For Power Stations, (Discussioin)", Proc. Instn. Civ. Engrs., Part 1, Vol. 64, pp 281-293.

167. Tullis, J.P. and Marschner, B.W. (1968). "Review Of Cavitation Research On Valves", A.S.C.E., Journal of Hydraulic Division, Vol. 94, No. HY1, pp 1-16.

168. Tullis, J.P. and Govindarajan, R. (1973). "Cavitation And Size Scale Effects For Orifices", A.S.C.E., Journal of Hydraulic Division, Vol. 99, No. HY3, pp 417-430.

169. Tullis, J.P. (1973). "Cavitation Scale Effects For Valves", A.S.C.E., Journal of Hydraulic Division, Vol. 99, No. HY7, pp 1109-1128.

170. Tullis, J.P. (1981). "Modelling Cavitation For Closed Conduit Flow", A.S.C.E., Journal of Hydraulic Division, Vol. 107, No. HY11, pp 1335-1349.

171. Tung, K.W. and Parlange, J.Y. (1976). "Note On The Motion Of Long Bubbles In Closed Tubes - Influence Of Surface Tension", Acta-Mechanica, Vol. 24, pp 313-317.

172. Tunstall, M.J. and Harvey, J.K. (1968). "The Effect Of A Sharp Bend In A Fully Developed Turbulent Flow", Journal of Fluid Mechanics, Vol. 34, Part 3, pp 595-608.

173. Vallentine, H.R. (1969). "Applied Hydrodynamics", S.I. Edition, Butterworth and Co. (Publishers) Limited.

174. Veronese, A. (1937). "Sul Motto Delle Bolle D'Aria Nelle Condotte D'Acqua", Estrato dal Fasciacolo X, Vol. XIV, Ottobre, p XV.

175. Viecelli, J.A. (1971). "A Computing Method For Incompressible Flows Bounded By Moving Walls", Journal of Computational Physics, Vol. 8, pp 119-143.

176. Wallis, G.B. (1962). General Electric Company, Schenectady, N.Y., Report 62 GL 130.

177. Wallis, G.B. (1969). "One-Dimensional Two-Phase Flow", McGraw Hill.

178. Wallis, G.B., Crowley, C.J. and Hagi, Y. (1977). "Conditions For A Pipe To Run Full When Discharging Liquid Into A Space Filled With Gas", A.S.M.E., Journal of Fluid Engineering, Vol. 99, pp 405-413.

179. Wallis, G.B. (1982). "Review - Theoretical Models Of Gas-Liquid Flows", A.S.M.E., Journal of Fluid Engineering, Vol. 104, pp 279-283.

180. Whillock, A.F. and Thorn, M.F.C. (1973). "Air Entrainment In Dropshafts", C.I.R.I.A. Tech. Note 48.

181. White, E.T. and Beardmore, R.H. (1962). "The Velocity Of Rise Of Single Cylindrical Air Bubbles Through Liquids Contained In Vertical Tubes", Chemical Engineering Science, Vol. 17, pp 351-361.

182. Whitham, G.B. (1961). "Mass, Momentum, And Energy Flux In Water Waves", Journal of Fluid Mechanics, Vol. 21, pp 135-147.

183. Wijnyaarden, L.V. (1968). "On The Equations Of Motion For Mixtures Of Liquid And Gas-Bubbles", Journal of Fluid Mechanics, Vol. 33, Part 3, pp 465-474.

184. Wilkinson, D.L. (1982). "Motion Of Air Cavities In Long Horizontal Ducts", Journal of Fluid Mechanics, Vol. 118, pp 109-122.

185. Williamson, J. (1939). "Considerations On Flow In Large Pipes, Conduits, Tunnels, Bends, And Siphons", Instn. Civ. Engrs, Journal, Paper 5189, pp 451-502.

186. Winn, W.P. and Johnson, D.E. (1970). "Cavitation Parameters For Outlet Valves", A.S.C.E., Journal of Hydraulic Division, Vol. 96, No. HY12, pp 2519-2533.

187. Wisner, P.E., Mohsen, F.N. and Kouwn, N. (1975). "Removal Of Air From Water Lines By Hydraulic Means", A.S.C.E. Journal of Hydraulic Division, Vol. 101, No. HY2, pp 243-257.

188. Wood, I.R. (1985). "Air Entrainment And Deaeration In Hydraulic Structures", Unpublished Monograph.

189. Wu, Th.Y.T. (1972). "Cavity And Wake Flows", Annual Review of Fluid Mechanics, Vol. 14, pp 243-284.

190. Zanker, K.J. and Brock, T.E. (1967). "A Review Of The Literature On Fluid Flow Through Closed Conduit Bends", The British Hydromechanics Research Association, TN901.

191. Zuber, N. and Findlay, J.A. (1965). "Average Volumetric Concentration In Two-Phase Flow Systems", A.S.M.E., Journal of Heat Transfer, pp 453-468.

192. Zukoski, E.E. (1966). "Influence Of Viscosity, Surface Tension, And Inclination Angle On Motion Of Long Bubbles In Closed Tubes", Journal of Fluid Mechanics, Vol. 25, Part 4, pp 821-837.

APPENDIX A

Correction Factor for the Momentum Flux β_o

The complete integration to obtain the correction factor applied for the momentum flux β_o will be given here as outlined earlier in Section (3.5.1). The momentum flux correction factor is applied to the momentum flux at the bend to account for the non-uniformity spacing of the stream lines. The equation used to derive β_o is as follows:

$$\beta_o = \frac{\int V^2 dA}{\bar{V}^2 A} \tag{3.13}$$

where $V = \frac{\bar{V}R'}{r}$ the velocity at any point (3.15)

and $\bar{V}$ = mean velocity, and $A = \frac{\pi D^2}{4}$ area of pipe. Substituting into equation (3.13) and arranging:

$$\beta_o = \frac{4R'^2}{\pi D^2} \int_o^{\pi} (\frac{1}{r})^2 dA \tag{A.1}$$

From equations (3.17), (3.18) and (3.19) the values of dA, dr and r respectively are used to substitute for their values in equation (A.1) to obtain:

$$\beta_o = \frac{4R'^2}{\pi D^2} \int_o^{\pi} \frac{1}{(R' - \frac{D}{2}\text{Cos}\theta)^2} \frac{D^2}{2} \text{Sin}^2\theta \, d\theta \tag{A.2}$$

let $K' = \frac{D}{2R'}$, then

$$\beta_o = \frac{2}{\pi} \int_0^{\pi} \frac{1}{(1-K'\cos\theta)^2} \sin^2\theta \, d\theta \qquad (A.3)$$

Now let $Z = (\frac{\theta}{2})$, then $\cos\theta = \frac{1-Z^2}{1+Z^2}$, $\sin\theta = \frac{2Z}{1+Z^2}$ and $d\theta = \frac{2dZ}{1+Z^2}$. The limit of integration will be from $0 \rightarrow \infty$. Substituting into equation (A.3) and rearranging:

$$\beta_o = \frac{16}{\pi} \int_0^{\infty} \frac{Z^2}{[(1-K') + Z^2(1+K')]^2} \frac{dZ}{1+Z^2} \qquad (A.4)$$

let $a = \sqrt{\frac{1-K'}{1+K'}}$, $b = (1+K')^{-2}$, then:

$$\beta_o = \frac{16b}{\pi} \int_0^{\infty} (\frac{Z}{a^2+Z^2})^2 \frac{dZ}{1+Z^2} \qquad (A.5)$$

Now let $Z = a\tan\phi$, $dZ = a \sec^2\phi \, d\phi$, the limit of integration will be from $0 \rightarrow \pi/2$. Substitute into equation (A.5):

$$\beta_o = \frac{16b}{\pi a} \int_0^{\frac{\pi}{2}} \frac{\tan^2\phi}{(1+\tan^2\phi)^2} \times \frac{\sec^2\phi \, d\phi}{(1+a^2\tan^2\phi)} \quad \text{or}$$

$$\beta_o = \frac{16b}{\pi a} \int_0^{\frac{\pi}{2}} \frac{\tan^2\phi}{(1+\tan^2\phi)^2} \times \frac{d(\tan\phi)}{(1+a^2\tan^2\phi)} \qquad (A.6)$$

Assuming that $x = \tan\phi$, then equation (A.6) can be written as follows:

$$\beta_o = \frac{16b}{\pi a} \int_0^{\frac{\pi}{2}} \frac{x^2\, dx}{(1+x^2)^2\,(1+a^2x^2)} \qquad (A.7)$$

Equation (A.7) is now integrated by parts after simplifying as follows:

$$\frac{x^2}{(1+x^2)^2(1+a^2x^2)} = \frac{Ax + B}{(1+x^2)^2} + \frac{Cx + D}{(1+x^2)} + \frac{Ex + F}{(1+a^2x^2)} \qquad (A.8)$$

where A, B, C, D, E and F are constants, simplifying the above equation:

$$x^2 = (Ax+B)(1+a^2x^2) + (Cx+D)(1+x^2)(1+a^2x^2) + (Ex+F)(1+x^2)^2 \qquad (A.9)$$

Arranging equation (A.9), the following is obtained:

$$x^2 = (B+D+F) + (A+C+E)\,x + (a^2B+a^2D+D+2F)x^2$$

$$+ (a^2A+a^2C+C+2E)x^3 + (a^2D+F)x^4 + (a^2C+E)x^5 \qquad (A.10)$$

Equating the coefficients on both sides of equation (A.10), and solving for the value of the constants A, B, C, D, E and F, the following is obtained:

$$A = 0 \quad , \quad C = 0 \quad \text{and} \quad E = 0$$

$$B = \frac{1}{a^2-1} \quad , \quad D = \frac{1}{(a^2-1)^2} \quad \text{and} \quad F = \frac{-a^2}{(a^2-1)^2}$$

The above constants appear to depend on the radius of the bend, since a is a function of the bend radius. Substituting into equation (A.8) and integrating:

$$\int_0^{\frac{\pi}{2}} \frac{x^2\,dx}{(1+x^2)^2(1+a^2x^2)} = \int_0^{\frac{\pi}{2}} \left[\frac{B}{(1+x^2)^2} + \frac{D}{(1+x^2)} + \frac{F}{(1+a^2x^2)} \right] dx$$

or:

$$\int_0^{\frac{\pi}{2}} \frac{\tan^2\phi\; d(\tan\phi)}{(1+\tan^2\phi)^2(1+a^2\tan^2\phi)} = \int_0^{\frac{\pi}{2}} \left[\frac{B}{(1+\tan^2\phi)^2} + \frac{D}{(1+\tan^2\phi)} + \frac{F}{(1+a^2\tan^2\phi)} \right] d(\tan\phi)$$

$$= B\int_0^{\frac{\pi}{2}} \frac{\mathrm{Sec}^2\phi\; d\phi}{\mathrm{Sec}^4\phi} + D\int_0^{\frac{\pi}{2}} \frac{\mathrm{Sec}^2\phi\; d\phi}{\mathrm{Sec}^2\phi} + \frac{F}{a^2}\int_0^{\frac{\pi}{2}} \frac{d(\tan\phi)}{(1/a^2+\tan^2\phi)}$$

$$= B\int_0^{\frac{\pi}{2}} \mathrm{Cos}^2\phi\; d\phi + D\int_0^{\frac{\pi}{2}} d\phi + \frac{F}{a^2}\int_0^{\frac{\pi}{2}} \frac{d(\tan\phi)}{(a'^2 + \tan^2\phi)}$$

where $a'^2 = 1/a^2$, integrating the final form above the following is obtained after substituting into equation (A.7):

$$\beta_o = \frac{16\,b}{\pi a}\left\{B\left(\frac{\phi}{2} + \frac{\mathrm{Sin}2\phi}{4}\right) + D\phi + \frac{F}{a^2}\left[\frac{1}{a'}\tan^{-1}\left(\frac{\tan\phi}{a'}\right)\right]\right\}_0^{\frac{\pi}{2}}$$

Substituting for a' and simplifying:

$$\beta_o = \frac{16\,b}{\pi a}\left(0.78539\;B + 1.57079D + 1.57079\,\frac{F}{a}\right) \qquad (A.11)$$

Substituting for the constants B, D and F values given in Table (3.1) and for a and b values, the following values for β_o are obtained:

For R'/D = 0.5 , $\beta_o \rightarrow \infty$

For R'/D = 1.0 , $\beta_o = 1.2389$

For R'/D = 1.5 , $\beta_o = 1.0868$
